LABORATORY OF MOLECULAR STRUCTURE AND SPECTRA

DEPARTMENT OF PHYSICS • THE UNIVERSITY OF CHICAGO

TECHNICAL REPORT

1969 - 70

D D C

RECEIVED

349

DOCUMENT CONTROL DATA - R & D		
1. Originating Activity Department of Physics and Department of Chemistry University of Chicago Chicago, Illinois 60637	2a. Report Security Classification UNCLASSIFIED	
	2b. Group	

3. Report Title

LABORATORY OF MOLECULAR STRUCTURE & SPECTRA TECHNICAL REPORT, 1969-70

4. Descriptive Notes

Joint Technical Report of the Laboratory of Molecular Structure & Spectra, reporting on the research accomplished under the sponsorship of the various contracts which support this Laboratory, for the period covering 1 January 1969 through 31 December 1970.

5. Authors

Mulliken, Robert S., Roothaan, Clemens C. J., and Hinze, Juergen (Principal Investigators). See Table of Contents for the complete listing of additional authors.

6. Report Date 1 January 1969 thru 31 December 1970	7a. Total No. of Pages 405	7b. No. of References N/A

8. Contracts or Grant Nos.
a. Contract N00014-67-A-0285-0001 a. Contract DA-31-124-ARO-D-447
b. RR 002-031   b. Project No. 3835-P
c. NR 014 101   c. ARPA Order No. 368
 	
  a. Contract DAHC 04-70-C-0037
  b. Project No. P-9421-P
  c. ARPA Order No. 62301D
	9a. Originators Report No.
	LMSS - 1969-70	

	9b. Other Report Nos.	

10. Availability/Limitation Notices

Qualified requesters may obtain copies of this report from LMSS and DDC.

11. Supplementary Notes	12. Sponsoring Military Activity Office of Naval Research Physics Branch Washington, D. C. 20360 Army Research Office (Durham) Box CM, Duke Station Durham, North Carolina 27706

13. Abstract

This Technical Report contains several papers on the qualitative and interpretive aspects of molecular orbital theory. Two papers are concerned with the interpretation of accurate H-F wavefunctions of small electronic molecules. Several papers give a detailed report of computed electronic and vibration rotational spectra and transition probabilities for some diatomic molecules. In addition there are a number of papers concerning high resolution UV spectroscopic studies of polyatomic molecules, and the interpretation of such spectra. In the case of some diatomics, UV spectra are more completely assigned and some bands are reinterpreted.

DD FORM 1 JAN.64 **1473**

| 14 | LINK A | | LINK B | | LINK C | |
KEY WORDS	ROLE	WT	ROLE	WT	ROLE	WT
SCF Wavefunctions						
Diatomic Molecules						
Hydrogen Molecules						
Charge-Transfer						
Molecular Compounds						
Absorption Spectra						
Vibrational Structure						
Ethylene						
Rydberg States						

INSTRUCTIONS

LABORATORY OF MOLECULAR STRUCTURE AND SPECTRA
DEPARTMENT OF PHYSICS • THE UNIVERSITY OF CHICAGO

TECHNICAL REPORT

1969 - 70

BLANK PAGE

LABORATORY OF MOLECULAR STRUCTURE AND SPECTRA PERSONNEL

(For the period 1 January 1969 thru 31 December 1970)

Faculty

†#   Robert S. Mulliken, Professor of Physics and Chemistry

*#   Clemens C. J. Roothaan, Professor of Physics and Chemistry

*   Juergen M. A. Hinze, Assistant Professor of Chemistry

Professional Staff

*#   Dr. Paul E. Cade, Physicist (thru 8/25/69). Now at the
      University of Massachusetts, Amherst, Massachusetts.

*   Dr. Nora H. Sabelli, Chemist (thru 6/11/69).

Research Associates

*   Dr. Reinhart Ahlrichs (thru 11/30/70). Now at Phys. Chemie
      Abt. Theoret. Chemie, 75 Karlsruhe, Kaiserstr. 12, W. Germany.

†#   Dr. David W. Green (from 9/30/68).

†   Dr. Ichiro Hanazaki (thru 12/31/70). Now at the Institute of
      Physical and Chemical Research, Hirosawa, Wako-shi, Saitama-ken,
      Japan

      Dr. William H. Henneker (thru 12/31/69). Now at the University
      of Massachusetts, Amherst, Massachusetts.

      Dr. Michiya Itoh (thru 7/31/69). Now at the Faculty of
      Pharmaceutical Sciences, The University of Tokyo, Bunkyo-ku,
      Tokyo, Japan.

*   Dr. Herbert E. Popkie (thru 12/31/70). Now at the IBM Research
      Laboratory, San Jose, California.

Research Assistants

*#   Mr. James Bass (thru 9/11/70). Physics Ph.D. Candidate.
      Now at the University of Florida, Gainesville, Florida.

†   Mr. Bei-dwo Chang (thru 12/31/70). Graduate Student in Physics.

*#   Mr. Brad Cox (thru 3/31/69). Chemistry Ph.D. Candidate.

*#   Mr. John Detrich (from 11/1/64). Physics Ph.D. Candidate.

*   Mrs. Kate K. Docken (from 9/1/67). Chemistry Ph.D. Candidate.

*§   Mr. Warren H. Kosman (from 9/1/67). Chemistry Ph.D. Candidate.

§   Mr. Chia-Ming Lee (thru 12/31/70). Graduate Student in Physics.

Mr. George Lie (from 9/1/67). Chemistry Ph.D. Candidate.

*#   Mr. Shiaw S. Lin (from 10/1/67). Physics Ph.D. Candidate.

iii

Research Assistants (continued)

* Mr. Bowen Liu (thru 6/11/69). Chemistry Ph.D. Candidate.

§ Mr. Bo-Ching Lu (from 10/1/70). Graduate Student in Physics.

†# Mr. Richard L. Lyke (thru 3/11/70). Now at the University of Minnesota, Minneapolis, Minnesota.

* Mr. Joseph Olive (thru 5/16/69). Physics Ph.D. degree, August 1969. Now at Bell Telephone Labs., Murray Hill, New Jersey.

*# Mr. Hideo Sambe (from 10/1/64). Physics Ph.D. Candidate.

†§ Mr. Lambert Schoonveld (thru 9/26/69). Graduate Student in Physics. Now at Illinois Circle Campus, Chicago, Illinois.

*# Mrs. Eugenia Schwartz (from 6/17/67). Physics Ph.D. Candidate.

* Mr. Kenneth J. Schwartz (from 9/1/68). Chemistry Ph.D. Candidate.

*# Mr. Zoran Sibincic (from 6/18/62). Physics Ph.D. Candidate.

*#§ Mr. George Soukup (from 10/1/61). Physics Ph.D. Candidate.

§ Mr. John Steinhoff (thru 9/30/69). Graduate Student in Physics. Now at Argonne National Laboratory, Argonne, Illinois.

*#§ Mr. Edward Weiss (from 10/1/66). Physics Ph.D. Candidate.

*# Mr. Irving Wladawsky (thru 5/31/70). Physics Ph.D. Candidate. Now at the IBM Thomas J. Watson Research Center, Yorktown Heights, New York.

Secretarial Staff

*# Mrs. Mary Fouts (thru 8/31/70).

†#§ Mrs. Helen Griffith (thru 5/31/70).

†# Mrs. Betty C. Miles (from 6/15/70). Editorial Secretary for this Report.

FOREWORD

Seven comprehensive Technical Reports were issued under Contract N6ori-20, Task Order IX, Project 019 101, with the Office of Naval Research: a Quarterly Report for the period 1 June 1947 to 31 August 1947; an Annual Report (in two parts) for the period from 1 September 1947 to 31 August 1948; a Report (in two parts) for the period 1 September 1948 to 31 March 1950; a Report (in two parts) for the period 1 April 1950 to 31 March 1951; a Report (in two parts) for the period 1 April to 31 March 1952.

The Technical Report for 1952-3, issued in two parts, and Part One of the Technical Report for 1953-4, which covered roughly the period 1 October 1953 to 31 March 1954, were issued jointly under this Laboratory's contract with the Office of Naval Research (ONR) and Contract DA-11-022-1002, Project TB2-0001 (505) with the Office of Ordnance Research (OOR). Part Two of the Technical Report for 1953-4 was issued jointly under these contracts and Contract AF18(600)-471, Project No. R-351-40-4 with the Office of Scientific Research (AFOSR) of the Air Research and Development Command (ARDC). The Technical Reports for 1955 and 1956 were issued jointly under the contracts with ONR, OOR, AFSOR, and under Contract AF19(604)-019 with the Geophysics Research Directorate (GRD) of the Air Force Cambridge Research Center. The OOR contract was extended without additional funds from 1 October 1957 through 30 September 1958 and a Final Report was issued.

The work under the original ONR contract N6ori-20, IX, Project 019 101 was completed on 30 September 1956, and a Final Report was issued. A new contract, Nonr-2121(01), went into effect 1 October 1956: work described in the 1956 and subsequent Technical Reports and supported by the ONR, was done under that contract. The contract was terminated on 30 November 1965, and a Final Report was issued. The work is being continued under a new contract, N00014-66-C0075 (A01) which became effective 1 October 1965. The contract was amended to N00014-67-A-0285-0001 on 1 October 1966.

The original GRD contract terminated 25 October 1967. This work was continued under GRD Contract AF19(604)-3478 which terminated 14 December 1959. The work was further continued, beginning 15 January 1960, under Contract AF19(604)-6662 with the Electronics Systems Division of the Air Force Systems Command (AFSC). At the termination of this contract on 14 January 1963, a final report was issued and work continued under Contract AF19(628)-2474 which began on 15 January 1963 and terminated on 31 March 1967, when a final report was issued. A new one-year Contract, F19628-67-C-0049 became effective on 1 April 1967 for the continuation of the work, but was terminated on 31 March 1968 without further funding from OAR, and a Final Report was issued.

The AFOSR contract was extended for two years from 1 October 1962 without added funds, but with the provision of ample computing time, for the completion of the work under the contract on the Univac Scientific (Remington-Rand 1103 and 1103A) electronic digital computers at Wright-Patterson Field Air Force Base (WADC); a Final Report was issued. With the availability of these computer facilities, new funded support from a National Science Foundation (NSF) grant, made it possible to carry this work further forward.

All the contracts mentioned thus far were under the direction of Professor Robert S. Mulliken as Principal Investigator. A one-year contract from WADC, AF33(616)-5608 with Professor C. C. J. Roothaan as Principal Investigator went into effect 1 April 1958, and the use of the computing facilities at WADC since 30 September 1958 on all the contracts and the NSF grant was under the auspices of this contract, extended on a no-cost basis through 31 May 1959. These computing facilities continued to be made available under a one-year contract AF49(638)-699 from AF Office of Scientific Research, Office of Aerospace Research which expired 30 June 1960. Continued use was made of the facilities under AFOSR, OAR Contract AF49(638)-1068 which commenced 1 April 1961 and terminated 30 April 1962. Under a new contract AF33(657)-8891 which was funded 1 May 1962, use of the computing facilities at WADC was continued through September 1962. In October 1962, all computation efforts were transferred to new facilities established at the University of Chicago Computation Center, with Professor C. C. J. Roothaan as Director. These facilities originally consisted of an IBM 7090 and IBM 1401 and peripheral equipment, but in June 1963 conversion of the IBM 7090 to a 7094 was carried out, and in December 1964 the 1401 was replaced by an IBM 7040. In August 1968 an IBM 360 Model 50 was added to the facilities available at the University of Chicago Computation Center. This machine was exchanged in January 1969 for a Model 65 and the IBM 7040 was returned. Professor C. C. J. Roothaan resigned from the directorship of the University of Chicago Computation Center in September 1968. The computing efforts in LMSS employ the University of Chicago Computer Center facilities, i.e. IBM 7094 and IBM 360/65 as well as those of Argonne National Laboratory, i.e. IBM 360/50 - 360/75.

Beginning 12 June 1959, a three-year contract with the OOR (now the Army Research Office, ARO), Contract DA-11-022-ORD-3119 went into effect, sponsored under auspices of the Advanced Research Projects Agency (ARPA), funded under ARPA Order 368, for theoretical computations on light molecules, and under the direction of Professor C. C. J. Roothaan and Dr. B. J. Ransil as Principal Investigators, with Professor R. S. Mulliken as Consultant. At its expiration on 11 June 1962, the contract was renewed for another three-year period from 12 June 1962 through 11 June 1965, with Professor Roothaan as Principal Investigator. The contract was renewed for an additional year on 12 June 1965

and was terminated on 11 June 1966, when a Final Report was issued. Work continued under a new contract DA-31-124-ARO-D-447, which became effective on 12 June 1966, and terminated 11 June 1970, when a Final Report was issued. For the last two years of this contract Professor Juergen Hinze was Co-principal Investigator. Since 12 June 1970, work is being supported by a new contract DAHC 04-07-C-0037 with Professor Juergen Hinze as Principal Investigator.

The present Technical Report for 1969-70 is issued under contracts from ONR (Office of Naval Research) and ARO (Army Research Office-Durham). These contracts have supported the research reported herein during the period 1 January 1969 through 31 December 1970. A number of the papers included have received partial support from National Science Foundation Grants (GP-9284, GP-15216 and GP-27138), and are included because of their close relation to the research reported on the ARO and ONR contracts. The ONR contract has supplied all the equipment and supported all the research carried out on molecular complexes for this period.

For a complete list of papers published from 1 January 1953 up to early 1960 by personnel of the Laboratory of Molecular Structure and Spectra, reference may be made to the Technical Report 1957-9, Part Two. Papers from this Laboratory published in the period 1947-52 are listed in the ONR Final Report of 30 September 1956.

TABLE OF CONTENTS

OTHER LMSS PUBLICATIONS NOT INCLUDED IN THIS REPORT

1. R. S. Mulliken, "Iodine Revisited". J. Chem. Phys. $\underline{55}$, 000 (1971).

2. R. S. Mulliken, "The Role of Kinetic Energy in the Franck-Condon Principle". J. Chem. Phys. $\underline{55}$, 000 (1971).

3. R. Ahlrichs, "Origin of the Dimerization Energy of $BH_3$2O B_2H_6". Chem. Phys. Letters $\underline{7}$, 503 (1970).

4. D. W. Green, "Electronic States of ScO, YO, and LaO", (submitted for publication).

Optimization of Exponents for Slater-Type Basis Functions

JÜRGEN HINZE

Department of Chemistry, University of Chicago,
Chicago, Illinois 60637

One of the bottlenecks in the computation of accurate atomic or molecular wavefunctions, using an expansion of the orbitals in Slater-type functions, is the determination of the "best" exponents to be used in these basis functions.[1] The use of large "saturated" basis sets has two practical disadvantages: (1) it does not yield the most compact description of the wavefunction desired, and (2) it becomes rapidly expensive in terms of computer time. The procedure generally used to find the "best" basis function exponents is a "brute-force" optimization, i.e., the energy hypersurface, which is a function of the basis function exponents, is searched for a minimum with procedures of various sophistication.[1-4] Since the computation of any one point on the energy surface is rather cumbersome, such "brute-force" minimization can become prohibitively expensive in terms of computer time required. We have successfully used an alternate method, based on the expansion of the Slater-type functions in terms of a truncated Taylor series, and have achieved significant time savings over the conventional "brute-force" methods.

The expansion of the spatial part of an orbital in terms of Slater-type basis functions is

$$\phi_i(\mathbf{r}) = \sum_p C_{ip}\chi_p(\mathbf{r}), \tag{1}$$

where the C_{ip}'s are the expansion coefficients, and the basis functions

$$\chi_p(\mathbf{r}) = R(n_p, \zeta_p; r) Y_{l_p,m_p}(\theta, \phi) \tag{2}$$

are generally centered on some atom. The Y_{lm}'s are normalized spherical harmonics and the $R(r)$'s are normalized Slater-type functions. The normalized Slater-type functions

$$R(n, \zeta; r) = [(2n)!]^{-1/2}(2\zeta)^{n+1/2}r^{n-1}\exp(-\zeta r) \tag{3}$$

depend on the origin of r (their center) and the parameters n and ζ. To achieve an optimization of ζ, we expand around ζ^0. Neglecting terms of second and higher

order in $\delta\zeta$, we obtain explicitly

$$R(n, \zeta^0+\delta\zeta; r) \approx [1+\tfrac{1}{2}(2n+1)(\delta\zeta/\zeta^0)]R(n, \zeta^0; r)$$
$$-\tfrac{1}{2}[(2n+1)(2n+2)]^{1/2}(\delta\zeta/\zeta^0)R(n+1, \zeta^0; r). \tag{4}$$

If $\delta\zeta_p$ is required to improve the basis function $\chi_p(n_p, \zeta_p^0; \mathbf{r})$, then it is only necessary to introduce into the calculation in addition the basis function $\chi_p(n_p+1, \zeta_p^0; \mathbf{r})$. A conventional SCF calculation will yield the expansion coefficients $C_{ip}^{(n)}$ and $C_{ip}^{(n+1)}$ corresponding to $\chi_p(n_p, \zeta_p^0; \mathbf{r})$ and $\chi_p(n_p+1, \zeta_p^0; \mathbf{r})$ respectively, for every orbital i.

Assume that C_{ip} is the unknown coefficient for the corrected basis function with exponent $\zeta_p^0+\delta\zeta_p$, then we obviously have

$$C_{ip}[1+\tfrac{1}{2}(2n+1)(\delta\zeta_{ip}/\zeta_p^0)]=C_{ip}^{(n)}, \tag{5a}$$

and

$$-\tfrac{1}{2}C_{ip}[(2n+1)(2n+2)]^{1/2}(\delta\zeta_{ip}/\zeta_p^0)=C_{ip}^{(n+1)}. \tag{5b}$$

Solving Eqs. (5) yields for the corrections to ζ_p^0 corresponding to orbital i,

$$\delta\zeta_{ip} = -\frac{2\zeta_p^0 C_{ip}^{(n+1)}}{C_{ip}^{(n)}[(2n+1)(2n+2)]^{1/2}+C_{ip}^{(n+1)}(2n+1)}. \tag{6}$$

If these $\delta\zeta_{ip}$'s differ only little, a weighted average (weighted by orbital occupation numbers N_i and expansion coefficients squared)

$$\langle\delta\zeta_p\rangle = \sum_i \delta\zeta_{ip}N_i C_{ip}^2 / \sum_i N_i C_{ip}^2 \tag{7}$$

will suffice. However, if the $\delta\zeta$'s for the same basis function but different orbitals differ widely, and the corresponding C_{ip}'s are significant, then it will be necessary to introduce a new basis function to satisfy the needs of the different orbitals.

The above procedure has been used successfully for the optimization of up to four basis functions simultaneously. Obviously, difficulties arise if two basis functions on the same center and with identical n and similar ζ are to be optimized simultaneously.

1

If the above procedure is used only for the optimization of one basis function at a time, then there is little advantage over "brute-force" methods. Clearly it is also not feasible to optimize all the basis functions in a given basis set simultaneously; the number of integrals to be computed would be excessive since the basis set would have been doubled. Also, the result with the doubled basis would obviously be better than the result with the reduced but optimized basis. It is most advantageous to optimize the basis set by optimizing blocks of three to five functions simultaneously and in turn.

[1] C. C. J. Roothaan and P. S. Bagus, Methods Comp. Phys. 2, 47 (1963).
[2] M. J. D. Powell, Computer J. 6, 163 (1963).
[3] R. J. Buehler, B. V. Shah, and O. Kempthorne, J. Soc. Ind. Appl. Math. 12, 74 (1964).

Potential Curves of Diatomic Rare-Gas Molecules and Their Ions, with Particular Reference to Xe₂*

ROBERT S. MULLIKEN

Laboratory of Molecular Structure and Spectra, Department of Physics, University of Chicago, Chicago, Illinois 60637

The excited and ionized states of the heavier rare-gas molecules are discussed, existing evidence on the dissociation energies of the ions are reviewed, and estimates of these dissociation energies are made. Estimated potential curves for the Xe₂⁺ ion and for the lower excited states of the Xe₂ molecule are given. Applications to the interpretation of the observed spectra of the heavier rare gases, especially Xe₂, are discussed.

I. INTRODUCTION

Rare-gas atoms in their ground states repel each other except for van der Waals attractions, which lead to weak molecular binding only for the heavier atoms (not for He₂). However, they all form fairly stable positive molecule–ions (He₂⁺, Xe₂⁺, HeNe⁺, etc.). By the addition of an electron in one or another Rydberg molecular orbital, any rare-gas molecule–ion should give rise to very numerous stable excited molecular electronic states. There should also be repulsive states of the molecule–ions and, in general,[1] very numerous repulsive excited states of the molecule. Numerous stable Rydberg states of He₂ have long been well known from a study of discrete band spectra in the infrared, visible, and near ultraviolet.[2] Continuous emission spectra and diffuse emission and absorption bands in the vacuum ultraviolet, known for all rare gases,[3,4] are attributable to transitions between stable excited states and the repulsive ground state. Except for He₂, only continuous emission spectra are definitely known in the visible and near ultraviolet,[5] although there are some indications of Xe₂ bands[3b] which, however, have not been further studied. Hence nothing has been known experimentally about the excited states of the heavier rare gases except the approximate location of the lowest. Recently, however, Tanaka and Yoshino[6] have obtained structured absorption spectra, and also corresponding emission spectra, of He atom pairs in which the upper states are highly vibrating excited He₂ molecules, and, as yet unpublished, they have obtained very numerous sharp absorption bands of van der Waals molecules of Ne₂ and Ar₂ leading to highly vibrating excited molecular states.

For the interaction of a normal with an excited or ionized He atom, the main features of the potential curves are believed to be known,[1] although more work is needed; in particular, the dissociation energies are known only approximately. For the heavier rare gases, because of their possession of a p^6 in addition to an s^2

shell, different and more complicated patterns of potential curves are expected, but until now, only brief preliminary discussions[1] of what the lowest of these may be have been published. In view of increasing interest in the rare gases in connection with electrical discharge mechanisms, plasma problems, shock-tube studies, vacuum spectroscopy, etc., it seemed worthwhile to attempt to predict some of the excited-state potential curves for a typical case.

Using qualitative theoretical considerations in combination with a variety of experimental data from related molecules and atoms, curves for Xe_2 and Xe_2^+ have been constructed and are shown in Figs. 1 and 2. These curves are being published in the belief that they can be helpful qualitatively, but it must be emphasized that no general quantitative reliance can be placed on them. This paper is devoted largely to an account of the various considerations used in drawing the curves, so that the reader may himself judge to what extent reliance can be placed on them. Potential curves for Ne_2, Ar_2, and Kr_2 and their ions should be similar to those for Xe_2 and Xe_2^+.

II. THE Xe_2^+ AND OTHER RARE-GAS MOLECULE-IONS

Just as for the excited states of He_2,[2] it is expected that for most of the stable Rydberg states of Xe_2, the forms of the potential curves near their minima should be nearly the same as that of the normal state of the Xe_2^+ ion (see Sec. III). For this reason and also because the predictions involve fewer uncertainties than for the Rydberg states, we begin with the Xe_2^+ ion.

To the extent that the ground states of the Xe atom and ion can be described by single-electron-configura-

tion wavefunctions (these will be assumed in the following discussion), the correct configurations and states are certainly $\cdots 5s^2 5p^6$, ^1S for the atom and $\cdots 5s^2 5p^5$, $^2P_{3/2}$ (lower) and $^2P_{1/2}$ (higher) for the ion. For a pair of normal Xe atoms in contact, the wavefunction then is a single-determinant expression corresponding to either of the two following equivalent descriptions:

$$\cdots 5s_a^2 5p\sigma_a^2 5p\pi_a^4 5s_b^2 5p\sigma_b^2 5p\pi_b^4, \quad {}^1\Sigma_g^+, \quad (1a)$$

$$\cdots (\sigma_g 5s)^2 (\sigma_u 5s)^2 (\sigma_g 5p)^2 (\pi_u 5p)^4 (\pi_g 5p)^4 (\sigma_u 5p)^2, \quad {}^1\Sigma_g^+. \quad (1b)$$

In (1b), $\sigma_g 5p$ and $\sigma_u 5p$ mean $2^{-1/2}(5p\sigma_a \pm 5p\sigma_b)$, while $\pi_u 5p$ and $\pi_g 5p$ mean $2^{-1/2}(5p\pi_a \pm 5p\pi_b)$.[7] It can be shown that the normalized single determinant wavefunction expressed in terms of AO's [configuration (1a)] is *identical* with that in terms of LCAO MO's [configuration (1b)].[7] Either (1a) or (1b) corresponds to a repulsive potential curve. In (1a), exchange repulsions between $5p\sigma_a^2$ and $5p\sigma_b^2$, between $5p\pi_a^4$ and $5p\pi_b^4$, and between $5s_a^2$ and $5s_b^2$, set in and increase as the internuclear distance R is decreased; the σ repulsions become important at larger R than the π repulsions. In (1b), the $\sigma_g 5s$, $\sigma_g 5p$, and $\pi_u 5p$ electrons are bonding, but their effect is always overbalanced,[8] increasingly as R decreases, by the antibonding effects of the equally numerous $\sigma_u 5s$, $\sigma_u 5p$, and $\pi_g 5p$ electrons.

By removing one electron from (1a) or (1b), the low-energy states of Xe_2^+ can be predicted. At sufficiently small R values, descriptions corresponding to removal of an electron from one or another of the MO's of (1b) should be appropriate.[7] The lowest four of the resulting states are listed and described in the inset in the lower right corner of Fig. 2. Two of these four states, the $B\,{}^2\Pi_g$ and $C\,{}^2\Pi_u$, should be widely split into two substates, a ${}^2\Pi_{3/2}$ (lower energy) and a ${}^2\Pi_{1/2}$ (higher energy). The interval ${}^2\Pi_{1/2}$–${}^2\Pi_{3/2}$ in each case should be approximately $\frac{2}{3}$ of that between the ${}^2P_{3/2}$ and ${}^2P_{1/2}$ substates of the p^5, ^2P ground states of the Xe^+ ion.[8]

The stability of the $A\,{}^2\Sigma_u^+$ state depends primarily on a predominance of the bonding effect of its two $\sigma_g 5p$ electrons over the antibonding effect of its one $\sigma_u 5p$ electron. This is expected theoretically and is supported experimentally by the stability of the analogous $\sigma_g 1s^2 \sigma_u 1s$ ground state of He_2^+. Matters are more complicated in Xe_2^+ because of the additional valence-shell electrons, but since overlap between $p\sigma$ AO's of two atoms is already fairly strong at R values sufficiently large that $p\pi$–$p\pi$ overlaps are still weak, and s–s overlaps weaker than $p\sigma$–$p\sigma$ overlap, it is to be expected that at the equilibrium distance R_e the loss of stability due to the net repulsion effect of the remaining valence shell electrons [in $(\sigma_g 5s)^2 (\sigma_u 5s)^2 (\pi_u 5p)^4 (\pi_g 5p)^4$] is not serious.

An additional complication is the fact that the doublet splitting in the ^2P state of Xe^+ is so large (see Fig. 1), due to strong spin–orbit coupling, that the coupling in the Xe_2^+ states even at R_e of the ground
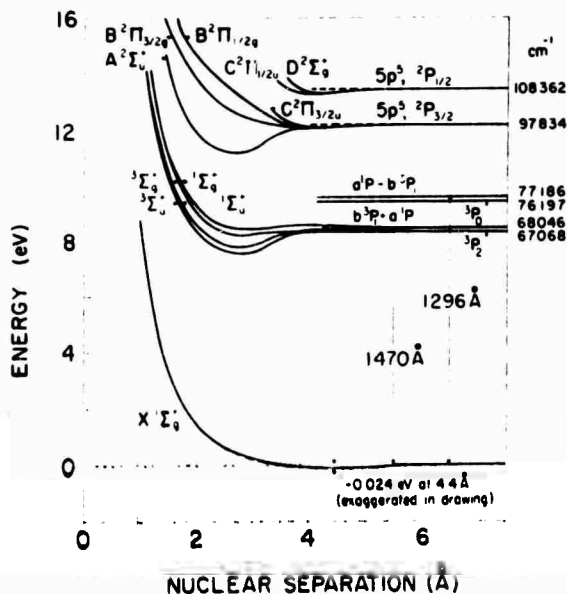
FIG. 1. Estimated potential curves for Xe_2^+ ion correlating with lowest states of $Xe^+ + Xe$, and for lowest states of Xe_2 molecule. See also inset in Fig. 2.
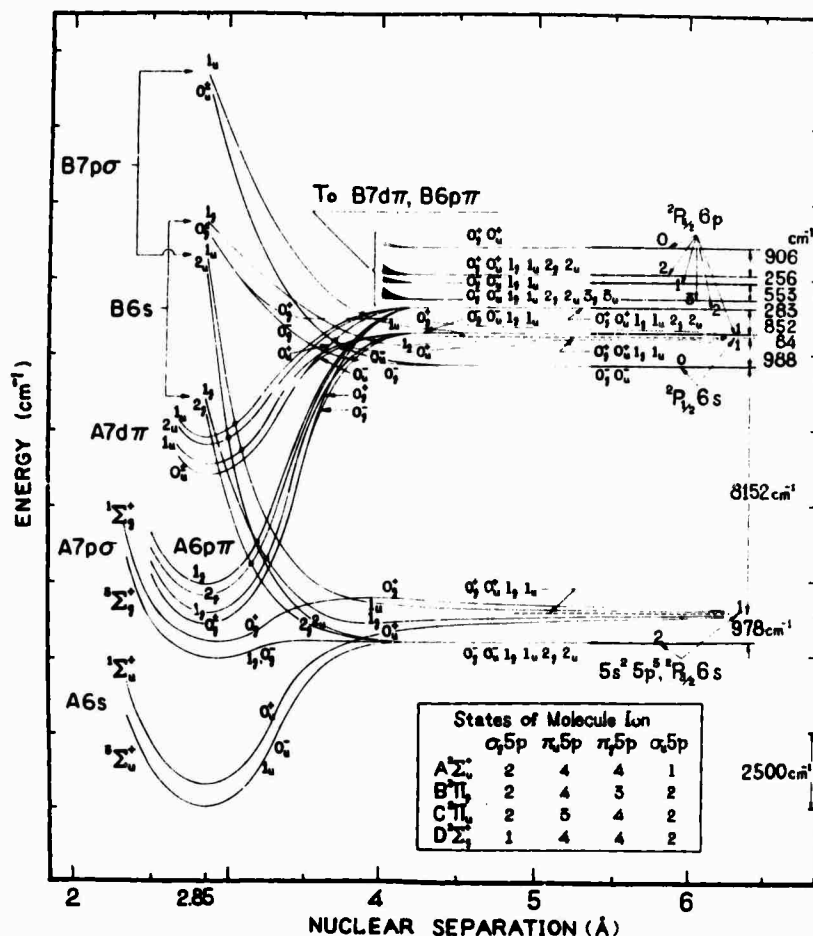
FIG. 2. Estimated potential curves for some of the lower excited states (Rydberg states) of Xe_2. For each state, the core (A or B) and the nature of the Rydberg orbital are given, also the case c labels of the substates. The positions of the curves are only estimated; for what are believed to be some improvements in the estimates, *see the last paragraph of Sec. III.* Some of the curves should be modified in one respect. Namely, as in the case of He_2 (see Ref. 1), those states (here $A\ 7p\sigma$, $A\ 7d\pi$, $B\ 7p\sigma$, $B\ 7d\pi$) which involve *promoted* MO's, but *not* those with un-promoted MO's, *should have major humps* (maxima) in their potential curves.

state must tend strongly toward the far-nuclei case c type.[10] The correlations of the Xe_2^+ states with those of $Xe^+ + Xe$ must accordingly be carried out in accordance with the case c rules. These show that $^2P_{3/2} + {}^1S$ must give a $\frac{1}{2}u$, a $\frac{3}{2}g$, a $\frac{1}{2}g$, and a $\frac{3}{2}u$, state, and $^2P_{1/2} + {}^1S$ a $\frac{1}{2}u$ and a $\frac{1}{2}g$, where the number $\frac{1}{2}$ or $\frac{3}{2}$ refers to the quantum number Ω. These case c states are, respectively, correlated with the MO-predicted states or substates $A\ ^2\Sigma_u^+$, $B\ ^2\Pi_{3/2g}$, $B\ ^2\Pi_{1/2g}$, and $C\ ^2\Pi_{3/2u}$ (from $^2P_{3/2} + {}^1S$), and $C\ ^2\Pi_{1/2u}$ and $D\ ^2\Sigma_g^+$ (from $^2P_{1/2} + {}^1S$), as shown in Fig. 1. At large R values the $\frac{1}{2}u$ wavefunctions from $^2P_{3/2} + {}^1S$ and $^2P_{1/2} + {}^1S$, respectively, can be shown to be 50:50 mixtures of $A\ ^2\Sigma_u^+$ and $C\ ^2\Pi_{1/2u}$, while as R decreases, the lower and upper $\frac{1}{2}u$ upper states must increasingly approach pure $A\ ^2\Sigma_u^+$ and pure $C\ ^2\Pi_{1/2u}$, respectively. However, even at R_e of the ground state of Xe_2^+, the purification is undoubtedly by no means complete. Similar considerations apply to the two $\frac{1}{2}g$ states. The $\frac{3}{2}g$ and $\frac{3}{2}u$ states, however, are pure $B\ ^2\Pi_{3/2g}$ and pure $C\ ^2\Pi_{3/2u}$ at all R values.

To estimate the dissociation energy D for the ground state of Xe_2^+, we note that Xe_2^+ is isoelectronic with I_2^-, and that the relationship of $I_2(\cdots\sigma_g 5p^2)$ to $Xe_2^+(\cdots\sigma_g 5p^2\sigma_u 5p)$ is analogous to that of $H_2(\sigma_g 1s^2)$ to $He_2^+(\sigma_g 1s^2\sigma_u 1s)$. Let us assume as a plausible relation that $D(He_2^+)/D(H_2) = D_{cg}(Xe_2^+)/D_{cg}(I_2)$, where in

order to take account of the distorting influences of strong spin–orbit coupling in the Xe^+ and I atoms, the assumed relation is taken to hold for D_{cg} of Xe_2^+ and I_2; that is, the dissociation energy measured with reference to the *centers of gravity*[9] of the ^2P states of Xe^+ and of I. This makes

$$D_{cg}(Xe_2^+) = D(Xe_2^+) + \tfrac{1}{3}[^2P_{1/2}(Xe^+) - {}^2P_{3/2}(Xe^+)],$$

$$D_{cg}(I_2) = D(I_2) + \tfrac{2}{3}[^2P_{1/2}(I) - {}^2P_{3/2}(I)] \qquad (2)$$

since $D(Xe_2^+)$ corresponds to dissociation to one $^2P_{3/2}\ Xe^+$ ion and one ^1S atom, while $D(I_2)$ corresponds to dissociation to two $^2P_{3/2}$ atoms.

$D(He_2^+)$ is 2.23 eV according to a rather accurate estimate based on a theoretical computation (Table I, Footnote g).[11] $D(H_2)$ is 4.48 eV, so that $D(He_2^+)/D(H_2)$ is about 0.50. $D(I_2)$ is 1.54 eV and $^2P_{1/2}(I) - {}^2P_{3/2}(I)$ is 0.94 eV, so that $D_{cg}(I_2)$ is $1.54 + 0.63 = 2.17$ eV. Multiplying by 0.50, one obtains $D(Xe_2^+) = 0.65$ eV for dissociation of $A\ ^2\Sigma_u^+$ into Xe plus $Xe^+(^2P_{3/2})$.

While the estimate of 0.65 eV for $D(Xe_2^+)$ thus obtained cannot be counted on as accurate, its basis seems to be fairly sound.[12] If the method used above for estimating $D(Xe_2^+)$ is applied to Ne_2^+, Ar_2^+, and Kr_2^+, then using $D(F_2) = 1.59$ eV,[13] $D(Cl_2) = 2.476$ eV, and $D(Br_2) = 1.971$ eV, together with $2P_{1/2} - {}^2P_{3/2}$

5

TABLE I. Rare-gas ion dissociation energies D_0.[a]

	b	c	d	e	f	g	h	i	j
He_2^+	$\geq 1.30\pm 0.1$[k]			2.06		2.07	2.23		2.23
Ne_2^+	$\geq 0.69\pm 0.2$ probably 0.7 ± 0.2			0.33–0.71	1.35 ± 0.07	1.65		0.78	1.1
Ar_2^+	$\geq 1.08\pm 0.1$ probably <1.503[l]	≥ 1.049		0.0035		1.25		1.21	1.4
Kr_2^+	$\geq 1.00\pm 0.1$ probably <1.641[l]	≥ 0.995	≥ 1.13					0.92	1.2
Xe_2^+	$\geq 0.91\pm 0.1$ probably <1.150[l]	≥ 0.967	0.99 ± 0.02					0.65	1.0

[a] In electron volts.

[b] M. S. B. Munson, J. L. Franklin, and F. H. F eld. J. Phys. Chem. 67, 1542 (1963), electron impact appearance potentials with mass spectroscopy.

[c] R. E. Huffman and D. H. Katayama, J. Chem. Phys. 45, 138 (1966), threshold of photoionization using rare gas atom resonance lines.

[d] J. A. R. Samson and R. B. Cairns, J. Opt. Soc. Am. 56, 1140 (1966), photoionization.

[e] From ion scattering data. E. A. Mason and J. T. Vanderslice, J. Chem. Phys. 29, 361 (1958) for He_2^+; 30, 599 (1959) for Ne_2^+; 36, 1103 (1962) for Ar_2^+.

[f] T. R. Connor and M. A. Biondi. Phys. Rev. 140, A778 (1965); L. Frommhold and M. A. Biondi, ibid. 185, 244 (1969), spectral line shapes.

[g] T. L. Gilbert and A. C. Wahl [unpublished theoretical calculations (self-consistent-field approximation)].

[h] Estimated from theoretical calculations: B. K. Gupta and F. A. Matsen, J. Chem. Phys. 47, 4860 (1967); C. Edmiston and M. Krauss, ibid 45, 1833 (1966). $D_e=2.33\pm 0.02$, $D_0=2.23\pm 0.02$.

[i] Semiempirical calculations of this paper.

[j] Writer's estimate of true values.

[k] The value $D_0=1.30$ eV corresponds to an appearance potential 23.1 eV, which may be identified with the $1s3p$, ^1P state of the He atom at 23.09 eV. However, the reliable theoretical value of 2.20 eV (cf. Footnote h) would correspond to an appearance potential A.P. (He_2^+) of ≥ 22.4 eV, with which the excitation energies $1s3s$, ^3S (22.72 eV), $1s3s$, ^1S (22.92), and $1s3p$, ^3P (23.01 eV) are also compatible. But as J. L. Franklin and F. A. Matsen point out [J. Chem. Phys. 41, 2948 (1964)], the cross section for electron impact excitation to these is very much less than to $1s3p$, ^1P; this seems sufficient to account for the failure in Footnote b to observe these lower A.P.'s.

[l] The indicated upper limit in each case is a value which corresponds to a transition to the next higher spectroscopically allowed atomic level which might have served as an A.P. if D were large enough, but which actually did not serve as an A.P.

data for Ne^+, Ar^+, and Kr^+, one obtains $D(Ne_2^+) = 0.78$ eV, $D(Ar_2^+) = 1.21$ eV, $D(Kr_2^+) = 0.92$ eV, $D(Xe_2^+) = 0.65$ eV.

The foregoing estimates were made some time ago when trustworthy experimental data appeared to be lacking. Fortunately there are now data which make possible some improved estimates of true D values. In the Hornbeck–Molnar process,[14] which apparently occurs for all rare-gas ions, one has, for example,

$$Xe^* + Xe \rightarrow Xe_2^+ + e, \qquad (3)$$
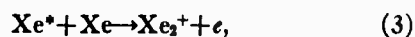
where Xe^* indicates an excited atom. The difference between the ionization energy of the atom and the lowest excitation energy (A.P.) of Xe^* for which the process occurs is evidently a lower limit to D for the molecule ion. The A.P. may be determined as an appearance potential of the molecule ion by electron impact excitation of the atom, as in the work of Munson, Franklin, and Field or, more accurately, by observation of the longest wavelength absorption line of the rare gas which produces photoionization (Huffman and Katayama). Values of D for the rare-gas ions resulting from the use of these and other perhaps less reliable methods, together with references to data sources, are set forth in Table I. In the last column of Table I the writer's judicious estimates of the true values are listed.

A value of R_e for the ground state of Xe_2^+ was roughly estimated in the following way. For the

$\cdots(\sigma_g 5p)^2(\pi_u 5p)^4(\pi_g 5p)^3\sigma_u 5p$, $^3\Pi_{0+u}$ state of I_{2e} R_e is 3.016 Å. It is estimated [by comparison with R_e data on Cl_2 and on the $\cdots(\pi_g 5p)^3$, $^2\Pi_g$ state of Cl_2^+] that the absence of one $\pi_g 5p$ electron in this state of I_2 has been responsible for a shortening of R_e by about 0.14 Å. If this electron were present $(\cdots\pi_g 5p^4\sigma_u 5p)$ one would have an I_2^- state isoelectronic with the ground state of Xe_2^+, with $R_e = 3.16$ Å. But by Slater's rules, the effective nuclear charge Z_{eff} governing the size of the atom (radius $a = a_0 n^2/Z_{eff}$) is 6.75 for Xe as compared with 6.10 for I. The estimated R_e of Xe_2^+ is then $(7.10/6.75)(3.16) = 2.85$ Å. Admittedly the procedure used to arrive at this estimate is crude, but it is not absurd.

Recalling that the force constant k for the vibration of a diatomic molecule is equal to $4\pi^2 c^2\omega_e^2\mu$, for ω_e in cm^{-1}, and where μ is the reduced mass (equal to $m/2$ for a homonuclear molecule), one may estimate

$$k(Xe_2^+) = [\omega_e^2(He_2^+)/\omega_e^2(H_2)](m_{He}/m_H)k(I_2)$$

$$= 0.58k(I_2).$$

$k(I_2)$ is about 2.04 $eV/Å^2$, so $k(Xe_2^+)$ is estimated as about 1.18 $eV/Å^2$.

With the estimates now available, a Morse curve for $A\ ^2\Sigma_u^+$ of Xe_2^+ was drawn, as shown in Fig. 1. Polarization of Xe by Xe^+ adds slightly to the attraction at large R values; this is also shown (exaggerated in magnitude and range) in Fig. 1.

Next we consider the curves for states B, C, D of

Xe_2^+. Configurationwise, states A and B differ from each other in the same way as the ground state $\cdots(\pi_g 5p)^4$, $^1\Sigma_g^+$, and the first excited states $\cdots(\pi_g 5p^3 \sigma_u 5p$, $^{3,1}\Pi_u$ of I_2. In I_2, the center of gravity of the $^{3,1}\Pi_u$ group of states, at R_e of its ground state (2.67 Å), is about 2.15 eV above the energy of the latter.[15] At a comparable R value for Xe_2^+ (about $2.67 \times 6.10/6.75$ Å = 2.11 Å) one might expect the *center of gravity* of the B state to be slightly more than this (say 2.3 eV) above the A state, because of the higher Z_{eff}. The $^2\Pi_{1/2}$ component of the B state should be lower, the $^2\Pi_{1/2}$ component higher, than the center of gravity, by approximately $\frac{1}{2}a$ of Xe^+, or $\frac{1}{3}(^2P_{1/2} - ^2P_{3/2})$ of Xe^+, or 0.44 eV.[9] The estimated positions of B $^2\Pi_{3/2g}$ and B $^2\Pi_{1/2g}$ at 2.11 Å are then 1.86 and 2.74 eV above A. The curves for these two substates have been drawn accordingly in Fig. 1.

States C and D are relatively unimportant for present purposes, and only their general trend at large R values has been indicated. The curves of the states and substates, B, C, D are almost certainly repulsion curves, except for a small polarization minimum at large R values. Two additional much higher energy states E $^2\Sigma_u^+$ and F $^2\Sigma_g^+$, respectively, corresponding to removal of a $\sigma_u 5s$ or a $\sigma_g 5s$ electron from configuration (1b), are not shown in Fig. 1. Of these two states, F must certainly be repulsive except for the weak polarization minimum, while E is almost certainly stable, although probably less so than the ground state.

III. THE Xe_2 MOLECULE

The ground state of Xe_2, aside from a van der Waals minimum with a depth of about 0.024 eV and with an equilibrium internuclear distance R_e of about 4.4 Å,[16] is a repulsive state. The exact form of the repulsion curve is uncertain. The lower part as shown in Fig. 1 is related to an interpretation of spectroscopic data discussed in Sec. IV.

All the excited states of Xe_2, like those of He_2, should be Rydberg states, with the excited electron in a MO much larger in diameter than the Xe–Xe internuclear distance and closely resembling a UAO (united-atom AO) except for a relatively small inner part lying within the Xe_2^+ core. The R_e values and force constants of typical stable Rydberg states should then be nearly the same as corresponding quantities for the stable ground state of the Xe_2^+ ion. In H_2, He_2, N_2, and NO, stable Rydberg states show these characteristics[17,18]; only the lowest stable Rydberg states of H_2 and He_2 show appreciable (and even then, not very large) deviations of these from those of the molecule–ion.

In accordance with the foregoing description, it is appropriate to designate the structure of Rydberg states of Xe_2 by using LCAO MO descriptions for the Xe_2^+ core electrons[19] (see the inset in Fig. 2) but using a UAO description for the Rydberg MO. This statement applies to internuclear distances R near or less than R_e of the stable state A of the core but for increasing R values leading toward dissociation the UAO

description for the Rydberg MO gives way to an LCAO description, while at the same time configuration mixing becomes important. A discussion of these changes is given for He_2 in an earlier paper.[20] Analogous changes may be expected in Ne_2, Ar_2, Kr_2, and Xe_2.

In He_2^+, one stable state of configuration $\sigma_g 1s^2 \sigma_u 1s$ (A) and one repulsion state of configuration $\sigma_g 1s \sigma_u 1s^2$ (B) are derived from the coming together of ground-state He and He$^+$. In an earlier paper,[1] it was concluded that core A is associated with a set of He_2 Rydberg states which on dissociation give one normal and one excited helium atom (He and He*). It was also predicted that core B, even though repulsive, gives rise to a set of Rydberg states (a) of which the lowest have stable minima; (b) all of whose potential curves on dissociation go asymptotically to a pair of ions: He$^+$+He$^-$, or rather, He$^+$+He+e. [Further consideration,[20a] however, indicates (1), that the B core states are higher in energy and less stable than previously supposed, because the potential curve of the B state of H_2^+, as computed by Gupta and Matsen,[20b] rises much more steeply at small R than was assumed in Ref. 1; (2), that because of the noncrossing rule, many of the B core states interact with the higher A core states so as in effect to dissociate into He+He* while making many of the higher A core states dissociate to He$^+$+He$^-$.]

With the heavier rare gases, matters must be more complicated. Analogous to state A of He_2^+, which is reached by removing one electron from the antibonding LCAO MO $\sigma_u 1s$, there are *two* states A and B which for Xe_2 (see the inset in Fig. 2) are obtained, respectively, by removing a $\sigma_u 5p$ or a $\pi_g 5p$ antibonding electron. Analogous to state B of He_2^+ there are two repulsion states C and D, respectively, obtained by removing a $\sigma_g 5p$ or a $\pi_u 5p$ bonding electron.[21] In analogy to He_2,[20] the Xe_2 states associated with both A and B cores may be expected to dissociate to give one normal and one excited atom (Xe+Xe*), while the Xe_2 states associated with the C and D cores may be expected to dissociate to a pair of ions: Xe$^+$+Xe$^-$, or Xe$^+$+Xe+e. The lowest-energy Rydberg states with C and D cores may then be stable states like the lowest of the states of He_2 with B core, but since these states must be of relatively high energy, they will not be further considered here. We then turn to the Xe_2 states with A and with B core. It seems clear that the states with A core are stable states but, because B is almost certainly a repulsive state of Xe_2^+ (see Sec. II and Fig. 1) yet the B-core states dissociate to Xe+Xe*, it is probable that the states with B core are all or mostly repulsive states. [In view of what was said at the end of the last paragraph, the dissociation correlations of A, B, C, and D core states may be less clear-cut than just outlined above.]

To obtain potential curves for Xe_2, we proceed by subtracting an appropriate estimated term value from the energy of the appropriate (A or B) potential curve of Xe_2^+ at each R value near R_e of state A of Xe_2^+. Thus the shape of each Xe_2 curve in this R neighborhood

TABLE II. Observed term values in $cm^{-1} \times 10^{-3}$.

He atom			He$_2$[a]			N atom		N$_2$[b]			NO[c]	
2s in 1s2s, ^3S:		38.46	2s in $^3\Sigma_u^+$:		34.30	3s (average)	32.57	3s in $E\,^1\Sigma_g^+$:	29.93		3s in A:	30.54
in 1s2s, ^1S:		32.03	in $^1\Sigma_u^+$:		31.96	3p (average)	20.48	in $a''\,^1\Sigma_g^+$:	26.80			
average:		35.24	average:		33.13			3s in $o\,^1\Pi_u$:	29.03			
2p (average)		28.30	2pπ					3pπ in $x\,^1\Sigma_g^-$:	21.48		3pπ in C:	23.37
			(average):		28.98							
3s in 1s3s, ^3S:		15.03	3pσ in $^3\Sigma_g^+$:		23.41			4pσ in $D\,^3\Sigma_u^+$:	23.83		4pσ in D:	21.45
			in $^1\Sigma_g^+$:		21.00			in $p'\,^1\Sigma_u^+$:	21.38		4dσ in H:	12.04
								in $y\,^1\Pi_g$:	20.53		4dπ in H':	12.02
											3dδ in F:	12.70
											4f$\sigma, \pi, \delta, \phi$:	5.86

[a] The MO symbols here are UAO symbols, the corresponding LCAO symbols being $\sigma_g 2s$, $\pi_u 2p$, and $\sigma_u 2s$.

[b] UAO symbols are given for the MO's; the corresponding LCAO symbols are $\sigma_g 3s$, $\pi_u 3p$, $\sigma_u 3s$. The states are: $E\,^3\Sigma_g^+$ and $a''\,^1\Sigma_g^+$ of configuration $X\,3s$, where X refers to the $\cdots \pi_u^4 \sigma_g$, $^2\Sigma_g^+$ ground state of N$_2^+$; $o\,^1\Pi_u$ is $A\,3s$, where A is the $\cdots \pi_u^3 \sigma_g^2$, $^2\Pi_u$ state of N$_2^+$; $x\,^1\Sigma_g^-$ is $A\,3p\pi$; $D\,^3\Sigma_u^+$ and $p'\,^1\Sigma_u^+$ are $X\,4p\sigma$; $y\,^1\Pi_g$ is $A\,4p\sigma$. For a'', see B. L. Lutz, J. Chem.

Phys. 51, 706 (1969); for the other states see Ref. 18 [but the energies of x and y have been revised on the basis of P. G. Wilkinson and R. S. Mulliken, ibid. 31, 674 (1959)].

[c] The states $A, C, \cdots$ are all doublet states, with ground-state $(^1\Sigma^+)$ NO$^+$ core. The UAO symbols $3s, 3p\pi, 4p\sigma, 4d\sigma, 4d\pi, 3d\delta, 4f\sigma, \pi, \delta, \phi$ correspond to the LCAO symbols $\sigma 3s, \pi 3p, \sigma^*3s, \sigma 3p, \pi^*3p, \delta 3d$, and $\sigma 2p, \pi 4f, \delta 4f, \phi 4f$. For data, see Ref. 18.

is determined by that of the Xe$_2^+$ core curve. At larger R values, the curves so obtained are connected smoothly to appropriate asymptotes (see below). The first task then is to obtain estimated term values.

The largest Rydberg term values should be for the unpromoted MO's $6s\sigma_g$ and $6p\pi_u$, which correlate as R increases with the LCAO forms $\sigma_g 6s$ and $\pi_u 6p$, and the promoted MO's $7p\sigma_u$, $7d\sigma_g$, and $7d\pi_g$ whose LCAO counterparts are $\sigma_u 6s$, $\sigma_g 6p$, and $\pi_g 6p$. All we can hope to do at present is to make crude estimates of these term values, guided by information on related or analogous Rydberg term values of other atoms and molecules. For this purpose, some information on term values of He, He$_2$, N, and N$_2$ is listed in Table II. One notes that the relation of molecular UAO to atomic AO term values is rather similar for N$_2$ versus N as compared with He$_2$ versus He. Also, the term values of $6s$ and $6p$ in the Xe atom are not far from those for $3s$ and $3p$ in the N atom. In making estimates for the $6s$, $6p\pi$, and $7p\sigma$ term values in Xe, some consideration has been given to the relative term values of $2s$, $2p\pi$, and

TABLE III. Observed term values for Xe and estimated values for Xe$_2$ in $cm^{-1} \times 10^{-3}$.

Xe atom[a]		Xe$_2$ molecule	
6s in $^3P_{3/2}6s$:	30.28	6s in $A\,6s, ^3\Sigma_u^+$:	29
in $^3P_{1/2}6s$:	31.67	in $A\,6s, ^1\Sigma_u^+$:	27
average:	30.74	6pπ in $A\,6p\pi$	
6p, average:	19.32	(average):	20.3
5d, average:	16.63	7pσ in $A\,7p\sigma, ^3\Sigma_u^+$:	24
		in $A\,7p\sigma, ^1\Sigma_g^+$:	22
		7dσ in $A\,7d\sigma$	
		(average):	16.5
		7dπ in $A\,7d\pi$	
		(average):	16.5
		5dδ (average):	17.2

[a] Weighted mean values for states of indicated kind.

$3p\sigma$ of He$_2$ but greater weight has been given to those of $3s$, $3p\pi$, and $4p\sigma$ of N$_2$ because Xe$_2$ more nearly resembles N$_2$ in respect to the nature of the closed-shell MO's which are the precursors of the several Rydberg MO's.[22] Some weight has also been given to the MO term values of NO, which include d and f UAO MO's.

Figure 2, which was drawn in 1958 or 1959, includes all states and substates of the electron configurations $A\,6s$, $A\,6p\pi$, $A\,7p\sigma$, and $A\,7d\pi$ located in accordance with Table II. In drawing Fig. 2, it was assumed that $A\,6s$ and $A\,7p\sigma$, since $6s$ and $7p\sigma$ correspond to $\sigma_g 6s$ and $\sigma_u 6s$, dissociate as $R \to \infty$ to Xe*$(\cdots 5p^5 6s)$+Xe. Similarly it was assumed that $A\,7p\pi$ and $A\,7d\pi$, which correspond to $A\,\pi_u 6p$ and $A\,\pi_g 6p$, dissociate to the lowest sublevels of Xe*$(\cdots 5p^5 6p)$+Xe. Corresponding assumptions were made for the states with B core.

The procedure just outlined does not always yield potential curves for the individual states or substates of Xe$_2$ but in general gives curves for the *center of gravity* of the states of given core and given Rydberg MO. For the $A\,6s$, $A\,7p\sigma$, $A\,7d\sigma$, and similar states, one expects a triplet state somewhat below, and a singlet state somewhat above, the center of gravity. However, in the cases of $A\,6s$ and $A\,7p\sigma$, separate estimates of term values for the triplet and singlet states have been made in Table III, so that the Xe$_2$ curves are obtained directly.

For the $B\,6s$ and $B\,6p\sigma$ states we have Ω, s (Jj-like) coupling between the $^2\Pi_g$ core, with its widely separated $^2\Pi_{3/2}$ (lower) and $^2\Pi_{1/2}$ (upper) substates, and the spin of the Rydberg electron; this should result in patterns of states approximately as shown in Fig. 2. For the $A\,6p\pi$ and $A\,7d\pi$ states the internal coupling of the orbital moment of the $6p\pi$ or $7d\pi$ electron with its own spin is so strong (as one can see from data on Xe-atom states with a $6p$ Rydberg electron) that the coupling with the spin of the $A\,^2\Sigma_u^+$ core must be of s, ω type (again Jj-like) with resulting patterns of substates as shown in Fig. 2. The spacings in these patterns have

been based on the aforementioned Xe-atom $6p$ data, and should be fairly reliable except for possible disturbances by configuration interaction with neighboring states of like far-nuclei case c symmetry.

As a final step, each potential curve is connected smoothly with an appropriate atom-pair asymptote. The latter is determined by first listing the far-nuclei case c states[10] obtainable for each given atom-pair state. These are given at the right of Fig. 2; for example, for $5s^2 5p^5$, $^2P_{3/2}6s$, $J=2$ (plus $5s^2 5p^6$, ^1S, $J=0$), one has one case c state of each of the types 0_g^-, 0_u^-, 1_g, 1_u, 2_g, and 2_u; this result is determined by standard correlation rules.[23] Next, the lowest case c state of each species at large R is correlated with the lowest of the same species at R_e and so on.

In Fig. 2 the rule that curves of the same species do not cross has been followed except in one respect. Namely, it has been assumed that potential curves coming from atomic Rydberg states with a $6s$ Rydberg orbital go only into molecular Rydberg states with a $6s$ or $7p\sigma$ MO ($\sigma_g 6s$ and $\sigma_u 6s$ in the LCAO region of R), and those with a $6p$ Rydberg AO only into those with a $6p\pi$ or $7d\pi$ ($\pi_u 6p$ or $\pi_g 6p$) or (*not shown*) a $7d\sigma$ or $8f\sigma$ ($\sigma_g 6p$ or $\sigma_u 6p$) MO. This assumption results in a number of crossings of curves of like species in Fig. 2. Each of these crossings is marked by a dot. It is questionable, although more so or less so in different cases and for crossings at different values of R, whether such crossings should have been allowed in Fig. 2. They have been allowed because it is believed that the wavefunctions of the curves involved in each such crossing are sufficiently different so that, even though of the same case c species, the interaction between them near the crossing point may be small; also, because the forms and identifications of the curves should in any event be essentially correct except close to crossing points.

However, it must then be recognized that for an otherwise stable state, all vibrational levels close to and above a crossing by a curve with a lower-energy asymptote (usually a repulsion curve) are unstable with respect to dissociation or predissociation along the latter. This fact is important for the spectroscopic behavior of the states involved (see Sec. IV).

A further point is the following. On the basis of experience obtained with He$_2$[1] some of the curves in Fig. 2 should be modified in one respect. Namely, those states which involve *promoted* MO's (but *not* those with unpromoted MO's) should have major humps (maxima) in their potential curves, similar to and for the same reasons as in corresponding curves of He$_2$. The most important *unpromoted* Rydberg MO's for Xe$_2$ are $6s\sigma_g$, $7p\pi_u$, and $5d\delta_g$, correlating, respectively, as R increases with the LCAO form $\sigma_g 6s$, $\pi_u 2p$, and $\delta_g 5d$. The most important promoted Rydberg MO's for Xe$_2$ are $7p\sigma_u$, $7d\sigma_g$, and $7d\pi_g$, which, respectively, correlate with LCAO MO forms $\sigma_u 6s$, $\sigma_g 6p$, and $\pi_g 6p$. The expected humps for the promoted MO states are *not shown* in Fig. 2, which was drawn prior to the realization of the

need of such humps, but the reader should add them to the figure.

Some further points concerning the forms of the curves at large R values must be discussed. For those atomic states which are the upper levels of atomic resonance lines such as $\lambda1470$ and $\lambda1296$, first-order dispersion forces[24] must cause appreciable splittings into distinct case c states already at R values much larger than those where valence forces become appreciable. The atomic states in question are the $J=1$ states of $(5p^5, {}^2P_{3/2})6s$ and $(5p^5, {}^2P_{1/2})6s$, which both are of mixed $^3P_1$, ^1P character. The shifts of the four case c molecular levels which arise from either of the two $J=1$ levels under discussion are given approximately by

$$\Delta E = \frac{k(\text{Ry}/\nu)f}{R^3}, \qquad (4)$$

where $k = +2$, $+1$, -1, and -2 for the 0_g^+, 1_u, 1_g, and 0_u^+ case c levels, respectively. Here R and ΔE are in atomic units (1 a.u. = 27.2 eV for ΔE, 1 a.u. = 0.529×10^{-8} cm for R), Ry is the Rydberg constant (109 737 cm^{-1}), ν is the wavenumber, and f the oscillator strength of the absorption line leading to the $J=1$ level considered.

At smaller R values, the effects of the first-order dispersion forces become swamped by those of the valence forces, and the curves in Fig. 2 were drawn accordingly. However, when Fig. 2 was drawn, it was assumed that the valence interactions begin to be appreciable only at about 4 Å. On further consideration, however (as can be seen from some of the discussion in Ref. 24), it was evident that they should become comparable with the first-order dispersion energies near 5 Å or perhaps even at 5.5 Å.

As noted above, the dispersion energies are proportional to the absolute f values of the resonance lines. Experimentally, $f = 0.26$ for the 1470-Å line and $f = 0.25$ for the 1296-Å line.[25] However, Fig. 2 was drawn before these values were known, and estimated values of 0.285 and 0.500, respectively, for $\lambda1470$ and $\lambda1296$ were used as a basis for drawing the curves in Fig. 2. so that the first-order dispersion splittings shown in Fig. 2 are about 50% exaggerated in the case of the curves dissociating to the $^2P_{1/2}6s$, $J=1$ atomic level. At $R = 4.5$ Å, Eq. (4) gives the following shifts for the four case c levels:

0_g^+, $+0.037$ eV; 1_u, $+0.019$ eV; 1_g, -0.019 eV;

$$0_u^+, -0.037 \text{ eV for } \lambda1470,$$

0_g^+, $+0.031$ eV; 1_u, $+0.016$ eV; 1_g, -0.016 eV;

$$0_u^+, -0.031 \text{ eV for } \lambda1296. \quad (5)$$

As can be seen from Fig. 2, these first-order dispersion shifts very often give rise to a hump in an attractive curve, or to an appreciable minimum at large R in an otherwise repulsive curve.

As has already been mentioned, Fig. 2 was drawn in

9

1959 using somewhat different Xe_2 term values than those listed in Table III, and with some differences in other data or assumptions. However, in view of various uncertainties, especially in the estimated term values of Table III, it has not seemed worthwhile to redraw it. The principal changes needed to bring Fig. 2 into agreement with the term value estimates of Table III are that at R_e of Xe_2^+ the energies for the various potential curves should be increased by the following amounts in 10^3 cm^{-1}: A $6s$, $^3\Sigma_u^+$, 0.9; A $6s$, $^1\Sigma_u^+$, 2.1; A $7p\sigma$, $^3\Sigma_g^+$, 1.0; A $7p\sigma$, $^1\Sigma_g^+$, 2.2; A $6p\pi$ (average), 2.8; A $7d\pi$ (average), 1.6; B $^2\Pi_{3/2}6s$, 1.3; B $^2\Pi_{3/2}7p\sigma$, 1.4; B $^2\Pi_{1/2}6s$, 1.2; B $^2\Pi_{1/2}7p\sigma$, 1.3. Further, it is possible that A $7d\sigma$ should occupy the place occupied by A $7d\pi$ in Fig. 2; in that event, the asymptotic correlations of their potential curves would need to be rearranged using the noncrossing rule in terms of case c states connected with $^2P_{3/2}6p$ atomic states. Also, it is probable that a $5d\delta$ (with LCAO correlate $A\delta g5d$) should lie below A $7d\sigma$ and A $7d\pi$; according to the rules followed in drawing Fig. 2, it should be correlated with atomic states $^2\Pi_{3/2}5d$ not shown in Fig. 2 and lying somewhat above the $^2\Pi_{3/2}6p$ levels shown. Further, the case c splittings for the $J=1$, $^2P_{1/2}6s$ atomic level should be decreased to about $\frac{2}{3}$ the values shown, to make them agree with (5). Finally, there should be pronounced humps in the states whose Rydberg MO's are of promoted type (in particular for the states of configurations A $7p\sigma$ and A $7d\pi$). *Regarding Fig. 1,* this *has* been redrawn in accordance with the estimates and specifications of the present paper.

IV. SPECTROSCOPIC APPLICATIONS

The molecular spectra of the heavier rare gases in the vacuum ultraviolet apparently all follow a similar pattern.[2] Most conspicuous is a continuous emission region extending from close to the first resonance line

$$[\cdots np^5, {}^2P_{3/2}(n+1)s]_{J=1} \rightarrow \cdots np^6, {}^1S$$

toward longer wavelengths. This continuum shows two major peaks, commonly referred to as the "first continuum"—nearer the resonance line—and the "second continuum"—at longer wavelengths. Under rather usual circumstances the first continuum is modulated by a series of diffuse bands. Under suitable conditions, these or similar bands are observed in absorption; at relatively high pressures the first continuum in emission can be more or less completely "eaten up" by this absorption. In general, the first continuum is favored by a silent or uncondensed discharge, the second by a disruptive condensed discharge and relatively high pressures (up to 1 atm), especially for the lighter of the heavy rare gases.[2] Both continua are increasingly stronger in the order $Xe_2 > Kr_2 > Ar_2 > Ne_2$.[2]

Associated with the forbidden atomic transition

$$[\cdots np^5, {}^2P_{3/2}(n+1)s]_{J=2} - \cdots np^6, {}^1S$$

in Kr_2 and Xe_2, an emission band has been observed as an intensification in the first continuum,[1c] and in Ar_2 a corresponding absorption band.[26] No emission or absorption associated with the second forbidden transition

$$[\cdots np^5, {}^2P_{3/2}(n+1)s]_{J=0} - \cdots np^6, {}^1S$$

has been observed.

The second resonance line

$$[\cdots np^5, {}^2P_{1/2}(n+1)s]_{J=1} - \cdots np^6, {}^1S$$

in emission is only moderately broadened, toward both shorter and longer wavelengths. In Ar_2 under conditions in which the two continua associated with the first resonance line are strongly developed, absorption bands have been observed[26] on the long-wavelength side of the second resonance line but extending only a limited distance from it. In the ultraviolet spectral regions farther in than the second resonance line there is very little observational evidence, except for absorption bands of Ar_2.[26]

Following are some more specific details on the Xe_2 spectrum. The resonance lines of the Xe atom are at 1470 and 1296 Å (cf. Fig. 1). When the emission spectrum is excited in xenon gas, the 1296-Å line broadens somewhat (a few angstroms on both sides) as the pressure is increased, while the 1470-Å line broadens tremendously toward longer wavelengths but only a little toward shorter wavelengths.[3] At 1 torr pressure the 1296-Å line is still sharp, while at 50 torr a series of at least 12 weak diffuse absorption bands extending from 1483 to 1400 Å is seen superposed on the emission continuum,[3b] while at 1491 Å there appears to be a distinct emission band rising somewhat above the continuum.[3a,3c] The broad continuum, which at high pressures (e.g., 350 mm) extends weakly to 2250 Å, is seen under suitable conditions to consist of two parts: the first starts at the resonance line and falls off gradually in intensity toward longer wavelengths, overlapping the second which has a broad rather symmetrical maximum near 1650 Å. At low pressures only the first continuum appears, at high pressures the second is favored, while self-absorption by the 1470-Å line and the adjacent bands eats up the shorter wavelength end of the first continuum. Under special conditions (e.g., 10 mm pressure, disruptive discharge), the spectrum consists mainly of the first continuum plus a series of diffuse emission bands degraded toward shorter wavelengths, between 1584 and 1621 Å.[3c]

All the phenomena just summarized appear to be explainable in terms of Figs. 1 and 2 together with expected selection rules and intensity relations. The first continuum in xenon, since it starts near λ1470 and extends toward longer wavelengths, may be attributed (see Fig. 2) in part to transitions from higher vibrational levels of the A $6s$, $^1\Sigma_u^+$ state to the repulsive ground state. The transition should be strongly allowed in the Xe_2 molecule, somewhat less so at large R values as dissociation is approached. (In krypton,

argon, and neon, the transition is decreasingly strongly allowed at large R values as the coupling gets more L, S-like.) The shortest-wavelength parts of the first continuum must come from vibrational levels close to the dissociation limit $(5p^5, {}^2P_{3/2}6s)_1$, while the absorption bands between $\lambda1483$ and $\lambda1500$ must represent transitions up to these same levels.[27] The emission spectrum may be explained by electron impact excitation of atoms followed by formation of ${}^1\Sigma_u^+$ molecules in three-body collisions. In further collisions, vibrational energy is lost leading to lower vibrational levels of the ${}^1\Sigma_u^+$ state, thus accounting for the longer-wavelength parts of the first continuum. The usual absence of sharply defined bands is perhaps understandable in terms of extensive overlapping of transitions from upper vibrational levels to a number of low-frequency vibrational levels of the ground-state van der Waals Xe_2 molecule.

Although the first continuum in Xe_2 starts at $\lambda1470$, it becomes intensified at $\lambda1491$, which is exactly the position of the forbidden line $(5p^5, {}^2P_{3/2}6s)_{J=2}\rightarrow5p^6, {}^1S$, as Tanaka has pointed out.[28,30] According to Fig. 2, this position is the asymptote of the potential curve of the $A\ 6s, {}^3\Sigma_u^+$ state of Xe_2. It appears then that the first continuum in Xe_2 includes emission from higher vibrational levels not only of the $A\ 6s, {}^1\Sigma_u^+$ but also of the $A\ 6s, {}^3\Sigma_u^+$ state, transitions from the latter to the ground state of Xe_2 being allowed because of the very strong spin–orbit coupling in Xe_2. An analogous $A\ 5s, {}^3\Sigma_u^+$ emission in Kr_2 is indicated by the presence of a $\lambda1250$-Å band.[30]

The broad and flat second continuum of Xe_2 with maximum near $\lambda\ 1650$ may be ascribed mainly to transitions from the lowest vibrational levels of the $A\ 6s, {}^3\Sigma_u^+$ and $A\ 6s, {}^1\Sigma_u^+$ states. The fact that the second continuum is favored by high pressures suggests that it may in part be produced like the first continuum by excited molecule formation from $J=1$ and $J=2$ $5p^5, {}^2P_{3/2}6s$ excited atoms,[28] followed by many collisions which deprive the excited molecules of vibrational energy. However, the fact that the second continuum is favored by a condensed discharge suggests an additional or alternative mechanism, namely capture of electrons by Xe_2^+ ions which have been formed by the Hornbeck–Molnar process[14] $(Xe^*+Xe\rightarrow Xe_2^++e$, see Sec. II) after Xe atoms have been excited to relatively high-energy states. By cascading down from initially formed higher-energy Xe_2^* states, with emission in the visible and near ultraviolet, the $A\ 6s, {}^1\Sigma_u^+$, and ${}^3\Sigma_u^+$ states are reached, and these then give rise to the second continuum. However, an inspection of Fig. 2, and the lack of evidence of discrete bands in the visible and near ultraviolet, raise doubts as to whether an effective cascade is possible. On the other hand, the occurrence of "dissociative recombination" of electrons $(Xe_2^++e\rightarrow Xe^*+Xe)$ seems probable.

Tanaka and others[3] earlier proposed that the second continuum in all the heavier rare gases is due mainly to transitions from the lowest vibrational levels of $A\ ns, {}^3\Sigma_u^+$

to the ground state. The progressive marked decrease in intensity of the rare-gas continua in the order $Xe_2>Kr_2>Ar_2>Ne_2$ is then explained by the decreasing transition probability of the intersystem transition involved. However, this explanation involves the assumption that $A\ ns, {}^3\Sigma_u^+$ molecules are soon quenched somehow if they do not emit promptly, and the explanation is thus seriously open to doubt. It seems more likely that the decreasing strength of the second and first continua in the order from Xe_2 to Ne_2 is a result of some aspect of the excitation mechanism. (Also it is open to some question as to whether the second continuum results mainly from transitions from $A\ ns, {}^3\Sigma_u^+$ or may also be due to an important extent to transitions from $A\ ns, {}^1\Sigma_u^+$.)

However this may be, the position $(\lambda1650)$ of the maximum of the second continuum of Xe_2 may plausibly be taken as a measure of the Franck–Condon vertical energy difference between the most probable emitting vibrational levels of the $A\ 6s, {}^3\Sigma_u^+$ and/or ${}^1\Sigma_u^+$ state and the potential curve of the ground state. $\lambda1650$ corresponds to a vertical distance of 7.49 eV. Fig. 1 has been drawn with a reasonable form for the ground state curve; this results in a vertical height of 7.0 eV from the latter to $v=0$ of $A\ 6s, {}^3\Sigma_u^+$. The maximum of the second continuum then corresponds to an excitation of 0.5 eV above $v=0$ of $A\ 6s, {}^3\Sigma_u^+$.

The series of well-defined diffuse Xe_2 emission bands between $\lambda1584$ and $\lambda1621$ obtained by Tanaka[30] with a condensed discharge at 10 torr may correspond to conditions intermediate between those which produce the first and second continua. These bands may perhaps represent transitions from low vibrational levels of $A\ 6s, {}^1\Sigma_u^+$, and/or ${}^3\Sigma_u^+$ down to vibrational levels of the van der Waals molecule Xe_2. The fact that they are degraded toward higher frequencies is in agreement with what is then expected from Fig. 1.

Turning now to higher frequencies, consider the second metastable atomic level $({}^2P_{1/2}6s)_{J=0}$ of Xe in Fig. 2. Associated with this level should be two molecular potential curves of 0_g^- and 0_u^- character. However, transitions between these and the ground state are rigorously forbidden by the molecular selection rules. Accordingly, no bands associated with this atomic level are expected; none are found, and the forbidden atomic transition to this level is also absent as expected.[29] This contrast to the behavior at the $({}^2P_{3/2}6s)_{J=2}$ level is in striking confirmation of what is expected theoretically.

In the case of the Xe_2 resonance line $\lambda1296$, which involves the atomic level $({}^2P_{1/2}6s)_{J=1}$, two associated molecular transitions are predicted. According to Fig. 2, allowed molecular transitions should occur for a 0_u^+ and a 1_u state, both of them repulsive at small R. However, as a result of first-order dispersion forces, the 1_u state is pushed up somewhat even at large R values, while the 0_u^+ state is pushed down so that it should have a minimum of appreciable depth [perhaps 0.05 eV: cf. Eq. (5)]. These two effects should lead to a

11

broadening of $\lambda1296$ toward both high and low frequencies but without the appearance of any extensive system of bands such as extend to long wavelengths from $\lambda1470$. What is observed is exactly as predicted here. A corresponding observation has been made by Tanaka and Yoshino[26] in connection with the absorption bands associated with the second resonance line of argon (analogous to λ 1296 of xenon), namely there are on the low-frequency side of the resonance line a limited number of bands belonging to a 0.052 eV deep Ar_2^* potential minimum, while there is on the high-frequency side just a broadening of the line.

Just as for the $\lambda1296$ line, molecular transitions involving a 0_u^+ and a 1_u state are predicted for the Xe_2 resonance line $\lambda1470$. The first continuum and bands associated with the $0_u^+(A\ 6s,\ ^1\Sigma_u^+)$ state have already been discussed. In contrast to its extensive broadening toward longer wavelengths in the first continuum, the $\lambda1470$ line is broadened only by several angstroms toward shorter wavelengths. This behavior is understandable from Fig. 2, according to which the 1_u state at small R is a repulsion state, but at large R is slightly elevated [perhaps 0.03 eV at $R=4$ Å—cf. Eq. (5)] by first-order dispersion forces.

The He_2 molecule shows both a strong continuum in the vacuum ultraviolet and structured band systems in the visible and near ultraviolet. The heavier rare gases show analogous vacuum-ultraviolet continua, but in the visible and near ultraviolet no structured bands have been identified with certainty. Extensive continua in this region are known for all the heavier rare gases, and these show a certain amount of diffuse structure but not much evidence for discrete bands. However, Wilkinson and Tanaka[8b] report in the microwave-power-excited Xe_2 emission spectrum, in addition to a background continuum extending from λ 2500 throughout the visible, a series of closely spaced bands at λ 3080, also strong maxima at λ 4600 and near λ 7000, and a sharp band near $\lambda5200$. Other workers[30,8] report spectra, presumably of Xe_2, of varying appearance in these wavelength regions. Under more severe conditions of excitation, the heavier rare gases give strong continuous spectra in the visible and near ultraviolet which are attributed to free–free and free–bound electronic transitions rather than molecular transitions.

Prince and Robertson[6] for all the heavier rare gases have obtained continua, from the positive column of a discharge, which they attribute to diatomic molecules. These extend from below λ 2900 throughout the visible, with a major peak near λ 3000 and indications of other minor peaks; the spectra are more or less similar for all the rare gases, with intensities in the order $Ar_2>Xe_2>Kr_2>Ne_2$. Prince and Robertson conclude that these spectra result from electronic excitation of metastable molecules to higher energy molecular states. Nichols and Vali[31] in a study of the Xe_2 continuum concur with this conclusion. Also they arrive at 10^{-7} sec for the lifetime of Xe_2^* molecules emitting at about 4350 Å.

It is somewhat difficult to reconcile the foregoing observations with what one must expect theoretically. However, the absence in the visible region of discrete bands like those of He_2 is probably understandable in terms of Fig. 2. On the basis of this figure, allowed transitions giving discrete bands should probably include, among others, transitions from $0_u^\pm$ of configuration $A\ 7d\pi$ to $0_g^\pm$ and 1_g of $A\ 6p\pi$ and $A\ 7p\sigma$, and from 0_g^+, 1_g, and 0_g^- of $A\ 6p\pi$ and $A\ 7p\sigma$ to 0_u^+, 0_u^-, and 1_u of $A\ 6s$, but these should lie rather far in the infrared. Discrete bands involving higher electronic levels with A and B cores cannot be predicted from Fig. 2, but are perhaps improbable. States whose potential curves in Fig. 2 are crossed by other curves of the same species, with crossing points indicated by dots in Fig. 2, are expected to be unstable toward dissociation or predissociation except perhaps for some of their lowest vibrational levels. In general, Fig. 2 makes understandable the absence of discrete band spectra in the visible and near ultraviolet, but definitely predicts that some such spectra should be present in the infrared (say at 2 or 3 μ).

A difficulty is the occurrence of continuous emission in Xe_2 at ultraviolet wavelengths below about $\lambda3500$, and of the bands reported by Wilkinson and Tanaka near $\lambda3080$. According to Fig. 1 and Table III, the energy of the Xe_2^+ ion above the state $A\ 6s,\ ^1\Sigma_u^+$ (see Fig. 1) is 29 000 cm^{-1}, which corresponds to $\lambda3450$, and all Xe_2 transitions involving Rydberg states with A core should come at longer wavelengths than this. For B core states, the available range extends to the difference in energy between Xe^++e and $A\ 6s,\ ^3\Sigma_u^+$ which corresponds to about $\lambda2700$. Although B core states (at least the lowest ones) are repulsive according to Fig. 2, some of them may have shallow minima at large R values from which transitions can occur. As already discussed above, first-order dispersion minima occur for some states, e.g., the 0_u^+ state derived from $(^2P_{1/2}6s)_{J=1}$; however, such minima would be less and less pronounced for analogous higher-energy states. Nevertheless, it would seem that there should be a minimum due to classical polarization by the Xe^+ core of the excited atom when a highly excited atom and a normal atom come together to form a molecular state corresponding to *any* sort of core $(A, B, C,$ or $D)$; note, however, that the model of a molecular core with a definite MO configuration plus an electron in a Rydberg MO loses meaning at large R values.[20] The nature of the high-energy molecular states postulated by Prince and Robertson and required to explain the short-wave parts of the molecular continua of Xe_2 and also of the other heavy rare gases, must here be left an open question.

Prince and Robertson's conclusion (after they had rejected three alternative proposals) that the spectra they observed result from electronic excitation of metastable molecules is open to a very serious objection, namely that according to Fig. 2 there are no Xe_2 states with expected lifetimes long enough to class them as metastable. Because of very strong spin–orbit coupling,

the $^3\Sigma_u^+$ lowest excited state of Xe_2 must be fairly short lived, and no one of the higher-energy states in Fig. 2 or predictable in the same way as those in Fig. 2 is metastable. Corresponding statements hold for the other heavier rare-gas molecules except perhaps Ne_2. Hence it seems that Prince and Robertson's reasoning on the mode of excitation of heavier rare-gas continua in the optical region needs to be re-examined.

V. SPECTRA OF CONDENSED PHASES

Several studies of emission[32] and absorption[33] spectra of liquid and solid heavier rare gases in the vacuum ultraviolet show considerable resemblances to gas-phase spectra. In the case of the emission spectra, the emitters may probably be described as diatomic molecules embedded in the liquid or solid matrix. However, correlations of the condensed phase spectra with the gas spectra are not easy and will not be attempted here.

[1] In He_2, there are apparently no strictly repulsive excited states, except perhaps B core states close to He_2^+ in energy, but there are many states such that the potential curve contains a maximum. See R. S. Mulliken, Phys. Rev. 136, A962 (1964).

[2] For recent work and literature, see M. L. Ginter, J. Chem. Phys. 42, 561 (1965); J. Mol. Spectry. 17, 224; 18, 32 (1965); J. Chem. Phys. 44, 950 (1966); 45, 248 (1966); 48, 2284 (1968).

[3] (a) Y. Tanaka and M. Zelikoff, J. Opt. Soc. Am. 44, 254 (1954); (b) P. G. Wilkinson and Y. Tanaka, ibid. 45, 344 (1955); (c) Y. Tanaka, ibid. 45, 710 (1955); (d) Y. Tanaka, A. S. Jursa, and F. J. LeBlanc, ibid. 47, 105 (1957); 48, 304 (1958); (e) R. E. Huffman, J. C. Larrabee, and Y. Tanaka, Appl. Opt. 4, 1581 (1965); (f) P. G. Wilkinson, Can. J. Phys. 45, 1715 (1967); 46, 315 (1968).

[4] (He_2): Y. Tanaka and K. Yoshino, J. Chem. Phys. 39, 3081 (1963); 50, 3087 (1969).

[5] J. F. Prince and W. W. Robertson, J. Chem. Phys. 45, 2577 (1966); 46, 3309 (1967). See also R. Turner and H. D. Riccius, ibid. 48, 4351 (1968).

[6] Y. Tanaka and K. Yoshino, J. Chem. Phys. 39, 3081 (1963), emission bands; 50, 3087 (1969), absorption bands. On the emission bands, see also F. H. Mies and A. L. Smith, ibid. 45, 994 (1966).

[7] However, when the atoms come closer together, the forms of the MO's are somewhat modified. The MO description is then no longer exactly identical with that of (1a).

[8] R. S. Mulliken, J. Chem. Phys. 23, 2343 (1955).

[9] The spin–orbit coupling energy is $+a$ for the $^2P_{1/2}$, $-\frac{1}{2}a$ for the $^2P_{3/2}$ substate of any p^5 atomic configuration, $+\frac{1}{2}a$ for the $^2\Pi_{1/2}$, $-\frac{1}{2}a$ for the $^2\Pi_{3/2}$ substate of any π^3 diatomic molecule configuration [cf. R. S. Mulliken, Rev. Mod. Phys. 4, 34 (1932)]. Thus for the center of gravity (i.e., the energy if there were no spin–orbit coupling) for a p^5, ^2P state, one may take the energy of $^2P_{3/2} + \frac{1}{2}(^2P_{1/2}-^2P_{3/2})$, and for a π^3, $^2\Pi$ state, $^2\Pi_{3/2}+\frac{1}{2}(^2\Pi_{1/2}-^2\Pi_{3/2})$.

[10] R. S. Mulliken, Rev. Mod. Phys. 3, 113 (1930); 4, 28 (1932).

[11] The D values here are D_0 values, that is, correspond to the vibrational level $v=0$.

[12] The greatest uncertainty lies perhaps in the question whether the relative effects of $\sigma_g 5p^2$ and $\sigma_u 5p$ on D_{0e} in Xe_2^+, in relation to those of $\sigma_g 5p^2$ in I_2, should be the same as those of $\sigma_g 1s^2$ and $\sigma_u 1s$ on D of He_2^+ in relation to those of $\sigma_g 1s^2$ in H_2. In other words, are $5p\sigma$ and $1s$ AO's sufficiently alike in their behavior in this respect? However, there seems to be no strong reason to doubt that they are. Another small question concerns the effect of the $5s$ and $5p\pi$ atomic shells; these, however, are formally the same in I_2 and Xe_2^+ and, if anything, should have somewhat less

effect in reducing D in Xe_2^+ (since R_e should be larger) than in I_2. Further, as noted in the text, there should be some admixture of $C^2\Pi_{1/2}$ in the $A^2\Sigma_u^+$ wavefunction of Xe_2^+, tending to increase $D(Xe_2^+)$, but this is paralleled in the case of I_2 by some admixtures of $^2\Pi_{u,g}$ into $^2\Sigma_g^+$ tending to increase $D(I_2)$; however, the effect should be greater for Xe_2^+ than for I_2 because D_{oe} is smaller.

[13] R. N. Doescher, J. Chem. Phys. 20, 330 (1952); J. G. Stamper and R. F. Barrow, Trans. Faraday Soc. 54, 1592 (1968).

[14] J. A. Hornbeck and J. P. Molnar, Phys. Rev. 84, 621 (1951).

[15] R. S. Mulliken, Phys. Rev. 57, 500 (1940), Interpretation I, as revised in view of new data [cf. J. S. Ham, J. Am. Chem. Soc. 76, 3386 (1954), and L. Mathieson and L. G. Rees, J. Chem. Phys. 25, 753 (1956), Fig. 3A].

[16] See, for example, A. Saran and A. K. Barua, Can. J. Phys. 42, 2026 (1964), and references given there; also Table V of R. J. Munn, J. Chem. Phys. 40, 1439 (1964).

[17] For H_2 and He_2, cf. R. S. Mulliken, J. Am. Chem. Soc. 91, 4615 (1969), Tables I and II.

[18] For N_2, see R. S. Mulliken, The Threshold of Space (Pergamon Press, Inc., New York, 1950), p. 169; the o, p', D, E, x, and y states are Rydberg states. For NO, see K. P. Huber, M. Huber, and E. Miescher, J. Mol. Spectry. 20, 130 (1966); R. Suter, Can. J. Phys. 47, 881 (1969); C. Juergen and E. Miescher, ibid. 46, 987 (1968).

[19] At least for the outer-shell core electrons. For the inner-shell core electrons, an alternative is to assign them all to AO's of the two atoms.

[20] R. S. Mulliken, J. Am. Chem. Soc. 88, 1849 (1966).

[20a] Initiated by a private communication from J. N. Bardsley, who has made MO configuration interaction computations on a number of the A and B core states as a function of internuclear distance.

[20b] B. K. Gupta and F. A. Matsen, J. Chem. Phys. 47, 4860 (1967).

[21] At higher energy are two additional states corresponding to removal of an antibonding $\sigma_u 5s$ or a bonding $\sigma_g 5s$ MO, respectively.

[22] Regarding precursors, see R. S. Mulliken, J. Am. Chem. Soc. 86, 3183 (1964).

[23] See G. Herzberg, Spectra of Diatomic Molecules (D. Van Nostrand, Co., Inc., New York, 1950), 2nd ed., p. 321.

[24] See R. S. Mulliken, Phys. Rev. 136, A962 (1964).

[25] D. K. Anderson, Phys. Rev. 137, A21 (1965): 0. 256±0.008 for λ 1470 and 0.238±0.015 for λ 1296. P. G. Wilkinson, J. Quant. Spectry. Radiation Transfer 5, 503 (1965): 0.260±0.02 for λ 1470 and 0.270±0.02 for λ1296.

[26] Y. Tanaka and K. Yoshino, J. Chem. Phys. (to be published). Absorption spectra of Ne_2, Kr_2, and Xe_2 will be published later by these authors.

[27] The strength of the emission and absorption is explained by the fact that the transition, which is ($A\,6s$, $^1\Sigma_u^+ - X\,^1\Sigma_g^+$) near R_e, $(0_u^+ - 0_g^+)$ at large R, $(5p^5, \,^2P_{3/2}6s)_1 - 5p^6$, ^1S at very large R, is strongly allowed at all R values. For the high vibrational levels involved, the potential curve of the 0_u^+ state is steep on its inner side but rather flat for a considerable range of R on its outer side, so that the Franck–Condon factor should strongly favor transitions at large R, hence to or from the nearly flat part of the ground-state potential curve near the van der Waals minimum. At the same time, the emission spectrum should receive some weak longer-wavelength contributions due to transitions from the inner side of the $^1\Sigma_u^+$ curve down to the repulsive part of the ground-state curve. The relative importance of these contributions must increase for the lower vibrational levels.

[28] Higher pressure favors the production of the metastable $J=2$ atoms by knocking down from $J=1$ atoms [cf., e.g., A. V. Phelps, Phys. Rev. 114, 1011 (1959)].

[29] Also in Ar_2, no absorption bands associated with this level are found, according to the work of Tanaka and Yoshino.[26]

[30] M. Laporte, J. Phys. Radium 9, 228 (1938); Compt. Rend. 226, 1265 (1948).

[31] L. C. Nichols and W. Vali, J. Chem. Phys. 49, 814 (1968).

[32] J. Jortner, L. Meyer, S. A. Rice, and E. G. Wilson, J. Chem. Phys. 42, 4250 (1965).

[33] O. Schnepp and K. Dressler, J. Chem. Phys. 33, 49 (1960); P. H. E. Meijer, ibid. 34, 2078 (1961); A. Gold and R. S. Knox, ibid. 36, 2805 (1962); G. Baldini, Phys. Rev. 128, 1562 (1962); J.-Y. Roncin, V Chandrasekharan, N. Damany, and B. Vodar, J. Chim. Phys. 10, 1212 (1963); Compt. Rend. 258, 2513 (1964). Theory for solid neon: A. Gold, J. Phys. Chem. Solids 18, 218 (1961).

13

Chapter 4

Heteropolar Bonds*

Juergen Hinze

I. Introduction

In homonuclear diatomic molecules like H_2 or O_2, the "bonding" electrons are shared equally by the atoms. Bonds of this type are called homopolar or covalent; however, the latter term is not completely satisfactory, since it is used differently in valence bond treatments of a molecule. In heteronuclear diatomic molecules like HF or LiH and in almost all polyatomic molecules, the "bonding" electrons are not shared equally by the two atoms connected by a bond. Bonds of this type, which are called heterovalent or, better, heteropolar, will be

discussed here in some detail. To do this we will start with some empirical considerations and concepts like electronegativity and ionic character. These concepts will be scrutinized later in qualitative discussions based on the simple forms of a valence bond and molecular orbital picture. Finally, we will see how these concepts appear in the light of a quantitative charge-distribution analysis of good Hartree–Fock functions of diatomic molecules.

Generally, in a heteropolar bond, one atom, the more electronegative one, withdraws electronic charge from the other atom, the less electronegative one. Therefore, the bonding electrons are unequally distributed between the two atoms, and the bond thus formed has some ionic character and a bond dipole moment. Can we determine the amount of the charge transferred from the less electronegative to the more electronegative atom? If yes, we could say how ionic the bond is, and how large the bond dipole is. However, such a determination cannot be done unambiguously, and the reader should be aware from the outset that concepts like electronegativity and ionic character, though very helpful in qualitative discussions and considerations, defy unambiguous quantitative definition and determination.

Heteropolar bonds range from one extreme where the bonding electrons are shared almost equally, as in the C—H bond, to the other extreme of the almost ionic bond, as in LiF, where one atom, F, has become almost a negative ion, while the other, Li, is left almost a positive ion. The transition between these two extremes is continuous: any intermediate shade may be realized. Discontinuous changes in ionic character may be found in transition-element complexes if the transition-element changes its oxidation number. We will not elaborate on this.

II. Empirical Considerations and Concepts

A. IONIC BONDS

If an atom with a low ionization potential, such as an alkali or alkaline earth, forms a bond with an atom which has a high electron affinity, such as a halogen, then the bond formed will be highly ionic. Such ionic bonds may be treated adequately by classical means without any resort to quantum mechanics. The principal contribution to the binding energy is the Coulomb attraction between the positive and negative ions formed. This attractive force will be counterbalanced at the equilibrium internuclear distance by the repulsion of the two ionic cores. If these

4. Heteropolar Bonds

cores are considered hard, and not polarizable, then the potential energy function per bond for the reaction

$$MX_n \rightleftharpoons M^{n+} + nX^- \tag{2.1}$$

in gas phase may be written, following Pearson and Gray (1963), as

$$E(R) = -\frac{f}{R} - \frac{d}{R^6} + b \exp(-aR). \tag{2.2}$$

Here, R is the internuclear distance, a, b, and d are constants which may be evaluated from virial coefficient data, and f is a geometric factor which is 1.00 for diatomic, 1.75 for symmetrical linear triatomic, and 2.44 for symmetrical trigonal planar tetraatomic molecules. The first term in Eq. (2.2) gives the Coulomb attraction of the positive and negative ions. The second term represents the van der Waals interaction of the ionic cores; its presence shows that the ion cores have not been considered as completely unpolarizable. The last term represents the repulsion of the ion cores, derived from a Buckingham potential. It is possible to calculate from Eq. (2.2) the equilibrium internuclear distances, as shown by Frost and Woodson (1958), as well as dissociation energies for highly ionic compounds. For dissociation energies to neutral atoms, Eq. (2.2) needs to be corrected by the appropriate ionization potentials and electron affinities.

In general, we expect that the negative ions in such a molecule will be highly polarized by their positive neighbors. The polarization of the positive ions may be neglected due to their much lower polarizability. This polarization of the negative ion is taken into consideration by writing the energy function per bond, following Rittner (1951) and Basolo and Pearson (1958), as

$$E(R) = -\frac{f}{R} - \frac{f^2\alpha}{2R^4[1 + (n\alpha/R^2)]} + \frac{B}{R^9}. \tag{2.3}$$

The first term here is the same as in Eq. (2.2), α is the polarizability of the negative ion, and n is another geometric factor which is 0.00 for diatomic, 0.25 for linear triatomic, and 1.01 for trigonal planar tetraatomic molecules. The ion core repulsion is represented here by the term B/R^9, where B is to be evaluated by setting $\partial E/\partial R = 0$ at the equilibrium internuclear distance. It is clear then that Eq. (2.3) cannot be used to calculate the internuclear separation.

Equations similar to Eqs. (2.2) and (2.3) are used to evaluate the energy of ionic crystals, where the geometric factor f has to be substituted by the Madelung constant. The reader is referred to Ketelaar

(1958) for a more detailed discussion of the ionic bond. We will turn our attention to heteropolar bonds, which are less ionic and therefore cannot be approached starting from an ionic model.

B. Extra Ionic Resonance Energy

We have seen that bonds which are highly ionic can be adequately described starting from the model of two interacting ions. The correction for the polarized negative ion allows for some reduction in ionic character, since the positive ion will polarize the negative ion such that the center of the negative charge on the negative ion will be shifted somewhat toward the positive ion. It is only natural to approach bonds which are only slightly ionic from the other extreme, the covalent bond found in homonuclear molecules. Thus, Pauling (1932a,b) wrote the dissociation energy D_{AB} of a heteropolar single bond A—B as

$$D_{AB} = \tfrac{1}{2}(D_{AA} + D_{BB}) + \Delta_{AB}, \tag{2.4}$$

the arithmetic mean of the homonuclear single-bond dissociation energies D_{AA} and D_{BB} plus a correction term, Δ_{AB}, which he called the extra ionic resonance energy. One expects the extra ionic resonance energy to be positive in all cases; that is what is found, with the only exception being the alkali hydrides, for which Δ_{AB} is found to be negative. If the geometric mean is substituted for the arithmetic mean, giving

$$D_{A^-} = (D_{AA}D_{BB})^{1/2} + \Delta'_{AB}, \tag{2.5}$$

then the extra ionic resonance energy, Δ'_{AB}, is found to be positive in all cases (Pauling and Sherman, 1937; Pauling, 1960). In Table I, some values for Δ_{AB} and Δ'_{AB} are listed.

C. Electronegativity

Pauling (1932a,b) found empirically that $\sqrt{\Delta_{AB}}$ is an additive quantity which is characteristic for the atoms A and B, i.e.,

$$\sqrt{\Delta_{HCl}} \approx \sqrt{\Delta_{HI}} + \sqrt{\Delta_{ICl}}. \tag{2.6}$$

Table II shows how well Eq. (2.6) is satisfied for Δ_{AB} and Δ'_{AB}. Guided by this relation, Pauling proposed to set $\sqrt{\Delta_{AB}}$ proportional to the difference of two numbers characteristic for the atoms A and B, and he called these numbers electronegativity. Thus

$$|\chi_A - \chi_B| = 0.208\sqrt{\Delta_{AB}} \tag{2.7}$$

17

4. Heteropolar Bonds

TABLE I[a]

	χ_A	χ_B	Δ	Δ'	D_{AB}	D'_{AB}	$D_{AB}^{(exp)}$	d_{theo}	d_{exp}	k_{theo}	k_{exp}
H_2	2.21	2.21	0	0	104	104	104	0.7417	0.7417	8.88	5.76
F_2	3.90	3.90	0	0	37	37	37	1.409	1.409	7.99	4.77
Cl_2	2.95	2.95	0	0	57	57	57	1.988	1.988	3.32	3.24
Br_2	2.62	2.62	0	0	45	45	45	2.283	2.283	2.35	2.45
I_2	2.52	2.52	0	0	36	36	36	2.66	2.66	1.83	1.71
Li_2	0.84	0.84	0	0	24	24	24	2.673	2.673	0.59	0.26
Na_2	0.74	0.74	0	0	17	17	17	3.078	3.078	0.50	0.17
K_2	0.77	0.77	0	0	12	12	12	3.923	3.923	0.44	0.10
LiH	0.84	2.21	43	58	107	108	58	1.58	1.595	1.62	1.024
NaH	0.74	2.21	50	67	110	109	50	1.78	1.886	1.23	0.781
KH	0.77	2.21	48	64	106	99	45	2.20	2.244	1.04	0.562
HF	2.21	3.90	66	88	136	150	135	0.92	0.917	9.87	9.65
HCl	2.21	2.95	13	17	93	94	103	1.30	1.274	5.04	5.1⁁
HBr	2.21	2.62	4	5	78	73	86	1.47	1.414	4.02	4.12
HI	2.21	2.52	2	2	72	63	71	1.67	1.604	3.28	3.14
LiF	0.84	3.90	216	289	245	319	136	1.76	1.564	2.38	2.50
NaF	0.74	3.90	231	308	258	330	114	1.96	1.926	1.68	1.93
KF	0.77	3.90	226	302	251	323	117	2.38	2.171	1.49	1.39
ClF	2.95	3.90	21	28	68	74	60	1.61	1.628	5.36	4.45
BrF	2.62	3.90	38	50	79	91	60	1.73	·1.755	4.40	4.09
IF	2.52	3.90	44	59	80	95	67	1.91	—	—	—
LiCl	0.84	2.95	103	137	143	174	112	2.14	2.022	1.45	1.404
NaCl	0.74	2.95	113	151	150	182	82	2.33	2.36	1.12	1.082
KCl	0.77	2.95	110	147	144	173	91	2.76	2.79	0.96	0.865
BrCl	2.62	2.95	2	3	53	54	53	2.10	2.136	2.78	2.84
ICl	2.52	2.95	4	6	51	51	50	2.28	2.33	2.41	2.36
LiBr	0.84	2.62	73	98	108	131	102	2.32	—	—	—
NaBr	0.74	2.62	82	109	113	137	86	2.51	2.502	0.99	0.959
KBr	0.77	2.62	79	106	108	129	91	2.94	2.94	0.86	0.702
IBr	2.52	2.62	0	1	41	41	42	2.46	2.47	2.07	2.04
LiI	0.84	2.52	65	87	95	116	81	2.52	—	—	—
NaI	0.74	2.52	73	98	100	123	73	2.71	2.90	0.84	0.938
KI	0.77	2.52	71	94	94	115	77	3.13	3.23	0.77	0.526

[a] χ_A and χ_B are the electronegativities of atoms A and B, respectively [from Hinze and Jaffé (1962)]. The extra ionic resonance energies from these electronegativities are $\Delta = (\Delta\chi/0.208)^2$ and $\Delta' = (\Delta\chi/0.18)^2$. The calculated dissociation energies are given in kcal/mole as $D_{AB} = \frac{1}{2}(D_{AA} + D_{BB}) + \Delta$ and $D'_{AB} = (D_{AA}D_{BB})^{1/2} + \Delta'$. The bond distances, d_{theo}, in Å, are calculated using Eq. (2.14), and the stretching force constants, k_{theo}, in (dyn/cm)·10^5, are calculated using Eq. (2.15).

TABLE II

Some Examples of the Additive Nature of $\sqrt{\Delta}$ and $\sqrt{\Delta'}$

	$\sqrt{\Delta}$	$\sqrt{\Delta'}$
HF	8.0	8.5
HCl + ClF	4.7 + 3.6 = 8.3	5.1 + 3.7 = 8.8
HBr + BrF	3.5 + 4.4 = 7.9	4.2 + 4.4 = 8.6
HI + IF	1.0 + 5.5 = 6.5	3.2 + 5.5 = 8.7
HCl	4.7	5.1
HBr + BrCl	3.5 + 1.4 = 4.9	4.2 + 1.7 = 5.9
HI + ICl	1.0 + 2.0 = 3.0	3.2 + 2.2 = 5.4
HBr	3.5	4.2
HI + IBr	1.0 + 1.4 = 2.4	3.2 + 1.4 = 4.6
IF	5.5	5.5
ICl + ClF	2.0 + 3.6 = 5.6	2.2 + 3.7 = 5.9
IBr + BrF	1.4 + 4.4 = 5.8	1.4 + 4.4 = 5.8
BrF	4.4	4.4
BrCl + ClF	1.4 + 3.6 = 5.0	1.7 + 3.7 = 5.4
ICl	2.0	2.2
IBr + BrCl	1.4 + 1.4 = 2.8	1.4 + 1.7 = 3.1

where χ_A and χ_B are, respectively, the electronegativities of atoms A and B, and the proportionality constant, according to Pauling, has been chosen to transform from kcal to eV.

Pauling defined electronegativity in words as the power of an atom in a molecule to attract electrons to itself. How such a measure can be obtained in the way described appears on first sight miraculous; however, we will see the required connections in the later qualitative molecular orbital discussion of the heteropolar bond. Using Eqs. (2.4) and (2.7), Pauling succeeded in setting up a relative electronegativity scale for the elements, which he fixed by arbitrarily assigning the value $\chi_H = 2.1$ to hydrogen.* This yielded the following simple numbers for the electronegativities of the first row elements: $\chi_B = 2.0$, $\chi_C = 2.5$, $\chi_N = 3.0$, $\chi_O = 3.5$, and $\chi_F = 4.0$. Equation (2.5), which overcomes the problem of a negative extra ionic resonance energy for the alkali hydrides, has apparently not been used to calculate electronegativities.

An absolute electronegativity scale was arrived at by Mulliken (1934), who considered the resonance structures

$$A^+B^- \leftrightarrow A—B \leftrightarrow A^-B^+$$

* Professor Mulliken pointed out to me that Pauling's original choice was $\chi_H = 0$, which he changed after the publication of Mulliken's absolute electronegativity scale to $\chi_H = 2.1$; thus, this choice may not have been so arbitrary.

of a molecule A—B. The energy required for the transition A—B → A$^+$B$^-$ is $I_A - E_B$, the ionization potential of atom A minus the electron affinity of atom B. The required energy for A—B → A$^-$B$^+$ is $I_B - E_A$. If both ionic structures contribute equally to the resonance hybrid, then we can say that A and B have the same electron attracting power. Thus we are led to the condition

$$I_A - E_B = I_B - E_A \tag{2.8}$$

as a necessary requirement for the equal electronegativity of the atoms A and B. In the preceding discussion, we have ignored the interaction energy of A and B as well as the ion-pair interactions. These contributions would appear equally on the right and left side of Eq. (2.8) and therefore cancel. The necessary condition for equal electronegativity, Eq. (2.8), may be rewritten:

$$I_A + E_A = I_B + E_B. \tag{2.9}$$

This led Mulliken to suggest

$$\chi_A = \tfrac{1}{2}(I_A + E_A) \tag{2.10}$$

as an equation defining an absolute electronegativity value of an atom. It must, however, be kept in mind here that I_A and E_A are not the ionization potential and electron affinity of atom A in its ground state, but are these values in its valence state (Mulliken, 1935), or better, of that orbital of A which forms the bond. For this reason, the term orbital electronegativity has been suggested by Hinze and Jaffe (1962).

Equation (2.10) has been used extensively for the evaluation of orbital electronegativities from valence state ionization potentials and electron affinities by Skinner and Pritchard (1953), Pilcher and Skinner (1962), and Hinze and Jaffe (1962, 1963a,b). These values correlate well with Pauling's electronegativities as well as with those electronegativity values obtained by other relations. We will not go into the details of the multitude of different electronegativity relations, nor do we want to discuss the physical meaning of electronegativity. Suffice it to state that electronegativity is an empirical concept which has become extremely useful in qualitative chemical considerations, but which defies an exact quantitative physical definition. These matters have been reviewed extensively by Pritchard and Skinner (1955) and more recently by Hinze (1968).

One more electronegativity definition, which is a generalization and refinement of Mulliken's formalism, should be mentioned, since it will be useful later in discussing ionic character. Here, electronegativity is defined as a potential and is obtained from the derivative of the energy of an atom with respect to its charge (Iczkowski and Margrave, 1961), or orbital

electronegativity is obtained as the derivative of the energy of an atom, W, with respect to the occupation number, n, of the orbital under consideration (Hinze *et al.*, 1963);

$$\chi(n) = \partial W/\partial n. \tag{2.11}$$

The energy of the atom is expanded into a power series of n,

$$W(n) = a + bn + cn^2, \tag{2.12}$$

in which the constants $a = 0$, $b = \frac{1}{2}(3I - E)$, and $c = \frac{1}{2}(E - I)$ are determined by setting $W(0) = 0$, $W(1) = I$ and $W(2) = I + E$, with I and E the orbital ionization potential and electron affinity, respectively. From Eqs. (2.11) and (2.12), we directly obtain the following for the normal orbital electronegativity:

$$\chi(1) = (\partial W/\partial n)_{n=1} = b + 2c = \frac{1}{2}(I + E). \tag{2.13}$$

For empty, virtual orbitals one obtains $\chi(0) = \frac{1}{2}(3I - E)$, and for doubly occupied orbitals the result is $\chi(2) = \frac{1}{2}(3E - I)$.

D. MOLECULAR PROPERTIES AND ELECTRONEGATIVITY

Using Eq. (2.11) or (2.13), electronegativities may be obtained from purely atomic data. It is now apparent that these values can be used in conjunction with Eqs. (2.7) and (2.4) or (3.5) to estimate the dissociation energies of heteropolar bonds once the homonuclear diatomic dissociation energies D_{AA} and D_{BB} are known. How well such estimates hold is demonstrated in Table I. It is also possible to estimate the bond distances, d_{AB}, in heteropolar bonds from covalent radii and electronegativities following the empirical relation found by Schomaker and Stevenson (1941):

$$d_{AB} = r_A + r_B - c\,|\chi_A - \chi_B|. \tag{2.14}$$

This relation has been carefully investigated by Polansky and Derflinger (1963), who find $c = 0.09$ for single bonds if d and r are in Å and χ is in Pauling's units. The covalent radii are roughly one-half of the bond distances of the corresponding homonuclear bonds, i.e., $r_A = \frac{1}{2}d_{AA}$; however, better values are obtained in a more detailed statistical study by Derflinger and Polansky (1963). In Table I, some results from Eq. (2.14) are listed and compared with experimental bond distances.

In addition, we demonstrate in Table I how well stretching-force constants can be estimated from electronegativities with the use of the empirical relation found by Gordy (1946a,b):

$$k_{AB} = \left[1.67N\left(\frac{\chi_A\chi_B}{d_{AB}}\right)^{0.75} + 0.3\right] \times 10^{-3}. \tag{2.15}$$

21

Here, k_{AB} is the stretching-force constant in dyn/Å, d_{AB} is the internuclear distance in Å, N is the bond order, and the electronegativities are to be used in the units of Pauling. The usefulness of the above-mentioned empirical relations should not be underestimated, although they do not add much to our understanding of the detailed electronic structure of a heteropolar bond. With these relations the chemist who wants an immediate answer can estimate dissociation energies, bond distances, and force constants without elaborate calculations. The answers he obtains are frequently better than those of exceedingly cumbersome, detailed quantum mechanical computations.

E. Ionic Character

The term "ionic character" of a bond, so much used in chemistry, is rather unfortunate, since it is associated with two distinct meanings.

(1) In the language of valence bond theory, where the total wave function of a diatomic molecule is written as

$$\Psi_{AB} = A\{\Phi_A\Phi_B\} + B\{\Phi_A{}^+\Phi_B{}^-\} + C\{\Phi_A{}^-\Phi_B{}^+\},$$

the ionic contribution $B\{\Phi_A{}^+\Phi_B{}^-\} + C\{\Phi_A{}^-\Phi_B{}^+\}$ is said to specify the ionic character of the bond, while $A\{\Phi_A\Phi_B\}$ is said to specify the covaient character. With this connotation, every bond has some ionic character, even the bonds in such homonuclear diatomic molecules as H_2 and O_2. Ionic character in this sense will not be discussed here.

(2) Ionic character as we would like to understand and discuss it here describes the partial charge distribution in a molecule, or, better, the amount of negative charge transferred upon bond formation from one atom to its neighbor. In this connection ionic character becomes equal to the partial positive and negative charges on the two atoms of a diatomic molecule, which will of course be zero for homonuclear diatomics.

This appears to be a clear definition of ionic character as we want to discuss it here. However, the distribution of the negative charge in a heteropolar molecule A—B into one part belonging to atom A and the other to atom B cannot be done unambiguously (Shull, 1962), because the atoms in a molecule have lost some of their identity. A definite assessment of the ionic character of a heteropolar bond can be made only in the frame of a particular restrictive model which specifies in detail how the charge is to be divided into the parts belonging to atoms A and B. For more details, see Sections IV,B and IV,C on population analysis and total charge analysis.

Keeping in mind that the "ionic character" of a bond A—B is merely an empirical concept, we expect it to be related to the

electronegativity difference, $\chi_A - \chi_B$. Thus, Pauling (1960) proposed to assess the ionic character of a bond A—B as

$$q = 1 - \exp\left[-\tfrac{1}{4}(\chi_A - \chi_B)^2\right]. \tag{2.16}$$

Gordy (1950) suggested the relation

$$q = \tfrac{1}{2}(\chi_A - \chi_B), \tag{2.17}$$

while, according to Wilmhurst (1958), the ionic character is given as

$$q = \frac{\chi_A - \chi_B}{\chi_A + \chi_B}. \tag{2.18}$$

Here, q is the amount of negative charge transferred from atom B to atom A, and is thus the partial negative charge on A. Equation (2.16) does not directly give the direction of the charge transfer.

If we start with the idea that electronegativity is a potential, then it is possible to derive a direct relation between electronegativity and ionic character. We expect that in a molecule A—B the charges will be in equilibrium if a test charge on atom A sees the same potential as a test charge on atom B. This requires, because of Eq. (2.11),

$$\chi_A(n_A) = \chi_B(n_B). \tag{2.19}$$

The idea that in a bond the electronegativities equalize has been postulated by Sanderson (1960). The same result may be obtained from the following consideration (Hinze *et al.*, 1963): Upon addition of the small negative charge dn to atom A the energy $(\partial W_A/\partial n)_{n_A}\, dn$ is liberated, while the removal of the charge dn from atom B requires the energy $(\partial W_B/\partial n)_{n_B}\, dn$. Charge transfer through the bond A—B will proceed as long as the energy liberated on A is larger than the energy required on B; equilibrium will be reached once both energies are equal. Thus, the condition for charge equilibrium is

$$\left(\frac{\partial W_A}{\partial n}\right)_{n_A} dn = \left(\frac{\partial W_B}{\partial n}\right)_{n_B} dn, \tag{2.20}$$

or, with the use of Eq. (2.11),

$$\chi(n_A) = \chi(n_B). \tag{2.19a}$$

If $n_A + n_B = 2$, we obtain from Eqs. (2.11) and (2.12) the following for the ionic character of the bond A—B:

$$q = n_A - 1 = \frac{\chi_A - \chi_B}{-2(c_A + c_B)} = \frac{\chi_A - \chi_B}{I_A - E_A + I_B - E_B}. \tag{2.21}$$

23

It is true that this line of argument, which leads to the equalization of electronegativity, is crude, since all changes in the interaction energy between the two atoms have been neglected. On these grounds, de Carvalho Ferreira (1963) and Pritchard (1963) have criticized the idea of electronegativity equalization. It is, however, interesting to note that an elementary description of the heteropolar bond in terms of molecular orbital theory yields a result quite similar to Eq. (2.21), as we will see in the following section. Any discussion of the finer details of the equations for the determination of ionic character and arguments about quantitative values appear rather meaningless in light of the ambiguity inherent in the definition of "ionic character."

III. Quantum Mechanical Considerations

A. GENERAL

If we want to investigate and understand the electronic structure of heteropolar bonds in any detail we are forced to resort to quantum mechanics. Ideally, we should solve the Schrödinger equation, a problem much too intricate to be practicable, since we would have to deal with the motion of at least two atomic nuclei and several electrons simultaneously. The first approximation introduced is to freeze the motion of the nuclei, i.e., the Born–Oppenheimer approximation. In addition, only Coulomb interactions are considered. Now we are left with the problem of dealing with the simultaneous motion of several electrons in the Coulomb field of, in the case of diatomics, two nuclei, a problem complicated because of the Coulomb interaction between electrons. This problem could be attacked directly, without any further approximations, in small, two-electron systems. However, we would not gain much insight into the more general structure of heteropolar bonds, insight which could be transferred to larger systems. The more useful approach is to break down the many-electron wave functions into one-electron functions, the orbitals, or, better, the spin-orbitals. The many-electron function is then constructed as an antisymmetrized product of these spin-orbitals in order to satisfy the Pauli principle. This procedure is known as the independent-particle approximation, and is more or less the starting point of the two approaches which have become useful in the interpretation of the electronic structure of molecules. The older of these two procedures is the valence bond method, which has been surpassed more and more by the molecular orbital method, mainly because the molecular orbital method becomes less complex if detailed computations are to be performed.

24

B. Valence Bond Theory

Valence bond (VB) theory takes a chemistry-like approach. In chemistry, a molecule is formed by combining atoms; in VB theory, the molecular wave function is formed by combining atomic wave functions. Thus the wave function of a diatomic molecule A—B is approximated by the product of the two atomic wave functions Φ_A and Φ_B:

$$\Psi_{AB} = \{\Phi_A \Phi_B\}. \tag{3.1}$$

We have written a curly bracket around the product as a reminder that this function has to be normalized and antisymmetrized. The atomic functions Φ_A and Φ_B, which describe particular stationary states of the atoms A and B, respectively, will be normal and antisymmetric in themselves; however, antisymmetry between the two functions has still to be achieved. This antisymmetrization can become rather involved, and we will avoid it for the moment by writing curely brackets.

It turns out that the simple product, Eq. (3.1), is a good approximation to the molecular wave function only if the atoms do not interact strongly. It will adequately describe the dissociation of the molecule A—B into the atoms A and B, each in a particular stationary state, for large internuclear distances only. At the molecular equilibrium internuclear distance, where the interactions are strong, it becomes necessary to add to the so-called covalent structure [AB], the ionic structures $[A^+B^-]$ and $[A^-B^+]$; hence

$$\Psi_{AB} = A\{\Phi_A \Phi_B\} + B\{\Phi_A^+ \Phi_B^-\} + C\{\Phi_A^- \Phi_B^+\}, \tag{3.2}$$

with Φ_A^+, Φ_A^-, Φ_B^+, and Φ_B^- being the wave functions of particular stationary states of the positive and negative ions of atoms A and B, respectively. The coefficients A, B, and C may now be determined by the variational principle so as to yield an energy minimum. This leads to the familiar set of secular equations with energy matrix elements of the form

$$\langle\{\Phi_A \Phi_B\}|\mathcal{H}|\{\Phi_A \Phi_B\}\rangle, \quad \langle\{\Phi_A \Phi_B\}|\mathcal{H}|\{\Phi_A^+ \Phi_B^-\}\rangle, \quad \text{etc.,}$$

with $\mathcal{H}$ being the total electrostatic Hamiltonian. The evaluation of these matrix elements is by no means trivial in the case of many-electron systems, even if the atomic state functions are known.

Initially, we will avoid this problem by just considering a two-electron heteropolar bond as if it were a two-electron heteropolar diatomic like HeH^+, ignoring all the other electrons in the molecule. In this case, Φ_A and Φ_B are simply single atomic spin orbitals φ_A and φ_B, respectively.

4. Heteropolar Bonds

In this case, the antisymmetrized and normalized function for the covalent structure may be written for a singlet as

$$\{\Phi_A\Phi_B\} = \frac{1}{2(1 + S^2)^{1/2}} \left\{ \begin{vmatrix} \varphi_A(1) & \bar{\varphi}_B(1) \\ \varphi_A(2) & \bar{\varphi}_B(2) \end{vmatrix} + \begin{vmatrix} \varphi_B(1) & \bar{\varphi}_A(1) \\ \varphi_B(2) & \bar{\varphi}_A(2) \end{vmatrix} \right\}, \quad (3.3)$$

where φ and $\bar{\varphi}$ are to represent the one particle orbital φ with α and β spin function respectively. This gives rise to the spatial two-electron probability function

$$P(1, 2) = \frac{1}{2 + 2S^2} [\varphi_A{}^2(1)\varphi_B{}^2(2) + \varphi_B{}^2(1)\varphi_A{}^2(2) + 2\varphi_A(1)\varphi_B(1)\varphi_A(2)\varphi_B(2)] \quad (3.4)$$

and a charge density of

$$\rho(1) = 2 \int_0^\infty P(1, 2) \, d(1) = 2 \int_0^\infty P(1, 2) \, d(2)$$

$$= \frac{2}{1 + S^2} [\varphi_A{}^2(1) + \varphi_B{}^2(1) + 2S\varphi_A(1)\varphi_B(1)]. \quad (3.5)$$

Here, S is the overlap integral

$$S = \int_0^\infty \varphi_A(1)\varphi_B(1) \, d(1). \quad (3.6)$$

We note in passing that the covalent charge density, Eq. (3.5), is by no means distributed symmetrically between the two nuclei, because the overlap charge density $\varphi_A(1)\varphi_B(1)$ is closer to the nucleus with the larger effective charge (see Fig. 1). This shows that the covalent structure in a heteropolar bond will give rise to a dipole moment, the covalent dipole.
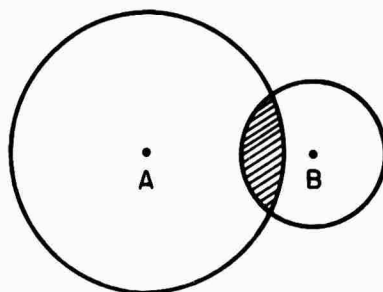
FIG. 1. Illustration of the asymmetry of an overlap charge distribution.

The dominant contribution to the dipole moment of a heteropolar bond is introduced by the ionic structures, which, in the case discussed, are

$$\{\Phi_A{}^+\Phi_B{}^-\} = \frac{1}{\sqrt{2}} \begin{vmatrix} \varphi_B(1) & \bar{\varphi}_B(1) \\ \varphi_B(2) & \bar{\varphi}_B(2) \end{vmatrix} \quad \text{and} \quad \{\Phi_A{}^-\Phi_B{}^+\} = \frac{1}{\sqrt{2}} \begin{vmatrix} \varphi_A(1) & \bar{\varphi}_A(1) \\ \varphi_A(2) & \bar{\varphi}_A(2) \end{vmatrix}. \quad (3.7)$$

Actually, these functions are rather poor approximations to the ionic structures. Even if we were satisfied with an independent-particle model for the description of the ionic structures, we would have to choose the Hartree–Fock orbitals for the positive and negative ions, which are quite different from the orbitals of the neutral atoms. This detail is disregarded in general, because it would only add to the complexity of VB calculations and not necessarily improve the results. The orbitals of the neutral atoms are already sufficient to permit the construction of an over-complete set of structures.

The total wave function for a singlet two-electron bond is now, following Eqs. (3.2), (3.3), and (3.7),

$$\Psi_{AB} = \frac{A}{2(1 + S^2)^{1/2}} \{\det |\varphi_A(1)\bar{\varphi}_B(2)| + \det |\varphi_B(1)\bar{\varphi}_A(2)|\}$$

$$+ \frac{B}{\sqrt{2}} \det |\varphi_B(1)\bar{\varphi}_B(2)| + \frac{C}{\sqrt{2}} \det |\varphi_A(1)\bar{\varphi}_A(2)|. \qquad (3.8)$$

This wave function gives rise to the spatial two-electron probability function

$$P(1, 2) = \frac{A^2}{2 + 2S^2} [\varphi_A{}^2(1)\varphi_B{}^2(2) + \varphi_B{}^2(1)\varphi_A{}^2(2)] + B^2\varphi_B{}^2(1)\varphi_B{}^2(2)$$

$$+ C^2\varphi_A{}^2(1)\varphi_A{}^2(2) + \left(\frac{A^2}{1 + S^2} + 2BC\right)\varphi_A(1)\varphi_B(1)\varphi_A(2)\varphi_B(2)$$

$$+ \frac{AB\sqrt{2}}{(1 + S^2)^{1/2}} [\varphi_A(1)\varphi_B(1)\varphi_B{}^2(2) + \varphi_B{}^2(1)\varphi_A(2)\varphi_B(2)]$$

$$+ \frac{AC\sqrt{2}}{(1 + S^2)^{1/2}} [\varphi_A(1)\varphi_B(1)\varphi_A{}^2(2) + \varphi_A{}^2(1)\varphi_A(2)\varphi_B(2)] \qquad (3.9)$$

and to the charge density

$$\rho(1) = 2\left(\frac{A^2}{2 + 2S^2} + C^2 + \frac{SAC\sqrt{2}}{(1 + S^2)^{1/2}}\right)\varphi_A{}^2(1)$$

$$+ 2\left(\frac{A^2}{2 + 2S^2} + B^2 + \frac{SAB\sqrt{2}}{(1 + S^2)^{1/2}}\right)\varphi_B{}^2(1)$$

$$+ 2\left[\frac{A\sqrt{2}}{(1 + S^2)^{1/2}} (B + C) + S\left(\frac{A^2}{1 + S^2} + 2BC\right)\right]\varphi_A(1)\varphi_B(1). \qquad (3.10)$$

The linear coefficients A, B, and C in the wave function, Eq. (3.8), are still to be determined. This may be done by the variational method, i.e., by minimizing the energy

$$E_{AB} = \langle \Psi_{AB} | \mathscr{H} | \Psi_{AB} \rangle, \qquad (3.11)$$

27

with

$$\mathscr{H} = h(1) + h(2) + (1/r_{12}), \tag{3.12}$$

where

$$h(1) = -\frac{\nabla^2(1)}{2} - \frac{Z_{A,eff}}{r_{A1}} - \frac{Z_{B,eff}}{r_{B1}}. \tag{3.13}$$

In addition, the restrictive normalization condition

$$\langle \Psi_{AB} | \Psi_{AB} \rangle = 1 \tag{3.14}$$

has to be maintained.

This process is relatively straightforward, but tedious; it requires the evaluation of a number of integrals over the orbitals φ_A and φ_B, which have to be specified, and the solution of the corresponding secular equation for its lowest root. It is found that if

$$\langle \{\Phi_A{}^+ \Phi_B{}^-\} | \mathscr{H} | \{\Phi_A{}^+ \Phi_B{}^-\} \rangle > \langle \{\Phi_A{}^- \Phi_B{}^+\} | \mathscr{H} | \{\Phi_A{}^- \Phi_B{}^+\} \rangle, \tag{3.15}$$

that is, if the electronegativity of atom A is larger than the electronegativity of atom B, then

$$C > B. \tag{3.16}$$

Thus the structure $\{\Phi_A{}^- \Phi_B{}^+\}$ will contribute more to the resonance hybrid than will the structure $\{\Phi_A{}^+ \Phi_B{}^-\}$. In this case, it may be seen from Eq. (3.10) that the charge density on atom A is larger than on atom B, and, from Eq. (3.9), that the probability of finding both electrons on atom A is higher than that of finding them both on atom B.

The introduction of many-electron functions for the description of covalent and ionic structures in larger molecules by and large leaves the conclusions reached unchanged. However, the construction of normalized and antisymmetrized structures is complicated, because several states of the neutral and ionized atoms are frequently required to describe a structure. In addition, the evaluation of the energy matrix elements, involving integrals over antisymmetric many-electron functions built from nonorthogonal orbitals, is rather more laborious. For details see Löwdin (1955) or Slater (1963). A possible way to avoid this complexity would be to initially orthogonalize the orbitals of atom A to the orbitals of atom B. This, however, leads to wave functions which represent the bonding rather poorly (McWeeny, 1954). In molecular orbital (MO) theory, all the foregoing problems are avoided because the MO's may be chosen mutually orthonormal. The MO formalism has therefore been favored recently whenever detailed computations are to be performed. VB calculations have been restricted to semiempirical methods, most notably the approach of "atoms in molecules" by Moffitt (1951) and its extension to "molecules in molecules" by Ellison (1963). Some small

28

systems have been treated a priori in a VB formalism, mainly by Matsen [see Matsen and Scott (1966)].

C. Molecular Orbital Theory

1. *Simple Two-Electron Model*

We again restrict ourselves initially to the treatment of the heteropolar bond as a separate two-electron problem. The electronic Hamiltonian will be the same as given by Eqs. (3.12) and (3.13). The bonding molecular orbital is approximated in the LCAO (linear combination of atomic orbitals) form of the theory by

$$\psi = a\varphi_A + b\varphi_B, \tag{3.17}$$

where φ_A and φ_B are atomic orbitals on atoms A and B, respectively. The antisymmetrized product function of the singlet two-electron bond is given by

$$\Psi(1, 2) = (1/\sqrt{2}) \det |\psi(1)\bar{\psi}(2)|. \tag{3.18}$$

The energy for the two bonding electrons is obtained from Eqs. (3.12) and (3.18) as

$$E = 2 \int \psi^*(1)h(1)\psi(1) \, d(1)$$
$$+ \iint \psi^*(1)\bar{\psi}^*(2)(1/r_{12})\psi(1)\bar{\psi}(2) \, d(1) \, d(2). \tag{3.19}$$

Substituting Eq. (3.17) gives

$$E = 2[a^2(\varphi_A|h|\varphi_A) + b^2(\varphi_B|h|\varphi_B) + 2ab(\varphi_A|h|\varphi_B)]$$
$$+ a^4(\varphi_A\varphi_A|1/r_{12}|\varphi_A\varphi_A) + b^4(\varphi_B\varphi_B|1/r_{12}|\varphi_B\varphi_B)$$
$$+ 2a^2b^2(\varphi_A\varphi_B|1/r_{12}|\varphi_A\varphi_B) + 4a^2b^2(\varphi_A\varphi_B|1/r_{12}|\varphi_B\varphi_A)$$
$$+ 4a^3b(\varphi_A\varphi_B|1/r_{12}|\varphi_B\varphi_B) + 4ab^3(\varphi_B\varphi_B|1/r_{12}|\varphi_B\varphi_A), \tag{3.20}$$

where we have used the abbreviated notation

$$(\varphi|h|\varphi) = \int \varphi^*(1)h(1)\varphi(1) \, d(1),$$

etc. With the consistent use of the Mulliken (1949) approximation for all integrals which contain an overlap charge distribution, i.e.,

$$(\varphi_A|h|\varphi_B) \approx \tfrac{1}{2}S[(\varphi_A|h|\varphi_A) + (\varphi_B|h|\varphi_B)]$$
$$= \tfrac{1}{2}S(h_A + h_B)$$
$$(\varphi_A\varphi_A|1/r_{12}|\varphi_A\varphi_B) \approx \tfrac{1}{2} S[(\varphi_A\varphi_A|1/r_{12}|\varphi_A\varphi_A) + (\varphi_A\varphi_B|1/r_{12}|\varphi_A\varphi_B)]$$
$$= \tfrac{1}{2}S(J_{AA} + J_{AB})$$

and

$$(\varphi_A\varphi_B|1/r_{12}|\varphi_B\varphi_A) \approx \tfrac{1}{4}S^2(J_{AA} + J_{BB} + 2J_{AB}), \tag{3.21}$$

where $S = (\varphi_A|\varphi_B)$ is again the overlap integral, we obtain

$$E = 2[(a^2 + abS)h_A + (b^2 + abS)h_B + abC] + (a^2 + abS)^2J_{AA}$$
$$+ (b^2 + abS)^2J_{BB} + 2(a^2 + abS)(b^2 + abS)J_{AB}. \tag{3.22}$$

The term

$$C = [2(\varphi_A|h|\varphi_B) - Sh_A - Sh_B] \tag{3.23}$$

has been introduced because the Mulliken approximation for the integral $(\varphi_A|h|\varphi_B)$ is not expected to hold too well; this term is expected to be small, however.

We may now identify $(2a^2 + 2abS)$ with the occupation number of the atomic orbital φ_A and $(2b^2 + 2abS)$ with the occupation number of φ_B. If q is defined as the negative charge shifted through the bond from B to A, then we obtain

$$q = a^2 + 2abS - b^2 - 2abS. \tag{3.24}$$

Since the normalization of the molecular orbital, Eq. (3.17), requires that

$$a^2 + 2abS + b^2 = 1, \tag{3.25}$$

we obtain

$$2(a^2 + abS) = 1 + q \quad\text{and}\quad 2(b^2 + abS) = 1 - q. \tag{3.26}$$

The energy of the two bond-forming electrons may now be written in terms of q, giving

$$E \approx h_A + h_B + \tfrac{1}{4}(J_{AA} + J_{BB} + 2J_{AB}) + q(h_A + \tfrac{1}{2}J_{AA} - h_B - \tfrac{1}{2}J_{BB})$$
$$+ \tfrac{1}{4}q^2(J_{AA} + J_{BB} - 2J_{AB}) + [1/(1 + S) - \tfrac{1}{4}(1 + S)q^2]C. \tag{3.27}$$

The last term is obtained by using the approximation

$$2ab \approx 1/(1 + S) - \tfrac{1}{4}(1 + S)q^2, \tag{3.28}$$

which holds for small q.

Now the optimum charge distribution may be found by setting $\partial E/\partial q = 0$, following the variational principle. This leads to

$$q = 2\frac{-(h_A + \tfrac{1}{2}J_{AA}) + (h_B + \tfrac{1}{2}J_{BB})}{J_{AA} + J_{BB} - 2J_{AB} - 2(1 + S)C}. \tag{3.29}$$

We may now specify the different terms in Eq. (3.29) in detail. We have

$$h_A = (\varphi_A|h|\varphi_A) = (\varphi_A|-\tfrac{1}{2}\nabla^2 - V_A|\varphi_A) + (\varphi_A|U_A|\varphi_A)$$
$$\approx I_A + (\varphi_A|U_A|\varphi_A), \tag{3.30}$$

where V_A is the potential of the core of atom A; the first integral may therefore be approximated by the negative ionization potential I_A of the orbital φ_A. The second integral, $(\varphi_A|U_A|\varphi_A)$, gives the potential energy of an electron in φ_A due to the field of all other atoms in the molecule. This term will be approximately canceled in Eq. (3.29) by the corresponding term arising from h_B, $(\varphi_B|U_B|\varphi_B)$. The Coulomb repulsion integrals on one center may be approximated, following Pariser (1953), by the difference between ionization potential and electron affinity of the orbital:

$$J_{AA} \approx I_A - E_A. \tag{3.31}$$

With these approximations and the electronegativity definition of Mulliken, Eq. (2.10), we obtain from Eq. (3.29) for the ionic character of the bond

$$q = 2\frac{(\chi_A - \chi_B)}{(I_A - E_A) + (I_B - E_B) - 2J_{AB} - 2(1 + S)C}. \tag{3.32}$$

This is rather close, save a factor of two, to Eq. (2.21) derived above from simple classical considerations, particularly since the term $-2J_{AB} - 2(1 + S)C$ is expected to be small, since J_{AB} will be positive and C negative.

The simple molecular orbital wave function, Eqs. (3.17) and (3.18), gives rise to the spatial two-electron probability function

$$
\begin{aligned}
P(1, 2) = {}& a^2b^2[\varphi_A{}^2(1)\varphi_B{}^2(2) + \varphi_B{}^2(1)\varphi_A{}^2(2)] + b^4\varphi_B{}^2(1)\varphi_B{}^2(2) \\
& + a^4\varphi_A{}^2(1)\varphi_A{}^2(2) + 4a^2b^2\varphi_A(1)\varphi_B(1)\varphi_A(2)\varphi_B(2) \\
& + 2ab^3[\varphi_A(1)\varphi_B(1)\varphi_B{}^2(2) + \varphi_B{}^2(1)\varphi_A(2)\varphi_B(2)] \\
& + 2a^3b[\varphi_A(1)\varphi_B(1)\varphi_A{}^2(2) + \varphi_A{}^2(1)\varphi_A(2)\varphi_B(2)]
\end{aligned}
\tag{3.33}
$$

and to the charge distribution

$$\rho(1) = 2[a^2\varphi_A{}^2(1) + b^2\varphi_B{}^2(1) + 2ab\varphi_A(1)\varphi_B(1)]. \tag{3.34}$$

These look rather similar to the equivalent quantities obtained from the valence bond function, Eqs. (3.9) and (3.10), respectively. However, in the molecular orbital wave function, there is only one independent variable parameter, the other being fixed by the normalization condition, while the valence bond function, Eq. (3.8), has two independent parameters. This gives rise to a shortcoming of a simple MO-function, like Eqs. (3.17) and (3.18), in that it is inadequate to describe the dissociation into neutral atoms. If the internuclear distance R goes to infinity, both a and b stay finite, and therefore we still have ionic contributions left, as evidenced by the terms $b^4\varphi_B{}^2(1)\varphi_B{}^2(2)$ and $a^4\varphi_A{}^2(1)\varphi_A{}^2(2)$ in Eq.

(3.33). This shortcoming of the simple MO-function is general whenever the molecular wave function is described by a single determinant constructed from molecular orbitals with the same MO's used for α and β spin. It is therefore expected that a single determinantal MO wave function of a stable molecule becomes a poor approximation as the internuclear distance becomes large. This has been overlooked even in recent detailed MO calculations by Sahni and Sawhney (1967).

This shortcoming of the simple molecular orbital wave function is easily overcome by permitting some configuration interaction. In the example of the two-electron bond, the total wave function would have to be written as

$$\Psi_{AB}(1, 2) = C \frac{1}{\sqrt{2}} \det |\psi(1)\bar{\psi}(2)| + C' \frac{1}{\sqrt{2}} \det |\psi'(1)\bar{\psi}'(2)|, \quad (3.35)$$

with ψ' the antibonding MO

$$\psi' = a'\varphi_A - b'\varphi_B, \quad (3.36)$$

which corresponds to ψ, the bonding MO of Eq. (3.17), and is orthogonal to it.

The two-electron probability function and charge density derived from an MO-function like Eq. (3.35) are equally as flexible as those obtained from the VB function. Dissociation leads correctly to two neutral atoms, and in an actual calculation, the MO and VB functions, Eqs. (3.35) and (3.8), respectively, give identical results if the same atomic orbitals φ_A and φ_B are used in both, showing that at this level of approximation, MO and VB theory merge. We will conclude this section by referring the reader for additional discussions of heteropolar bonds under different aspects to Peters (1963–1966), O-Ohata (1961), and Hamano (1964).

2. *Self-Consistent Field Approach*

The major advantage of the MO theory is that with it, all electrons of many-electron systems may be treated simultaneously without the additional complications which arise in a VB treatment. This is so because in MO theory, in the frame of the independent-particle approximation, the molecular orbitals may be chosen mutually orthonormal without loss of generality (Roothaan, 1951). An a priori all-electron molecular orbital treatment of the electronic structure of a molecule, hetero- or homopolar, starts in general with the expansion of the molecular orbitals in terms of some basis functions

$$\psi_i = \sum_p \varphi_p c_{ip}. \quad (3.37)$$

The index i labels different MO's, and p is used as a basis function index. The separation of the MO's into sets belonging to different irreducible representations of the point group of the molecule will be ignored here. Such a separation will, in general, significantly reduce the amount of computational work required but in this discussion it would only clutter the notation. The basis functions may be of various types: those most commonly used are:

(a) Atomic orbitals, in general of Slater type, centered at the atoms of the molecule. This leads to the LCAO-MO (linear combination of atomic orbitals) approximation.

(b) Slater-type functions centered on the atoms of the molecule. This leads to the more flexible description of MO's, and most calculations on diatomics and linear molecules have been performed in this LCSTF-MO (linear combination of slater-type functions) approximation. Results of computations with this type of orbital are the most accurate available for many molecules, and they will be close to the Hartree–Fock limit if the basis functions are chosen carefully and their exponents are optimized.

(c) Gaussian-type basis functions, which need not be centered on the atoms of the molecule (floating Gaussians). These basis functions have the advantage that the molecular integrals required for a detailed calculation are much easier to evaluate than with Slater-type basis functions. Gaussian-type basis functions have become dominant in the calculation of larger molecules with less than linear symmetry, where the integral evaluation with Slater-type functions is still rather cumbersome. The results obtained are, in general, inferior to those obtainable with STF-MO's unless exceedingly large basis sets are chosen.

The molecular orbitals, Eq. (3.37), are in general chosen to be mutually orthonormal and are multiplied by either spin function, α or β. The many-electron wave function of the molecule is then constructed as an antisymmetrized product of the MO's, which, in the case of a closed-shell system, may be written as a single Slater determinant, giving the following for a molecule with $2N$ electrons:

$$\Psi = \frac{1}{[(2N)!]^{1/2}} \det |\psi_1(1)\bar{\psi}_1(2) \cdots \psi_N(2N - 1)\bar{\psi}_N(2N)|. \quad (3.38)$$

The expectation value of the electronic energy for a closed-shell system characterized by a single determinantal wave function such as Eq. (3.38) is

$$E = \langle \Psi | \mathscr{H} | \Psi \rangle = \sum_i n_i \left(H_i + \tfrac{1}{2} \sum_j n_j P_{ij} \right), \quad (3.39)$$

33

with the total electronic Hamiltonian

$$\mathcal{H} = \sum_{i}^{2N} \left(-\tfrac{1}{2}\nabla^2(i) - \sum_{s} \frac{Z_s}{r_{si}} \right) + \sum_{i>j}^{2N} \frac{1}{r_{ij}}. \tag{3.40}$$

Here n_i is the occupation number of the ith orbital, and the integrals used are defined as

$$H_i = \int \psi_i^*(1) \left(-\tfrac{1}{2}\nabla^2(1) - \sum_{s} \frac{Z_s}{r_{s1}} \right) \psi_i(1)\, d(1) \tag{3.41}$$

and

$$P_{ij} = \iint \psi_i^*(1)\psi_j^*(1) \frac{1}{r_{12}} \psi_i(1)\psi_j(2)\, d(1)\, d(2)$$

$$-\tfrac{1}{2} \iint \psi_i^*(1)\psi_j^*(2) \frac{1}{r_{12}} \psi_j(1)\psi_i(2)\, d(1)\, d(2). \tag{3.42}$$

In order to obtain the linear expansion coefficients [c_{ip} in Eq. (3.37)] of the molecular orbitals, Eq. (3.39) is expanded in terms of basis functions and the variational principle is applied with respect to variations of the c_{ip}. This leads to the Hartree–Fock-like equations for the molecular orbitals (Roothaan, 1951). We will not go into the details, and just give the final equations in matrix form

$$\mathbf{FC}_i = \epsilon_i \mathbf{SC}_i, \tag{3.43}$$

where ϵ_i is the energy of the ith orbital, $\mathbf{S}$ is the overlap matrix defined by its elements

$$S_{pq} = \int \varphi_p^*(1)\varphi_q(1)\, d(1), \tag{3.44}$$

and the Fock matrix $\mathbf{F}$ is given by

$$F_{pq} = H_{pq} + \sum_{rs} P_{pq,rs} D_{rs}. \tag{3.45}$$

In Eq. (3.45) we have used the integrals

$$H_{pq} = \int \varphi_p^*(1) \left(-\tfrac{1}{2}\nabla^2(1) - \sum_{s} \frac{Z_s}{r_{s1}} \right) \varphi_q(1)\, d(1), \tag{3.46}$$

$$P_{pq,rs} = \int \varphi_p^*(1)\varphi_r^*(2) \frac{1}{r_{12}} \varphi_q(1)\varphi_s(2)\, d(1)\, d(2)$$

$$-\tfrac{1}{2} \int \varphi_p^*(1)\varphi_r^*(2) \frac{1}{r_{12}} \varphi_s(1)\varphi_q(2)\, d(1)\, d(2), \tag{3.47}$$

and the density matrix elements

$$D_{rs} = \sum_{i} n_i c_{ir} c_{is}, \tag{3.48}$$

where the sum i extends over all occupied orbitals.

An extension of this formalism to open-shell systems does not cause any major complications [see Roothaan (1960)]. The solution of Eq. (3.43) (which has to be performed iteratively until self-consistency is obtained) with flexible enough basis functions will yield molecular wave functions and energies close to the Hartree–Fock limit. Computations of this type have been done for a large number of molecules; references to these, and wave functions, may be found in the comprehensive compilation by Krauss (1967), and in the work of Cade and Huo (1967) for first- and second-row hydrides; in addition, many wave functions of linear molecules are given by McLean and Yoshimine (1967).

Hartree–Fock wave functions are good to first order [Brillouin (1933, 1934), or Møller and Plesset (1934)]. This is known as Brillouin's theorem. The expectation values of single-electron operators obtained from Hartree–Fock functions will also be good to first order (Cohen and Dalgarno, 1961). Therefore, we expect that charge distributions, dipole moments, etc., will be represented rather well by the wave functions obtained in the Hartree–Fock approximation. Total energies obtained are about 1% too high; this error, mainly due to the electron correlation energy, is too large, however, if dissociation energies are required, because dissociation energies arise in these calculations as the difference of two large numbers, the total molecular energy minus the energy of the dissociation products, each calculated in the Hartree–Fock approximation. In this case, the intraatomic correlation energy will roughly cancel; however, the interatomic correlation energy, which cannot be obtained in this approximation, is of the order of the total dissociation energy, 1–2 eV. For a detailed discussion of the correlation energy problem see Löwdin (1959).

It is expedient to point out again that the molecular orbital approximation, in the Hartree–Fock formalism discussed, will lead to poor results for large internuclear distances because the dissociation products are described with an excess of "ionic contributions." This inadequacy of the MO wave function may be corrected for by introducing some configuration interaction, as shown above [Eq. (3.35)]. This can be done systematically following the recently developed multiconfiguration self-consistent-field formalism (Das and Wahl, 1966; Das, 1967). Such calculations are capable of giving good dissociation energies by accounting for the interatomic correlation without increasing the complexity of the wave function significantly. The Hartree–Fock functions of molecules are already complex enough, and a means of interpreting them is necessary to make the problem of bond formation more lucid.

IV. Interpretation of Molecular Wave Functions

A. Localized Orbitals

Molecular orbitals as obtained from the Hartree–Fock approximation are, in general, delocalized over the entire molecule. This is an artifact introduced into the calculation for mathematical convenience by forcing the matrix of Lagrange multipliers, ϵ_{ij}, to be diagonal in closed-shell cases. Little physical significance can be attributed to single orbitals thus obtained, since a unitary transformation among the orbitals will neither change the total wave function nor any of its expectation values. An exception is provided by the diagonal Lagrange multipliers, ϵ_{ii}, of the delocalized MO's, which are physically significant because they are approximately equal to the negative of the different ionization potentials of the molecule (Koopmans, 1933). This is known as Koopmans' theorem, and holds due to a fortuitous cancellation of terms neglected in the approximation.

The delocalized MO's, however, do not yield readily to a direct interpretation of the computational results in terms of common chemical nomenclature, such as bond orbitals, lone pairs, or atomic core orbitals. Now, as pointed out above, unitary transformations among the occupied MO's may be applied without changing the total wavefunction. A unitary transformation may be chosen so as to yield well-localized orbitals, which are amenable to a direct chemical interpretation. Several criteria which may be used to specify a particular unitary transformation to localized orbitals have been proposed, most notably by Hall (1950) and Edmiston and Ruedenberg (1963, 1965). Similar criteria may also be used from the start in order to derive self-consistent-field equations analogous to Eq. (3.45) which will lead to localized orbitals directly (Gilbert, 1964; Ruedenberg, 1965). None of these localization criteria are unique, however, and their application requires, in general, a significant amount of extra computational labor. In the author's opinion, it is hardly worthwhile to succumb to the extra labor required to obtain orbitals which fit better into our traditional chemical language. Orbitals are an artifact of the mathematical model used in the interpretation of the electronic structure of atoms and molecules; they are, in particular, an artifact of the independent-particle approximation. Orbitals have no really fundamental physical significance, only the total wave function is meaningful. This, however, is not to say that orbitals are useless. They are useful as convenient entities in detailed calculations and, in particular, as an easily visualized conceptual aid in the rough and qualitative discussion of the electronic structure of atoms and molecules. However,

36

they do not appear to be useful in the interpretation of the results of detailed a priori computations.

B. POPULATION ANALYSIS

A procedure known as electronic population analysis has been proposed by Mulliken (1955) as an aid in the interpretation of results obtained from detailed molecular orbital calculations. This procedure has the advantage that it is readily applied to MO-type wave functions provided the MO's are constructed as linear combinations of atomic orbitals or functions. In this method the first-order charge density obtained from the many-electron MO-type wave function is analyzed in terms of net and gross atomic populations and overlap populations. The general first-order charge density of a wavefunction like Eqs. (3.37) and (3.38) is

$$\rho(1) = \sum_i n_i \sum_{p,q} c_{ip} c_{iq} \varphi_p(1) \varphi_q(1), \qquad (4.1)$$

with n_i the occupation number of the ith MO and p and q indexing the basis functions, φ, which are assumed here to be centered on the different atoms of the molecule. The net atomic population (NAP) on a particular atom, say A, is defined as

$$\mathrm{NAP}_A = \sum_i n_i \sum_{p \subset \mathscr{R}(A)} \sum_{q \subset \mathscr{R}(A)} c_{ip} c_{iq} S_{pq}, \qquad (4.2)$$

where we have used the symbolism $p \subset \mathscr{R}(A)$ (p part of the set A) to indicate that the summation over p runs only over those basis functions which are centered on atom A. S_{pq} is the one-center overlap integral, which becomes δ_{pq} if the basis functions are atomic orbitals which are mutually orthonormal.

The overlap population (OLP) between atoms A and B is defined as

$$\mathrm{OLP}_{AB} = 2 \sum_i n_i \sum_{p \subset \mathscr{R}(A)} \sum_{q \subset \mathscr{R}(B)} c_{ip} c_{iq} S_{pq}, \qquad (4.3)$$

where S_{pq} is now a two-center overlap integral. The overlap population may now be divided equally between atoms A and B and added to the corresponding net atomic populations. The gross atomic population on atom A, say, is thus obtained by adding one-half of the overlap populations between A and any other atom of the molecule to its net population,

$$\mathrm{GAP}_A = \mathrm{NAP}_A + \tfrac{1}{2} \sum_{B \neq A} \mathrm{OLP}_{AB} = \sum_i n_i \sum_{p \subset \mathscr{R}(A)} \sum_q c_{ip} c_{iq} S_{pq}. \qquad (4.4)$$

37

4. Heteropolar Bonds

These atomic and overlap population may be split up further into contributions from different MO's or atomic orbitals or functions. In this case, however, the same ambiguities arise which are discussed in Section IV,A. Even the total populations defined in Eqs. (4.2)–(4.4) are not unique; they obviously depend on the particular choice of basis functions made in constructing the MO's. This choice can be quite arbitrary. Therefore, not too much emphasis should be placed on the "exact" numerical values of the populations. All we can hope to get from a population analysis is a rough idea of the charge distribution in the molecule and of the bonding characteristics. To illustrate this we will discuss the results of a population analysis of a few simple heteropolar molecules, LiH, HF, and CO, which are listed in Table III. We see that the differences between the corresponding values obtained for different basis sets, Slater AO's, best minimal AO's, and best minimal MO's, are only small. From the gross atomic populations we can estimate the ionic character of a bond. We find that in LiH, the lithium

TABLE III

GROSS ATOMIC POPULATIONS (GAP), OVERLAP POPULATIONS (OLP), AND IONIC CHARACTER, q, IN LIH, HF, AND CO[a]

LiH	GAP(Li)	GAP(H)	OLP	q
Slater AO's	2.690	1.310	0.741	0.310
Best min AO's	2.686	1.314	0.736	0.314
Best min MO's	2.646	1.354	0.726	0.354

HF	GAP(F)	GAP(H)	OLP	q
Slater AO's	σ 5.154 π 4.000	0.846	0.261	0.154
Best min AO's	σ 5.219 π 4.000	0.781	0.272	0.219
Best min MO's	σ 5.229 π 4.000	0.771	0.381	0.229

CO	GAP(C)	GAP(O)	OLP	q
Best min AO's	σ 4.639 π 1.250	5.361 2.750	0.332 0.742	0.111
Best min MO's	σ 4.591 π 1.234	5.409 2.766	0.286 0.766	0.175

[a] Different entries correspond to a different basis function choice in the SCF-MO calculation.

atom has a fractional positive charge of $+0.3$, while hydrogen carries a fractional negative charge of -0.3. Similarly, we find the ionic character in HF to be about 0.2, with F more negative and H more positive, as expected. In CO, the total ionic character is found to be roughly 0.15, with O more negative than C; however, in CO we may discuss the contributions from σ- and π-type MO's separately. This division of the charge distribution into parts arising from orbitals which belong to different irreducible representations of the point group of the molecule can be done unambiguously. If we make this separation, we may consider the bond formation from two distinct starting points:

(1) Initially, carbon, $(1s^2 2s^2 2p\sigma 2p\pi)$, has 5 σ-type and 1 π-type electrons and oxygen, $(1s^2 2s^2 2p\sigma 2p\pi^3)$, has 5 σ-type and 3 π-type electrons. Upon bond formation, a charge of about 0.4 will be transferred in the σ-MO from carbon to oxygen, while a charge of 0.25 is transferred in the π-MO from oxygen to carbon.

(2) Initially, carbon, $(1s^2 2s^2 2p\pi^2)$, has 4 σ-type and 2 π-type electrons and oxygen, $(1s^2 2s^2 2p\sigma^2 2p\pi^2)$, has 6 σ-type and 2 π-type electrons. Upon bond formation, a charge of about 0.6 will be transferred in the σ-MO from oxygen to carbon, while a charge of 0.75 is transferred in the π-MO from carbon to oxygen.

This is one freedom one has to be aware of when making such an analysis. Both points of view are correct, and naturally the total charge distribution arrived at is the same.

Attempts have been made to correlate the overlap populations with bond dissociation energies (Mulliken, 1955). Such a correlation is not too good, however, and can be used at most as a qualitative guide.

C. Charge Distribution Analysis

The most promising and least ambiguous interpretation of molecular wave functions obtained from detailed a priori computations is based on an analysis of the first-order charge density, which, for a general N-electron function $\Psi(1, 2, \ldots, N)$, is given as

$$\rho(1) = \int \Psi^*(1, 2, \ldots, N)\Psi(1, 2, \ldots, N) \, d(2, \ldots, N). \qquad (4.5)$$

In the case of closed-shell systems, with MO's expressed as linear combinations of atomic or other basis functions as in Eq. (3.37), this reduces to the expression given in Eq. (4.1). From these charge densities, contour maps can be derived which give insight into the size and shape of molecules (Fig. 2 gives examples for LiH, HF, and CO).

LiH   HF

CO
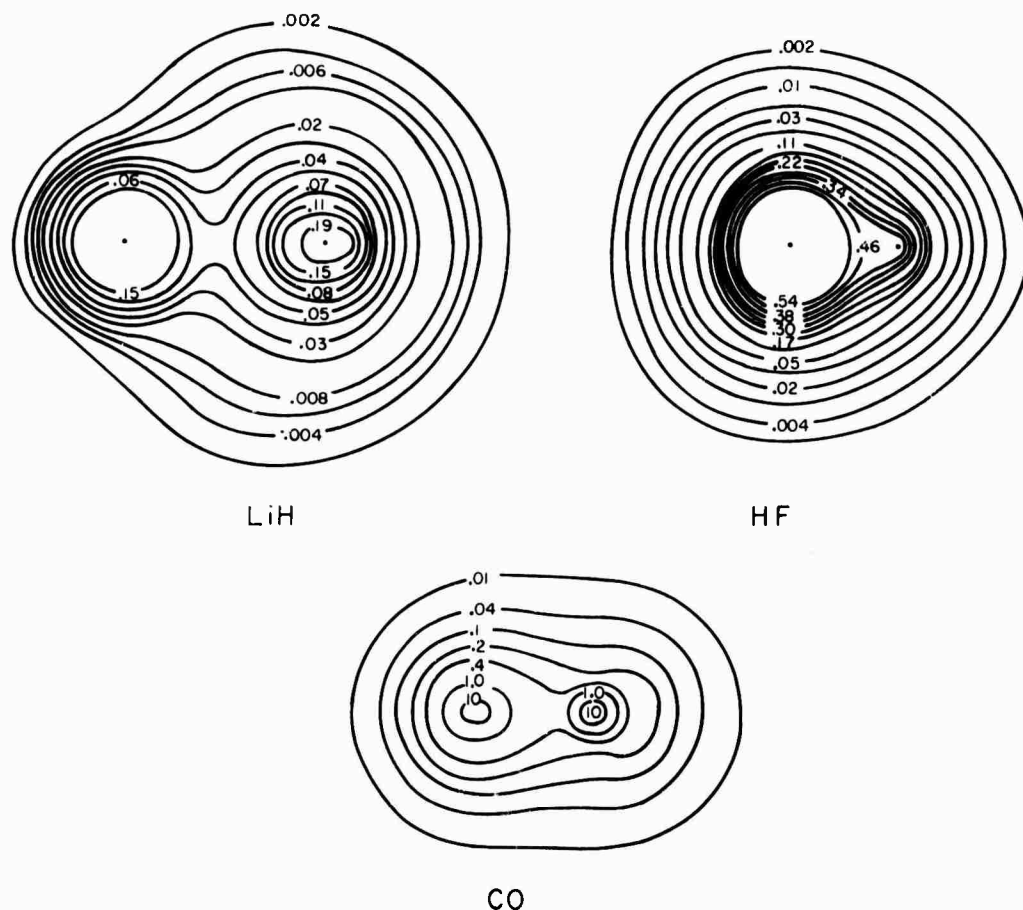
FIG. 2. Total charge-density maps from SCF wave functions of LiH, HF, and CO. The normalization of the CO charge density is different from those of LiH and HF.

In order to obtain more information about the detailed charge migrations upon bond formation, a charge-density difference-function is defined (Roux *et al.*, 1956)

$$\Delta\rho(1) = \rho_M(1) - \rho_A(1) \tag{4.6}$$

as the difference between the molecular charge density, $\rho_M(1)$, and the hypothetical atomic charge density, $\rho_A(1)$. This atomic charge density is obtained by placing the atoms in the same geometry as they are in the molecule and calculating $\rho_A(1)$ from the unperturbed atomic wave functions.

An interpretation of chemical bonding in terms of charge densities and charge-density difference-functions has the advantage that it is based on quantities which are physically real and invariant. Total charge densities are largely independent of the orbitals or basis functions used; they will depend only on the overall quality of the total wave function.

Many authors have recently presented charge density and charge-density-difference contours constructed mainly from SCF-type molecular wave functions of various molecules, Bader (1963, 1964), Bader and Jones (1961, 1963a,b), Bader and Henneker (1965, 1966), Ransil and Sinai (1967), Smith and Richardson (1965, 1967), to name a few. Figures 2, 3, and 4 show some examples for LiH, HF, and CO. We will restrict ourselves here to a merely descriptive interpretation of these contours.
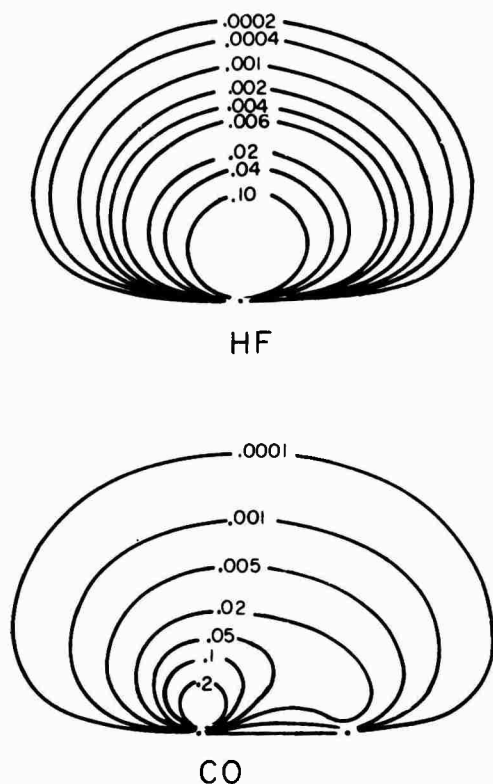
FIG. 3. π-Electron charge-density maps of HF and CO.

The total charge densities of LiH and HF clearly show the characteristics of a heteropolar bond, with a strong polarization of the charge cloud toward H and F in LiH and HF, respectively. This becomes clearer from the charge-density-difference maps, Fig. 4, where a strong pile-up of charge behind the more electronegative atom is observed. This pile-up occurs at the expense of the regions behind the less electronegative atom, and it is generally observed in heteropolar bonds. It is striking to note in the total charge-density map of HF how the proton is engulfed by the charge; it merely produces small dents in the contour lines, resulting in a molecule which is almost spherically symmetric. A simple inspection of the total charge-density map of HF makes it abundantly clear that a
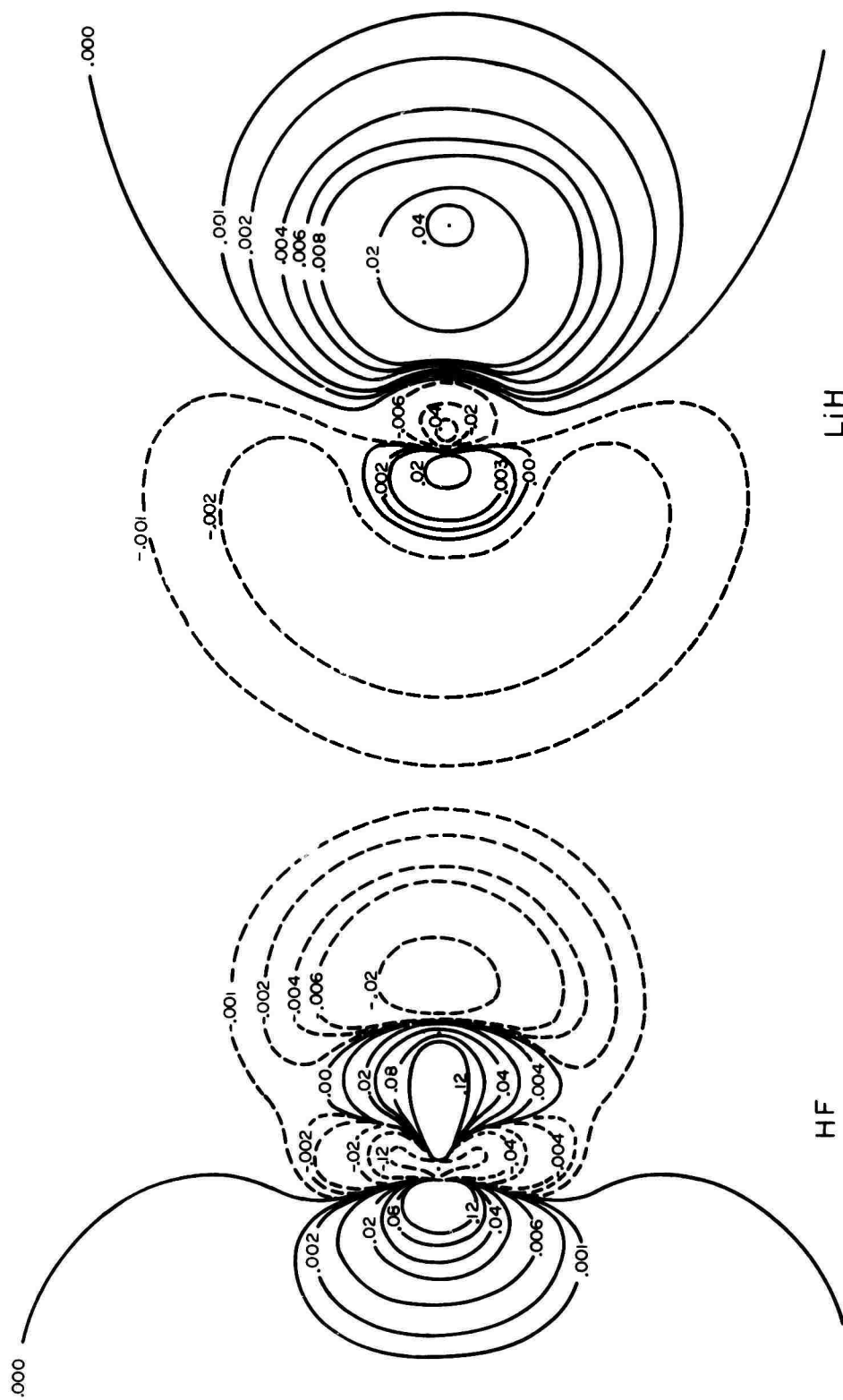
Fig. 4. Charge-density-difference maps of HF and LiH. Total molecular charge density and hypothetical atomic charge density are both from SCF wavefunctions.

42

division of the negative charge into one part belonging to the F atom and another belonging to the H atom requires more artistic imagination than scientific rigor. The total charge-density map of CO appears different from those of the strongly polar HF and LiH; it almost resembles the contours obtained for homonuclear diatomics. However, the π density alone (Fig. 3) is strongly polarized and it is dominant in the vicinity of the O atom.

Unfortunately, up to now no clear and unique concepts have evolved which permit the abstraction of useful chemical information from charge-density contour maps. Attempts to arrive at such concepts are actively being pursued; Bader and Henneker (1966) advocate an analysis in terms of forces on the nuclei; Ransil and Sinai (1967) emphasize, in addition, electron populations in different regions of space. It is impossible to go into all these details here, and it would be presumptuous at this time to predict to what results and concepts the molecular charge-density analysis will lead. It is hoped that the concepts developed will become as useful, but less ambiguous, than the familiar concepts in chemistry of orbitals, ionic character, charge transfer, electronegativity, and the like.

References

Bader, R. F. W. (1963). *Can. J. Chem.* **41**, 2303.

Bader, F. R. W. (1964). *J. Am. Chem. Soc.* **86**, 5070.

Bader, R. F. W., and Henneker, W. H. (1965). *J. Am. Chem. Soc.* **87**, 3063.

Bader, R. F. W., and Henneker, W. H. (1966). *J. Am. Chem. Soc.* **88**, 280.

Bader, R. F. W., and Jones, G. A. (1961). *Can. J. Chem.* **39**, 1253.

Bader, R. F. W., and Jones, G. A. (1963a). *Can. J. Chem.* **41**, 586, 2251.

Bader, R. F. W., and Jones, G. A. (1963b). *J. Chem. Phys.* **38**, 2791.

Basolo, F., and Pearson, R. G. (1958). "Mechanisms of Inorganic Reactions." Wiley, New York (in particular Chapter 2).

Brillouin, L. (1933). *Actualités Sci. et Ind.* No. 71.

Brillouin, L. (1934). *Actualités Sci. et Ind.* No. 159.

Cade, P. E., and Huo, W. M. (1967). *J. Chem. Phys.* **47**, 614, 649.

Cohen, M., and Dalgarno, A. (1961). *Proc. Phys. Soc. (London)* **77**, 748.

Das, G. (1967). *J. Chem. Phys.* **46**, 1568.

Das, G., and Wahl, A. C. (1966). *J. Chem. Phys.* **44**, 87.

de Carvalho Ferriera, R. (1963). *Trans. Faraday Soc.* **59**, 1064, 1075.

Derflinger, G., and Polansky, O. E. (1963). *Theoret. Chim. Acta* **1**, 316.

Edmiston, C., and Ruedenberg, K. (1963). *Rev. Mod. Phys.* **34**, 457.

Edmiston, C., and Ruedenberg, K. (1965). *J. Chem. Phys.* **43**, S97.

Ellison, F. O. (1963). *J. Am. Chem. Soc.* **85**, 3540 (and other publications by this author).

Frost, A. A., and Woodson, J. H. (1958). *J. Am. Chem. Soc.* **80**, 2617.

Gilbert, T. L. (1964). "Molecular Orbitals in Chemistry, Physics and Biology," p. 405. Academic Press, New York.

4. Heteropolar Bonds

GORDY, W. (1946a). *Phys. Rev.* **69**, 130.

GORDY, W. (1946b). *J. Chem. Phys.* **14**, 305.

GORDY, W. (1950). *J. Chem. Phys.* **19**, 792.

HALL, G. G. (1950). *Proc. Roy. Soc.* **A202**, 336.

HAMANO, H. (1964). *Bull. Chem. Soc. Japan* **37**, 1574, 1583, 1592.

HINZE, J. (1968). "Fortschritte der Chemischen Forschung," Vol. 9.3, "Theoretische Organische Chemie," p. 447. Springer, Berlin.

HINZE, J., and JAFFÉ, H. H. (1962). *J. Am. Chem. Soc.* **84**, 540.

HINZE, J., and JAFFÉ, H. H. (1963a). *Canad. J. Chem.* **41**, 1315.

HINZE, J., and JAFFÉ, H. H. (1963b). *J. Phys. Chem.* **67**, 1501.

HINZE, J., WHITEHEAD, M. A., and JAFFÉ, H. H. (1963). *J. Am. Chem. Soc.* **85**, 148.

ICZOWSKI, R. P., and MARGRAVE, J. L. (1961). *J. Am. Chem. Soc.* **83**, 3547.

KETELAAR, J. A. A. (1958). "Chemical Constitution," Chapter 2. Van Nostrand, Princeton, New Jersey.

KOOPMANS, T. A. (1933). *Physica* **1**, 104.

KRAUSS, M. (1967). Compendium of ab initio calculations of molecular energies and properties. *Nat. Bur. Std. (U.S.) Tech. Note* **438**.

LÖWDIN, P. -O. (1955). *Phys. Rev.* **97**, 1474.

LÖWDIN, P. -O. (1959). *Advan. Chem. Phys.* **2**, 207.

McLEAN, A. D., and YOSHIMINE, M. (1967). Tables of linear molecular wave functions. Suppl. to *IBM J. Res. Develop.* **12**, 206 (1968).

McWEENY, R. (1954). *Proc. Roy. Soc.* **A223**, 63, 306.

MATSEN, F. A., and SCOTT, D. R. (1966). "Quantum Theory of Atoms, Molecules and the Solid State." Academic Press, New York (and other publications by F. A. Matsen).

MOFFITT, W. E. (1951). *Proc. Roy. Soc.* **A210**, 245.

MØLLER, C., and PLESSET, M. S. (1934). *Phys. Rev.* **46**, 618.

MULLIKEN, R. S. (1934). *J. Chem. Phys.* **2**, 782.

MULLIKEN, R. S. (1935). *J. Chem. Phys.* **3**, 573.

MULLIKEN, R. S. (1949). *J. Chim. Phys.* **46**, 497.

MULLIKEN, R. S. (1955). *J. Chem. Phys.* **23**, 1833, 1841, 2338, 2343.

O-OHATA, K. (1961). *Progr. Theoret. Phys. (Kyoto)* **25**, 215.

PARISER, R. (1953). *J. Chem. Phys.* **21**, 568.

PAULING, L. (1932a). *Proc. Natl. Acad. Sci.* **84**, 415.

PAULING, L. (1932b). *J. Am. Chem. Soc.* **54**, 3570.

PAULING, L. (1960). "The Nature of the Chemical Bond," 3rd ed. Cornell Univ. Press, Ithaca, New York.

PAULING, L., and SHERMAN, J. (1937). *J. Am. Chem. Soc.* **59**, 1450.

PEARSON, R. G., and GRAY, H. B. (1963). *Inorg. Chem.* **2**, 358.

PETERS, D. (1963). *J. Chem. Soc.* pp. 2003, 2015, 4017.

PETERS, D. (1964). *J. Chem. Soc.* pp. 2901, 2908, 2916.

PETERS, D. (1965). *J. Chem. Soc.* p. 3026.

PETERS, D. (1966). *J. Chem. Soc.* pp. 644, 652, 656.

PILCHER, G., and SKINNER, H. A. (1962). *J. Inorg. Nucl. Chem.* **24**, 937.

POLANSKY, O. E., and DERFLINGER, G. (1963). *Theoret. Chim. Acta* **1**, 308.

PRITCHARD, H. O. (1963). *J. Am. Chem. Soc.* **85**, 1875.

PRITCHARD, H. O., and SKINNER, H. A. (1955). *Chem. Rev.* **52**, 747.

RANSIL, B. J., and SINAI, J. J. (1967). *J. Chem. Phys.* **46**, 4050.

RITTNER, E. S. (1951). *J. Chem. Phys.* **19**, 1030.

ROOTHAAN, C. C. J. (1951). *Rev. Mod. Phys.* **23**, 69.

ROOTHAAN, C. C. J. (1960). *Rev. Mod. Phys.* **32**, 179.

Juergen Hinze

ROUX, M., BOSNAINOU, S., and DAUDEL, R. (1956). *J. Chim. Phys.* **54**, 218.

RUEDENBERG, K. (1965). "Modern Quantum Chemistry," Vol. 1, p. 85. Academic Press, New York.

SAHNI, R. C., and SAWHNEY, B. C. (1967). *Intern. J. Quant. Chem.* **1**, 251.

SANDERSON, R. T. (1960). "Chemical Periodicity." Reinhold, New York.

SCHOMAKER, V., and STEVENSON, D. P. (1941). *J. Am. Chem. Soc.* **63**, 37.

SHULL, H. (1962). *J. Phys. Chem.* **66**, 2320.

SKINNER, H. A., and PRITCHARD, H. O. (1953). *Trans. Faraday Soc.* **49**, 1254.

SLATER, J. C. (1963). "Quantum Theory of Molecules and Solids," Vol. 1, Appendix 9. McGraw-Hill, New York.

SMITH, P. R., and RICHARDSON, J. W. (1965). *J. Phys. Chem.* **69**, 3346.

SMITH, P. R., and RICHARDSON, J. W. (1967). *J. Phys. Chem.* **71**, 924.

WILMHURST, J. K. (1958). *J. Phys. Chem.* **62**, 631.

45

MOLECULAR CHARGE DISTRIBUTIONS AND CHEMICAL BONDING.V.

MOLECULAR EXCITATION, IONIZATION, AND ELECTRON ATTACHMENT [+]

Paul E. Cade*

Laboratory of Molecular Structure and Spectra

Department of Physics, University of Chicago

Chicago, Illinois 60637

AND

R.F.W. Bader and Jocelyn Pelletier

Department of Chemistry, McMaster University

Hamilton, Ontario, Canada

ABSTRACT

The detailed changes in the electronic charge distributions upon electronic excitation, ionization, and electron attachment are studied for selected diatomic molecules. The processes considered involve the following systems and states $O_2(X^3\Sigma_g^-, a^1\Delta_g, b^1\Sigma_g^+)$, $O_2^+(X^2\Pi_g)$, $O_2^-(^2\Pi_g)$; BeH and MgH $(X^2\Sigma_g$, and $A^2\Pi_r)$; OH and SH $(X^2\Pi_i, A^2\Sigma)$, OH^+ and SH^+ $(X^3\Sigma^-)$, and OH^- and SH^- $(X^1\Sigma^+)$. It is shown that metastable excitation in the oxygen molecule produces only a very small change in the electronic charge distribution of the system. This suggests an important rôle for the spin density in determining the differential behavior of these systems. The $A^2\Pi_r \leftarrow X^2\Sigma^+$ and $A^2\Sigma^+ \leftarrow X^2\Pi_i$ excitations for the (BeH; MgH) and (OH; SH) pairs are examined and compared to the "active" electron approximation.

The changes in binding of the system associated with these various excitations, ionization, or electron attachments is examined in terms of the partial forces exerted by the various molecular orbitals. In particular, the sharp conversion to a pronounced "ionic" molecule is evident in the BeH and MgH excitations. The $A^2\Pi_r$ states of BeH and MgH are as ionic as the LiH and NaH systems in their ground states. It is demonstrated that the binding ability or properties of a given orbital shows a simple graduated trend in a sequence $(AB^+; AB; AB^-)$ which is not strongly dependent on the particular state symmetry of the system. The binding role assigned to a particular molecular orbital in a molecule is shown to depend on the particular state, and charge situation. The implications of these results towards providing a role for the excited states and molecular ions in the theory of chemical bonding is briefly discussed.

I. Introduction

The excited states of molecules and positive or negative molecular ions have not played any <u>major</u> role in shaping our ideas about chemical bonding. The basic notions of chemical bonding were developed primarily for the <u>ground</u> states of neutral molecules. The well-known molecular orbital theory does employ excited states of molecules together with changes in energy values and geometrical parameters to characterize the salient features of molecular orbitals and hence chemical bonding. This approach is applicable to excited states, although it has primarily been used to elucidate the bonding in ground states of molecules [see R. S. Mulliken[1] and A. C. Hurley[2] for recent discussions and references].

The chemical bonding in excited states or ions ($\pm$) of molecules has until recently been of little consequence since it is the <u>ground</u> states of neutral molecules which are usually involved, or in evidence, in most chemical phenomena or measurements. In recent years, however, the differential reactivity of excited states versus ground states has become an added factor in consideration of photochemical processes, flames, gas discharges, upper atmosphere phenomena, etc. As examples pertinent here, one might consider the properties and reactivity of metastable $O_2(a^1\Delta_g$ or $b^1\Sigma_g^+)$ relative to the ground state $O_2(X^3\Sigma_g^-)$ and the role and importance of the $OH(A^2\Sigma^+)$ excited state in flames. Wayne[3] has prepared a lengthy survey of the chemistry of $O_2(a^1\Delta_g$ and $b^2\Sigma_g^+)$. The very recent conference on "Singlet Molecular Oxygen and Its Role in Environmental Sciences"[4] and the rapid developments in "Chemical Lasers" further emphasize the increasing importance of excited states of molecules.

In addition to the fundamental property of a molecule, the molecular geometry, the electric dipole moment is now known for an <u>excited</u> electronic state in a few cases. In fact, electric dipole moments are known experimentally

for some molecules in excited states, but <u>not</u> in the ground electronic state. Bogaard and Orr[5] have proposed a method for measuring electric quadrupole moments of excited states of molecules and the method of Buckingham[6] or the molecular beam method[7,8] can perhaps be applied to metastable systems, e.g., $O_2(a^1\Delta_g$ and $b^1\Sigma_g^+)$. Very few examples can be quoted from experimental sources, but one can expect rather large changes in electric multipole moments with excitation, e.g., the dipole moment in CO changes such that $CO(X^1\Sigma^+, \mu = 0.112D, C^-O^+) \rightarrow CO(a^3\Pi_i, \mu = 1.38D, C^+O^-)$[9] and $CN(X^2\Sigma^+, \mu = 1.45D) \rightarrow CN(B^2\Sigma^+, \mu = -1.15D)$.[10] Only recently a procedure has been proposed for obtaining the electric quadrupole moment of a positive ion from a Rydberg sequence and tested for NO^+ by Lefebvre-Brion and Jungen.[11] Finally, we may mention that very recently the possibility has been demonstrated that hyperfine structure can be observed in very high resolution electronic spectra of simpler molecules, so that in principle the same repertory of expectation values and properties now routinely obtainable from high resolution microwave spectra of ground electronic states[12] are a possibility. Innes et al[13] have demonstrated this for $I_2(B^3\Pi_{ou})$ by obtaining the electric field gradient at the I nucleus in this excited state. Research is in progress to attempt to carry out electron diffraction from free radicals and positive ions.[14] Similar naiscent efforts have not been attempted for long-lived metastable states although they may not prove an impossible task.

Coulson[15] has given a very useful survey on the theoretical aspects of electronic excitation in molecules and is recommended for an additional general perspective of the bonding in electronically excited molecules.

On a lower plateau of "excitation", not involving electronic excitation, various physical properties such as dipole moments, electric field gradients, etc., are now being measured for specific (and usually lower) vibrational states

of simpler molecules. The rapid growth of techniques and the growing emphasis on the study of "definite state" physical or chemical processes imply increasing attention to the understanding of the variation of the electronic charge distribution with specific quantum state.

However, in addition to the above "diagonal" physical properties, information relevant to the changes in chemical binding, changes in the charge distribution, or changes in certain physical properties is directly or indirectly available through transition processes. The most obvious and useful physical properties of excited states determined in such processes are energy quantities, bond lengths, and molecular geometry. In this aspect the usual molecular orbital theory has been the means to explain the observed changes since MO theory is intrinsically adapted for treating excited and ground states within a common framework. However, we advocate the inclusion also of non-diagonal properties, i.e., transition moments, into an understanding of chemical binding in excited states. The use of such information has played little or no role in the theory of chemical binding previously. This last aspect is not considered in detail here except in certain gross features and will be considered more fully elsewhere.

Positive and negative molecular ions are important species in certain experimental situations and it is of interest to understand how ionization or electron attachment may modify the molecular charge distribution or physical properties. Information relating to the properties of molecular ions is very limited, being derived mostly from molecular spectroscopy or ions in crystal lattices, and therefore makes theoretical considerations more valuable. However, one expects that the usual canons relating to chemical binding developed from neutral ground state molecules to be generally applicable but subject to some modifications. The extent and precise nature of these modifications are largely

50

unknown.

It is convenient to make the following rough classification of excited states of a diatomic molecule:

i) Vibrational-rotational excited states within a common electronic state, e.g., $H_2(X^1\Sigma_g^+, \nu = 1,2,3,...,J = 0)$.

ii) Metastable electronic excited states; i.e., the same orbital configuration is involved, but different electronic states, e.g., $O_2(KK2\sigma_g^2 2\sigma_u^2 1\pi_u^4 3\sigma_g^2 1\pi_g^2, a^1\Delta_g, b^1\Sigma_g^+)$, $CH(K2\sigma^2 3\sigma 1\pi^2, a^4\Sigma^-, A^2\Delta, B^2\Sigma^-, C^2\Sigma^+)$, etc.

iii) Electronic excitation - One electron in an open-shell jumps to another open shell; for example, $BeH(K2\sigma^2 3\sigma, X^2\Sigma^+ \to K2\sigma^2 1\pi, A^2\Pi_r)$. This class of excitations is particularly interesting in case there is little inter-shell correlation between the electron in the open-shell and the underlying closed shells in <u>both</u> the ground and excited states. In such a situation the Hartree-Fock <u>and</u> "active" electron approximation <u>may</u> be exceptionally reliable as regards quantities associated with the transition.

iv) Electronic excitation - One or two electrons are redistributed among the <u>same</u> orbitals, e.g., $OH(K2\sigma^2 3\sigma^2 1\pi^3, X^2\Pi_i \to K2\sigma^2 3\sigma 1\pi^4, A^2\Sigma^+)$. This involves somewhat more complications than iii) in most cases as far as the expected quality of Hartree-Fock or the "active" electron approximation is concerned. At issue is the extent to which the symmetry of the paired electrons versus the unpaired electron affects various properties.

v) Electronic excitation - An electron in a closed-shell orbital jumps to an orbital not occupied in the ground configuration, for example almost any of the very important transitions of CO or N_2. These changes expose the worst in the Hartree-Fock approximation as such differential correlation effects are ordinarily large.

vi) Electronic excitation or ionization - An electron jumps either to a high Rydberg orbital or into a continuum orbital. The electron moves in the field of a slightly perturbed AB^+ parent system. Such a transition from a ground state to an $[AB^+;e^-]$ system may or may not be reasonably described by an independent particle model.

This rough classification has several faults. It assumes separability of electronic and nuclear motion, it emphasizes an orbital perspective with occupancy of orbitals in a key role, and cases could arise which are not covered or are ambiguous. These classes are much less useful when it is clear that one or both of the states involved in the excitation cannot be associated with a single molecular orbital configuration. The difficulties of this classification thus parallels the similar situation in dicusssing electronic transitions in molecular spectroscopy. In consideration of excitation processes we will ignore whether or not the transition is allowed in the usual spectroscopic sense.

The states and systems involved in the excitation, ionization or electron attachment processes considered in this final paper of a sequence[16] are listed in Table I. In the molecular density difference maps the R values used correspond to the R_e(exp.) of the ground state or neutral species. The excitation versus emission processes give slightly different $\Delta\rho$ maps, but the major features considered are substantially unchanged. Throughout then, vertical excitation, ionization, or electron attachment processes are involved in the $\Delta\rho(x,y)$ maps constructed from two total molecular density maps, $\rho(x,y)$. The partial force components in Tables II-V involve adiabatic changes for excitations if both R_e are known and vertical changes otherwise. In several cases both results are given. Following the actual vibrational distribution or the relax-

atlon to the upper state R_e value is best considered by other means. The

electronic wavefunctions employed here are all alledged to be to Hartree-Fock

accuracy and always involve large basis sets of Slater-type-functions and

extensive optimization of orbital exponents for the excited state or ions

involved as well as for the ground states of the systems. Only the wave-

functions for $BeH(X^2\Sigma^+)$, $MgH(X^2\Sigma^+)$, $OH(X^2\Pi_i)$, $SH(X^2\Pi_i)$, $OH^-(X^1\Sigma^+)$, and $SH(X^1\Sigma^+)$

have been published.[17] The remainder are either contained in forthcoming works

or available upon request.

II. The Molecular Charge Density; Total, Partial and Difference Densities

and Binding Analysis via Partial Forces

A. General Aspects

The rearrangement of the electronic charge distribution accompanying

electronic excitation or the gain or loss of an electron is expected to take

place very rapidly compared to the motion of the nuclei in coming to their new

equilibrium separation (or configuration). In principle one expects to see

first of all a rapid change of the electronic density upon excitation or

ionization followed by a adiabatic relaxation as the nuclei assume the new R_e

value. On the basis of the Franck-Condon principle the vertical rearrangement

of charge density therefore assumes a central role. If one is employing an

orbital perspective (Hartree-Fock or otherwise beyond the Hartree-Fock model),

the various orbitals in common between the two states involved also change;

some change slightly and some change considerably. This brief synopsis of what

happens neglects at least two factors. The first is probably not very important

and concerns the perturbation of the final state by the outgoing electron(s) in

the case of an excitation to a continuum orbital; any slight effects due to the

electromagnetic field other than the transition process are also neglected. The

second factor involves the explicit inclusion of the vibrational state.[18]

The chief elements in this study are the actual molecular charge distributions themselves, certain key differences between two charge distributions, and the forces exerted on the nuclei by electrons in the various molecular orbitals. The gross changes in a molecular charge distribution caused by a change in electronic state are characterized by the dimensions and nonbonded radii and charges of the distributions given in Table I. That the changes in these parameters on electronic excitation can be substantial is seen by comparing their value for the $X^2\Sigma^+$ and $A^2\Pi_r$ states of BeH or MgH, a comparison which in addition indicates that the excitation is spatially localized in the region of the Be or Mg nucleus. Primary attention however is paid to the usual molecular bond density maps defined by

$$\Delta\rho_{SA}(x,y) = \rho_{AB}(x,y;R_e) - [\rho_A(x,y) + \rho_B(x,y)]_{R=R_e} \qquad (1)$$

where $\rho_A(x,y)$ and $\rho_B(x,y)$ are the separated atoms (but, not spherically averaged, however) the molecule dissociates into. These atomic densities are to Hartree-Fock quality. The $\Delta\rho_{SA}$ maps reveal the nature of the chemical binding for the excited versus the ground state of the molecule. The other key quantity used here directly gauges the change in the molecular charge distribution upon excitation, ionization, or electron attachment and is defined, respectively, by:

$$\Delta\rho_{\Lambda,\Lambda'}(x,y) = \rho_{AB}^{(\Lambda')}(x,y;R) - \rho_{AB}^{(\Lambda)}(x,y;R),$$

$$\Delta\rho_I(x,y) = \rho_{AB^+}(x,y;R) - \rho_{AB}(x,y;R), \qquad (2)$$

or

$$\Delta\rho_{E.A.}(x,y) = \rho_{AB^-}(x,y;R) - \rho_{AB}(x,y;R).$$

The superscripts (Λ) and (Λ') refer to the ground and excited state designations,

54

respectively. These quantities are defined so that the $\Delta\rho$ maps exhibit the
change in the final state relative to the initial state and always involve
$\rho_{Final} - \rho_{initial}$. Even though $\Delta\rho_I$ and $\Delta\rho_{E.A.}$ integrate to give one electron
charge totally and $\Delta\rho_{\Lambda,\Lambda'}$ integrates over all space to give zero, the actual
magnitudes of changes in the three cases are generally comparable.

The partial force, $f_{iA}(R)$, acting on nucleus A in the molecule when R is
the internuclear separation is defined by[16]

$$f_{iA}(R) = R^2 N_i \int |\phi_i(\vec{r}_\mu)|^2 r_{\mu A}^{-2} \cos\theta_{\mu A} d\vec{r}_\mu \ . \tag{3}$$

The partial force is actually not a force (since R^2 occurs) but has the dimensions
of a charge in au. Thus $f_{iA}(R)$ is numerically equivalent to a point charge at the
B nucleus in the AB molecule which will exert the same electrostatic force on the
A nucleus as the charge distribution in the ith molecular orbital. The actual
force exerted on nucleus A by a single electron in the ϕ_i molecular orbital is
$f_{iA}(R)/R^2$. N_i is the orbital occupation number. The partial forces are a
quantitative measure of how effective the electrons (all N_i) in the ϕ_i molecular
orbital are in opposing a share of the electrostatic repulsion of the nuclei. The
binding, antibinding, or nonbinding labels characterize the effectiveness of a
given orbital relative to the separated atoms situation which the molecular
orbital correlates with. A more complete discussion is given in (I) and (II)
for the A_2 and AH systems, respectively. In these studies we will consider in
some detail the comparative changes of $f_{iA}^{(\Lambda)}(R)$ versus $f_{iA}^{(\Lambda')}(R')$ or $f_{iA}^{(\Lambda')}(R)$ and
$f_{jA}^{(\Lambda')}(R)$ where j refers to a new orbital occupied in the excited state. The
binding of the excited state or ion is treated in a comparative manner relative
to the ground state neutral parent. Such an approach has the merit, as do the
$\Delta\rho_{\Lambda,\Lambda'}$ maps, that it is free from any concern about the separated atoms situation

55

and provides the means of directly comparing molecular systems. The question
of chemical bonding is in practice more a case of comparative situations in
two molecules (or parts of two molecules) than between the same two molecules
and their separated atoms individually.

B. Metastable Excitation, Ionization, and Electron Attachment of

$O_2(KK2\sigma_g^2 2\sigma_u^2 3\sigma_g^2 1\pi_u^4 1\pi_g^2, X^3\Sigma_g^-)$
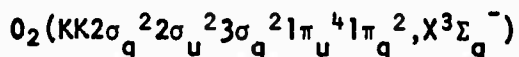
In the metastable excitation of $O_2(X^3\Sigma_g^-)$ to the $a^1\Delta_g$ and $b^1\Sigma_g^+$ state no
new orbitals are involved, all three states arising from the $1\pi_g^2$ open-shell
configuration. The $\Delta\rho_{\Lambda,\Lambda'}(x,y)$ and $\Delta\rho_{\Lambda,\Lambda'}(x,o)$ maps (in Fig. 1) and the data
in Table 1 reveal an apparently very small change in the molecular charge density
upon excitation $(a^1\Delta_g - X^3\Sigma_g^-)$ or $(b^1\Sigma_g^+ - X^3\Sigma_g^-)$. [It should be carefully noted
that the excitation maps for oxygen are given on a much finer scale, by ~~about~~ a
factor of ten, than are other maps in this and earlier papers.] The "active"
electron $\Delta\rho_{\Lambda,\Lambda'}(x,y)$ maps very closely resemble these as well as little changes
are observed in each orbital. The value of $\Delta\rho_{\Lambda,\Lambda'}(x,y)$ is less than 0.1% of the
value of the total charge density itself in any region of space and contour maps
of $\rho(r)$ for the three states, illustrating density contours with values down to
0.002 au, are superimposable.

The insensitivity of $\rho_m(r)$ to changes in the values of Λ and/or S within a
given configuration is not unique for O_2, but appears to be general, for diatomic
molecules at least. Because of the Hellmam Feynman theorem and the near
constancy of $\rho(r)$, it follows that states arising from the same configuration
should possess nearly the same bond length, or in the case of polyatomic systems,
nearly the same geometry. The experimental verification of the constancy

of $\rho(r)$ is illustrated by the nearly identical values for the equili-
brium bond lengths, the values being 2.282, 2.297 and 2.318 B. respectively for

56

the $^3\Sigma_g^-$, $^1\Delta_g$ and $^1\Sigma_g^+$ states.

The potential constants of a system are determined by the changes in the forces exerted on the nuclei when they are displaced from their equilibrium positions.[19,20] The changes in the forces are in turn determined by the changes in $\rho(r)$. In particular if the X coordinates of the nuclei in a diatomic molecule are denoted as X_A and X_B, then

$$k_2 = -\partial^2 E/\partial X_A \partial X_B = 2Z_A Z_B/R_e^3 + Z_A \int (\partial\rho/\partial X_B)(\cos\theta_A/r_A^2)d\tau.$$

The last term states that the total electronic contribution to k_2 may be equated to the change in the force on nucleus A resulting from the change in $\rho(r)$ caused by a displacement of nucleus B from its equilibrium position. If the near identity in $\rho(r)$ for states within the same configuration extends over a range of internuclear separations around R_e it should be reflected in similar values of the harmonic frequency ν_o for these states. The values of ν_o for the $^3\Sigma_g^-$, $^1\Delta_g$ and $^1\Sigma_g^+$ states of O_2 are 1580, 1509, and 1433 cm^{-1} respectively.

The wavefunctions employed are to Hartree-Fock accuracy, but this is to restricted Hartree-Fock accuracy so that not only are the spatial parts of the spin-orbitals $\psi_{1\pi}^+(\vec{x}) = \phi_{1\pi}^+(\vec{r})\alpha(s)$ and $\psi_{1\pi}'^+(\vec{x}) = \phi_{1\pi}^+(\vec{r})\beta(s)$ assumed identical, but in addition the spatial parts $\phi_{1\pi}^+(\vec{r})$ and $\phi_{1\pi}^-(\vec{r})$ not involving the ϕ-dependence (angular dependence around the internuclear axis) are taken to be the same.[21] In the calculations of Cade and Malli,[22] separate and relatively independent wavefunctions were obtained for the $X^3\Sigma_g^-$, $a^1\Delta_g$, and $b^1\Sigma_g^+$ states, with orbital exponents optimized for each case, and all questions of internal consistency considered afterwards. In short, these wavefunctions and $\Delta\rho_{\Lambda,\Lambda'}(x,y)$ maps are as flexible as the restricted Hartree-Fock approximation permits.

It is difficult to convincingly attribute physical reasons to the specific features in $\Delta\rho_{\Lambda,\Lambda'}$ for oxygen. The excitation to the $a^1\Delta_g$ state implies orbital changes ($1\pi'_{g+}\alpha 1\pi'_{g+}\beta \leftarrow 1\pi_{g+}\alpha 1\pi_{g-}\alpha$), i.e., a change from $1\pi_{g-}$ to $1\pi_{g+}$ plus a spin change, whereas excitation to the $b^1\Sigma_g^+$ state involves only a change in the spin state, i.e., ($1\pi'_{g+}\alpha 1\pi'_{g-}\beta \leftarrow 1\pi_{g+}\alpha 1\pi_{g-}\alpha$). It would be desirable to have some qualitative notion regarding the relative or comparative failure of the RHF approximation for these three configurations in order to estimate the contributions of artifacts to the $\Delta\rho_{\Lambda,\Lambda'}$ maps in Fig. 1. If we consider only the $1\pi_g^2$ part, which is of key significance here, then symmetry equivalence (assuming $1\pi_{g+} = 1\pi_{g-}$) only is invoked in the $^3\Sigma_g^-$ ground state and in the $b^1\Sigma_g^+$ state and spin equivalence only is invoked in the $a^1\Delta_g$ state. This may suggest that the $\Delta\rho_{\Lambda,\Lambda'}$ maps involving $^3\Sigma_g^-$ and $^1\Sigma_g^+$ involve approximately the same order of RHF errors for both states and hence artifacts are less pronounced than in the $^3\Sigma_g^- - a^1\Delta_g \ \Delta\rho_{\Lambda,\Lambda'}$ maps. This train of argument is perilous and we do not feel can lead to any useful suggestions as to the extent to which errors, differential errors, arising from the use of the RHF approximation affect the $\Delta\rho_{\Lambda,\Lambda'}$ maps in Fig. 1. Unrestricted Hartree-Fock calculations on atoms lead to only slightly different orbitals which are normally spin equivalent so great changes in $\Delta\rho_{\Lambda,\Lambda'}$ are probably not to be expected even in a more complete study. The only safe conclusion Fig. 1 suggests is that the changes in the usual molecular charge distribution is not great - even with a more general independent particle model - so that changes in physical properties and/or reactivity which do not depend primarily on spin cannot be great among these three $1\pi_g^2$ electronic states. This implies that a $\Delta\rho_{\Lambda,\Lambda'}$ map involving spin densities (and better wavefunctions) must give indications of any marked changes in physical properties associated with spin.

And conversely, properties showing pronounced variability for these three systems are probably primarily explicable in terms of spin density differences. These suggestions are consistent with the close similarity of spin-independent expectation values,[22] the small differences in R_e, etc., for these three states. It is further likely that these three states have very similar interactions and transport properties and the three charge distributions are perhaps indistinguishable to usual electron diffraction. Unfortunately no physical properties of the $a^1\Delta_g$ and $b^1\Sigma_g^+$ are experimentally known (other than D_e and spectroscopic properties). The spin density of the $a^1\Delta_g$ and $b^1\Sigma_g^+$ are both zero in our approximation because of the spin equivalence in the first case and because of the symmetry equivalence in the latter. Therefore any $\Delta\rho_{\Lambda,\Lambda'}$ map presented using the RHF wavefunctions will simply be the spin density of the $X^3\Sigma_g^-$ state or just the $1\pi_g^2$ charge density again.

The $\Delta\rho_I$ and $\Delta\rho_{E.A.}$ density difference maps [for vertical ionization or electron attachment of $O_2(X^3\Sigma_g^-)$] show the loss and gain, respectively, of another $1\pi_g$ electron. There is not, however, a very noticeable contraction or expansion accompanying these processes as the total $\rho(x,y)$ density maps (not shown) indicate. The overall contraction upon ionization is $\sim$2-5% whereas an expansion of 5-10% accompanies vertical electron attachment. The addition (or loss) of a $1\pi_g$ electron causes a considerable _loss_ of charge along the molecular axis and between the nuclei (or conversely cause a considerable _accumulation_ of charge in the same region upon ionization). The later reaction-reorganizations of the sigma charge density is a substantial effect. The $O_2^-;O_2(X^3\Sigma_g^-);O_2^+$ sequence forms a graduated triple as electrons are successively detached. For each of the two steps [reverse the senses of the $\Delta\rho_{E.A.}$ map for comparison in this sequence] the sigma density substantially tightens about the molecular

59

axis and between the nuclei to offset the decreased shielding of the inter-
nuclear repulsion due to the loss of the $1\pi_g$ electrons. These aspects are
quantitatively discussed next in terms of partial forces or effective charges
acting to bind the nuclei.

The analysis of the binding of the nuclei in terms of partial forces is
transparent for the metastable excitations of $O_2(X^3\Sigma_g^-)$. The pertinent
numbers are summarized in Table II for the vertical excitations. (In this
case the R_e values are so similar that the partial forces for adiabatic
excitation, which are shown in parentheses, are almost identical to the
vertical values.) In a few words the results, as well as the $\Delta\rho_{\Lambda,\Lambda'}$ maps,
indicate that the binding in the $a^1\Delta_g$ and $b^1\Sigma_g^+$ states is almost exactly the
same as in the ground state. Accordingly, invoking the "active" electron
approximation and even neglecting all orbital reorganization would be an excellent
substitute. The partial forces are simply very nearly independent of the
electronic configuration, and the differences in Table II are probably too small
to be given physical visage. Is the binding in these three states actually so
very similar? Probably not, and this reveals either a weakness of the methods
of force analysis[16] or a particularly sensitive situation which exposes the
relative inflexibility of the RHF. The latter seems a much more reasonable
alternative and it is likely that an analysis in terms of the partial forces,
or equivalent charges, employing a more general independent particle approx-
imation would show small, but significant changes in the binding of the nuclei.

The changes in the binding forces as electrons are added or taken from
$O_2(X^3\Sigma_g^-)$ are indicated in Table II and Fig. 2. The O_2^{++} results have been
included as well, although the system may not be bound (the large attractive
net force as $O_2 \rightarrow O_2^{++}$ in the N_2 configuration does suggest it is bound,

60

however.[23]) The smooth trends suggest that the relative chemical binding in

this sequence is explained in terms of the relative degrees of binding of the

nuclei by the various molecular orbitals. The O_2^+; O_2; O_2^- situation was

also previously discussed (in I) for different purposes. Although the curves

in Fig. 2 connect points for <u>vertical</u> excitation, the adiabatic forces also

shown would not significantly change the key trends indicated. (For O_2^- these

differences are expected to be, and are, greatest.)

In this sequence the very slight binding of the nuclei by the $1\sigma_g^2$ and

$1\sigma_u^2$ decreases a few percent as $O_2^{++} \rightarrow O_2^+ \rightarrow O_2(X^3\Sigma_g^-) \rightarrow O_2^-$. The "core"

binding is almost unaffected by successive addition of $1\pi_g$ electrons, but the

change is greater than that associated with the metastable excitation of

$O_2(X^3\Sigma_g^-)$. All of the partial forces in Fig. 2 are given for pair occupancy

for internal comparison and hence all effective charges, f_i values, exceeding

1.00 are binding as usual (I). Across the sequence $O_2^{+2} \rightarrow O_2^+ \rightarrow O_2 \rightarrow O_2^-$ the

general picture emerges that all orbitals decrease their binding strength as

electrons are added except for the $3\sigma_g^2$ density which counters this trend and

the $2\sigma_u^2$ density which doesn't change much. The $2\sigma_g^2$ is strongly binding across

the sequence and remains the mainstay of the binding force. The $1\pi_u$ charge

density which was previously classed as only weakly binding for B_2, C_2, N_2, O_2,

and F_2 with a peak at O_2 actually is significantly more binding in O_2^{++} and O_2^+

than for any other $1\pi_u$ orbital in a first-row A_2 system (neutral or ion), i.e.,

the $1\pi_u$ orbital in O_2^{+2} is the most strongly binding $1\pi_u$ orbital known. The $2\sigma_u^2$

density unresponsively neglects <u>any</u> shielding and provides the most serious

electronic <u>opposition</u> to binding the nuclei. The $3\sigma_g^2$ density, often assigned

to "spectator" role in the molecule, but held to be definitely <u>antibinding</u> in

earlier work (I), displays an <u>increased</u> binding tendency, but still falls by a

large margin to shield one nuclear charge. Paralleling this behavior the $1\pi_g$ density/pair is still sharply antibinding and increasingly as $O_2^{++} \rightarrow O_2^{+} \rightarrow O_2 \rightarrow O_2^{-}$. All indices lead straightforwardly to the conclusion that the binding role of almost all orbitals (except $3\sigma_g$) decrease as another $1\pi_g$ orbital is added. As ineffectual as the additional $1\pi_g$ electrons are in screening nuclear charge, as long as the nuclear charges are unchanged, they afford a relaxation of the binding ability of the key binding orbitals ($2\sigma_g$ and $1\pi_u$). This regular change as $1\pi_g$ electrons are added is very nearly additive except for the incorrigible $2\sigma_u$ density.

C. The $BeH(A^2\Pi_r \leftarrow X^2\Sigma^+)$ and $MgH(A^2\Pi_r \leftarrow X^2\Sigma^+)$ Excitations

The most prominent transitions observed for the BeH and MgH molecules are the $(A \rightarrow X)$ band systems considered herein. In the Hartree-Fock approximation these transitions may be represented

$$BeH[K(2\sigma)^2(3\sigma)^1, X^2\Sigma^+ \rightarrow K'(2\sigma')^2(1\pi)^1, A^2\Pi_r]$$

and

$$MgH[KL(4\sigma)^2(5\sigma)^1, X^2\Sigma^+ \rightarrow K'L'(4\sigma')^2(2\pi), A^2\Pi_r]$$
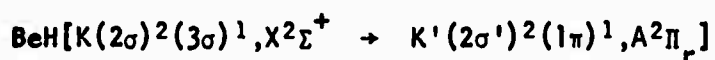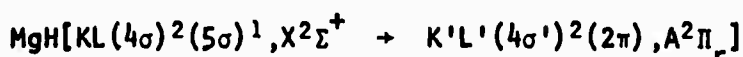
where the inner, atomic-like, shells are designated by $K \cdot \equiv \cdot 1\sigma^2$ and $KL \cdot \equiv \cdot 1\sigma^2 2\sigma^2 3\sigma^2 1\pi^4$ and the primes emphasize the common orbitals which have readjusted to the new electronic configuration and state. In Fig. 3 the actual total changes in the charge distribution for the excitation in BeH is shown (the data in Table I show that corresponding changes occur in the MgH system) and in particular the bond density maps are shown for BeH and MgH. The latter are as usual indices of how the charge (in the excited state, $^2\Pi_r$) has rearranged itself relative to the separated atoms - in short the chemical bonding in this excited state. It is especially noteworthy that the $\Delta\rho_{SA}(x,y)$ and $\Delta\rho_{SA}(x,o)$ maps for the $^2\Pi_r$ states are very good examples of the "ionic"

type $\Delta\rho_{SA}$ maps and are remarkably similar to the $\Delta\rho_{SA}$ maps for LiH($X^1\Sigma^+$) and NaH($X^1\Sigma^+$) respectively (see Figs. 3, 4, paper II and Figs. 3, 4, paper IV). When BeH($A^2\Pi_r$) and MgH($A^2\Pi_r$) are contrasted to the ground $X^2\Sigma^+$ states a very substantial change in bonding attributes is seen and also demonstrable in terms of physical properties. Actually the $\Delta\rho_{SA}$ maps for the $^2\Pi_r$ state of BeH and MgH are very similar to the $\Delta\rho_{SA}$ maps for BeH$^+$ and MgH$^+$ suggesting that the transition 3σ (or 5σ) $\to$ 1π (or 2π) is as effective as complete loss of the 3σ (or 5σ) electron in pushing the BeH (or MgH) molecule emphatically in the direction of a strong ionic molecule characterized by a nearly perfect transfer of an electron from the vicinity of the Be nucleus to the vicinity of the proton. The details of this aspect of the $\Delta\rho_{SA}$ maps, the back-polarization of the "core", etc., are discussed fully below.

The major new and revealing aspects concern the $\Delta\rho_{\Lambda,\Lambda'}(x,y)$ maps for several approximations. The two figures on the left-hand side of Fig. 4 represent the full single configuration Hartree-Fock results for the two states--everything is included. It should be noted that $\Delta\rho_{\Lambda,\Lambda'}(x,y)$ maps do not depend intrinsically on an orbital approximation or any special functional form of the electronic wavefunction, so in a real sense Fig. 4 should be a direct gauge of the success of the independent particle model. The main feature of the $\Delta\rho_{\Lambda,\Lambda'}(x,y)$ maps is, as might be expected in a $\Sigma \to \Pi$ transition, a transfer of electronic charge from along the molecular axis to perpendicular to the molecular axis with the focus of the origin of this change near the Be nucleus in BeH and less near the Mg nucleus in MgH. It roughly corresponds to an electron in a $2p\sigma$ (or $3p\sigma$) atomic-like orbital jumping to a $2p\pi$ (or $3p\pi$) atomic-like orbital centered on the Be (or Mg) nucleus. Both atomic-like orbitals are distortions of any ancestral atomic orbitals, however. These particular figures support

the idea that some features of certain molecules might be understood very approximately in terms of analogous features of one of the atoms from which the molecule was formed. In the case of BeH, it suggests that the electron in the 3σ orbital, which is much like a $2p\sigma$ on Be, is mainly a "spectator" or opponent of molecule formation and to some extent can jump to other orbitals of like behavior. The results are electronic transitions for the molecule being essentially remnants of the related atomic transitions, but now taking place in an unusual environment. The $\Delta\rho_{\Lambda,\Lambda'}(x,y)$ map for MgH also reveals a significant change in the core charge density as contrasting polarization influences are involved in the $5\sigma \rightarrow 2\pi$ transition.

The right-hand side of Fig. 4 displays directly the effectiveness of an "active" electron approximation using the actual 1π orbital calculated for the $^2\Pi_r$ state in BeH on the one hand (upper) and the 2π "virtual" orbital from the $^2\Sigma^+$ for MgH on the other hand (lower). (These should be contrasted with the complete $\Delta\rho_{\Lambda,\Lambda'}(x,y)$ maps on the left hand side.) Both approximations to $\Delta\rho_{\Lambda,\Lambda'}(x,y)$ are qualitatively correct, as necessary simply by symmetry, but generally both approximations underestimate the amount of charge removed from around the proton and the amount of charge accumulated in the doughnut-like region perpendicular to the page around the Be or Mg nucleus. Thus neglecting readjustment of the orbital charge density not involved and/or neglecting the change in the π-orbital, the excitation would appear to involve less transfer of charge than is really the case in the $^2\Pi_r \leftarrow {}^2\Sigma^+$ excitation. It would be very desirable to correlate these shortcomings of the "active" or "virtual" electron $\Delta\rho_{\Lambda,\Lambda'}$ maps to the calculated transition probabilities, but no straightforward correlation is apparent employing diagonal reduced density matrices.[24] Another very significant, and expected, deficiency in the "active"

electron $\Delta\rho_{\Lambda,\Lambda'}(x,y)$ maps occurs in the region near the A nucleus. This is most strikingly seen for BeH and for MgH; neglects$_{\Lambda}$ the very important effect of a new "core" polarization upon excitation.

The partial force or effective charges (Table III) permit a quantitative expression of the changes in the chemical binding situation in BeH and MgH in the $^2\Sigma^+ \rightarrow {}^2\Pi$ transition. These partial forces are all at R_e(exp.), for the system in question. Hence adiabatic excitation or ionization is studied. The effective charges for BeH$^+$ and MgH$^+$ molecule-ions are also included for comparison and these closely resemble the LiH and NaH values published previously. As always, the $K(1\sigma^2)$ core (for the first-row) and the $KL(1\sigma^2 2\sigma^2 3\sigma^2 1\pi^4)$ core (for the second-row) appears to the proton as simply a sphere of negative charge cancelling either 2 nuclear charges (for the first-row) or 10 nuclear charges (for the second-row). This characteristic behavior is essentially unaffected by excitation or ionization of BeH and MgH. As is characteristic of the second-row hydrides, however, the $3\sigma^2$ density cancels 2.137, not 2.000 nuclear charges, and the $1\pi^4$ density cancels 3.863, not 4.000 nuclear charges, so that the net total shielding very near 10.000 nuclear charges reflects some mutual internal balancing.

The force exerted on the A nucleus by the "core" orbitals, i.e., orbitals tightly localized around the A nucleus, is changed quite substantially in the $^2\Sigma^+ \rightarrow {}^2\Pi$ excitation. In Table III it is apparent that in the $^2\Pi$ state the effective charge on the A nucleus by the "core" orbitals is strongly repulsive in effect. That is, the "core" orbitals act to pull the A nucleus away from the proton. In the BeH($^2\Sigma^+$) state the effective charge acting on the Be nucleus due to the $K(1\sigma^2)$ core is -0.127 and it changes to -0.520 upon excitation to the $^2\Pi_r$ state and -0.629 upon ionization (compare with a value of -0.489 for LiH).

A parallel situation obtains in MgH with the effective charge acting on the Mg nucleus due to the $KL(1\sigma^2 2\sigma^2 3\sigma^2 1\pi^4)_{\text{core}}$ changes from -0.217 to -0.488 upon excitation and to -0.716 upon ionization (for NaH the value is -0.724). The core polarizations provide a sensitive probe of the fields experienced in the region of a given nucleus and hence a measure of the direction and extent of transfer of valence charge density. The core density must exert a field at its' own nucleus equal in magnitude but opposite in direction to the net field exerted by the valence density and the second nucleus and its core density if the force on the nucleus is to equal zero. The f_1 values for the core orbitals on Be and Mg in the $^2\Sigma^+$ states indicate that the net dipolar field experienced by the Be or Mg cores from the valence density and the proton is quite small in magnitude; the field of the proton and its accumulated charge density being largely balanced by the field exerted by the nonbonded charge density on the Be or Mg nuclei. In the $^2\Pi$ excited or ionized states of BeH and MgH, however, the core densities are strongly polarized away from the proton, a reflection of the net negative field exerted on the cores by the localization of the valence charge density on the bonded side of the heavy nuclei in these states. These changes demonstrate the sharp change from a "covalent" type situation to an "ionic" type upon excitation or ionization. Comparatively viewed, the BeH($^2\Pi_r$) state appears beyond even LiH in behavior, whereas the trend for MgH($^2\Pi_r$) is much less than for NaH again a reflection of the difference of the BeH(3σ) and MgH(5σ) orbitals.

The $2\sigma^2$ (BeH) and $4\sigma^2$ (MgH) molecular orbitals are not changed a great deal in the excitation or even upon ionization. This is reflected in the partial forces exerted on the A nucleus and the proton in Table III. The effective charge (which is zero for $R \to \infty$) giving rise to the strong binding of the A

66

decreases only slightly on excitation or ionization. The effective charge due to the $2\sigma^2$ (or $4\sigma^2$) orbital density acting on the proton as $R \to \infty$ is just 2.000, of course, as it shields two positive charges on the A nucleus. In these molecular systems the $2\sigma^2$ (or $4\sigma^2$) density is slightly _more_ antibinding with respect to the proton in the excited state relative to the ground state and in the BeH$^+$ and MgH$^+$ ion the $2\sigma^2$ and $4\sigma^2$ density, respectively, are actually slightly _binding_ with respect to the proton. Therefore the changes in the partial forces on the proton and the A nucleus due to the $2\sigma^2$ (or $4\sigma^2$) density in the $(^2\Sigma^+ \to {}^2\Pi_r)$ excitation are quite small and the binding or anti-binding characteristics are slightly affected by this excitation. In fact the change in the "core" orbital (s), and especially as relates to the A nucleus, upon excitation is about four times as large as that of the $2\sigma^2$ (or $4\sigma^2$) charge density.

The "active" electron perspective may, of course, be cast in terms of the changes in partial forces or effective charges. Clearly since the force on each nucleus must vanish at R_e for both the ground or the excited state, the "active" electron approximation would imply that in the $^2\Sigma^+ \to {}^2\Pi_r$ transition $f_{3\sigma,A} = f_{1\pi,A}$ or $f_{5\sigma,A} = f_{2\pi,A}$ and $f_{3\sigma,H} = f_{1\pi,H}$ or $f_{3\sigma,H} = f_{2\pi,H}$. Table III indicates that this is roughly true for the partial forces on the _proton_. . Thus the force on the proton due to each individual orbital needs only small modification in the excitation ($3\sigma \to 1\pi$ or $5\sigma \to 2\pi$), and for MgH these individual changes are quite small. However, the _changes_ in the effective charges acting on the A nucleus by the "active" orbitals is large and non-cancelling, i.e., for BeH, $f_{3\sigma,A} = -0.513$ and $f_{1\pi,A} = -0.055$ and for MgH, $f_{5\sigma,A} = -0.699$ and $f_{2\pi,A} = -0.019$, results which demand that there be balancing changes in the partial forces on A due to "non-active" orbitals which we have

67

seen above is accomplished principally through the "core" orbitals and not the $2\sigma^2$ (in BeH) or $4\sigma^2$ (in MgH) orbitals.

In the earlier studies of the AH systems the 1π (or 2π) orbitals were generally viewed as an unimportant feature of the binding of the nuclei. Those views also hold for the 1π (or 2π) orbital in the $^2\Pi_r$ state - i.e., the orbital is slightly polarized, but now surprisingly it is not polarized towards the proton as usual, but it is polarized in the opposite sense. As a result the π-orbital in the excited state actually exerts a force on the A nucleus equivalent to enhancement of the internuclear repulsion. The effect is very small, however, -0.055 in BeH and -0.019 in MgH and is a very rare feature of the AH hydrides. The π-orbital is antibinding with respect to the proton as well, failing to shield a single nuclear charge on Be- or Mg-nucleus.

The major quantitative features in the $(X^2\Sigma^+ - A^2\Pi_r)$ excitation for BeH and MgH can be briefly summarized. The effective charges acting on the proton are almost unchanged, orbital for orbital, with the 1π (or 2π) simply assuming the role of the 3σ (or 5σ) orbital. As regards the A nucleus the $z\sigma \to w\pi$ electron jump eliminates the strongly antibinding $z\sigma$ orbital and the force balance is achieved not by a substantial weakening of the strongly binding $y\sigma^2$ orbital or a strongly antibinding $w\pi$ orbital, but by a sharply back-polarized K or KL "core". A charge transfer effect results, but the transferred charge is not localized on the proton, but between the nuclei.

D. The OH and SH$(A^2\Sigma^+ \Leftarrow X^2\Pi_i)$ Excitation and Ionization and Electron Attachment of OH and SH

The processes or net changes involved here can be represented by

$$\text{OH}[K(2\sigma)^2(3\sigma)^2(1\pi)^3_i X^2\Pi_i \to K'(2\sigma')^2(3\sigma')^1(1\pi')^4, A^2\Sigma^+]$$

68

and

$$SH[KL(4\sigma)^2(5\sigma)^2(2\pi)^3,X^2\Pi_i \rightarrow K'L'(4\sigma')^2(5\sigma')^1(2\pi')^4,A^2\Sigma^+]$$
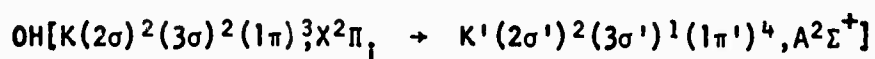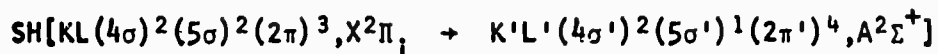
for the excitation process and by

$$AH[C(y\sigma)^2(z\sigma)^2(w\pi)^3,X^2\Pi_i] \rightarrow AH^+[C'(y\sigma')^2(z\sigma')^2(w\pi')^2,X^3\Sigma^-] + e^-$$

and

$$AH[C(y\sigma)^2(z\sigma)^2(w\pi)^3,X^2\Pi_i] + e^- \rightarrow AH^-[C'(y\sigma')^2(z\sigma')^2(w\pi')^4,X^1\Sigma^+]$$
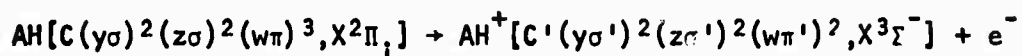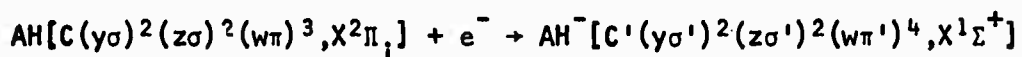
for the ionization and electron attachment processes. The latter are written
in Mulliken's general form and C (or C') is the particular core involved and
A·≡·O or S nuclei.

The total electron density, $\Delta\rho_{SA}(x,y)$, and $\Delta\rho_{SA}(x,o)$ for the $A^2\Sigma^+$ excited
state (at its R_e value) in Fig. 5 should be compared with the corresponding
figures for the ground state (1,3,4 in paper II for OH and 1,6,7 in paper IV
for SH). The changes in the molecular dimensions and in the nonbonded radii
and charges (Table I) between $^2\Pi_i$ ground and $^2\Sigma^+$ excited states of OH and SH
reflect the expected consequences of a $\sigma \rightarrow \pi$ transition; a decrease in length
and an increase in width of the distribution and a decrease in the nonbonded
populations on oxygen and sulphur and on the proton in both molecules.

The most significant changes are in the $\Delta\rho_{SA}$, or bond density maps of
the excited state compared to the ground state.[25] Compared to the $^2\Pi_i$ states
of OH and SH, the distribution of charge accumulated in the internuclear
region for the $^2\Sigma^+$ states is more diffuse and much less contracted along the
internuclear axis. In addition, more charge is removed from the region of
the proton and the proton itself resides in a region of charge deficit.
Finally, the pattern of charge reorganization in the region of the A nucleus

69

differs radically between the ground and excited states. In the formation of the bond in the $^2\Sigma^+$ state charge density is removed from the nonbonded region of A and accumulated in a belt-like region around the A nucleus, a reversal of that found for the $^2\Pi_i$ ground states. The accumulation of charge density in the binding region in the form of a diffuse equitorial distribution characterizes a binding situation with a dominant π component. The surprising features are the increased extent to which charge density is removed from the proton and the loss of charge density from the nonbonded region of the A nucleus. A $\Delta\rho_{SA}$ map for a system bonded primarily by the sigma density is characterized by an axial charge increase in both the bonded and nonbonded regions of the A nucleus and an equitorial region of charge removal. Thus the bond density maps clearly illustrate the change in the binding of the nuclei in the OH and SH systems from one which is primarily sigma in character in their ground states to one which is principally of π character in their excited states.

The net force binding the nuclei in both ground and excited states is exerted by the charge density accumulated between and shared by both nuclei. Thus on the basis of the $\Delta\rho_{SA}$ maps the binding in both the $^2\Pi_i$ and $^2\Sigma^+$ states is classified as covalent. However, the difference in the spatial distribution of this charge increase between the two states, one axial and contracted, the other diffuse and equitorial, clearly reveals a difference in the manner in which the charge density is shared in the two cases, a difference which is reflected in the lower dissociation energies of the $^2\Sigma^+$ states. [The ratio of the dissociation energies $D_o(A^2\Sigma^+)/D_o(X^2\Pi_i)$ is 2.35/4.39 for OH and ~1.00/3.53 for SH.]

The four $\Delta\rho_{\Lambda,\Lambda'}(x,y)$ maps at the top of Fig. 6 suggest that the "active"

70

electron approximation is qualitatively reliable. The main features of the $\Pi \rightarrow \Sigma^+$ transition (which again involve a $z\sigma \rightarrow w\pi'$ electron jump) are clearly evidenced by a sharp transfer of electronic charge from a region along the molecular axis to one perpendicular to it. Comparison of the 3σ and 1π orbitals (or 5σ and 2π orbitals) in Fig. 7 and 8 of paper II (or Fig. 3 and 4, paper IV) does indicate that the major features are as expected in a $z\sigma \rightarrow w\pi'$ transition and especially the close similarity of the deficit region with the 3σ or 5σ orbital of the ground state.

The two upper $\Delta\rho_{\Lambda,\Lambda'}(x,y)$ maps on the right afford a more direct gauge of the validity of the "active" electron approximation. These are simply the differences between the $w\pi$ orbital in the excited state (or $w\pi'$) and the $z\sigma$ orbital of the ground state. The two $\Delta\rho_{\Lambda,\Lambda'}(x,y)$ maps are very similar and the "active" electron approximation of $\Delta\rho_{\Lambda,\Lambda'}$ seems more quantitatively correct for the OH and SH systems than for the BeH and MgH systems. Thus the "active" electron $\Delta\rho_{\Lambda,\Lambda'}$ map does not appreciably misrepresent the region of deficit near the proton as in BeH and MgH. In fact, for OH and SH the "active" electron approximation slightly <u>overestimates</u> (not <u>underestimates</u> as in BeH and MgH) the amount of charge removed from around the proton in the $^2\Pi \rightarrow {}^2\Sigma$ excitation. Generally, for OH and SH the "active" electron $\Delta\rho_{\Lambda,\Lambda'}$ map gives a slight overestimate of both deficit and accumulation regions when closely compared to the complete $\Delta\rho_{\Lambda,\Lambda'}$ maps on the left. Again the significance of this contrast of the "active" electron versus the complete $\Delta\rho_{\Lambda,\Lambda'}$ maps only distantly suggests a connection with the corresponding transition $(^2\Pi_1 \rightarrow {}^2\Sigma^+)$ probabilities. Perhaps it suggests that the "active" electron transition probabilities are nearer the complete calculations for OH and SH than for BeH and MgH--a conclusion opposite to expectations based on other, qualitative considerations.

71

The gross changes in the charge distributions of OH and SH caused by the loss or gain of an electron are given in Table III. The valence charge density becomes increasingly diffuse through both series $OH^+ \rightarrow OH^-$ and $SH^+ \rightarrow SH^-$ with an accompanying increase in the amount of charge density in the region of the proton. The removal of an electron from OH or SH causes an overall tightening of the charge distribution and a shift in the values of the nonbonded radii towards values characteristic of HF ($r_F = 2.7$, $r_H = 1.9$) or HCl ($r_{Cl} = 3.3$, $r_H = 2.0$) respectively. Similarly, the addition of an electron to OH or SH results in an expansion of the charge distribution and in sets of nonbonded radii close in value to those for the preceeding neutral hydride NH ($r_N = 3.2$, $r_H = 2.1$) or PH ($r_P = 3.8$, $r_H = 2.3$). The _changes_ in the nonbonded charges in OH or SH upon ionization or electron attachment also reflect a shift in the properties of the charge distribution towards those characteristic of HF and HC or NH and PH respectively. For example, the increase in the nonbonded charge on O (+0.34 compared to O^+) and its decrease for H (0.26) in OH^+ indicates the presence of a greater degree of charge polarization than is found in HF where the corresponding changes are +0.22 and -0.20 respectively. Thus the neutral systems OH and SH become more or less polar as the number of electrons is decreased or increased respectively.

This shift in bonding character away from the neutral parent toward HF and HCl for the positive ion and towards NH and PH for the negative ions is evidenced most clearly in a comparison of the bond density maps. These maps show only the charge reorganization on bond formation and are free of the complicating feature of different numbers of electrons for the systems to be compared. While the general pattern of charge reorganization depicted in the $\Delta\rho_{SA}$ maps for NH, OH and HF are all similar, the extent of charge transfer and

72

the degree of contraction of the charge increase towards the A nucleus in OH^+ is much more pronounced than in OH and instead is very similar to that found in HF. In fact, the $\Delta\rho_{SA}$ map for OH^+ indicates (as do the data in Table I) a greater transfer of charge from the proton than is found in HF. The SH^+ and $HC\ell$ pair of $\Delta\rho_{SA}$ maps are nearly identical in all respects. Similarly, the character of the $\Delta\rho_{SA}$ maps for OH^- and SH^- is shifted away from that for the neutral parent species towards that found for the NH and PH molecules.

The manner in which the electron charge distribution or chemical binding changes when the system is ionized or attaches an electron is succintly summarized for OH and SH in the lower four $\Delta\rho_{\Lambda,\Lambda'}(x,y)$ maps of Fig. 6. The OH ionization map especially reveals the loss of a π-electron and the contraction of sigma charge density to counterbalance the loss of shielding of internuclear repulsion. The SH ionization map shows similar but less pronounced features and more asymmetry. [Apparently the OH^+ and SH^+ ions have dissociation energies greater than the ground states of OH and SH.] In both OH and SH charge is removed also from around the proton and this is an indirect, or reorganizational, effect as the π-density at the proton is insignificant.

The $\Delta\rho_{\Lambda,\Lambda'}(x,y)$ maps for the electron attachment process show in detail the enlargement of the distribution perpendicular to the axis at the expense of regions along the axis. The sigma-like charge density gives an accumulation at the proton and a deficit in the dumb-bell region around the A nucleus and along the molecular axis. Indeed, if one instead considers the sequence $OH^- \rightarrow OH \rightarrow OH^+$ (or $SH^- \rightarrow SH \rightarrow SH^+$) and presents the $\Delta\rho_{\Lambda,\Lambda'}(x,y)$ maps for the first electron detachment, which would reverse the regions of accumulation and deficit given here, a rather smooth process would be observed. In this two-

73

step process charge is progressively lost from off the molecular axis
(π-density) and accumulated along the axis as the sigma orbitals progressively
must shield more nuclear charge to keep the nuclei together or form a stable
molecule.

The ionization and electron attachment can also be discussed in terms of
an "active" electron approximation. In this case the $\Delta\rho_{\Lambda,\Lambda'}(x,y)$ maps would
simply be the 1π (or 2π) orbital of the parent neutral system (Fig. 8 of paper
II and Fig. 4 of paper IV). The reorganization of non-active orbitals, however,
seems to dominate as the comparison of the $w\pi$ orbital density with the
$\Delta\rho_{\Lambda,\Lambda'}(x,y)$ maps in Fig. 5 shows. An $w\pi$ orbital <u>can</u> be traced out on the
$\Delta\rho_{\Lambda,\Lambda'}$ map and does account for some major features of the molecular axis
around the A nucleus, but the important reaction-reorganization localized along
the molecular axis is completely neglected for AH^+ and AH^- molecular-ions.

There is in these excitations, ionizations, and electron attachments
rather substantial feedback effects in the "core" polarizations of the $SH(A^2\Sigma^+)$,
SH^+ and SH^- systems. [Such changes are less pronounced in the OH systems.]
These details are best appreciated in the more quantitative perspective to
follow.

The quantitative aspects of the binding changes considered here for the
OH and SH systems are summarized in Tables IV and V. For OH all partial forces
are for the appropriate R_e value. For SH all are for the same R value except
$SH(A^2\Sigma^+)$ is at R_e(exp.). The changes in binding associated with ionization
and electron attachment will be considered first due to the more straightforward
nature of the changes relative to the neutral parent molecule. The graduated
changes in the chemical binding for the sequence AH^+; AH; AH^-, i.e.,
$...z\sigma^2 w\pi^2; ...z\sigma^2 w\pi^3; ...z\sigma^2 w\pi^4$, will be of prime concern. For this purpose

Fig.78 gives a useful sketch of the changes in the partial forces, or the effective charges, and summarizes the counterbalancing trends as electrons are successively added to the system. One may note first that as electrons are added to the 1π orbital the partial force, or effective charge, of the K-shell "core" of the OH sequence drops sharply and becomes slightly less forward polarized and less <u>binding</u> with respect to the oxygen nucleus. The KL "core" in the SH sequence exerts a small binding force on the sulphur nucleus which changes only very slightly through the sequence. The cores in these cases screen either 2 (for the OH sequence) or 10 (for the SH sequence) nuclear charges from the proton and there is almost negligible change in this efficient screening across the AH^+;AH;AH^- sequence. Briefly then, the only changes in the core behavior as electrons are added to the π orbital is a slightly decreased forward polarization of the charge around the oxygen nucleus in the OH sequences $OH^+ \rightarrow OH \rightarrow OH^-$.

The upper three diagrams in Fig.76 reveal the smooth variation of the $f_{2\sigma,A}$, $f_{3\sigma,A}$, and $f_{1\pi,A}$ (or the second-row congeners $f_{4\sigma,A}$, $f_{5\sigma,A}$, and $f_{2\pi,A}$) values as electrons are added to the $w\pi$ orbital. The internal changes, i.e., within the OH- or SH- sequence, are almost the same in the two sequences although the absolute scales differ. The $2\sigma^2$ (or $4\sigma^2$) charge density is strongly binding for the A nucleus and the strength of this binding ability <u>decreases</u> monatonically as electrons are added to the $w\pi$ shell of OH^+ or SH^+ (a decrease of some $\sim 10\%$ from OH^+ to OH^- and $\sim 8\%$ from SH^+ to SH^-). However, as the $2\sigma^2$ (or $4\sigma^2$) charge density binds the A nucleus less, the $3\sigma^2$ (or $5\sigma^2$), which is strongly antibinding towards the A nucleus, becomes less antibinding, largely cancelling the decreased ability of the $2\sigma^2$ (or $4\sigma^2$) density to bind the A nucleus into the molecule. Thus the net contribution of the $2\sigma^2$ plus

75

$3\sigma^2$ (or $4\sigma^2$ plus $5\sigma^2$) charge densities to the total force on the A nucleus goes $OH^+(0.965 - 0.384 = +0.581)$; $OH(0.905 - 0.347 = +0.558)$; $OH^-(0.862 - 0.305 = +0.557)$ and $SH^+(1.088 - 0.478 = +0.610)$; $SH(1.034 - 0.435 = +0.599)$; $SH^-(0.999 - 0.397 = +0.602)$. Briefly then, these two orbital charge densities acting as a unit bind the A nucleus about the same for both sequences. [This is not to say that the $3\sigma^2$ (or $5\sigma^2$) density is binding, it remains strongly antibinding.] In terms of the atomic, overlap, and screening contribution (Table III) one may describe these trends in more detail. Thus for the $2\sigma^2$ orbital density in the $OH^+ \rightarrow OH \rightarrow OH^-$ sequence, the decreased binding of the A nucleus arises from a sharply decreasing atomic contribution only partially offset by a gradually increasing overlap contribution. As π-electrons are added the locl of the $2\sigma^2$ charge density is moving towards the proton and off of the oxygen nucleus. The large antibinding character of the $3\sigma^2$ charge density is due to a large, negative atomic contribution. In the sequence $OH^+ \rightarrow OH \rightarrow OH^-$, this large negative contribution of the $3\sigma^2$ orbital _increases_, but this increase is overcome by the increases in the positive overlap and screening contributions. The electrons in the $w\pi^n$ density increase their binding of the A nucleus almost strictly additively ($2,3,4$ $w\pi$ electrons) and this _increase_ has a significant overlap contribution although most of the binding arises from the atomic contribution.

The lower three diagrams of Fig.76 indicate a more substantial change in the binding of the proton in the OH- and SH-sequences. There is still a balancing effect, but in the case of the proton the binding ability of the $2\sigma^2$ and $3\sigma^2$ (or $4\sigma^2$ and $5\sigma^2$) density _both_ decrease sharply in the sequence $AH^+ \rightarrow AH \rightarrow AH^-$. The binding of the $2\sigma^2$ (or $4\sigma^2$) charge density, i.e., $f_{2\sigma,H}(R_e)$ versus $f_{2\sigma,H}(R \rightarrow \infty) = 2$, is substantial for the proton and is composed

76

largely of a screening part. Across the sequence, however, the screening contribution decreases more rapidly than the overlap contribution increases, so that a net decrease in binding of the proton occurs in the OH and SH sequence. This is exactly the situation also in the binding of the proton by the $3\sigma^2$ (or $5\sigma^2$) charge density--the orbital charge density becomes less localized on the A nucleus, screening decreases, and overlap contributions increase. The decrease in the sigma binding of the proton is accompanied by a $\sim 50\%$ increase in the screening of the nuclear charge on A from the proton as the $w\pi$ density is increased 100%. The $w\pi^m$ density remains antibinding for the proton through the sequence and even four $w\pi$ electrons do not shield three nuclear charges. Obviously the shielding increases as more electrons are added, and this increase is nearly additive, but the diagram in Fig.76 does not suggest that the $w\pi$-density becomes binding although it does become less antibinding for the proton.

In summary, we may conclude that as electrons are added to the $w\pi$ orbital in the OH and SH sequences $AH^+;AH;AH^-$ the chemical bond becomes progressively weaker and the two separated atoms become a more attractive alternative. The smoothly varying trends above indicate that the binding situation depends less directly on the particular state symmetry than on the net charge of the system in conjunction with the kind and number of occupied valence-shell molecular orbitals. In particular the above indicates that as electrons are added to OH^+ the key valence molecular orbitals become less binding with the $2\sigma^2$ (or $4\sigma^2$) density less able to play a dominant role in strongly binding both nuclei. The antibinding elements decrease in effectiveness, but at a slower pace. The result is a weaker chemical bond in the order $AH^+;AH;AH^-$.

The excitation process $X^2\Pi_i$ - $A^2\Sigma^+$ can be analyzed in terms of the "active" electron perspective with reorganization effects or non-active electron contributions considered later. The active electron approximation here would require strictly applied, that $\frac{1}{2}f_{3\sigma,A} = \frac{1}{4}f_{1\pi',A}$ or $\frac{1}{2}f_{5\sigma,A} = \frac{1}{4}f_{2\pi',A}$ and also $\frac{1}{2}f_{3\sigma,H} = \frac{1}{4}f_{1\pi',H}$ or $\frac{1}{2}f_{5\sigma,H} = \frac{1}{4}f_{2\pi',A}$ where the fractions arise since $f_{i,A}$ is defined with the occupation number, N_i, contained and we require <u>no</u> change in force with the electron jump $3\sigma \rightarrow 1\pi'$ (or $5\sigma \rightarrow 2\pi'$). A more reasonable requirement, which is the only one considered here, is to consider the degree to which the sum of the partial forces of the $z\sigma$ and $w\pi$ orbitals is conserved in the transition. The sum of the partial forces acting on the proton are very nearly conserved and change (as $^2\Pi_i \rightarrow {}^2\Sigma^+$) from 3.765 to 3.854 in OH and from 3.619 to 3.528 in SH. Expectedly, the electrons in nonactive orbitals exert partial forces on the proton that are also changed very little (see Tables IV and V). The data in Tables IV and V also indicate that the binding of the proton <u>per</u> $z\sigma$-electron and the antibinding of the proton <u>per</u> $w\sigma$-electron are also approximately conserved.

The active electron view fails badly to characterize the situation at the A nucleus, however, as the sum of the $z\sigma$ and $w\pi$ partial forces change from -0.120 → -0.012 for OH and from -0.304 → +0.259 for SH. There is not even an approximate conservation of the partial forces in this excitation as regards the A nucleus and one expects changes also in the non-active orbital electrons. For example, in the transition $X^2\Pi_i$ - $A^2\Sigma^+$ the core polarization, and forces on the A nucleus from the core, almost completely vanish.

In summary, the $z\sigma$-$w\pi'$ excitation in OH and SH demonstrates a simple additive effect with regard to binding properties of the $w\pi$ density as one more electron is added (binding the A nucleus and antibinding the proton by 1/3

more). The "core" polarization of the ground state largely vanishes upon excitation and the effects of the "core" on both nuclei closely parallels that for the free atoms. The $y\sigma^2$ charge density binds the proton almost the same in ground and excited states, but the $4\sigma^2$ density in SH is considerably less binding for the S nucleus in the excited state. The $z\sigma$-$w\pi'$ excitation strengthens the antibinding character of the 3σ density, per electron, for the O nucleus but additively decreases the binding of the proton. In contrast the 5σ density is now non-bonding for the S nucleus. The excitation serves to weaken key characteristics serving to hold the nuclei together, the emergence of the SH 5σ density in a non-bonding role emphasizes this, so that the nuclear binding force is neutralized in the excited state in a means closer to the separated atoms than in the ground state.

IV General Conclusions

These studies support the established evidence that very substantial changes in the electronic charge distribution, and chemical binding, may accompany electronic excitation. The repertory oi this study restricts the generality of any tentative conclusions, but further unpublished results are consistent with the discussions in Section III. The example of a type III) electronic excitation (see part I) shows how "ionic" BeH and MgH really are although this characteristic of the charge density of the molecule was effectively masked by the $z\sigma$ electron which is largely an atomic relic of A and strongly antibinding. Doubtlessly, other such systems or cases arise in which such a sharp apparent change in the bonding character is likely upon electronic excitation. The OH and SH excitation demonstrates no less absolute rearrangement or changes upon an internal shift of electronic populations among

79

already occupied orbitals. However, in this type iv) electronic excitation, a precipitate change in bonding type, and indeed many physical properties, is less likely to occur since only a change in degree of already present influences is implied.

The electronic charge distribution changes only very slightly upon metastable excitations involving states arising from π_g^2 (and perhaps also π_u^2) configurations. Apparently, then if RHF predictions are reliable, all bonding, reactive, or property distinctions must be associated with differences in the spin densities of the systems. Indeed, although it is predicted[22] that the electric quadrupole moments of $O_2(X^3\Sigma_g^-, a^1\Delta_g,$ and $b^1\Sigma_g^+)$ are very similar it is possible to define electric spin quadrupole moments, Q^α and Q^β, which should vary much more within these systems (and especially for wavefunctions, beyond RHF), but is not easily determined or inferred experimentally. These basic ideas are being pursued further.

The evidence here for the $O_2^{+2}; O_2^+; O_2(X^3\Sigma_g^-); O_2^-$ and $AH^+; AH; AH^-$ systems implies that the electronic charge distributions behave very regularly and in a closely additive fashion as π-electrons are added. The graduated change in the binding or antibinding characteristics of each molecular orbital is apparent. One expects then that their bonding properties and physical properties are similarly graduated.

ACKNOWLEDGEMENT

References and Footnotes

[*]Present address: Department of Chemistry, University of Massachusetts, Amherst, Massachusetts 01002.

1. R. S. Mulliken, In Quantum Theory of Atoms, Molecules, Solid State (Academic Press, Inc., New York, 1966), Edited by P.-O. Löwdin, p. 231, with extensive early references on p. 241.

2. A. C. Hurley, In Molecular Orbitals in Chemistry, Physics and Biology (Academic Press, Inc., New York, 1964), Edited by P.-O. Löwdin and B. Pullman, p. 161 ff.

3. R. P. Wayne, In Advances in Photochemistry (Interscience Publishers, New York, 1969), Edited by J. N. Pitts, Jr., et al, pp. 311-371, with extensive references.

4. International Conference on Singlet Molecular Oxygen and Its Role In Environmental Sciences, New York Academy of Sciences, October 23-25, 1969; M. Kasha and A. U. Khan, "The Physics, Chemistry, and Biology of Singlet Molecular Oxygen". (Proceedings to be published.)

5. M. P. Bogaard and B. J. Orr, Mol. Phys. 14, 557 (1968) -- But no experimental attempts have been published.

6. A. D. Buckingham, J. Chem. Phys. 30, 1580 (1959); A. D. Buckingham and R. L. Disch, Proc. Royal Soc. A273, 275 (1963); A. D. Buckingham, R. L. Disch, and D. A. Dunmur, J. Am. Chem. Soc. 90, 3104 (1968).

7. N. F. Ramsey, Molecular Beams (Oxford University Press, Osford, England, 1956), Chapter VIII.

8. J. R. P. Angel, P. G. H. Sanders, and G. K. Woodgate, J. Chem. Phys. 47, 1552 (1967) - First direct measurement of Q for an atom.

9. R. S. Freund and W. Klemperer, J. Chem. Phys. 43, 2422 (1965).

10. R. Thomson and F. W. Dalby, Can. J. Phys. $\underline{46}$, 2815 (1968). These authors also give the change $BH(X^1\Sigma^+, \mu = 1.27\ D) \rightarrow BH(A^1\Pi_r, \mu = 0.58\ D)$.

11. Ch. Jungen and H. Lefebvre-Brion, J. Mol. Spectros. $\underline{33}$, 520 (1970). A value of $+0.79 \times 10^{-26}$ esu cm^2 is given for $NO^+(X^1\Sigma^+)$. This procedure is also applicable for Rydberg series converging on an excited state of the ion "core".

12. W. H. Flygare, Record Chem. Prog. $\underline{28}$, 63 (1967).

13. K. Innes (private communication to P.E.C.).

14. B. Turman, J. Ingram and H. P. Hansen, Proceedings of the Second Austin Symposium on Gas Phase Molecular Structure (unpublished); for N_2^+ molecular-ion. See also E. M. A. Peixoto, Phys. Rev. $\underline{177}$, 204 (1969). Also R. A. Bonham (private communication to P.E.C.).

15. C. A. Coulson, in Reactivity of the Photoexcited Organic Molecule (Interscience Publishers, New York, 1967), 13th Solvay Conference on Chemistry, October, 1965, pp. 1-49.

16. (a) R. F. W. Bader, W. H. Henneker and P. E. Cade, J. Chem. Phys. $\underline{46}$, 3341 (1967) (I);

    (b) R. F. W. Bader, I. Keaveny and P. E. Cade, ibid $\underline{47}$, 3381 (1967) (II);

    (c) R. F. W. Bader and A. D. Bandrauk, ibid $\underline{49}$, 1653 (1968) (III); and

    (d) P. E. Cade, R. F. W. Bader, W. H. Henneker and I. Keaveny, ibid $\underline{50}$, 5313 (1969) (IV).

17. P. E. Cade and W. Huo, J. Chem. Phys. $\underline{47}$, 634 (1967).

18. If would be desirable to consider an excitation from and to a specific vibrational state instead of merely from R_e(exp.) for the ground state to the same R value for the excited state. Such a study is underway to introduce vibrational states explicitly and therefore more closely

approach the actual physical situation, but it will not be considered here.

19. R. F. W. Bader and A. D. Bandrauk, J. Chem. Phys. $\underline{49}$, 1666 (1968).

20. R. F. W. Bader and J. L. Ginsburg, Can. J. Chem. $\underline{47}$, 3061 (1969).

21. These are the spin and symmetry equivalence restrictions discussed, for example, by R. K. Nesbet, Proc. Royal Soc. A$\underline{230}$, 312 (1955).

22. P. E. Cade and G. Malli, unpublished calculations of O_2 and $O_2^{\pm}$ systems.

23. D. R. Bates and T. R. Carson, Proc. Phys. Soc. (London), __, 1199 (1956) and A. C. Hurley et al, J. Chem. Phys. $\underline{34}$, 1919 (1961); J. Mol. Spectros. $\underline{9}$, 18 (1962) have indicated how the potential curve of O_2^{++} might behave. There is a long-range repulsive part of coulombic origin which is sharply reserved at smaller R values. The large attractive force for O_2^{++} here may correspond to a point on the steep down side of the potential curve but well inside the hump in $E(R)$.

24. Careful studies of the $^2\Sigma^+$ - $^2\Pi_r$ transition probabilities have been carried out by W. H. Henneker and H. E. Popkie (to be published).

25. The $^2\Sigma^+$ states dissociate into ^1D states of O and S. The molecular electronic configuration are most closely approximated by the $M_L = 0$ component $(np\sigma^{2/3}np\pi^{1)/3})$ of the ^1D states and this component is used in the construction of the $\Delta\rho_{SA}$ maps. The $\Delta\rho_{SA}$ maps for the ground states employ the configurations $np\sigma^1np\pi^3$ corresponding to the $M_L = \pm 1$ components of the ^3P states of O and S. The differences between the $\Delta\rho_{SA}$ maps for the $^2\Pi_i$ and $^2\Sigma^+$ states noted in the following discussion would all be enhanced if both $\Delta\rho_{SA}$ maps were referred to either of the above configurations as a common atomic component.

83

TABLE I

PROPERTIES OF THE TOTAL CHARGE DISTRIBUTIONS

A2, AH or AB	State	R_e	L	W	nonbonded radius r_A	r_B	nonbonded charge on A	on B
	$X^3\Sigma_g^-$	2.282	7.9	5.9	2.83		4.14	
O_2	$a^1\Delta_g$	2.297	7.9	5.9	2.82		4.14	
	$b^1\Sigma_g^+$	2.318	7.9	5.9	2.82		4.14	
O_2^-	$X^2\Pi_g$	2.4	8.4	6.4	2.98		4.49	
O_2^+	$X^2\Pi_g$	2.122	7.5	5.5	2.69		3.81	
O_2^{++}	$^1\Sigma_g^+$	(2.282)	7.6		2.64		3.47	
BeH	$X^2\Sigma^+$	2.538	9.2	6.4	4.1	2.5	1.96	0.66
	$A^2\Pi_r$	2.519	6.4	7.5	1.4	2.4	1.69	0.62
BeH$^+$	$X^1\Sigma^+$	2.497	6.1	5.9	1.4	2.3	1.41	0.51
MgH	$X^2\Sigma^+$	3.271	10.5	7.0	4.5	2.7	5.93	0.72
	$A^2\Pi_r$	3.173	8.2	8.1	2.3	2.6	5.65	0.68
MgH$^+$	$X^1\Sigma^+$	3.116					5.15	0.58

84

Table I (cont'd.)

A_2, AH or AB	State	R_e	L	W	nonbonded radius r_A	nonbonded radius r_B	nonbonded charge on A	nonbonded charge on B
OH	$X^2\Pi_i$	1.8342	6.7	6.0	2.9	1.9	4.22	0.37
	$A^2\Sigma^+$	1.912	6.2	6.3	2.2	1.7	4.12	0.25
OH$^+$	$X^3\Sigma^-$	1.944	6.4	5.3	2.8	1.6	3.79	0.22
OH$^-$	$X^1\Sigma^+$	1.781	7.1	7.0	3.1	2.2	4.66	0.54
SH	$X^2\Pi_i$	2.551	8.2	7.5	2.2	3.5	8.12	0.48
	$A^2\Sigma^+$	2.689	7.2	7.8	2.0	3.2	8.05	0.35
SH$^+$	$X^3\Sigma^-$	2.551	8.0	6.9	2.0	3.4	7.66	0.38
SH$^-$	$X^1\Sigma^+$	2.551	8.6	8.4	2.3	3.7	8.58	0.60

Table II. Comparative Partial Forces for O_2, O_2^*, O_2^+, and O_2^- Systems[a]

System MO	$O_2(X^3\Sigma_g^-)$	$O_2(a^1\Delta_g)$ (2.297 B.)	$O_2(b^1\Sigma_g^+)$ (2.318 B.)	$O_2^+(X^2\Pi_g)$ (2.122 B.)	$O_2^-(X^2\Pi_g)$ (2.400 B.)	$O_2^{++}(^1\Sigma_g^+)$
$1\sigma_g$	1.232	1.243 (1.244)	1.234 (1.237)	1.263 (1.244)	1.211 (1.220)	1.290
$2\sigma_g$	2.934	2.938 (2.934)	2.941 (2.931)	3.055 (3.056)	2.859 (2.810)	3.194
$3\sigma_g$	0.174	0.174 (0.178)	0.171 (0.180)	0.098 (0.082)	0.239 (0.277)	-0.006
$1\sigma_u$	1.138	1.144 (1.145)	1.145 (1.146)	1.146 (1.138)	1.134 (1.136)	1.154
$2\sigma_u$	-0.517	-0.511 (-0.511)	-0.512 (-0.512)	-0.504 (-0.492)	-0.515 (-0.513)	-0.345
$1\pi_u$	2.605	2.611 (2.611)	2.614 (2.616)	2.808 (2.785)	2.409 (2.407)	3.013
$1\pi_g$	0.426	0.413 (0.418)	0.411 (0.424)	0.245 (0.215)	0.501 (0.557)	
$\Sigma_i f_i$	7.992	8.012 (8.019)	8.005 (8.022)	8.111 (8.029)	7.838 (7.894)	8.299
Total net force (au)	0.0128	-0.0181 (-0.0294)	-0.0083 (-0.0323)	-0.1710 (-0.0508)	0.2487 (0.1467)	-0.4593

[a] All results outside parentheses are for $R = R_e$(exp.) for $O_2(X^3\Sigma_g^-) = 2.282$ Bohr. The values in parentheses are for R_e(exp.), or R_e(calc.) for O_2^-, as indicated in the column heading.

86

Table III. Comparative Partial Forces for BeH, BeH*, BeH⁺ and MgH, MgH*, MgH⁺ Systems[a]

System MO	$BeH(X^2\Sigma^+)$ R = 2.538 B.	$BeH(A^2\Pi_r)$ R = 2.519 B.	$BeH^+(X^1\Sigma^+)$ R = 2.479 B.	$MgH(X^2\Sigma^+)$ R = 3.271 B.	$MgH(A^2\Pi_r)$ R = 3.173 B.	$MgH^+(X^1\Sigma^+)$ R = 3.116 B.
Force on A						
1σ	-0.127	-0.520	-0.629	-0.064	-0.285	-0.276
2σ	1.625	1.505	1.542	-0.161	-0.523	-0.514
3σ	-0.513			0.124	0.423	0.413
4σ				1.960	1.831	1.878
5σ				-0.696		
1π		-0.055		-0.115	-0.103	-0.339
2π					-0.019	
Total	0.984	0.930	0.913	1.048	1.324	1.162
Net Force	0.0098	0.0440	0.0567	-0.0534	-0.3863	-0.2008
Force on H						
1σ	1.999	1.995	1.994	2.000	2.000	2.000
2σ	1.699	1.670	2.041	1.995	1.982	1.982
3σ	0.313			2.137	2.153	2.158
4σ				1.783	1.760	2.056
5σ				0.265		
1π		0.361		3.863	3.853	3.837
2π					0.277	
Total	4.012	4.027	4.035	12.043	12.026	12.032
Net Force	-0.0019	-0.0042	-0.0057	-0.0041	-0.0026	-0.0033

[a] All R values are R_e(exp.) for the system in question.

Table IV. Comparative Partial Forces for OH, OH⁺, OH* and OH⁻ Systems[a]

		OH($3\sigma^2 1\pi^3$)X²Π R_e = 1.8342 B.				OH($3\sigma 1\pi^4$)A²Σ⁺ R_e = 1.912 B.				OH⁺($3\sigma^2 1\pi^2$)X³Σ⁻ R_e = 1.944 B.				OH⁻($3\sigma^2 1\pi^4$)X¹Σ⁺ R_e = 1.781 B.			
	MO	Atomic	Overlap	Screening	Total	Atomic	Overlap	Screening	Total	Atomic	Overlap	Screening	Total	Atomic	Overlap	Screening	Total
Force on O	1σ	0.245	0.002	0.000	0.247	0.003	0.001	0.000	0.004	0.289	0.001	0.000	0.290	0.213	0.001	0.000	0.214
	2σ	0.581	0.292	0.031	0.904	0.676	0.310	0.034	1.020	0.704	0.238	0.022	0.965	0.481	0.339	0.043	0.862
	3σ	-1.430	0.915	0.169	-0.347	-0.889	0.487	0.105	-0.297	-1.285	0.784	0.117	-0.384	-1.473	0.959	0.209	-0.305
	1π	0.130	0.045	0.001	0.226	0.209	0.071	0.002	0.282	0.144	0.022	0.000	0.167	0.176	0.063	0.002	0.241
	Total	-0.425	1.254	0.202	1.031	-0.002	0.868	0.142	1.008	-0.148	1.046	0.139	1.037	-0.604	1.362	0.253	1.011
Total force on nucleus			-0.0731				-0.0186				-0.0782				-0.0289		
Force on H	1σ	0.000	0.000	2.000	2.001	0.000	0.000	2.000	2.000	0.000	0.000	2.001	2.001	0.000	0.000	2.000	2.001
	2σ	0.040	0.381	1.894	2.314	0.046	0.402	1.939	2.386	0.038	0.333	2.056	2.428	0.047	0.420	1.744	2.211
	3σ	0.068	0.472	1.141	1.681	0.044	0.252	0.556	0.852	0.084	0.553	1.452	2.089	0.066	0.377	0.939	1.382
	1π	0.001	0.044	2.039	2.084	0.001	0.068	2.733	2.802	0.000	0.022	1.534	1.557	0.001	0.058	2.354	2.413
	Total	0.109	0.897	7.074	8.080	0.091	0.723	7.228	8.041	0.123	0.908	7.043	8.074	0.114	0.857	7.037	8.008
Total force on nucleus			-0.0237				-0.0113				-0.0197				-0.0024		

[a]All results are for R_e(exp) of the system in question except OH⁻ which is given for R_e(calc).

Table V. Comparative Partial Forces for SH, SH*, SH$^+$ and SH$^-$ Systems[a]

MO \ State	SH($X^2\Pi_r$) R = 2.551 B.	SH($A^2\Sigma^+$) R = 2.689 B.	SH$^+$($X^3\Sigma^-$) R = 2.551 B.	SH$^-$($X^1\Sigma^+$) R = 2.551 B.
Force on S				
1σ	0.142	0.014	0.159	0.143
2σ	0.162	-0.006	0.170	0.150
3σ	-0.135	0.007	-0.146	-0.125
4σ	1.034	0.744	1.088	0.999
5σ	-0.435	0.026	-0.478	-0.397
1π	0.013	-0.002	0.014	0.012
2π	0.131	0.233	0.103	0.148
Total	0.911	1.016	0.911	0.930
Net Force	0.218	-0.036	0.220	0.173
Core	0.1818	0.013	0.1945	0.1797
Force on H				
1σ	2.000	2.000	2.000	2.000
2σ	2.004	2.000	2.004	2.004
3σ	2.087	2.081	2.086	2.087
4σ	2.474	2.369	2.595	2.372
5σ	1.806	0.997	2.146	1.541
1π	3.911	3.920	3.911	3.911
2π	1.813	2.531	1.308	2.179
Total	16.094	15.898	16.050	16.094
Net Force	-0.0145	0.0141	-0.0078	-0.0144

[a]All results are for R_e(exp) of SH($X^2\Pi_i$) except for SH($A^2\Sigma^+$) which is at R_e(exp) for that system.

Figure Captions

Fig. 1 ; $\Delta\rho_{\lambda,\lambda'}(x,y)$ density difference maps for vertical excitation, ionization, and electron attachment for oxygen molecule.

Fig. 2 ; Partial forces, f_i, for the sequence O_2^{++}; O_2^+; O_2; O_2^- resulting from successive addition of $1\pi_g$ electrons.

Fig. 3 ; Total electron charge distribution and bonding, density maps for BeH and MgH($A^2\Pi_r$) excited state.

Fig. 4 ; $\Delta\rho_{\lambda,\lambda'}(x,y)$ density difference maps for vertical $A^2\Pi_r \leftarrow X^2\Sigma^+$ excitation in BeH and MgH. Left-hand-side employs total densities, Right-hand-side employs only "active" orbital density differences.

Fig. 5 ; Total electron charge distribution and bonding, density maps for OH and SH($A^2\Sigma^+$) excited state.

Fig. 6 ; $\Delta\rho_{\lambda,\lambda'}(x,y)$ density difference maps for vertical $A^2\Sigma^+ \leftarrow X^2\Pi_i$ excitation in OH and SH and ionization and electron attachment of OH and SH. Upper right two figures only involve "active" electron density differences.

Fig. 7 ; Partial forces, f_{iA} and f_{iH}, for the sequence AH^+; AH; AH^- resulting from successive addition of 1π electrons to OH^+ and SH^+.
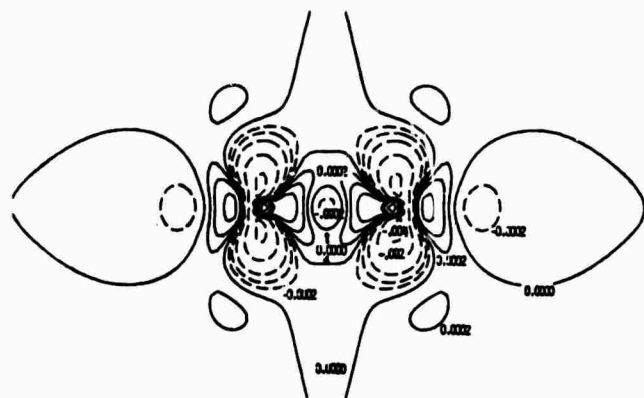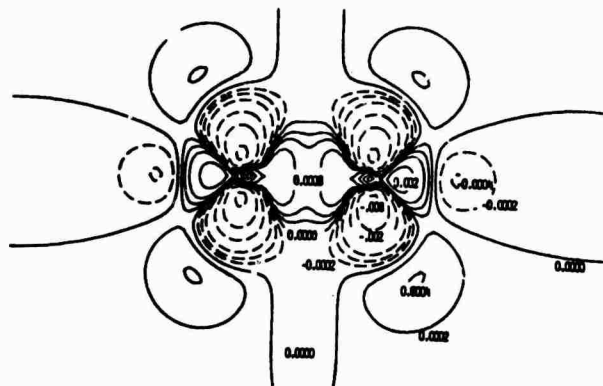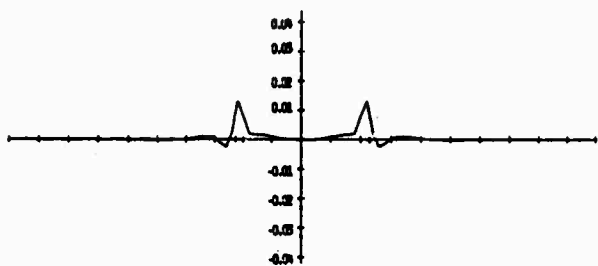
$\Delta\rho_m(x,y)$ O_2 $(^1\Delta_g - ^3\Sigma_g^-)$ $\Delta\rho_m(x,y)$ O_2 $(^1\Sigma_g^+ - ^3\Sigma_g^-)$
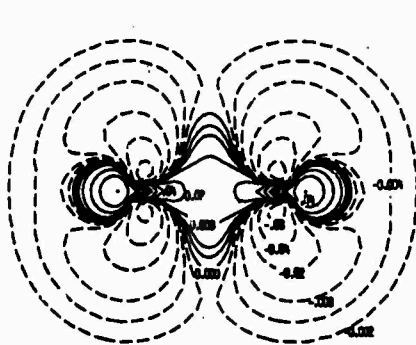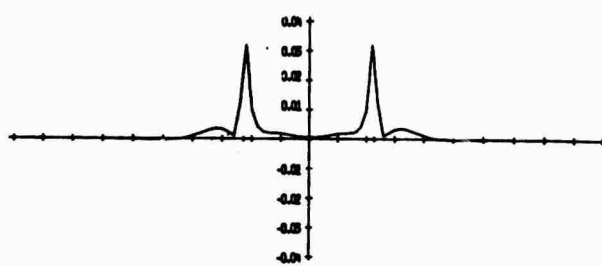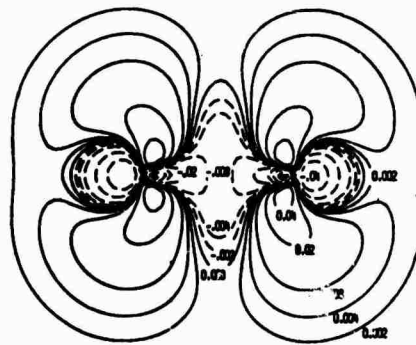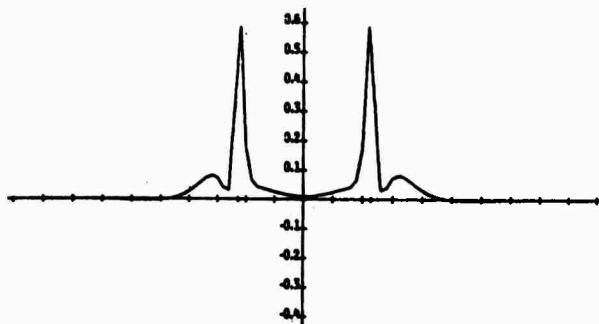
$\Delta\rho_m(x,y)$ O_2^+ $(^2\Pi_g)$ $-$ $O_2(^3\Sigma_g^-)$ $\Delta\rho_m(x,y)$ O_2^- $(^2\Pi_g)$ $-$ $O_2(^3\Sigma_g^-)$
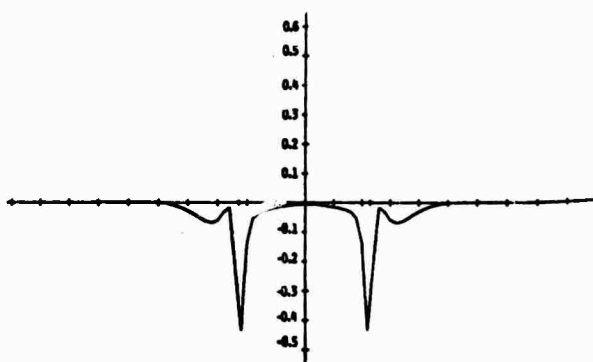
FIGURE 1

91

PARTIAL FORCES FOR VALENCE ORBITALS FOR THE
O_2^{++}; O_2^+; O_2; O_2^- SEQUENCE
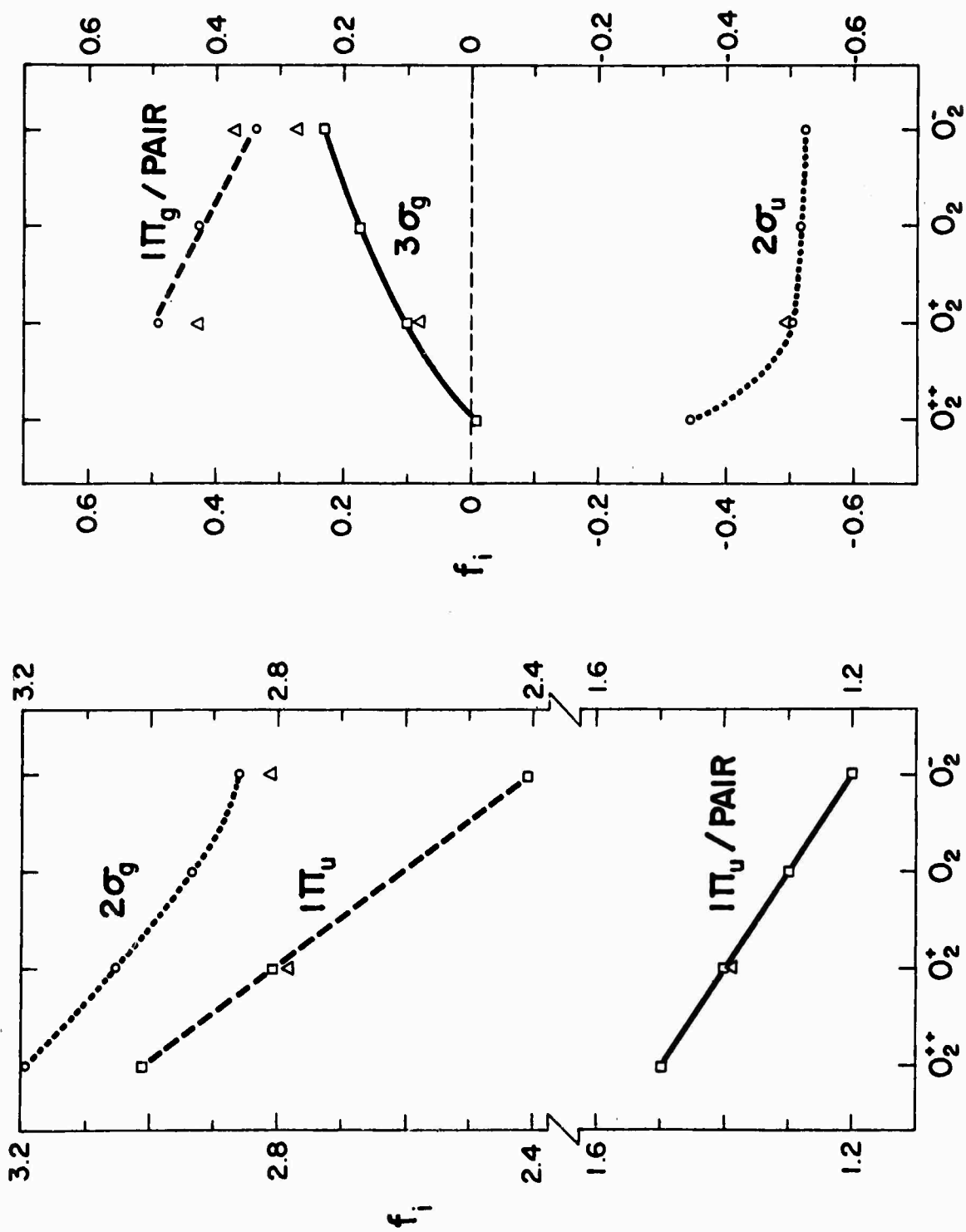
FIGURE 2
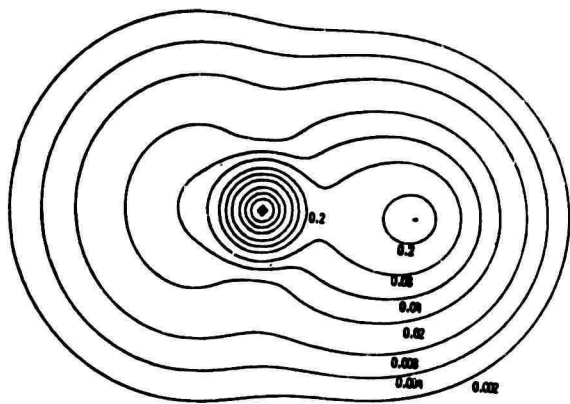
$\rho(x,y)$ BeH $^2\Sigma^+$
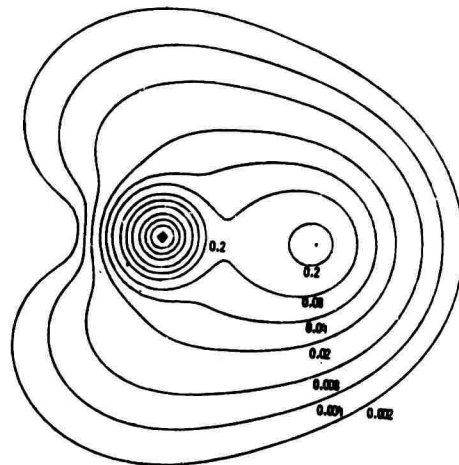
$\rho(x,y)$ BeH $^2\Pi_r$
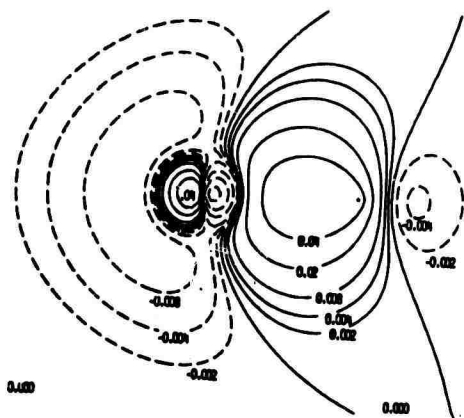
$\Delta\rho_{oo}(x,y)$ BeH $^2\Pi_r$
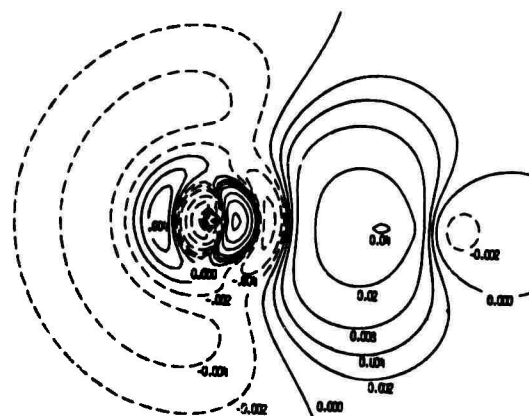
$\Delta\rho_{oo}(x,y)$ MgH $^2\Pi_r$
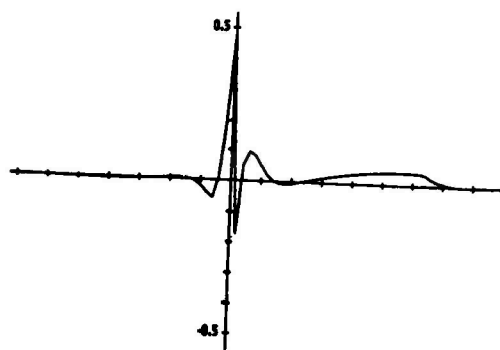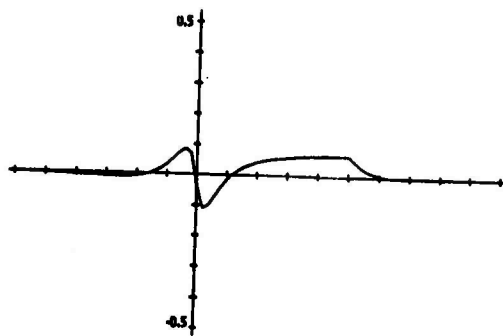
FIGURE 3

FIGURE 4

$\rho(x,y)$ OH $^2\Sigma^+$

$\rho(x,y)$ SH $^2\Sigma^+$

$\Delta\rho_{ee}(x,y)$ OH $^2\Sigma^+$

$\Delta\rho_{ee}(x,y)$ SH $^2\Sigma^+$

FIGURE 5

$\Delta \rho_\pi(x,y)$ OH $(^2\Sigma^+ - ^2\Pi_1)$

$\Delta \rho_{\pi.\sigma}(x,y)$ OH $(1\pi - 3\sigma)$

$\Delta \rho_\pi(x,y)$ SH $(^2\Sigma^+ - ^2\Pi_1)$

$\Delta \rho_{\pi.\sigma}(x,y)$ SH $(2\pi - 5\sigma)$

$\Delta \rho_\pi(x,y)$ OH$^+ (^3\Sigma^-) - $ OH $(^2\Pi_1)$

$\Delta \rho_\pi(x,y)$ OH$^- (^1\Sigma^+) - $ OH $(^2\Pi_1)$

$\Delta \rho_\pi(x,y)$ SH$^+ (^3\Sigma^-) - $ SH $(^2\Pi_1)$

$\Delta \rho_\pi(x,y)$ SH$^- (^1\Sigma^+) - $ SH $(^2\Pi_1)$
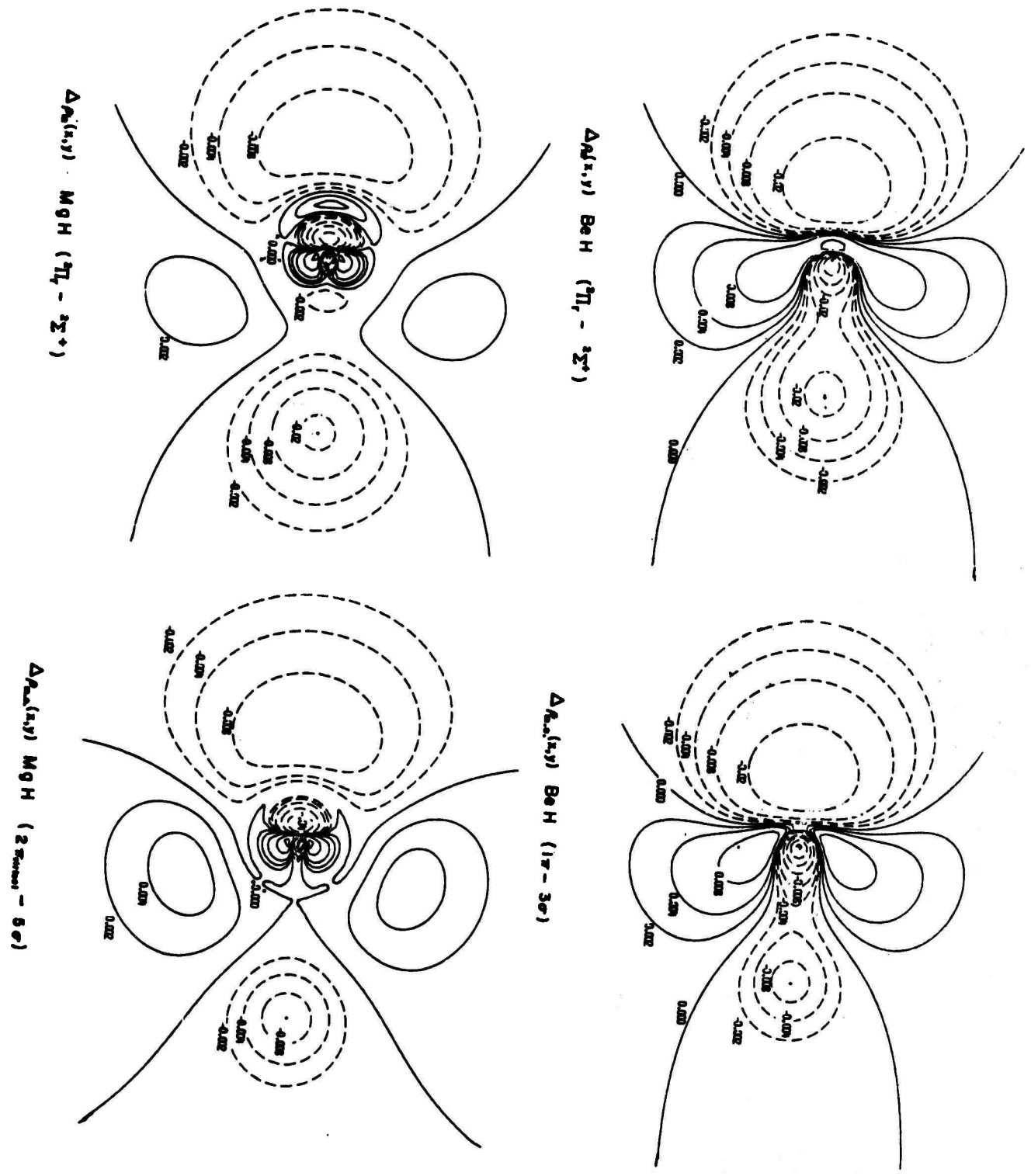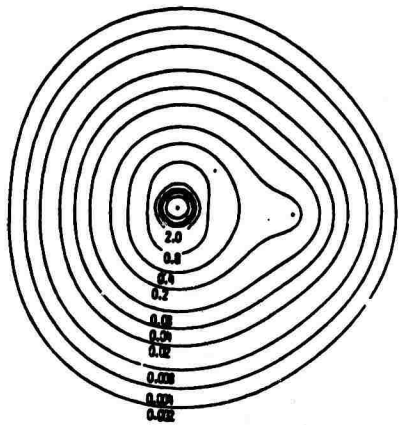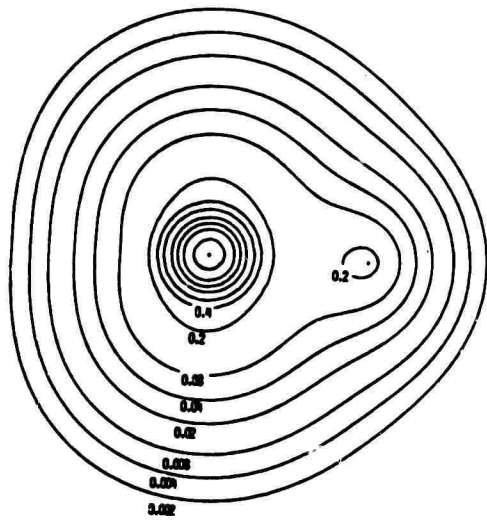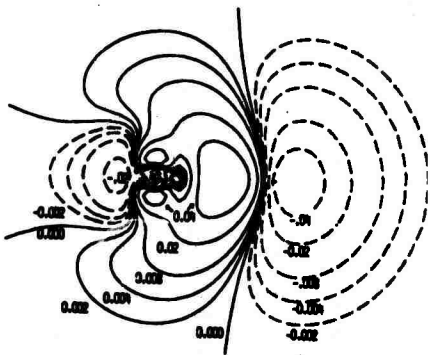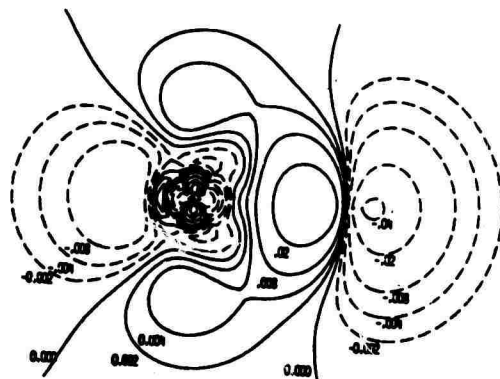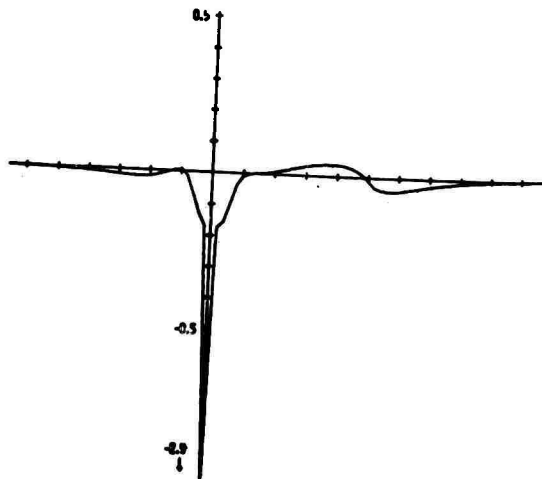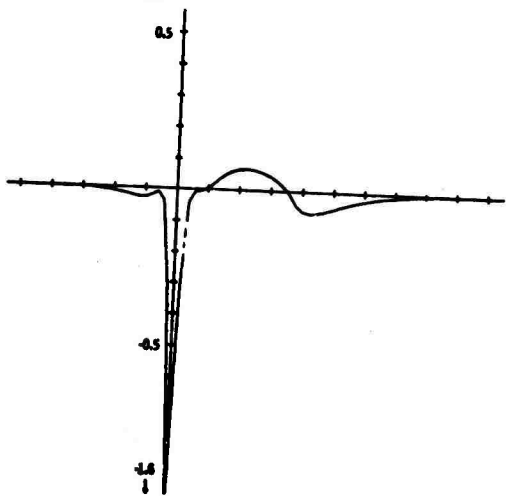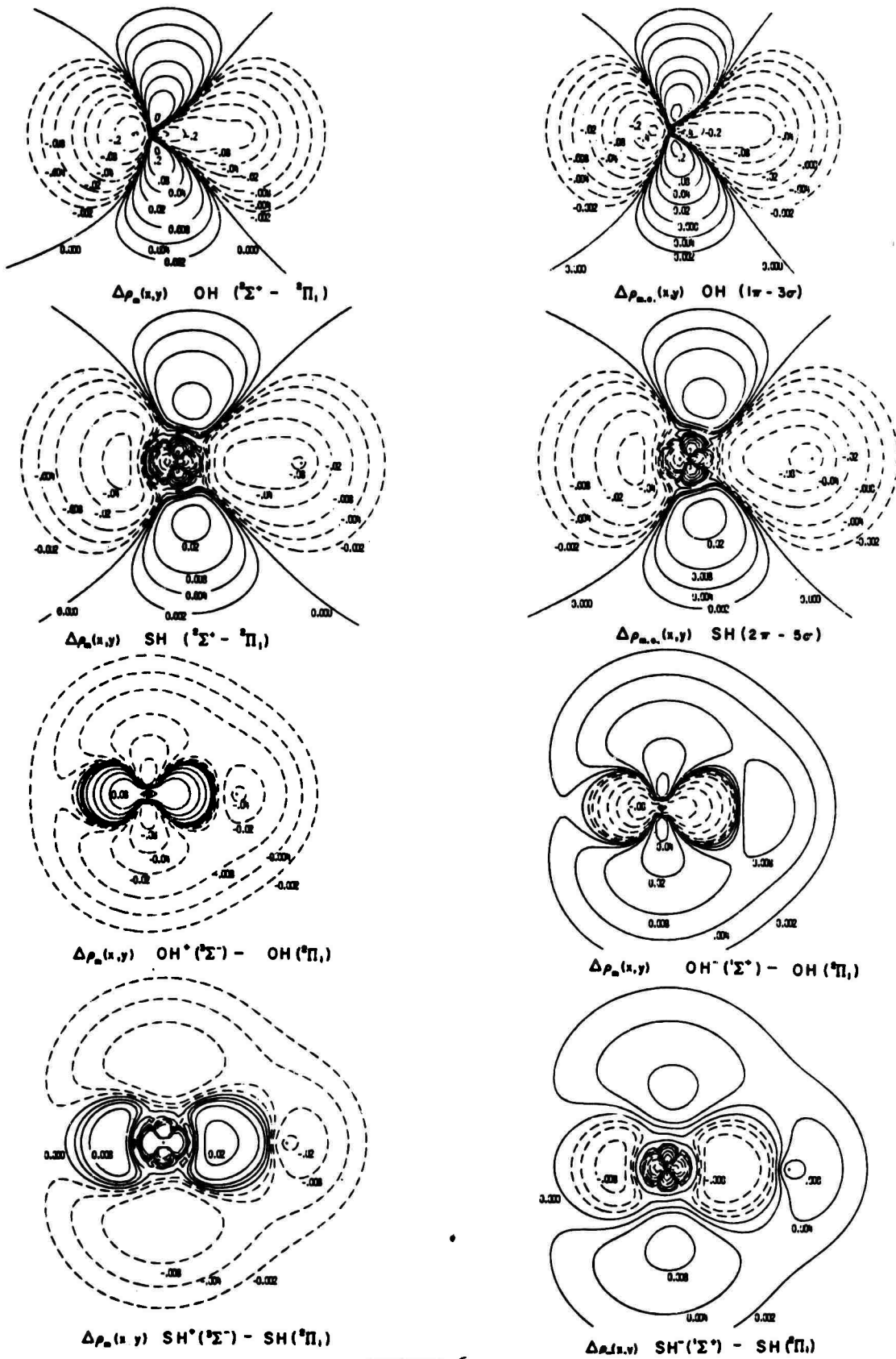
FIGURE 6

96

PARTIAL FORCES FOR VALENCE ORBITALS FOR THE OH⁺; OH; OH⁻ AND SH⁺; SH; SH⁻ SEQUENCES
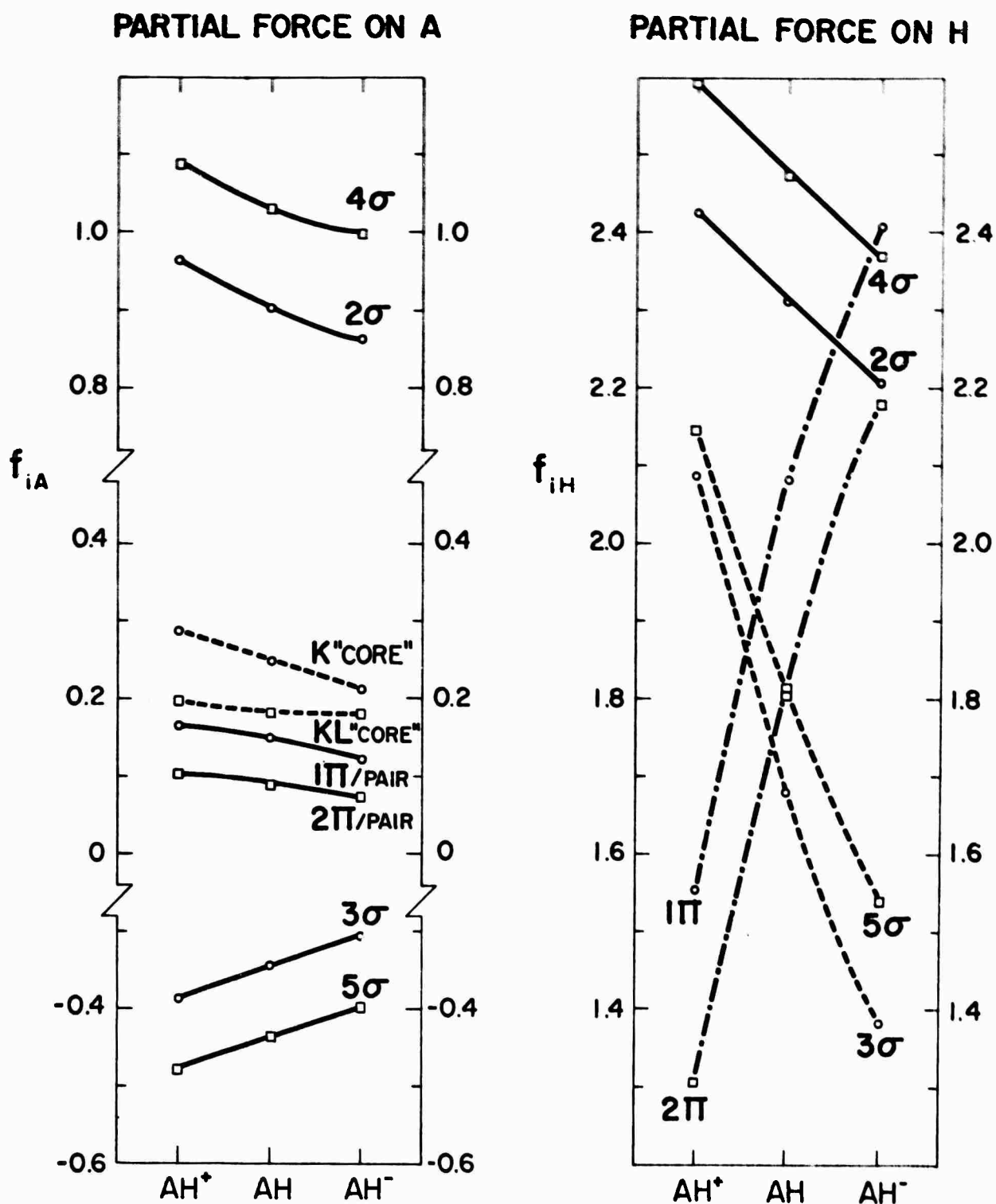
FIGURE 7

Theoretical Investigation of the Transition Probabilities in the Hydrogen Molecule*

L. WOLNIEWICZ†

Laboratory of Molecular Structure and Spectra, Department of Physics, University of Chicago, Chicago, Illinois 60637

The electronic transition moments for the $B-X$, $C-X$, and E, $F-B$ transitions in the hydrogen molecule are given for several internuclear separations, $R \leq 12$ a.u. The electronic transition moments are used for the computation of the transition moments for individual vibrational and rotational lines. The results show that, except for the Werner bands, the relative intensities cannot be accurately represented by the Franck–Condon factors. It is not possible to make a definite quantitative comparison of the present results with experiment due to a significant R dependence of the electronic moments. Qualitatively, the results agree well with experiment. However, they do not explain the fact that the lowest vibrational levels in the F state have not yet been observed.

I. INTRODUCTION

Although the electronic dipole transition probabilities in the hydrogen molecule are of considerable interest in molecular spectroscopy and also in astrophysics,[1] there are relatively few theoretical results concerning their numerical values. In addition the most complete results available at present[2] for the Lyman and Werner bands give little information about the dependence of the electronic transition moments on the internuclear distance R. Knowledge of the electronic transition moment over a wide range of R is essential for determining the relative intensities of the individual lines unless the transition moment is constant. However, the experimental results of Geiger and Topschowsky[3] show clearly that, for the Lyman bands at least, the moment changes quite appreciably with R. Therefore, one cannot expect the transition probabilities in hydrogen to be proportional to the Franck–Condon factors, and an accurate computation of the transition moments for the known Lyman $(B \, {}^1\Sigma_u{}^+ - X \, {}^1\Sigma_g{}^+)$ and Werner $(C \, {}^1\Pi_u - X \, {}^1\Sigma_g{}^+)$ bands seems desirable.

In the present work we investigate the two transitions mentioned above and also the transition from the first excited E, $F \, {}^1\Sigma_g{}^+$ state to the $B \, {}^1\Sigma_u{}^+$ state. The latter transition, studied experimentally by Dieke,[4] is of considerable interest since some lines predicted theoretically[5,6] have not yet been found experimentally.

II. COMPUTATIONAL DETAILS

The electronic wavefunctions employed in the present work are those obtained previously by Kolos and the present author.[6,7,8] Since all the functions are real, the electronic transition moment is given by[9]

$$M_{nm}{}^e = \left| e \int \Psi_n (r_1 + r_2) \Psi_m d\tau \right|, \qquad (1)$$

where r_1, r_2 are the coordinates of the two electrons in the molecule-fixed reference system, and Ψ_n, Ψ_m are the electronic wavefunctions of the corresponding states.

As is well known,[9] $M_{nm}{}^e$ can be equivalently expressed as

$$M_{nm}{}^e = \left| \frac{e}{\Delta E} \int \Psi_n (\nabla_1 + \nabla_2) \Psi_m d\tau \right|,$$

$$\Delta E = E_n(R) - E_m(R), \qquad (2)$$

and Eq. (2) is believed[10] to give more accurate results if variational wavefunctions are used. However, this is not necessarily the case if one uses the electronic wavefunctions from Refs. 6–9. Since the wavefunctions have the general form of a linear combination

$$\Psi_n = \sum_k c_k{}^n g_k(r_1, r_2), \qquad (3)$$

$M_{nm}{}^e$ is expressed as

$$M_{nm}{}^e = \sum_{k,l} c_k{}^n c_l{}^m D_{kl}, \qquad (4)$$

where D_{kl} are the appropriate matrix elements. The basis functions g_k in Eq. (3) are obviously not eigenfunctions of the Hamiltonian, and so Eqs. (1) and (2) lead to quite different matrix elements D_{kl}. In the present computations the matrix elements resulting

* This research was supported in part by the Advanced Research Projects Agency of the Department of Defense and was monitored by the U.S. Army Research Office—Durham, Box CM, Duke Station, Durham, N.C. 27706, under Contract DA-31-124-ARO-D-447, and in part by a grant from the National Science Foundation, GP-9284.

† Present and permanent address: Department of Theoretical Physics, Nicholas Copernicus University, Toruń, Poland.

[1] G. B. Field, W. B. Somerville, and K. Dressler, Ann. Rev. Astron. Astrophys. 4, 207 (1966).

[2] S. Rothenberg and E. R. Davidson, J. Mol. Spectry. 22, 1 (1967).

[3] J. Geiger and M. Topschowsky, Z. Naturforsch. 21a, 626 (1966).

[4] G. H. Dieke, Phys. Rev. 50, 797 (1936); 76, 50 (1949).

[5] E. R. Davidson, J. Chem. Phys. 33, 1577 (1960); 35, 1189 (1961).

[6] W. Kolos and L. Wolniewicz, "Theoretical Investigation of the Lowest Double-Minimum State E, F of the Hydrogen Molecule," J. Chem. Phys. (to be published).

[7] W. Kolos and L. Wolniewicz, J. Chem. Phys. 43, 2409 (1965).

[8] W. Kolos and L. Wolniewicz, J. Chem. Phys. 45, 509 (1966).

[9] See for instance R. W. Nicholls and A. L. Steward in *Atomic and Molecular Processes*, D. R. Bates, Ed. (Academic Press Inc., New York, 1962), p. 47.

[10] See for instance H. A. Bethe and E. E. Salpeter in *Handbuch der Physik*, S. Flügge, Ed. (Springer-Verlag, Berlin, 1957), Vol. 35/1, p. 338.

from the use of Eq. (2) were, in all tested cases, larger than those obtained from Eq. (1). This means that the final results obtained from Eq. (4) may suffer more from the cancellation of significant figures if Eq. (2) is used rather than Eq. (1). Therefore, it is difficult to decide if Eq. (2) is more reliable than Eq. (1). Since the dipole velocity operator requires significantly more computer time we decided to use Eq. (1) for the main computations. Equation (2) was employed only to test the accuracy of some numerical results. A comparison of the numerical values of $\Delta E M_{nm}$ obtained from Eq. (1) and from Eq. (2) is made in Table I, where R is the internuclear distance and ΔE is the difference of the corresponding variational energies from Refs. 6–8.

Though the agreement of numerical values obtained from Eqs. (1) and (2) is not a sufficient condition for the accuracy of the wavefunctions employed, the systematic agreement seen in Table I strongly suggests that the results presented in this paper do not differ much from the true values.

From the electronic transition moment M_{nm} one can obtain the line strength as[9]

$$S_{mv''j''\Lambda''}{}^{nv'j'\Lambda'} = S_{j''\Lambda''}{}^{j'\Lambda'} p_{v'v''}{}^{j'j''}, \qquad (5)$$

where $S_{j''\Lambda''}{}^{j'\Lambda'}$ is the Hönl–London factor, and $p_{v'v''}{}^{j'j''}$ is given by

$$p_{v'v''}{}^{j'j''} = \left| \int \chi_{v'j'}{}^{n} M_{nm} \chi_{v''j''}{}^{m} dR \right|^{2} \qquad (6)$$

with $\chi_{vj}{}^{n}$ being the vibrational wavefunction in the electronic state n. The primed and double primed quantum numbers have the usual meaning, i.e., they refer to the upper and lower states, respectively.

In cases where $p_{v'v''}{}^{j'j''}$ is practically independent of the rotational quantum numbers, $p_{v'v''}{}^{j'j''} \cong p_{v'v''}{}^{0,0}$, it represents the vibrational band strength.[9] However, for the hydrogen molecule the j dependence of $p_{v'v''}{}^{j'j''}$ is appreciable and was not neglected in the present work. Nevertheless, in this paper we will use the term band strength for $p_{v'v''}{}^{j'j''}$.

To evaluate the integral in Eq. (6) use has been made of the vibrational wavefunctions computed

TABLE I. Comparison of dipole velocity and dipole length transition moments (in atomic units).

R	$\Delta E M$		Diff in %	Transition
	Velocity	Length		
1.4	0.4604	0.4593	0.2	
5.0	0.3146	0.3136	0.3	$B\,{}^{1}\Sigma_{u}{}^{+}$–$X\,{}^{1}\Sigma_{g}{}^{+}$
9.0	0.1983	0.1972	0.6	
2.0	0.08253	0.08109	1.8	$E, F\,{}^{1}\Sigma_{g}{}^{+}$–$B\,{}^{1}\Sigma_{u}{}^{+}$
4.0	0.07084	0.07089	0.07	
10.0	0.3937	0.3936	0.03	$C\,{}^{1}\Pi_{u}$–$X\,{}^{1}\Sigma_{g}{}^{+}$

TABLE II. Electronic transition moments M, in atomic units.[a]

R	$B\,{}^{1}\Sigma_{u}{}^{+}$–$X\,{}^{1}\Sigma_{g}{}^{+}$	$E, F\,{}^{1}\Sigma_{g}{}^{+}$–$B\,{}^{1}\Sigma_{u}{}^{+}$	$C\,{}^{1}\Pi_{u}$–$X\,{}^{1}\Sigma_{g}{}^{+}$
0	0.4208	2.918	0.4208
1.	0.7625	2.905	0.6442
1.4	0.9799		
1.5		2.703	0.7648
1.6	1.094		
2.	1.312	2.401	0.8629
2.4		2.097	
2.5	1.519		0.9342
2.8		1.982	
3.0	1.607	2.063	0.9760
3.5	1.567	2.510	0.9919
4.	1.433	3.001	0.9932
4.5	1.256	3.494	0.9926
5.	1.085	3.949	0.9966
6.	0.8210	4.764	1.015
7.	0.6521	5.474	1.032
8.	0.5805	6.061	1.042
9.	0.5635	6.431	
10.	0.5937	6.428	1.048
12.		4.734	
∞	1.054	3.	1.054

[a] The results for $R = 0$ are from B. Schiff and C. L. Pekeris, Phys. Rev. 134, A638 (1964).

earlier[6,11,12] by Cooley's method. Since these functions are given at intervals of $\Delta R = 0.01$ a.u. and the electronic transition moments were computed for much fewer internuclear separations, a quadratic interpolation was made to yield M_{nm} at intervals of $\Delta R = 0.01$ and the integrations were performed by means of Simpson's rule.

The numerical computations were carried out on the 7094 IBM computer at the Computation Center of The University of Chicago. The band strengths $p_{v'v''}{}^{j'j''}$ were computed for the P and R branches ($j', j'' \leq 10$) in the three electronic transitions mentioned above. All computations were carried out for H_2, HD, and D_2 molecules. In the following we give some of the results obtained for H_2.

III. RESULTS AND DISCUSSION

The electronic transition moments computed for various internuclear distances from Eq. (1) are given in Table II. They are also shown graphically on Figs. 1 and 2. It is seen immediately from the figures that if one writes instead of Eq. (6)

$$p_{v'v''}{}^{j'j''} = M \cdot F_{v'v''}{}^{j'j''},$$

$$F_{v'v''}{}^{j'j''} = \left| \int \chi_{v'j'}{}^{n} \chi_{v''j''}{}^{m} dR \right|^{2}, \qquad (7)$$

M will depend both on the vibrational and rotational quantum numbers. Since in the interpretation of experimental data one must usually use the band strength in the form of the product (7), it is interesting to know the variation of M with the quantum numbers.

[11] W. Kolos and L. Wolniewicz, J. Chem Phys. 48, 3672 (1968).
[12] W. Kolos and L. Wolniewicz, J. Chem. Phys. 49, 404 (1968).
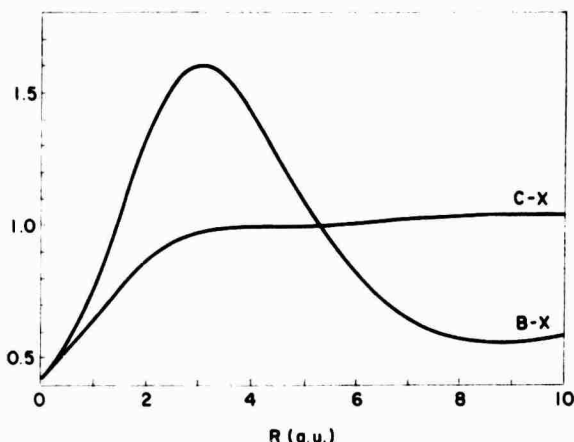
FIG. 1. Electronic transition moments, M_{nm}, for the Lyman $(B-X)$ and Werner $(C-X)$ bands.

This variation is shown in Fig. 3, where we give the ratio

$$M_{v'v''}{}^{j'j''} = p_{v'v''}{}^{j'j''}/F_{v'v''}{}^{j'j''} \qquad (8)$$

for some transitions in the Lyman bands. The notation in Fig. 3 is defined by Eq. (8), i.e., $M_{0,0}{}^{n,n+1}$, for instance, corresponds to the P branch of the 0–0 transition.

From Table II and from Refs. 6–8 one can readily get the electronic matrix elements of the dipole velocity operator, i.e.,

$$\Delta EM_{nm} \cong \int \Psi_n (\nabla_1 + \nabla_2) \Psi_m d\tau. \qquad (9)$$

The ΔEM_{nm} versus R curves are given in Fig. 4. It is seen that in the region important for transition probabilities, the matrix element for the Werner bands is practically constant. Therefore, as was already stated by Rothenberg and Davidson,[2] one may assume

$$(E_{v''j''} - E_{v'j'})^2 p_{v'v''}{}^{j'j''} = \text{const} \times F_{v'v''}{}^{j'j''}$$

for these bands without making an error of more than a few percent.

The present electronic transition moments can be compared for several internuclear separations with
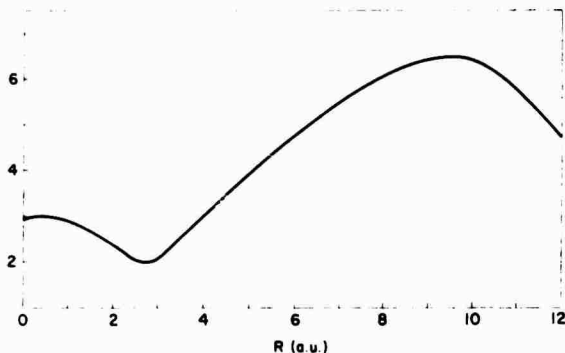
FIG. 2. Electronic transition moment, M_{nm}, for the E, $F-B$ transition.
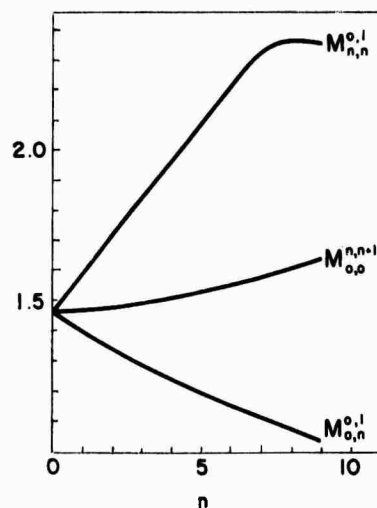
FIG. 3. The ratios of band strengths and Franck–Condon factors, defined by Eq. (8), for the $B-X$ transition.

the results of Ref. 2. If one uses for the comparison the results obtained in Ref. 2 from the dipole length formula, the agreement is very good. Our transition moments are slightly larger but the differences never exceed 2%.

The transition moments for the Lyman and Werner bands also agree qualitatively with the experimental results of Ref. 3. Unfortunately, due to the significant variation of the computed electronic transition moments with R, it does not seem possible to make a quantitative comparison with experiment.

Below we give some results of the computations of the band strength as given by Eq. (6). In Table III the results for the $v'-0$ Lyman bands are given. Similar results for the Werner bands are presented in Table IV.

Comparison of the present results with experiment is difficult. As we have mentioned above, due to the R dependence of the electronic transition moments, a comparison of experimental and theoretical electronic
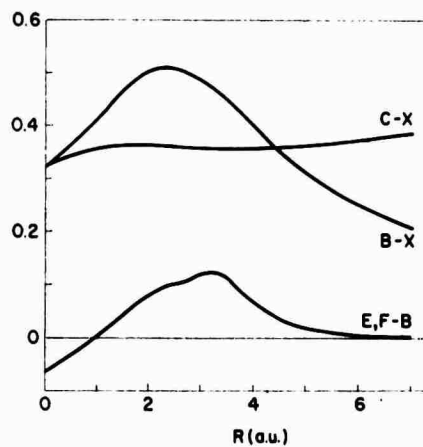
FIG. 4. Dipole velocity transition moments, as given by Eq. (9), for $C-X$, $B-X$, and E, $F-B$ electronic transitions.

TABLE III. Band strengths $p_{v'v''}{}^{j'j''}$, for the $B-X$ transition (in 10^{-2} a.u.).

j	0-0 $P(j)$	0-0 $R(j)$	1-0 $P(j)$	1-0 $R(j)$	2-0 $P(j)$	2-0 $R(j)$	3-0 $P(j)$	3-0 $R(j)$	4-0 $P(j)$	4-0 $R(j)$
0		0.5955		2.020		3.993		6.015		7.648
1	0.6341	0.5701	2.130	1.950	4.177	3.884	6.244	5.887	7.882	7.527
2	0.6461	0.5413	2.170	1.873	4.250	3.764	6.343	5.750	7.994	7.402
3	0.6528	0.5100	2.197	1.789	4.307	3.636	6.430	5.606	8.102	7.274
4	0.6539	0.4769	2.211	1.700	4.349	3.500	6.505	5.454	8.206	7.142
5	0.6494	0.4428	2.213	1.608	4.374	3.357	6.566	5.295	8.303	7.006
6	0.6395	0.4083	2.202	1.513	4.383	3.211	6.613	5.130	8.394	6.864
7	0.6246	0.3741	2.178	1.417	4.375	3.061	6.644	4.961	8.476	6.718
8	0.6053	0.3408	2.142	1.322	4.349	2.909	6.659	4.787	8.549	6.567
9	0.5822	0.3090	2.096	1.229	4.308	2.757	6.658	4.610	8.610	6.410
10	0.5562		2.040		4.252		6.640		8.660	

TABLE IV. Band strengths $p_{v'v''}{}^{j'j''}$, for the $C-X$ transition (in 10^{-2} a.u.).

j	0-0 $P(j)$	0-0 $R(j)$	1-0 $P(j)$	1-0 $R(j)$	2-0 $P(j)$	2-0 $R(j)$	3-0 $P(j)$	3-0 $R(j)$	4-0 $P(j)$	4-0 $R(j)$
0		7.771		11.69		11.04		8.525		5.949
1		7.644		11.58		11.00		8.551		5.999
2	8.205	7.527	12.09	11.49	11.20	10.98	8.502	8.585	5.839	6.057
3	8.367	7.420	12.25	11.40	11.27	10.97	8.512	8.628	5.818	6.121
4	8.534	7.322	12.41	11.33	11.36	10.97	8.532	8.678	5.805	6.191
5	8.708	7.233	12.58	11.26	11.45	10.97	8.561	8.735	5.800	6.267
6	8.886	7.152	12.76	11.21	11.55	10.99	8.599	8.800	5.803	6.349
7	9.067	7.079	12.94	11.16	11.66	11.01	8.646	8.870	5.815	6.436
8	9.617	7.013	13.13	11.13	11.78	11.04	8.702	8.945	5.836	6.527
9	9.433	6.954	13.32	11.10	11.90	11.08	8.766	9.025	5.865	6.622
10	9.617		13.51		12.03		8.838		5.902	

oscillator strengths is not very meaningful. In principle one could compare the calculated intensities of individual lines, or bands, with experimental values. However, a quantitative comparison requires a detailed knowledge of the population of the upper states. Therefore in the present work it was not possible to draw any definite conclusions concerning the agreement of computed and observed intensities. Even so, for the Lyman and Werner bands, one may compare the present results semiquantitatively with the transition probabilities obtained by Hesser.[18] Since Hesser's results represent some kind of averaging over v' of the transition probabilities, $A_{v'}$ defined as

$$A_{v'} = \sum_{v''j''j'} w_{j'} A_{v'j'v''j''} \qquad (10)$$

with $w_{j'}$ being the unknown distribution function for j', it would be pointless to evaluate $A_{v'}$ very accurately. Thus we have made the following simplifying assumption:

$$A_{v'v''} = \sum_{j'j''} w_{j'} A_{v'j'v''j''}$$
$$= [4(E_{v''_,0} - E_{v'_,0})^3 / 3\hbar^4 c^3] p_{v'v}{}^{j,j+1} \qquad (11)$$

with j equal to 0 and 1 for the Lyman and Werner bands, respectively. In addition, since the present computations were restricted to $v'' \leq 12$, it was necessary to extrapolate $A_{v'v''}$ for $v'' = 13$ and 14 for the Lyman bands. This was done by assuming

$$p_{v'v''}{}^{j'j''} = |M^e(R_{v''})|^2 F_{v'v''}{}^{j'j''}, \qquad (12)$$

where R_v is the expectation value of R in the vibrational state v, and the Franck–Condon factors appearing in Eq. (12) were taken from Ref. 14.

TABLE V. Transition probabilities $A_{v'}$ in 10^9 sec^{-1}.

v'	$C-X$	$B-X$
0	1.19	
1	1.17	
2	1.15	
3	1.13	1.55
4		1.47
5		1.34
6		1.19
7		0.98
Exptl[a]	1.16	1.25

[a] From Ref. 13.

[18] J. E. Hesser, J. Chem. Phys. 48, 2518 (1968).

[14] D. Villarejo, R. Stockbauer, and M. G. Inghram, Chem. Phys. Letters 2, 11 (1968); J. Chem. Phys. 50, 1754 (1969), and private communication.

101

TABLE VI. Band strengths $p_{v'v''}{}^{j'j''}$ for the E-B transition (in 10^{-2} a.u.).

j	$P(j)$	$R(j)$	$P(j)$	$R(j)$	$P(j)$	$R(j)$
	0–0		1–0		2–0	
0		173.2		178.5		71.23
1	168.6	174.1	178.9	177.4	75.81	63.22
2	164.9	173.9	179.2	171.9	75.50	44.49
3	160.4	172.8	178.8	176.1	69.84	53.10
4	155.1	170.9	172.7	177.3	51.59	63.74
5	149.3	168.2	177.4	179.2	61.05	66.31
6	143.0	165.3	178.8	136.9	76.22	44.77
7	136.5	160.8	181.1	175.8	82.59	42.07
8	130.6		144.3		40.43	
	0–1		1–1		2–1	
0		176.3		0.1102		147.7
1	175.2	176.1	0.5098	0.0181	141.8	148.9
2	173.9	175.7	0.7272	0.4979	142.3	131.5
3	172.0	174.6	0.4838	0.0945	141.9	66.26
4	169.8	173.0	3.755	0.0118	127.1	99.90
5	166.9	170.8	3.369	0.0374	50.33	125.8
6	163.4	163.8	3.678	11.41	77.53	19.84
7	159.4	165.4	3.442	0.0663	100.1	111.2
8	149.8		3.802		41.36	

The results obtained for $A_{v'}$ are presented in Table V. The second and third columns contain $A_{v'}$ for the Werner and Lyman bands, respectively. The numbers in the last row are the average transition probabilities from Hesser. In view of the experimental error, amounting to about 25%, the agreement is quite satisfactory.

It is well known[4,15] that the two minima in the potential-energy curve of the $E,F\,{}^1\Sigma_g{}^+$ state give rise to two band systems: $E\,{}^1\Sigma_g{}^+-B\,{}^1\Sigma_u{}^+$ and $F\,{}^1\Sigma_g{}^+-B\,{}^1\Sigma_u{}^+$. The band strengths $p_{v'v''}{}^{j'j''}$ for the former bands are given in Table VI. The F state is of special interest because, as we have mentioned above, some of the vibrational levels have not yet been observed. Therefore, to facilitate the comparison between the expected intensities of the observed and not observed lines in the F–B bands we give in Table VII, instead of $p_{v'v''}{}^{j'j''}$, the Einstein coefficients defined by

$$A_{v'j'v''j''}=[4(E_{v''j''}-E_{v'j'})^3/3\hbar^4c^3(2j'+1)]$$
$$\times S_{j''\Lambda''}{}^{j'\Lambda'}p_{v'v''}{}^{j'j''}. \quad (13)$$

The numbers in Table VII correspond to the lowest rotational states, i.e., to $j''=0$ and $j''=1$ for the R and P branches, respectively. For higher rotational quantum numbers one gets a similar picture of the v' dependence of the Einstein coefficients, though in general $A_{v'j'v''j''}$, change rather irregularly with j. This is due to the irregularities in $p_{v'v''}{}^{j'j''}$ that are visualized in Table VI and also in Table VIII, where we present the variation with j of $p_{v'v''}{}^{j'j''}$ for some vibrational bands in the F–B transition.

It is seen from Table VII that our results do not explain the fact that in the $F\,{}^1\Sigma_g{}^+$ state the lowest observed vibrational level is that for $v=4$. Except for the lowest v'', the transition probabilities given in Table VII are not as much larger for $v'=4$ compared with the lower vibrational states as was expected.[6] Therefore, since Dieke observed the transitions from the $v'=4$ state, it seems strange that it was not possible to observe transitions from the $v'<4$ vibrational states, unless the conditions of excitation were such that the population of the states in question was very low.

TABLE VII. Einstein coefficients (in 10^6 sec^{-1}) for the F–B transition.

v''	$v'=0$		$v'=1$		$v'=2$		$v'=3$		$v'=4$	
	P	R	P	R	P	R	P	R	P	R
0	0.009	0.003	0.081	0.026	0.060	0.003	1.32	0.405	1.96	1.05
1	0.153	0.050	0.854	0.279	2.94	0.958	8.84	2.88	0.635	0.019
2	0.871	0.286	3.45	1.14	8.19	2.80	11.6	3.92	26.82	9.15
3	2.37	0.790	5.93	1.99	6.69	2.20	4.77	1.56	1.56	0.674
4	3.06	1.04	3.41	1.18	1.22	0.468	0.041	0.008	4.22	1.50
5	1.77	0.615	0.143	0.057	1.05	-0.347	3.43	1.15	0.417	0.089
6	0.348	0.126	0.525	0.173	1.35	0.461	0.205	0.083	0.101	0.081
7	0.007	0.003	0.492	0.174	0.007	0.004	0.531	0.246	2.75	0.986

[15] G. Herzberg, *Spectra of Diatomic Molecules* (D. Van Nostrand Co., Inc., Princeton, N.J., 1950), 2nd ed.

TABLE VIII. Band strengths for the $F–B$ transition in 10^{-4} a.u.

j	$P(j)$	$R(j)$	$P(j)$	$R(j)$	$P(j)$	$R(j)$	$P(j)$	$R(j)$
	0–0		0–2		4–2		3–3	
0		0.0537		14.92		99.92		36.60
1	0.0587	0.0399	15.47	14.99	99.11	101.2	35.74	36.19
2	0.0619	0.0755	16.29	16.09	102.4	69.62	34.47	35.12
3	0.0532	0.0760	17.34	17.11	107.2	22.63	32.53	33.21
4	0.0997	0.0846	19.62	18.66	10?.8	36.35	29.82	30.08
5	0.1104	0.0985	21.96	20.78	16.57	43.58	26.25	24.23
6	0.1332	0.1188	25.12	23.59	28.64	89.13	21.64	0.531
7	0.1668	0.1477	29.20	27.22	34.52	50.30	15.21	30.74
8	0.2148		34.40		95.87		0.386	

In view of the irregular behavior of the band strengths presented in Table VI and VIII, there arises the question of the accuracy of the numerical results. This point requires some additional comments.

The irregular behavior of $p_{v'v''}^{j'j''}$ may be due to three different causes. One of them, affecting only the E, $F–B$ transitions, lies in the fact that some of the vibrational states considered are only partly localized[6] in one of the minima of the potential-energy curve, and thus belong only partly to the $E–B$ or $F–B$ bands. Obviously, in such cases one should expect irregularities such as are seen in Table VI in the bands originating from the $v'=1$ and $v'=2$ levels. Note, however, that since the lowest vibrational state in the inner minimum is always well localized, the 0–0 and 0–1 bands in Table VI are quite regular.

One would also expect irregular behavior of the band strengths whenever they are small, since then a minor change in the vibrational wavefunctions introduced by the increase in j may cause a relatively large change in the integral appearing in Eq. (6). However, it is necessary to distinguish two cases, since $p_{v'v''}^{j'j''}$ may be small either due to the smallness of the integrand in Eq. (6) or due to cancellation of positive and negative contributions to the integral. The former situation is illustrated by the 0–0 band in Table VIII. The latter can always occur when there are many nodes in the wavefunctions. Therefore, the accuracy of the computed transition probabilities between highly excited vibrational states may be in some cases rather low.

The above holds also in the case of computation of the Franck–Condon factors. Consequently, one can get an idea of the accuracy of the computed transition probabilities by comparing the Franck–Condon factors obtained in this work with those computed by Villarejo et al.[14] for the Lyman band. Although the vibrational wavefunctions used in Ref. 14 were also obtained by Cooley's method, we used a different interpolation of the potential energy and also assumed the proton mass to be 1836.12 electron masses as compared with 1836.09 used in Ref. 14. Thus the rounding errors must be different in the two cases. In Table IX we give the Franck–Condon factors for the R branch of the 0–4 and 6–4 bands. Table IX is quite typical, i.e., except when they are very small, our Franck–Condon factors agree well with those given in Ref. 14.

The good agreement of the Franck–Condon factors seems to justify the opinion that the errors introduced by the integration over R in Eq. (6) are in most cases smaller than the probable errors in the electronic moments M^e. In cases where the integration over R may introduce large relative errors, the transition probability is very small and thus practically unmeasurable.

When this paper was being completed, the present writer was unaware of the recent work of Browne.[16] The electronic transition moments for the Lyman band reported in Ref. 16 are only in qualitative agreement with the present ones given in Table II. The discrepancies, amounting to about 20% for some internuclear separations, are probably due to the fact that the wavefunctions used in Ref. 16 are not very accurate.

TABLE IX. Comparison of Franck–Condon factors for the Lyman bands in 10^{-2} a.u.

j	0–4		6–4	
	This work	Ref. 14	This work	Ref. 14
0	24.10	24.09	0.1803	0.1818
1	24.02	24.01	0.1267	0.1278
2	23.93	23.92	0.0775	0.0783
3	23.82	23.82	0.0372	0.0377
4	23.70	23.69	0.0100	0.0102
5	23.57	23.56	8×10^{-7}	3×10^{-4}
6	23.41	23.40	0.0107	0.0105
7	23.24	23.23	0.0446	0.0444

[16] J. C. Browne, Astrophys. J. 156, 397 (1969).

L . WOLNIEWICZ

ACKNOWLEDGMENTS

Introductory remarks

By R. S. Mulliken, For.Mem.R.S.

University of Chicago

It is for me a great pleasure to be here and to have the privilege of opening this first international meeting of workers in the flourishing new field of photoelectron spectroscopy. It is a special pleasure to be able to meet here with the pioneers of the field, in particular Dr Turner, Professor Price, and Professor McDowell, who have worked with ultraviolet photons, and Professor Siegbahn who has worked mainly with X-rays.

Photoelectron spectroscopy has already shown, and will continue to show, unique ability to see down into the depths of molecules. It has given a new reality to the idea of molecular orbitals, by determining quantitative values for their binding energies, and also by giving information about their bonding characteristics.

Strictly speaking, molecular orbitals are no more than convenient theoretical building blocks for *approximate* descriptions of the electronic structures of molecules. When we speak of the binding energy, or the orbital energy, of a molecular orbital, the actual physical reality is an *ionization energy*, that is to say, the energy required to create a stationary state of the positive ion of a molecule by removing one electron from that molecule. In general, these are excited states of the molecular ion. However, the molecular ion states which are disclosed by photoelectron spectroscopy correspond, for the most part at least, to the removal of an electron from a particular molecular orbital.

It has been quite usual up to now to speak of *the* ionization potential of an atom or molecule. What is really meant is the *minimum* ionization potential, corresponding to production of the molecular ion in its ground state. Because there was relatively little possibility of determining deeper, i.e. inner-shell, ionization potentials, they were largely ignored. To be sure, in a few cases, especially for diatomic and a few triatomic molecules, two or three inner-shell ionization energies have been determined before the advent of photoelectron spectroscopy. This method now makes possible for the first time the wholesale exploration of inner-shell orbital energies.

We are interested here, I believe, primarily in individual molecules in the gaseous or vapour state. As simple examples, consider the nitrogen and carbon monoxide molecules, whose electron configurations in terms of molecular orbitals can be written as

$$1\sigma_g^2\ 1\sigma_u^2\ 2\sigma_g^2\ 2\sigma_u^2\ 1\pi_u^4\ 3\sigma_g^2 \quad \text{and} \quad 1\sigma^2\ 2\sigma^2\ 3\sigma^2\ 4\sigma^2\ 1\pi^4\ 5\sigma^2.$$

The minimum ionization potential corresponds to removal of an electron from the $3\sigma_g$ m.o. (molecular orbital) in N_2, or the 5σ in CO. The resulting ground state of the N_2^+ molecular ion can be called $(3\sigma_g)^{-1}$. But there are other states $(1\pi_u)^{-1}$, $(2\sigma_u)^{-1}$, and so on. One way in which we can learn about these is through a study of the band spectrum of N_2^+, where emission spectra $(1\pi_u)^{-1} \rightarrow (3\sigma_g)^{-1}$ and $(2\sigma_u)^{-1} \rightarrow (3\sigma_g)^{-1}$ are known. From data on these, if the minimum ionization potential, that for $3\sigma_g$, is accurately known, those for $1\pi_u$ and $2\sigma_u$ can be determined accurately. Analogous statements apply to CO. X-ray spectroscopy, both in absorption and emission, has been used in a similar way to optical spectroscopy, but not very much for gaseous molecules; it is difficult to obtain accurate results.

I-2

To determine the *minimum* ionization potentials of molecules, electron impact methods have been widely used. However, these usually result in values that are of limited accuracy. More accurate is the photoionization method, in which the molecule is allowed to absorb almost monochromatic light of varying frequency until a frequency is reached at which ionization begins and ions can be collected; this (with rare exceptions) gives the minimum ionization potential, usually determined to within 0.01 or 0.02 V.

A direct method of determining accurately not only the minimum but also some of the inner-shell ionization potentials of molecules is the observation of the limits, i.e. the convergence points, of Rydberg series absorption spectra. Professor Price was one of the pioneers in using this method for many molecules. The method has been employed successfully for the $3\sigma_g$, $1\pi_u$ and $2\sigma_u$ m.o. of the nitrogen molecule. However, because of the complexity of their spectra or sometimes for other reasons, the use of this method has largely been limited to the simplest molecules, and has not always been successful even for these. Photoelectron spectroscopy is in theory a related procedure but by-passes all the complexity of the Rydberg series, going directly, for each inner shell excitation, to what would be the limit of the Rydberg series, namely the ionization potential.

Paralleling the development of experimental methods for determining molecular ionization potentials there has been an outburst of activity in theoretical computations on molecular electronic structure, using large digital computers. In particular, the forms and the orbital energies of m.o. in the s.c.f. (self consistent field) approximate descriptions of larger and larger molecules are now being computed with considerable accuracy. On the basis of Koopmans's theorem, the s.c.f. orbital energy of a m.o. is approximately, but not exactly, equal to the ionization energy for removal of an electron from that m.o. Thus s.c.f. theory gives values of inner-shell ionization energies which, while rather rough, are usually good enough to corroborate or to serve as a guide if needed, to the identity of the m.o. whose energies are being determined accurately by photoelectron spectroscopy. The theory tells us not only the energy but also the symmetry type (e.g. π_u or σ_g in the example of N_2), and beyond this, the detailed form of each m.o. with, as a corollary, an *approximate* indication as to whether it should be bonding, non-bonding, or anti-bonding. In favourable cases photoelectron spectroscopy gives amazingly *accurate* evidence about the bonding characteristics of m.o. and at the same time gives detailed information on the vibrational levels of the molecular ion states.

S.c.f. theory predicts the approximate characteristics not only of outer-shell m.o. but also of inner-shell m.o. down to the K shell orbitals. It makes interesting approximate predictions about how the K shell energies corresponding to various atoms differ in different molecules. For example, in N_2, the m.o. $1\sigma_g$ and $1\sigma_u$ are approximately N atom's a.o. (atomic orbitals), or rather, linear combinations of these, $1\sigma_g \approx 1s_a + 1s_b$, $1\sigma_u \sim 1s_a - 1s_b$, where a and b refer to the two nuclei. In CO, 1σ is, very nearly, 1s of oxygen and 2σ is, very nearly, 1s of carbon. In N_2, the orbital energy is predicted to be slightly less for $1\sigma_u$ than for $1\sigma_g$. In CO, the predicted K shell orbital energies for C and O differ from those for CO_2, and for C from those for CH_4, C_2H_4, C_2H_2, and other carbon compounds. However, the theoretical predictions, even with the most accurate s.c.f. wave functions, cannot give accurate ionization potentials, while X-ray photoelectron spectroscopy as developed by Professor Siegbahn, does give accurate values.

In the course of time, accurate theoretical calculation of outer- and inner-shell ionization potentials will become possible, first for various small molecules, then for larger and larger ones. This course of events will proceed in two steps; the first of these will be the making of

more accurate s.c.f. calculations for larger molecules; at present, really accurate s.c.f. approximation calculations are available only for diatomic and perhaps some triatomic molecules. Later will come the introduction of configuration mixing, going beyond the s.c.f. approximation, to get really accurate molecular wave functions. But the second step will take a very long time, and I think we shall have to rely on experimental information from photoelectron spectroscopy for accurate ionization energies and, clearly, for an amazing variety of other interesting and important information about molecules and their ions.

THE PARAMETRIZATION OF SEMI-EMPIRICAL π-ELECTRON MOLECULAR ORBITAL CALCULATIONS; π-SYSTEMS CONTAINING C, N, O AND F[1]

David L. Beveridge[2] and Juergen Hinze[3]

Contribution from the Department of Chemistry

University of Chicago, Chicago, Illinois 60637

ABSTRACT

A uniform parametrization is suggested for π-electronic structure calculations of conjugated systems containing carbon, nitrogen, oxygen and fluorine. All parameters are related directly to atomic data. The parametrization scheme is substantiated by comparing computed and observed uv spectral data and proton hyperfine coupling constants for a large number of different π electron systems. The good correlations obtained suggests that π electronic structure calculations, in conjunction with the proposed parametrization scheme, can be used reliably for the prediction of uv spectra and proton hyperfine coupling constants. Arguments are presented that singlet-triplet transition energies, as well as ionization potentials, cannot be predicted with equal reliability using the scheme proposed.

THE PARAMETRIZATION OF SEMI-EMPIRICAL π-ELECTRON MOLECULAR ORBITAL CALCULATIONS; π-SYSTEMS CONTAINING C, N, O AND F[1]

I. INTRODUCTION

The application of semi-empirical π-electron molecular orbital calculations to the study of chemical and spectroscopic properties of unsaturated hydrocarbons has been extensive and in general successful. The method of calculation used commonly is the semi-empirical scheme of Pariser-Parr and Pople, which is a SCF-LCAO procedure based on the independent particle model, grossly simplified by the assumption of Σ Π separability and the approximation of "zero differential overlap" between atomic orbitals on different centers.[4] The effect of these rather severe approximations is hopefully compensated somewhat by the introduction of semi-empirical parameters into the calculation. Computations following the PPP method result in π-electron molecular wavefunctions, describing many important phenomena not accommodated by the simpler Hückel theory, such as separations between excited states of different multiplicity, excitation energies for electronic transitions giving rise to α and β bands in the absorption spectra of aromatic hydrocarbons, and positive as well as negative spin densities in free radicals and ions. Although computations using the PPP method are in principle no more difficult than Hückel calculations, the choice of suitable parameters for PPP calculations is more arduous, especially if hetero systems are to be treated.

Often, when π-electron calculations are performed for a limited group of similar molecules, a parametrization is effected such as to give good agreement between computed and experimental data for some molecules in the group considered. Proceeding in this manner results in a certain loss of objectivity, such as is commonly encountered in Hückel theory. In addition it is more difficult to judge the relative reliability of calculations from different sources, when different approximations have been made in the selection of the basic parameters. If the PPP theory is general enough that it allows correlation of computed results with experimental data over a wide variety of unsaturated compounds, there must be at least one consistent choice of parameters which will yield a general and wide reaching correlation. It is felt that there exists a need for such a unified parameterization scheme, which is generally applicable, without additional modifications, to all types of atoms routinely encountered in different π-electron systems.

In order to deal with this problem we propose herein a generalized parameter scheme for PPP type calculations, and detail its application to π-electron systems containing carbon, nitrogen, oxygen and fluorine. Due to the empirical nature of π-electron theory, it was felt that a direct theoretical parameter choice was not feasible, but the validity of an empirical parameter scheme, though derived with some theoretical reasoning, had to be demonstrated by showing its capability to predict or correlate observables. Therefore in section (4) a number of representative calculations of electronic excitation energies and proton isotopic hyperfine coupling constants for different types of unsaturated systems are presented to substantiate the

111

parameter scheme proposed in section (3). To clarify our notation and to avoid confusion, section (2) allows for a brief review of the π-electron formalism as it is used here.

2. SEMI-EMPIRICAL π ELECTRON THEORY

In the π-electron approximation the Σ part of the total electronic wavefunction of a molecule is assumed to be invariant to changes in the π-electron distribution and therefore considered as constant and disregarded. A molecular wavefunction, Ψ_s, of a stationary state, describing the π-electron cloud only, is then written in general as a sum of configurational functions, Φ_n. The configurational functions are Slater determinants constructed from molecular orbitals ψ_i. These MO's are given as linear combinations of basis functions φ_μ as

$$\psi_i = \Sigma_\mu \varphi_\mu c_{\mu i},\tag{1}$$

where the $c_{\mu i}$ are linear expansion coefficients. As a basis set φ_μ, atomic $2p\pi$ orbitals are chosen, centered one on each atom which is participating in the π structure of the system.

a.) <u>Closed Shell Ground State</u>. The π-electron molecular wavefunction for a closed shell ground state of a molecule with n (n = even) π-electrons is written as a single Slater determinant, constructed from m = n/2 doubly occupied spatial orbitals:

$$\Psi_o = \Phi_o = \frac{1}{\sqrt{n!}} \; \det\left\{ \psi_1(1)\,\psi_1(2)\ldots\psi_i(2i-1)\,\psi_i(2i)\ldots\psi_m(n) \right\} \qquad (2)$$

where barred orbitals are β spin, unbarred, α spin. Ψ_o is an eigenfunction of S^2 and S_z with the eigenvalues 0, representing a singlet state.

The ψ_i's in Eq. (2) are determined by the eigenvectors of the Fock equation

$$\mathbb{F}\, C \cdot \mathcal{S}\, C\, \mathcal{E} \qquad (3)$$

where $\mathcal{E}$ is diagonal.

In the zero differential overlap approximation of Pariser-Parr and Pople we have $\varphi_\mu \varphi_\nu \, d\tau = 0$ unless $\nu = \mu$. Thus $\mathcal{S}$ is a unit matrix, and the matrix elements of $\mathbb{F}$ are given by

113

$$F_{\mu\nu} = H_{\mu\nu} - \frac{1}{2} P_{\mu\nu} \gamma_{\mu\nu} + \delta_{\mu\nu} \Sigma_\sigma \ P_{\sigma\sigma} \gamma_{\mu\sigma'} \tag{4}$$

where

$$\gamma_{\mu\nu} = \iint \varphi_\mu(1)\varphi_\nu(2) \ \frac{1}{r_{12}} \ \varphi_\mu(1) \varphi_\nu(2) \, d\tau_1 \, d\tau_{2'} \tag{5}$$

$$H_{\mu\mu} = -I_\mu(V, n) - \Sigma_{\sigma \neq \mu} Z_\sigma \gamma_{\mu\sigma'} \tag{6}$$

and

$$P_{\mu\nu} = 2 \sum_i^m c_{\mu i} c_{\nu i} . \tag{7}$$

The $\gamma_{\mu\nu}$ are one and two center coulomb repulsion integrals, $I(V, n)$ the nth ionization potential of atom μ in valence state V, Z_σ the core charge of atom σ (equal to the number of electrons contributed to the π electron system) and $p_{\mu\nu}$ the elements of the charge density-bond order matrix $\mathbb{P}$. $H_{\mu\nu} (= \beta_{\mu\nu})$ for $\mu \neq \nu$ is known as a core resonance integral and enters as a parameter, as does $I_\mu(V, n)$ and $\gamma_{\mu\nu}$.

b.) <u>Open Shell Ground States.</u> For open shell systems of π-electron free radicals and radical anions and cations, we choose the spin unrestricted Hartree-Fock description, because we would like to retain the simplicity of a single determinantal wave function, but at the same time be able to describe negative spin densities, central in the description of electron spin resonance spectroscopy.

An unrestricted molecular wavefunction for p α electrons and q β electrons (putting arbitrarily $p > q$) has the form:

$$\Psi_o^U = \frac{1}{\sqrt{n!}} \det \left\{ \psi_1^\alpha (1) \, \psi_2^\alpha (2) \ldots \psi_p^\alpha (p+1) \ldots \psi_q^\beta (p+q) \right\}, \tag{10}$$

where the molecular orbitals comprising the elements of the determinant form two different orthonormal sets,

$$\psi_i^\alpha = \Sigma_\mu \, \varphi_\mu \, c_{\mu i}^\alpha , \qquad\qquad \psi_i^\beta = \Sigma_\mu \, \varphi_\mu \, c_{\mu i}^\beta . \tag{11}$$

determined by the solution

$$F^\alpha c^\alpha = S \, c^\alpha \varepsilon^\alpha \quad , \quad F^\beta c^\beta = S \, c^\beta \varepsilon^\beta \tag{12}$$

with

$$F_{\mu\nu}^\alpha = H_{\mu\nu} - p_{\mu\nu}^\alpha \, \gamma_{\mu\nu} + \delta_{\mu\nu} \Sigma_\sigma (p_{\sigma\sigma}^\alpha + p_{\sigma\sigma}^\beta) \, \gamma_{\mu\sigma} \tag{13}$$

and

$$p_{\mu\nu}^\alpha = \Sigma_i^{\alpha occ} c_{\mu i}^\alpha \, c_{\nu i}^\alpha \tag{14}$$

The matrix elements F^β are obtained by interchanging the superscripts α with the superscripts β in Eqs. (13, 14). The π electronic energy of the system is

$$E_o^U = \frac{1}{2} \Sigma_{\mu\nu} [p_{\mu\nu}^\alpha (H_{\mu\nu} + F_{\mu\nu}^\alpha) + p_{\mu\nu}^\beta (H_{\mu\nu} + F_{\mu\nu}^\beta)]. \qquad (15)$$

The wavefunction Ψ_o^U is an eigenfunction of S_z but not of S^2 and contains in addition to the state of the multiplicity desired, contamination from spin components of higher multiplicity. However, the extent of contamination from higher multiplets is generally not large and Ψ_o^U may usually be considered a reasonable approximation to the state desired. By annihilating contaminating states of higher multiplicity one can obtain a ground state function from Ψ_o^U, which is an eigenfunction of S^2. Such an annihilation will in general change the energy and charge distribution little; however, it may have a marked effect on spin densities (see results).

c.) <u>Excited States</u>. A simple formulation of the molecular wavefunction
for an excited singlet or triplet state, arising from a single excitation of a closed shell
ground state may be given as the sum or difference of two determinantal functions:

$$^{3,1}\Phi_{i\to k} = \frac{1}{\sqrt{2n}} \left[\det \left\{ \psi_1(1)\,\bar{\psi}_1(2)\ldots \psi_k(2i-1)\,\bar{\psi}_i(2i)\ldots \bar{\psi}_m(n) \right\} \right.$$

$$\left. \pm \det \left\{ \psi_1(1)\,\bar{\psi}_1(2)\ldots \psi_i(2i-1)\,\bar{\psi}_k(2i)\ldots\bar{\psi}_m(n) \right\} \right]. \tag{16}$$

Eq. (16) describes a spin proper configuration arising from a single excitation of an
electron out of the orbital ψ_i, occupied in the ground state, into a virtual (unoccupied)
orbital ψ_k. The positive sign refers to a singlet and the negative sign to a triplet
configuration. A single configuration represented by Eq. (16) will be in general a
poor approximation to an excited state. A better, and frequently a sufficiently good
approximation to an excited state, is obtained by writing the excited state wavefunction
as a linear combination of many such spin proper configurations of a given multiplicity,

$$\Psi_p = \sum_n \Phi_n A_{np}, \tag{17}$$

and determining the linear expansion coefficients A_{np} by the variational method

118

(configuration interaction calculation). In this investigation the summation in Eq. (17) will be limited to singly excited configurations from the restricted Hartree-Fock ground state function of Eq. (2), and the parametrization will be effected accordingly. The energies of the electronic excited states and the linear expansion coefficients A_{np} are the eigenvalues and eigenvectors respectively of the matrix $|H|$ of the total π-electron operator $\mathcal{H}^\pi$ of the system, having the elements $\langle \Phi_m | \mathcal{H}^\pi | \Phi_n \rangle$. Since the orbitals from which the spin proper configurations are constructed are Hartree-Fock orbitals, the interaction elements between ground state and singly excited configurations will vanish, and the $|H|$ matrix elements may be written for singlets as:

$$\langle {}^1\Phi_m | \mathcal{H}^\pi | {}^1\Phi_n \rangle = \langle {}^1\Phi_{i \to k} | \mathcal{H}^\pi | {}^1\Phi_{j \to \ell} \rangle = \delta_{ij} \delta_{k\ell} E_o$$

$$+ \delta_{k\ell} \, \epsilon_k - \delta_{ij} \, \epsilon_i - (jk|i\ell) + 2(jk|\ell i), \tag{18}$$

and for triplets as:

$$\langle {}^3\Phi_m | \mathcal{H}^\pi | {}^3\Phi_n \rangle = \langle {}^3\Phi_{i \to k} | \mathcal{H}^\pi | {}^3\Phi_{j \to \ell} \rangle = \delta_{ij} \delta_{k\ell} E_o$$

$$+ \delta_{k\ell} \, \epsilon_k - \delta_{ij} \, \epsilon_i - (ik|i\ell), \tag{19}$$

where δ_{ij} is the Kronecker delta. Due to the "zero differential overlap" approximation, we have,

$$(ij|k\ell) = \iint \psi_i(1) \, \psi_j(2) \, \frac{1}{r_{12}} \, \psi_k(1) \, \psi_\ell(2) \, d\tau_1 \, d\tau_2$$

$$\approx \sum_{\mu\nu} c_{\mu i} \, c_{\mu k} \, c_{\nu j} \, c_{\nu \ell} \, \gamma_{\mu\nu} \, . \tag{20}$$

By subtracting the ground state energy, E_o, from the diagonal matrix elements, the eigenvalues obtained will be the excitation energies.

Analogously excited doublet and quartet states could be constructed from the unrestricted Hartree-Fock functions of ions and radicals, Eq. (10); however, this possibility is not considered in this work.

3. PARAMETRIZATION

From the preceding review of the formalism of semiempirical π-electron molecular orbital theory it is seen that the same basic parameters enter into each type of calculation considered, namely the valence state ionization potentials I_μ, the coulomb repulsion integrals $\gamma_{\mu\nu}$, and the core resonance integrals $\beta_{\mu\nu}$. We proceed now to a detailed discussion and specification of the particular parameter choice proposed for the atoms carbon, nitrogen, oxygen and fluorine.

a.) <u>Valence State Ionization Potentials and One Center Coulomb Repulsion Integrals</u>. The valence state ionization potentials and the one center coulomb repulsion integrals are interrelated through the elegant argument due to Pariser,[5]

120

who pointed out that the energetics of a charge transfer disproportionation of two identical neutral atoms into an ion pair require approximately

$$\gamma_{\mu\mu} = I_\mu - A_\mu, \tag{21}$$

where I_μ and A_μ are the proper ionization potential and electron affinity of atom μ. The validity of Pariser's argument has been questioned frequently; it has been criticized particularly because the rearrangement in the electronic core (analogous to the Σ core in π-electron theory) of the atoms is not considered. Neglect of core rearrangement, however, is consistent with the entire framework of π-electron theory. Eq. (21) is attractive by its simplicity and especially through the fact that with it good results can be obtained. To our knowledge there is in semiempirical π-theory no procedure of obtaining the one center coulomb integral, which yields results significantly better; therefore, Eq. (21) has been adopted for the determination of the one center coulomb repulsion integrals.

The determination of valence state ionization potentials and electron affinities is accomplished by combining the proper valence state promotional energies with the corresponding ground state ionization potentials and electron affinities respectively. For example the valence state ionization potential and electron affinity for carbon in its (tr tr tr π) valence state is given by

$$I_C(\text{tr tr tr } \pi, 1) = I_C + P_C^+(\text{tr tr tr}) - P_C^o(\text{tr tr tr } \pi)$$

$$A_C(\text{tr tr tr } \pi, 1) = A_C + P_C^o(\text{tr tr tr } \pi) - P_C^-(\text{tr tr tr } \pi^2)$$

121

where $P_C(v)$ is the promotion energy to valence state v. For an atom contributing two electrons to the π electron system of a molecule, it is necessary to have the second valence state ionization potential and corresponding electron affinity, i.e., the first ionization potential. As an example for a pyrrole nitrogen, with a valence state tr tr tr π^2 it is

$$I_N(tr\ tr\ tr\ \pi^2, 2) = I_N^2 + P_N^{++}(tr\ tr\ tr) - P_N^+(tr\ tr\ tr\ \pi)$$

$$A_N(tr\ tr\ tr\ \pi^2, 2) = I_N^1 + P_N^+(tr\ tr\ tr\ \pi) - P_N^0(tr\ tr\ tr\ \pi^2).$$

Selection of the ground state ionization potentials and electron affinities and calculations of the appropriate promotion energies has been considered in detail in an earlier publication,[6] and the valence state quantities employed herein are based on these results.

It is in general not necessary to consider fine details in the hybridization of the underlying core of the atoms considered, since such changes affect the pπ-electron ionization potential and electron affinity only little. As an example, $I_C(tr\ tr\ tr\ \pi, 1) = 11.16$ e.V. and $A_C(tr\ tr\ tr\ \pi, 1) = .03$ e.V., while for acetylene type carbon the values would be $I_C(di\ di\ \pi\ \pi, 1) = 11.19$ e.V. and $A_C(di\ di\ \pi\ \pi, 1) = .10$ e.V. It is therefore sufficient to use general pπ-electron ionization potentials and electron affinities. In Table 1 the required pπ-electron ionization potentials and electron affinities are listed together with the corresponding one center coulomb repulsion integrals, evaluated from Eq. (21), for the atoms considered in this investi-

TABLE 1. Valence State Ionization Potentials, Electron Affinities and One-Center Coulomb Integrals Used.[6]

Atom	Valence State Electronic Configuration	Valence State Ionization Potential eV	Valence State Electron Affinity eV	One-Center Coulomb Integral eV
C	trtrtrπ	11.16	0.03	11.13
N (I)	tr^{2}trtrπ	14.12	1.78	12.34
N (II)	trtrtrπ^2	28.72	11.96	16.76
O (I)	tr^{2}tr^{2}trπ	17.70	2.47	15.23
O (II)	tr^{2}trtrπ^2	34.12	15.30	18.82
F (II)	sp^{2}p^{2}p^2	40.70	18.52	22.18

gation. The values given correspond to an underlying trigonally hybridized core, as it is most commonly encountered.

b.) <u>Two Center Coulomb Repulsion Integrals.</u> The one center coulomb repulsion integrals, when determined semiempirically from Eq. (21) are lower than the corresponding theoretical values, computed from Slater type orbitals using Slater-Zehner exponents or from atomic Hartree-Fock orbitals, and thus correspond to somewhat more diffuse orbitals. The two center coulomb integrals must be determined with recognition of their proper limiting values, i.e. they should join smoothly the purely electrostatic value $r_{\mu\nu}^{-1}$ for large distances $r_{\mu\nu}$ and also go to $\gamma_{\mu\mu}$ at $r_{\mu\nu} = 0$ in the homonuclear case. A general formula for $\gamma_{\mu\nu}$ may be obtained by treating the problem purely theoretically and evaluating the coulomb integral using Slater type functions with an exponent that would give the empirical $\gamma_{\mu\mu}$ for the one center case. Such a procedure would complicate π-electron calculations considerably, and not necessarily yield better results than the alternative method of treating the integrals empirically. This can be done by choosing a flexible function with the required limiting behavior and implementing it from experience. We have chosen the latter method, and our suggested general formula for $\gamma_{\mu\nu}$ in atomic units is

$$\gamma_{\mu\nu} = \frac{1}{a \ \exp(-r_{\mu\nu}^2/2a^2) + r_{\mu\nu}} \ , \tag{22}$$

where

$$a = \frac{2}{\gamma_{\mu\mu} + \gamma_{\nu\nu}} \tag{23}$$

124

with γ's in Hartrees and r in Bohr. (Atomic units are chosen here to avoid the appearance of conversion factors in the formulas.)

This expression is similar to a suggested formula by Mataga and Nishimoto,[7] and has been inspired by it. An equation of similar form has been suggested by Knowlton and Carper.[8] The exponential factor introduced into the denominator was found necessary to dampen the influence of a at intermediate values of $r_{\mu\nu}$, because Mataga type formulas, without the exponential factor, result in the prediction of triplet states which are in general more than 1 e.V. too low. The reason for this is apparently that Mataga type $\gamma_{\mu\nu}$'s show initially a too rapid decrease of $\gamma_{\mu\nu}$ with $r_{\mu\nu}$, giving too large differences between one center coulomb integrals and nearest neighbor coulomb integrals. Another formula for $\gamma_{\mu\nu}$ tested in this work has been

$$\gamma_{\mu\nu} = \frac{1}{\sqrt{a^2 + r^2}} \quad , \tag{24}$$

as suggested by Ohno.[9] However results obtained with such $\gamma_{\mu\nu}$'s were completely unacceptable. In Fig. 1 the dependence of different $\gamma_{\mu\nu}$ formulas on $r_{\mu\nu}$ is illustrated for $C(2p\pi)$ – $C(2p\pi)$ coulomb repulsion.

c.) <u>Core Resonance Integrals</u>. A semi-theoretical method of estimating $\beta_{\mu\nu}$ has been proposed by Ohno.[9] Using Löwdin orbitals and assuming that the major contribution to $\beta_{\mu\nu}$ comes from the region near the midpoint of internuclear separation, he derives

125

$$\beta_{\mu\nu} = \frac{1}{2} (Z_\mu + Z_\nu) \, S_{\mu\nu} \left\{ \gamma_{\mu\nu} - \frac{2 \, C}{r_{\mu\nu}} \right\} , \qquad (25)$$

where C is a disposable parameter. We have chosen to implement Eq. (25) in its present form into the overall parametrization scheme proposed herein, choosing the basic functions for the evaluation $S_{\mu\nu}$ in a manner consistent with the semiempirical $\gamma_{\mu\nu}$. This is accomplished by evaluating $S_{\mu\nu}$ over Slater orbitals, using the theoretical value of the orbital exponents corresponding to the semiempirical value for the one-center coulomb repulsion integral, i.e. evaluating the one center coulomb repulsion integral $\gamma_{\mu\mu}$ from a 2pπ orbital, which is represented by a single 2p Slater type basis function with exponent ζ_μ gives the relation

$$\zeta_\mu = \frac{1280}{501} \gamma_{\mu\mu} , \qquad (26)$$

which is used to obtain the ζ_μ's required for the determination of the overlap integrals $S_{\mu\nu}$. This procedure leads to relatively large values for the overlap integrals, but has the advantage of leaving the parameter scheme proposed internally consistent, and based entirely on the atomic energy data. That $S_{\mu\nu}$ used in Eq. (25) may be too large is remedied by the parameter C, which is left unspecified to this point. This parameter has been chosen empirically such as to give the best overall fit to the electronic excitation energies in a small set of selected compounds, namely ethylene, benzene and the monocyclic azines. The best value found is C = .545, and this value has been used in all following calculations performed, to substantiate the parameter scheme proposed herein.

4. RESULTS OF SAMPLE CALCULATIONS

As pointed out in the introduction, the authors feel that a rigorous

theoretical justification of a parameter scheme in the Pariser-Parr and Pople method

cannot be achieved, due to the many approximations in this semi-empirical MO

procedure. Numerical experimentation is therefore the only method to test the

merits of the parametrization scheme proposed in Section 3. Any parameter scheme

is useful only, if with it several experimental observables can be calculated reliably

for a large class of molecules. It is, however, asking too much to expect a particular

scheme to overcome the limitations inherent in the Pariser-Parr and Pople method. The

method is based on the independent particle model and therefore incapable to yield

effects, which depend critically on electron correlation. Fortunately it appears

possible to compensate some of this shortcoming by an appropriate parameter choice.

However, if parameters are chosen to compensate for one particular correlation error,

one should not expect the same parameters to compensate other correlation errors. To

be more specific, let us discuss correlation errors in the description of electron excitation

and ionization.

A particular singly excited configuration of a closed shell molecules gives

rise to a singlet and a triplet state. We ask, what is the electron correlation error, if

we calculate term values, i.e.,

$$\Delta E \;=\; E^* - E^o \;.$$

127

Identifying the correlation energy as ϵ (a negative quantity), we obtain

$$\Delta\epsilon = \epsilon^* - \epsilon^o.$$

If the transition energy is calculated within the framework of the independent particle model, we should get ΔE_{HF} which in general will be smaller than ΔE, since ϵ^o is in general smaller than ϵ^* (ϵ^o and ϵ^* are negative energy quantities), and

$$\Delta E = \Delta E_{HF} + \Delta\epsilon.$$

If we effect the parametrization such that we obtain in the frame of the independent particle model directly $\Delta E^{(1)}$ for singlet states, then we should expect to obtain $\Delta E^{(3)}$, the term values for triplet states too low, because we calculate approximately

$$\Delta E^{(3)} = \Delta E^{(3)}_{HF} + \Delta\epsilon^{(1)},$$

the corrections $\Delta\epsilon^{(1)}$ resulting from our parameter choice; however $\Delta\epsilon^{(1)}$ is in general smaller than $\Delta\epsilon^{(3)}$ since the Fermi hole in the triplet state results in $\epsilon^{*(1)} < \epsilon^{*(3)}$ (ϵ's are negative quantities.).

The parametrization scheme suggested in this paper is adjusted such as to yield good correlation between experimental and computed values for singlet-singlet transition energies and for ground state properties, i.e. proton isotopic hyperfine coupling constants. It must be expected therefore that singlet-triplet excitations will be calculated consistently too low. Such a consistent discrepancy has been observed in all cases where experimental singlet triplet transition energies are known.

128

TABLE 2.—Computed and Experimental UV-Excitation Energies in eV.

Type	Compound	Ref.	Excitation 1		Excitation 2		Excitation 3		Excitation 4		Excitation	
			Calc.	Exp.	Calc.	Exp.	Calc.	Exp.	Calc.	Exp.	Calc.	Exp.
Hydrocarbons alternant	T-Butadiene	a	5.51	5.80–6.10	6.64	6.60–6.70	7.13	7.05–7.15				
	Styrene	b	4.39	4.30–4.50	4.82	5.00–5.10	5.83	5.75–5.90	6.08	5.95–6.30		
	Naphthalene	b	3.97	3.90–4.15	4.35	4.40–4.60	5.80	5.60–5.70	6.17	5.90–6.20		
	Phenanthrene	b	3.71	3.55–3.85	4.21	4.15–4.30	5.14, 5.16	4.85–5.10	5.56, 5.71	5.70–6.00		
non alternant	Azulene	b,d	2.03, 2.13	2.00–2.20	3.36	3.50–3.80	4.31	4.35–4.60	4.98	5.05–5.15		
	Acenaphthylene	c,e	2.90	2.80–3.00	3.77	3.65–3.75	3.81	3.80–3.90	4.87	4.50–4.80	5.55	5.30–5.50
N^+	Pyrazine	b	-	3.95–4.05	4.67	4.70–4.85	6.18	6.15–6.25	7.22	7.05–7.25		
	Isoquinoline	f	3.77	3.85–4.00	4.31	4.50–4.80	5.22	5.25–5.40	5.61, 5.66	5.60–5.80		
	Acridine	c	3.38	3.40–3.50	3.47	3.55–3.70	4.15, 4.85	-	5.11, 5.12, 5.15	4.90–5.10		

Type	Compound	Ref.	Excitation 1		Excitation 2		Excitation 3		Excitation 4		Excitation 5	
			Calc.	Exp.	Calc.	Exp.	Calc.	Exp.	Calc.	Exp.	Calc.	Exp.
N⁺	Aniline	b,c	4.41	4.25–4.40	5.30	5.20–5.35	6.22, 6.23	6.20–6.35				
	Pyrrole	b,g	5.12	5.10–5.20	5.47	5.35–5.60						
	Indole	b	2.38	–	3.97	4.25–4.35	4.50	4.55–4.70	5.28	5.55–5.80		
O⁺	o–Benzoquinone	h	2.79	2.40–2.55	3.87	3.60–3.90	5.22	5.00–5.30				
	p–Benzoquinone	c,h	2.71	2.70–2.80	4.07	4.25–4.40	5.67	5.10–5.35				
	Benzaldehyde	b	–	3.65–3.85	4.34	4.30–4.5C	4.97	4.90–5.15	5.94	5.75–5.90		
O⁺	Phenol	b,c	4.61	4.50–4.65	5.64	5.50–5.75						
	Hydroquinone	b,i	4.58	4.15–4.30	5.60	5.45–5.60						
	Furan	b,i	4.71	4.40–4.60	5.67	5.60–5.80						
F⁺	Fluorobenzene	b	4.62	4.65–4.80	5.67	5.80–5.90						

Type	Compound	Ref.	Excitation 1		Excitation 2		Excitation 3		Excitation 4		Excitation 5	
			Calc.	Exp.	Calc.	Exp.	Calc.	Exp.	Calc.	Exp.	Calc.	Exp.
	α-Fluoronaphthalene	k	3.95	3.90–4.00	4.34	4.30–4.50						
	β-Fluoronaphthalene	k	3.95	3.90–4.05	4.34	4.30–4.50						
Mixed	p-Aminopyridine	l	4.36	4.35–4.50	5.10	4.95–5.15						
	Benzoic acid	b,j	3.84	–	4.42	4.40–4.60	5.16	5.35–5.55	6.11, 6.20	6.15–6.30		
	Nitrobenzene	b	4.49, 4.56	4.65–4.85	5.26	5.70–5.85	6.01, 6.20	6.10–6.30				
	p-Nitroaniline	m	4.37, 4.53	4.10–4.30	5.76	5.40–5.65						
	p-Nitrophenole	m	4.48, 4.55	3.85–4.15	5.19	5.25–5.60	5.94, 6.16	6.20–6.35				

References to Table 2.

a. L. C. Jones, Jr. and L. W. Taylor, Analyt. Chem. 27, 228 (1955).

b. J. R. Platt, "Systematics of Electronic Spectra of Conjugated Molecules,"
    John Wiley (1964).

c. R. A. Friedel and M. Orchin, "Ultraviolet Spectra of Aromatic Compounds,"
    John Wiley (1951).

d. E. K. Jensen, E. Kovats, A. Eschenmoser and E. Heilbronner, Helv. Chim.
    Acta. 39, 1051 (1956).

e. A. Pullman et al., J. Chim. Phys. 48, 359 (1951).

f. R. Müller and F. Dorr, Z. f. Elekfroehem., 63, 1150 (1959).

g. S. Menezel, Z. f. Phys. Chem. 125, 161 (1927).

h. L. Horner and H. Lang, Chem. Ber., 89, 2768 (1956).

i. J. C. Dearden and W. F. Forbes, Can. J. Chem. 37, 1294 (1959).

j. "UV Atlas of Organic Compounds," Plenum Press, New York, 1966.

k. T. Iredale and J. W. White, Trans. Faraday Soc. 56, 1719 (1960).

l. P. Grammaticakis, Bull. Soc. Chim. France, 1959, 480.

m. "Absorption Spectra in the Ultraviolet and Visible Region", L. Lang, Ed.,
    Academic Press, N. Y. (1965).

It can be concluded from an argument quite analogous to the one presented above that ionization potentials calculated from orbital energies, following Koopmans' theorem, should be too large, if the orbital energies are obtained with parameters chosen for singlet-singlet transitions. This was also consistent with the results obtained in this work. Thus the parameter scheme presented here will yield only ground state properties and singlet singlet transition energies reliably. We believe, due to the arguments presented above, that such limitations should apply to any general parameter scheme for the Pariser-Parr and Pople method. The arguments presented above apply only if, as done here, the ground state is described by a single, spin restricted HF function, and the excited states are expressed as combinations of Slater determinants, singlet excited with respect to the ground state. If doubly and higher excited configurations are used in the expansion of the total wave function, these shortcomings of the conventional Pariser-Parr-Pople method can be overcome. Work along these lines is in progress.

Results for singlet-singlet excitations: Singlet-Singlet excitation energies were calculated for organic π-electron systems containing the atoms C, N, O and F. The results are given in Figure 2 and Table 2. All systems were assumed to be planar, and if known, the ground state bond distances and angles were used; otherwise idealized structures were assumed with standard internuclear distances. It was found that the results did not depend critically on these assumed geometries. The computed transition energies should correspond to the energies of the absorption maxima, since these Franck-Condon maxima in general correspond to excitations from the zero'th vibrational state, which corresponds most closely to the ground state geometry assumed in our calculations. Unfortunately most of the observed absorption maxima are rather broad; therefore, we have compared an observed absorption range with the computed transition energies. This we believe is more meaningful than comparing the exact observed absorption maxima. Frequently weak absorptions, which are symmetry or

133

overlap forbidden, do not show up in the system as absorption maxima. If such absorptions appeared as shoulders of stronger peaks, we have included them in Table 2 together with the corresponding computed excitation energies. If, however, symmetry or overlap forbidden excitations resulted in the computation of energy values where neighboring strong lines completely obscured the appearance of a weak absorption, then such computed excitations are left out in Table 2, since no meaningful comparison would be possible. It should be kept in mind that the purpose of this presentation is to compare computed and observed spectra to justify a parameter scheme, and it is not even attempted to interpret in detail any one particular UV spectrum of a compound. Only in the latter case it would be necessary to report also computed weak transition energies which clearly are obscured in the observed spectrum. It is seen from Table 2 and from the correlation diagram, Fig. 2, that the computed transition energies correlate well with the observed absorption maxima ranges.

It is clear that a parameter scheme can be tailored such as to yield better results for a particular small class of compounds, the discrepancies for compounds outside this class would then surely be larger. In addition to the transition energies, we have also computed the transition moments, using the point dipole approximation. The results obtained correlate rather well with the observed molar extinction coefficients. This permitted a less ambiguous assignment of computed and observed transition energies. Besides the results reported here we computed the spectra of 40 more hydro-carbons and azines, and the results obtained agreed equally well with the observed spectra as those reported here. We will report on these results in the future, with an attempt of detailed spectral assignments.

134

Results for proton isotopic hyperfine coupling constants. It is clear that within the PPP method the proton hyperfine coupling constant, which depends on the electron spin probability at specific protons, cannot be obtained directly. The protons are generally located in the molecular plane where the π electron wave function, which is the part of the electronic wavefunction considered explicitly, has a nodal plane. It is expected however that the proton hyperfine coupling constants, a_H, observed in esr spectra, correlate well with $\rho_{c\pi}$, the electron spin density in the π orbital of the carbon atom, to which the specific hydrogen atoms are bonded. This is generally known as the McConnel relation[10]

$$a_H = Q \rho_{c\pi}$$

which can be justified theoretically.[11] Correlated are therefore the calculated spin densities of the carbon atoms with the observed proton isotopic hyperfine coupling constants of the corresponding hydrogen atoms (see Fig. 3 and 4).

It is well known that PPP calculations within the restricted SCF frame, i.e. each spatial orbital is occupied with spin α and spin β electrons excepting on singly occupied orbital, cannot yield negative spin densities. It is therefore necessary to resort to an unrestricted SCF formalism, as outlined above, if spin densities at the carbon atoms are to be computed in a more realistic manner. It is well known also that unrestricted SCF functions are not eigenfunctions of the S^2 operator. Thus the wavefunctions which are obtained directly by solving Eq. (12) will in general not

135

represent pure doublet states as they should for the radicals and positive and negative ions considered here. In principle, it is possible to project out the components of the wavefunction which corresponds to states of higher multiplicity. This, however, is rather arduous, and it is in general sufficient to annihilate the next higher multiplicity component, here a quartet. This is so because the higher spin components are in general only small contaminations of the wavefunctions, which in our case are in general of more than 98% doublet character. It should in general not be expected that the projected wavefunction or the function with the dominant contamination, here the quartet, annihilated yields a more true representation of the electron or spin distribution. Because the orbitals of the projected function were obtained by solving Eq. (12), in which the electron interaction potential is obtained from the unprojected total wavefunction, thus projected or annihilated functions are in general no more self-consistent functions. In addition, the generation of wavefunctions which are eigenfunctions of S^2 from the unrestricted SCF function is necessarily arbitrary. The mechanical procedures of projection or annihilation do not always yield functions which give a potential in the SCF equations, which is most closely related to the potential used when solving the SCF equations. Thus the unrestricted SCF functions are afflicted with inadequacies if used directly or after projection or annihilation of the contaminating spin components. Fortunately these inadequacies are in general not serious, since the contribution of high spin components in the unrestricted SCF functions is rather small. An inspection and statistical evaluation of the correlations in Fig. (3) and (4) shows that the correlation of experimental and computed results

136

before and after annihilation of quartet states is equally good. For spin density

proton hyperfine coupling constant correlation derived from a single determinantal

function, Fig. (3), the slope is $Q = -17.09$, and the standard error is 1.05 Gauss,

while for the function after quartet annihilation, Fig. (4), the slope is $Q = -23.66$,

with the standard error 0.84 Gauss. Thus we conclude that our parameter scheme is

adequate to yield reliably proton hyperfine coupling constants within the unrestricted

SCF frame of the PPP approximation and the McConnel relation. It may be concluded

further that a projection or annihilation of contaminating high multiplicity in the

wavefunction is unnecessary labor if esr spectral data are to be correlated or predicted.

REFERENCES

1.   Research supported in part by the National Science Foundation.

2.   Department of Chemistry, Hunter College, 695 Park Ave., New York, N. Y. 10021.

3.   To whom correspondence should be addressed.

4.   a) J. A. Pople, Proc. Phys. Soc. (London) A68, 81 (1955).

      b) R. Pariser and R. G. Parr, J. Chem. Phys. 21, 466, 767 (1953).

      c) For additional references see general reviews, e.g. L. Salem, "The Molecular Orbital Theory of Conjugated Systems", W. A. Benjamin, Inc. New York, 1966; K. Jug, Theoret. Chim. Acta. 14, 91 (1969).

5.   R. Pariser, J. Chem. Phys. 21, 568 (1953).

6.   J. Hinze and H. H. Jaffe, J. Am. Chem. Soc. 84, 540 (1962). J. Hinze, Ph.D. Dissertation, University of Cincinnati, 1962.

7.   K. Nishimoto and N. Mataga, Z. Physik. Chem. (Frankfurt) 12, 335 (1957), ibid. 13, 140 (1957).

8.   P. Knowlton and W. R. Cooper, Mol. Phys. 11, 213 (1966).

9.   K. Ohno, Theoret. Chim. Acta. 2, 219 (1964).

10.   H. M. McConnell, J. Chem. Phys. 24, 764 (1956).

11.   H. M. McConnell, J. Chem. Phys. 28, 1188 (1958).

FIGURE 1

139

FIGURE 2

140
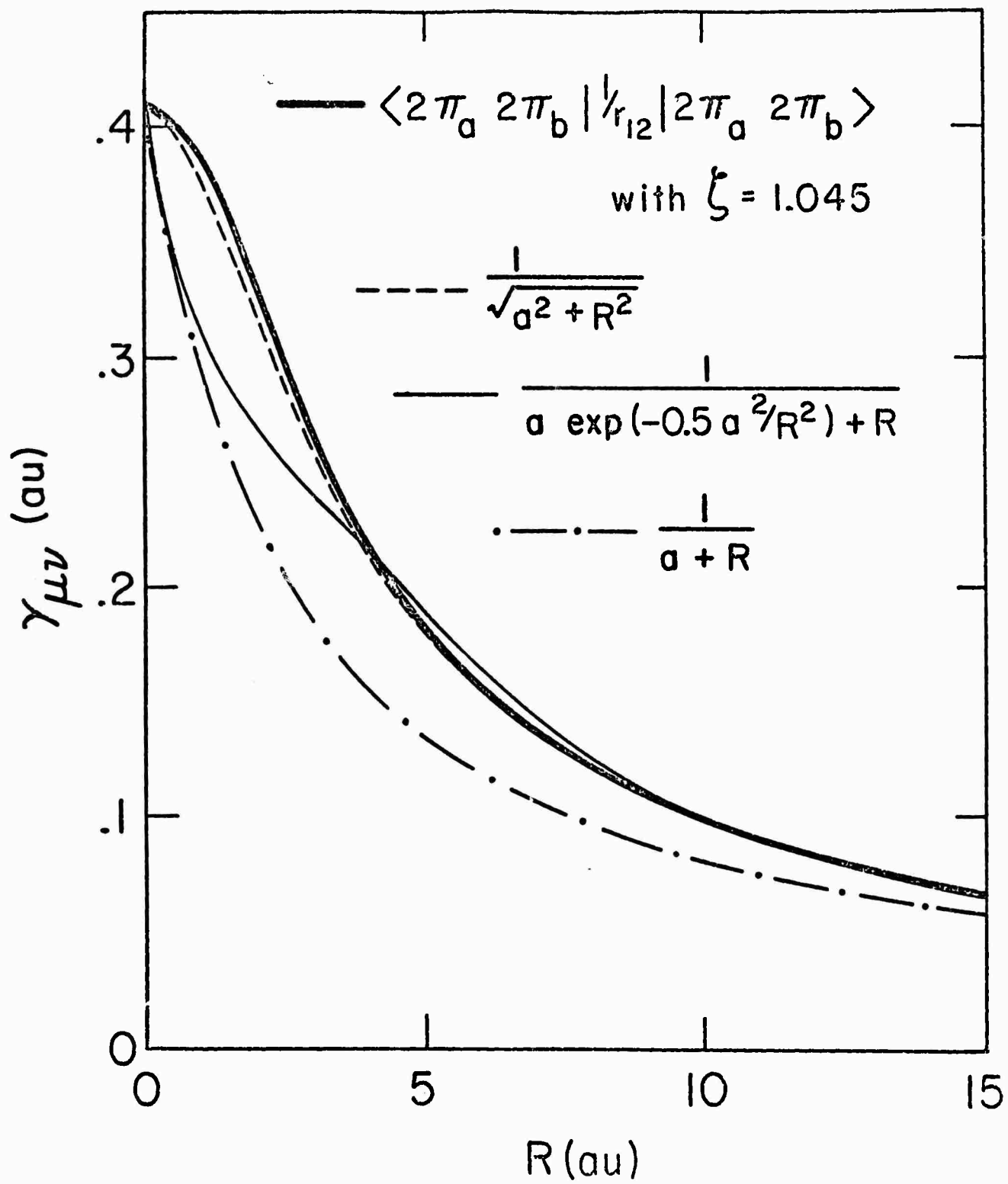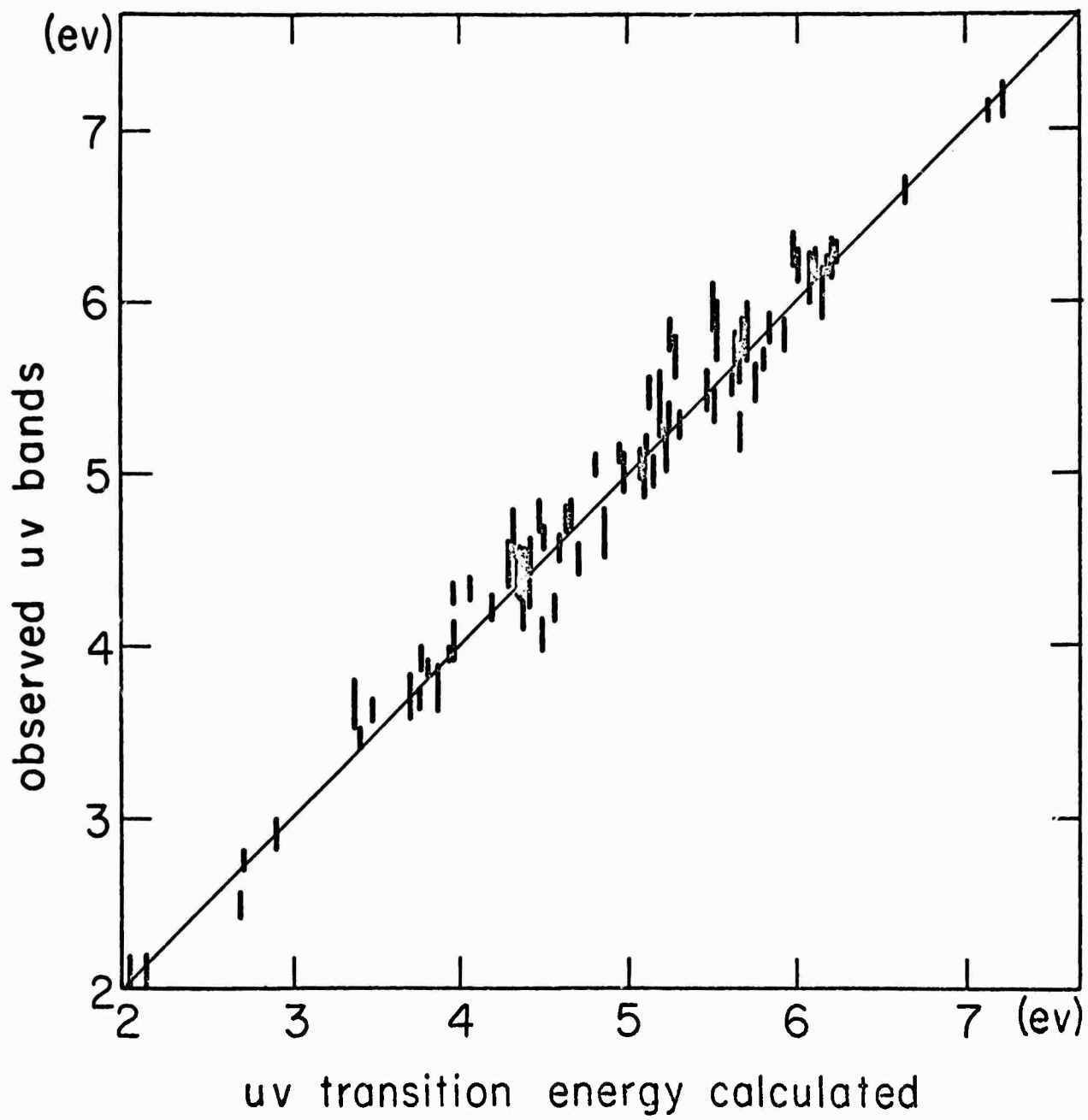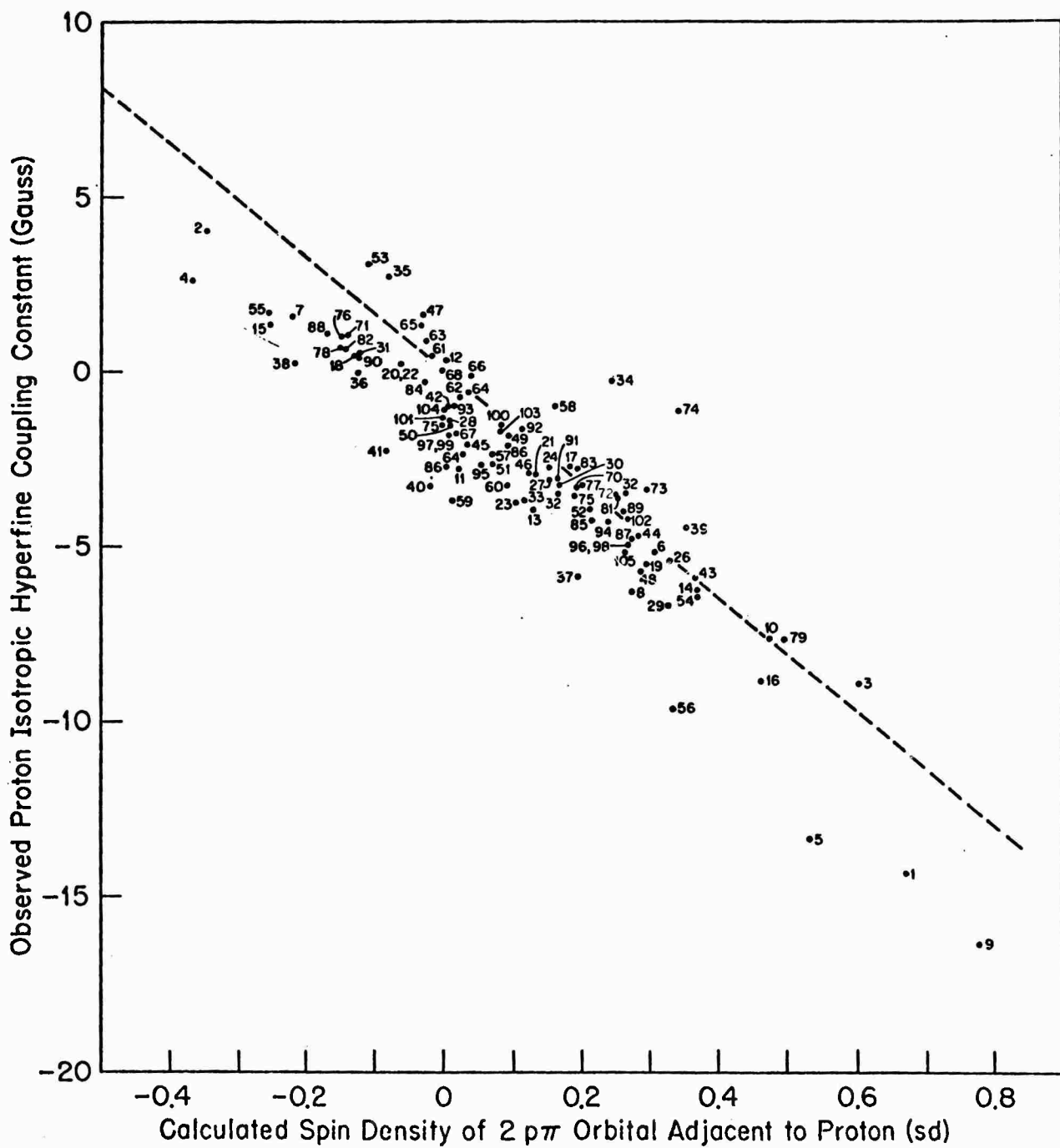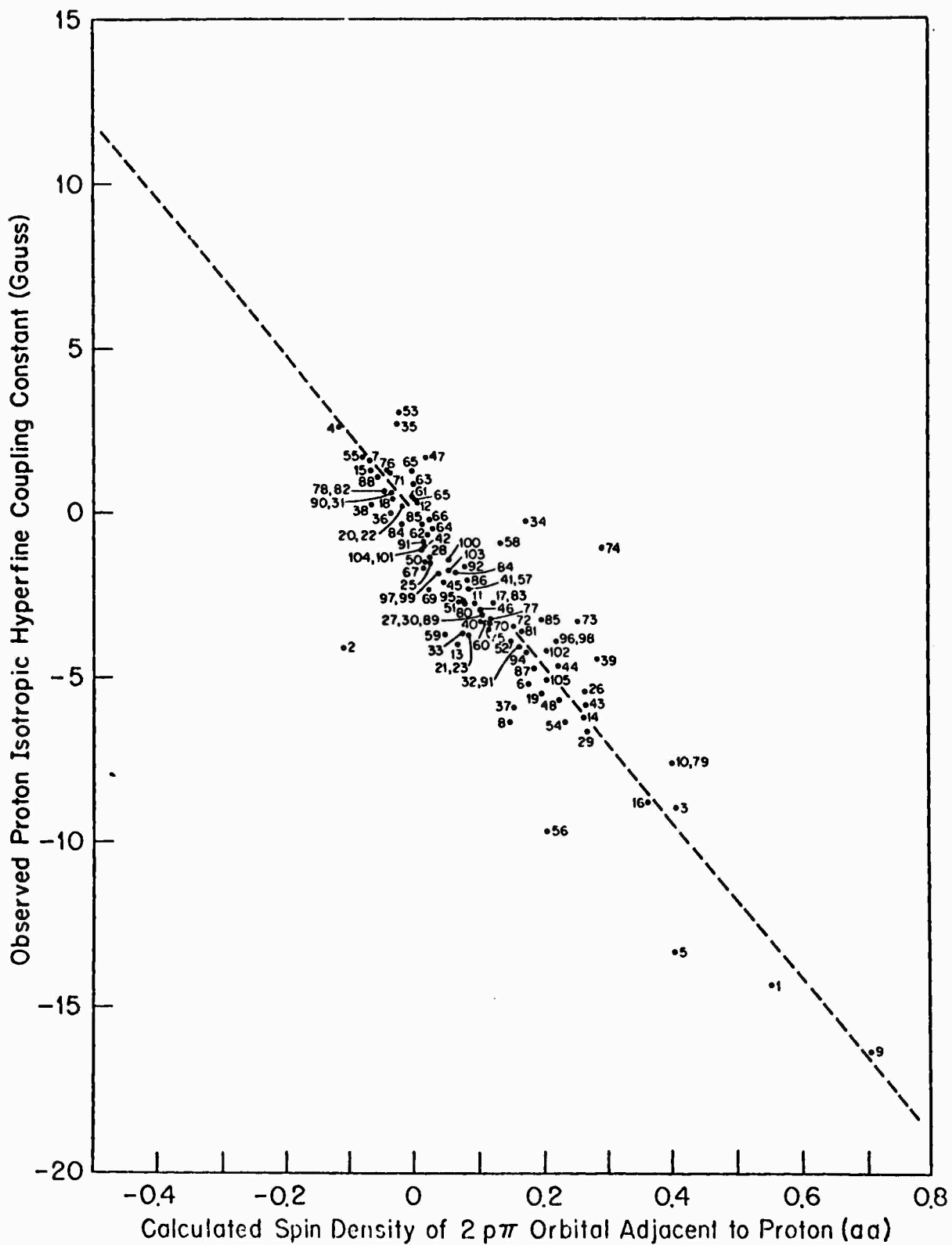
FIGURE 3

FIGURE 4

Captions for Figures

Fig. 1.   Dependence of $\gamma_{\mu\nu}$ on $r_{\mu\nu}$ as computed for $2p\pi$ orbitals, and as given by different approximate formulas.

Fig. 2.   Observed uv absorption bands versus computed singlet term energies for molecules given in Table 2.

Fig. 3.   Observed proton isotropic hyperfine coupling constant vs. calculated $2p\pi$ orbital spin density (sd = single determinant). Dotted line is linear least squared correlation line, constrained to origin. Key: (1) allyl radical, 1 position[a], (2) allyl radical, 2 position[a], (3) pentadienyl radical, 1 position[a], (4) pentadienyl radical, 2 position[a], (5) pentadienyl radical, 3 position[a], (6) benzyl radical, 2 position[b], (7) benzyl radical, 3 position[b], (8) benzyl radical, 4 position[b], (9) benzyl radical, 7 position[b], (10) trans-butadiene radical anion, 1 position[c], (11) trans-butadiene radical anion, 2 position[c], (12) azulene radical anion, 1 position[c], (13) azulene radical anion, 2 position[c], (14) azulene radical anion, 4 position[c], (15) azulene radical anion, 5 position[c], (16) azulene radical anion, 6 position[c], (17) diphenyl radical anion, 2 position[d], (18) diphenyl radical anion, 3 position[d], (19) diphenyl radical anion, 4 position[d], (20) biphenylene radical anion, 1 position[e], (21) biphenylene radical anion, 2 position[e], (22) biphenylene radical cation, 1 position[f,g], (23) biphenylene radical cation, 2 position[f,g], (24) anthracene radical anion, 1 position[h,i], (25) anthracene radical anion, 2 position[h,i], (26) anthracene radical anion, 9 position[h,i], (27) anthracene radical cation, 1 position[h,i],

(28) anthracene radical cation, 2 position[h, i], (29) anthracene radical cation, 9 position[h, i], (30) perylene radical anion, 1 position[h, i], (31) perylene radical anion, 2 position[h, i], (32) perylene radical anion, 3 position[h, i], (33) dibenzobiphenylene radical cation, 1 position[e], (34) dibenzobiphenylene radical cation, 5 position[e], (35) meta-dinitrobenzene, 2 position[z], (36) pyridazine radical anion, 3 position[l], (37) pyridazine radical anion, 4 position[l], (38) s-tetrazine radical anion, 3 position[m], (39) meta-dinitrobenzene, 4 position[z], (40) 1,4-diazanaphthalene radical anion, 2 position[n], (41) 1,4-diazanaphtalene radical anion, 5 position[n], (42) 1,4-diazanaphthalene radical anion, 6 position[n], (43) phthalazine radical anion, 1 position[m], (44) phthalazine radical anion, 5 position[m], (45) phthalazine radical anion, 6 position[m], (46) 1,5-diazanaphthalene radical anion, 2 position[l], (47) 1,5-diazanaphthalene radical anion, 3 position[l], (48) 1,5-diazanaphthalene radical anion, 4 position[l], (49) phenazine radical anion, 1 position[l], (50) phenazine radical anion, 2 position[l], (51) 1,4,5,8-tetraazaanthracene radical anion, 2 position[n], (52) 1,4,5,8-tetraazaanthracene radical anion, 9 position[n], (53) dihydrophyrazine radical cation, 2 position[o], (54) phenoxy radical, 2 position[p], (55) phenoxy radical, 3 position[p], (56) phenoxy radical, 4 position[p], (57) para-benzoquinone radical anion, 2 position[q, r], (58) ortho-benzoquinone radical anion, 3 position[q, s, t], (59) ortho-benzoquinone radical anion, 4 position[q, s, t], (60) 1,4-naphthoquinone radical anion, 2 position[q], (61) 1,4-naphthoquinone radical anion, 5 position[q], (62) 1,4-naphthoquinone radical anion, 6 position[q], (63) 9,10-

anthraquinone radical anion, 1 position[q], (64) 9,10-anthraquinone radical anion, 2 position[q], (65) 9,10-phenanthrenequinone radical anion, 1 position[u], (66) 9,10-phenanthrenequinone radical anion, 2 position[u], (67) 9,10-phenanthrenequinone radical anion, 3 position[u], (68) 9,10-phenanthrenequinone radical anion, 4 position[u], (69) hydroquinone radical cation, 2 position[v], (70) nitrobenzene radical anion, 2 position[w], (71) (72) nitrobenzene radical anion, 4 position[w], (73) 1-nitro-4-aminobenzene radical anion, 2 position[w], (74) 1-nitro-4-aminobenzene radical anion, 3 position[w], (75) 1-nitro-4-fluorobenzene radical anion, 2 position[y], (76) 1-nitro-4-fluorobenzene radical anion, 3 position[y], (77) 1-nitro-4-hydroxybenzene radical anion, 2 position[x], (78) 1-nitro-4-hydroxybenzene radical anion, 3 position[x], (79) cis-butadiene radical anion, 1 position[c], (80) cis-butadiene radical anion, 2 position[c], (81) phenanthrene radical anion, 1 position[i], (82) phenanthrene radical anion, 2 position[i], (83) phenanthrene radical anion, 3 position[i], (84) phenanthrene radical anion, 4 position[i], (85) phenanthrene radical anion, 9 position[i], (86) pyrene radical anion, 1 position[g], (87) pyrene radical anion, 3 position[g], (88) pyrene radical anion, 4 position[g], (89) perylene radical cation, 1 position[h, i], (90) perylene radical cation, 2 position[h, i], (91) perylene radical cation, 3 position[h, i], (92) dibenzobiphenylene radical anion, 1 position[e], (93) dibenzobiphenylene radical anion, 2 position[e], (94) dibenzobiphenylene radical anion, 5 position[e], (95) pyrazine radical

anion, 2 position[k], (96) naphthalene radical anion, 1 position[d], (97)

naphthalene radical anion, 2 position[d], (98) naphthalene radical cation,

1 position[d], (99) naphthalene radical cation, 2 position[d], (100) tetracene

radical anion, 1 position[d], (101) tetracene radical anion, 2 position[d],

(102) tetracene radical anion, 5 position[d], (103) tetracene radical cation,

1 position[d], (104) tetracene radical cation, 2 position[d], (105) tetracene

radical cation, 5 position[d].

Fig. 4.   Observed proton isotropic hyerpfine coupling constant vs. calculated $2p\pi$

orbital spin density (aa = after annihilation of quartet contamination).

Dotted line is linear least squares correlation line, constrained to origin.

Key to Figure 3 applies also to Figure 4.

References for Isotropic Hyperfine Coupling Constants

a. R. W. Fessenden and R. H. Schuler, J. Chem. Phys. 39, 2147 (1963).

b. W. T. Dixon and R. O. C. Norman, J. Chem. Soc. 1964, 4857.

c. D. H. Levy and R. J. Meyers, J. Chem. Phys. 41, 1062 (1964).

d. A. Carrington, F. Dravnieks and M. C. R. Symons, J. Chem. Soc. 1959, 947.

e. A. Carrington and J. dos Santos-Veiga, Mol. Phys. 5, 285 (1962).

f. G. J. Hoijtink, Mol. Phys. 1, 157 (1958).

g. G. J. Hoijtink, J. Townsend and S. I. Weissman, J. Chem. Phys. 34, 507 (1961).

h. J. P. Colpa and J. R. Bolton, Mol. Phys. 6, 273 (1963).

i. L. C. Snyder and T. Amos, J. Chem. Phys. 42, 3670 (1965).

j. S. H. Glarum and L. C. Snyder, J. Chem. Phys. 36, 2989 (1962).

k. N. M. Atherton, F. Gerson and J. N. Murrell, Mol. Phys. 5, 509 (1962).

l. J. C. M. Henning, J. Chem. Phys. 44, 2139 (1966).

m. E. W. Stone and A. H. Malsi, J. Chem. Phys. 39, 1635 (1963).

n. A. Carrington and J. dos Santos-Veiga, Mol. Phys. 5, 21 (1962).

o. H. M. McConnell and D. B. Chestnut, J. Chem. Phys. 27, 984 (1957).

p. W. T. Dixon and R. O. C. Norman, Proc. Chem. Soc. 1963, 97.

q. G. Vincow and G. K. Fraenkel, J. Chem. Phys. 34, 1333 (1961).

r. B. Venkataraman, B. G. Segal and G. K. Fraenkel, J. Chem. Phys. 30, 1006 (1959).

s. G. Vincow, J. Chem. Phys. 38, 917 (1963).

t. M. Adams, M. S. Blois Jr., and H. R. Sands, J. Chem. Phys. 28, 774 (1958).

u. R. Dehl and G. K. Fraenkel, J. Chem. Phys. $\underline{39}$, 1793 (1963).

v. J. R. Bolton, A. Carrington and J. dos Santos-Veiga, Mol. Phys. $\underline{5}$, 465 (1962).

w. L. H. Piette, P. Ludwig and R. N. Adams, J. Anal. Chem. Soc. $\underline{84}$, 4212 (1962).

x. K. Umemoto, Y. Deguchi and T. Fujinaga, Bull. Chem. Soc. Japan $\underline{36}$, 1539 (1963).

y. A. H. Maki and D. H. Geski, J. Am. Chem. Soc. $\underline{83}$, 1852 (1961).

z. P. H. Reiger and G. K. Fraenkel, J. Chem. Phys. $\underline{39}$, 609 (1963).

THE PATH TO MOLECULAR ORBITAL THEORY

R. S. Mulliken

Laboratory of Molecular Structure and Spectra,
Department of Physics,
University of Chicago, Chicago, Illinois 60637

ABSTRACT

The early history of the development of molecular orbital
(MO) theory is reviewed. Aided by analogies to atomic spectra
and based on evidence from molecular spectra in connection with
the old quantum theory, a classification of electronic states
of many diatomic molecules was effected early in 1926. This
classification was clarified and extended with the advent of
quantum mechanics, using the new concept of molecular orbitals
(not so named until 1932): Hund, Mulliken. The bonding power
of electrons in MOs was discussed, and with the help of the
LCAO approximation, MOs were classified as bonding or anti-
bonding. Herzberg proposed that one half the number of bonding
less half the number of antibonding electrons is equal to the
number of chemical bonds in not too polar diatomic molecules.
As an alternative to the use of general or non-localized MOs,
Hund showed the usefulness of localized σ and π MOs in des-
cribing the structures of single and multiple chemical bonds.
The close correspondence of a pair of electrons in a localized
MO to G. N. Lewis's earlier concept of an electron-pair bond is
pointed out. The 'semi-united-atom' MO concept, e.g. for N_2
and CO, is related to Langmuir's earlier description of the

structures of polyatomic molecules using non-localized MOs,
the criterion of maximum overlap in MO theory, the electro-
negativity scale, and the prediction of MO ionization potentials
are discussed briefly.

150

THE PATH TO MOLECULAR ORBITAL THEORY

By Robert S. Mulliken

In a discussion of "Fifty Years of Valence Theory", it is
necessary to go back a little further to the chemical theory
of valence developed by G. N. Lewis in 1916. The essential
features of this theory still to a considerable extent form a
useful framework for understanding the role of electrons in
chemical bonding. Lewis's theory spanned the previously un-
bridged gap between ionic valence and the kind of valence that
is typical of carbon compounds. This it accomplished by using
the idea of pairs of electrons shared either equally or
unequally between two atoms, permitting each atom either by
transfer or sharing to be surrounded by a completed electron
shell, usually of two or eight. Figure 1 summarizes the rela-
tions of Lewis's theory to earlier valence theories and to
Bohr's theory of atomic structure, and points to its relations
to the subsequent quantum-mechanical theories of molecular
electronic structure.

Lewis's theory showed electrons distributed in pairs shared
by two atoms, and in unshared "lone pairs". As I have discussed
elsewhere,[1] molecular orbital (MO) theory provides close
counterparts to Lewis's shared pairs and lone pairs if we use
localized MO's or chemical orbitals, as I have called them.

---

1. R. S. Mulliken, Science 157, 13 (1967).

In the Lewis theory, electrons in shared pairs are bonding electrons, those in lone pairs are non-bonding. In Lewis's description of coordination compounds, initially lone pairs become shared pairs. In such compounds, as also in all polar bonds, there is unequal sharing between two atoms; the same thing is true of electrons in 2-center localized MO's.

Langmuir in 1919 in extending Lewis's theory introduced the term isostere to designate molecules which have the same number of electrons and are believed to have essentially the same electronic structure as judged by their properties.[2] As examples Langmuir gave, among others, N_2, CO, CN^-; CO_2, N_2O, N_3^-, NCO^-. In particular, N_2 and CO have very similar physical properties in spite of their very different atomic composition and their very different structure in terms of early ideas of valence bonding. In retrospect, we may find here a strong hint of the need for a new type of molecular description such as MO theory now gives.

Langmuir described the structure of N_2 and CO as consisting of two K shells surrounded by a valence octet, plus what he called an "imprisoned pair".[3] Langmuir's picture of the structure of N_2 differs considerably from Lewis's (see Fig.2). In NO, there is an additional imprisoned electron.[3] Langmuir's picture of N_2 can nowadays be translated into orbital language by writing the electron configuration shown by item (1) in Fig. 3, corresponding to a "semi-united atom", with $3d\sigma^2$ as the imprisoned pair. I shall discuss this identification later. In NO, an imprisoned $3d\pi$ electron is added.

2. I. Langmuir, J. Am. Chem. Soc. 41, 868, 1543 (1919).
3. I. Langmuir, l.c. p. 901-906.

Let us now turn to Bohr's quantum theory of atomic structure and spectra in terms of electron orbits, — as further developed by Sommerfeld, Main Smith, Stoner, Pauli, Landé, and others. Although this theory met with much success in explaining atoms and the periodic system of the elements, it did not help in understanding valence except in ionic molecules. Bohr's early papers[4] included some pictures of pairs of electrons circulating in orbits to form chemical bonds, for example in H_2 and in CH_4, but these pictures led to no progress.

Nevertheless, certain features of the spectra of diatomic molecules (for example, Rydberg series of the He_2 molecule, and electronic doublets resembling those in the spectra of alkali metal atoms) pointed to the existence in molecules of electronic states and perhaps orbits more or less similar to those of atoms.[5] There was some discussion about the possibility of the interaction of electronic and nuclear-rotational angular momentum, and Kramers and Pauli[6] proposed the formula

$$E_{rot} = B(\sqrt{m^2 - \sigma^2} - \epsilon)^2 \tag{1}$$

4. See the reprinted 1913 papers with introduction and discussion by L. Rosenfeld (Benjamin, New York, 1963).

5. A. Sommerfeld, Atombau und Spektrallinien, (Friedr. Vieweg, 1924). See Chap. 9, on band spectra, in the 4th Edition. On the possibility of electronic angular momentum in molecules, see p. 743.

6. H.A. Kramers and W. Pauli,Jr., Zeits. f. Physik 13, 351 (1923).

for the nuclear rotational energy. Here $mh/2\pi$ is the total angular momentum, and $\sigma h/2\pi$ and $\epsilon h/2\pi$ are components of electron angular momentum along and perpendicular to the line joining the nuclei. Kratzer[7] interpreted empirical features of certain band spectra in terms of an electronic quantum number $\epsilon = \frac{1}{2}$ and ascribed the paramagnetism of O_2 and some features of its band spectrum to an electronic angular momentum $\sigma h/2\pi$ around the line joining the nuclei. While these particular conclusions were incorrect, they pointed the way toward later valid developments. R. Mecke[8] also made efforts to carry over the systematics of atomic spectra to diatomic molecular spectra.

It should be kept in mind that the foregoing developments occurred in the period 1923-5 before there was a clear under-standing of the nature of the various components of electronic angular momentum even in <u>atoms</u>. In particular, it was not until late 1925 and early 1926 that Uhlenbeck and Goudsmit[9] proposed that each electron has a quantized spin of $\frac{1}{2}h/2\pi$.

---

7. A. Kratzer, Naturwiss. <u>27</u>, 577 (1923), Ann. Physik. <u>71</u>, 72 (1923), and elsewhere.

8. R. Mecke, Zeits. f. Physik <u>28</u>, 261 (1924) and elsewhere.

9. S. Goudsmit and G. E. Uhlenbeck, Nature <u>117</u>, 264 (1926); Naturwiss. <u>13</u>, 953 (1925).

In 1925 I called attention to what I called "a class of one-valence-electron emitters of band spectra", one series of which includes BeF, BO, CN, CO$^+$,... while another includes MgF, AℓO, SiN,...[10] These molecules each showed three low-energy electronic levels, and I suggested that those of the first series are analogous to the levels of a sodium atom; the middle one of the levels shows a doublet structure reminiscent of ^{2}P of the Na atom, while the other two levels resemble ^{2}S levels (see Fig. 4). The analogy could be understood in terms of Langmuir's description of N$_2$ and CO if the "imprisoned pair" in these molecules is identified as analogous to the valence electrons of Mg; removing one leaves a structure like Na. Adding one makes a structure like Aℓ, with a ^{2}P normal state; actually, NO was soon found to have a ^{2}P-like normal state. Mecke also discussed some of these analogies and other relations of molecular to atomic electron levels.[11]

R. T. Birge then proposed that "the energy levels associated with the valence electrons of molecules agree in all essential aspects with those associated with the valence electrons of atoms", and proposed that the molecular levels should be given the same letter designations s, p, etc. as in atomic spectra.

In a systematic survey and analysis of available data on diatomic spectra beginning in 1926, I found that the electronic states involved could be classified as what are now called

---

10. R. S. Mulliken, Phys. Rev. 26, 561 (1925); earlier,
    Phys. Rev. 25, 290 and 26, 29 (1925).

11. R. Mecke, Naturwiss. 13, 698, 755 (1925).

$^1\Sigma$, $^1\Pi$, $^1\Delta$, $^2\Sigma$, $^2\Pi$ (with sublevels $^2\Pi_{\frac{1}{2}}$ and $^2\Pi_{3/2}$), $^3\Pi$.[12] At that time they were called ^1S, ^1P, ^1D, ^2S, ^2P, ^3P in accordance with Birge's proposal, although it was clear that in the states called P and D the symbol referred not to an atomic quantum number L but to a quantum number belonging to an electronic angular momentum component directed along the internuclear axis, corresponding to σ of the Kramers-Pauli equation.

Meanwhile quantum mechanics was discovered, and Hund in 1926-7 applied it to a detailed understanding of atoms and their spectra and of major aspects of diatomic spectra (in particular, the delineation of his well-known cases $\underline{a}$, $\underline{b}$, $\underline{c}$, $\underline{d}$).[13] He also discussed the general relations of separate-atom to diatomic electron states, with applications to BO, CN, N_2, etc. Somewhat later, Wigner and Witmer published their well-known group-theoretically derived rules for specifying the types of diatomic states derivable from two atomic states of given types.[14]

During the above-outlined developments, there was much semi-empirical groping, especially before quantum mechanics became available, but even after that it took a few years before things settled down to a point where all major important features were fairly well clarified.

12. R.S. Mulliken, Proc. Nat. Acad. Sci. 12, 144, 151, 158, 338 (1926); Phys. Rev. 28, 481, 1202 (1926) and subsequent papers in Phys. Rev.

13. F. Hund, Zeits. f. Physik. 36, 657 (1926); 40, 742 (1927); 42, 93 (1927).

14. E. Wigner and E.E. Witmer, Zeits.f.Physik. 51, 859 (1928).

Molecular orbitals, for diatomic molecules, first emerged clearly in 1928 in a paper by myself [15] and independently in one by Hund.[16] In my paper, "the essential ideas and methods were those already successfully used by Hund" in earlier papers,[13] "the chief difference being in the attempt to assign individual quantum numbers to the electrons" (that is, to specify electron configurations, analogous to those customary for atoms). The quantum number symbols used were chosen to correspond to electrons of the united-atom as modified by separating the united-atom nucleus into two. Hund's paper discussed more or less the same subject matter from more theoretical and general viewpoints.

My paper originated in an attempt to explain an important defect in the analogy of the three observed states of BO, CO^+ and CN to Na, namely this: that the $^2\Pi$ states are _inverted_ (see Fig. 4), whereas the supposedly analogous ^2P state of sodium is _normal_. Careful consideration led to (2) in Fig. 2 as the most probable electron configuration[17] for the normal states of N_2 and CO. Although because of the "non-crossing rule" the

15. R.S. Mulliken, Phys. Rev. 32, 186 (1928): The Assignment of Quantum Numbers for Electrons in Molecules. I. Later, Phys. Rev. 32, 761 (1928), on correlation of molecular and atomic electron states, and Phys. Rev. 33, 730 (1929) on diatomic hydrides.

16. F. Hund, Zeits. f. Physik. 51, 759 (1928). Later, Zeits. f. Physik. 47, 719 (1930). Hund's 1928 paper included a discussion of MO's and states of hydrides.

17. In the original paper, the configuration was written $(1s)^2(2s^p)^2(2s^s)^2(3s^p)^2(2p^p)^4(3s^s)^2$.

assignment for the last MO as $3s\sigma$ was favored, the possibility of that it is $3d\sigma$ (as suggested by the MO diagram of H_2^+) was also considered. The electrons in $2p\sigma$, $3p\sigma$, and $3s\sigma$ were called _promoted_ electrons, because they correspond to $1s$, $2s$, and $2p\sigma$ electrons of the separated atoms. The electron configurations for BO, CN, and CO^+ were now explained as corresponding to (2) of Fig. 2 less one electron from $3s\sigma$, from $2p\pi$, or from $3p\sigma$ for the normal, the first excited, and the second excited states respectively. The key point was that for the second excited, $^2\Pi$, state, the grouping $(2p\pi)^3$ explains the observed inverted character of that state.

Proceeding further, electron configurations for NO^+, NO, O_2^+, O_2, and F_2 were obtained by adding from one to four electrons in a $3p\pi$ MO. (Later it was seen that this should be $3d\pi$, not $3p\pi$.) Electron configurations for various excited states of these molecules were also assigned. The paramagnetism of O_2 was explained by the fact that _two_ electrons in a π MO yield a $^3\Sigma$, a $^1\Delta$, and a $^1\Sigma$ state, of which the $^3\Sigma$ should be the lowest "if the order of levels is as in atoms".

The current notation σ, π, δ, .. $^1\Sigma$, $^2\Pi$, .. was first introduced by Hund in his 1928 paper. The notations Σ^+ and Σ^-, σ_g and σ_u, Σ_g and Σ_u, and so on, were introduced somewhat later,[18] although the distinctions involved had already been recognized by Wigner and Witmer[14] and by Hund.

---

18. F. Hund, Ergebnisse der exakten Naturwiss. **8**, 147 (1929) and Zeits. f. Physik. **63**, 719 (1930).

My paper introduced the concept of the <u>bonding power</u> of electrons in MO's. Classically, only bonding and non-bonding electrons were distinguished. Quoting (with a few unsubstantial omissions or minor changes) "while the present work does not indicate any such sharp division, it is nevertheless possible to assign, roughly, various degrees of <u>bonding power</u> for various orbit types. For this purpose, electrons whose presence in a molecule tends to make the dissociation energy D large, or the internuclear distance r_0 small, as judged by the fact that their <u>removal</u> causes decrease in D or increase in r_0, may be said to have positive bonding power, or to be bonding electrons; and conversely." Also, "unpromoted electrons whose 'orbits' are of the order of size of r_0 show strong bonding power. Electrons in large non-penetrating orbits should be as good as ionized, and should show zero bonding power. Promoted electrons should show small or negative bonding power unless orbit size or other conditions are very favorable." The term "antibonding electrons" for those with negative bonding power was introduced only somewhat later.

In the papers just discussed, the MO concept appeared in its general form. The usefulness of the LCAO approximation in estimating the energies and bonding powers of MO's was not yet recognized. In his discussion of the resonance between HH^+ and H^+H wave functions, Pauling[19] obtained approximate wave functions

19. L. Pauling, Chem. Rev. 5, 173 (1928).

which may be considered as the prototypes of MO's approximated

in LCAO form as simple linear combinations of AO's (atomic orbitals)

of the two separate atoms involved (see $\sigma_g 1s$ and $\sigma_u 1s$ in Fig. 5).

Here $\sigma_g 1s$ and $\sigma_u 1s$ are respectively unpromoted ($\sigma_g 1s \rightarrow 1s$) and

bonding, and promoted ($\sigma_u 1s \rightarrow 2p\sigma$) and antibonding. Bloch[20]

used the LCAO method for metallic MO's.

Lennard-Jones[21] introduced the systematic use of LCAO-

approximated MO's for valence electrons, but employed these only

for bonding electrons; for example he described the structure of

N_2 as in (3) of Fig. 3, where in current notation $2p\pi$ and $2p\sigma$ are

written as $\pi_u 2p$ and $\sigma_g 2p$. These symbols refer to LCAO forms

built from separate-atom AO's as shown in Fig. 5. It is to be

understood in Fig. 5 that the AO's in any LCAO expression are

to be defined in such a way that <u>the parts which overlap</u> are

both positive. In particular, $2p\sigma_a$ and $2p\sigma_b$ are to be defined

so that that lobe of each which faces and overlaps the other is

positive.

In line (4) of Fig. 3, LCAO-MO symbols have replaced the

corresponding UA (united-atom) MO symbols in line (2) of Fig. 3.[22]

Each type of symbol embodies a rough description of the forms of

the MO's. The UA symbols are more nearly appropriate at small,

the LCAO symbols at larger, internuclear distances. Figure 5

brings out the important fact that MO's approximated by <u>additive</u>

or by <u>subtractive</u> LCAO expressions are respectively <u>bonding</u> or

<u>antibonding</u>.

---

20. F. Bloch, Zeits. f. Physik <u>52</u>, 555 (1928)

21. J.E. Lennard-Jones, Trans. Faraday Soc. <u>25</u>, 668 (1929).

22. As later became clear, $\sigma_g 2s$ and $\sigma_g 2p$ are strongly modified
     by mutual interaction (hybridization), likewise $\sigma_u 2s$ is
     modified by interaction with the unoccupied $\sigma_u 2p$.

Lennard-Jones avoided assigning electrons to antibonding MO's, for example by using atomic shells $(2s_a)^2 2s_b)^2$ in (3) of Fig. 3 instead of $(\sigma_g 2s)^2 (\sigma_u 2s)^2$. Where interactions between atomic closed shells are weak, as in the case of the two 1s shells in N_2, or in general for these and for completed octet shells like the L shells in Na_2, Lennard-Jones' practice has much to recommend it.[23] However, as applied to molecules like O_2 with incomplete MO shells, it created difficulties. Further, for strongly interacting atomic shells like the 2s shells of the N atoms in N_2, it is clearly better to replace them by corresponding MO shells containing antibonding $\sigma_u 2s$ as well as bonding $\sigma_g 2p$ MO's. Then, as proposed by Herzberg,[24] "It seems sensible to define it [the number of bonds in a molecule such as O_2 or F_2] as half the difference in the number of electrons which tighten the bonding and the number which are working in the opposite direction." In other words, half the difference in the numbers of bonding and antibonding electrons.

The electron configurations of C_2, N_2^+, N_2, O_2^+, O_2, and F_2 are all of the form given in Fig. 5. (Instead of $(\sigma_g 1s)^2 (\sigma_u 1s)^2$, the atomic-closed-shell expression $(1s_a)^2 (1s_b)^2$ can be substituted.)

---

23. However, for systematic all-electron self-consistent-field MO calculations as now carried out, it is necessary to use MO's for all the electrons.

24. G. Herzberg, Zeits. f. Physik 57, 601 (1929); Leipziger Vorträge 1931, p. 167 (S. Hirzel, Leipzig).

The σ_g and π_u MO's, of additive LCAO-approximate form, are bonding, the σ_u and π_g MO's, of subtractive form, are antibonding. (The K shell MO's of course are essentially non-bonding.) Herzberg's rule then gives for the number of bonds 2, $2\frac{1}{2}$, 3, $2\frac{1}{2}$, 2, and 1 in the respective molecules.

Herzberg's rule glosses over the fact that, especially because of hybridization,[22] different bonding or antibonding MO's differ considerably in their bonding or antibonding power, as indicated in Fig. 5, for example $\sigma_g 2s$ is very strongly bonding but $\sigma_g 2p$ only weakly bonding, while $\sigma_u 2p$ is only weakly antibonding. In general, especially when we come to the MO's in heteropolar and in polyatomic molecules, the general concept of bonding power is perhaps better than a sharp division into bonding and antibonding MO's.

Herzberg's rule can be applied not only to homopolar molecules but also to moderately heteropolar molecules, e.g., NO and CO with configurations as shown in the first line of Fig. 6, where $p = 2$, $n = 0$ for CO and $p = 2$, $q = 1$ for NO, giving 3 bonds in CO and $2\frac{1}{2}$ in NO. However, if we go to successively more polar molecules, — consider for example the series C_2, BN, BeO, LiF, — covalent bonding in the MO's becomes very weak, and in LiF (where, also, σ^*2s is replaced by $\sigma 2p$, see Fig. 6) the bonding is largely ionic. In any event, however, additive and subtractive LCAO forms $a\chi_a + b\chi_b$ and $a'\chi_a - b'\chi_a$ respectively (with $a > b$ and $a' > b'$ if a is the more electronegative of the two atoms) remain qualitatively well correlated with positive or negative bonding powers of MO's.

A comprehensive view of the forms and binding energies of MO's as a varying function of the particular nuclei involved and of the internuclear distance is obtained by use of so-called correlation diagrams. These were first introduced in simple form by Hund to show correlations between the limiting cases of united atom and two separated atoms. Figures 7 and 8 reproduce some more elaborate correlation diagrams taken from a review paper.[25] These Figures show,besides the united-atom and LCAO notations, a semi-empirical notation (see item 5 in Fig. 3) which has the advantage that it can be used equally for homopolar and heteropolar molecules (e.g., N_2 and CO, or C_2 and BeO), and can also be extended to corresponding valence-shell MO's of molecules whose atoms belong in higher rows of the periodic system. Item (6) in Fig. 3 shows still another notation introduced more recently, one that is now used in connection with systematic theoretical computations. Here the MO's of each different group-theoretical species (e.g., σ_g, σ_u, π_u) are numbered in order of decreasing binding energy.

I have now presented a variety of viewpoints and symbolisms for describing the structures of N_2 and other diatomic molecules. Let us now return to the "semi-united atom" viewpoint on N_2 as expressed in (1) of Fig. 3. First of all, in (2) or (4) of Fig. 3 the first two MO shells can very nearly exactly be replaced by $(1s_a)^2(1s_b)^2$; in (2) of Fig. 3, 2pσ is only incipiently promoted. Next, because 2pσ in (2) of Fig. 3 is essentially unpromoted, 3pσ in (2) or σ_u2s in (4) of Fig. 3 has a form which when laid out in

---

25. R.S. Mulliken, Rev. Mod. Phys. $\underline{4}$, 1 (1932). For some qualifications on the meaning of such correlation diagrams, see R.S. Mulliken, J. Am. Chem. Soc. $\underline{88}$, 1849 (1966), and for some critical comments on bonding power, see "Quantum Theory of Atoms, Molecules, Solid State", Academic Press, Inc., New York (1966), p. 231.

ir a graph is seen to closely resemble a $2p\sigma$ rather than a $3p\sigma$ AO. Similarly the form of $2s\sigma$ of (2) of Fig. 3 or $\sigma_g 2s$ of (4) of Fig. 3 after allowance for hybridization[22] is found when laid out to resemble a 2s (or equally an enlarged 1s) AO. Further, $2p\pi$ of (2) or $\pi_u 2p$ of (4) of Fig. 3 actually rather strongly resembles in form a $2p\pi$ AO. The last MO in (3), $\sigma_g 2p$ of (4), the MO occupied by Langmuir's "imprisoned pair", after allowance for hybridization, is found to strongly resemble a shrunken $3d\sigma$ AO.[26] All these resemblances have been determined by Huzinaga[27] in a comparison between the actual forms of the MO's, as determined from computer calculations, and the AO's of an atom. Further, the MO $\pi_g 2p$ in O_2^+ or O_2 in Fig. 5, — correspondingly π^*2p in NO, — shows an obvious strong resemblance to a (shrunken) $3d\pi$ AO.

The discussion so far has dealt with diatomic orbitals. As we have seen, diatomic MO's in general extend around both nuclei. In heteropolar molecules, however, even when we do not voluntarily prescribe replacement of inner-shell MO's by AO's, some of the

---

26. "Shrunken" means that it is much smaller in size than, though of similar shape to, a $3d\sigma$ AO of an N atom. This difference, here in the semi-united atom, is explained by the fact that the MO is strongly penetrating, unlike the 3d AO's of a free atom.

27. S. Huzinaga, Memoirs of the Faculty of Science, Kyusyu University, B 3, 57 (1962). See also R.S. Mulliken, Int. J. Quantum Chem. 1, 103 (1967), p. 113.

MO's <u>automatically</u> become nearly the same as AO's of one atom. For example, in LiF, the special description given in Fig. 6 is rather nearly correct, although the outer-shell MO's do all extend to an appreciable degree around the Li atom. In polyatomic molecules, automatic localization occurs to a varying extent, from slight to complete, in some of the MO's. Also, while fully <u>non-localized</u> or "best" MO's which spread at least to some slight extent over all atoms, give the most accurate electronic structure description, we can arbitrarily impose various kinds of transformations or constraints to obtain useful approximate localized MO descriptions which correlate instructively with the older valence theory. However, in the case of conjugated and aromatic so-called π-electron molecules, as Hückel showed,[28] the use of nonlocalized MO's in LCAO approximation is desirable even for approximate calculations.

Nevertheless in molecules whose bonds can be well expressed by simple classical dot or dash formulas, electrons in non-localized bonding MO's form a useful counterpart. This type of representation was developed by Hund.[29] Each MO is approximated as an LCAO expression $\lambda\psi_a + \mu\psi_b$ which is applicable to polar $(\lambda \neq \mu)$ as well as to homopolar bonds $(\lambda = \mu)$; the ψ's here are AO's of the two atoms. I believe that the placing of two electrons in such a localized MO represents the best quantum-mechanical counterpart for a Lewis electron pair bond.[30]

28. E. Hückel, Zeits. f. Physik 70, 204 (1931).

29. F. Hund, Zeits. f. Physik 73, 1 (1931); 73, 565 (1932).

30. For maximum accuracy, somewhat modified AO's (MAO's) must be used; R. S. Mulliken, J. Am. Chem. Soc. 88, 1849 (1966); Science 157, 13 (1967).

Hund classified these localized bond MO's under two types, σ and π. Single bonds are always σ bonds (structure σ^2), in which the AO's involved may be s, pσ, or q, where q is some s, pσ hybrid. They are approximately cylindrically symmetrical, which accounts for "free rotation"; in linear molecules, they are _exactly_ cylindro-symmetric. Triple bonds are cylindrosymmetric, of structure $\sigma^2\pi^4$. Double bonds are of structure $\sigma^2\pi^2$ and involve a plane of symmetry which prevents free rotation. Empirically, they are never of structure $\sigma^2\sigma^2$.[31]

The symbol π referred originally to a two-fold degenerate MO in a linear (at first a diatomic) molecule; it embraces two independent MO's which may be taken in the linear case as π^+ and π^- or as π_x and π_y. In Hund's description of unsaturated and aromatic molecules, it refers to just one, say π_x, of these two orbitals. This use of the same symbol for a degenerate and for a non-degenerate MO is unfortunate. A new symbol, say τ, really should be introduced for the non-degenerate type of π.

In his papers on chemical bonding, Hund showed how the observed shapes of various molecules, for example H_2O and NH_3, that were first explained by Slater and Pauling using valence-bond-theory, can be explained just as well in terms of MO's.

---

31. An interesting case is that of C_2 (Fig. 5 with p = q = 0) where the bonding is essentially π^4 (the net effect of $\sigma_g 2s^2 \sigma_u 2s^2$ is approximately non-bonding).

In a series of papers entitled "Electronic Structures of Polyatomic Molecules and Valence,"[32] I assigned electron configurations using nonlocalized MO's expressed in LCAO approximation to a considerable variety of types of molecules (especially, CH_2, C_2H_4, CH_4, NH_3, H_2O, C_2H_6, C_2H_2, H_2CO, CO_2, $HgCl_2$, and derivatives and analogues of these). I proposed the name <u>orbital</u> as an abbreviation for one-electron orbital wave function in the second of these papers. Following a suggestion by Van Vleck, I used group-theoretical methods in classifying the MO's; I adopted a system of MO species symbols similar to one used by Placzek for classifying molecular vibrations. I used various other less formal symbols to indicate the approximate forms of the MO's and their relations to AO's or to MO's of constituent groups or radicals. I also gave interpretations of electronic spectra in terms of MO excitations.

I called attention to the applicability in LCAO MO theory of the criterion of maximum overlap of AO's, first used by Slater and Pauling in the AO form of valence-bond theory, as a measure of the bonding power of a MO. (Later, I pursued this idea further in papers on "Overlap integrals and chemical binding".)[33]

---

32. R. S. Mulliken, Phys. Rev. 40, 55 (1932); 49, 751 (1932); 43, 279 (1933); J. Chem. Phys. 1, 492 (1933); 3, 375, 506, 514, 517, 564, 573, 586, 635, 720 (1935).

33. R. S. Mulliken, J. Am. Chem. Soc. 72, 4493 (1950); J. Chem. Phys. 19, 900, 912 (1951).

In these and related papers,[34] I set up and applied a
new electronegativity scale. In setting up this scale, I made
use of a criterion first stated by Hund,[35] also of the idea
of "valence states", first proposed by Van Vleck.[36] I ap-
plied LCAO MO theory to show the relation of this scale to
Pauling's electronegativity scale, and to give a theoretical
derivation of the latter, I also set forth relations of the
polarity coefficients in LCAO-MO's to charges on the atoms
participating in a bond, and to dipole moments. (Later[37]
I developed these ideas further in a "population analysis"
which used overlap populations as measures of bonding power,
and used atomic populations to yield charges on atoms.)

---

34. R. S. Mulliken, J. Chem. Phys. $\underline{2}$, 782 (1935,; Phys. Rev.
     $\underline{46}$, 549 (1934); Phys. Rev. $\underline{47}$, 413 (1935).

35. On p. 17 of (29) Hund pointed out that for strongest inter-
     action of the AO's in a localized LCAO-MO, the terms of
     the electrons in the two atoms should not be very different,
     "and this means not that the ionization energies should be
     approximately equal, but that the average between atomic
     term and ionic term" [that is, of ionization energy and
     electron affinity] should be about the same for the two atoms.

36. J. H. Van Vleck, J. Chem. Phys. $\underline{2}$, 22 (1934).

37. R. S. Mulliken, J. Chem. Phys. $\underline{23}$, 1833, 1840, 2338, 2343
     (1955).

168

I made estimates of polarity coefficients as a basis for
conclusions as to bonding. For example, in molecules CX_4,
the MO structure may be written as $1s_C{}^2[2s]^2[2p]^6 \cdots$, where
the dots refer to MO's largely restricted to the X atoms, and
the symbols [2s] and [2p] refer to 2s-like and 2p-like non-
localized bonding MO's. At one extreme, probably approached in
CI_4, the [s] MO's have very strong C^-X^+ polarity and so are
almost unshared 2s carbon AO's, while the [p] MO's are nearly
homopolar and strongly bonding, so that the four C—X bonds of
classical valence theory are provided almost entirely by three
pairs of [p] electrons. At the other extreme, as in CF_4
(better, SiF_4), the [s] orbitals are nearly homopolar and give
strong covalent bonding while the [p] orbitals have strong R^+A^-
polarity so that their bonding is to a large extent heteropolar.

I made approximate predictions of ionization potentials (I)
on the basis of the specification $I > (I_a^o + I_b^o)/2$ for two-center
bonding MO's, $I < (I_a^o + I_b^o)/2$ for antibonding MO's, and $I \approx I^*$
for non-bonding MO's (lone-pair or nearly lone-pair orbitals,
localized more or less on one atom or on a set of equivalent
atoms); here I^o and I^* refer to appropriate valence-state AO's.
The rules just given must be modified to allow for charge
transfer. For example, in volts, for the lone-pair MO's in
HI, HBr, and HCl, the I^* values are 10.38, 12.28, and 13.62,
the corresponding I values are 9.28, 10.55, and 11.48. In all
HX, $I < I^*$ corresponding to charge transfer in the sense H^+X^-,

increasing in the series from HI to HCℓ.[38] Similar comparisons hold for CH_3X and C_2H_5X.

---

38. See especially J. Chem. Phys. $\underline{3}$, 515 (1935), but with I values here considerably changed, to current reliable values. The I* values above are also subject to some correction.

FIG. 1.   Historical Flow Diagram of Ideas Leading to MO and AO
Theories of Molecular Electronic Structure, and on to
Accurate Wave Functions.

171

:N::N:
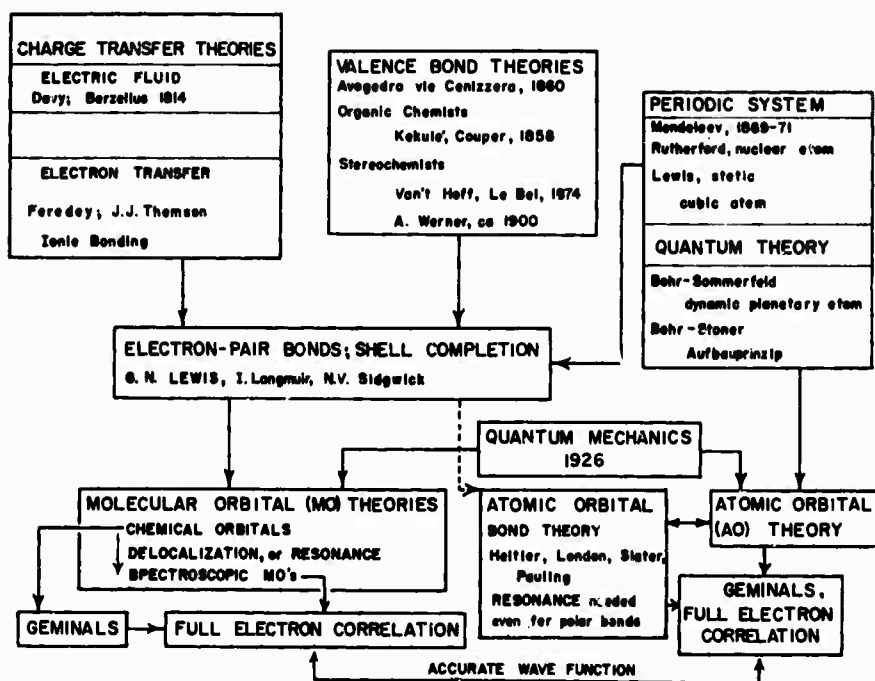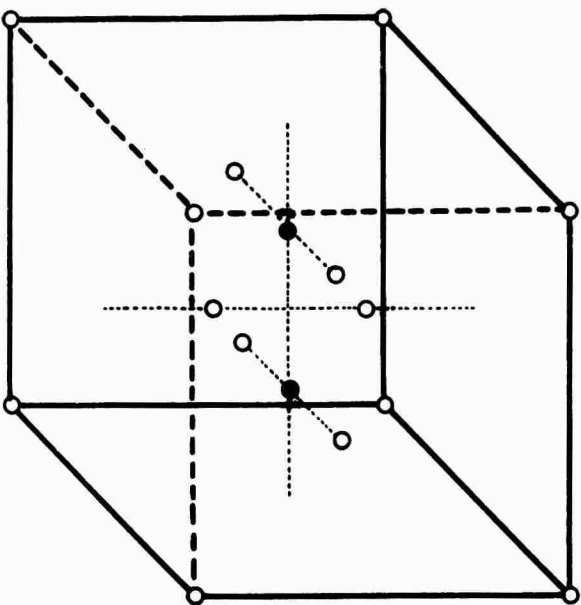
LEWIS

LANGMUIR

Models of the N₂ Molecule (CO similar)

FIG. 2. Models of the N₂ molecule (CO similar)

FIG. 3. ELECTRON CONFIGURATION OF N_2

(1) Semi-united Atom: $(1s)^2(1s)^2(2s)^2(2p\sigma)^2(2p\pi)^4(3d\sigma)^2$

(2) United-Atom: $(1s\sigma)^2(2p\sigma)^2(2s\sigma)^2(3p\sigma)^2(2p\pi)^4(3s\sigma \text{ or } 3d\sigma)^2$

(3) Lennard-Jones[*] $(1s)^2(1s)^2(2s)^2(2s)^2(2p\pi)^4(2p\sigma)^2$

(4) Rough LCAO[†] $(\sigma_g 1s)^2(\sigma_u 1s)^2(\sigma_g 2s)^2(\sigma_u 2s)^2(\pi_u 2p)^4(\sigma_g 2p)^2$

(5) Semi-Empirical: $(kz\sigma)^2(ky\sigma)^2(z\sigma)^2(y\sigma)^2(w\pi)^4(x\sigma)^2$

(6) Formal MO: $(1\sigma_g)^2(1\sigma_u)^2(2\sigma_g)^2(2\sigma_u)^2(1\pi_u)^4(3\sigma_g)^2$

[*]Lennard-Jones' $2p\pi$ and $2p\sigma$ mean the same as $\pi_u 2p$ and $\sigma_g 2p$.

[†]Mutual hybridization modifies $\sigma_g 2s$ and $\sigma_g 2p$; likewise $\sigma_u 2s$ and $\sigma_u 2p$.
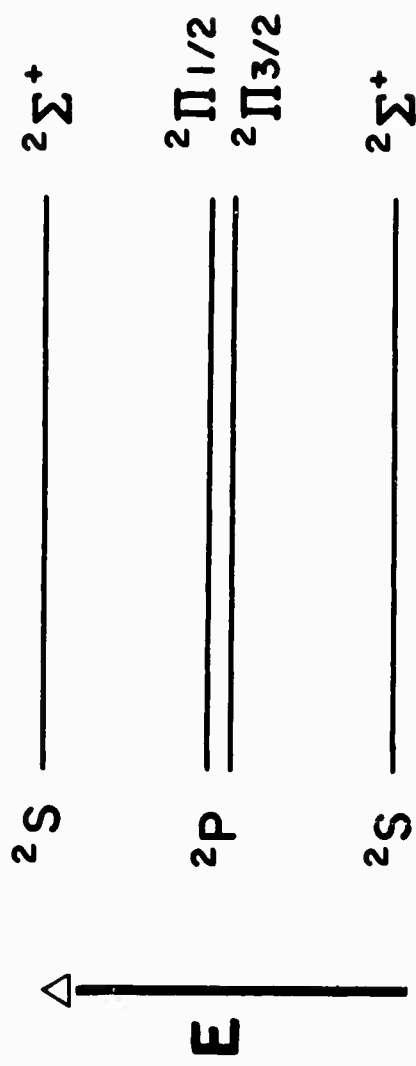
Electronic levels of BO
(old notation at left, current notation at right)

FIG. 5. ELECTRON CONFIGURATIONS AND BONDING
(HOMOPOLAR MOLECULES)

Rough LCAO: $(\sigma_g 1s)^2(\sigma_u 1s)^2(\sigma_g 2s)^2(\sigma_u 2p)^2(\pi_u 2p)^4(\sigma_g 2p)^p(\pi_g 2p)^q(\sigma_u 2p)^r$

n: $\sigma_g 1s = 1s_a + 1s_b$ n: $\sigma_u 1s = 1s_a - 1s_b$

BB: $\sigma_g 2s = 2s_a + 2s_b$ a: $\sigma_u 2s = 2s_a - 2s_b$

B: $\pi_u 2p = 2p\pi_a + 2p\pi_b$ A: $\pi_g 2p = 2p\pi_a - 2p\pi_b$

b: $\sigma_g 2p = 2p\sigma_a + 2p\sigma_b$ AA: $\sigma_u 2p = 2p\sigma_a - 2p\sigma_b$

$\acute{n}$ = nonbonding; b, B, BB = bonding; a, A, AA = antibonding

In C_2, $p = q = 0$; in N_2, O_2, F_2, $p = 2$; in O_2, F_2, $q = 2, 4$

175

FIG. 6.   HETEROPOLAR MOLECULES

General: $(1s_a)^2(1s_b)^2(\sigma 2s)^2(\sigma *2s)^2(\pi 2p)^4(\sigma 2p)^P(\pi *2p)^q(\sigma *2p)^0$

LiF: $(1s_F)^2(1s_{Li})^2(2s_F)^2(2p\sigma_F)^2(2p\pi_F)^4$ nearly

176

FIG. 7. Binding scheme of electron orbits for molecules whose nuclei are of the same element. Neither the abscissas ξ (distance between nuclei divided by mean diameter of electron orbit) nor the ordinates (negative energy of ionization of the electron) are plotted or a uniform scale, as will be seen from the figure. Also, from the nature of the figure, it is not possible for either ordinates or abscissas, especially the former, to have a quantitative significance. The ordinates on the right are, however, proportional to the logarithms of the binding energies of electrons in the N atom, except for the 2s level which has been arbitrarily shifted downward. Those on the left, except 2s, are proportional to a function of the logarithms of the binding energies of electrons in the Si atom, which is the united-atom corresponding to N₂. Thus the diagram is especially suited to the N₂ molecule, but is also satisfactory in a somewhat more qualitative way for other molecules. The thin lines going upward and to the left indicate roughly for various molecules the actual ξ values of various orbits, for stable molecular states. From these lines, the qualitative order of binding of orbit-types in each molecule can be seen, and at least a rough idea can often be obtained of the relative energy-differences between different orbit-types.

Fig 8 Binding scheme of electron orbits for molecules with nuclei of moderately unequal charge. The figure is in most respects like Fig. 7 The ordinates on the right are proportional to the logarithms of the binding energies of electrons in the O atom (lower 1s, 2s, 2p, etc.) and in the C atom (upper 1s, 2s, 2p, etc.), those on the left correspond to the united-atom Si in the same way as in Fig. 7 The figure is qualitatively fairly correct also for other molecules composed of atoms which do not differ too much in the numbers and nature of their outer electrons.

178

A PREDISPERSER SYSTEM AND ORDER-SORTER FOR USE WITH A PLANE
GRATING SPECTROGRAPH[*]

by

David W. Green

Laboratory of Molecular Structure and Spectra
Department of Physics, University of Chicago
Chicago, Illinois   60637

A PREDISPERSER SYSTEM AND ORDER-SORTER FOR USE WITH A PLANE
GRATING SPECTROGRAPH

Table of Contents

D. W. Green
February 2, 1970

180

INTRODUCTION

In order to maximize the dispersion of a plane grating spectrograph, a high grating angle and corresponding high order must be employed. The visible spectrum is typically covered in 15th through 9th order of the grating. It is desirable for the high-resolution analysis of complex moleular spectra to eliminate all overlapping orders and photograph exclusively one order. It is difficult to find filters that will transmit only the range of wavelengths corresponding to one-free spectral range without seriously attenuating the wavelengths of interest. To adequately accomplish order separation over the entire photographic spectral region would require an enormous number of filters.

The predisperser system described here provides a convenient and versatile method for passing a wavelength region into the spectrograph with little attenuation while eliminating those wavelengths outside the free-spectral range.

The free-spectral range, the range of wavelengths without overlap from other orders, is approximately

$$\Delta\lambda = \frac{\lambda^2}{d} \left(\sin \theta + \sin \vartheta \right) = \frac{\lambda}{n} \tag{1}$$

where d is the grating spacing; θ and ϑ are the angle of incidence and diffraction, respectively and n, the grating order. In order to pass one free-spectral range into the spectrograph for any wavelength, it is desirable to have a predisperser whose dispersion is proportional to the inverse of the free-spectral range, $1/\lambda^2$. Since a grating's dispersion is roughly independent of λ, a prism, which has a dispersion approximately proportional to $1/\lambda^3$ in the visible spectral region, more nearly fulfills the requirement.

181

PELLIN-BROCA PRISM

It has been shown[2] that a quadrilateral prism of the Pellin-Broca type[3] can be mounted and rotated so as to remain in the position of minimum deviation for any wavelength. This prism provides a dispersing element for a predisperser which is superior to a triangular prism[1] since the source need not be moved to change the central wavelength entering the spectrograph at minimum deviation of the prism.

Fig. 1 shows that path of collimated light entering the prism on the X-axis and exiting on the Y-axis for two different wavelengths. Point R is the point of rotation[2] of the prism. The X-axis, Y-axis and the point R are fixed.

For the fused silica prism used here the refractive index as a function of wavelength is known.[4] The incident angle, θ_1, for which a wavelength, λ_o, will exit the prism at right angles is given by

$$\theta_1 = \arcsin[n(\lambda_o)/2] \tag{2}$$

where $n(\lambda_o)$ is the refrective index at λ_o. The reciprocal linear dispersion of a predisperser system using this prism is

$$\frac{d\lambda}{dx} = \frac{\sqrt{1-(n/2)^2}}{f \cdot (dn/d\lambda)} \tag{3}$$

where f is the focal length of the exit lens.

The Appendix tabulates the properties from 2000 to 8000 Å for the predisperser system described.
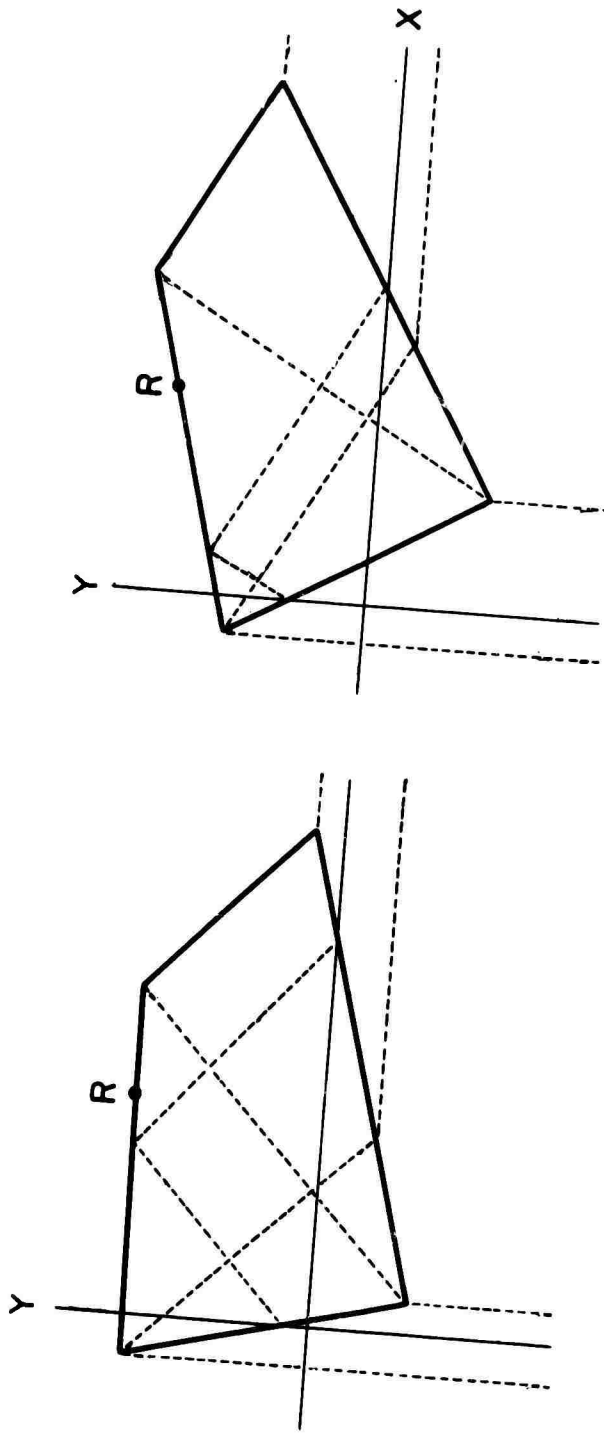
Fig. I. ROTATION OF THE PELLIN-BROCA PRISM

PREDISPERSER DESIGN

Fig. 2 shows the elements of the predisperser assembly:
holders for an entrance slit, a collimating lens, a Pellin-Broca
prism and an exit lens. Fig. 3 shows a photograph of the entire
assembled predisperser system.

The predisperser slit is a calibrated unilateral slit on a
cylindrical mount which fits the slit assembly of Fig. 2. The
slit may then be rotated relative to the vertical axis. A cali-
bration on the mount allows the rotation to be measured to one
degree accuracy. The slit width is accurate to about 3 μm.

A spherical, ultra-violet grade fused silica lens of focal
length 10 cm is used as the collimating lens. Its holder moves
on the X-axis (see Fig. 1) on a small calibrated optical bench.

The Pellin-Broca prism is Corning 7940 fused silica with
2.54 cm faces, and is 5.0 cm on its longest side. It is mounted
with small adjustable stops on a circular rotating table. The
angle of incidence is calibrated and can be read to about 0.2°.
The exact prism position is determined experimentally as dis-
cussed later. The rotation is controlled and measured by a
vernier parallel to and below the Y-axis. A vertical bar from
the rotating prism table extends downward. A second bar at right
angles to the first extends parallel to the X-Y plane beneath
the optical axes to the vernier.

A cylindrical, ultra-violet grade fused silica lens of focal
length 10 cm is used as the exit lens. The lens is held in a
cylindrical mount which fits the holder of Fig. 2 such that the
lens will rotate about the Y-axis to match the tilt, if any, of
the spectrograph entrance slit. The entire exit lens assembly
is adjustable along the Y-axis and is calibrated.

The entire predisperser assembly is mounted on an optical
bench extending from the spectrograph along the Y-axis.

SLIT HOLDER

COLLIMATING
LENS HOLDER

PRISM
TABLE

PELLIN-BROCA
PRISM

EXIT LENS
HOLDER
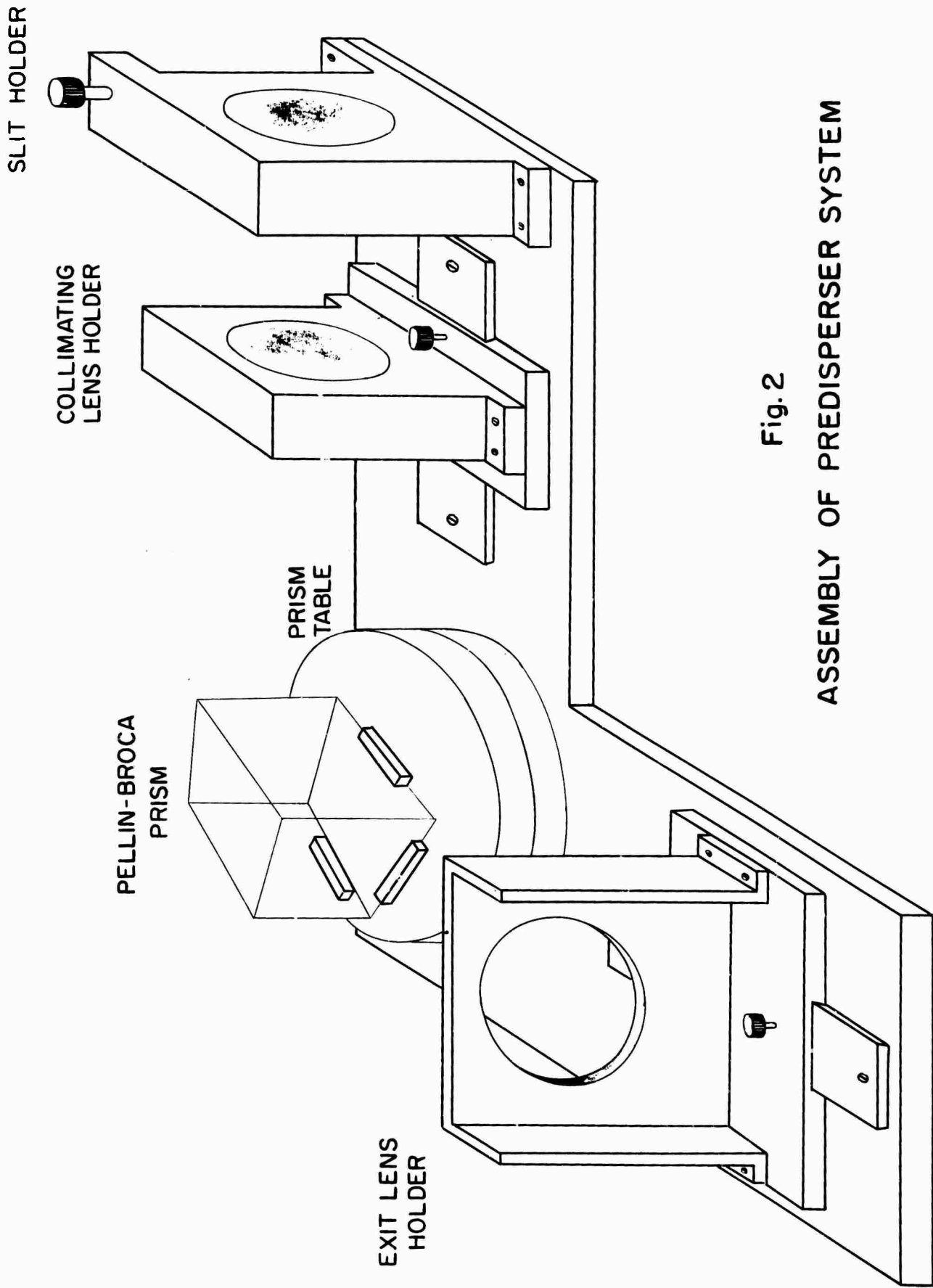
Fig.2

ASSEMBLY OF PREDISPERSER SYSTEM
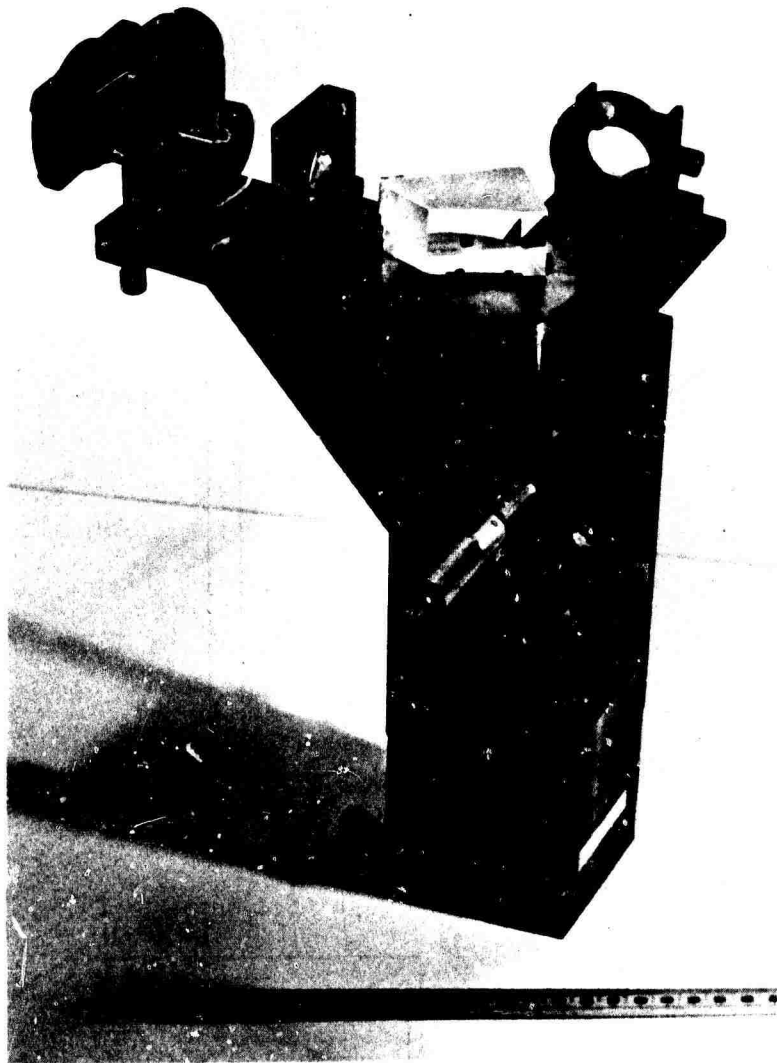
FIG. 3. THE ASSEMBLED PREDISPERSER SYSTEM

ALIGNMENT AND CALIBRATION

The Y-axis is defined by the line from the center of the collimating mirror through the entrance slit of the spectrograph. The predisperser was placed with the cylindrical lens on this axis. The X-axis is determined experimentally by directing a He/Ne laser beam along the Y-axis from inside the spectrograph. The prism is rotated such that the beam exits the center of the predisperser slit with the spherical lens removed. For the Pellin-Broca prism, the X-axis is at right angles to the Y-axis. The spherical lens is then centered on the X-axis so that it collimates light from the predisperser entrance slit.

The rotation of the predisperser slit was determined by temporarily replacing the cylindrical lens with a spherical lens of the same diameter and focal length. The slit was rotated so that the image of the slit illuminated by monochromatic light was parallel to the spectrograph slit.

The cylindrical lens was centered on the Y-axis again so that it focused light at the spectrograph slit and it was rotated so that the image of the predisperser slit illuminated with monochromatic light was parallel to the spectrograph slit.

In order to locate the prism on the rotating table, the laser is used in the manner described above. Small aperature stops with 1 mm diameter holes were placed on the lenses and predisperser slit, so that only light from the laser on the axes passed through the predisperser system. Light from a mercury discharge tube was passed through a monochromator to select the 4358 Å line, and then was passed into the masked predisperser system along the X-axis. The prism was rotated until the light beam exited through the aperature of the masked cylindrical lens. If the prism is properly positioned, the light will be focused on the spectrograph slit. Small adjustments in

187

the prism position were made until light from both the laser
line and mercury line were on the predisperser axes with the
proper prism rotation.

The lens positions on the X and Y-axes will be small func-
tions of wavelength, since they are not achromatic. Except for
this adjustment, no change of source or predisperser other than
prism rotation is required to change the central wavelength
entering the spectrograph.

The prism rotation can be calculated from Eq. (2) for any
desired wavelength. However, the exact position is better deter-
mined experimentally because $(d\lambda/d\theta)$ is so large. An experimen-
tal calibration was obtained for wavelength regions of interest
by using a thorium discharge tube as a light source and exposing
photographic plates at different prism positions.

OPERATION

Define the following quantities for a given prism rotation:

S = reciprocal linear dispersion of the system;

D_P = predisperser slit width;

D_J = spectrograph slit width;

λ_o = wavelength centered on Y-axis;

$\Phi_{max}(\lambda)$ = maximum possible useful light flux passing
into spectrograph at wavelength λ;

$\Phi(\lambda)$ = actual flux passing into spectrograph at wavelength
λ for a particular arrangement of slits.

Assume S is a constant over the wavelength range of interest.

The fraction of flux passing through the predisperser that is useful at any wavelength (i.e. is incident upon the spectrograph collimator), is given by the ratio of the f/-numbers of the predisperser and spectrograph. The f/-numbers of the predisperser is smaller than that of the spectrograph. The maximum useful flux is obtained at any wavelength when the image of the predisperser slit illiminates the entire spectrograph slit. Φ/Φ_{max} is approximately a linear function of λ when the predisperser slit image does not illuminate the entire spectrograph slit.

Three general cases may now be considered: (a) $D_P = D_J$; (b) $D_J < D_P$ and (c) $D_J > D_P$. The flux ratio, Φ/Φ_{max}, for each of these cases is plotted in Fig. 4 (a), (b) and (c), respectively. For minimum exposure times with the spectrograph, one would operate with $D_J < D_P$.

If F is the f/-number of the spectrograph, then the spectrograph slit width is chosen on the basis of resolution considerations.[5]

$$D_J = \lambda_o \cdot F \tag{4}$$

This choice leaves the predisperser slit width as the independent variable affecting the performance of the predisperser.

$$\lambda_2 = \lambda_0 - S \cdot (D_P + D_J) / 2$$

$$\lambda_3 = \lambda_0 - S \cdot (D_P - D_J) / 2$$

$$\lambda_4 = \lambda_0 - S \cdot (D_J - D_P) / 2$$
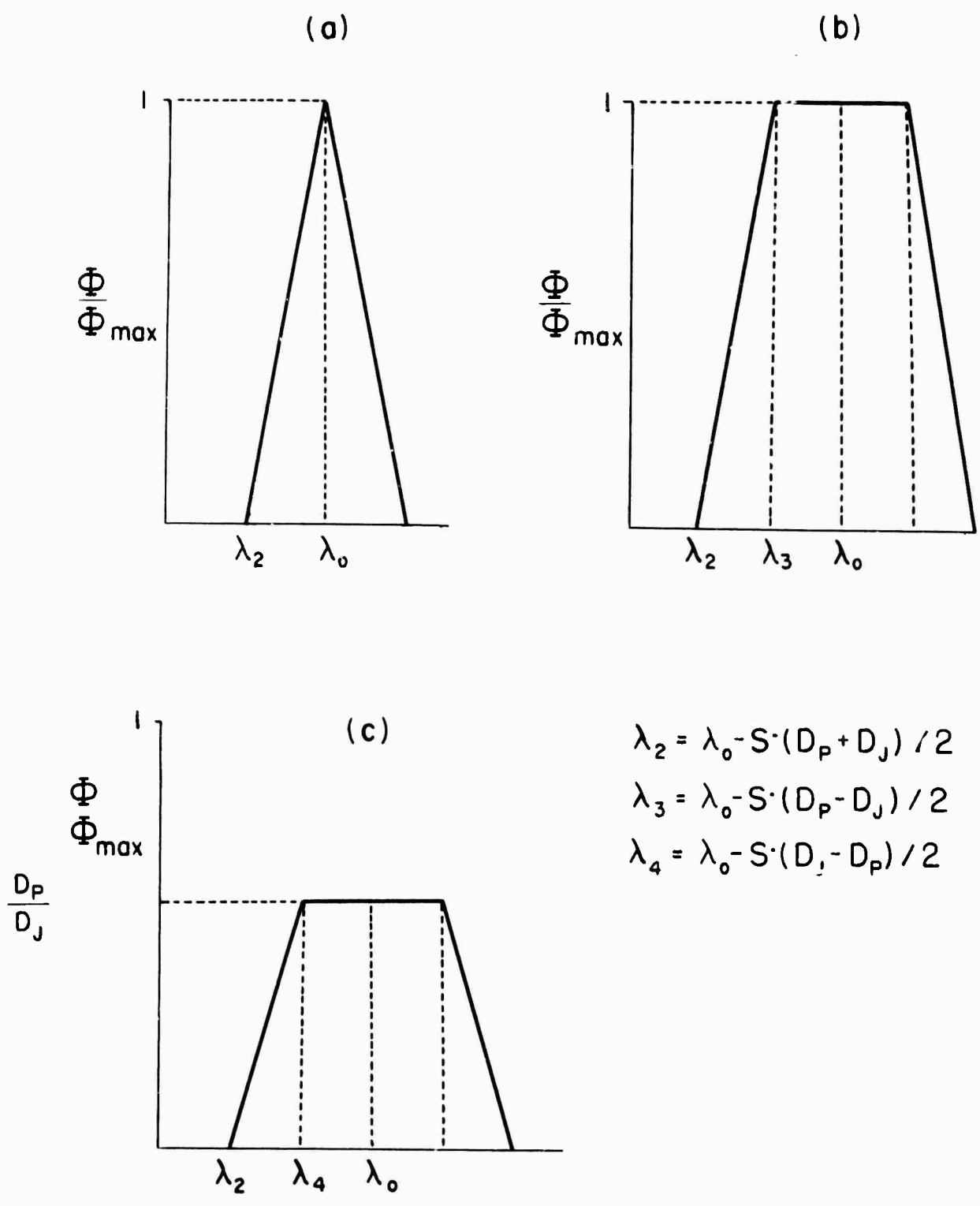
Fig. 4. RELATIVE FLUX PASSING INTO SPECTROGRAPH:
(a) $D_J = D_P$; (b) $D_J < D_P$; (c) $D_J > D_P$

190

For molecular spectra analysis one would typically want to pass into the spectrograph an unattenuated range of wavelengths from 20 to 150 Å. So the predisperser slit width is large compared to the spectrograph slit width determined by Eq. (4), and the relative flux distribution of Fig. 4 (b) closely approaches a step function. The predisperser slit width for such an application is given as

$$D_P = \frac{\Delta\lambda}{S} + D_J \tag{5}$$

where $\Delta\lambda$ is the unattenuated range of wavelengths.

USE AS AN ORDER-SORTER

An order-sorter provides a vertical dispersion at the spectrograph slit, so that in one photographic plate exposure, different grating orders appear displaced vertically. Some order-sorters have previously been described[1,6] for applications in atomic spectroscopy and Fabry-Perot interferometry.

The predisperser system described here is easily adapted for use as an order-sorter by tilting the predisperser slit and cylindrical lenses relative to the spectrograph slit. Lines from different orders of the spectrograph will appear at different heights on the plate, and will either overlap or be entirely separated. The following considerations allow one to choose the scheme of order sorting most suited to a particular application.

The tilt of the predisperser slit determines the vertical separation between orders on the plate. Its width determines the vertical height of the lines of each order which is prescribed by the desired spacing between lines of different orders or the degree of overlapping of different orders. The number of orders which can be simultaneously photographed is limited by the predisperser dispersion and ℓ_{max}.

The maximum useful slit heigth, ℓ_{max}, depends on the method of illuminating the spectrograph slit.[7] For the predisperser system described vertical filling of the Ebert spectrograph collimator is done with a fused silica cylindrical lens placed at the spectrograph slit with its axis perpendicular to the slit. The limiting vertical aperture is the length of the grating grooves, ℓ_g. To a good approximation

$$\ell_{max} = f_v \cdot \ell_g / (F_c - f_v) \qquad (6)$$

where f_v is the cylindrical lens focal length and F_c is the collimator focal length. For the predisperser in combination with the f/35 Ebert spectrograph of this laboratory, ℓ_{max} is about 10 mm.

For other method of spectrograph illumination Eq. (6) will be somewhat different.

If h is the desired vertical separation between the central wavelength of consecutive orders, then the angle of tilt of the predisperser slit, θ_p, relative to the spectrograph slit is given approximately by

$$\sin \theta_p = \frac{\lambda_o}{h \cdot n_o} \cdot \frac{1}{(d\lambda/dx)_o} \qquad (7)$$

Eq. (7) is accurate only at the central wavelength, λ_o, of the predisperser since both the free-spectral range and the reciprocal linear dispersion are functions of λ. In general, h is approximately proportional to n.

The predisperser slit width is chosen to control the overlapping of orders. If L is the desired image length, then

$$D_P = \frac{L \sin \theta_P}{M} \qquad (8)$$

M is the magnification (=1 for the system described) of the predisperser.

193

REFERENCES

1. Joseph Reader, Louis C. Marquet and Sumner P. Davis, Appl. Opt. $\underline{2}$, 963 (1963).

2. W. E. Forsythe, Astrophys. J., $\underline{45}$, 278 (1917).

3. M. Pellin and A. Broca, J. de Phys. $\underline{8}$, 314 (1899).

4. I. H. Malitson J. Opt. Soc. Am. $\underline{44}$, 1205 (1965); B. Brixner, J. Opt. Soc. Am. $\underline{57}$, 654 (1967).

5. Ralph A. Sawyer, <u>Experimental Spectroscopy</u>, 3rd ed., Dover Publications, New York, 1963.

6. R. F. Jarrell, J. Opt. Soc. Am. $\underline{45}$, 259 (1955).

7. G. R. Harrison, R. C. Lord and J. R. Loofbourow, <u>Practical Spectroscopy</u>, Prentice-Hall, Inc., New York, 1948, p. 126.

APPENDIX: PREDISPERSER PROPERTIES

Using the known refractive index of fused silica as a function of wavelength[4] we may derive the following formulas:

$$n = (1 + a_1 \cdot z/b_1 + a_3 \cdot z/b_2 + a_5 \cdot z/b_4) \qquad (A1)$$

where

$$z = \lambda^2 \ (\lambda \text{ in } \mu m) \qquad a_1 = 0.6961663$$

$$b_1 = z - a_2 \qquad a_2 = (0.0684043)^2$$

$$b_2 = z - a_4 \qquad a_3 = 0.4079426$$

$$b_3 = z - a_6 \qquad a_4 = (0.1162414)^2$$

$$a_5 = 0.8975794$$

$$a_6 = (9.896161)^2$$

From Eq. (2)

$$\theta = \arcsin(n/2) \qquad (A2)$$

$$dn/d\lambda = -(\lambda/n) \cdot (a_1 \cdot a_2/b_1^2 + a_3 \cdot a_4/b_2^2 + a_5 \cdot a_6/b_3^2 \qquad (A3)$$

$$d\lambda/d\theta = 2 \cdot \sqrt{1 - (n/2)^2} \ /(dn/d\lambda) \qquad (A4)$$

From Eq. (3)

$$d\lambda/dx = (d\lambda/d\theta)/2 \cdot f \qquad (A5)$$

The focal length, f, was treated as a function of wavelength.

The results of calculating (A1) through (A5) for the predisperser system described as a function of wavelength are tabulated for 2000 to 8000 Å. Also included is the focal length of the two fused silica lenses as a function of wavelength for

195

a focal length of 100.0 mm at 5890 Å. The lenses are moved to their proper positions for any central wavelength of the pre-disperser.

$$f_\lambda = f_{5890} \cdot \left(\frac{n_{5890} - 1}{n_\lambda - 1}\right) \qquad (A6)$$

ACKNOWLEDGEMENT

λ (Å)	n	θ ° '	$(dn/d\lambda)$ μm^{-1}	$(d\lambda/d\theta)$ (Å/min)	$(d\lambda/dx)$ (Å/mm)
2000	1.55051	50 49.7	-1.3514	-2.72	46.74
2010	1.54917	50 46.0	-1.3216	-2.78	47.86
2020	1.54786	50 42.5	-1.2927	-2.85	48.99
2030	1.54658	50 39.0	-1.2648	-2.92	50.13
2040	1.54533	50 35.6	-1.2377	-2.98	51.29
2050	1.54411	50 32.3	-1.2114	-3.05	52.46
2060	1.54291	50 29.1	-1.1860	-3.12	53.65
2070	1.54174	50 25.9	-1.1613	-3.19	54.85
2080	1.54059	50 22.8	-1.1374	-3.26	56.07
2090	1.53946	50 19.8	-1.1142	-3.33	57.30
2100	1.53836	50 16.8	-1.0916	-3.41	58.54
2110	1.53728	50 13.9	-1.0697	-3.48	59.80
2120	1.53622	50 11.1	-1.0485	-3.55	61.07
2130	1.53518	50 8.3	-1.0278	-3.63	62.36
2140	1.53416	50 5.5	-1.0078	-3.70	63.66
2150	1.53316	50 2.9	-0.9883	-3.78	64.98
2160	1.53219	50 0.3	-0.9693	-3.86	66.31
2170	1.53123	49 57.7	-0.9508	-3.94	67.66
2180	1.53028	49 55.2	-0.9329	-4.02	69.02
2190	1.52936	49 52.7	-0.9154	-4.10	70.39
2200	1.52845	49 50.3	-0.8984	-4.18	71.78
2210	1.52756	49 47.9	-0.8819	-4.26	73.19
2220	1.52669	49 45.6	-0.8658	-4.34	74.61
2230	1.52583	49 43.3	-0.8501	-4.42	76.05
2240	1.52499	49 41.1	-0.8348	-4.51	77.50
2250	1.52416	49 38.9	-0.8199	-4.59	78.97
2260	1.52335	49 36.7	-0.8054	-4.68	80.45
2270	1.52255	49 34.6	-0.7913	-4.77	81.95
2280	1.52177	49 32.5	-0.7775	-4.86	83.46
2290	1.52099	49 30.5	-0.7640	-4.94	84.99
2300	1.52024	49 28.5	-0.7509	-5.03	86.54
2310	1.51949	49 26.5	-0.7381	-5.13	88.10
2320	1.51876	49 24.6	-0.7256	-5.22	89.67
2330	1.51804	49 22.7	-0.7134	-5.31	91.27
2340	1.51733	49 20.8	-0.7015	-5.40	92.87
2350	1.51664	49 19.0	-0.6898	-5.50	94.50
2360	1.51595	49 17.2	-0.6785	-5.59	96.14
2370	1.51528	49 15.4	-0.6674	-5.69	97.79
2380	1.51462	49 13.7	-0.6566	-5.79	99.46
2390	1.51397	49 11.9	-0.6460	-5.88	101.15
2400	1.51333	49 10.3	-0.6357	-5.98	102.86
2410	1.51270	49 8.6	-0.6255	-6.08	104.58
2420	1.51208	49 7.0	-0.6157	-6.18	106.31
2430	1.51147	49 5.4	-0.6060	-6.29	108.07
2440	1.51086	49 3.8	-0.5966	-6.39	109.83
2450	1.51027	49 2.2	-0.5873	-6.49	111.62
2460	1.50969	49 0.7	-0.5783	-6.60	113.42
2470	1.50912	48 59.2	-0.5694	-6.70	115.24
2480	1.50855	48 57.7	-0.5608	-6.81	117.08
2490	1.50799	48 56.3	-0.5523	-6.92	118.93

λ (Å)	n	θ ° '	(dn/dλ) μm⁻¹	(dλ/dθ) (Å/min)	(dλ/dx) (Å/mm)
2500	1.50745	48 54.8	-0.5440	-7.03	120.80
2510	1.50691	48 53.4	-0.5359	-7.14	122.69
2520	1.50637	48 52.0	-0.5280	-7.25	124.59
2530	1.50585	48 50.7	-0.5202	-7.36	126.51
2540	1.50533	48 49.3	-0.5126	-7.47	128.45
2550	1.50482	48 48.0	-0.5051	-7.59	130.40
2560	1.50432	48 46.7	-0.4978	-7.70	132.37
2570	1.50383	48 45.4	-0.4907	-7.82	134.36
2580	1.50334	48 44.1	-0.4837	-7.93	136.36
2590	1.50286	48 42.9	-0.4768	-8.05	138.39
2600	1.50239	48 41.6	-0.4700	-8.17	140.43
2610	1.50192	48 40.4	-0.4634	-8.29	142.49
2620	1.50146	48 39.2	-0.4570	-8.41	144.56
2630	1.50101	48 38.0	-0.4506	-8.53	146.65
2640	1.50056	48 36.9	-0.4444	-8.65	148.76
2650	1.50012	48 35.7	-0.4383	-8.78	150.89
2660	1.49968	48 34.6	-0.4323	-8.90	153.04
2670	1.49925	48 33.5	-0.4265	-9.03	155.20
2680	1.49883	48 32.4	-0.4207	-9.16	157.38
2690	1.49841	48 31.3	-0.4150	-9.28	159.58
2700	1.49800	48 30.2	-0.4095	-9.41	161.80
2710	1.49759	48 29.2	-0.4041	-9.54	164.03
2720	1.49719	48 28.1	-0.3987	-9.67	166.29
2730	1.49680	48 27.1	-0.3935	-9.81	168.56
2740	1.49641	48 26.1	-0.3883	-9.94	170.85
2750	1.49602	48 25.1	-0.3833	-10.07	173.16
2760	1.49564	48 24.1	-0.3783	-10.21	175.48
2770	1.49526	48 23.1	-0.3735	-10.35	177.83
2780	1.49489	48 22.2	-0.3687	-10.48	180.19
2790	1.49453	48 21.2	-0.3640	-10.62	182.57
2800	1.49416	48 20.3	-0.3594	-10.76	184.97
2810	1.49381	48 19.4	-0.3548	-10.90	187.39
2820	1.49345	48 18.5	-0.3504	-11.04	189.83
2830	1.49311	48 17.6	-0.3460	-11.19	192.28
2840	1.49276	48 16.7	-0.3417	-11.33	194.76
2850	1.49242	48 15.8	-0.3375	-11.48	197.25
2860	1.49209	48 14.9	-0.3333	-11.62	199.76
2870	1.49176	48 14.1	-0.3293	-11.77	202.29
2880	1.49143	48 13.2	-0.3253	-11.92	204.84
2890	1.49111	48 12.4	-0.3213	-12.07	207.41
2900	1.49079	48 11.6	-0.3174	-12.22	210.00
2910	1.49047	48 10.8	-0.3136	-12.37	212.60
2920	1.49016	48 10.0	-0.3099	-12.52	215.23
2930	1.48985	48 9.2	-0.3062	-12.68	217.87
2940	1.48955	48 8.4	-0.3026	-12.83	220.54
2950	1.48925	48 7.6	-0.2990	-12.99	223.22
2960	1.48895	48 6.8	-0.2955	-13.14	225.92
2970	1.48865	48 6.1	-0.2921	-13.30	228.65
2980	1.48836	48 5.3	-0.2887	-13.46	231.39
2990	1.48808	48 4.6	-0.2853	-13.62	234.15

λ (Å)	n	θ °	θ '	$(dn/d\lambda)$ μm^{-1}	$(d\lambda/d\theta)$ (Å/min)	$(d\lambda/dx)$ (Å/mm)
3000	1.48779	48	3.9	-0.2821	-13.78	236.93
3010	1.48751	48	3.1	-0.2788	-13.95	239.73
3020	1.48724	48	2.4	-0.2757	-14.11	242.55
3030	1.48696	48	1.7	-0.2725	-14.28	245.39
3040	1.48669	48	1.0	-0.2694	-14.44	248.25
3050	1.48642	48	0.3	-0.2664	-14.61	251.13
3060	1.48616	47	59.7	-0.2634	-14.78	254.03
3070	1.48590	47	59.0	-0.2605	-14.95	256.95
3080	1.48564	47	58.3	-0.2576	-15.12	259.89
3090	1.48538	47	57.7	-0.2548	-15.29	262.85
3100	1.48513	47	57.0	-0.2520	-15.47	265.83
3110	1.48488	47	56.4	-0.2492	-15.64	268.82
3120	1.48463	47	55.7	-0.2465	-15.82	271.84
3130	1.48438	47	55.1	-0.2438	-15.99	274.88
3140	1.48414	47	54.5	-0.2412	-16.17	277.94
3150	1.48390	47	53.9	-0.2386	-16.35	281.02
3160	1.48366	47	53.3	-0.2360	-16.53	284.12
3170	1.48343	47	52.7	-0.2335	-16.71	287.24
3180	1.48320	47	52.1	-0.2310	-16.89	290.39
3190	1.48297	47	51.5	-0.2286	-17.08	293.55
3200	1.48274	47	50.9	-0.2262	-17.26	296.73
3210	1.48251	47	50.3	-0.2238	-17.45	299.93
3220	1.48229	47	49.7	-0.2215	-17.64	303.16
3230	1.48207	47	49.2	-0.2191	-17.83	306.40
3240	1.48185	47	48.6	-0.2169	-18.02	309.66
3250	1.48164	47	48.1	-0.2146	-18.21	312.95
3260	1.48142	47	47.5	-0.2124	-18.40	316.26
3270	1.48121	47	47.0	-0.2103	-18.59	319.58
3280	1.48100	47	46.5	-0.2081	-18.79	322.93
3290	1.48080	47	45.9	-0.2060	-18.98	326.30
3300	1.48059	47	45.4	-0.2039	-19.18	329.69
3310	1.48039	47	44.9	-0.2019	-19.38	333.10
3320	1.48019	47	44.4	-0.1998	-19.58	336.53
3330	1.47999	47	43.9	-0.1978	-19.78	339.99
3340	1.47979	47	43.4	-0.1959	-19.98	343.46
3350	1.47960	47	42.9	-0.1939	-20.18	346.95
3360	1.47940	47	42.4	-0.1920	-20.39	350.47
3370	1.47921	47	41.9	-0.1901	-20.60	354.01
3380	1.47902	47	41.4	-0.1883	-20.80	357.57
3390	1.47884	47	40.9	-0.1864	-21.01	361.15
3400	1.47865	47	40.4	-0.1846	-21.22	364.75
3410	1.47847	47	40.0	-0.1828	-21.43	368.37
3420	1.47829	47	39.5	-0.1811	-21.64	372.02
3430	1.47811	47	39.0	-0.1793	-21.86	375.68
3440	1.47793	47	38.6	-0.1776	-22.07	379.37
3450	1.47775	47	38.1	-0.1759	-22.29	383.08
3460	1.47758	47	37.7	-0.1742	-22.50	386.81
3470	1.47740	47	37.3	-0.1726	-22.72	390.56
3480	1.47723	47	36.8	-0.1710	-22.94	394.34
3490	1.47706	47	36.4	-0.1693	-23.16	398.13

λ (Å)	n	θ ° '	(dn/dλ) μm⁻¹	(dλ/dθ) (Å/min)	(dλ/dx) (Å/mm)
3500	1.47689	47 36.0	-0.1678	-23.38	401.95
3510	1.47672	47 35.5	-0.1662	-23.61	405.79
3520	1.47656	47 35.1	-0.1647	-23.83	409.65
3530	1.47640	47 34.7	-0.1631	-24.06	413.54
3540	1.47623	47 34.3	-0.1616	-24.29	417.44
3550	1.47607	47 33.9	-0.1601	-24.51	421.37
3560	1.47591	47 33.5	-0.1587	-24.74	425.32
3570	1.47575	47 33.1	-0.1572	-24.97	429.29
3580	1.47560	47 32.7	-0.1558	-25.21	433.28
3590	1.47544	47 32.3	-0.1544	-25.44	437.30
3600	1.47529	47 31.9	-0.1530	-25.68	441.33
3610	1.47514	47 31.5	-0.1516	-25.91	445.39
3620	1.47499	47 31.1	-0.1503	-26.15	449.47
3630	1.47484	47 30.7	-0.1489	-26.39	453.58
3640	1.47469	47 30.3	-0.1476	-26.63	457.70
3650	1.47454	47 30.0	-0.1463	-26.87	461.85
3660	1.47440	47 29.6	-0.1450	-27.11	466.02
3670	1.47425	47 29.2	-0.1437	-27.36	470.21
3680	1.47411	47 28.9	-0.1425	-27.60	474.43
3690	1.47397	47 28.5	-0.1412	-27.85	478.67
3700	1.47383	47 28.1	-0.1400	-28.10	482.93
3710	1.47369	47 27.8	-0.1388	-28.34	487.21
3720	1.47355	47 27.4	-0.1376	-28.60	491.51
3730	1.47341	47 27.1	-0.1364	-28.85	495.84
3740	1.47328	47 26.7	-0.1352	-29.10	500.19
3750	1.47314	47 26.4	-0.1340	-29.35	504.56
3760	1.47301	47 26.1	-0.1329	-29.61	508.96
3770	1.47288	47 25.7	-0.1318	-29.87	513.37
3780	1.47274	47 25.4	-0.1307	-30.13	517.81
3790	1.47261	47 25.1	-0.1296	-30.38	522.28
3800	1.47248	47 24.7	-0.1285	-30.65	526.76
3810	1.47236	47 24.4	-0.1274	-30.91	531.27
3820	1.47223	47 24.1	-0.1263	-31.17	535.80
3830	1.47210	47 23.8	-0.1253	-31.44	540.36
3840	1.47198	47 23.5	-0.1242	-31.70	544.93
3850	1.47186	47 23.1	-0.1232	-31.97	549.53
3860	1.47173	47 22.8	-0.1222	-32.24	554.15
3870	1.47161	47 22.5	-0.1212	-32.51	558.80
3880	1.47149	47 22.2	-0.1202	-32.78	563.47
3890	1.47137	47 21.9	-0.1192	-33.05	568.16
3900	1.47125	47 21.6	-0.1182	-33.33	572.87
3910	1.47113	47 21.3	-0.1173	-33.60	577.61
3920	1.47102	47 21.0	-0.1163	-33.88	582.37
3930	1.47090	47 20.7	-0.1154	-34.16	587.15
3940	1.47079	47 20.4	-0.1145	-34.44	591.95
3950	1.47067	47 20.1	-0.1136	-34.72	596.78
3960	1.47056	47 19.9	-0.1127	-35.00	601.63
3970	1.47045	47 19.6	-0.1118	-35.29	606.51
3980	1.47034	47 19.3	-0.1109	-35.57	611.40
3990	1.47023	47 19.0	-0.1100	-35.86	616.32

λ (Å)	n	θ °	θ '	(dn/dλ) μm^{-1}	(dλ/dθ) (Å/min)	(dλ/dx) (Å/mm)
4000	1.47012	47	18.7	-0.1091	-36.14	621.27
4010	1.47001	47	18.5	-0.1083	-36.43	626.23
4020	1.46990	47	18.2	-0.1074	-36.72	631.22
4030	1.46979	47	17.9	-0.1066	-37.01	636.24
4040	1.46969	47	17.6	-0.1058	-37.31	641.27
4050	1.46958	47	17.4	-0.1049	-37.60	646.33
4060	1.46948	47	17.1	-0.1041	-37.90	651.41
4070	1.46937	47	16.8	-0.1033	-38.19	656.52
4080	1.46927	47	16.6	-0.1025	-38.49	661.65
4090	1.46917	47	16.3	-0.1018	-38.79	666.80
4100	1.46907	47	16.1	-0.1010	-39.09	671.97
4110	1.46897	47	15.8	-0.1002	-39.40	677.17
4120	1.46887	47	15.6	-0.0995	-39.70	682.39
4130	1.46877	47	15.3	-0.0987	-40.01	687.64
4140	1.46867	47	15.1	-0.0980	-40.31	692.91
4150	1.46857	47	14.8	-0.0972	-40.62	698.20
4160	1.46847	47	14.6	-0.0965	-40.93	703.51
4170	1.46838	47	14.3	-0.0958	-41.24	708.85
4180	1.46828	47	14.1	-0.0951	-41.55	714.21
4190	1.46819	47	13.8	-0.0944	-41.86	719.59
4200	1.46809	47	13.6	-0.0937	-42.18	725.00
4210	1.46800	47	13.4	-0.0930	-42.49	730.43
4220	1.46791	47	13.1	-0.0923	-42.81	735.89
4230	1.46782	47	12.9	-0.0916	-43.13	741.36
4240	1.46772	47	12.7	-0.0910	-43.45	746.86
4250	1.46763	47	12.4	-0.0903	-43.77	752.39
4260	1.46754	47	12.2	-0.0896	-44.09	757.93
4270	1.46745	47	12.0	-0.0890	-44.42	763.50
4280	1.46737	47	11.8	-0.0883	-44.74	769.10
4290	1.46728	47	11.5	-0.0877	-45.07	774.71
4300	1.46719	47	11.3	-0.0871	-45.40	780.35
4310	1.46710	47	11.1	-0.0865	-45.73	786.02
4320	1.46702	47	10.9	-0.0859	-46.06	791.71
4330	1.46693	47	10.7	-0.0852	-46.39	797.42
4340	1.46685	47	10.5	-0.0846	-46.73	803.15
4350	1.46676	47	10.2	-0.0840	-47.06	808.91
4360	1.46668	47	10.0	-0.0835	-47.40	814.69
4370	1.46660	47	9.8	-0.0829	-47.73	820.49
4380	1.46651	47	9.6	-0.0823	-48.07	826.31
4390	1.46643	47	9.4	-0.0817	-48.41	832.16
4400	1.46635	47	9.2	-0.0811	-48.76	838.04
4410	1.46627	47	9.0	-0.0806	-49.10	843.93
4420	1.46619	47	8.8	-0.0800	-49.44	849.85
4430	1.46611	47	8.6	-0.0795	-49.79	855.80
4440	1.46603	47	8.4	-0.0789	-50.14	861.76
4450	1.46595	47	8.2	-0.0784	-50.48	867.75
4460	1.46587	47	8.0	-0.0779	-50.83	873.76
4470	1.46580	47	7.8	-0.0773	-51.18	879.80
4480	1.46572	47	7.6	-0.0768	-51.54	885.86
4490	1.46564	47	7.4	-0.0763	-51.89	891.94

λ (Å)	n	θ ° '	(dn/dλ) μm^{-1}	(dλ/dθ) (Å/min)	(dλ/dx) (Å/mm)
4500	1.46557	47 7.2	-0.0758	-52.25	898.05
4510	1.46549	47 7.0	-0.0753	-52.60	904.17
4520	1.46542	47 6.8	-0.0748	-52.96	910.33
4530	1.46534	47 6.6	-0.0743	-53.32	916.5C
4540	1.46527	47 6.5	-0.0738	-53.68	922.70
4550	1.46519	47 6.3	-C.0733	-54.04	928.92
4560	1.46512	47 6.1	-C.0728	-54.41	935.16
4570	1.46505	47 5.9	-G.0723	-54.77	941.43
4580	1.46498	47 5.7	-0.0718	-55.14	947.72
4590	1.46490	47 5.5	-0.0714	-55.50	954.03
4600	1.46483	47 5.4	-0.0709	-55.87	960.37
4610	1.46476	47 5.2	-0.0704	-56.24	966.73
4620	1.46469	47 5.0	-0.0700	-56.61	973.11
4630	1.46462	47 4.8	-0.0695	-56.99	979.51
4640	1.46455	47 4.7	-C.0691	-57.36	985.94
4650	1.46448	47 4.5	-0.0686	-57.74	992.39
4660	1.46442	47 4.3	-0.0682	-58.11	998.87
4670	1.46435	47 4.1	-0.0677	-58.49	1C05.36
4680	1.46428	47 4.0	-C.0673	-58.87	1C11.88
4690	1.46421	47 3.8	-0.0669	-59.25	1018.42
4700	1.46415	47 3.6	-C.0665	-59.63	1024.99
4710	1.46408	47 3.5	-0.0660	-60.01	1C31.58
4720	1.46401	47 3.3	-C.0656	-60.40	1038.19
4730	1.46395	47 3.1	-0.0652	-60.79	1C44.82
4740	1.46388	47 3.0	-C.0648	-61.17	1051.48
4750	1.46382	47 2.8	-C.0644	-61.56	1058.15
4760	1.46375	47 2.6	-C.0640	-61.95	1064.86
4770	1.46369	47 2.5	-C.0636	-62.34	1C71.58
4780	1.46363	47 2.3	-C.0632	-62.73	1078.32
4790	1.46356	47 2.2	-C.0628	-63.13	1085.09
48C0	1.46350	47 2.0	-C.0624	-63.52	1091.89
4810	1.46344	47 1.8	-0.0620	-63.92	1098.70
4820	1.46338	47 1.7	-C.0617	-64.32	1105.54
4830	1.46332	47 1.5	-C.0613	-64.72	1112.39
4840	1.46326	47 1.4	-C.0609	-65.12	1119.27
4850	1.46319	47 1.2	-C.0605	-65.52	1126.18
4860	1.46313	47 1.1	-C.0602	-65.92	1133.10
4870	1.46307	47 0.9	-G.0598	-66.33	1140.05
4880	1.463C1	47 0.8	-C.0594	-66.73	1147.C2
4890	1.46296	47 0.6	-C.0591	-67.14	1154.01
4900	1.46290	47 0.5	-C.0587	-67.55	1161.03
4910	1.46284	47 0.3	-C.0584	-67.96	1168.07
4920	1.46278	47 0.2	-C.0580	-68.37	1175.12
4930	1.46272	47 0.0	-C.0577	-68.78	1182.2C
4940	1.46266	46 59.9	-C.0573	-69.19	1189.31
4950	1.46261	46 59.7	-C.0570	-69.61	1196.43
4960	1.46255	46 59.6	-C.0567	-70.02	1203.58
4970	1.46249	46 59.5	-C.0563	-70.44	1210.75
4980	1.46244	46 59.3	-C.0560	-70.86	1217.94
4990	1.46238	46 59.2	-C.0557	-71.28	1225.15

λ (Å)	n	θ ° '	(dn/dλ) μm⁻¹	(dλ/dθ) (Å/min)	(dλ/dx) (Å/mm)
5000	1.46233	46 59.0	-0.0554	-71.70	1232.38
5010	1.46227	46 58.9	-0.0550	-72.12	1239.64
5020	1.46222	46 58.8	-0.0547	-72.54	1246.92
5030	1.46216	46 58.6	-0.0544	-72.97	1254.21
5040	1.46211	46 58.5	-0.0541	-73.39	1261.53
5050	1.46205	46 58.4	-0.0538	-73.82	1268.88
5060	1.46200	46 58.2	-0.0535	-74.25	1276.24
5070	1.46195	46 58.1	-0.0532	-74.68	1283.62
5080	1.46189	46 57.9	-0.0529	-75.11	1291.03
5090	1.46184	46 57.8	-0.0526	-75.54	1298.46
5100	1.46179	46 57.7	-0.0523	-75.97	1305.91
5110	1.46174	46 57.6	-0.0520	-76.41	1313.38
5120	1.46168	46 57.4	-0.0517	-76.84	1320.87
5130	1.46163	46 57.3	-0.0514	-77.28	1328.38
5140	1.46158	46 57.2	-0.0511	-77.72	1335.91
5150	1.46153	46 57.0	-0.0508	-78.16	1343.47
5160	1.46148	46 56.9	-0.0505	-78.60	1351.04
5170	1.46143	46 56.8	-0.0502	-79.04	1358.64
5180	1.46138	46 56.7	-0.0500	-79.49	1366.25
5190	1.46133	46 56.5	-0.0497	-79.93	1373.89
5200	1.46128	46 56.4	-0.0494	-80.38	1381.55
5210	1.46123	46 56.3	-0.0491	-80.82	1389.23
5220	1.46118	46 56.2	-0.0489	-81.27	1396.93
5230	1.46113	46 56.0	-0.0486	-81.72	1404.65
5240	1.46108	46 55.9	-0.0483	-82.17	1412.39
5250	1.46104	46 55.8	-0.0481	-82.62	1420.15
5260	1.46099	46 55.7	-0.0478	-83.07	1427.93
5270	1.46094	46 55.6	-0.0476	-83.53	1435.73
5280	1.46089	46 55.4	-0.0473	-83.98	1443.55
5290	1.46085	46 55.3	-0.0471	-84.44	1451.40
5300	1.46080	46 55.2	-0.0468	-84.90	1459.26
5310	1.46075	46 55.1	-0.0466	-85.35	1467.14
5320	1.46071	46 55.0	-0.0463	-85.81	1475.04
5330	1.46066	46 54.8	-0.0461	-86.28	1482.96
5340	1.46061	46 54.7	-0.0458	-86.74	1490.90
5350	1.46057	46 54.6	-0.0456	-87.20	1498.87
5360	1.46052	46 54.5	-0.0453	-87.66	1506.85
5370	1.46048	46 54.4	-0.0451	-88.13	1514.85
5380	1.46043	46 54.3	-0.0449	-88.60	1522.87
5390	1.46039	46 54.2	-0.0446	-89.06	1530.91
5400	1.46034	46 54.0	-0.0444	-89.53	1538.97
5410	1.46030	46 53.9	-0.0442	-90.00	1547.04
5420	1.46026	46 53.8	-0.0439	-90.47	1555.14
5430	1.46021	46 53.7	-0.0437	-90.95	1563.26
5440	1.46017	46 53.6	-0.0435	-91.42	1571.39
5450	1.46012	46 53.5	-0.0433	-91.89	1579.55
5460	1.46008	46 53.4	-0.0430	-92.37	1587.72
5470	1.46004	46 53.3	-0.0428	-92.85	1595.92
5480	1.46000	46 53.2	-0.0426	-93.32	1604.13
5490	1.45995	46 53.1	-0.0424	-93.80	1612.36

203

λ (Å)	n	θ ° '	(dn/dλ) μm⁻¹	(dλ/dθ) (Å/min)	(dλ/dx) (Å/mm)
5500	1.45991	46 53.0	-0.0422	-94.28	1620.61
5510	1.45987	46 52.9	-0.0420	-94.76	1628.87
5520	1.45983	46 52.7	-0.0418	-95.25	1637.16
5530	1.45979	46 52.6	-0.0415	-95.73	1645.46
5540	1.45974	46 52.5	-0.0413	-96.21	1653.79
5550	1.45970	46 52.4	-0.0411	-96.70	1662.13
5560	1.45966	46 52.3	-0.0409	-97.18	1670.49
5570	1.45962	46 52.2	-0.0407	-97.67	1678.86
5580	1.45958	46 52.1	-0.0405	-98.16	1687.26
5590	1.45954	46 52.0	-0.0403	-98.65	1695.67
5600	1.45950	46 51.9	-0.0401	-99.14	1704.10
5610	1.45946	46 51.8	-0.0399	-99.63	1712.55
5620	1.45942	46 51.7	-0.0397	-100.12	1721.02
5630	1.45938	46 51.6	-0.0395	-100.62	1729.50
5640	1.45934	46 51.5	-0.0393	-101.11	1738.00
5650	1.45930	46 51.4	-0.0392	-101.61	1746.52
5660	1.45926	46 51.3	-0.0390	-102.10	1755.05
5670	1.45922	46 51.2	-0.0388	-102.60	1763.61
5680	1.45918	46 51.1	-0.0386	-103.10	1772.18
5690	1.45915	46 51.0	-0.0384	-103.60	1780.76
5700	1.45911	46 50.9	-0.0382	-104.10	1789.37
5710	1.45907	46 50.8	-0.0380	-104.60	1797.99
5720	1.45903	46 50.7	-0.0379	-105.11	1806.63
5730	1.45899	46 50.7	-0.0377	-105.61	1815.28
5740	1.45896	46 50.6	-0.0375	-106.11	1823.95
5750	1.45892	46 50.5	-0.0373	-106.62	1832.64
5760	1.45888	46 50.4	-0.0371	-107.13	1841.34
5770	1.45884	46 50.3	-0.0370	-107.63	1850.06
5780	1.45881	46 50.2	-0.0368	-108.14	1858.80
5790	1.45877	46 50.1	-0.0366	-108.65	1867.55
5800	1.45873	46 50.0	-0.0365	-109.16	1876.32
5810	1.45870	46 49.9	-0.0363	-109.67	1885.10
5820	1.45866	46 49.8	-0.0361	-110.18	1893.90
5830	1.45863	46 49.7	-0.0360	-110.70	1902.72
5840	1.45859	46 49.6	-0.0358	-111.21	1911.55
5850	1.45855	46 49.6	-0.0356	-111.72	1920.40
5860	1.45852	46 49.5	-0.0355	-112.24	1929.26
5870	1.45848	46 49.4	-0.0353	-112.76	1938.14
5880	1.45845	46 49.3	-0.0351	-113.27	1947.03
5890	1.45841	46 49.2	-0.0350	-113.79	1955.93
5900	1.45838	46 49.1	-0.0348	-114.31	1964.86
5910	1.45834	46 49.0	-0.0347	-114.83	1973.79
5920	1.45831	46 48.9	-0.0345	-115.35	1982.75
5930	1.45827	46 48.8	-0.0344	-115.87	1991.71
5940	1.45824	46 48.8	-0.0342	-116.40	2000.69
5950	1.45821	46 48.7	-0.0341	-116.92	2009.69
5960	1.45817	46 48.6	-0.0339	-117.44	2018.70
5970	1.45814	46 48.5	-0.0338	-117.97	2027.72
5980	1.45810	46 48.4	-0.0336	-118.49	2036.76
5990	1.45807	46 48.3	-0.0335	-119.02	2045.81

λ (Å)	n	θ (°)	(′)	$(dn/d\lambda)$ μm^{-1}	$(d\lambda/d\theta)$ (Å/min)	$(d\lambda/dx)$ (Å/mm)
6000	1.45804	46	48.3	−0.0333	−119.55	2054.88
6010	1.45800	46	48.2	−0.0332	−120.08	2063.96
6020	1.45797	46	48.1	−0.0330	−120.61	2073.05
6030	1.45794	46	48.0	−0.0329	−121.14	2082.16
6040	1.45791	46	47.9	−0.0327	−121.67	2091.28
6050	1.45787	46	47.8	−0.0326	−122.20	2100.42
6060	1.45784	46	47.8	−0.0325	−122.73	2109.56
6070	1.45781	46	47.7	−0.0323	−123.26	2118.72
6080	1.45778	46	47.6	−0.0322	−123.80	2127.90
6090	1.45774	46	47.5	−0.0320	−124.33	2137.08
6100	1.45771	46	47.4	−0.0319	−124.87	2146.28
6110	1.45768	46	47.4	−0.0318	−125.40	2155.49
6120	1.45765	46	47.3	−0.0316	−125.94	2164.72
6130	1.45762	46	47.2	−0.0315	−126.48	2173.96
6140	1.45759	46	47.1	−0.0314	−127.01	2183.20
6150	1.45755	46	47.0	−0.0312	−127.55	2192.47
6160	1.45752	46	47.0	−0.0311	−128.09	2201.74
6170	1.45749	46	46.9	−0.0310	−128.63	2211.02
6180	1.45746	46	46.8	−0.0308	−129.17	2220.32
6190	1.45743	46	46.7	−0.0307	−129.71	2229.63
6200	1.45740	46	46.6	−0.0306	−130.26	2238.95
6210	1.45737	46	46.6	−0.0305	−130.80	2248.28
6220	1.45734	46	46.5	−0.0303	−131.34	2257.62
6230	1.45731	46	46.4	−0.0302	−131.89	2266.98
6240	1.45728	46	46.3	−0.0301	−132.43	2276.34
6250	1.45725	46	46.3	−0.0300	−132.98	2285.72
6260	1.45722	46	46.2	−0.0298	−133.52	2295.11
6270	1.45719	46	46.1	−0.0297	−134.07	2304.51
6280	1.45716	46	46.0	−0.0296	−134.62	2313.92
6290	1.45713	46	46.0	−0.0295	−135.17	2323.33
6300	1.45710	46	45.9	−0.0294	−135.71	2332.76
6310	1.45707	46	45.8	−0.0292	−136.26	2342.20
6320	1.45704	46	45.8	−0.0291	−136.81	2351.65
6330	1.45701	46	45.7	−0.0290	−137.36	2361.11
6340	1.45698	46	45.6	−0.0289	−137.92	2370.58
6350	1.45695	46	45.5	−0.0288	−138.47	2380.06
6360	1.45693	46	45.5	−0.0287	−139.02	2389.55
6370	1.45690	46	45.4	−0.0286	−139.57	2399.05
6380	1.45687	46	45.3	−0.0284	−140.12	2408.56
6390	1.45684	46	45.2	−0.0283	−140.68	2418.08
6400	1.45681	46	45.2	−0.0282	−141.23	2427.61
6410	1.45678	46	45.1	−0.0281	−141.79	2437.14
6420	1.45676	46	45.0	−0.0280	−142.34	2446.69
6430	1.45673	46	45.0	−0.0279	−142.90	2456.24
6440	1.45670	46	44.9	−0.0278	−143.45	2465.80
6450	1.45667	46	44.8	−0.0277	−144.01	2475.37
6460	1.45664	46	44.8	−0.0276	−144.57	2484.95
6470	1.45662	46	44.7	−0.0275	−145.13	2494.54
6480	1.45659	46	44.6	−0.0274	−145.68	2504.13
6490	1.45656	46	44.5	−0.0273	−146.24	2513.73

λ (Å)	n	θ ° '	(dn/dλ) μm⁻¹	(dλ/dθ) (Å/min)	(dλ/dx) (Å/mm)
6500	1.45653	46 44.5	-0.0272	-146.80	2523.34
6510	1.45651	46 44.4	-0.0271	-147.36	2532.96
6520	1.45648	46 44.3	-0.0270	-147.92	2542.59
6530	1.45645	46 44.3	-0.0269	-148.48	2552.22
6540	1.45643	46 44.2	-0.0268	-149.04	2561.86
6550	1.45640	46 44.1	-0.0267	-149.60	2571.51
6560	1.45637	46 44.1	-0.0266	-150.17	2581.17
6570	1.45635	46 44.0	-0.0265	-150.73	2590.83
6580	1.45632	46 43.9	-0.0264	-151.29	2600.50
6590	1.45629	46 43.9	-0.0263	-151.85	2610.17
6600	1.45627	46 43.8	-0.0262	-152.42	2619.85
6610	1.45624	46 43.7	-0.0261	-152.98	2629.54
6620	1.45622	46 43.7	-0.0260	-153.54	2639.23
6630	1.45619	46 43.6	-0.0259	-154.11	2648.93
6640	1.45616	46 43.6	-0.0258	-154.67	2658.64
6650	1.45614	46 43.5	-0.0257	-155.24	2668.35
6660	1.45611	46 43.4	-0.0256	-155.80	2678.07
6670	1.45609	46 43.4	-0.0255	-156.37	2687.79
6680	1.45606	46 43.3	-0.0254	-156.94	2697.52
6690	1.45604	46 43.2	-0.0253	-157.50	2707.26
6700	1.45601	46 43.2	-0.0252	-158.07	2716.99
6710	1.45599	46 43.1	-0.0251	-158.64	2726.74
6720	1.45596	46 43.0	-0.0251	-159.20	2736.49
6730	1.45594	46 43.0	-0.0250	-159.77	2746.24
6740	1.45591	46 42.9	-0.0249	-160.34	2756.00
6750	1.45589	46 42.9	-0.0248	-160.91	2765.76
6760	1.45586	46 42.8	-0.0247	-161.47	2775.53
6770	1.45584	46 42.7	-0.0246	-162.04	2785.30
6780	1.45581	46 42.7	-0.0245	-162.61	2795.08
6790	1.45579	46 42.6	-0.0244	-163.18	2804.85
6800	1.45576	46 42.5	-0.0244	-163.75	2814.64
6810	1.45574	46 42.5	-0.0243	-164.32	2824.42
6820	1.45572	46 42.4	-0.0242	-164.89	2834.21
6830	1.45569	46 42.4	-0.0241	-165.46	2844.01
6840	1.45567	46 42.3	-0.0240	-166.03	2853.80
6850	1.45564	46 42.2	-0.0239	-166.60	2863.60
6860	1.45562	46 42.2	-0.0239	-167.17	2873.40
6870	1.45560	46 42.1	-0.0238	-167.74	2883.21
6880	1.45557	46 42.1	-0.0237	-168.31	2893.02
6890	1.45555	46 42.0	-0.0236	-168.88	2902.83
6900	1.45552	46 41.9	-0.0235	-169.45	2912.64
6910	1.45550	46 41.9	-0.0235	-170.02	2922.45
6920	1.45548	46 41.8	-0.0234	-170.59	2932.27
6930	1.45545	46 41.8	-0.0233	-171.16	2942.09
6940	1.45543	46 41.7	-0.0232	-171.74	2951.91
6950	1.45541	46 41.7	-0.0232	-172.31	2961.73
6960	1.45538	46 41.6	-0.0231	-172.88	2971.56
6970	1.45536	46 41.5	-0.0230	-173.45	2981.38
6980	1.45534	46 41.5	-0.0229	-174.02	2991.21
6990	1.45532	46 41.4	-0.0229	-174.59	3001.04

λ (Å)	n	θ ° '	$(dn/d\lambda)$ μm^{-1}	$(d\lambda/d\theta)$ (Å/min)	$(d\lambda/dx)$ (Å/mm)
7000	1.45529	46 41.4	-0.0228	-175.17	3010.86
7010	1.45527	46 41.3	-0.0227	-175.74	3020.69
7020	1.45525	46 41.3	-0.0226	-176.31	3030.52
7030	1.45522	46 41.2	-0.0226	-176.88	3040.35
7040	1.45520	46 41.1	-0.0225	-177.45	3050.19
7050	1.45518	46 41.1	-0.0224	-178.02	3060.02
7060	1.45516	46 41.0	-0.0223	-178.60	3069.85
7070	1.45513	46 41.0	-0.0223	-179.17	3079.68
7080	1.45511	46 40.9	-0.0222	-179.74	3089.51
7090	1.45509	46 40.9	-0.0221	-180.31	3099.34
7100	1.45507	46 40.8	-0.0221	-180.88	3109.17
7110	1.45505	46 40.7	-0.0220	-181.46	3119.00
7120	1.45502	46 40.7	-0.0219	-182.03	3128.83
7130	1.45500	46 40.6	-0.0219	-182.60	3138.66
7140	1.45498	46 40.6	-0.0218	-183.17	3148.48
7150	1.45496	46 40.5	-0.0217	-183.74	3158.31
7160	1.45494	46 40.5	-0.0217	-184.31	3168.13
7170	1.45492	46 40.4	-0.0216	-184.89	3177.96
7180	1.45489	46 40.4	-0.0215	-185.46	3187.78
7190	1.45487	46 40.3	-0.0215	-186.03	3197.60
7200	1.45485	46 40.3	-0.0214	-186.60	3207.42
7210	1.45483	46 40.2	-0.0213	-187.17	3217.23
7220	1.45481	46 40.2	-0.0213	-187.74	3227.05
7230	1.45479	46 40.1	-0.0212	-188.31	3236.86
7240	1.45477	46 40.0	-0.0211	-188.88	3246.67
7250	1.45474	46 40.0	-0.0211	-189.45	3256.47
7260	1.45472	46 39.9	-0.0210	-190.02	3266.28
7270	1.45470	46 39.9	-0.0209	-190.59	3276.08
7280	1.45468	46 39.8	-0.0209	-191.16	3285.87
7290	1.45466	46 39.8	-0.0208	-191.73	3295.67
7300	1.45464	46 39.7	-0.0208	-192.30	3305.46
7310	1.45462	46 39.7	-0.0207	-192.87	3315.25
7320	1.45460	46 39.6	-0.0206	-193.44	3325.03
7330	1.45458	46 39.6	-0.0206	-194.01	3334.81
7340	1.45456	46 39.5	-0.0205	-194.58	3344.59
7350	1.45454	46 39.5	-0.0205	-195.15	3354.36
7360	1.45452	46 39.4	-0.0204	-195.72	3364.13
7370	1.45450	46 39.4	-0.0203	-196.29	3373.90
7380	1.45448	46 39.3	-0.0203	-196.85	3383.66
7390	1.45446	46 39.3	-0.0202	-197.42	3393.41
7400	1.45444	46 39.2	-0.0202	-197.99	3403.17
7410	1.45442	46 39.2	-0.0201	-198.56	3412.91
7420	1.45440	46 39.1	-0.0201	-199.12	3422.65
7430	1.45438	46 39.1	-0.0200	-199.69	3432.39
7440	1.45436	46 39.0	-0.0199	-200.25	3442.12
7450	1.45434	46 39.0	-0.0199	-200.82	3451.85
7460	1.45432	46 38.9	-0.0198	-201.39	3461.57
7470	1.45430	46 38.9	-0.0198	-201.95	3471.28
7480	1.45428	46 38.8	-0.0197	-202.52	3480.99
7490	1.45426	46 38.8	-0.0197	-203.08	3490.69

λ (Å)	n	θ ° '	(dn/dλ) μm⁻¹	(dλ/dθ) (Å/min)	(dλ/dx) (Å/mm)
7500	1.45424	46 38.7	-C.0196	-203.64	3500.39
7510	1.45422	46 38.7	-C.0196	-204.21	3510.08
7520	1.45420	46 38.6	-C.0195	-204.77	3519.77
7530	1.45418	46 38.6	-C.0195	-205.33	3529.45
7540	1.45416	46 38.5	-C.0194	-205.90	3539.12
7550	1.45414	46 38.5	-C.0193	-206.46	3548.78
7560	1.45412	46 38.4	-C.0193	-207.02	3558.44
7570	1.45410	46 38.4	-0.0192	-207.58	3568.09
7580	1.45408	46 38.3	-C.0192	-208.14	3577.74
7590	1.45406	46 38.3	-C.0191	-208.70	3587.37
7600	1.45404	46 38.2	-0.0191	-209.27	3597.00
7610	1.45402	46 38.2	-0.0190	-209.82	3606.63
7620	1.45401	46 38.1	-0.0190	-210.38	3616.24
7630	1.45399	46 38.1	-C.0189	-210.94	3625.85
7640	1.45397	46 38.0	-C.0189	-211.50	3635.45
7650	1.45395	46 38.0	-0.0188	-212.06	3645.04
7660	1.45393	46 38.0	-C.0188	-212.62	3654.62
7670	1.45391	46 37.9	-0.0187	-213.17	3664.19
7680	1.45389	46 37.9	-C.0187	-213.73	3673.76
7690	1.45387	46 37.8	-C.0186	-214.29	3683.32
7700	1.45385	46 37.8	-0.0186	-214.84	3692.87
7710	1.45384	46 37.7	-C.0185	-215.40	3702.41
7720	1.45382	46 37.7	-C.0185	-215.95	3711.94
7730	1.45380	46 37.6	-0.0185	-216.51	3721.46
7740	1.45378	46 37.6	-0.0184	-217.06	3730.97
7750	1.45376	46 37.5	-C.0184	-217.61	3740.48
7760	1.45374	46 37.5	-C.0183	-218.16	3749.97
7770	1.45373	46 37.4	-C.0183	-218.72	3759.46
7780	1.45371	46 37.4	-C.0182	-219.27	3768.93
7790	1.45369	46 37.4	-C.0182	-219.82	3778.40
7800	1.45367	46 37.3	-C.0182	-220.37	3787.85
7810	1.45365	46 37.3	-C.0181	-220.92	3797.30
7820	1.45364	46 37.2	-0.0180	-221.47	3806.73
7830	1.45362	46 37.2	-C.0180	-222.01	3816.16
7840	1.45360	46 37.1	-C.0180	-222.56	3825.57
7850	1.45358	46 37.1	-C.0179	-223.11	3834.97
7860	1.45356	46 37.0	-C.0179	-223.66	3844.37
7870	1.45355	46 37.0	-C.0178	-224.20	3853.75
7880	1.45353	46 36.9	-C.0178	-224.75	3863.12
7890	1.45351	46 36.9	-0.0177	-225.29	3872.48
7900	1.45349	46 36.9	-C.0177	-225.84	3881.83
7910	1.45347	46 36.8	-C.0177	-226.38	3891.17
7920	1.45346	46 36.8	-C.0176	-226.92	3900.49
7930	1.45344	46 36.7	-0.0176	-227.46	3909.81
7940	1.45342	46 36.7	-0.0175	-228.00	3919.11
7950	1.45340	46 36.6	-C.0175	-228.55	3928.40
7960	1.45339	46 36.6	-C.0174	-229.09	3937.68
7970	1.45337	46 36.6	-C.0174	-229.62	3946.95
7980	1.45335	46 36.5	-C.0174	-230.16	3956.21
7990	1.45333	46 36.5	-C.0173	-230.70	3965.45

Singlet–Triplet Absorption Bands of Methyl-Substituted Ethylenes[1]

by Michiya Itoh[2] and Robert S. Mulliken[3]

*Institute of Molecular Biophysics, Florida State University, Tallahassee, Florida 32306 and
Laboratory of Molecular Structure and Spectra, Department of Physics, University of Chicago, Chicago, Illinois 60637
(Received June 25, 1969)*

In the absorption spectra of the methylated ethylenes propene and 2-methylpropene in the gas state plus 70 atm of oxygen, banded structures are found which can be identified as triplet ← singlet (T ← N) transitions analogous to that found for ethylene itself. A similar absorption but without structure is found for *trans*-butene. At shorter wavelengths, and also even at longer wavelengths in 2-methyl-2-butene and in 2,3-dimethyl-2-butene vapor in the presence of 70 atm of oxygen, relatively strong absorption was found which can probably be attributed to contact charge-transfer transitions from the ethylene to O_2. This absorption defeated attempts to determine by oxygen enhancement whether the extremely weak bands which have been observed by others at 2100–2500 Å on the long wavelength side of the Rydberg bands of the methylated ethylenes are the triplet ← singlet analogs of the Rydberg bands. To determine the location of the T ← N bands of 2-methyl-2-butene and 2,3-dimethyl-2-butene, enhancement in the liquid state by CH_2Br_2 was used.

Introduction

Writing the normal state (N) electron configuration of ethylene as ⸺ π^2, the first excited states are a triplet (T) and a singlet (V) of respective vertical excitation energies 4.6 and 7.6 eV, both of configuration ⸺$\pi\pi^*$, and another singlet, a Rydberg state (R) with vertical energy 7.1 eV.[4] States analogous to R and V are also known in the alkyl-substituted ethylenes. The V ← N bands, and to a greater extent the R ← N bands, are progressively shifted to longer wavelengths with each additional alkyl substitution.

In the absorption spectra of ethylene and the alkylated ethylenes, the V ← N band system is very strong, the R ← N system moderately strong, the T ← N system[5,6] extremely weak. In the methylated ethylenes, absorption bands very much weaker than the R ← N systems, and at somewhat longer wavelengths (2100–2500 Å) have long been known,[7] although the possibility that they may be due to impurities has not been entirely disproved. These bands if genuine can be ascribed to the transition T_R ← N, where T_R means the triplet Rydberg state corresponding to the singlet Rydberg state R.[8] The vibrational spacing in these bands (about 1400 cm^{-1}) is approximately the same as in the R ← N bands and their positions, which correspond to an energy separation of 0.7 eV between T_R and R levels, are in good agreement[9] with theoretical expectation. A proposal by Berry[10] that the tentative T_R ← N bands may be analogous to the π^* ← n transition in formaldehyde has been shown not to be correct.[4]

The T ← N band was first discovered by Reid[5] in the absorption spectrum of a 1.4-m path in liquid ethylene. This identification was confirmed by Evans[6] using a mixture of ethylene at 50 atm and oxygen at 25 atm; it is well known that oxygen causes marked intensification of otherwise weak singlet–triplet transitions. The present paper originated in an attempt to use the

oxygen-intensification technique to confirm the triplet–singlet nature of the tentative T_R ← N bands in several methylated ethylenes. We found new weak absorption bands, but only in the wavelength region where T ← N bands should occur. Relatively strong absorption also occurred in the T_R ← N wavelength region, but it was entirely continuous—no bands could be identified. We attribute this absorption to contact charge-transfer transitions, which as well as triplet ← singlet bands are known to be brought out by oxygen.[11]

Experimental Section

We have investigated the near-ultraviolet absorption of propene, 2-methylpropene, and *trans*-butene in the gas phase by the oxygen enhancement method using a high-pressure optical cell, and that of 2-methyl- and 2,3-dimethyl-2-butene in the liquid state using the external heavy atom effect[12] of CH_2Br_2. Commercial research grade cylinders (The Matheson Co., Inc.) were

(1) This research was assisted by a contract between the Division of Biology and Medicine, U. S. Atomic Energy Commission and the Florida State University, and by the Office of Naval Research, Physics Branch, under Contract No. N00014-67-A-0285-0001 with theUniversity of Chicago.

(2) Faculty of Pharmaceutical Sciences, University of Tokyo, Bunkyo-ku, Tokyo, Japan.

(3) To whom requests for reprints should be addressed.

(4) See A. J. Merer and R. S. Mulliken, *Chem. Rev.*, 69, 639 (1969).

(5) C. Reid, *J. Chem. Phys.*, 18, 1299 (1950).

(6) D. F. Evans, *J. Chem. Soc.*, 1735 (1960).

(7) W. J. Potts, *J. Chem. Phys.*, 23, 65 (1955).

(8) R. S. Mulliken, *ibid.*, 33, 1597 (1960). Before the discovery[5,6] of the T ← N bands, it had been thought that the bands now attributed to T_R ← N were T ← N bands.

(9) P. G. Wilkinson and R. S. Mulliken, *ibid.*, 23, 1895 (1955).

(10) R. S. Berry, *ibid.*, 38, 1934 (1963).

(11) Cf. H. Tsubomura and R. S. Mulliken, *J. Amer. Chem. Soc.*, 82, 5966 (1960).

(12) M. Kasha, *J. Chem. Phys.*, 20, 71 (1952).
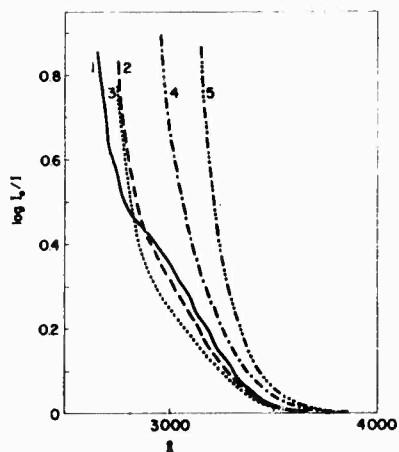
Figure 1. Absorption spectra of oxygen at 70 atm pressure and several methylethylenes (~6.5 cm cell): (1) propene, ~10 atm; (2) 2-methylpropene, ~1.5 atm; (3) *trans*-butene, ~1.0 atm; (4) 2-methyl-2-butene, ~0.5 atm (vapor pressure at room temperature); (5) 2,3-dimethyl-2-butene, ~0.2 atm (vapor pressure at room temperature).

Figure 2. Absorption spectra of 2-methyl-2-butene plus CH_2Br_2: (1) 2-methyl-2-butene and CH_2Br_2, 1:1 mixture, (5-cm cell); (2) 2-methyl-2-butene (2.5-cm cell); (3) CH_2Br_2 (2.5-cm cell); (4) absorption spectrum obtained by subtracting curves 2 and 3 from curve 1.

Figure 3. Absorption spectra of 2,3-dimethyl-2-butene plus CH_2Br_2: (1) 2,3-dimethyl-2-butene and CH_2Br_2, 1:1 mixture (5-cm cell); (2) 2,3-dimethyl-2-butene (2.5-cm cell); (3) CH_2Br_2 (2.5-cm cell); (4), absorption spectrum obtained by subtracting curves 2 and 3 from curve 1.

used without further purification for the three gaseous samples, and API standard samples were used for the other two methylated ethylenes. Absorption spectra of propene, 2-methylpropene, and *trans*-butene in the gas phase with oxygen at 70 atm pressure were taken at room temperature with a Cary recording spectrophotometer 14 M. A high-pressure optical cell with a light path of approximately 6.5 cm was used.

Results

The spectra of several methylethylenes are shown in Figure 1. A weak absorption band with vibrational structure was observed in propene and in 2-methylpropene, and a very weak band without structure in *trans*-butene. There is no reasonable doubt that the bands shown in curves 1–3 in Figure 1 are due to T ← N transitions, especially since the vibrational spacing, 960–970 cm^{-1} in both propene and 2-methylpropene, is almost identical with that of ethylene as reported by Reid[5] and Evans.[6]

However, there was also relatively very strong absorption beginning near 4000 Å in the case of 2-methyl- and 2,3-dimethyl-2-butene with compressed oxygen gas (curves 4 and 5 in Figure 1). Contact charge-transfer absorption between methylethylenes and oxygen should shift to longer wavelengths with decrease in ionization potentials of the methylethylene; these vary from 10.507 to about 8.3 eV[13] in going from ethylene to 2,3-dimethyl-2-butene. The relatively strong absorption beginning near 4000 Å in the 2-methyl- and 2,3-dimethyl-2-butenes, and also *trans*-butene, may probably be ascribed to contact charge-transfer absorption masking the weak T ← N bands, and at shorter wavelengths the T_R ← N bands. In the cases of propene, 2-

methylpropene, and *trans*-butene, the increasingly intense absorption at wavelengths beginning at almost 2600–2700 Å may also probably be attributed to charge-transfer absorption, or perhaps also to V ← N absorption.

We also examined the spectra of 1:1 mixed solutions of 2-methylbutene and of 2,3-dimethyl-2-butene with methylene bromide. In each case a weak absorption band was obtained by subtracting the individual absorptions of CH_2Br_2 and the methylethylene from that of the mixed solution, see Figures 2 and 3. It seems to us that these absorption bands can be identified as T ← N bands enhanced by the heavy atom effect. Possible charge-transfer bands between the methylethylenes and CH_2Br_2 should be at much shorter wave-

(13) Roughly estimated from the data of *trans*-butene (9.13 eV) and 3-methyl-2-butene (8.67 eV); see K. Watanabe, T. Nakayama and J. Mottl. *J. Quant. Spectrosc. Radiat. Transfer*, **2**, 369 (1962).

Table I: Absorption Maxima of V ← N and T ← N bands, and the T-V Energy Separations

	V ← N (λ_{max}, cm^{-1})	T ← N (λ_{max}, cm^{-1})	T-V (eV)
Ethylene	61,400[e]	37,000[e]	3.0[e]
Propene	57,800[b]	33,900	2.96
2-Methylpropene	53,100[c]	33,000	(2.3)
trans-Butene	56,270[c]	32,800	2.9
2-Methyl-2-butene	56,340[b] (53,000)[d]	29,850[f]	2.87[f]
2,3-Dimethyl-2-butene	53,500[c] (52,250)[d]	29,400[f]	2.82[f]

[a] P. G. Wilkinson and H. L. Johnston, *J. Chem. Phys.*, **18**, 190 (1950). [b] L. C. Jones, Jr., and L. W. Taylor, *Anal. Chem.*, **27**, 228 (1955). [c] J. T. Cary and L. W. Pickett, *J. Chem. Phys.*, **22**, 599, 1266 (1954). [d] Data in solution, see ref 7. [e] See ref 6. [f] Data from the CH₃Br solution.

lengths. On the other hand, the considerable absorption shown by the liquid methylethylenes themselves (curve 1 in Figures 2 and 3) may perhaps be ascribed to the relatively weak long wavelength tail of the V ← N transition; in ethylene itself this absorption begins at almost 2700 Å.

Table I summarizes the absorption maxima estimated from the spectra and also gives the T–V energy separation in the several ethylenes, using the liquid state data in the case of 2-methyl- and 2,3-dimethyl-2-butene. Table I shows that this energy separation decreases slowly with increase in the number of alkyl substituents, as seems reasonable.

<u>Correction</u> (see J. Am. Chem. Soc. <u>92</u>, 7239 (1970)):

Interpretation of the formation of the dimer anion is unfortunately incorrect, and the anion dimer, (TCNE⁻)₂, may be formed in that experimental condition, because further investigations of epr and absorption spectra of TCNE⁻,M⁺ (Na, K, and Cs) both in the solution and in the solid state show the formation of the anion dimer of which detail will be submitted to the journal in the near future. Concentration dependence of the visible absorption spectra on pages 887–888 can be also interpreted in the monomer-dimer equilibrium (see ref. 7 on page 886).

Formation and Spectrum of Tetracyanoethylene Dimer Anion (TCNE)$_2$$^-$ [1]

Michiya Itoh[2]

Contribution from the Laboratory of Molecular Structure and Spectra, Department of Physics, University of Chicago, Chicago, Illinois 60637. Received June 11, 1969

Abstract: The reversible complex formation of TCNE (tetracyanoethylene) anion radical with its parent molecule in MTHF (methyltetrahydrofuran) or in THF was confirmed spectroscopically at low temperature. The complex, (TCNE)$_2$$^-$, shows a strong visible absorption band at 5330–5350 Å (ϵ_{max} 15,500). Analysis of the spectra yields an equilibrium constant in MTHF for TCNE⁻, Na⁺ + TCNE $\rightleftharpoons$ (TCNE)$_2$$^-$, Na⁺ at 161 °K of 1.32 × 10^5 l./mol, $-\Delta H°$ of 1.46 kcal, and $\Delta S°$ of 3.95 eu. Thermodynamic data depend very strongly on the metal cation and also on the solvent composition. Using the equilibrium constant, the spectrum of pure (TCNE)$_2$$^-$, M⁺ was obtained. The equilibrium of the complex formation and the absorption spectrum are discussed.

R ecently, electronic spectra and structures of the dimers of anion,[3–5] neutral,[6–8] and cation[6,10,11] radicals have been reported in both liquid and solid states. However, only a few spectroscopic studies of complexes (such as the naphthalene dimer cation) between anion or cation radicals and their parent molecules have been reported[12–15] although this kind of complex formation was rather often suggested, and also electron-transfer rates have been determined between anion radical and parent molecule in the liquid state. Among such studies, Ishitani and Nagakura[16] reported the electronic spectrum and structure of paracyclophane monoanion radical as a model for CT (charge-transfer) interaction between benzene anion and neutral molecule. Complex formation of tetracyanoethylene with its anion was first suggested by Phillips and Powell[17] on the basis of the reversible color change of THF (tetrahydrofuran) solution with temperature.

In this paper, the equilibrium of the formation of (TCNE)$_2$$^-$ from TCNE and TCNE⁻ was studied for Li, Na, and K salts in MTHF (2-methyltetrahydrofuran), and in mixtures with THF at low temperature. Thermodynamic quantities of the equilibrium are reported. The absorption spectrum of the pure dimer anion, (TCNE)$_2$$^-$, M⁺, was obtained from the analysis of this equilibrium.

Experimental Section

A good commercial sample of TCNE was used after sublimation in high vacuum. 2-Methyltetrahydrofuran was distilled over sodium metal after refluxing with sodium metal for 10 hr. The refluxing and distillation were repeated two times. THF was also purified using the same procedures as for MTHF. These solvents were kept with a Na mirror in bottles connected to the vacuum system.

The TCNE anion radical was prepared by reduction with a sodium or potassium mirror for about 5 or 10 sec, respectively. The TCNE anion and TCNE mixed solution was obtained. After that, the tube containing the Na or K mirror was sealed off from the solution tube with the 1-cm optical cell. For TCNE⁻, Li⁺, freshly cut lithium metal was used.

Alternatively, TCNE⁻,Na⁺ solid was prepared in acetonitrile from NaCN and TCNE *in vacuo* following the method reported by Webster, *et al.*[18] The molar absorption coefficient of the TCNE anion was determined from the solution of the solid salt dissolved in MTHF or THF, and also from the solution made by contacting TCNE with sodium or potassium. The coefficient was also determined by the following electron-transfer reaction from 1-methyl-4-carbomethoxypyridinyl radical[6,19] to TCNE. The absorption spectrum of an MTHF solution of the 1-methyl-4-carbomethoxypyridinyl radical was carefully determined at room temperature. The molar coefficient of the absorption band at 3920 Å of this radical has been reported (ϵ_{max} 4500).[7,19] TCNE was added to the MTHF solution of the pyridinyl radical through a breakable seal. Complete electron transfer from the pyridinyl radical to

(1) This research was assisted by the Office of Naval Research, Physics Branch, under Contract No. N00014-67-A-0285-0001.
(2) Address correspondence to: Faculty of Pharmaceutical Sciences, University of Tokyo, Bunkyo-ku, Tokyo, Japan.
(3) N. Hirota and S. I. Weissman, *J. Amer. Chem. Soc.*, **86**, 2538 (1964).
(4) R. H. Boyd and W. D. Phillips, *J. Chem. Phys.*, **43**, 2927 (1965).
(5) K. Kimura, H. Yamada, and H. Tsubomura, *ibid.*, **48**, 440 (1968).
(6) K. H. Hausser and J. N. Murrell, *ibid.*, 27, 500 (1957).
(7) M. Itoh and S. Nagakura, *J. Amer. Chem. Soc.*, **89**, 3959 (1967).
(8) M. Itoh and E. M. Kosower, *ibid.*, **89**, 3955 (1967); *ibid.*, **90**, 1843 (1968).
(9) D. A. Wiersma and J. Kommandeur, *Mol. Phys.*, 13, 241 (1967).
(10) See references in ref 5.
(11) E. M. Kosower and J. L. Cotter, *J. Amer. Chem. Soc.*, **86**, 5521 (1964).
(12) I. C. Lewis and L. S. Singer, *J. Chem. Phys.*, 43, 2712 (1965).
(13) O. W. Howarth and G. K. Fraenkel, *J. Amer. Chem. Soc.*, **88**, 4514 (1966).
(14) B. Badger, B. Brocklehurst, and R. D. Russell, *Chem. Phys. Lett.*, 1, 122 (1967).
(15) L. R. Melby, R. J. Harder, W. R. Hertler, W. Mahler, R. E. Benson, and W. E. Mochel, *J. Amer. Chem. Soc.*, **84**, 3374 (1962).
(16) A. Ishitani and S. Nagakura, *Mol. Phys.*, 12, 1 (1967).
(17) W. D. Phillips and J. C. Powell, *J. Chem. Phys.*, 33, 626 (1960).

(18) O. W. Webster, W. Mahler, and R. E. Benson, *J. Amer. Chem. Soc.*, **84**, 3678 (1962).
(19) E. M. Kosower and E. J. Poziomek, *ibid.*, **86**, 5515 (1964).
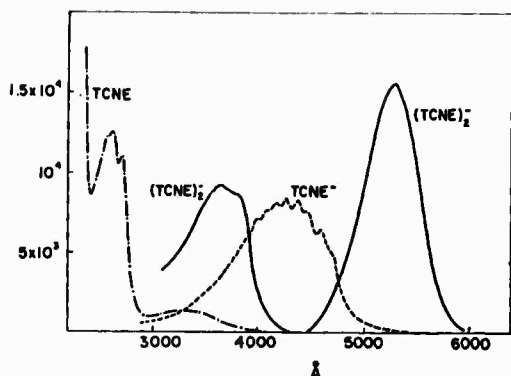
Figure 1. The spectra of TCNE and its anion radical in MTHF, and the spectrum of pure $(TCNE)_2^-$ complex constructed from the equilibrium investigation. The unit of ordinate is ϵ.

TCNE occurred very rapidly to give TCNE anion and pyridinium cation. The absorption spectrum of the pyridinyl radical was completely replaced by that of the TCNE anion in the visible region, and that of the pyridinium cation in the uv region. From this spectrum, the molar absorption coefficient of the TCNE anion was calculated. No interaction between TCNE anion and pyridinium cation was detected in a large temperature range from room temperature to 77°K. The TCNE⁻ spectra from the Na⁺, K⁺, and pyridinium salt solutions were substantially identical.

All of the absorption measurements were made on a Beckman DK-2 spectrophotometer. Low-temperature spectra were taken by using a quartz or vicole dewar. Intermediate temperatures (173–123°K) were controlled by a flow of nitrogen gas cooled by liquid N_2.

Results and Discussion

Webster, et al.,[18] reported the absorption spectrum of TCNE⁻, Na⁺ prepared from sodium cyanide and TCNE in acetonitrile. In the present paper, the electronic absorption spectrum of the TCNE anion made by conventional sodium metal reduction in MTHF (THF) is shown in Figure 1, together with the spectrum of TCNE itself. The spectrum of TCNE in MTHF or THF is considered as that of a complex with the solvent molecule.[20] The absorption coefficient of the TCNE anion was determined as already described above. The spectrum of the TCNE⁻,Na⁺ solution shows no significant spectral change at low temperature except very much sharpening of vibrational structure.

However, the MTHF solution of TCNE⁻,Na⁺ plus an excess amount of TCNE shows reversibly intense absorption in the 5000–5500-Å region on decreasing the temperature. This can be attributed to $(TCNE)_2^-$,Na⁺. The temperature dependence of the intensity of the visible and uv absorption of TCNE⁻,Na⁺ plus TCNE in MTHF is shown in Figure 2, taking into account volume changes with temperature. No absorption in this spectrum at 77°K was observed at longer wavelengths up to 13,000 Å.

Using the intensity of the ~5300-Å band as an index of the amount of $TCNE_2^-$, the equilibrium constant K for the formation of the 1:1 complex was determined from the spectrophotometric analysis by using Scott's equation, $ab/d = 1/K\epsilon + b/\epsilon$. Here a and b are the initial concentrations of TCNE⁻ and TCNE, d is the measured absorbance at a certain wavelength, and ϵ is

(20) R. Vars, L. A. Tripp, and L. W. Pickett, J. Phys. Chem., 66, 1754 (1962).
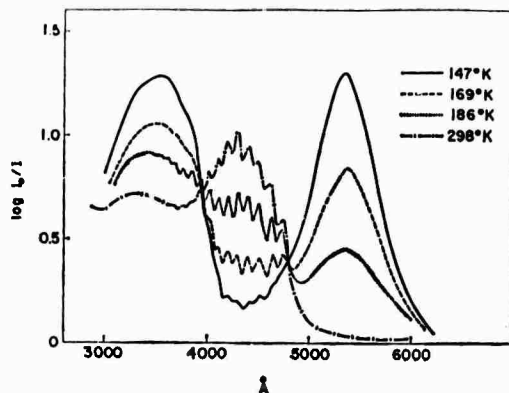
Figure 2. Temperature dependence of absorption spectrum of the TCNE-TCNE⁻, Na⁺ system in MTHF; concentration of TCNE, 4.9×10^{-4}, concentration of TCNE⁻, Na⁺, 0.88×10^{-4}, light pathlength, 1 cm.
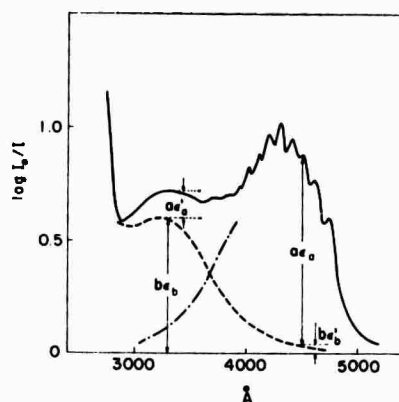
Figure 3. Determination of the concentration of TCNE⁻ (a) and TCNE (b) from the absorption spectrum. Concentrations, a and b, were determined from the following equations: $d = a\epsilon_a + b\epsilon_b'$ $(\epsilon_a \gg \epsilon_b')$ and $d' = b\epsilon_b + a\epsilon_a'$ $(\epsilon_b \gg \epsilon_a')$ $(b \gg a)$, where d and d' are observed absorbances of the solution of the TCNE-TCNE⁻, Na⁺ system at 4500 and 3300 Å, respectively, ϵ_a and ϵ_a' are molar absorption coefficients of TCNE⁻ at 4500 and 3300 Å, respectively, and ϵ_b' and ϵ_b are molar coefficients of TCNE at 4500 and 3300 Å, respectively, as shown in Figure 3.

the molar absorption coefficient. Absorptions of TCNE and of TCNE⁻,Na⁺ at 5300 Å (λ_{max}) were negligible (see Figure 1), especially since b was greater than a ($b \approx 15a$). The concentration of TCNE⁻,Na⁺, a, was determined from the room-temperature absorbance at 4500 Å of the MTHF solution containing TCNE⁻, Na⁺, and TCNE mentioned above, and the concentration TCNE, b, was determined from the absorbance at 3300 Å of the same solution, because no complex formation occurred at room temperature, as is seen from Figure 2. In this determination of a and b, the absorption of TCNE at 4500 Å and also that of TCNE⁻ at 3300 Å were taken into account, respectively, as shown in Figure 3.

Figure 4 shows Scott plots for the absorption maximum at 5340 Å of the TCNE-TCNE⁻,Na⁺ system in MTHF at several temperatures. The linearity of this kind of plot may be regarded as evidence for a 1:1 com-
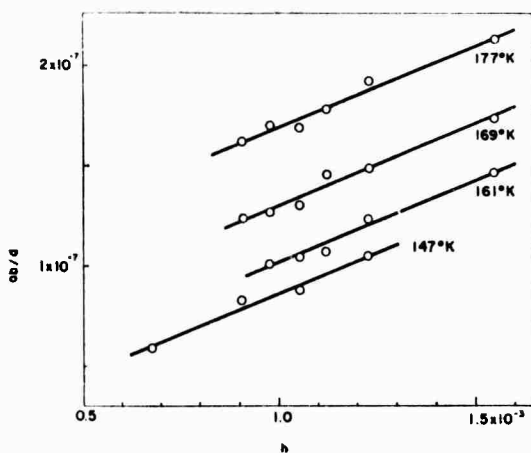
Figure 4. Scott plots for the TCNE-TCNE⁻, Na⁺ system in MTHF at various temperatures.

Figure 5. The log of the equilibrium constant for the complex formation of (TCNE)₂⁻, Na⁺ against $1/T$.

plex at the low concentrations used, although a complex with other stoichiometry than 1:1 might be considered at high concentrations. From the Scott plot, the molar absorption coefficient of the 5340-Å band of the complex was calculated by a least-squares fit at each of several temperatures between ∼173 and ∼123°K. No significant variation in the value of ϵ_{max} was obtained, although one would expect a little increase of ϵ_{max} with decreasing temperature. In this paper, the average value of ϵ_{max} at several temperatures was adopted in order to calculate the equilibrium constant, K, of complex formation.

Alternatively, the spectrum of the TCNE⁻,Na⁺ and TCNE mixed solution ($b \gg a$) in MTHF was taken at room temperature and at 77°K. The value of ϵ_{max} of the complex at 5340 Å was evaluated from these spectra, because at 77°K the TCNE anion may be assumed to be almost completely in the complex form (TCNE)₂⁻, but completely uncomplexed at room temperature (see Figure 1). The value of ϵ_{max} (15,000) thus obtained at 77°K shows good agreement with the data (15,500) calculated from a Scott plot. This confirms that the TCNE⁻ really makes a 1:1 complex with its parent molecule within experimental error.

To determine $-\Delta H°$ for the complex, the equilibrium constant was evaluated from each of a series of Scott plots at various temperatures, and log K was plotted against $1/T$ as shown in Figure 5. As seen in Figure 5, the plots of log K against $1/T$ are not straight lines at temperatures below ∼140°K. Supposedly, this is because MTHF and also the MTHF-THF mixed system showed gradually increasing viscosity below ∼140°K. Constant low viscosity of the solvent within a temperature range is required for this kind of determination. In this paper, the data for less than ∼140°K were excluded from the calculation of $-\Delta H°$.

The spectrum of the complex (TCNE)₂⁻,Na⁺ was constructed using the equilibrium constant K and the molar absorption coefficient. The constructed spectrum is shown in Figure 1, together with those of TCNE and TCNE⁻,Na⁺.

The room temperature spectra of TCNE⁻,Li⁺ and TCNE⁻,K⁺ in MTHF were next recorded. In neither case was any significant difference observed in the spec-

tra compared with that of the sodium salt. The low-temperature spectrum of the MTHF solution of TCNE⁻,Li⁺ plus a large excess of TCNE showed no new spectrum attributable to complex formation of (TCNE)₂⁻,Li⁺. On the other hand, the equilibrium constant, K, and absorption coefficient of the visible band of the complex (TCNE)₂⁻,K⁺ were obtained by similar procedures to that of the Na salt. The K obtained for the potassium salt in MTHF is approximately one-tenth of that of the sodium salt, while the absorption maximum and intensity of the ∼5340-Å band do not depend on the metal cation within experimental error.
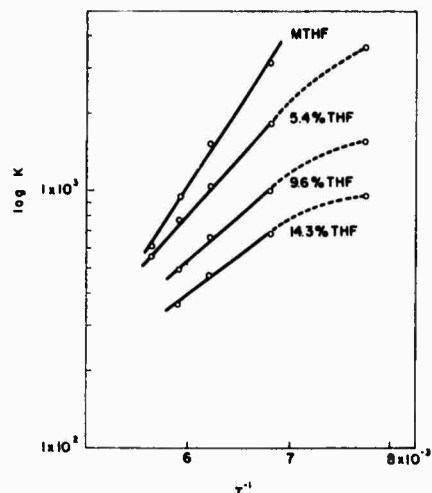
As shown in Figure 5 and Table I, the complex formation of (TCNE)₂⁻,M⁺ also depends very much on the solvent composition. No observable complex formation was found in other solvents including 1,2-dimethoxyethane and acetonitrile, although a color change from yellow to red could be seen from a solidified acetonitrile solution at 77°K. Even in THF at ∼170°K, visible spectrum shows only very faint formation of (TCNE)₂⁻,M⁺. Not many solvents could be used for this kind of experiment, because the solvent should be transparent at low temperature, and also dissolve TCNE⁻,M⁺ and the complex. Further, the TCNE⁻ is unstable in a mixed solvent such as EPA containing ethanol.

Table I. Thermodynamic Data for the Formation of (TCNE)₂⁻

Solvent	(TCNE)₂⁻, K⁺		(TCNE)₂⁻,Na⁺		
	MTHF	MTHF	5.45% THF	9.6% THF	14.5% THF
ϵ_{max} (5340 Å)	15,800	15,500	16,070	15,400	15,515
K, mol⁻¹ (161°K)	144	1322	971	575	407
$-\Delta H°$, kcal	1.30	1.46	0.85	0.52	0.39
$\Delta S°$, eu	1.78	3.95	8.39	9.39	9.47

The thermodynamic quantities for the complex formation obtained here are summarized in Table I. The heat of formation shows that (TCNE)₂⁻ is a weaker complex than the anion radical dimers; for example,

214

$-\Delta H^{\circ}$ is reported to be ~ 10 kcal for the dimer of the tetracyanoquinodimethane anion, $(TCNQ)_2^{2-}$.[4] However, the formation of $(TCNE)_2^-$ reported here may be competing with CT complex formation of TCNE with the solvent molecule. Here TCNE$^-$ and the solvent both are electron donors. The heat of complex formation of TCNE with an ethereal solvent such as THF has been reported to be 1–2 kcal.[19] Although TCNE and its anion are a strong acceptor and donor, respectively, the $-\Delta H^{\circ}$ obtained here is very similar to that of a weak CT complex. As summarized in Table I, $-\Delta H^{\circ}$ does not depend very much on the metal cation, while K depends very much as mentioned above. This difference of K is attributed to a change of the entropy terms, as will be mentioned below.

Hogen-Esch and Smid[21] reported the existence of contact and solvent-separated ion pairs in solutions of carbanions and of radical ions, and also reported the effect of a counterion on the absorption spectrum of the metal fluorenide, and on the equilibrium constant between two types of ion pairs, contact and solvent-separated ion pairs. On the other hand, Hirota[22] reported epr studies of the different types of ion pairs in metal–cation naphthalenide and anthracenide in ethereal solvents. The absorption spectra of metal–cation tetracyanoethylenide and its dimer anion neither depend on the solvent (MTHF, THF, and CH_3CN), nor on the metal (Li, Na, and K). From the viewpoint of the ion pairs reported by Hogen-Esch and Smid, and by Hirota, it is likely that both TCNE$^-$,M$^+$ and $(TCNE)_2^-$,M$^+$ may be solvent-separated or much solvated ion pairs rather than contact pairs in MTHF or THF. On the basis of these assumptions, it is of interest to compare the entropy of formation of $(TCNE)_2^-$ with that of radical dimers, and with that of numerous CT complexes with TCNE as acceptor. Boyd and Phillips reported -19.5 eu for dimerization of the 7,7′,8,8′-tetracyanoquinodimethane anion in aqueous solution.[4] Furthermore, numerous papers show considerable entropy loss in formation of the CT complexes of TCNE. It seems that these results mean increased solvation or more ordering of the solvent in the complexes than in the uncomplexed molecules. Hirota and Weissman[3] reported a large *negative* entropy change for *dissociation* of sodium fluorenone anion dimer. According to their argument, the solvation of the Na ion in the ethereal solvent has been considered to be one of the main causes of the large entropy decrease, and the solvation of the Na ion is greatly hindered in the dimer, while in the monomer more space is accessible for the solvent molecule. The considerable *positive* entropy change obtained here in *formation* of $(TCNE)_2^-$ means stronger solvation of TCNE$^-$,M$^+$ in the uncomplexed state. In $(TCNE)_2^-$,M$^+$, the solvation of the metal ion is hindered by the complex anion, and also the complex anion may be much less solvated than TCNE$^-$, because the negative charge is more distributed in the large dimer anion compared with the monomer. In addition to these arguments, partial ordering of the solvent molecule (THF or MTHF) as electron donor[20] by the CT interaction with TCNE could be partly responsible for the entropy change.

As seen in Table I, the equilibrium constant of the $(TCNE)_2^-$ complex is much larger in the Na salt than in the K salt. This increase of K is mainly attributed to the increase of the entropy term from the K to the Na salts, which may be ascribed to the size of the counterion. The smaller cation means more solvation by the ethereal solvent, and causes more increase of the entropy.[11] This behavior is similar to that found in the dissociation of metal naphthalenide[23] and of the diamagnetic dimers of ketyls.[3] From these arguments, the entropy of $(TCNE)_2^-$ formation seems to increase in the order K$^+$ < Na$^+$ < Li$^+$. If $-\Delta H^{\circ}$ of the $(TCNE)_2^-$ complex formation does not depend very much on the counterion, K would be expected to increase in the same order as in the entropy change. Nevertheless, the equilibrium constant of $(TCNE)_2^-$,Li$^+$ complex formation is abnormally too small to be determined. It seems that the structure of the complex from the Li salt might be different from those of the other salts, and therefore the heat of formation might be different.

Table I shows considerable solvent dependence of $-\Delta H^{\circ}$ and ΔS°. This seems to confirm strong electronic interaction of TCNE$^-$,Na$^+$ or TCNE with the solvent mentioned above. When MTHF was mixed with a small amount of THF, which is more polar than MTHF, the heat of complex formation decreased, while the entropy change considerably increased. The solvent dependence of $-\Delta H^{\circ}$ can be well understood from the argument that $(TCNE)_2^-$ formation may compete with the formation of the CT complex of TCNE with the solvent molecule. The change of ΔS° with solvent composition is also explained by the supposition that TCNE$^-$,Na$^+$ is more solvated than $(TCNE)_2^-$,Na$^+$, as mentioned above.

Lewis and Singer[12] reported the epr spectrum in methylene chloride at -85 to -90° of the naphthalene dimer cation, which was made by oxidation with antimonyl pentachloride. The purple color of the solution was tentatively ascribed to $(C_{10}H_8)_2^+$. Recently, Badger, *et al.*,[14] have observed the 9600 cm^{-1} band of $(C_{10}H_8)_2^+$ in a methylcyclohexane–isopentane system, generated by γ irradiation at low temperature.

As mentioned above, Ishitani and Nagakura[16] reported a strong absorption band at 13200 cm^{-1} of the paracyclophane monoanion and attributed it to a CT band between two benzene rings on the basis of theoretical considerations. If $(TCNE)_2^-$ is assumed to be a sandwich-type complex as proposed for substituted pyridinyl dimers in previous papers[7,8,14] and in other numerous complexes, the charge-resonance band due to the transition between the following two states should be observed in visible or ir regions: (A$^-$, B $\pm$ A, B$^-$) I, II, where A$^-$ and B are TCNE$^-$ and TCNE, respectively. However, it seems that the strong band at ~ 5340 Å of the $(TCNE)_2^-$ is too short a wavelength to be assigned to this transition. It is more likely that the visible band of the complex is tentatively ascribed to the transition from I to the lower of the two states III, IV: (A^{-*},B $\pm$ A,B^{-*}) III, IV, where A^{-*} and B^{-*} are excited states of TCNE$^-$.

(21) T. E. Hogen-Esch and J. Smid, *J. Amer. Chem. Soc.*, **88**, 307 (1966).
(22) N. Hirota, *ibid.*, **90**, 3603 (1968).
(23) A. Mathias and E. Warhurst, *Trans. Faraday Soc.*, **59**, 345 (1960).
(24) M. Itoh, *Mol. Phys. Lett.*, **2**, 371 (1968).

Theoretical Electronic Transition Probabilities in Diatomic Molecules. I. Hydrides*

W. H. Henneker†‡ AND H. E. Popkie†

Laboratory of Molecular Structure and Spectra, Department of Physics, University of Chicago, Chicago, Illinois 60637

(Received 3 September 1970)

Hartree–Fock (HF) electronic transition moments calculated in both the position and momentum representations are presented as a function of the internuclear separation R for the BeH, MgH, OH, and SH ($A-X$) systems. The vibrational averages of these quantities are obtained and the results are used to calculate some absorption band oscillator strengths. For the OH ($A-X$) system several independent experimental determinations of the 0–0 band oscillator strength have been reported in the literature. Our theoretical value of 20.6×10^{-4} differs from experiment by a factor of 2.5. Active electron and virtual orbital approximations to the HF transition moment integrals are given. Consideration of the united and separated atom limits and the region of the equilibrium internuclear separation for the states involved leads to an abbreviated discussion of the effect of correlation on the HF transition moments. HF transition moment calculations at a single value of R are also reported for the BH+, AlH+, HF+, and HCl+ ($A-X$) systems.

I. INTRODUCTION

The literature contains a wide selection of papers in which authors have addressed themselves to the subject of atomic transition probabilities.[1] In recent years, people have converged on the problem of correlation and its effect on this important physical quantity. Accurate calculations on He by Schiff and Pekeris[2] and a series of atomic multiconfiguration calculations by Weiss[3] have resulted in empirical observations concerning correlation sensitive transitions. Sinanoğlu and his colleagues[4] have applied the "many-electron theory" to the calculation of atomic transition probabilities in an attempt to give some insight into the physical processes that constitute correlation. We note also the related efforts of Kim and Inokuti[5] to characterize the generalized oscillator strengths that describe the scattering of fast electrons by atomic and molecular targets.

The description of molecular electronic transition probabilities is far from complete. Part of the problem has arisen because of the lack of accurate molecular wavefunctions that describe excited states. The qualified success of the Hartree–Fock–Roothaan procedure for ground-state diatomic molecules has been demonstrated in the past five years by the calculative efforts of several people at the University of Chicago[6] and the IBM Research Laboratory in San Jose.[7] Further, a series of interpretative papers by Bader *et al.*[8] and Ransil and Sinai[9] has helped focus attention on the electron density distributions and "bond maps" describing these molecules. There has been no vigorous, systematic, theoretical attempt to characterize diatomic molecular excited states, although isolated examples can be found in the literature.[10] The study of a molecule is not complete until an effort has been made to predict the ordering of its various excited states and the transition probabilities influencing the intensities of its molecular band spectra. Also, the mechanisms governing chemical binding in excited states merit the same attention given to ground states. Such a program is more easily stated

than accomplished. Excited electronic states are usually represented by open-shell wavefunctions whose properties are not as simple to classify as those for closed-shell ground states. The open-shell Hartree–Fock (HF) problem as formulated by Roothaan and Bagus[11] allows for one open shell per symmetry. Within this restriction, a large number of low-lying excited electronic states differing from the ground state by single excitations has been considered by Cade.[12] The molecular electronic transition probabilities discussed in this paper, in addition to the extensive interpretative results of Cade *et al.*,[13] represent an attempt to bridge the gap that has existed between ground and excited states because of the lack of accurate HF wavefunctions. The results form part of a continuing effort to evaluate the effectiveness of the wavefunctions reported by Cade *et al.*[6,12]

Aside from the previous neglect of excited states as fundamental blocks to be used in building an interpretation of molecular structure, the question of nuclear motion has received little attention. Since molecular HF calculations are carried out within the framework of the Born–Oppenheimer approximation, the electronic energy and other properties calculated from a diatomic wavefunction depend parametrically on the internuclear distance. In order to obtain a property that one can identify with experiment, a final average over the nuclear coordinate must be performed. If there is considerable variation in a particular property as a function of R such averaging is essential.

For many years spectroscopists have been measuring the intensities of spectral bands and interpreting them in terms of oscillator strengths and Franck–Condon factors.[14] Such measurements play a leading role in estimating the concentration of absorbing species, and hence in the calculation of rate constants characterizing certain chemical reactions occurring in the upper atmosphere.[15] In the case of diatomic molecules, only recently has it been possible to attempt accurate calculations within the formalism of the semiclassical theory of radiation[16] to obtain *a priori* values of the oscillator strengths of given transitions or the lifetimes

1763

TABLE I. Summary of ground and low-lying excited configurations for diatomic molecules.

Molecule	Lowest electron configuration	States generated	Low-lying excited configurations	States generated
H_2	$1\sigma_g^2$	$X\,^1\Sigma_g^+$	$1\sigma_g1\sigma_u$ $1\sigma_g1\pi_u$ $1\sigma_g2s;\,1\sigma_u^2$	$B\,^1\Sigma_u^+$ $C\,^1\Pi_u$ $E\,^1\Sigma_g^+;\,F\,^1\Sigma_g^+$
BeH, BH⁺	$K2\sigma^23\sigma$ [a]	$X\,^2\Sigma^+$	$K2\sigma^21\pi$	$A\,^2\Pi_r$
CH	$K2\sigma^23\sigma^21\pi$	$X\,^2\Pi_r$	$K2\sigma^23\sigma1\pi^2$	$a\,^4\Sigma^-;\,A\,^2\Delta;\,B\,^2\Sigma^-;\,C\,^2\Sigma^+$
NH	$K2\sigma^23\sigma^21\pi^2$	$X\,^3\Sigma^-;\,a\,^1\Delta;\,b\,^1\Sigma^+$	$K2\sigma^23\sigma1\pi^3$	$A\,^3\Pi_i;\,c\,^1\Pi$
OH; HF⁺	$K2\sigma^23\sigma^21\pi^3$	$X\,^2\Pi_i$	$K2\sigma^23\sigma1\pi^4$	$A\,^2\Sigma^+$
C_2	$KK2\sigma_g^22\sigma_u^21\pi_u^4$ [b]	$a\,^1\Sigma_g^+$	$KK2\sigma_g^22\sigma_u^23\sigma_g1\pi_u^3$ $KK2\sigma_g^22\sigma_u3\sigma_g^21\pi_u^3$	$X\,^1\Pi_u;\,b\,^1\Pi_u$ $A\,^1\Pi_g;\,c\,^1\Pi_g$
BeO	$KL4\sigma^2$ [c]	$X\,^1\Sigma^+$	$KL4\sigma5\pi$	$^1\Sigma^+;\,B\,^1\Sigma^+$
MgH; AlH⁺; BeF; BF⁺; BO; CO⁺; CN	$KL4\sigma^25\sigma$	$X\,^2\Sigma^+$	$KL4\sigma^22\pi$ $K2\sigma^23\sigma^21\pi^44\sigma^25\sigma^2$	$^2\Pi_r$ $^2\Pi_i$
C_2^-; N_2^+	$KK2\sigma_g^22\sigma_u^23\sigma_g^21\pi_u^4$	$X\,^2\Sigma_g^+$	$KK2\sigma_g^22\sigma_u^23\sigma_g1\pi_u^3$ $KK2\sigma_g^22\sigma_u3\sigma_g^21\pi_u^4$	$A\,^2\Pi_u$ $B\,^2\Sigma_u^+$
N_2	$KK2\sigma_g^22\sigma_u^23\sigma_g^21\pi_u^4$	$X\,^1\Sigma_g^+$	$KK2\sigma_g^22\sigma_u^23\sigma_g^21\pi_u^31\pi_g$ $KK2\sigma_g^22\sigma_u^23\sigma_g1\pi_u^41\pi_g$ $KK2\sigma_g^22\sigma_u3\sigma_g^21\pi_u^41\pi_g$	$A\,^3\Sigma_u^+;\,B'\,^3\Sigma_u^-;\,^3\Delta_u;$ $b'\,^1\Sigma_u^+;\,a'\,^1\Sigma_u^-;\,w\,^1\Delta_u$ $B\,^3\Pi_g;\,a\,^1\Pi_g$ $C\,^3\Pi_u;\,b\,^1\Pi_u$
CO	$KL4\sigma^25\sigma^2$	$X\,^1\Sigma^+$	$KL4\sigma^25\sigma2\pi$	$a\,^3\Pi_r;\,A\,^1\Pi$
O_2	$KK2\sigma_g^22\sigma_u^23\sigma_g^21\pi_u^41\pi_g^2$	$X\,^3\Sigma_g^-;\,b\,^1\Sigma_g^+;\,a\,^1\Delta_g$	$KK2\sigma_g^22\sigma_u^23\sigma_g^21\pi_u^31\pi_g^3$	$A\,^3\Sigma_u^+;\,B\,^3\Sigma_u^-;\,C\,^3\Delta_u;$ $c\,^1\Sigma_u^-;\,^1\Sigma_u^+;\,^1\Delta_u$
SH; HCl⁺	$KL4\sigma^25\sigma^22\pi^3$	$X\,^2\Pi_i$	$KL4\sigma^25\sigma2\pi^4$	$A\,^2\Sigma^+$

[a] $K=1\sigma^2$.
[b] $KK=1\sigma_g^21\sigma_u^2$.
[c] $KL=1\sigma^22\sigma^23\sigma^21\pi^4$.

of excited species. A recent report by Wolniewicz[17] has yielded definitive theoretical results for the $(B\text{-}X)$, $(C\text{-}X)$, and $(E, F\text{-}B)$ transitions in the H_2 molecule. In another study Huo[10b] has considered theoretical transition probabilities for the NH($A\text{-}X$, $c\text{-}a$, $c\text{-}b$) and CH($A\text{-}X$, $B\text{-}X$, $C\text{-}X$) systems. She concluded that the oscillator strengths calculated from molecular HF wavefunctions can be expected to have order-of-magnitude accuracy only.

Since the transition moment is a one-electron property depending on the transition density matrix, it is not correct to first order in perturbation theory.[4a] However, this is also true for the dipole moment calculated from an open-shell HF wavefunction. A comparison of this quantity for the first-row hydride ground states[18a] with the accurate results of Bender and Davidson[18b] indicates that the HF dipole moments are as reliable for the open-shell states as they are for the closed-shell states. This implies that double excitations are more important than single excitations in the correlation correction to the open-shell HF wavefunctions as is the case for closed-shell wavefunctions. But configurations that are doubly excited with respect to one HF configuration can still be singly excited with respect to another HF configuration and thus considerably affect the transition moment between the states represented by the HF configurations. It is difficult to predict how the approximations inherent in the HF wavefunctions will manifest themselves in the transition density. If one considers

the extensive calculations on atoms carried out by Weiss[3] (see the results for Li and B [3a,3a]) one may argue that the transitions of a single electron outside a closed-shell core are insensitive to correlation effects present in the accurate ground- and excited-state wavefunctions. The probabilities characterizing these transitions should be adequately described by the employment of HF wavefunctions in the semiclassical radiation theory formalism. Such transitions form a particular subclass of the class of all transitions for which the total number of electron pairs is conserved. In this paper we consider two examples from this subclass, namely the BeH and MgH $(A\text{-}X)$ transitions. We also consider the OH and SH $(A\text{-}X)$ transitions that are within the same general class. Although the latter systems are such that electron pair conservation is maintained, the effects of correlation on the transition probability are difficult to predict. Analogies with the atomic calculations of Weiss[3] and Sinanoğlu et al.[4] are inconclusive. The only comment that seems to evoke general agreement is that correlation effects in this type of transition, although highly specific, are not predictable a priori. The same qualifications are applicable to the CH and NH transitions studied by Huo.[10b]

Table I presents a list of the ground and low-lying excited configurations for some diatomic molecules composed of first- and second-row atoms and the term symbols of the states generated by these configurations. The compilation represents a good portion of the

diatomic molecules for which intensity studies are available, and transitions between the given configurations are representative of the types found. As indicated in the previous paragraph, the BeH, MgH, OH, and SH (A–X) systems considered in this paper are examples of dipole-allowed transitions involving the excitation of a single electron where the number of paired electrons is the same in both of the configurations involved in the transition. The N_2^+ (A–X) Meinel and N_2^+ (B–X) first negative systems also fall into this category and are discussed in a separate paper[19] along with transitions involving other members of the 13 electron isoelectronic sequence. The N_2 (B–A) first positive, N_2 (C–B) second positive, and O_2 (B–X) Schumann–Runge systems are members of the above-mentioned class; however, present programming aids at the Laboratory of Molecular Structure and Spectra only permit the calculation of HF wavefunctions for the O_2 ($X\,^3\Sigma_g^-$) state. It is tempting to consider the wider class of single electron excitations in which the restriction of pair conservation is removed. One could then deal with such well-known transitions as the CO (A–X) fourth positive and BeO (B–X) systems. However, the inability to predict the effects of correlation on the HF oscillator strengths would again make any conclusions very tentative. Also, further programming efforts are necessary in order to make possible the calculation of open-shell wavefunctions such as CO (A $^1\Pi$) and BeO (B $^1\Sigma^+$).

This paper is solely concerned with electric-dipole-allowed transitions. Additional examples are transitions involving a single configuration, namely the vibration–rotation spectra for various ground states where the intensity depends on the dipole moment, and transitions involving the excitation of more than one electron. A recent review by Herzberg[20] has dealt with many forbidden transitions of astrophysical interest. Further studies by one of the authors[21] will be aimed at a discussion of some electric-quadrupole-allowed transitions: the vibration–rotation spectra of H_2 and N_2 and the O_2 (a–b) Noxon band system. The N_2 (a–X) Lyman–Birge–Hopfield system is typical of the case of a magnetic dipole transition, although recently a small quadrupole contribution to the intensity has been observed.[22] The present HF formalism is capable of yielding wavefunctions from which such transition probabilities could be calculated. However, the HF wavefunctions would inadequately describe the spin-orbit interactions that influence these magnetic transitions. Finally, the O_2 (a–X) infrared atmospheric, O_2 (b–X) atmospheric, and N_2 (A–X) Vegard–Kaplan systems are examples of spin-forbidden transitions that involve spin-orbit interaction. To calculate wavefunctions for the two states connected by such a transition would require a formalism that either included spin-orbit interactions in the HF Hamiltonian or as a perturbation of the zeroth-order single-particle states. Such calculations are beyond the scope of this

report. The O_2 (A–X) Herzberg system involves even more subtle electronic-rotational interactions which seem at the moment quite beyond our resolution.

The exhaustive studies reported in this paper include the transition moment as a function of R and a final average over the nuclear vibrations. There is a great variety of experimental data available for the OH (A–X) transition. The first oscillator strengths were reported in 1939 by Oldenberg and Rieke,[23a] while the most recent study is that of Smith.[23k] In addition, Hurley[24] has calculated the oscillator strength for this transition. There are two experimental results concerning the MgH (A–X) oscillator strength. Schadee[25a] first gave a value of $f=8.0\times10^{-3}$. More recently Main et al.[25b] have placed an upper limit of $f\leq2.0\times10^{-3}$ on the intensity of this transition. Chan and Davidson[26] have reported fairly accurate theoretical results for both the BeH and MgH (A–X) oscillator strengths based on multiconfiguration wavefunctions. Apparently no experimental efforts have been made to determine the oscillator strengths for the BeH and SH (A–X) transitions.

A description of the theory used in this paper is given in the next section, and computational details can be found in Sec. III. In Sec. IV numerical results are presented and discussed.

II. THEORY

Consider two wavefunctions $\Psi_{\Gamma'}(\mathbf{R},\mathbf{r}^n)$ and $\Psi_{\Gamma''}(\mathbf{R},\mathbf{r}^n)$ describing an upper state Γ' and a lower state Γ'' of an N-electron diatomic molecule AB. The internuclear axis vector $\mathbf{R}$ is directed from A to B and gives the orientation of the molecule relative to a set of coordinate axes whose origin is at the nuclear center of mass. The y axis of the latter is chosen to be parallel to the wave vector $\mathbf{K}$ describing the direction of propagation of incident radiation. It is assumed that the center of mass of the molecular system is at rest with respect to the laboratory frame of reference. In this coordinate system, the operator describing a single photon absorption process is

$$0=\sum_{\mu=1}^{N}\mathbf{p}_\mu\exp(i\mathbf{K}\cdot\mathbf{r}_\mu)-\left(\frac{m_e}{M}\right)\mathbf{P}_R\left[\frac{M}{M_B}Z_B\exp\left(\frac{iM_A\mathbf{K}\cdot\mathbf{R}}{M}\right)\right.$$
$$\left.-\frac{M}{M_A}Z_A\exp\left(\frac{-iM_B\mathbf{K}\cdot\mathbf{R}}{M}\right)\right].\quad(1)$$

Z_A and Z_B are the nuclear charges, M_A and M_B the nuclear masses, M the nuclear reduced mass, and the electronic coordinates $\mathbf{r}_\mu$ are measured relative to the laboratory-fixed coordinate system. The position coordinates $\mathbf{r}_\mu$ and $\mathbf{R}$ are related through the commutation relations

$$\mathbf{p}_\mu=i[H,\mathbf{r}_\mu],\quad(2)$$

$$\mathbf{P}_R=i(M/m_e)[H,\mathbf{R}]\quad(3)$$

to their conjugate momenta $\mathbf{p}_\mu$ and $\mathbf{P}_R$. H is the non-

relativistic molecular Hamiltonian and m_e the electronic mass. The smallness of the ratio of electronic mass to nuclear reduced mass $(m_e/M \approx 10^{-4})$ allows us to neglect the second term in Eq. (1). Furthermore, in the Born–Oppenheimer approximation this term gives zero contribution to the transition moment for electronic transitions.

The Einstein A coefficient describing a spontaneous transition from Γ' to Γ'' accompanied by the emission of a light quantum $h\nu_{\Gamma'\Gamma''}$ is given as

$$A_{\Gamma'\Gamma''} = (4e^4/3c^3 a_0^3 m_e^2)(\Delta E_{\Gamma'\Gamma''}/\omega_{\Gamma'}) S_{\Gamma'\Gamma''}, \quad (4)$$

where $\Delta E_{\Gamma'\Gamma''}$ and $S_{\Gamma'\Gamma''}$ are in atomic units. In Eq. (4) e is the electronic charge, c the velocity of light, and a_0 the Bohr radius. $\Delta E_{\Gamma'\Gamma''}$ is the energy difference between the upper molecular state (with degeneracy factor $\omega_{\Gamma'}$) and the lower state (with degeneracy factor $\omega_{\Gamma''}$). The line strength $S_{\Gamma'\Gamma''}$ is equal to the square of the transition moment summed over all degenerate components of the molecular states Γ' and Γ'':

$$S_{\Gamma'\Gamma''} = \sum_{\alpha'\alpha''} |\int \{\gamma(\mathbf{p}'|\mathbf{p})\mathbf{p}\}_{\mathbf{p}'=\mathbf{p}+\mathbf{K}} d\mathbf{p}|^2. \quad (5)$$

The semiclassical theory of radiation yields a transition moment integral that depends explicitly on the non-diagonal element of the first-order spinless transition density matrix in momentum space given by

$$\gamma(\mathbf{p}'|\mathbf{p}) = N \int \Psi_{\Gamma'}(\mathbf{p}', \mathbf{p}_2, \cdots, \mathbf{p}_N, \mathbf{P}_R)$$
$$\times \Psi_{\Gamma''}(\mathbf{p}, \mathbf{p}_2, \cdots, \mathbf{p}_N, \mathbf{P}_R)(d\mathbf{P}_R d\mathbf{p}^N ds^N/d\mathbf{p}_1). \quad (6)$$

The volume element in (6) involves integration over the spin coordinates of all electrons and the momentum coordinates of all electrons except the first one. If $\mathbf{p}'$ is approximated by $\mathbf{p}$ in (5) the electric dipole approximation to $S_{\Gamma'\Gamma''}$ is obtained.[27]

The Einstein B coefficient describing an induced transition from Γ'' to Γ' accompanied by the absorption of a light quantum $h\nu_{\Gamma'\Gamma''}$ is given as

$$B_{\Gamma'\Gamma''} = (2\pi\hbar^2/3c e^2 m_e^2)\{S_{\Gamma'\Gamma''}/[\Delta E_{\Gamma'\Gamma''}]^2 \omega_{\Gamma''}\}. \quad (7)$$

The absorption oscillator strength $f_{\Gamma'\Gamma''}$[14] is related to the Einstein B coefficient and can be defined as

$$f_{\Gamma'\Gamma''} = \tfrac{2}{3}(1/\Delta E_{\Gamma'\Gamma''})(S_{\Gamma'\Gamma''}/\omega_{\Gamma''}). \quad (3)$$

From Eqs. (8) and (5) it follows that the transition moment integral involving the operator $\mathbf{p}$ in momentum space is taken to be the fundamental quantity of interest[28] rather than the usual integral involving $\mathbf{r}$ in position space.[29]

After a suitable transformation of the electronic and nuclear coordinates to a molecule-fixed coordinate system,[30] one obtains for the dipole line strength [Hund's case (a)][14,17,21]

$$S_{\Omega''v''j''}^{\Omega'v'j'} = S_{j''\Omega''}^{j'\Omega'} \sum_{\alpha'\alpha''} P_{\Omega''v''j''}^{\Omega'v'j'}. \quad (9)$$

$S_{j''\Omega''}^{j'\Omega'}$ are the Hönl–London factors and

$$P_{\Omega''v''j''}^{\Omega'v'j'} = |N \int \Psi_{\Omega'v'j'}(P_R, \mathbf{p}^N) \mathbf{p}_1 \Psi_{\Omega''v''j''}(P_R, \mathbf{p}^N) P_R^2 dP_R d\mathbf{p}^N|^2. \quad (10)$$

In Eq. (10) the nuclear momentum is a scalar and the electronic momenta are referred to a molecule-fixed coordinate system whose z axis is parallel to $\mathbf{R}$. Ω, v, and j are the quantum numbers characterizing electronic angular momentum along the internuclear axis, vibration, and total angular momentum, respectively. For *exact* wavefunctions, the commutation relation (2) allows one to express Eq. (10) equally well as

$$P_{\Omega''v''j''}^{\Omega'v'j'} = [\Delta E_{\Omega''v''j''}^{\Omega'v'j'}]^2 |N \int \Psi_{\Omega'v'j'}(R, \mathbf{r}^N) \mathbf{r}_1 \Psi_{\Omega''v''j''}(R, \mathbf{r}^N) R^2 dR d\mathbf{r}^N|^2, \quad (11)$$

where $\Delta E_{\Omega''v''j''}^{\Omega'v'j'}$ is the exact energy difference between the two states of total angular momentum j' and j'', respectively.

An infinite number of expressions for $P_{\Omega''v''j''}^{\Omega'v'j'}$ may be obtained by the successive use of commutators of the form $[H, [H, \cdots, [H, \mathbf{p}_\mu]]]^n$ where $n \geq 1$ is the number of brackets to the right of $\mathbf{p}_\mu$. Thus, in general we have

$$P_{\Omega''v''j''}^{\Omega'v'j'} = \{1/[\Delta E_{\Omega''v''j''}^{\Omega'v'j'}]^{2n}\} |N \int \Psi_{\Omega'v'j'}(P_R, \mathbf{p}^N)[H, [H, \cdots, [H, \mathbf{p}_\mu]]^n \Psi_{\Omega''v''j''}(P_R, \mathbf{p}^N) P_R^2 dP_R d\mathbf{p}^N|^2.$$

$$(11')$$

For $n = 1$, the acceleration form of $P_{\Omega''v''j''}^{\Omega'v'j'}$ is obtained. Previous studies[2,2a] have indicated that the acceleration operator is much more sensitive to wavefunction deficiencies in the region of the nuclei than either the momentum or position operator. Consequently it is not considered further in this paper.

In the Born–Oppenheimer approximation, a diatomic molecular wavefunction can be written:

$$\Psi_{\Omega,j}(\mathbf{r}^N, R) = R^{-1} P_{\Omega,j}(R) \Psi_{\Omega}(R, \mathbf{r}^N). \quad (12)$$

Ψ_{Ω} is an eigenfunction of the electronic Hamiltonian H_e (obtained from H by setting the nuclear masses equal to infinity) with eigenvalue $E_{\Omega}(R)$. Substitution of (12) into (10) and (11) gives two expressions for $P_{\Omega''v''j''}^{\Omega'v'j'}$:

$$P_{\Omega''v''j''}^{\Omega'v'j'} = |\int P_{\Omega'v'j'}(R) M_{\Omega'\Omega''}^{\mathbf{p}}(R) P_{\Omega''v''j''}(R) dR|^2 \quad (13a)$$

and

$$P_{\Omega''v''j''}^{\Omega'v'j'} = [\Delta E_{\Omega''v''j''}^{\Omega'v'j'}]^2 |\int P_{\Omega'v'j'}(R) M_{\Omega'\Omega''}^{\mathbf{r}}(R) P_{\Omega''v''j''}(R) dR|^2. \quad (13b)$$

219

$M_{\Omega'\Omega''}{}^{\mathcal{O}}(R)$ is the electronic dipole transition moment integral connecting states of angular momentum Ω' and Ω''. The superscript $\mathcal{O}$ indicates in which representation this integral is calculated.

There is some ambiguity[28,32] as to the order of application of the commutation relations and the Born–Oppenheimer approximation in Eq. (10). Equation (13b) results from first applying the commutation relation (2) and then the Born–Oppenheimer approximation (12). This procedure is consistent with the definition of the oscillator strength in Eq. (8). However, the order of application can be reversed. If one first applies the Born–Oppenheimer approximation (12) to Eq. (10) and then uses the commutation relation

$$\mathbf{p}_\mu = i[H_e, \mathbf{r}], \tag{14}$$

one obtains the following result:

$$P_{\Omega''v''j'',\Omega'v'j'} = \mid \int P_{\Omega''v''j'}(R) \Delta E_{\Omega'\Omega''}(R) M_{\Omega'\Omega''}{}^{r}(R) P_{\Omega''v''j''}(R) dR \mid^2. \tag{13c}$$

Equation (13c) is not used in this paper although the quantity $\Delta E_{\Omega'\Omega''}(R) M_{\Omega'\Omega''}{}^{r}(R)$ is discussed in Sec. IV.

Equations (13a) and (13b) together with (8) and (9) provide two expressions for the oscillator strength:

$$f_{\Omega''v''j'',\Omega'v'j'} = \tfrac{2}{3}(1/\Delta E_{\Omega''v''j'',\Omega'v'j'})[\sum_{\alpha'\alpha''} P_{\Omega''v''j'',\Omega'v'j'} S_{j''\Omega'',}{}^{j'\Omega'}]/\{(2-\delta_{0,\Lambda''})(2S''+1)(2j''+1)\} \tag{15a}$$

and

$$f_{\Omega''v''j'',\Omega'v'j'} = \tfrac{2}{3}[\Delta E_{\Omega''v''j'',}{}^{\Omega'v'j'} \sum_{\alpha'\alpha''} \bar{P}_{\Omega''v''j'',}{}^{\Omega'v'j'} S_{j''\Omega'',}{}^{j'\Omega'}]/\{(2-\delta_{0,\Lambda''})(2S''+1)(2j''+1)\}. \tag{15b}$$

The degeneracy factor $(2-\delta_{0,\Lambda''})(2S''+1)(2j''+1)$, where S'' is the spin quantum number and Λ'' is the component of orbital angular momentum along R for the lower state, is that used by Schadee[20a] and Tatum[33] and corresponds to the case where spin splitting and Λ doubling are ignored. In (15b) the line strength $\bar{P}_{\Omega''v''j'',}{}^{\Omega'v'j'}$ has a form identical to Eq. (13a) with $M_{\Omega'\Omega''}{}^{p}(R)$ replaced by $M_{\Omega'\Omega''}{}^{r}(R)$.

Hansen[34] has suggested the use of a mixed oscillator strength expression:

$$f_{\Omega''v''j'',\Omega'v'j'} = \tfrac{2}{3}[\sum_{\alpha'\alpha''} \mid \bar{P}_{\Omega''v''j'',}{}^{\Omega'v'j'} P_{\Omega''v''j'',}{}^{\Omega'v'j'}\mid^{1/2} S_{j''\Omega'',}{}^{j'\Omega'}]/\{(2-\delta_{0,\Lambda''})(2S''+1)(2j''+1)\}. \tag{15c}$$

He argues that for approximate wavefunctions this combination of (15a) and (15b) is less sensitive to correlation effects since it provides the geometric average of two oscillator strength quantities that have correlation errors of opposite sign. A small number of exploratory calculations performed by La Paglia et al.[35] tentatively confirm this hypothesis. The mixed oscillator strength expression possesses the advantage that it does not contain the energy term $\Delta E_{\Omega''v''j'',}{}^{\Omega'v'j'}$.

If vibration–rotation interaction is neglected, vibrational band oscillator strengths can be defined as

$$f_{\Omega''v'',\Omega'v'} = \tfrac{2}{3}[\sum_{\alpha'\alpha''} \mid \bar{P}_{\Omega''v''0}{}^{\Omega'v'0} P_{\Omega''v''0}{}^{\Omega'v'0}\mid^{1/2}]/\{(2-\delta_{0,\Lambda''})(2S''+1)\}. \tag{16}$$

Equation (16) results from summing over all j' levels and averaging over all j'' levels making use of the sum rule:

$$\sum_{j'} S_{j''\Omega'',}{}^{j'\Omega'} = (2j''+1). \tag{17}$$

III. COMPUTATIONAL DETAILS

All wavefunctions used in this study have been calculated by Cade and Huo[6,12] with the Hartree–Fock–Roothaan procedure. The electronic transition moment is expressed as

$$M_{\Omega'\Omega''}{}^{\mathcal{O}}(R) = \sum_{j,\mu,\beta,i,\lambda,\alpha} D(j\mu\beta \mid i\lambda\alpha) \langle \psi_{j\mu\beta} \mid \mathcal{O} \mid \psi_{i\lambda\alpha}\rangle a_{\Omega'\Omega''}. \tag{18a}$$

The indices $(i\lambda\alpha)$ and $(j\mu\beta)$ characterize lower- and upper-state molecular spin orbitals, respectively. $\psi_{i\lambda\alpha}$ is the ith molecular spin orbital of symmetry λ and subspecies α. $D(j\mu\beta \mid i\lambda\alpha)$ is the signed minor[36] of the overlap matrix

$$S_{i\lambda\alpha}{}^{j\mu\beta} = \langle \psi_{j\mu\beta} \mid \psi_{i\lambda\alpha}\rangle \tag{19}$$

formed by the removal of row $(j\mu\beta)$ and column

$(i\lambda\alpha)$. $\mathcal{O}$ is the operator $\mathbf{r}$ or $\mathbf{p}$, and $a_{\Omega'\Omega''}$ are coefficients characteristic of the wavefunctions $\Psi_{\Omega'}$ and $\Psi_{\Omega''}$ describing open-shell configurations. $M_{\Omega'\Omega''}{}^{\mathcal{O}}(R)$ is not state averaged. It represents the expectation value of the operator $\mathcal{O}$ for given degenerate components of Ω' and Ω'' and is to be contrasted with the expression for a pure state expectation value of $\mathcal{O}$ obtained by averaging over all degenerate components of Ω:

$$M_\Omega = \sum_{i,\lambda} (n_{i\lambda}/d_\lambda)\sum_\alpha \langle \phi_{i\lambda\alpha} \mid \mathcal{O} \mid \phi_{i\lambda\alpha}\rangle. \tag{18b}$$

The $n_{i\lambda}$ are shell populations while d_λ is the dimension of the representation spanned by orbitals of symmetry λ. In the restricted Hartree–Fock formalism, the molecular orbitals $\phi_{i\lambda\alpha}$ multiplied by spin functions α or β give the spin orbitals $\psi_{i\lambda\alpha}$.

Since the molecular orbitals are expanded as a finite
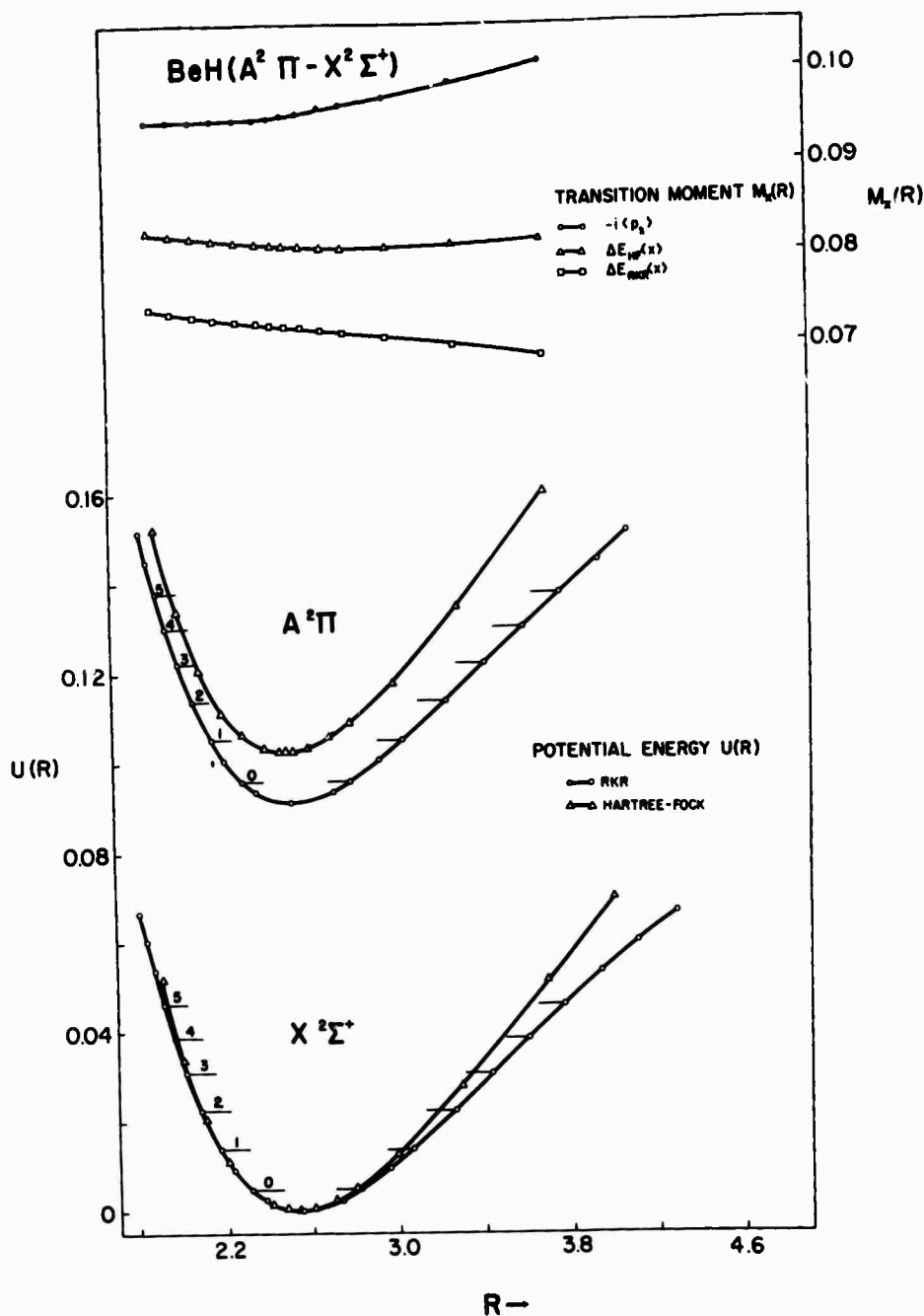
FIG. 1. BeH(A $^2\Pi$-X $^2\Sigma^+$) transition moment and potential energy curves. The transition moment $M_x(R)$ is represented as $-i\langle p_x \rangle$ and $\Delta E \langle x \rangle$ with ΔE computed from both the Hartree–Fock and RKR potential curves. The excited state potential energy curves are measured relative to the minimum in the ground state curves. For the RKR curves the lower vibrational levels are indicated.

sum of basis functions,

$$\phi_{i\lambda\alpha} = \sum_p \chi_{p\lambda\alpha} C_{i\lambda p},$$ (20)

one can express the matrix elements in (18a) as

$$\langle \psi_{j\mu\beta} | \Theta | \psi_{i\lambda\alpha} \rangle = \delta_{\alpha i, \alpha j} C_{j\mu}^\dagger OC_{i\lambda}.$$ (21)

$C_{i\lambda}$ is a column vector of coefficients and O is the matrix of the operator Θ evaluated over the Slater-type functions. The matrix O is not necessarily Hermitian in the case of a transition moment.

The $D(j\mu\beta | i\lambda\alpha)$ were evaluated using the method suggested by Prosser and Hagstrom.[37] r and p matrix

221
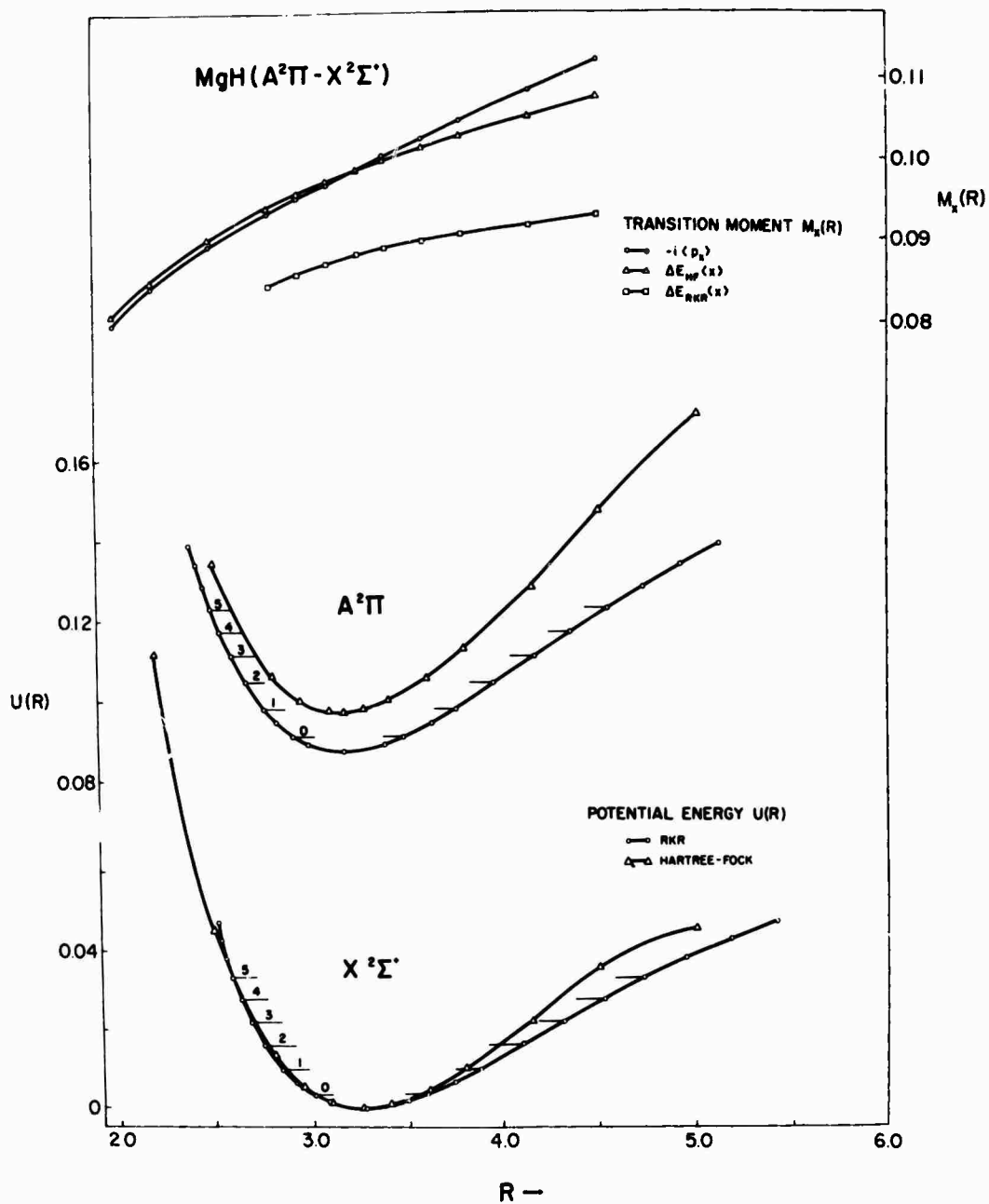
FIG. 2. MgH(A $^2\Pi$-X $^2\Sigma^+$) transition moment and potential energy curves. The transition moment $M_x(R)$ is represented as $-i\langle p_x\rangle$ and $\Delta E\langle x\rangle$ with ΔE computed from both the Hartree–Fock and RKR potential curves. The excited-state potential energy curves are measured relative to the minimum in the ground state curves. For the RKR curves the lower vibrational levels are indicated.

elements represented by O in Eq. (21) were calculated by standard methods.[38] The $\mathbf{r}$ matrix elements were compared with results available from similar computer programs at the Laboratory of Molecular Structure and Spectra. The $\mathbf{p}$ matrix elements were also calculated by

a different method that derives from suggestions indicated by Geller[39] and involves numerical evaluation of the integrals

$$\langle g_{e\mu\beta} \mid \mathbf{p} \mid g_{\Omega\alpha}\rangle.$$

222
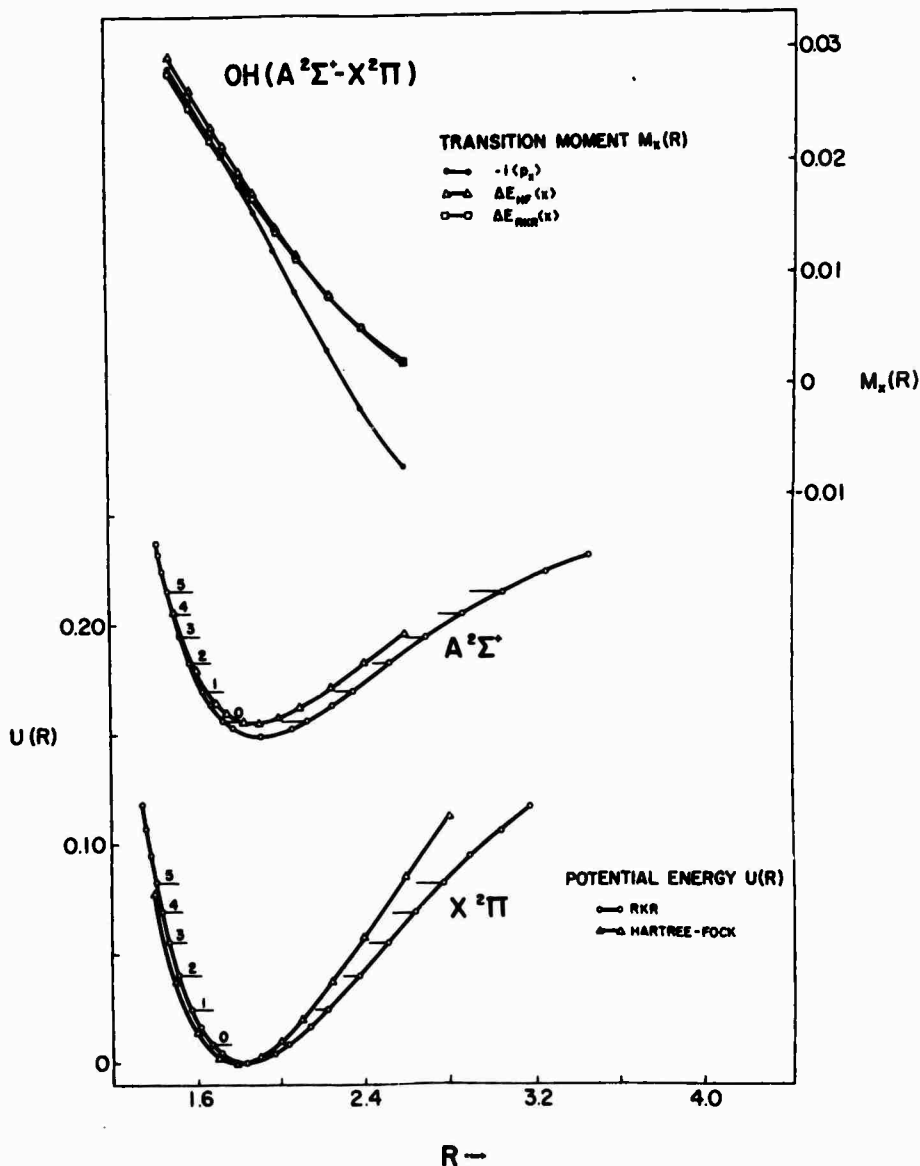
FIG. 3. OH($A\,^2\Sigma^+$-$X\,^2\Pi$) transition moment and potential energy curves. The transition moment $M_x(R)$ is represented as $-i\langle p_x \rangle$ and $\Delta E_{\backslash x}\rangle$ with ΔE computed from both the Hartree–Fock and RKR potential curves. The excited state potential energy curves are measured relative to the minimum in the ground state curves. For the RKR curves the lower vibrational levels are indicated.

The $g_{\lambda\alpha}$ represent Slater-type functions in momentum space discussed by Geller,[39] Silverstone,[40] and Henneker and Cade.[41]

The vibrational wavefunctions $P_{\Omega vj}(R)$ in (12) satisfy

$$[(d^2/dR^2) - 2M(U_\Omega(R) + \{[j(j+1) - \Omega^2]/2MR^2\}$$
$$- E_{\Omega vj})]P_{\Omega vj}(R) = 0. \quad (22)$$

If $U_\Omega(R)$ is known, Eq. (22) can be solved to yield vibration–rotation energy levels $E_{\Omega vj}$ and wavefunctions

$P_{\Omega vj}(R)$. "Experimental" RKR potential energy curves $U_\Omega(R)$ were constructed using the method proposed by Zeleznik.[42] The spectroscopic constants employed were obtained from Olsson[43] for the BeH states, Guntsch[44a] and Khan[44b] for the MgH states, Chamberlain and Roesler[45a] and Barrow[45b] for the OH states, and Ramsay[46] for the SH states.

The $P_{\Omega vj}(R)$ were obtained by numerical integration of equation (22) using the procedure of Cooley[47] that is based on the Numerov[48] method. The integration grid consisted of 1001 equally spaced points R_i. Points

223

$U(R_i)$ on the potential energy curves were calculated by piecewise interpolation of the RKR turning points using a cubic polynomial four-point formula. Simpson's rule was used to calculate the vibrational transition moment integrals occurring in Eqs. (13a) and (13b). Points $M_x(R_i)$ on the transition moment curves corresponding to the integration grid used were obtained by quadratic polynomial interpolation of the available points $M_x(R_k)$.

RESULTS AND DISCUSSION

Figures 1–4 show $-i\langle p_x \rangle$, the momentum representation of the x-component M_x of the dipole transition moment, as a function of the internuclear distance R for the BeH, MgH, OH, and SH $(A-X)$ transitions. Also presented for comparison are curves showing the position representation $\Delta E_{HF}\langle x \rangle$ as a function of R where $\Delta E_{HF}(R)$ is the Hartree–Fock transition energy. For exact Born–Oppenheimer electronic wavefunctions these two forms of the transition moment would yield the same result. However, this equality does not hold for approximate wavefunctions. It is well known[22a,40–51] that HF wavefunctions are eigenfunctions of a state-dependent effective Hamiltonian H_e^0 that does not fulfill the commutation relation (14) because of the exchange operator present. As has been found for some atomic transitions where comparison between theory and experiment is possible,[3] the momentum and position representations of the transition moment may be approximately equal for HF wavefunctions while being poor approximations to more accurate values. Thus agreement between the two forms of the transition moment is not a reliable indication of the accuracy of the wavefunctions employed.

For the MgH transition the two quantities $-i\langle p_x \rangle$ and $\Delta E_{HF}\langle x \rangle$ differ by less than 1% over the range $R = 2.2$ to 3.4 a.u. For OH they differ by less than 10% for $R < 1.9$ a.u., while for BeH an almost constant difference of approximately 15% is obtained. For SH the agreement between the two theoretical curves is rather poor, the smallest difference being $\approx 30\%$.

In Figs. 1–4 the semiempirical curve $\Delta E_{RKR}\langle x \rangle$ is also shown, where $\Delta E_{RKR}(R)$ is the "experimental" transition energy obtained from the RKR procedure. It has been speculated that this quantity should more closely approximate the experimental result than $\Delta E_{HF}\langle x \rangle$ because ΔE_{RKR} is free from correlation corrections. For the BeH and MgH transitions $\Delta E_{RKR}\langle x \rangle$ lies substantially below $\Delta E_{HF}\langle x \rangle$. If one accepts the empirical evidence that HF transition probabilities tend to overestimate experimental values, then a substitution of ΔE_{HF} by ΔE_{RKR} in the oscillator strength expression defined by Mulliken and Rieke[29] yields a result more compatible with experiment. For OH and SH $\Delta E_{RKR}\langle x \rangle$ and $\Delta E_{HF}\langle x \rangle$ lie quite close together and no benefit is derived from using the experimental transition energies.

For OH and SH the $-i\langle p_x \rangle$ curve lies below the $\Delta E_{HF}\langle x \rangle$ curve over the entire range of R studied, while for BeH the situation is reversed. For MgH the two curves are very close together and actually cross. The transition moments for BeH and MgH are almost independent of R, while for OH and SH M_x varies considerably with R and approaches zero as R increases. The latter behavior is what is expected for a so-called "perpendicular" Σ–Π transition. In the vicinity of the equilibrium internuclear distance R_e of the states involved the slope of the function $\langle {}^2\Sigma^+ | x | {}^2\Pi \rangle$ for the OH $(A-X)$ transition compares favorably with the experimental result of Nicholls.[52]

Figures 1–4 also show HF and "experimental" RKR potential curves $U(R)$ for the electronic states involved in the $(A-X)$ transitions under consideration. The energies are measured relative to the minimum in the ground-state curve. It is interesting to note that the energy differences $\Delta E_{HF}(R)$ between the Hartree–Fock curves are quite close to the experimental $\Delta E_{RKR}(R)$ values, especially for the OH transition.

The transition moment integrals calculated from Eq. (18a) and presented in this paper represent the best results obtainable within the bounds set by the restricted HF model. A consideration of the sum in Eq. (18a) usually indicates the dominance of a single term and it is of interest to evaluate and criticize the approximation in which this active electron matrix element is identified with the total transition moment integral. The assignment of electron configurations to the various states of atoms and molecules and the interpretation of their spectra in terms of a single active electron jumping between configurations are very appealing ideas that have been with us since the early 1900's. When these concepts are applied to the calculation of transition probabilities, the quantity to be evaluated is

$$\int \phi'(\mathbf{r}) \mathbf{r} \phi(\mathbf{r}) d\mathbf{r},$$

where $\phi'(\mathbf{r})$ and $\phi(\mathbf{r})$ are the single-particle functions describing the active electron in the upper and lower states, respectively. In the case of atoms ϕ' and ϕ are solutions of a radial Schrödinger equation similar to (22) in which the potential due to the remaining inactive electrons must be estimated. For alkali and alkaline-earth metals this potential has been determined in the past by the Hartree self-consistent field procedure (with and without exchange) and by empirical methods. The inactive electrons are termed a frozen core because they are constrained to be unresponsive to transitions of the active electron. As early as 1928 estimates of transition probabilities involving the valence electrons in Li and Na were available.[53] More recently the idea of the frozen core has been revived by McEachran et al.[54] and Cohen and Kelly.[55] For transitions involving the valence electrons of Li and Na, these investigators have described the inactive electrons by HF wavefunctions for the closed-shell parent ions Li^+ and Na^+, respectively. They
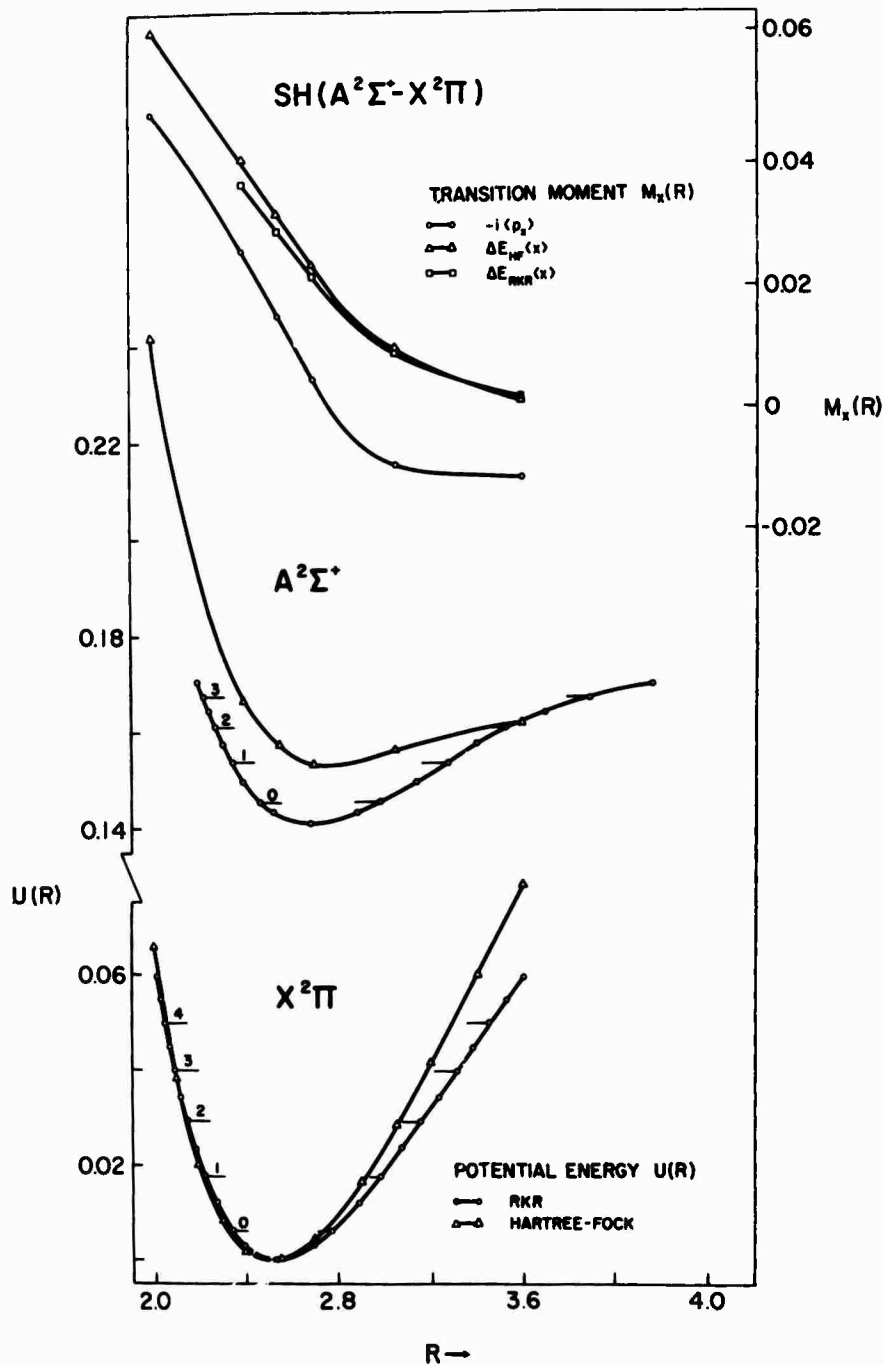
FIG. 4. $SH\langle A\,^2\Sigma^+-X\,^2\Pi\rangle$ transition moment and potential energy curves. The transition moment $M_x(R)$ is represented as $-i\langle p_x\rangle$ and $\Delta E\langle x\rangle$ with ΔE computed from both the Hartree–Fock and RKR potential curves. The excited state potential energy curves are measured relative to the minimum in the ground state curves. For the RKR curves the lower vibrational levels are indicated.

have shown[54b] that the transition moment integral is rigorously given by the active electron matrix element for the case of a single electron moving outside a closed-shell frozen core. An even simpler estimation of the

potential governing the motion of an active electron has been suggested by Bates and Damgaard.[55]

Tables II–V and X give a summary of transition moment integrals obtained during the course of this

225

TABLE II. BeH(A $^1\Pi$–X $^1\Sigma^+$) Hartree–Fock and active electron transition moment integrals.[a]

R	$\langle ^1\Pi \mid x \mid ^1\Sigma^+\rangle$	$\langle 1\pi' \mid x \mid 3\sigma\rangle$[b]	$-i\langle ^1\Pi \mid p_x \mid ^1\Sigma^+\rangle$	$-i\langle 1\pi' \mid p_x \mid 3\sigma\rangle$[b]
1.90	0.8280	0.8666	0.0949	0.1059
2.00	0.8220	0.8628	0.0948	0.1062
2.10	0.8159	0.8589	0.0948	0.1066
2.20	0.8097	0.8550	0.0949	0.1070
2.30	0.8037	0.8513	0.0950	0.1074
2.40	0.7978	0.8477	0.0952	0.1079
2.47	0.7938	0.8453	0.0953	0.1083
2.528	0.7906	0.8434	0.0955	0.1086
2.60	0.7868	0.8411	0.0957	0.1090
2.70	0.7818	0.8381	0.0960	0.1096
2.80	0.7770	0.8354	0.0964	0.1101
3.00	0.7687	0.8306	0.0973	0.1113
3.30	0.7589	0.8246	0.0989	0.1128
3.70	0.7506	0.8177	0.1011	0.1143

[a] Atomic units (a.u.) are used throughout this paper. [b] Active electron approximation.

study. The fourth column of Table II and fifth column of Tables III–V give values of the x component of the **p** integral plotted in Figs. 1–4. The integral values in the second column of these tables multiplied by ΔE_{HF} and ΔE_{RKR} yield the two **r** transition moment curves. The third and fifth columns of Table II and the third and sixth columns of Tables III–V contain values of the active electron approximation to the accurate HF **r** and **p** integrals, respectively. As noted above, this approximation is obtained by deleting all minors in Eq. (18a) except the one multiplying the active electron matrix element which is set equal to unity. The molecular orbitals contained in the matrix element are somewhat more accurate than those obtained by the frozen core method. They are not eigenfunctions of some one-electron Schrödinger equation where the potential is due to the parent ion. In each state the active electron moves in the SCF field generated by the remaining electrons. The deletion of the remaining

minors in (18a) in effect means that no allowance is made for the fact that the inactive electron orbitals adjust to the excited-state SCF potential.

For BeH, MgH, and SH the active electron approximation overestimates the accurate HF **p** and **r** integrals. For the case of the transition of a single electron outside a closed shell the approximation is expected to work quite well. There is an average 6% difference between the HF **r** integrals and the active electron approximation to them for BeH and MgH. The percent difference is doubled if one compares the **p** integral values obtained. For OH, where the active electron approximation underestimates the HF integrals, there is an average 14% difference for the **r** integral values and a 60% difference for the **p** values. Similarly for SH there is poor agreement between the HF values and the active electron approximation to them. As R increases the agreement deteriorates very rapidly.

A particularly inviting procedure that simplifies the

TABLE III. MgH(A $^1\Pi$–X $^1\Sigma^+$) Hartree–Fock, active electron and virtual orbital transition moment integrals.

R	$\langle ^1\Pi \mid x \mid ^1\Sigma^+\rangle$	$\langle 2\pi' \mid x \mid 5\sigma\rangle$[a]	$\langle 2\pi \mid x \mid 5\sigma\rangle$[b]	$-i\langle ^1\Pi \mid p_x \mid ^1\Sigma^+\rangle$	$-i\langle 2\pi' \mid p_x \mid 5\sigma\rangle$[a]	$-i\langle 2\pi \mid p_x \mid 5\sigma\rangle$[b]
2.00	0.9885	1.0431	0.9424	0.0796	0.0923	0.0767
2.20	1.0035	1.0567	0.9561	0.0842	0.0966	0.0805
2.50	1.0119	1.0657	0.9679	0.0893	0.1016	0.0859
2.80	1.0117	1.0682	0.9751	0.0934	0.1058	0.0911
2.95	1.0100	1.0681	0.9779	0.0953	0.1078	0.0936
3.10	1.0076	1.0675	0.9806	0.0970	0.1096	0.0962
3.259	1.0047	1.0665	0.9832	0.0989	0.1115	0.0988
3.40	1.0018	1.0653	0.9854	0.1004	0.1131	0.1012
3.60	0.9977	1.0632	0.9883	0.1026	0.1152	0.1044
3.80	0.9937	1.0606	0.9908	0.1048	0.1172	0.1075
4.15	0.9878	1.0546	0.9939	0.1085	0.1202	0.1123
4.50	0.9842	1.0455	0.9939	0.1122	0.1223	0.1162
5.00	0.8696	0.3620	0.3356	0.0840	0.0040	0.0036

[a] Active electron approximation. [b] Virtual orbital approximation.

TABLE IV. OH$(A\,^2\Sigma^+-X\,^2\Pi)$ Hartree–Fock, active electron and virtual orbital transition moment integrals.

R	$\langle^2\Sigma^+|x|^2\Pi\rangle$	$\langle1\pi'|x|3\sigma\rangle^a$	$\langle1\pi|x|3\sigma\rangle^b$	$-i\langle^2\Sigma^+|p_x|^2\Pi\rangle$	$-i\langle1\pi'|p_x|3\sigma\rangle^a$	$-i\langle1\pi|p_x|3\sigma\rangle^b$
1.50	0.1741	0.1621	0.1583	0.0283	0.0202	0.0154
1.60	0.1588	0.1441	0.1413	0.0253	0.0156	0.0120
1.70	0.1434	0.1266	0.1250	0.0222	0.0115	0.0090
1.75	0.1356	0.1182	0.1172	0.0206	0.0095	0.0077
1.8342	0.1226	0.1046	0.1045	0.0178	0.0065	0.0056
1.90	0.1125	0.0945	0.0952	0.0155	0.0044	0.0042
2.00	0.0972	0.0802	0.0819	0.0120	0.0017	0.0025
2.10	0.0822	0.0672	0.0699	0.0085	−0.0005	0.0011
2.25	0.0605	0.0504	0.0541	0.0031	−0.0028	−0.0004
2.40	0.0402	0.0368	0.0409	−0.0020	−0.0040	−0.0014
2.60	0.0175	0.0235	0.0270	−0.0072	−0.0040	−0.0019

ᵃ Active electron approximation.   ᵇ Virtual orbital approximation.

calculation of molecular transition probabilities is the virtual orbital approximation that involves choosing the lowest virtual molecular orbital of correct symmetry generated in the ground-state HF calculation as an approximation to the orbital describing the active electron in the excited state. Since the ground-state orbitals are orthonormal, all but one of the minors in Eq. (1°ₐ) disappear and one obtains the transition moment rigorously as the active electron matrix element. This virtual orbital approximation is again slightly different from most frozen core calculations in that the molecular orbitals appearing in the active electron matrix element are not eigenfunctions of the same Fock operator for the molecules studied. The virtual orbital approximation results if no consideration is given to orbital adjustments required to describe the excited-state SCF potentials. In this restricted sense we are dealing with a frozen core approximation.

The fourth and seventh columns of Tables III–V present virtual orbital approximations to the HF transition moment integrals for MgH, OH, and SH, respectively. The HF calculations for the BeH ground state do not produce a virtual orbital of the correct symmetry to describe the excited state. For MgH there is an average 2% difference between the approximate and accurate integral values and the virtual orbital approximation gives better values than the previously noted active electron values. For OH the

virtual orbital approximation underestimates the HF r integrals by 13% on the average while the percent difference between p integral values is some five times larger. The results for SH are similar. However the agreement rapidly deteriorates at larger R values to the point where no sensible comparison is possible.

Tables VI–IX present our results for the band oscillator strengths calculated from Eq. (16) using the accurate HF transition moment integrals given in Tables II–V and vibrational wavefunctions obtained from the RKR potential energy curves shown in Figs. 1–4. A comparison of the HF and RKR $U(R)$ curves in Figs. 1–4 shows that their shapes and R_e values are quite similar. Consequently, the theoretical vibrational averages based on the HF $U(R)$ curves will be quite close to the semiempirical averages using the RKR $U(R)$ curves.

The BeH band oscillator strengths, and to a lesser extent the MgH strengths, are indicative of transitions where the Franck–Condon principle is operative. The f values in Tables VI and VII are slowly varying along the diagonal and rapidly fall off as one moves away from the diagonal. This behavior is typical of the case where the transition moment is essentially constant and the ground- and excited-state potential energy curves have similar R_e values and are approximately parallel over the R range of interest. In effect, the Franck–Condon principle prevents the intensity from being distributed

TABLE V. SH$(A\,^2\Sigma^+-X\,^2\Pi)$ Hartree–Fock, active electron and virtual orbital transition moment integrals.

R	$\langle^2\Sigma^+|x|^2\Pi\rangle$	$\langle2\pi'|x|5\sigma\rangle^a$	$\langle2\pi|x|5\sigma\rangle^b$	$-i\langle^2\Sigma^+|p_x|^2\Pi\rangle$	$-i\langle2\pi'|p_x|5\sigma\rangle^a$	$-i\langle2\pi|p_x|5\sigma\rangle^b$
2.00	0.3523	0.3439	0.3462	0.0487	0.0445	0.0471
2.40	0.2491	0.2537	0.2624	0.0256	0.0273	0.0333
2.551	0.2025	0.2198	0.2305	0.0148	0.0216	0.0284
2.70	0.1567	0.1882	0.2005	0.0045	0.0167	0.0241
3.05	0.0746	0.1262	0.1389	−0.0096	0.0093	0.0164
3.60	0.0145	0.0629	0.0715	−0.0115	0.0055	0.0097

ᵃ Active electron approximation.   ᵇ Virtual orbital approximation.

TABLE VI. BeH($A\ ^2\Pi-X\ ^2\Sigma^+$) absorption band oscillator strengths.

v'	v''			
	0	1	2	3
0	0.2008	0.55−3	0.18−4	0.3−6
1	0.72−2	0.2001	0.87−3	0.53−4
2	0.3−5	0.12−3	0.1998	0.98−3
3	0.5−7	0.12−4	0.83−3	0.1998

TABLE VIII. OH($A\ ^2\Sigma^+-X\ ^2\Pi$) absorption band oscillator strengths.

v'	v''			
	0	1	2	3
0	0.206−2	0.7−5	0.9−6	0.1−6
1	0.57−3	0.122−2	0.26−4	0.4−5
2	0.88−4	0.88−3	0.62−3	0.46−4
3	0.12−4	0.25−3	0.93−3	0.27−3

over some of the nondiagonal vibrational combinations. It should be pointed out that if the HF transition moment curves for BeH and MgH differ significantly from the experimental curves with regard to their variation with R, the experimental band intensity pattern will be quite different from that in Tables VI and VII.

The transition moment integrals for OH and SH are much smaller than the analogous quantities for BeH and MgH. Also, the transition moment varies considerably with R and Tables VIII and IX bear evidence to this fact. Although the 0–0 band oscillator strength for OH in Table VIII is still predominant, a variation of the diagonal elements across the table is much more evident than in the two previous tables. Furthermore the rate of decay of the f values on moving away from the diagonal is much more gradual here. For example, the 2–1 band oscillator strength is $\frac{2}{3}$ of the value of the diagonal 1–1 band strength while that for the 3–2 band is actually 50% larger than the diagonal 3–3 band strength. Table IX for SH presents even more convincing evidence of the smearing out of intensity that occurs for the case where the transition moment varies considerably with R.

As indicated in the Introduction, experimentally the OH $(A-X)$ transition has been extensively studied. There is some disagreement with regard to the oscillator strength of this aeronomically important transition. A summary of experimental determinations of the 0–0 band oscillator strength has been presented by Anketell and Pery-Thorne.[21] These investigators obtained a value of $f=(14.3\pm1.3)\times10^{-4}$ that can be compared with our theoretical value of 20.6×10^{-4} from Table VIII. They also obtained $f=(8.9\pm1.7)\times10^{-4}$ for the

1–0 band oscillator strength compared with the theoretical value of 5.7×10^{-4}. We shall not attempt to give a detailed critique of the numerous experimental 0–0 band oscillator strengths published for OH.[22] If Watson's[22b] rather large value is ignored, an unweighted average of the remaining values gives $f\approx8\times10^{-4}$. Thus an estimate of the accuracy of our theoretical value is that it differs from experiment by a factor of 2.5. This indicates that the HF transition moment $M_z(R)$ is approximately 60% too large in the region of R_e for the OH A and X states.

The SCF electronic f values for OH reported by Hurley[24] are based on a minimal basis set calculation performed by Krauss[37] on the ground state and the virtual orbital approximation to the excited state. He obtained a semitheoretical (experimental ΔE) dipole length f value of 1.8×10^{-3} and a dipole velocity f value of 9.5×10^{-2} for $R=1.8342$ a.u. These values can be compared with f values of 2.99×10^{-3} and 2.83×10^{-3}, respectively, calculated using the HF integrals given in Table IV. It is interesting to note that the r integral is hardly changed if one uses accurate HF wavefunctions, whereas the p integral decreases by an order of magnitude. For OH the momentum operator p appears to be more sensitive to improvements in the SCF wavefunctions than the position operator r. However, for accurate HF wavefunctions the dipole length and velocity f values are quite close together and neither is to be preferred in comparison with experiment.

Chin and Davidson[26] define an electronic oscillator strength similar to Eq. (15b) in this paper. Using their definition we calculate a HF electronic oscillator strength of 0.086 at $R=2.528$ a.u. for BeH $(A-X)$ that is approximately 60% larger than the value of 0.053 at

TABLE VII. MgH($A\ ^2\Pi-X\ ^2\Sigma^+$) absorption band oscillator strengths.

v'	v''			
	0	1	2	3
0	0.2501	0.126−1	0.87−3	0.79−4
1	0.159−1	0.2240	0.228−1	0.249−2
2	0.66−4	0.316−1	0.1983	0.314−1
3	0.3−6	0.91−3	0.484−1	0.1714

TABLE IX. SH($A\ ^2\Sigma^+-X\ ^2\Pi$) absorption band oscillator strengths.

v'	v''			
	0	1	2	3
0	0.163−2	0.26−3	0.22−4	0.9−6
1	0.159−2	0.55−3	0.35−3	0.7−4
2	0.75−3	0.131−2	0.20−3	0.26−3
3	0.27−3	0.121−2	0.62−3	0.4−5

TABLE X. A comparison of the transition moment $M_z(R)$ in the position and momentum representations for the BeH, BH$^+$, MgH, AlH$^+$, OH, HF$^+$, SH, and HCl$^+$ ($A-X$) systems.

System	R	x	$-i\langle p_z \rangle$	$\Delta E\langle x \rangle$
BeH($A\,^2\Pi-X\,^2\Sigma^+$)	2.30	0.8037	0.0950	0.0815
BH$^+$($A\,^2\Pi-X\,^2\Sigma^+$)	2.296	0.3920	0.0737	0.0536
MgH($A\,^2\Pi-X\,^2\Sigma^+$)	2.95	1.0100	0.0953	0.0957
AlH$^+$($A\,^2\Pi-X\,^2\Sigma^+$)	3.027	0.6606	0.0996	0.0918
OH($A\,^2\Sigma^+-X\,^2\Pi$)	1.75	0.1356	0.0206	0.0216
HF$^+$($A\,^2\Sigma^+-X\,^2\Pi$)	1.7328	0.0779	0.0102	0.0112
SH($A\,^2\Sigma^+-X\,^2\Pi$)	2.40	0.2491	0.0256	0.0409
HCl$^+$($A\,^2\Sigma^+-X\,^2\Pi$)	2.4087	0.1463	0.0089	0.0229

$R=2.50$ a.u. reported by these researchers using multiconfiguration wavefunctions. Our electronic HF f value of 0.132 at $R=3.259$ a.u. for MgH ($A-X$) is only slightly larger than the Chan–Davidson value of 0.110 at $R=3.25$ a.u. These results seem to indicate that correlation will not affect the HF electronic oscillator strengths in the region of R_e for the states involved by more than a factor of 2 to 5, although it should be pointed out that the atomic orbital basis sets employed by Chan and Davidson[26] in their multiconfiguration studies of BeH and MgH give absolute electronic energies that are actually higher than the HF energies for both the A and X states.

As noted in the Introduction, the most recent experimental intensity measurements[25a] give an upper bound of 2.0×10^{-3} for the MgH ($A-X$) 0–0 absorption band oscillator strength. Our theoretical value of 2.501×10^{-1} in Table VII differs from experiment by two orders of magnitude. Westhaus and Sinanoğlu[4b] note that for atoms the inclusion of correlation usually influences HF oscillator strengths by factors of 2–3. For diatomic hydrides where experimental oscillator strengths are available, the results of Huo[10b] for some CH and NH systems and the results for OH ($A-X$) given in this paper seem to indicate that HF oscillator strengths can be expected to have at least order-of-magnitude accuracy. These arguments together with the considerations of the previous paragraph lead the authors to believe that the effect of correlation on the HF transition moment will not resolve the discrepancy between theory and experiment for the MgH ($A-X$) system. Clearly, additional experimental efforts are highly desirable to resolve this dilemma.

In Table X values of the transition moment integrals at a single value of R are presented for the ($A-X$) transition in the singly ionized species that are isoelectronic to the neutral molecules studied in this paper. The value of R is in the region of the R_e values for the states involved. If we assume that the behavior of the transition moment as a function of R and the correlation corrections will be similar for the neutral and charged isoelectronic species, we can make qualitative predictions concerning the electronic oscillator strengths

of the ions with respect to the neutral molecules. We use the mixed oscillator strength that corresponds to the geometric mean of the third and fourth columns of Table X. The BeH and MgH oscillator strengths will be roughly 50% larger than the strengths for BH$^+$ and AlH$^+$, respectively, while the OH and SH oscillator strengths will be approximately twice as large as the strengths for HF$^+$ and HCl$^+$, respectively.

An estimation of the error in a molecular HF transition moment due to correlation requires a consideration of two factors. A knowledge of the correlation in the vicinity of the ground- and excited-state R_e values is necessary. Also, it must be determined whether or not the correlation correction varies considerably as a function of R. It is difficult to predict the magnitude of the correction to the HF transition moment in the region of R_e for the states involved. The work of Chan and Davidson[26] indicates that there is a substantial number of important configurations in the BeH and MgH $A\,^2\Pi$ multiconfiguration wavefunctions. Consequently a simple interpretation of the defects in the HF model will not be possible. Transition moments as a function of R for the BeH and MgH ($A-X$) systems based on the Chan–Davidson wavefunctions will be given by one of the authors[58] and a more detailed discussion of correlation effects will be presented.

The analogy between the BeH and MgH ($A-X$) transitions and certain atomic transitions was suggested in order to strengthen our hypothesis that the probabilities characterizing such molecular transitions are adequately described by HF calculations. Such comparisons are not always effective. HF and multiconfiguration calculations performed by Weiss[1e] indicate that the $2p-3s$ transition probability in $B\,I$ is relatively insensitive to correlation. However, for the isoelectronic $C\,II$ ion the configuration $2s2p^2$ plays a considerable role in lowering the oscillator strength by a factor of 5 from its HF value. The analogy between atoms and molecules is also dependent on how much s character is present in σ orbitals and how much p character is present in π orbitals.
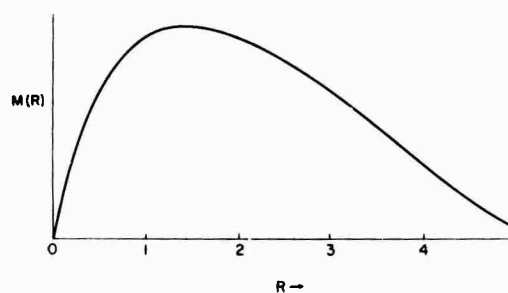
FIG. 5. A schematic representation of the accurate Born–Oppenheimer transition moment for the BeH, OH, MgH, and SH ($A-X$) systems (R scale arbitrary).

229

For the $(A-X)$ systems considered in this paper the united $(R=0)$ and separated $(R=\infty)$ atom limits for the ground and excited states are

$$B\ (^2P)\rightarrow BeH\ (X\ ^2\Sigma^+)\rightarrow Be\ (^1S)+H\ (^2S)$$
$$\rightarrow BeH\ (A\ ^2\Pi)\rightarrow Be\ (^1P)+H\ (^2S),$$

$$Al\ (^2P)\rightarrow MgH\ (X\ ^2\Sigma^+)\rightarrow Mg\ (^1S)+H\ (^2S)$$
$$\rightarrow MgH\ (A\ ^2\Pi)\rightarrow Mg\ (^1P)+H\ (^2S),$$

$$F\ (^2P)\rightarrow OH\ (X\ ^2\Pi)\rightarrow O\ (^3P)+H\ (^2S)$$
$$\rightarrow OH\ (A\ ^2\Sigma^+)\rightarrow O\ (^1D)+H\ (^2S),$$

$$Cl\ (^2P)\rightarrow SH\ (X\ ^2\Pi)\rightarrow S\ (^3P)+H\ (^2S)$$
$$\rightarrow SH\ (A\ ^2\Sigma^+)\rightarrow S\ (^1D)+H\ (^2S).$$
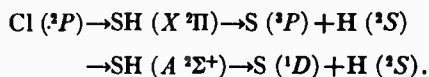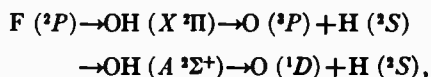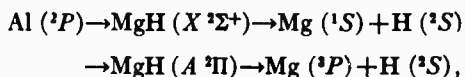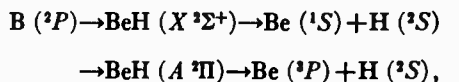
At $R=0$ the transition for these systems is forbidden because the upper and lower states are degenerate, while at $R=\infty$ the transition probability is zero if the dissociation products are described within the LS-coupling scheme. Figure 5 gives a schematic representation of the shape of the transition moment curve that is to be expected for a transition that is forbidden in the united and separated atom limits but allowed at intermediate R values. The curve rises fairly rapidly to a maximum in the vicinity of the R_e values of the states involved and decreases to zero at a slower rate for large R.

The general shape suggested by Fig. 5 is not evident in the transition moment curves for BeH and MgH in Figs. 1 and 2. A consideration of the curves over the limited range of R values for which HF calculations were carried out gives no indication that $M_x(R)$ approaches zero for large R. This fact together with the earlier suggestion of a reasonably accurate transition moment in the region of R_e for the states involved leads us to predict a considerable variation with R of the correlation correction to the HF transition moments. The correction should increase on going from intermediate to larger values of R.

Figures 3 and 4 for OH and SH seem to indicate a more acceptable variation of $M_x(R)$ for large R. It is difficult to predict the atomic components of a molecular restricted HF wavefunction in the limit of large R. However, arguments similar to those used by Green[59] yield $O^-(1s^22s^22p^5)$ and H^+ as the principle dissociation products of both the A and X states of OH and $S^-(1s^22s^22p^63s^23p^5)$ and H^+ as the principle dissociation products of the SH states. If these were the only dissociation products the HF potential curves in Figs. 3 and 4 would become degenerate at large R and the transition moment would go to zero in the limit. The fact that the $M_x(R)$ curves for OH and SH appear to be approaching zero for large R together with the knowledge that the M_x values for OH are too large in

the region of R_e for the states involved leads us to predict a sizeable variation with R of the correlation correction to the HF $M_x(R)$ curves. The correction should decrease on going from intermediate to larger values of R. Again this very qualitative conclusion is reached from a knowledge of the HF $M_x(R)$ curves over a rather limited range of internuclear distances.

The mixed oscillator strength expression gives essentially the geometric mean of the dipole length and velocity quantities. Inherent in the definition of the mixed oscillator strength is the idea that approximate f values calculated using the length and velocity transition moments bracket the accurate value. Hence their mean should be a more reliable measure of the transition probability and should be less sensitive to correlation effects. However, this rationalization does not account for the many instances where approximate length and velocity f values are both higher or lower than experiment and consequently their mean is subject to considerable correction. Our use of the mixed oscillator strength is based on the fact that the formal energy term is absent in its definition. We do not propose that it provides a satisfactory solution to the problem of correlation corrections to molecular HF transition probabilities.

ACKNOWLEDGMENTS

* This research was supported by the Advanced Research Projects Agency of the Department of Defence and was monitored by the U.S. Army Research Office—Durham, Box CM, Duke Station, Durham, N.C. 27706, under Contract No. DA-31-124-ARO-D-447.

† National Research Council, Canada, Postdoctoral Fellow (1968-1969).

‡ Present address: Department of Chemistry, University of Massachusetts, Amherst, Mass. 01002.

[1] For recent reviews see: (a) R. J. S. Crossley, Advan. At. Mol. Phys. 5, 237 (1969); (b) W. L. Wiese, in *Methods of Experimental Physics*, edited by B. Bederson and W. L. Fite (Academic, New York, 1968), Vol. 7A, p. 117; (c) A. Dalgarno, in *Atomic Physics, Proceedings of the First International Conference on Atomic Physics*, edited by B. Bederson, V. W. Cohen, and F. M. J. Pichanick (Plenum, New York, 1969), p 101.

[2] B. Schiff and C. L. Pekeris, Phys. Rev. A134, 638 (1964).

[3] (a) A. W. Weiss, Astrophys. J. 138, 1262 (1963); (b) A. W. Weiss, Phys. Rev. 162, 71 (1967); (c) A. W. Weiss, J. Chem. Phys. 47, 3573 (1967); (d) W. L. Wiese and A. W. Weiss, Phys. Rev. 175, 50 (1968); (e) A. W. Weiss, *ibid.* 188, 119 (1969).

[4] (a) S. R. La Paglia and O. Sinanoğlu, J. Chem. Phys. 44, 1888 (1966); (b) P. Westhaus and O. Sinanoğlu, Astrophys. J. 157, 997 (1969); (c) P. Westhaus and O. Sinanoğlu, Phys. Rev. 183, 56 (1969).

[5] (a) Y.-K. Kim and M. Inokuti, Phys. Rev. 175, 176 (1968); (b) 181, 205 (1969); (c) 184, 38 (1969); (d) M. Inokuti and Y.-K. Kim, *ibid.* 186, 100 (1969).

[6] (a) P. E. Cade and W. M. Huo, J. Chem. Phys. 47, 614, 649 (1967); (b) P. E. Cade, "Hartree–Fock–Roothaan Wavefunctions for First-Row Diatomic Molecules. AH, A₂, and AB," Special Tech. Rept., Laboratory of Molecular Structure and Spectra (to be published).

[7] A. D. McLean and M. Yoshimine, "Tables of Linear Molecule Wavefunctions" [a supplement to the paper by A. D. McLean and M. Yoshimine, IBM J. Res. Develop. 12, 206 (1968)].

[8] (a) R. F. W. Bader, W. H. Henneker, and P. E. Cade, J. Chem. Phys. 46, 3341 (1967); (b) R. F. W. Bader, I. Keaveny, and P. E. Cade, ibid. 47, 3381 (1967); (c) R. F. W. Bader and A. D. Bandrauk, ibid. 49, 1653 (1968); (d) P. E. Cade, R. F. W. Bader, W. H. Henneker, and I. Keaveny, ibid. 50, 5313 (1969).

[9] B. J. Ransil and J. J. Sinai, J. Chem. Phys. 46, 4050 (1967).

[10] (a) W. M. Huo, J. Chem. Phys. 45, 1554 (1966); (b) 49, 1482 (1968).

[11] C. C. J. Roothaan and P. S. Bagus, Methods Computational Phys. 2, 47 (1963).

[12] P. E. Cade (unpublished).

[13] P. E. Cade, R. F. W. Bader, and J. Pelletier, J. Chem. Phys. (to be published).

[14] R. W. Nicholls and A. L. Stewart, in Atomic and Molecular Processes, edited by D. R. Bates (Academic, New York, 1962), p. 47.

[15] E. M. Bulewicz, P. J. Padley, and R. E. Smith, Proc. Roy. Soc. (London) A315, 129 (1970).

[16] W. Heitler, The Quantum Theory of Radiation (Oxford U. P., Oxford, England, 1953), 3rd ed., Chap. 5.

[17] L. Wolniewicz, J. Chem. Phys. 51, 5002 (1969).

[18] (a) P. E. Cade and W. M. Huo, J. Chem. Phys. 45, 1063 (1966). (b) C. F. Bender and E. R. Davidson, Phys. Rev. 183, 23 (1969).

[19] H. E. Popkie and W. H. Henneker, J. Chem. Phys. (to be published).

[20] G. Herzberg, Mem. Soc. Roy. Sci. Liege 54, 121 (1969).

[21] P. E. Cade and H. E. Popkie, Mem. Soc. Roy. Sci. Liege 54, 161 (1969).

[22] P. G. Wilkinson and R. S. Mulliken, Astrophys. J. 126, 10 (1957).

[23] (a) O. Oldenburg and F. F. Rieke, J. Chem. Phys. 6, 439, 779 (1939); (b) R. J. Dwyer and O. Oldenburg, ibid. 12, 351 (1944); (c) P. J. Dyne, ibid. 28, 999 (1958); (d) T. Carrington, ibid. 31, 1243 (1959); (e) P. M. Golden, F. P. Del Greco, and F. Kaufman, ibid. 39, 3034 (1963); (g) W. Bennett and R. W. Dalby, ibid. 40, 1414 (1964). (h) R. Watson, J. Quant. Spectry. Radiative Transfer 4, 1 (1964); (i) J. Anketell and A. Pery-Thorne, Proc. Roy. Soc. (London) A301, 343 (1967); (j) K. R. German and R. N. Zare, Phys. Rev. Letters 23, 1207 (1969); (k) W. H. Smith, J. Chem. Phys. 53, 792 (1970).

[24] A. C. Hurley, Proc. Roy. Soc. (London) A249, 402 (1959).

[25] (a) A. Schadee, Bull. Astron. Inst. Neth. 5, 311 (1964); (b) R. P. Main, D. J. Carlson, and R. A. Dupuis, J. Quant. Spectry. Radiative Transfer 7, 805 (1967).

[26] (a) A. C. H. Chan and E. R. Davidson, J. Chem. Phys. 49, 727 (1968); (b) 52, 4108 (1970).

[27] H. A. Bethe and E. E. Salpeter, Quantum Mechanics of One- and Two-Electron Atoms (Springer, Berlin, 1957), p. 270.

[28] S. Rothenberg and E. R. Davidson, J. Mol. Spectry. 22, 1 (1967).

[29] R. S. Mulliken and C. A. Rieke, Rept. Progr. Phys. 8, 231 (1941).

[30] (a) R. T. Pack and J. O. Hirschfelder, J. Chem. Phys. 49, 4009 (1968); (b) W. Kolos and L. Wolniewicz, Rev. Mod. Phys. 35, 473 (1963); (c) P. R. Bunker, J. Mol. Spectry. 28, 422 (1968).

[31] I. Kovacs, Rotational Structure in the Spectra of Diatomic Molecules (American Elsevier, New York, 1969).

[32] (a) N. V. Cohan and H. F. Hameka, J. Chem. Phys. 45, 4392 (1966); (b) C. A. Mead and A. Moscowitz, Intern. J. Quantum Chem. 1, 243 (1967); (c) R. A. Harris, J. Chem. Phys. 50, 3947 (1969).

[33] J. B. Tatum, Astrophys. J. Suppl. Ser. 14, 21 (1967).

[34] A. E. Hansen, Mol. Phys. 13, 425 (1967).

[35] W. Lamb, R. Young, and S. R. La Paglia, J. Chem. Phys. 49, 2868 (1968).

[36] P.-O. Lowdin, Phys. Rev. 97, 1474 (1955).

[37] F. Prosser and S. Hagstrom, Intern. J. Quantum Chem. 2, 89 (1968).

[38] C. C. J. Roothaan, J. Chem. Phys. 19, 1445 (1951).

[39] (a) M. Geller, J. Chem. Phys. 39, 84 (1963); (b) 41, 4006 (1964).

[40] H. J. Silverstone, J. Chem. Phys. 45, 4337 (1966).

[41] W. H. Henneker and P. E. Cade, Chem. Phys. Letters 2, 575 (1968).

[42] F. J. Zeleznik, J. Chem. Phys. 42, 2836 (1965).

[43] E. Olsson, Z. Physik 73, 732 (1932).

[44] (a) A. Guntsch, Z. Physik 104, 584 (1937); (b) M. A. Khan, Proc. Phys. Soc. (London) 80, 523 (1962).

[45] (a) J. W. Chamberlain and F. L. Roesler, Astrophys. J. 121, 541 (1955); (b) R. F. Barrow, Arkiv Fysik 11, 281 (1956).

[46] D. A. Ramsay, J. Chem. Phys. 20, 1920 (1952).

[47] (a) J. W. Cooley, Math. Computation 15, 363 (1961); (b) J. M. Blatt, J. Computational Phys. 1, 382 (1967); (c) L. Wolniewicz, J. Chem. Phys. 45, 515 (1966).

[48] B. Numerov, Publ. Observatoire Central Astrophys. Russia 2, 188 (1933).

[49] E. S. Chang and M. R. C. McDowell, Phys. Rev. 176, 126 (1968).

[50] A. V. Ivanova, Liet. Fiz. Rink 3, 185 (1963).

[51] S. R. La Paglia, J. Mol. Spectry. 24, 302 (1967).

[52] R. W. Nicholls, Proc. Phys. Soc. (London) A69, 741 (1956).

[53] (a) J. Hargreaves, Proc. Cambridge Phil. Soc. 25, 75 (1928); (b) V. K. Prokof'ev, Z. Physik 58, 255 (1929).

[54] (a) R. P. McEachran, C. E. Tull, and M. Cohen, Can. J. Phys. 47, 835 (1969); (b) 46, 2675 (1968).

[55] (a) M. Cohen and P. S. Kelly, Can. J. Phys. 45, 1661, 2079 (1967).

[56] D. R. Bates and A. Damgaard, Phil. Trans. Roy. Soc. London A242, 101 (1949).

[57] M. Krauss, J. Chem. Phys. 28, 1021 (1958).

[58] H. E. Popkie, J. Chem. Phys. (to be published).

[59] S. Green, J. Chem. Phys. 52, 3100 (1970).

231

THEORETICAL ELECTRONIC TRANSITION

PROBABILITIES IN DIATOMIC MOLECULES

II. 13-ELECTRON SEQUENCE[*]

H. E. Popkie[†#]

and

W. H. Henneker[†‡]

Laboratory of Molecular Structure and Spectra
Department of Physics
University of Chicago
Chicago, Illinois 60637

ABSTRACT

Hartree-Fock (HF) electronic dipole-momentum and dipole-length transition moments, $M(R)$ and $\bar{M}(R)$ respectively, are presented as a function of the internuclear distance R for the N_2^+ ($B^2\Sigma_u^+ - X^2\Sigma_g^+$) first negative and ($A^2\Pi_u - X^2\Sigma_g^+$) Meinel systems. They are compared with 'experimental' $M(R)$ and $\bar{M}(R)$ curves obtained by using relative band transition probability and upper state lifetime measurements recently reported in the literature. Vibrational averages of both the theoretical and 'experimental' transition moments are computed and used to calculate some relative band oscillator strengths $f_{v'v''}/f_{00}$. The HF f_{00} value of 0.1370 for the first negative system differs from experiment by a factor of 5.6. For the Meinel system the HF f_{00} value of 1.065×10^{-2} is too large by a factor of 3.3 or 7.3 depending on whether the lifetime data of O'Neil and Davidson or that of Hollstein et al. are used to determine the experimental value. HF transition moment calculations at a single value of R are also reported for the ($B^2\Sigma_u^+ - X^2\Sigma_g^+$) and ($A^2\Pi_u - X^2\Sigma_g^+$) systems of C_2^- and for the ($^2\Pi_i - X^2\Sigma^+$) and ($^2\Pi_r - X^2\Sigma^+$) systems of CN, CO$^+$, BO, BF$^+$ and BeF. Electronic absorption oscillator strengths are presented and compared with experiment where possible.

I. INTRODUCTION

In the first paper[1] of this series (hereafter referred to as I) the current status of the theoretical calculation of diatomic transition probabilities was briefly reviewed. Transition moment calculations using Hartree-Fock (HF) wave functions were presented for the BeH, MgH, OH, and SH (A-X) systems. These results together with the results of Huo[2] for some CH and NH systems indicate that for diatomic hydrides HF oscillator strengths can be expected to have only order of magnitude accuracy. For the cases where reliable experimental data were available for comparison, HF f values differed from experiment by factors of 2-5. Also, for the systems studied in I, a considerable variation with internuclear distance R was predicted for the correlation correction to the HF transition moments on going from intermediate to larger values of R.

In the present paper we are principally concerned with the N_2^+ $(B^2\Sigma_u^+ - X^2\Sigma_g^+)$ first negative and N_2^+ $(A^2\Pi_u - X^2\Sigma_g^+)$ Meinel systems. The states involved in these transitions arise from the following MO configurations:

$$X^2\Sigma_g^+: \quad KK'2\sigma_g^2 2\sigma_u^2 1\pi_u^4 3\sigma_g \quad (KK' \equiv 1\sigma_g^2 1\sigma_u^2)$$

$$A^2\Pi_u: \quad KK'2\sigma_g^2 2\sigma_u^2 1\pi_u^3 3\sigma_g^2$$

$$B^2\Sigma_u^+: \quad KK'2\sigma_g^2 2\sigma_u 1\pi_u^4 3\sigma_g^2$$
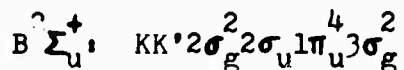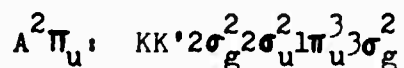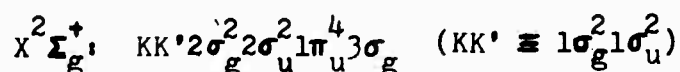
These transitions belong to the class discussed in I for which the number of electron pairs is conserved. Previous theoretical work dealing with the transition probabilities of these systems consists

234

of the approximate N_2^+ (B-X) electronic oscillator strength calcula-
tions reported by Bates[3] and Shull[4].

Also considered are transitions involving other members
of the diatomic 13-electron sequence, namely C_2^-, CN, CO^+, BO, BF^+,
BeF, MgH, and AlH^+. For the last two members, the $(A^2\Pi - X^2\Sigma^+)$
system has been considered in I. The ground states of CN, CO^+, BO
and BeF have been known experimentally for many years[5]. They were
reviewed in 1932 by Mulliken[6] who ascribed the normal states to the
MO configuration:

$$X^2\Sigma^+: \quad KL4\sigma^2 5\sigma \quad (KL \equiv 1\sigma^2 2\sigma^2 3\sigma^2 1\pi^4)$$
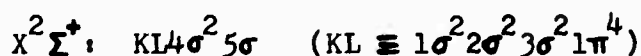
For the 13-electron heteronuclear diatomics there are two low-
lying excited states of interest to us arising from the following
configurations:

$$^2\Pi_r: \quad KL4\sigma^2 2\pi$$

$$^2\Pi_i: \quad K2\sigma^2 3\sigma^2 1\pi^3 4\sigma^2 5\sigma^2$$
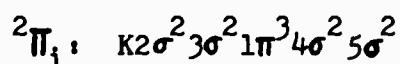
For MgH, AlH^+ and BeF the lowest excited doublet state, $A^2\Pi$, arises
from the $^2\Pi_r$ configuration[6,7]. However, as one considers members of
the isoelectronic sequence such that $Z_A - Z_B$ decreases, the $^2\Pi_i$
configuration achieves greater stability than the $^2\Pi_r$ configuration.
For BO, CO^+, CN and N_2^+ the $A^2\Pi$ state arises from the $^2\Pi_i$ configur-
ation[6]. HF calculations[8] actually predict that the $A^2\Pi$ state is
more stable than the $X^2\Sigma^+$ state for N_2^+, CN and C_2^-.[9] The $^2\Pi_r$ config-
uration gives rise to the $H^2\Pi$ state in CN[10].

Extensive HF calculations as a function of R for the $X^2\Sigma_g^+$,

235

$A^2\Pi_u$ and $B^2\Sigma_u^+$ states of N_2^+ have been reported by Cade, Sales and Wahl[8a]. Calculations at one or more R values for the $X^2\Sigma_g^+$, $A^2\Pi_u$ and $B^2\Sigma_u^+$ states of C_2^- and for the $X^2\Sigma^+$, $^2\Pi_r$ and $^2\Pi_i$ states of the heteronuclear members of the 13-electron sequence have been documented by Cade[8b] and are the subject of a paper being prepared for publication[8c]. These HF wave functions are used to calculate the electronic transition moments reported in this paper.

A completely general theoretical analysis of isoelectronic sequences in diatomic molecules has proven to be largely an unsolved problem. The Z-expansion technique[11] that has been useful in the classification of atomic properties has so far not been successfully extended to diatomic molecules, although Hall and Rees[12] have made an attempt in the case of 2- and 4-electron hydrides. Alternatively, the empirical analysis of a large number of molecular properties within a given isoelectronic sequence can be attempted. Such internal comparisons hopefully might lead to an ad hoc parameter that would be the analogue of $1/Z$ in the atomic case. One of the purposes of this paper is to provide HF transition probabilities for certain members of the 13-electron sequence and thereby enlarge the repertory of molecular properties that can be used in an analysis of this sequence.

The first negative and Meinel bands of N_2^+ are common features of the auroral and upper atmosphere spectra[13]. The 0-0 band of the (B-X) system is also observed in the twilight airglow. The CO^+ (A-X) system is a prominent component of the spectra of comets. These afore-mentioned systems and CN (A-X) bands are all observed in the emission spectra of shock-heated air. A recent review by Ortenberg and Antropov[14] provides a concise summary of the three principle methods of obtaining transition probabilities and a bibliography

of experimental data. For the N_2^+ (B-X) system, a considerable number of experimental studies have been reported in the literature dealing with the measurement of relative band transition probabilities[15] and intensities[16], lifetimes of upper state vibrational levels[17], and absolute intensities[18] and oscillator strengths[19]. Tyte and Nicholls[20] have presented a summary of experimental work until 1964. A recent review by Srivastava and Mirza[15c] of relative band intensity measurements for the v'=0 progression shows that there is fairly good agreement among the results of different workers using various excitation mechanisms. Bennett and Dalby[17a] were the first investigators to attempt to measure the lifetime of the $B^2\Sigma_u^+$ state. Numerous subtly refined versions of their experiment have been performed in the last eleven years[17] and these have been reviewed by Hesser[21] and Johnson and Fowler[17k]. Several workers[18,22] have used experimental data to determine the variation of the dipole-length transition moment $\overline{M}(R)$ with R and hence to obtain 'smoothed' arrays of vibrational transition probabilities and oscillator strengths. For the N_2^+ (A-X) system, the situation is less satisfactory from an experimental point of view. Some results have been reported concerning relative band transition probability[15e] and intensity[23], lifetime[24], and oscillator strength[25] measurements. However, there is some disagreement among the results of various researchers. Attempts[23cd,26] to determine the variation of $\overline{M}(R)$ with R appear to be inconclusive. Wentink et al.[27] have obtained electronic oscillator strengths for the CN and CO^+ (A-X) transitions using available experimental data[28,29] for these systems. The CO^+ $A^2\Pi$ lifetime has also recently been measured

237

by Desesquelles et al.[17h]. There appear to be no absolute measurements for any of the other systems studied, although it is thought[30] that $f_{el} > 10^{-3}$ for the BO (A-X) system.

In the present paper relative band transition probabilities measured by Stanton and St. John[15e] are used to determine the variation with respect to R of both the dipole-momentum and dipole-length transition moments for the N_2^+ first negative and Meinel systems. These semiempirical curves are put on an absolute basis using available lifetime data[17,24] and are compared with theoretical ones resulting from quantum mechanical calculations. A brief summary of pertinent theoretical expressions is given in Section II (for a more detailed account, see I). The methods used to calculate HF electronic transition moments, to construct RKR potential energy curves, and to compute vibrational wave functions have been described in I and are not repeated here. For the $X^2\Sigma_g^+$, $A^2\Pi_u$ and $B^2\Sigma_u^+$ states of N_2^+, the spectroscopic constants employed in the calculation of RKR curves were those used by Gilmore[31]. Section III outlines the procedure used to determine 'experimental' transition moment curves for the N_2^+ systems. Theoretical results are presented and compared with experiment in Section IV.

238

II. THEORY

In the semi-classical theory of radiation[32], the probability for a spontaneous transition from the upper state Γ' to the lower state Γ'' of a diatomic system accompanied by the emission of a light quantum $\hbar\omega_{\Gamma'\Gamma''}$ is given by

$$A_{\Gamma'\Gamma''} = \frac{4e^4}{3c^3 a_0^3 m_e^2} \frac{\Delta E_{\Gamma'\Gamma''}}{\omega_{\Gamma'}} S_{\Gamma'\Gamma''} \tag{1}$$

where $\Delta E_{\Gamma'\Gamma''}$, $S_{\Gamma'\Gamma''}$ are in a.u. and $A_{\Gamma'\Gamma''}$ is in $\sec^{-1}$. $\Delta E_{\Gamma'\Gamma''}$ is the energy difference between state Γ' (with degeneracy factor $\omega_{\Gamma'}$) and state Γ'' (with degeneracy factor $\omega_{\Gamma''}$). In the dipole approximation, the line strength $S_{\Gamma'\Gamma''}$ is equal to the square of the momentum transition moment summed over all degenerate components of Γ' and Γ'':

$$S_{\Gamma'\Gamma''} = \sum_{\alpha'\alpha''} \left| \int \{ \gamma(\vec{p}' | \vec{p}) \, \vec{p} \}_{\vec{p}'=\vec{p}} \, d\vec{p} \right|^2 . \tag{2}$$

$\gamma(\vec{p}' | \vec{p})$ is the first order spinless transition density matrix in momentum space:

$$\gamma(\vec{p}' | \vec{p}) = N \int \Psi_{\Gamma'}^*(\vec{p}', \vec{p}_2, \ldots \vec{p}_N, \vec{P}_R) \, \Psi_{\Gamma''}(\vec{p}, \vec{p}_2, \ldots \vec{p}_N, \vec{P}_R) \, \frac{d\vec{P}_R d\vec{p}^N ds^N}{d\vec{p}_1} . \tag{3}$$

In equation (3), the $\vec{p}_\mu$ represent the electronic momentum vectors conjugate to the position vectors $\vec{r}_\mu$ measured relative to a space-fixed coordinate system. The nuclear momentum vector $\vec{P}_R$ is conjugate to the internuclear axis vector $\vec{R}$ (directed from nucleus A to nucleus B). The integration is over the spin coordinates of

239

all electrons and the space coordinates of all particles except electron 1. For a transition from Γ'' to Γ', the absorption oscillator strength is defined as

$$f_{\Gamma'\Gamma''} = \frac{2}{3}\frac{1}{\Delta E_{\Gamma'\Gamma''}}\frac{S_{\Gamma'\Gamma''}}{\omega_{\Gamma''}} \quad . \tag{4}$$

After transforming to a molecule-fixed frame of reference and applying the Born-Oppenheimer approximation, one obtains for the oscillator strength[33]:

$$f^{\Omega'v'j'}_{\Omega''v''j''} = \frac{2}{3}\frac{1}{\Delta E^{\Omega'v'j'}_{\Omega''v''j''}}\frac{\sum\limits_{\alpha'\alpha''} P^{\Omega'v'j'}_{\Omega''v''j''} S^{j'\Omega'}_{j''\Omega''}}{(2-\delta_{0,\Lambda''})(2S''+1)(2j''+1)} \quad . \tag{5}$$

Ω, Λ, v, and j are the quantum numbers for the total and orbital electronic angular momentum about the internuclear axis, vibration, and total angular momentum respectively, $2S''+1$ is the spin multiplicity of the lower state, $S^{j'\Omega'}_{j''\Omega''}$ is the Hönl-London factor, and

$$P^{\Omega'v'j'}_{\Omega''v''j''} = \left| \int P_{\Omega'v'j'}(R)\, M_{\Omega'\Omega''}(R)\, P_{\Omega''v''j''}(R)\, dR \right|^2 \quad . \tag{6}$$

In (6), the $P_{\Omega v j}(R)$ are vibration-rotation wave functions and $M_{\Omega'\Omega''}(R)$ is the electronic dipole-momentum transition moment:

$$M_{\Omega'\Omega''}(R) = -i\, N \int \Psi^*_{\Omega'}(\vec{r}^N,R)\, \vec{p}\, \Psi_{\Omega''}(\vec{r}^N,R)\, d\vec{r}^N\, ds^N \tag{7}$$

In (7), the $\Psi_{\Omega}(\vec{r}^N,R)$ are electronic wave functions, $\vec{p} = -i\vec{\nabla}$, and the integration is over the spin and space coordinates of all electrons.

As discussed in I, application of the commutator relation between electronic position and momentum coordinates and the Born-Oppenheimer approximation leads to another expression for the oscillator strength:

$$f^{\Omega'v'j'}_{\Omega''v''j''} = \frac{2}{3} \frac{\Delta E^{\Omega'v'j'}_{\Omega''v''j''} \sum\limits_{\alpha'\alpha''} \overline{P}^{\Omega'v'j'}_{\Omega''v''j''} S^{j'\Omega'}_{j''\Omega''}}{(2-\delta_{0,\Lambda''})(2S''+1)(2j''+1)} \tag{8}$$

where $\overline{P}^{\Omega'v'j'}_{\Omega''v''j''}$ is given by expression (6) with $M_{\Omega'\Omega''}(R)$ replaced by the electronic dipole-length transition moment $\overline{M}_{\Omega'\Omega''}(R)$:

$$\overline{M}_{\Omega'\Omega''}(R) = N \int \Psi^*_{\Omega'}(\vec{r}^N,R) \, \vec{r} \, \Psi_{\Omega''}(\vec{r}^N,R) \, d\vec{r}^N \, ds^N \quad . \tag{9}$$

If vibration-rotation interaction is neglected and the mixed expression for the oscillator strength that corresponds to the geometric average of (5) and (8) is used, vibrational band oscillator strengths can be defined as:

$$f^{\Omega'v'}_{\Omega''v''} = \frac{2}{3} \frac{\sum\limits_{\alpha'\alpha''} \left| \overline{P}^{\Omega'v'0}_{\Omega''v''0} P^{\Omega'v'0}_{\Omega''v''0} \right|^{1/2}}{(2-\delta_{0,\Lambda''})(2S''+1)} \quad . \tag{10}$$

Expression (10) is used exclusively for the calculation of band oscillator strengths. In the remainder of this paper, the labels $M_{\Omega'\Omega''}(R)$, $\overline{M}_{\Omega'\Omega''}(R)$, and $f^{\Omega'v'}_{\Omega''v''}$ are replaced by $M(R)$, $\overline{M}(R)$ and $f_{v'v''}$ respectively and the dependence on the quantum numbers Ω' and Ω'' of the two electronic states under consideration is implicitly understood.

241

III. DETERMINATION OF 'EXPERIMENTAL' TRANSITION MOMENT CURVES

The procedure used to determine the variation of the electronic transition moment with R from experimental relative band transition probability or intensity measurements differs somewhat from that usually employed[34] in that the R-centroid approximation[35] is not used and both the dipole-length and dipole-momentum transition moments are considered. If the moments are expanded as polynomials in R,

$$M(R) = \sum_i m_i R^i \tag{11a}$$

and

$$\bar{M}(R) = \sum_i \bar{m}_i R^i \quad, \tag{11b}$$

vibrational matrix elements can be expressed as

$$M_{v'v''} = \sum_i m_i \langle v'|R^i|v''\rangle \tag{12a}$$

and

$$\bar{M}_{v'v''} = \sum_i \bar{m}_i \langle v'|R^i|v''\rangle \quad. \tag{12b}$$

Experimental matrix elements are defined as

$$M'_{v'v''} = (\tilde{I}_{v'v''}/\Delta E^2_{v'v''})^{\frac{1}{2}} \tag{13a}$$

and

$$\bar{M}'_{v'v''} = (\tilde{I}_{v'v''}/\Delta E^4_{v'v''})^{\frac{1}{2}} \quad, \tag{13b}$$

where $\tilde{I}_{v'v''}$ is the relative intensity of the v'-v" band measured in emission. Since $\tilde{I}_{v'v''}$ is proportional to $N_{v'}\Delta E^2_{v'v''}M^2_{v'v''}$, $N_{v'}$ being the population of the upper vibrational level, the following identity is valid (to within the accuracy of the experimental data):

242

$$M'_{v'v''} = c_{v'}M_{v'v''}. \tag{14a}$$

242

The constant $c_{v'}$ in (14a) depends on the population $N_{v'}$ and also on the absolute intensity of the band used as the standard of reference for the experimental $\widetilde{I}_{v'v''}$ measurements. Similarly, since $\widetilde{I}_{v'v''}$ is also proportional to $N_{v'}\Delta E_{v'v''}^{4}\overline{M}_{v'v''}^{2}$:

$$\overline{M}_{v'v''}' = \overline{c}_{v'}\overline{M}_{v'v''} . \tag{14b}$$

If relative band transition probabilities in the form of optical cross sections $\widetilde{Q}_{v'v''}$ are available, $M_{v'v''}'$ and $\overline{M}_{v'v''}'$ are defined by (13a) and (13b) with $\widetilde{I}_{v'v''}$ replaced by $\Delta E_{v'v''}\widetilde{Q}_{v'v''}$. Since $\widetilde{Q}_{v'v''}$ is proportional to $Q_{v'}\Delta E_{v'v''}M_{v'v''}^{2}$, $Q_{v'}$ being the apparent cross section of the upper vibrational level, the identities (14a) and (14b) remain valid with $c_{v'}$ and $\overline{c}_{v'}$ depending on $Q_{v'}$.

Equations (14a) and (14b) imply that the experimental matrix elements are normalized differently for the various v' sequences. If the transition moment expansions given by (11a) and (11b) are to be used for all sequences, it is necessary to scale the sequences respect to one of them , say the v^* one, and then to scale expansion (11a) to the $M_{v^*v''}'$ values and (11b) to the $\overline{M}_{v^*v''}'$ values. To accomplish this we introduce the factors $c_{v'}' = c_{v^*}/c_{v'}$, $\overline{c}_{v'}' = \overline{c}_{v^*}/\overline{c}_{v'}$ and the scaled polynomial coefficients $m_i' = c_{v^*}m_i$, $\overline{m}_i' = \overline{c}_{v^*}\overline{m}_i$. Δ and $\overline{\Delta}$ are defined by:

$$\Delta = \sum_{v'}\sum_{v''}\left[c_{v'}'M_{v'v''}' - \sum_i m_i'\langle v'|R^i|v''\rangle\right]^2 \tag{15a}$$

and

$$\overline{\Delta} = \sum_{v'}\sum_{v''}\left[\overline{c}_{v'}'\overline{M}_{v'v''}' - \sum_i \overline{m}_i'\langle v'|R^i|v''\rangle\right]^2 . \tag{15b}$$

The double sum in (15a) and (15b) is over all bands for which

243

measurements have been carried out. The unknown constants m_i', c_v', and $\bar{m}_i'$, $\bar{c}_v'$, are varied to minimize Δ and $\bar{\Delta}$ respectively, thereby giving the best fit to the experimental data in the least squares sense. Expression (15b) is similar to that used by Cunio and Jansson[36] in their study of $\bar{M}(R)$ for the N_2 first positive system. However, the R-centroids appearing in equation (6) of their paper are replaced by the matrix elements $\langle v'|R^i|v''\rangle$. The latter are evaluated using vibrational wave functions derived from the RKR potential curves for the electronic states involved in the transition under consideration.

The transition moment curves determined by the above procedure can be put on an absolute basis by evaluating $m_i = m_i'/c_{v*}$ and $\bar{m}_i = \bar{m}_i'/\bar{c}_{v*}$. However, a knowledge of N_{v*} and an absolute measurement on at least one of the $v*-v''$ bands are required for the calculation of c_{v*} and $\bar{c}_{v*}$. Alternatively, if the lifetime $\tau_{v'}$ of one of the upper state vibrational levels is known, the product $c_{v*}\bar{c}_{v*}$ can be determined by making use of the relations:

$$\tau_{v'}^{-1} = \sum_{v''} A_{v'v''} \tag{16}$$

and

$$A_{v'v''} = \frac{4e^4}{3c^3 a_0^3 m_e^2} \Delta E_{v'v''}^2 \frac{\displaystyle\sum_{\alpha'\alpha''} M_{v'v''}\bar{M}_{v'v''}}{(2-\delta_{0,\Lambda'})(2S'+1)} \quad , \tag{17}$$

with $M_{v'v''}$ and $\bar{M}_{v'v''}$ given by (12a) and (12b) respectively. If the lifetimes of several upper state levels are available, a least squares procedure can be used to determine $c_{v*}\bar{c}_{v*}$. To within the accuracy of the Born-Oppenheimer approximation the following identity is valid (see I):

$$M(R) = \Delta E(R) \, \overline{M}(R) \tag{18}$$

where $\Delta E(R)$ is the difference in energy between the upper and lower electronic states. Also, the dipole-length and dipole-momentum vibrational matrix elements are connected by

$$M_{v'v''} = \Delta E_{v'v''} \, \overline{M}_{v'v''} \, . \tag{19}$$

The ratio $c_{v*}/\overline{c}_{v*}$ can be evaluated by a least squares fit of (19) with $v'-v''$ values used in the determination of the variation of $M(R)$ and $\overline{M}(R)$ with R.

If $M(R)$ and $\overline{M}(R)$ are determined by fitting experimental data, equation (18) is satisfied to within a given tolerance over a rather limited range of R. Equation (19) is only approximately satisfied for various bands with the result that different sets of $A_{v'v''}$ and $f_{v'v''}$ values are obtained depending on whether one uses $M_{v'v''}^2$ or $\overline{M}_{v'v''}^2$ to evaluate them. The approach taken in the present paper is to use the mixed expression (17) for $A_{v'v''}$ in terms of the product $M_{v'v''}\overline{M}_{v'v''}$ to obtain a single set of values.

In Table I polynomial transition moment curves obtained by the procedure outlined above are reported for the N_2^+ (A-X) and (B-X) systems. The following format is used:

$$M(R) = B \left[\frac{m_0}{|m_0|} + \frac{m_1}{|m_0|} R + \frac{m_2}{|m_0|} R^2 \right] \tag{20a}$$

and

$$\overline{M}(R) = \overline{B} \left[\frac{\overline{m}_0}{|\overline{m}_0|} + \frac{\overline{m}_1}{|\overline{m}_0|} R + \frac{\overline{m}_2}{|\overline{m}_0|} R^2 \right] \tag{20b}$$

where $B = |m_0|$ and $\overline{B} = |\overline{m}_0|$.

The experimental $\widetilde{Q}_{v'v''}$ values reported by Stanton and St. John[15e] for some Meinel and first negative bands were used to determine the variation of $M(R)$ and $\overline{M}(R)$ with R. For the (B-X) system a linear $\overline{M}_z(R)$ curve was found to be sufficient to fit the experimental data. Relative band cross sections calculated with the polynomial transition moments are compared with the experimental ratios in Tables II and III. Also presented for comparison are relative cross sections calculated with $\overline{M}(R)$ curves recently reported in the literature. For the (B-X) system the dipole-length transition moment curve of Jain and Sahni[22c] was used, while for the (A-X) system the curve used was that of Koppe et al.[23d].

For the Meinel system the $M_x(R)$ and $\overline{M}_x(R)$ curves in Table I are valid for only a very limited range of R. They cannot be used for $R \gtrsim 2.1$ a.u. because the quadratic polynomials start to increase very rapidly with R for larger values of R. The $A^2\Pi_u$ and $X^2\Sigma_g^+$ states of N_2^+ both dissociate into $N(^4S^o)$ + $N^+(^3P)$ atomic states and consequently the 'experimental' (A-X) transition moment curves should approach zero in the limit of large R. In order to calculate vibrational matrix elements for the Meinel system we used the quadratic polynomials for small to intermediate R values and linearly extrapolated $M_x(R)$ and $\overline{M}_x(R)$ to zero for large R. We assumed that $M_x(5.0)$ = 0 and $\overline{M}_x(5.0)$ = 0, and for each curve we matched the slope of the linear part to the slope of the quadratic part at the point where they meet. This procedure is somewhat arbitrary but some form of extrapolation is required. In Table II relative band cross sections resulting from this procedure are compared with cross sections obtained by using the quadratic polynomials in Table I over the entire range of R. It can be seen that there is not sufficient experimental

246

data available to permit a determination of the variation of $M_X(R)$ and $\bar{M}_X(R)$ with R for large R.

The scale factors B and $\bar{B}$ in Table I for the first negative system were obtained by assuming that $\tau_0 = 65.0$ nsec for the $B^2\Sigma_u^+$ state of N_2^+. This value corresponds to an unweighted average of reported τ_0 measurements[17] if we disregard Anton's[17d] rather low value and reinterpret Fink and Welge's[17b] results in the manner prescribed by Johnson and Fowler[17k]. The lifetimes for the v' = 0,1,2 vibrational levels of the $A^2\Pi_u$ state reported by O'Neil and Davidson[24b] result in the first pair of B,$\bar{B}$ values for the Meinel system given in Table I. However, the second pair is required to fit the v' = 3,4 lifetimes reported by Hollstein et al.[24c]. Tables IV and V present a summary of calculated and experimentally measured lifetimes for the $A^2\Pi_u$ and $B^2\Sigma_u^+$ states of N_2^+.

The 'experimental' dipole-momentum transition moment curves given in Table I are plotted in Figs. 1 and 2 for the N_2^+ (A-X) and (B-X) systems respectively. The upper 'experimental' curve in Fig. 1 corresponds to the first pair of B,$\bar{B}$ values for the Meinel system, whereas the lower curve corresponds to the second pair. The ratio $M(R)/\Delta E(R)\bar{M}(R)$ differs from unity by less than $2\frac{1}{2}\%$ for $1.95 \leqslant R \leqslant 2.10$ a.u. For the first negative system the ratio differs from unity by less than 1% for $1.85 \leqslant R \leqslant 2.40$ a.u.

247

IV. THEORETICAL RESULTS AND COMPARISON BETWEEN THEORY AND EXPERIMENT

Tables VI and VII contain transition moment integrals calculated at various R values for the N_2^+ systems. The second column of Table VI gives $\bar{M}_x(R)$, the x-component of the HF dipole-length transition moment, and the fifth column gives $M_x(R)$, the x-component of the HF dipole-momentum transition moment, for the Meinel system. The corresponding columns of Table VII give $\bar{M}_z(R)$ and $M_z(R)$, the z-component of the HF transition moments for the first negative system.

The third and sixth columns of Tables VI and VII contain values for the active electron (AE) approximation to $\bar{M}(R)$ and $M(R)$. As discussed in I, this is the approximation where the transition moment is represented by the integral between the MO's $\phi'(r)$ and $\phi(r)$ describing the single excited electron in the upper and lower states respectively. The AE approximation works quite well for the first negative system. For the Meinel system the HF $\bar{M}_x(R)$ values are fairly well approximated by the AE values. However, there is only order of magnitude agreement between the HF and AE $M_x(R)$ values.

The electronic configurations for the X, A and B states of N_2^+ are composed of the same set of MO's and differ only in the number of electrons in the $2\sigma_u$, $1\pi_u$ and $3\sigma_g$ orbitals. The (A-X) and (B-X) transition moment integrals can be estimated by using the ground state $3\sigma_g$ orbital to describe the excited electron in the upper state. Such a procedure is a special case of the more general virtual orbital (VO) approximation discussed in I. The fourth and seventh columns of Tables VI and VII give VO values for $\bar{M}(R)$ and $M(R)$ respectively. The VO approximation works remarkably well for the first negative system, especially for the $\bar{M}_z(R)$ values.

248

It is rather surprising that the VO approximation is better than the AE approximation for both N_2^+ systems and for both the dipole-length and dipole-momentum transition moments. In the independent-particle scheme one would expect that the active electron is more accurately described in the excited state by an MO that results from applying the SCF procedure to that state rather than one resulting from the ground state SCF calculation. In I, the VO values for the MgH (A-X) transition moments were closer to the accurate HF values than the AE values, while the opposite was the case for the OH and SH (A-X) systems. It is impossible to predict on an a priori basis which approximation will work better for a given system.

In Figs. 1 and 2 dipole-momentum transition moment and potential energy curves are shown for the N_2^+ Meinel and first negative systems. The theoretical M(R) curves are obtained from the accurate $\vec{p}$- and $\vec{r}$-integrals in Tables VI and VII and $\Delta E_{HF}(R)$ values. The semitheoretical curve results from using $\Delta E_{RKR}(R)$ instead of $\Delta E_{HF}(R)$. As discussed in I, for exact Born-Oppenheimer wave functions equation (18) holds, but for approximate wave functions the identity is no longer valid and the expressions M(R), $\Delta E_{HF}(R)\bar{M}(R)$ and $\Delta E_{RKR}(R)\bar{M}(R)$ yield different dipole-momentum transition moment curves.

For the Meinel system the $M_x(R)$ curves in Fig. 1 all exhibit the same qualitative behaviour as a function of R. In spite of the experimental uncertainty, several facts are evident. The HF x-integrals are fairly accurate and the consideration of correlation should not change them by more than about 50%. On the other hand, the HF p_x-integrals are too large by a factor of 4-5. The correlation correction to $M_x(R)$ and $\bar{M}_x(R)$ does not vary considerably with R over the range for which the 'experimental' transition moment curves are

valid. For the first negative system several observations result from comparing the calculated $M_z(R)$ curves with the 'experimental' one in Fig. 2. The HF model yields slightly better z-integrals than p_z-integrals. The correlation correction to the dipole-momentum curves, say $\Delta M_z(R)$, varies considerably with R and increases on going from intermediate to large values of R. Moreover, the $\Delta M_z(R)$ values are of the same order of magnitude as the $M_z(R)$ values over the R range studied.

Band oscillator strengths were calculated using the mixed expression (10) with vibrational matrix elements derived from wave functions for the RKR potential curves shown in Figs. 1 and 2. HF $f_{v'v''}$ values were obtained by averaging the HF transition moment curves, while 'experimental' oscillator strengths resulted from the use of the polynomial curves given in Table I. For the first negative system, the HF $\langle 0|M_z|0 \rangle$ value is too large by a factor of 2.6 and the $\langle 0|\overline{M}_z|0 \rangle$ value by a factor of 2.2, resulting in a HF f_{00} values of 0.1370 that is 5.6 times larger than the experimental value of 0.0246. For the Meinel system, if the lifetimes of O'Neil and Davidson[24b] are used to put the experimental data on an absolute basis and a comparison between theory and experiment is made, the HF $\langle 0|M_x|0 \rangle$ value is 3.6 times too large while the $\langle 0|\overline{M}_x|0 \rangle$ value differs from the experimental value by a factor of 0.9. The HF matrix elements lead to a f_{00} value of 1.065×10^{-2} that is 3.3 times larger than the experimental value of 3.28×10^{-3}. Alternatively, if experimental data scaled to fit the lifetimes of Hollstein et al.[24c] are used as the standard for comparison, the HF $\langle 0|M_x|0 \rangle$ and $\langle 0|\overline{M}_x|0 \rangle$ values are too large by factors of 5.4 and 1.4 respectively,

resulting in a f_{00} value that is 7.3 times larger than the experimental value of 1.46×10^{-3}.

In Tables VIII and IX 'experimental' and semitheoretical relative band oscillator strengths $f_{v'v''}/f_{00}$ are compared with relative Franck-Condon factors $q_{v'v''}/q_{00}$ for the v'-v" ($0 \leqslant v',v'' \leqslant 5$) bands of the Meinel and first negative systems. $f_{v'v''}$ is proportional to $\langle v'|M|v''\rangle\langle v'|\bar{M}|v''\rangle$. Because of equation (18) it is unreasonable to expect that for a given system $M(R)$ and $\bar{M}(R)$ can both be taken to be nearly independent of R and consequently that $f_{v'v''}/f_{00}$ values can be adequately approximated by $q_{v'v''}/q_{00}$ values. However, it may happen that the variation of $M(R)$ and $\bar{M}(R)$ with R is such that for some bands $\langle v'|M|v''\rangle\langle 0|0\rangle/\langle 0|M|0\rangle\langle v'|v''\rangle$ is approximately equal to $\langle 0|\bar{M}|0\rangle\langle v'|v''\rangle/\langle v'|\bar{M}|v''\rangle\langle 0|0\rangle$ and hence the ratio $f_{v'v''}q_{00}/f_{00}q_{v'v''}$ is close to unity. For these bands the Franck-Condon factors will give good estimates of relative oscillator strengths.

For the Meinel system $\bar{R}_{v'v''} < 2.2$ a.u. for $v' > v''$ and $\bar{R}_{v'v''} > 2.2$ a.u. for $v' < v''$, where $0 \leqslant v',v'' \leqslant 5$ and $\bar{R}_{v'v''}$ is the R-centroid[35] for the v'-v" band. This indicates that the oscillator strengths below the diagonal ($v' > v''$) in Table VIII will be mainly influenced by the behaviour of $M_x(R)$ and $\bar{M}_x(R)$ for small to intermediate values of R whereas the oscillator strengths above the diagonal ($v' < v''$) will depend to a large extent on transition moment values at intermediate to large values of R. As mentioned in Section III, the polynomial curves for $M_x(R)$ and $\bar{M}_x(R)$ given in Table I are not valid for $R \gtrsim 2.1$ a.u. and consequently the 'experimental' oscillator strengths in the upper right corner of Table VIII are expected to be the least reliable. Two qualitative observations can be made by considering the numbers in this table. Firstly, for

251

all bands except the 5-4 one such that $v' > v''$, $\tilde{f}_{expt} > \tilde{f}_{HF} > \tilde{q}$, where $\tilde{q}$ and $\tilde{f}$ denote relative Franck-Condon factor and relative oscillator strength respectively. The reason for this is that for small R values the variation with R for the HF transition moment curves is not as great as that for the 'experimental' curves and hence the HF $\tilde{f}$ values do not deviate as much from the $\tilde{q}$ values as the experimental $\tilde{f}$ values. Secondly, for all bands such that $v' < v''$, $\tilde{f}_{expt} \approx \tilde{f}_{HF} < \tilde{q}$. For intermediate to large values of R, the theoretical curves slowly decrease as a function of R and so do the 'experimental' curves because of the procedure used to extrapolate the latter.

For the first negative system $\bar{R}_{v'v''} > 2.1$ a.u. for $v' > v''$ and $\bar{R}_{v'v''} < 2.1$ a.u. for $v' < v''$. The $\tilde{f}$ values below the diagonal in Table IX reflect the behaviour of the $M_z(R)$ and $M_z(R)$ curves in the intermediate to large R region while the $\tilde{f}$ values above the diagonal are influenced considerably by the behaviour of the transition moment curves in the small to intermediate R region. The HF $\bar{M}_z(R)$ curve is relatively flat in the R_e region whereas the $M_z(R)$ curve is approximately linear and varies considerably with R as evidenced by the fact that $M_z'(\bar{R}_{00})/M_z(\bar{R}_{00}) = 1.4$ where M' is the derivative of M with respect to R. The 'experimental' $M_z(R)$ and $\bar{M}_z(R)$ curves vary slightly as a function of R with $M_z'(\bar{R}_{00})/M_z(\bar{R}_{00})$ = 0.46 and $\bar{M}_z'(\bar{R}_{00})/\bar{M}_z(\bar{R}_{00})$ = -0.49. These factors can be used to explain two qualitative observations made by considering the entries in Table IX. First of all, $\tilde{f}_{HF} > \tilde{f}_{expt} \approx \tilde{q}$ for all but the weakest bands such that $v' > v''$. Secondly, $\tilde{f}_{HF} < \tilde{f}_{expt} \approx \tilde{q}$ for bands with $v' < v''$. The remarkable agreement between the $\tilde{f}_{expt}$ and $\tilde{q}$ values, especially for the strongest bands, is not to be viewed as an indication of the constancy of the 'experimental' transition

252

moments $M_z(R)$ and $\bar{M}_z(R)$. In the region of $\bar{R}_{00}$, $M_z'/M_z \approx -\bar{M}_z'/\bar{M}_z$ and the variation of $M_z(R)$ with R counterbalances the variation of $\bar{M}_z(R)$ so that the 'experimental' $\tilde{f}_{v'v''}$ values are fortuitously close to the relative Franck-Condon factors $\tilde{q}_{v'v''}$.

In Table X values of $\bar{M}(R)$ and $M(R)$, the HF dipole-length and dipole-momentum transition moments respectively, at a single value of R are presented for the $^2\Pi-^2\Sigma^+$ and $^2\Sigma^+-^2\Sigma^+$ transitions of some members of the diatomic 13-electron sequence. These are used to calculate the electronic absorption oscillator strength $f_{el}(R)$:

$$f_{el}(R) = \frac{8}{3} M_x(R)\,\bar{M}_x(R) \qquad (^2\Pi-^2\Sigma^+) \qquad (21a)$$

and

$$f_{el}(R) = \frac{2}{3} M_z(R)\,\bar{M}_z(R) \qquad (^2\Sigma^+-^2\Sigma^+). \qquad (21b)$$

Also presented for comparison are experimental values of the electronic oscillator strength f_{el} for the systems where absolute measurements have been reported in the literature. These are computed using

$$f_{expt} = f_{00}/q_{00}. \qquad (22)$$

Equation (22) results from assuming that $M(R)\bar{M}(R)$ is independent of R and assigning an 'average' value to the product for the system under consideration.

For the N_2^+ (B-X) system, if f_{00} and q_{00} are calculated using the polynomial transition moments given in Table I a value of 3.8×10^{-2} for f_{el} results from equation (22). Several workers[19]

have reported absolute oscillator strength measurements and an unweighted average of the f_{el} values given in references 19d-h equals 3.8×10^{-2}, in excellent agreement with the f_{el} value determined from $B^2\Sigma_u^+$ lifetime measurements . For the N_2^+ (A-X) system the $A^2\Pi_u$ lifetimes of O'Neil and Davidson[24b] lead to $f_{el} = 6.4 \times 10^{-3}$ whereas those of Hollstein et al.[24c] result in $f_{el} = 2.9 \times 10^{-3}$. The absolute band strength reported by Kuprianova et al.[25c] for the Meinel system corresponds to an electronic oscillator strength of 8.4×10^{-3} and implies even shorter lifetimes for the upper state than those of O'Neil and Davidson[24b]. In Table X it can be seen that the f_{el} values for the CN and CO^+ (A-X) systems are nearly the same. The HF f_{el} values are also quite close together but are too large by a factor of about 3.

A few qualitative observations can be made by considering the HF transition moments in Table X. For the $^2\Pi_i - ^2\Sigma^+$ and $^2\Pi_r - ^2\Sigma^+$ systems the molecules and ions are arranged in order of increasing $Z_A - Z_B$. There is no systematic behaviour in the M_x and $\bar{M}_x$ values for the $^2\Pi_i - ^2\Sigma^+$ transitions as one goes from C_2^- ($Z_A - Z_B = 0$) to BeF ($Z_A - Z_B = 5$). The dipole-momentum moment varies considerably more than the dipole-length moment as one progresses from one member to the next. The HF oscillator strengths for the $^2\Pi_i - ^2\Sigma^+$ systems considered are all of the order of 10^{-2}. For the $^2\Pi_r - ^2\Sigma^+$ systems the CN f_{el} value is an order of magnitude smaller than that for any of the others. There is a considerable variation in M_x and $\bar{M}_x$ values as one progresses from CN ($Z_A - Z_B = 1$) to AlH^+ ($Z_A - Z_B = 12$). The values increase, go through a maximum, and then decrease.

254

ACKNOWLEDGMENTS

255

REFERENCES

1. W. H. Henneker and H. E. Popkie, J. Chem. Phys. (in press).

2. W. M. Huo, J. Chem. Phys. 49, 1482 (1968).

3. D. R. Bates, Proc. Roy. Soc. (London) A196, 562 (1949).

4. a) H. Shull, Astrophys. J. 112, 352 (1950).

    b) H. Shull, Astrophys. J. 114, 546 (1951).

    c) H. Shull, J. Chem. Phys. 20, 1095 (1952).

5. G. Herzberg, "Spectra of Diatomic Molecules", (D. Van Nostrand Co., New York, 1950).

6. R. S. Mulliken, Rev. Mod. Phys. 4, 1 (1932).

7. a) T. E. H. Walker and R. F. Barrow, J. Phys. B 2, 102 (1969).

    b) T. E. H. Walker and W. G. Richards, J. Phys. B 3, 271 (1970).

8. a) P. E. Cade, K. D. Sales, and A. C. Wahl, J. Chem. Phys. 44 1973 (1966).

    b) P. E. Cade, "Hartree-Fock-Roothaan Wave Functions for First Row Diatomic Molecules: AH, A_2, and AB", Special Technical Report, Laboratory of Molecular Structure and Spectra, University of Chicago (to be published).

    c) P. E. Cade (to be published).

9. For a recent tentative description of C_2^-, see G. Herzberg and A. Lagerqvist, Can. J. Phys. 46, 2363 (1968).

10. a) A. E. Douglas and P. M. Routly, Astrophys. J. Suppl. Ser. 1, 295 (1954).

    b) B. L. Lutz, Can. J. Phys. 48, 1192 (1970).

11. a) E. A. Hylleraas, Z. Physik 65, 209 (1930).

    b) J. O. Hirschfelder, W. B. Brown, and S. T. Epstein, Advan. Quantum Chem. 1, 255 (1964).

256

c) M. Cohen and A. Dalgarno, Proc. Roy. Soc. (London) $\underline{A280}$, 258 (1964).

d) W. L. Wiese and A. W. Wiess, Phys. Rev. $\underline{175}$, 50 (1968).

12. G. G. Hall and D. Rees, Theoret. Chim. Acta $\underline{1}$, 448 (1963).

13. a) M. J. McEwan and L. F. Phillips, Acc. Chem. Res. $\underline{3}$, 9 (1970).

b) For other general reviews, see "I.A.G.A. Symposium on Laboratory Measurements of Aeronomic Interest, York University, Toronto, 1968", Can. J. Chem. $\underline{47}$, 1703 (1969).

14. F. S. Ortenberg and E. T. Antropov, Sov. Phys. Usp. $\underline{9}$, 717 (1967).

15. a) J. L. Philpot and R. H. Hughes, Phys. Rev. $\underline{133}$, A107 (1964).

b) J. W. McConkey and I. D. Latimer, Proc. Phys. Soc. (London) $\underline{86}$, 463 (1965).

c) B. N. Srivastava and I. M. Mirza, Phys. Rev. $\underline{176}$, 137 (1968).

d) D. L. Judge and G. L. Weissler, J. Chem. Phys. $\underline{48}$, 4590 (1968).

e) P. N. Stanton and R. M. St. John, J. Opt. Soc. Am. $\underline{59}$, 252 (1969).

16. a) G. Herzberg, Ann. Physik $\underline{86}$, 191 (1928).

b) H. D. Smythe and E. G. F. Arnot, Phys. Rev. $\underline{36}$, 1023 (1930).

c) O. S. Duffendack, R. W. Revans, and A. S. Roy, Phys. Rev. $\underline{45}$, 807 (1934).

d) L. V. Wallace and R. W. Nicholls, J. Atmospheric Terrest. Phys. $\underline{7}$, 101 (1955); $\underline{24}$, 749 (1962).

e) D. T. Stewart, Proc. Phys. Soc. (London) $\underline{A69}$, 437 (1956).

f) D. C. Tyte, Proc. Phys. Soc. (London) $\underline{80}$, 1364 (1962).

g) J. R. Sheridan and K. C. Clark, Phys. Rev. $\underline{140}$, A1033 (1965).

h) S. Hayakawa, T. Kumazaki, H. Nishimura, and M. Otsuku, Rep. Ionosphere and Space Research (Japan) 19, 311 (1965).

i) R. F. Holland, Los Alamos Scientific Laboratory Report No. LA-3783 (1967).

j) G. N. Polyakova, V. I. Tatus' and Ya. M. Fogel', Sov. Phys. JETP 25, 430 (1967).

k) H. Nishimura, J. Phys. Soc. Japan 24, 130 (1968).

17. a) R. G. Bennett and F. W. Dalby, J. Chem. Phys. 31, 434 (1959).

b) E. Fink and K. H. Welge, Z. Naturforsch. 199, 1193 (1964).

c) D. I. Sebacher, J. Chem. Phys. 42, 1368 (1965).

d) H. Anton, Ann. Physik 18, 178 (1966).

e) M. Jeunehomme, J. Chem. Phys. 44, 2672 (1966).

f) R. G. Fowler and T. M. Holzberlein, J. Chem. Phys. 45, 1124 (1966).

g) J. E. Hesser and K. Dressler, J. Chem. Phys. 45, 3149 (1966).

h) J. Desesquelles, M. Dufay, and M. C. Poulizac, Phys. Lett. 27A, 96 (1968).

i) L. L. Nichols and W. E. Wilson, Appl. Opt. 7, 167 (1968).

j) T. Sawada and H. Kamada, Bull. Chem. Soc. Japan 43, 325 (1970).

k) A. W. Johnson and R. G. Fowler, J. Chem. Phys. 53, 65 (1970).

18. L. I. Kiselyovskii and V. D. Simanovich, Opt. Spectry. (USSR) 24, 266 (1968).

19. a) J. C. Keck, J. C. Camm, B. Kivel, and T. Wentink, Jr., Ann. Phys. (N.Y.) 7, 1 (1959).

b) R. A. Allen, J. C. Camm, and J. C. Keck, J. Quant. Spectry. Radiative Transfer 1, 269 (1961).

c) J. C. Keck, R. A. Allen, and R. L. Taylor, J. Quant. Spectry. Radiative Transfer 3, 335 (1963).

d) J. B. Shumaker, Jr., in "Proc. 6th Conf. on Ionization Phenomena in Gases", (S.E.R.M.A., Paris, 1963), Vol. 3, p. 170.

e) V. H. Reis, J. Quant. Spectry. Radiative Transfer 4, 783 (1964).

f) T. Wentink, Jr., L. Isaacson, and R. J. Spindler, AVCO Corporation Technical Report No. AFWL-TR-65-139 (1965).

g) R. A. Allen, J. Quant. Spectry. Radiative Transfer 5, 511 (1965).

h) K. L. Wray and T. J. Connolly, J. Quant. Spectry. Radiative Transfer 5, 633 (1965).

20. D. C. Tyte and R. W. Nicholls, "Identification Atlas of Molecular Spectra, No. 3", Molecular Excitation Group, Department of Physics, University of Western Ontario (1965).

21. J. E. Hesser, J. Chem. Phys. 48, 2518 (1968).

22. a) R. W. Nicholls, J. Atmospheric Terrest. Phys. 25, 218 (1963).

b) A. L. Broadfoot, Planetary Space Sci. 15, 1801 (1967).

c) D. C. Jain and R. C. Sahni, Int. J. Quantum Chem. 1, 721 (1967).

23. a) A. B. Meinel, Astrophys. J. 113, 583 (1951); 114, 431 (1951).

b) A. Omholt, J. Atmospheric Terrest. Phys. 10, 320 (1957).

c) N. I. Fedorova, in "Polar Aurorae and Emission of the Night Sky", No. 10 (1963).

d) V. T. Koppe, A. G. Koval, V. V. Gritsyna, and Ya. M. Fogel', Opt. Spectry. (USSR) 24, 440 (1968).

259

24. a) W. F. Sheridan, O. Oldenberg, and N. P. Carleton, in "Atomic
       Collision Processes", M. R. C. McDowell, ed. (North-Holland
       Publishing Co., Amsterdam, 1964), p. 440.

    b) R. O'Neil and G. Davidson, U. S. Air Force Cambridge Research
       Laboratories Report No. AFCRL-67-0277 (1968).

    c) M. Hollstein, D. C. Lorents, J. R. Peterson, and J. R.
       Sheridan, Can. J. Chem. 47, 1858 (1969).

25. a) W. H. Wurster, J. Chem. Phys. 36, 2111 (1962).

    b) R. P. Main and E. Bauer, J. Quant. Spectry. Radiative Transfer
       6, 1 (1966).

    c) E. B. Kuprianova, V. N. Kolesnikov, and N. N. Sobelev,
       J. Quant. Spectry. Radiative Transfer 9, 1025 (1969).

26. R. W. Nicholls, J. Atmospheric Terrest. Phys. 12, 211 (1958).

27. T. Wentink, Jr., E. P. Marram, L. Isaacson, and R. J. Spindler,
    AVCO Corporation Technical Report No. AFWL-TR-67-30 (1967).

28. a) T. Wentink, Jr. L. Isaacson, and J. Morreal, J. Chem. Phys.
       41, 278 (1964).

    b) E. G. Gippius, E. M. Kudryavtsev, A. N. Pechenov, N. N.
       Sobolev, and V. P. Fokeyev, Teplofiz. Vysokikh Temperatur
       Akad. Nauk SSSR 2, 181 (1964).

    c) G. Poletto and M. Rigutti, Z. Astrophys. 60, 199 (1964).

    d) M. Jeunehomme, J. Chem. Phys. 42, 4086 (1965).

    e) A. P. Droncv, N. N. Sobolev, F. S. Faizullov, and V. A.
       Boiko, Opt. Spectry. (USSR) 21, 397 (1966).

29. R. G. Bennett and F. W. Dalby, J. Chem. Phys. 32, 1111 (1960).

30. O. Engvold, Solar Physics 11, 183 (1970).

31. F. R. Gilmore, J. Quant. Spectry. Radiative Transfer 5, 369
     (1965).

32. a) W. Heitler, "The Quantum Theory of Radiation", 3rd edn.
         (Oxford University Press, 1953).

     b) H. A. Bethe and E. E. Salpeter, "Quantum Mechanics of One-
        and Two-Electron Atoms" (Springer-Verlag, Germany, 1957).

33. a) R. W. Nicholls and A. L. Stewart, in "Atomic and Molecular
         Processes", D. R. Bates, ed. (Academic Press, New York,
         1962).

     b) I. Kovacs, "Rotational Structure in the Spectra of Diatomic
        Molecules" (American Elsevier, New York, 1969).

34. See, for example, references (16d) and (26).

35. a) P. A. Fraser, Can. J. Phys. 32, 515 (1954).

     b) R. W. Nicholls and W. R. Jarmain, Proc. Phys. Soc. (London)
        A69, 253 (1956).

36. B. E. Cunio and R. E. W. Jansson, J. Quant. Spectry. Radiative
     Transfer 8, 1763 (1968).

TABLE I. N_2^+ ($A^2\Pi_u - X^2\Sigma_g^+$) and ($B^2\Sigma_u^+ - X^2\Sigma_g^+$) 'Experimental' Transition Moments

System	$m_0'/|m_0'|$	$m_1'/|m_0'|$	$m_2'/|m_0'|$	$\bar{m}_0'/|\bar{m}_0'|$	$\bar{m}_1'/|\bar{m}_0'|$	$\bar{m}_2'/|\bar{m}_0'|$	B	$\bar{B}$
A-X	1.0	-0.8958	0.2028	1.0	-0.9225	0.2177	0.880[a]	10.51[a]
B-X	-1.0	1.0369	-0.2319	1.0	-0.2432	------	0.587[b] 0.535	7.00[b] 1.42

[a] Derived from lifetime measurements of O'Neil and Davidson (Ref. 24b).

[b] Derived from lifetime measurements of Hollstein et al. (Ref. 24c).

TABLE II. N_2^+ $(A^2\Pi_u - X^2\Sigma_g^+)$ Relative Band Cross Sections

$v'v_1''/v''v_2''$	$Q_{v'v_1''}/Q_{v'v_2''}$			
20/21	0.78[a]	0.786[b]	0.817[c]	0.98[d]
30/31	0.42	0.369	0.345	0.23
40/41	0.23	0.227	0.214	0.11
51/52	0.46	0.508	0.473	0.29

[a] Determined from experimental measurements of Stanton and St. John (Ref. 15e).

[b] Calculated using polynomial $M_\chi(R)$ and $\bar{M}_\chi(R)$ given in Table I over entire R range.

[c] Calculated using polynomial $M_\chi(R)$ and $\bar{M}_\chi(R)$ given in Table I for small to intermediate R values and linear extrapolation to zero for large R (see text).

[d] Calculated using polynomial $\bar{M}_\chi(R)$ of Keppe et al. (Ref. 23d).

TABLE III. N_2^+ ($B^2\Sigma_u^+ - X^2\Sigma_g^+$) Relative Band Cross Sections

$v'v_1''/v'v_2''$	$Q_{v'v_1''}/Q_{v'v_2''}$			
01/00	0.34[a]	0.35[b]	0.343[c]	0.365[d]
02/00	0.08	0.071	0.075	0.082
03/00	0.01	0.013	0.013	0.015
11/10	----	0.61	0.581	0.615
12/10	0.78	0.69	0.684	0.789
13/10	0.37	0.27	0.265	0.316
14/10	0.08	0.065	0.067	0.081
20/21	0.13	----	0.138	0.120
23/21	0.41	0.41	0.401	0.471
24/21	0.24	----	0.252	0.306

[a] Determined from experimental measurements of Wallace and Nicholls (Ref. 16d).

[b] Determined from experimental measurements of Stanton and St. John (Ref. 15e).

[c] Calculated using polynomial $M_z(R)$ and $\bar{M}_z(R)$ given in Table I.

[d] Calculated using polynomial $\bar{M}_z(R)$ of Jain and Sahni (Ref. 22c).

TABLE IV. N_2^+ ($A^2\Pi_u$) Lifetimes

v'	$\tau_{v'}$ (sec)			
0	8.5[a]	-----	8.09[c]	18.21[d]
1	6.8	-----	7.22	16.25
2	6.3	-----	6.34	14.26
3	---	12.23[b]	5.57	12.54
4	---	11.42	4.91	11.06
5	---	12.2	4.36	9.81

[a] Experimental measurements of O'Neil and Davidson (Ref. 24b).

[b] Experimental measurements of Hollstein et al. (Ref. 24c).

[c] Calculated using polynomial $M_x(R)$ and $\bar{M}_x(R)$ given in Table I with B=0.880, $\bar{B}$=10.51 and linear extrapolation to zero for large R (see text).

[d] Calculated using polynomial $M_x(R)$ and $\bar{M}_x(R)$ given in Table I with B=0.587, $\bar{B}$=7.00 and linear extrapolation to zero for large R (see text).

TABLE V. N_2^+ ($B^2\Sigma_u^+$) Lifetimes

v'	$\tau_{v'}$(nsec)			
0	71.5[a]	59.2[b]	65.0[c]	65.0[d]
1	75.8	58.5	63.8	65.9
2	70.2	----	62.9	67.3
3	63.5	----	62.2	69.3
4	66.8	----	61.8	72.1

[a] Experimental measurements of Jeunehomme (Ref. 17e).

[b] Experimental measurements of Johnson and Fowler (Ref. 17b).

[c] Calculated using polynomial $M_z(R)$ and $\bar{M}_z(R)$ given in Table I.

[d] Calculated using polynomial $\bar{M}_z(R)$ of Jain and Sahni (Ref. 22c).

TABLE VI. $N_2^+(A^2\Pi_u-X^2\Sigma_g^+)$ Hartree-Fock, active electron and virtual orbital transition moment integrals*

R	$\langle^2\Pi_u\|x\|^2\Sigma_g^+\rangle$	$\langle3\sigma_g'\|x\|1\pi_u\rangle^\dagger$	$\langle3\sigma_g\|x\|1\pi_u\rangle^\ddagger$	$-i\langle^2\Pi_u\|p_x\|^2\Sigma_g^+\rangle$	$-i\langle3\sigma_g'\|p_x\|1\pi_u\rangle^\dagger$	$-i\langle3\sigma_g\|p_x\|1\pi_u\rangle^\ddagger$
1.80	0.2526	0.2810	0.2380	0.0486	0.0277	0.0331
1.85	0.2485	0.2778	0.2338	0.0465	0.0251	0.0311
1.95	0.2387	0.2698	0.2239	0.0428	0.0206	0.0279
2.00	0.2331	0.2651	0.2183	0.0413	0.0187	0.0266
2.0132	0.2316	0.2638	0.2168	0.0408	0.0182	0.0263
2.05	0.2272	0.2601	0.2125	0.0398	0.0169	0.0254
2.15	0.2143	0.2489	0.2000	0.0374	0.0139	0.0237
2.30	0.1931	0.2298	0.1797	0.0346	0.0107	0.0221
2.40	0.1781	0.2158	0.1656	0.0332	0.0093	0.0216
2.60	0.1477	0.1860	0.1370	0.0310	0.0079	0.0212

* Atomic units (a.u.) are used throughout this paper

† Active electron approximation

‡ Virtual orbital approximation

TABLE VII. $N_2^+(B^2\Sigma_u^+-X^2\Sigma_g^+)$ Hartree-Fock, active electron and virtual orbital transition moment integrals

R	$\langle^2\Sigma_u^+|z|^2\Sigma_g^+\rangle$	$\langle 3\sigma_g'|z|2\sigma_u\rangle^*$	$\langle 3\sigma_g|z|2\sigma_u\rangle^\dagger$	$-i\langle^2\Sigma_u^+|p_z|^2\Sigma_g^+\rangle$	$-i\langle 3\sigma_g'|p_z|2\sigma_u\rangle^*$	$-i\langle 3\sigma_g|p_z|2\sigma_u\rangle^\dagger$
1.80	1.4619	1.4914	1.4621	0.1281	0.1114	0.1261
1.85	1.4732	1.5055	1.4734	0.1435	0.1257	0.1413
1.95	1.4916	1.5304	1.4918	0.1738	0.1539	0.1713
2.00	1.4989	1.5411	1.4989	0.1886	0.1677	0.1860
2.0132	1.5006	1.5438	1.5006	0.1925	0.1713	0.1898
2.05	1.5046	1.5507	1.5046	0.2033	0.1813	0.2005
2.15	1.5117	1.5659	1.5115	0.2318	0.2078	0.2287
2.30	1.5106	1.5788	1.5105	0.2721	0.2458	0.2690
2.40	1.5026	1.5804	1.5025	0.2970	0.2696	0.2940
2.60	0.0483	0.7199	1.4707	0.0455	0.8917	0.3382

* Active electron approximation

† Virtual orbital approximation

TABLE VIII. $N_2^+(A^2\Pi_u - X^2\Sigma_g^+)$ Relative Franck-Condon Factors and Band Oscillator Strengths

v' \ v"	0	1	2	3	4	5
0	1.000*	0.713	0.208	0.324-1	0.294-2	0.153-3
	1.000†	0.591	0.170	0.266-1	0.183-2	0.537-4
	1.000‡	0.642	0.166	0.227-1	0.177-2	0.761-4
1	0.619	0.103	0.691	0.426	0.104	0.129-1
	0.715	0.128	0.575	0.336	0.824-1	0.862-2
	0.675	0.100	0.612	0.336	0.718-1	0.762-2
2	0.236	0.481	0.196-1	0.422	0.558	0.204
	0.336	0.598	0.636-2	0.356	0.429	0.158
	0.278	0.515	0.197-1	0.367	0.432	0.139
3	0.733-1	0.376	0.202	0.174	0.167	0.578
	0.137	0.547	0.281	0.131	0.145	0.435
	0.928-1	0.436	0.212	0.168	0.142	0.441
4	0.206-1	0.180	0.356	0.305-1	0.296	0.260-1
	0.528-1	0.328	0.538	0.607-1	0.248	0.257-1
	0.278-1	0.224	0.405	0.309-1	0.281	0.212-1
5	0.556-2	0.688-1	0.258	0.237	0.530-2	0.311
	0.199-1	0.166	0.470	0.380	0.133-2	0.276
	0.795-2	0.914-1	0.316	0.265	0.585-2	0.291

* RKR $q_{v'v''}/q_{00}$ ($q_{00} = 0.511$).

† 'Experimental' $f_{v'v''}/f_{00}$ ($f_{00} = 1.46 \times 10^{-3}$ or 3.28×10^{-3}, see text).

‡ Hartree-Fock $f_{v'v''}/f_{00}$ ($f_{00} = 1.065 \times 10^{-2}$).

TABLE IX. $N_2^+(B^2\Sigma_u^+ - X^2\Sigma_g^+)$ Relative Franck-Condon Factors and Band Oscillator Strengths

v' \ v''	0	1	2	3	4	5
0	1.000* 1.000† 1.000‡	0.409 0.409 0.358	0.111 0.108 0.852-1	0.249-1 0.233-1 0.166-1	0.506-2 0.455-2 0.291-2	0.979-3 0.797-3 0.483-3
1	0.470 0.467 0.534	0.326 0.320 0.335	0.448 0.447 0.399	0.214 0.209 0.167	0.689-1 0.648-1 0.470-1	0.183-1 0.163-1 0.108-1
2	0.769-1 0.731-1 0.996-1	0.628 0.617 0.726	0.663-1 0.611-1 0.715-1	0.346 0.344 0.312	0.265 0.259 0.211	0.116 0.109 0.804-1
3	0.434-2 0.362-2 0.656-2	0.176 0.165 0.232	0.637 0.616 0.749	0.177-2 0.824-3 0.265-2	0.224 0.220 0.204	0.267 0.261 0.215
4	0.159-4 0.320-5 0.386-4	0.118-1 0.942-2 0.184-1	0.269 0.247 0.360	0.597 0.565 0.716	0.871-2 0.119-1 0.638-2	0.127 0.124 0.117
5	0.764-5 0.897-5 0.956-5	0.173-5 0.871-5 0.771-5	0.186-1 0.139-1 0.300-1	0.346 0.310 0.471	0.559 0.517 0.687	0.273-1 0.340-1 0.223-1

*RKR $q_{v'v''}/q_{00}$ ($q_{00} = 0.645$).

†'Experimental' $f_{v'v''}/f_{00}$ ($f_{00} = 2.46 \times 10^{-2}$).

‡Hartree-Fock $f_{v'v''}/f_{00}$ ($f_{00} = 1.370 \times 10^{-1}$).

TABLE **X.** Hartree-Fock electronic transition moments and absorption oscillator strengths for some 13-electron systems

SYSTEM	R	$\bar{M}_X(R)$	$M_X(R)$	$\Delta E\bar{M}_X(R)$	$f_{el}(R)$	f_{expt}
$C_2^-(A^2\Pi_u - X^2\Sigma_g^+)$	2.20	0.3436	0.0230	-0.0021	2.11×10^{-2}	
	2.42	0.3184	0.0195	-0.0087	1.66×10^{-2}	
	2.50	0.3039	0.0181	-0.0068	1.47×10^{-2}	
$N_2^+(A^2\Pi_u - X^2\Sigma_g^+)$	2.0132	0.2316	0.0408	-0.0029	2.52×10^{-2}	2.9×10^{-3}c 6.4×10^{-3}d
$CN(A^2\Pi_i - X^2\Sigma^+)$	2.214	0.2611	0.0231	-0.0003	1.61×10^{-2}	5.8×10^{-3}e
$CO^+(A^2\Pi_i - X^2\Sigma^+)$	2.107	0.2267	0.0292	0.0176	1.77×10^{-2}	5.6×10^{-3}e
$BO\ (A^2\Pi_i - X^2\Sigma^+)$	2.275	0.2627	0.0419	0.0250	2.94×10^{-2}	
$BF^+(^2\Pi_i - X^2\Sigma^+)$	2.391	0.1635	0.0529	0.0421	2.31×10^{-2}	
$BeF\ (^2\Pi_i - X^2\Sigma^+)$	2.512	0.2031	0.0701	0.0583	3.80×10^{-2}	
$CN\ (H^2\Pi_r - X^2\Sigma^+)$	2.214	0.1284	0.0462	0.0465	1.58×10^{-2}	
$CO^+(^2\Pi_r - X^2\Sigma^+)$	2.107	0.3212	0.1231	0.1215	1.05×10^{-1}	
$BO\ (^2\Pi_r - X^2\Sigma^+)$	2.275	0.5353	0.1333	0.1687	1.90×10^{-1}	
$BF^+(^2\Pi_r - X^2\Sigma^+)$	2.391	0.5847	0.1411	0.1434	2.20×10^{-1}	
$BeF(A^2\Pi_r - X^2\Sigma^+)$	2.572	0.9759	0.1424	0.1674	3.71×10^{-1}	
$MgH(A^2\Pi_r - X^2\Sigma^+)$ a	3.259	1.0047	0.0989	0.0987	2.65×10^{-1}	
$AlH^+(A^2\Pi_r - X^2\Sigma^+)$ a	3.027	0.6606	0.0996	0.0918	1.75×10^{-1}	
$C_2^-(B^2\Sigma_u^+ - X^2\Sigma_g^+)$ b	2.3481	1.8750	0.1795	0.2301	2.24×10^{-1}	
$N_2^+(B^2\Sigma_u^+ - X^2\Sigma_g^+)$ b	2.0132	1.5006	0.1925	0.2164	1.93×10^{-1}	3.8×10^{-2}f

a) See I.
b) Columns 3 to 5 give values of $\bar{M}_z(R)$, $M_z(R)$ and $\Delta E\bar{M}_z(R)$ respectively.
c) Calculated using τ measurements of reference (24c) (see text).
d) Calculated using τ measurements of reference (24b) (see text).
e) See reference (27).
f) Calculated using τ measurements of reference (17)(see text).
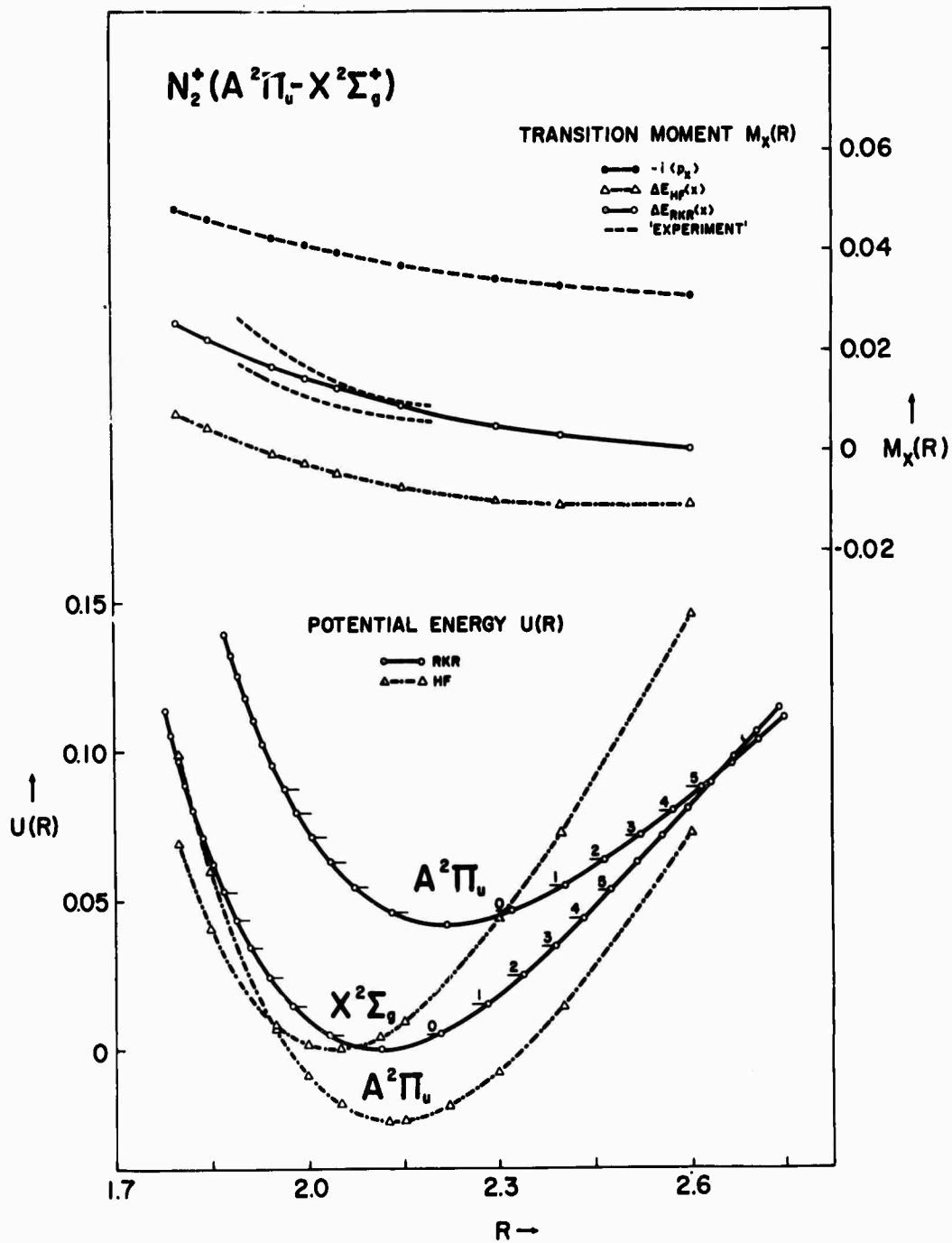
FIGURE 1. $N_2^+(A^2\Pi_u—X^2\Sigma_g^+)$ dipole-momentum transition moment and
potential energy curves. The excited state U(R) curves
are measured relative to the minimum in the ground state
curves. For the RKR curves the lower vibrational levels
are indicated. The theoretical M_x(R) curves result from
use of the expressions $-i\langle p_x\rangle$ and $\Delta E\langle x\rangle$ with Hartree-Fock
p_x- and x-integrals and with ΔE determined from the Hartree-
Fock and RKR U(R) curves. The procedure used to obtain
the 'experimental' M_x(R) curves is given in the text.

272
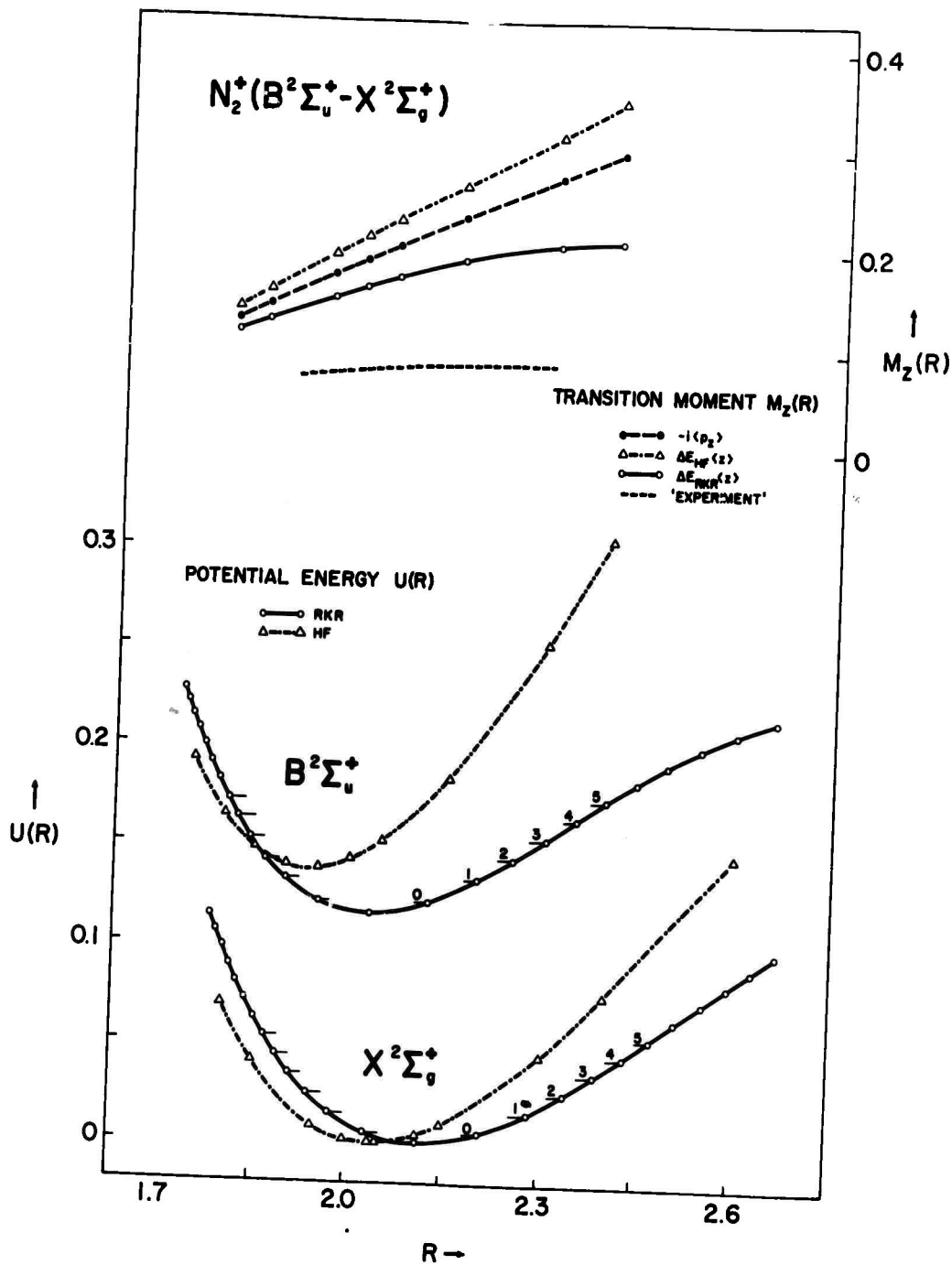
FIGURE 2. $N_2^+(B^2\Sigma_u^+ - X^2\Sigma_g^+)$ dipole-momentum transition moment and potential energy curves. The excited state U(R) curves are measured relative to the minimum in the ground state curves. For the RKR curves the lower vibrational levels are indicated. The theoretical $M_z(R)$ curves result from use of the expressions $-i\langle p_z \rangle$ and $\Delta E \langle z \rangle$ with Hartree-Fock p_z- and z-integrals and with ΔE determined from the Hartree-Fock and RKR U(R) curves. The procedure used to obtain the 'experimental' $M_z(R)$ curve is given in the text.

273

THEORETICAL ELECTRONIC TRANSITION

PROBABILITIES IN DIATOMIC MOLECULES

III. BeH and MgH $(A^2\Pi - X^2\Sigma^+)$ Systems[*]

H. E. Popkie[†]

Laboratory of Molecular Structure and Spectra
Department cf Physics
University of Chicago
Chicago, Illinois 60637

275

ABSTRACT

Electronic dipole-momentum and dipole-length transition moment curves obtained from the multiconfiguration (MC) wave functions of Chan and Davidson are presented for the BeH and MgH ($A^2\Pi - X^2\Sigma^+$) systems. They are used to discuss the correlation correction to the Hartree-Fock (HF) curves previously reported. The MC transition moments and vibrational wave functions derived from both the theoretical MC and 'experimental' RKR potential energy curves for the $A^2\Pi$ and $X^2\Sigma^+$ states are used to calculate band oscillator strengths. A table of band wavelengths and semitheoretical transition-probabilities is presented for each system and the predicted band spectrum is briefly discussed.

I. INTRODUCTION

In the first two papers[1,2] of this series (hereafter referred to as I and II) transition moment calculations using single configuration Hartree-Fock (HF) wave functions were presented for the BeH, MgH OH and SH (A-X) and N_2^+ (A-X; B-X) systems. These results and those of Huo[3] for some CH and NH systems indicate that for diatomics composed of first and second row atoms HF oscillator strengths have order of magnitude accuracy only. For the cases where experimental data is available for comparison, HF f values differ from experiment by factors of 2-7. These observations are consistent with the exploratory investigations of LaPaglia[4] using relatively crude multiconfiguration (MC) wave functions. He found that for $^1\Sigma-^1\Sigma$ transitions in some first row diatomics the correlation correction to the SCF transition moments can have the same order of magnitude as the transition moment itself.

Recently Wolniewicz[5] has reported accurate theoretical dipole-length transition moments for the H_2 (B-X; C-X; E,F-B) systems. They have been used by Allison and Dalgarno[6] to compute vibrational band oscillator strengths and transition probabilities for the Lyman and Werner systems. It has not been possible to calculate reliable transition moments for other diatomics due to the lack of wave functions that adequately take in to account the effect of correlation. However, this situation is changing and good wave functions are becoming available for the ground and excited states of first and second row diatomics. A review by Wahl and Das[7] summarizes the methods currently in use for calculating wave functions that go beyond the HF approximation.

Chan and Davidson[8] have carried out MC calculations on the ground and low-lying excited states of BeH and MgH at several values of the internuclear separation R. The wave functions are expanded as a linear combination of configurations composed of the occupied and virtual MO's generated in an SCF run for the ground state. For all states, the MO's describing the inner shell electrons are the same in each configuration, i.e., the core is 'frozen', and only the valence shell electrons are correlated. The configuration coefficients were determined by straightforward use of the conventional configuration interaction (CI) procedure. In the present paper, the Chan-Davidson wave functions for the lowest $^2\Sigma^+$ and $^2\Pi$ states are used to calculate electronic dipole-momentum $M_x(R)$ and dipole-length $\bar{M}_x(R)$ transition moment curves for the BeH and MgH ($A^2\Pi - X^2\Sigma^+$) systems. The MC curves are compared with the HF ones given in I. The transition moments and vibrational wave functions derived from both the theoretical MC and 'experimental' RKR potential energy $U(R)$ curves are used to calculate band oscillator strengths $f_{v'v''}$. A table of band wavelengths $\lambda_{v'v''}$ and semitheoretical transition probabilities $A_{v'v''}$ is presented for each system and the predicted band spectrum is briefly discussed.

No absolute oscillator strength measurements for the BeH (A-X) system appear in the literature. There are two papers dealing with experimental investigations of the strength of the MgH (A-X) system. Schadee[9] first gave a value of $f_{00} \approx 0.008$ for the 0-0 band oscillator strength that was subsequently revised to $f_{00} \approx 0.035$ by Main et al.[10] on the basis of a more recent value of the dissociation energy of the MgH $X^2\Sigma^+$ ground state. The

277

latter authors report absolute emission intensity studies of the MgH system and place an upper limit of $f_{\Delta v=0} \lesssim 0.002$ on the absorption oscillator strength of the $\Delta v=0$ sequence.

In Section II, the theoretical expressions and computational methods used are briefly reviewed. A more complete description is given in I. Numerical results are presented and discussed in Section III.

II. THEORY AND COMPUTATIONAL DETAILS

In the semiclassical theory of radiation[11], the probability for a spontaneous transition from the upper state Γ' to the lower state Γ'' of a diatomic system is given by:

$$A_{\Gamma'\Gamma''} = \frac{4e^4}{3c^3 a_0^3 m_e^2} \frac{\Delta E_{\Gamma'\Gamma''}}{\omega_{\Gamma'}} S_{\Gamma'\Gamma''} \tag{1}$$

where $\Delta E_{\Gamma'\Gamma''}$, $S_{\Gamma'\Gamma''}$ are in atomic units (a.u.) and $A_{\Gamma'\Gamma''}$ is in $\sec^{-1}$. $\Delta E_{\Gamma'\Gamma''}$ is the transition energy and $\omega_{\Gamma'}$ the degeneracy of the upper state. In the dipole approximation, the line strength $S_{\Gamma'\Gamma''}$ is equal to the square of the momentum transition moment summed over all degenerate components of Γ' and Γ'':

$$S_{\Gamma'\Gamma''} = \sum_{\alpha'\alpha''} \left| \int \left\{ \gamma(\vec{p}'|\vec{p}) \ \vec{p} \right\}_{\vec{p}'=\vec{p}} d\vec{p} \right|^2 . \tag{2}$$

$\gamma(\vec{p}'|\vec{p})$ is the first order spinless transition density matrix in momentum space:

$$\gamma(\vec{p}'|\vec{p}) = N \int \Psi_{\Gamma'}^*(\vec{p}',\vec{p}_2,\ldots\vec{p}_N,\vec{P}_R) \Psi_{\Gamma''}(\vec{p},\vec{p}_2,\ldots\vec{p}_N,\vec{P}_R) \frac{d\vec{P}_R d\vec{p}^N ds^N}{d\vec{p}_1} . \tag{3}$$

The electronic momentum vectors $\vec{p}_\mu$ are conjugate to the position vectors $\vec{r}_\mu$ and the nuclear momentum vector $\vec{P}_R$ is conjugate to the internuclear axis vector $\vec{R}$. All vectors are measured relative to a space-fixed coordinate system. In equation (3) the integration is over the spin coordinates of all electrons and over all momentum vectors except that of electron 1. For a transition from Γ'' to Γ' the absorption oscillator strength is defined as:

$$f_{\Gamma'\Gamma''} = \frac{2}{3} \frac{1}{\Delta E_{\Gamma'\Gamma''}} \frac{S_{\Gamma'\Gamma''}}{\omega_{\Gamma''}} . \qquad (4)$$

Transformation to a molecule-fixed coordinate system and application of the Born-Oppenheimer approximation results in the following expression for the oscillator strength[12],

$$f_{\Omega''v''j''}^{\Omega'v'j'} = \frac{2}{3} \frac{1}{\Delta E_{\Omega''v''j''}^{\Omega'v'j'}} \frac{\sum\limits_{\alpha'\alpha''} P_{\Omega''v''j''}^{\Omega'v'j'} S_{j''\Omega''}^{j'\Omega'}}{(2-\delta_{0,\Lambda''})(2S''+1)(2j''+1)} . \qquad (5)$$

Ω, Λ, v, and j are the quantum numbers for the total and orbital electronic angular momentum about the internuclear axis, vibration, and total angular momentum respectively, $2S''+1$ is the spin multiplicity of the lower state, $S_{j''\Omega''}^{j'\Omega'}$ is the Hönl-London factor, and

$$P_{\Omega''v''j''}^{\Omega'v'j'} = \left| \int P_{\Omega'v'j'}(R) M_{\Omega'\Omega''}(R) P_{\Omega''v''j''}(R) \, dR \right|^2 . \qquad (6)$$

In (6), the $P_{\Omega v j}(R)$ are vibration-rotation wave functions and $M_{\Omega'\Omega''}(R)$ is the electronic dipole-momentum transition moment:

$$M_{\Omega'\Omega''}(R) = -i \, N \int \Psi_{\Omega'}^*(\vec{r}^N, R) \, \vec{p} \, \Psi_{\Omega''}(\vec{r}^N, R) \, d\vec{r}^N \, ds^N \qquad (7)$$

In (7), the $\Psi_\Omega(\vec{r}^N, R)$ are electronic wave functions, $\vec{p} = -i\vec{\nabla}$, and the integration is over the spin and space coordinates of all electrons.

Application of the commutator relation between $\vec{r}_\mu$ and $\vec{p}_\mu$ and the Born-Oppenheimer approximation leads to another expression for the oscillator strength (see I):

280

$$f^{\Omega'v'j'}_{\Omega''v''j''} = \frac{2}{3}\frac{\Delta E^{\Omega'v'j'}_{\Omega''v''j''} \displaystyle\sum_{\alpha'\alpha''} \bar{P}^{\Omega'v'j'}_{\Omega''v''j''} S^{j'\Omega'}_{j''\Omega''}}{(2-\delta_{0,\Lambda''})(2S''+1)(2j''+1)} \quad , \tag{8}$$

where
$$\bar{P}^{\Omega'v'j'}_{\Omega''v''j''} = \left| \int P_{\Omega'v'j'}(R)\, \bar{M}_{\Omega'\Omega''}(R)\, P_{\Omega''v''j''}(R)\, dR \right|^2 \quad . \tag{9}$$

$\bar{M}_{\Omega'\Omega''}(R)$ is the electronic dipole-length transition moment:

$$\bar{M}_{\Omega'\Omega''}(R) = N \int \Psi^*_{\Omega'}(\vec{r}^N,R)\, \vec{r}\, \Psi_{\Omega''}(\vec{r}^N,R)\, d\vec{r}^N\, ds^N \quad . \tag{10}$$

If vibration-rotation interaction is neglected and the mixed expression for the oscillator strength derived from (5) and (8) is used, vibrational band oscillator strengths can be defined as:

$$f^{\Omega'v'}_{\Omega''v''} = \frac{2}{3}\frac{\displaystyle\sum_{\alpha'\alpha''} \left| \bar{P}^{\Omega'v'0}_{\Omega''v''0}\, P^{\Omega'v'0}_{\Omega''v''0} \right|^{1/2}}{(2-\delta_{0,\Lambda''})(2S''+1)} \quad . \tag{11}$$

Similarly, band transition probabilities are defined as:

$$A^{\Omega'v'}_{\Omega''v''} = \frac{4e^4}{3c^3 a_0^3 m_e^2}\left[\Delta E^{\Omega'v'0}_{\Omega''v''0}\right]^2 \frac{\displaystyle\sum_{\alpha'\alpha''} \left| \bar{P}^{\Omega'v'0}_{\Omega''v''0}\, P^{\Omega'v'0}_{\Omega''v''0} \right|^{1/2}}{(2-\delta_{0,\Lambda''})(2S''+1)} \tag{12}$$

In the remainder of this paper the labels $M_{\Omega'\Omega''}(R)$, $\bar{M}_{\Omega'\Omega''}(R)$, $f^{\Omega'v'}_{\Omega''v''}$ and $A^{\Omega'v'}_{\Omega''v''}$ are replaced by $M(R)$, $\bar{M}(R)$, $f_{v'v''}$ and $A_{v'v''}$ respectively, and the dependence on the quantum numbers Ω' and Ω'' is implicitly understood.

For the $^2\Pi$ and $^2\Sigma^+$ states of BeH and MgH the MC wave functions have the form:

$$\Psi(^2\Pi) = \sum_I c'_I \Phi'_I \tag{13a}$$

281

and
$$\Psi(^2\Sigma^+) = \sum_J C_J \bar{\Phi}_J \tag{13b}$$

where Φ_I' is a MO configuration of $^2\Pi$ symmetry, Φ_J a MO configuration of $^2\Sigma^+$ symmetry, and C_I', C_J are CI coefficients. The x-components of the transition moments are given by:

$$\langle ^2\Pi|x|^2\Sigma^+\rangle = \sum_I \sum_J C_I' \, C_J \langle \Phi_I'|x|\Phi_J\rangle \tag{14a}$$

and
$$\langle ^2\Pi|-ip_x|^2\Sigma^+\rangle = \sum_I \sum_J C_I' \, C_J \langle \Phi_I'|-ip_x|\Phi_J\rangle. \tag{14b}$$

The MC transition moment calculations differ from the HF computations described in I in that each wave function is represented by a linear combination of configurations rather than a single configuration and hence the moments are given by a double sum of terms involving integrals between excited state configurations and ground state configurations. The BeH and MgH calculations have been simplified by the fact that Chan and Davidson[8] used a single orthonormal set of MO's to construct both $\Psi(^2\Pi)$ and $\Psi(^2\Sigma^+)$ at a given value of R and consequently the signed minors of the MO overlap matrix appearing in equation (18a) of I are either 0 or ±1.

The methods used to construct RKR potential energy U(R) curves and to compute vibration-rotation wave functions $P_{vj}(R)$ are given in I. Experimental spectroscopic constants were taken from Olsson[13] for the BeH states and from Guntsch[14] and Khan[15] for the MgH states.

282

III. RESULTS AND DISCUSSION

In Figs. 1 and 2 potential energy U(R) curves for the BeH and MgH $A^2\Pi$ and $X^2\Sigma^+$ states are shown. Theoretical curves based on the HF energies of Cade and Huo[16] and on the MC energies reported by Chan and Davidson[8] are compared with 'experimental' curves obtained by the RKR procedure. The AO basis sets used by the latter authors in their MC studies of BeH and MgH lead to total electronic energies that are actually higher than the HF energies for both the A and X states. However, as is evident from Figs. 1 and 2, the energy difference $\Delta E(R)$ between the $A^2\Pi$ and $X^2\Sigma^+$ states is closer to experiment for the MC energies than for the HF energies.

In Table I spectroscopic constants are presented for the BeH and MgH A and X states. The theoretical constants are based on $\Delta G(v)$ and B_v values obtained by numerically integrating the one-dimensional Schrödinger equation for nuclear motion using the U(R) curves depicted in Figs. 1 and 2. For a given theoretical curve, only a small number of points $U(R_i)$ are available and consequently the results are dependent on the method used to interpolate and extrapolate U(R), especially for the higher vibrational levels. For each state U(R) was represented by a single polynomial in R passing through all available points, and only the three lowest vibrational levels were used to determine the constants in Table I.

For the BeH states the MC ω_e and $\omega_e x_e$ values are closer to experiment than the HF values. It can be seen in Fig. 1 that the shapes of the MC curves are quite similar to that of the RKR curves resulting in good vibrational constants. The HF curves rise too sharply for large R because of the incorrect dissociation of the

283

states in the HF approximation and this behaviour is reflected in the poorer ω_e and $\omega_e x_e$ values. On the other hand, the HF B_e values are closer to experiment than the MC values. The MC R_e values are larger than the experimental equilibrium separations for both the A and X states resulting in B_e values that are too small. Fig. 2 shows that the shapes of the HF and MC potential energy curves for the MgH $X^2\Sigma^+$ state are practically the same for intermediate values of R and both curves rise too sharply for large R in comparison with the RKR curve. The HF and MC ω_e and $\omega_e x_e$ values are similar and neither pair is to be preferred. The theoretical R_e values are too large, with the HF equilibrium separation closer to experiment than the MC separation. Consequently the HF B_e rotational constant is more accurate. For the MgH $A^2\Pi$ state, the characteristics (shape and position of the minimum) of the RKR potential energy curve are better approximated by the MC curve than the HF curve with the result that more accurate spectroscopic constants are obtained using the former. In summary, the theoretical spectroscopic constants computed with the Chan-Davidson potential energy curves are fairly good in comparison with experiment and are of similar quality to the HF values even though, on an absolute scale, the MC electronic energies are poorer than the HF energies.

Tables II and III contain values of the dipole-momentum and dipole-length transition moments for the BeH and MgH (A-X) systems obtained from expressions (7) and (10) using the Chan-Davidson MC wave functions. Also presented are values of the transition energy $\Delta E(R)$. The $M_x(R)$ and $\bar{M}_x(R)$ curves are plotted in Figs. 3 and 4 and are labelled MC $-i\langle p_x\rangle$ and MC $\langle x\rangle$ respectively. For exact Born-Oppenheimer electronic wave functions the following relationship holds (see I):

$$-i \langle p_x \rangle = \Delta E \langle x \rangle \ . \qquad (15)$$

The identity is not valid for approximate wave functions and $\Delta E \langle x \rangle$ leads to a different $M_x(R)$ curve than $-i \langle p_x \rangle$. The expression $-i \, \Delta E^{-1} \langle p_x \rangle$ can be used for $\overline{M}_x(R)$ provided that ΔE is nonzero, i.e., provided that the potential curves for the two states do not cross. The MC dipole-momentum and dipole-length transition moment curves obtained from using the expressions containing ΔE are plotted in Figs. 3 and 4. Also shown are the HF curves reported in I.

As discussed in I, for BeH and MgH the (A-X) transition is dipole forbidden in the united and separated atom limits and consequently the $M_x(R)$ and $\overline{M}_x(R)$ curves should go to zero in the limit of small and large R. The HF curves in Figs. 3 and 4 give no indication of approaching zero for large R, although it should be kept in mind that the HF calculations have been performed over a rather limited range of R. On the other hand, it can be seen that the MC curves appear to be approaching zero for $R=0$ and $R=\infty$. Thus the MC $M_x(R)$ and $\overline{M}_x(R)$ curves exhibit the behaviour expected of a transition that is forbidden in the united and separated atoms.

Using the MC curves as the basis for comparison, it is possible to obtain the correlation correction to the HF transition moment curves:

$$\Delta M_x(R) = M_x^{HF}(R) - M_x^{MC}(R) \qquad (16a)$$

and

$$\Delta \overline{M}_x(R) = \overline{M}_x^{HF}(R) - \overline{M}_x^{MC}(R) \ , \qquad (16b)$$

285

where $M_X(R)$ and $\overline{M}_X(R)$ are calculated using expressions (7) and (10). For the BeH and MgH (A-X) systems $\Delta M_X(R)$ and $\Delta\overline{M}_X(R)$ increase monotonously on going from intermediate to larger values of R. For BeH, $\Delta M_X(R)$ increases from 0.022 a.u. to 0.059 a.u. and $\Delta\overline{M}_X(R)$ from 0.113 a.u. to 0.343 a.u. in the interval R = 2.00 a.u. to R = 3.70 a.u. For MgH, $\Delta M_X(R)$ increases from 0.009 a.u. to 0.051 a.u. and $\Delta\overline{M}_X(R)$ from -0.003 a.u. to 0.259 a.u. on going from R = 2.50 a.u. to R = 4.50 a.u. Thus for both systems $\Delta M_X(R)$ and $\Delta\overline{M}_X(R)$ vary considerably as a function of R. These results are in agreement with the qualitative predictions made in I concerning the behaviour of the correlation correction to the HF transition moments.

As noted earlier, the AO basis sets used by Chan and Davidson[8] for BeH and MgH were not as flexible as those of Cade and Huo[16] with the result that the MC electronic energies are poorer than the HF energies. Hence the question arises as to whether the differences between the HF and MC transition moment curves in Figs. 3 and 4 are indeed due to correlation effects and not to the use of different AO basis sets. The author carried out some SCF runs on the BeH $A^2\pi$ and $X^2\Sigma^+$ states using the Chan-Davidson AO basis set and found that the calculated transition moments were quite close to the HF moments reported in I. SCF $M_X(R)$ values of 0.096, 0.097, 0.099, 0.102, 0.105 a.u. and $\overline{M}_X(R)$ values of 0.838, 0.819, 0.795, 0.776, 0.765 a.u. were obtained for R = 2.00, 2.50, 3.00, 3.50 and 4.00 a.u. respectively. These can be compared with the HF $M_X(R)$ values of 0.095, 0.095, 0.097, 0.101 a.u. and $\overline{M}_X(R)$ values of 0.822, 0.794, 0.769, 0.751 a.u. at R = 2.00, 2.47, 3.00 and 3.70 a.u. respectively in I. Thus in the independent particle approximation the AO set used by

Chan and Davidson[8] for the BeH (A-X) system is adequate for the calculation of the dipole-length and dipole-momentum transition moments. This should also be true for the MgH (A-X) system.

For the transition moments studied in this paper it was found that at a given R value a relatively small number of terms contribute substantially to the double sums in (14a) and (14b) while the remaining terms are of smaller magnitude and tend to cancel one another. For intermediate values of R the term involving the $K2\sigma^2 1\pi$ configuration in the $^2\pi$ state and the $K2\sigma^2 3\sigma$ configuration in the $^2\Sigma^+$ state dominates the BeH (A-X) $M_x(R)$ and $\bar{M}_x(R)$ transition moments. This is to be expected because the HF approximation is fairly good in the neighborhood of R_e for the two states as is evident in Fig. 3. On going to larger values of R the $K2\sigma 3\sigma 1\pi$ - $K2\sigma^2 3\sigma$ term increases and is of opposite sign to the $K2\sigma^2 1\pi$ - $K2\sigma^2 3\sigma$ term. For R = 5.00 a.u. the two terms have essentially the same magnitude and cancel each other. Thus the qualitative behaviour of the $M_x(R)$ and $\bar{M}_x(R)$ curves in Fig. 3 can be arrived at by considering the terms between the $K2\sigma^2 1\pi$ and $K2\sigma 3\sigma 1\pi$ configurations of the $A^2\pi$ state and the $X^2\Sigma^+$ $K2\sigma^2 3\sigma$ configuration. For BeH, the sum of the terms between the $K2\sigma^2 1\pi$, $K2\sigma^2 2\pi$, $K2\sigma^2 3\pi$, $K2\sigma^2 4\pi$, $K2\sigma 3\sigma 1\pi$ and $K2\sigma 3\sigma 2\pi$ configurations of the $A^2\pi$ state and the $K2\sigma^2 3\sigma$, $K2\sigma^2 4\sigma$, $K2\sigma^2 5\sigma$, $K2\sigma^2 8\sigma$ and $K2\sigma 1\pi^2$ configurations of the $X^2\Sigma^+$ state is given in columns four and six in Table II for M_x and $\bar{M}_x$ respectively. It can be seen that the partial sums are quite close to the total sums in columns three and five.

For the MgH $X^2\Sigma^+$ state the HF configuration $KL4\sigma^2 5\sigma$ dominates the MC wave function at all values of R and accounts for the simi-

larity between the HF and MC potential energy curves in Fig. 2. However, for the $A^2\Pi$ state the $KL4\sigma^2 5\pi$ configuration is dominant while the $KL4\sigma^2 2\pi$ one is the next most important. The sum of the $KL4\sigma^2 5\pi - KL4\sigma^2 5\sigma$ and $KL4\sigma^2 2\pi - KL4\sigma^2 5\sigma$ contributions to the transition moments is of similar magnitude to the HF transition moments for intermediate values of R. The $KL4\sigma 5\sigma 5\pi - KL4\sigma^2 5\sigma$ term is of opposite sign and increases in magnitude on going from intermediate to larger values of R. The qualitative behaviour of the $M_x(R)$ and $\overline{M}_x(R)$ curves in Fig. 4 can be accounted for by considering the $KL4\sigma^2 2\pi$, $KL4\sigma^2 5\pi$ and $KL4\sigma 5\sigma 5\pi$ configurations of the $A^2\Pi$ state and the $X^2\Sigma^+$ $KL4\sigma^2 5\sigma$ configuration. Columns four and six in Table III give partial sums that also include the $KL4\sigma^2 6\pi - KL4\sigma^2 5\sigma$ and $KL4\sigma 5\sigma 7\pi - KL4\sigma^2 5\pi$ contributions. It can be seen that the entries in columns four and six are quite close to the corresponding entries in columns three and five.

For the BeH and MgH (A-X) systems the small number of configurations in the $A^2\Pi$ and $X^2\Sigma^+$ states that contribute substantially to the dipole-length and momentum transition moments are also important on the basis of the magnitude of their coefficients in the configuration expansions of the state wave functions. Hence reliable transition moments can be obtained with fairly short multiconfiguration expansions for the A and X states especially if the MO's in the configurations are optimized in some fashion to better describe the state under consideration.

Electronic dipole-momentum and dipole-length matrix elements and Franck-Condon factors, $M_{v'v''}$, $\overline{M}_{v'v''}$ and $q_{v'v''}$ respectively, were calculated using vibrational wave functions obtained from the

MC and RKR U(R) curves in Figs. 1 and 2 and the MC $-i\langle p_x \rangle$ and $\langle x \rangle$ curves in Figs. 3 and 4. The latter curves were extrapolated to zero for small and large R as shown. Band oscillator strengths $f_{v'v''}$ were determined from the $M_{v'v''}$ and $\overline{M}_{v'v''}$ values using expression (11). Tables IV and V give relative Franck-Condon factors $q_{v'v''}/q_{00}$ and oscillator strengths $f_{v'v''}/f_{00}$ for the v'-v'' (v',v'' $\leqslant$ 5) bands of the BeH and MgH (A-X) systems. The theoretical values result from the use of the MC U(R) curves while the semi-theoretical values are obtained by using the RKR potential energy curves.

For a given band, two factors influence the value of the product $M_{v'v''}\overline{M}_{v'v''}$. First of all, the product will depend on the magnitude of the electronic transition moments M(R) and $\overline{M}(R)$ and their variation with R. Secondly, the value of $M_{v'v''}\overline{M}_{v'v''}$ will be affected by the vibrational wave functions used and these depend on the shapes and R_e values of the U(R) curves for the states under consideration. If M(R) and $\overline{M}(R)$ were constant, the relative oscillator strengths $f_{v'v''}/f_{00}$ would equal the relative Franck-Condon factors $q_{v'v''}/q_{00}$. A comparison of the semitheoretical $f_{v'v''}/f_{00}$ values with the RKR $q_{v'v''}/q_{00}$ values gives an indication of the effect on the band oscillator strengths of the variation of M(R) and $\overline{M}(R)$ with R. On the other hand, if the semitheoretical $f_{v'v''}/f_{00}$ values are compared with the theoretical values we see the effect of approximating the RKR U(R) curves by the MC ones.

For the BeH (A-X) system the $A^2\Pi$ and $X^2\Sigma^+$ potential energy curves have nearly identical R_e values and their shapes in the vicinity of the minimum are quite similar as evidenced by the

vibrational spectroscopic constants. Consequently the ground and
excited state vibrational wave functions are almost orthonormal
($q_{v'v''} \approx 1$ for $v'=v''$; $q_{v'v''} \approx 0$ for $v' \neq v''$) and the band oscillator
strengths are mainly determined by the Franck-Condon factors.
However, for the $\Delta v=0$ sequence $f_{v'v''}$ decreases as v' increases
because both $M_x(R)$ and $\bar{M}_x(R)$ approach zero for large R.
For the MgH (A-X) system the RKR $q_{v'v''}/q_{00}$ values for $v' < v''$
are closer to the semitheoretical $f_{v'v''}/f_{00}$ values than the
theoretical $f_{v'v''}/f_{00}$ values indicating that for these bands the
oscillator strengths are influenced more by the U(R) curves than by
the $M_x(R)$ and $\bar{M}_x(R)$ curves. The $f_{v'v''}/f_{00}$ values for the $\Delta v=0$
sequence fall off more rapidly than the $q_{v'v''}/q_{00}$ values as v'
increases due to the variation of M(R) and $\bar{M}(R)$ with R. For the
$\Delta v=1$ sequence we have the unexpected result that the MC $q_{v'v''}/q_{00}$
values are closer to the semitheoretical $f_{v'v''}/f_{00}$ values than either
the RKR $q_{v'v''}/q_{00}$ values or the theoretical $f_{v'v''}/f_{00}$ values. The
entries in Tables IV and V indicate that accurate potential energy
and transition moment curves are required to arrive at reliable
oscillator strengths for the BeH and MgH (A-X) systems.

The semitheoretical f_{00} values are 0.114 and 0.188 for the BeH
and MgH (A-X) systems respectively. These can be compared with the
HF f_{00} values of 0.201 and 0.250 reported in I. As mentioned in the
Introduction no absolute oscillator strength measurements have been
reported in the literature for BeH. For MgH Main et al.[10] have
determined that $f_{\Delta v=0} \lesssim 0.002$ on the basis of absolute emission
intensity measurements of a portion of the flame of a rocket engine.
Schadee[9] has analysed the 0-0 band absorption in the solar proto-
sphere and attempted to deduce f_{00} from an atmospheric model. As

pointed out by Main et al.[10], Schadee's results indicate that $f_{00} \approx 0.008$ or $f_{00} \approx 0.035$ depending on the value used for the dissociation energy of the MgH $X^2\Sigma^+$ state. Thus for MgH there appears to be at least an order of magnitude discrepancy between the calculated and experimental f_{00} values. The author believes that the use of more accurate wave functions will not change the calculated value by more than $\approx 50\%$ and that more precise experimental measurements are required to resolve this dilemma.

In Tables VI and VII band wavelengths $\lambda_{v'v''}$ and semitheoretical transition probabilities $A_{v'v''}$ are presented for the BeH and MgH (A-X) systems. This information is useful to spectroscopists attempting to obtain the band spectra. In emission the band intensities $I_{v'v''}$ are proportional to $N_{v'}A_{v'v''}/\lambda_{v'v''}$ where $N_{v'}$ is the population of the excited state vibrational level. For BeH the $\Delta v = 0$ sequence will be strongest while the $\Delta v = -1$ sequence will be about two orders of magnitude less intense. All other sequences are predicted to have an intensity that is at least three orders of magnitude smaller than the $\Delta v = 0$ sequence and will be extremely difficult to observe. Experimentally, the 0-0, 1-1, 2-2, 3-3, 4-4, 0-1, 1-2, 2-3 and 3-4 bands have been observed[13]. For MgH the $\Delta v = 0$ sequence is again predicted to be the most intense while the $\Delta v = -1$ and $\Delta v = 1$ sequences are about an order of magnitude less intense and the $\Delta v = -2$ sequence another order of magnitude weaker. Experimentally, only the 0-0, 1-1, 2-2, 0-1, 1-2, 1-0 and 2-1 bands have been observed[14].

ACKNOWLEDGMENTS

REFERENCES

1. W. H. Henneker and H. E. Popkie, J. Chem. Phys. 54, 0000 (1971).

2. H. E. Popkie and W. H. Henneker, J. Chem. Phys. (to be published).

3. W. M. Huo, J. Chem. Phys. 49, 1482 (1968).

4. a) S. R. LaPaglia, Theoret. Chim. Acta 8, 185 (1967).

    b) M. A. Marchetti and S. R. LaPaglia, J. Chem. Phys. 48, 434 (1968).

5. L. Wolniewicz, J. Chem. Phys. 51, 5002 (1969).

6. A. C. Allison and A. Dalgarno, Atomic Data 1, 289 (1970).

7. A. C. Wahl and G. Das, Adv. Quantum Chem. 5, 261 (1970).

8. a) A. C. H. Chan and E. R. Davidson, J. Chem. Phys. 49, 727 (1968).

    b) A. C. H. Chan and E. R. Davidson, J. Chem. Phys. 52, 4108 (1970).

9. A. Schadee, Bull. Astron. Inst. Neth. 5, 311 (1964).

10. R. P. Main, D. J. Carlson and R. A. Dupuis, J. Quant. Spectry. Radiative Transfer 7, 805 (1967).

11. a) W. Heitler, "The Quantum Theory of Radiation", 3rd edn. (Oxford University Press, 1953).

    b) H. A. Bethe and E. E. Salpeter, "Quantum Mechanics of One- and Two-Electron Atoms" (Springer-Verlag, Germany, 1957).

12. a) R. W. Nicholls and A. L. Stewart, in "Atomic and Molecular Processes", D. R. Bates, ed. (Academic Press, New York, 1962).

    b) I. Kovacs, "Rotational Structure in the Spectra of Diatomic

Molecules" (American Elsevier, New York, 1969).

13. E. Olsson, Z. Physik $\underline{73}$, 732 (1932).

14. A. Guntsch, Z. Physik $\underline{104}$, 584 (1937).

15. M. A. Khan, Proc. Phys. Soc. (London) $\underline{80}$, 523 (1962).

16. a) P. E. Cade and W. M. Huo, J. Chem. Phys. $\underline{47}$, 614 (1967).

    b) P. E. Cade and W. M. Huo, J. Chem. Phys. $\underline{47}$, 649 (1967).

    c) P. E. Cade, "Hartree-Fock-Roothaan Wave Functions for First-Row Diatomic molecules: AH, A_2 and AB", Special Technical Report, Laboratory of Molecular Structure and Spectra (to be published).

    d) P. E. Cade (to be published).

TABLE I. Theoretical and experimental spectroscopic constants for the $A^2\Pi$ and $X^2\Sigma^+$ states of BeH and MgH

State*		$\omega_e(cm^{-1})$	$\omega_e x_e(cm^{-1})$	$B_e(cm^{-1})$	$\alpha_e(cm^{-1})$	$R_e(bohr)$
BeH ($A^2\Pi$)	HF	2236	29.3	10.673	0.255	2.495
	MC	2058	40.0	9.949	0.316	2.584
	RKR	2088	39.9	10.470	0.329	2.519
BeH ($X^2\Sigma^+$)	HF	2142	28.2	10.396	0.257	2.528
	MC	2032	40.7	9.873	0.318	2.594
	RKR	2059	35.5	10.308	0.300	2.538
MgH ($A^2\Pi$)	HF	1742	22.4	6.266	0.134	3.153
	MC	1692	30.0	6.231	0.172	3.162
	RKR	1598	31.9	6.178	0.188	3.175
MgH ($X^2\Sigma^+$)	HF	1598	21.5	5.860	0.129	3.259
	MC	1597	25.7	5.940	0.166	3.238
	RKR	1497	32.4	5.818	0.167	3.271

*The experimental spectroscopic constants are from Olsson[13] for the BeH states and from Guntsch[14] and Khan[15] for the MgH states.

TABLE II. BeH $(A^2\Pi - X^2\Sigma^+)$ Electronic dipole-momentum and dipole-length transition moments and transition energy [*]

R	ΔE	$-i\langle p_x\rangle$	†	$\langle x\rangle$	‡
1.00	0.0956	0.069	0.062	0.627	0.686
1.50	0.0928	0.075	0.076	0.725	0.772
2.00	0.0918	0.072	0.077	0.709	0.751
2.50	0.0924	0.068	0.070	0.655	0.691
3.00	0.0931	0.061	0.058	0.576	0.621
3.50	0.0938	0.049	0.042	0.465	0.519
4.00	0.0942	0.031	0.028	0.311	0.371
4.50	0.0931	0.012	0.010	0.153	0.230
5.00	0.0893	0.004	0.001	0.066	0.139

[*] Entries are in a.u.

[†] Contribution to $-i\langle p_x\rangle$ arising from terms between the $K2\sigma^2 1\pi$, $K2\sigma^2 2\pi$, $K2\sigma^2 3\pi$, $K2\sigma^2 4\pi$, $K2\sigma 3\sigma 1\pi$ and $K2\sigma 3\sigma 2\pi$ configurations of the $A^2\Pi$ state and the $K2\sigma^2 3\sigma$, $K2\sigma^2 4\sigma$, $K2\sigma^2 5\sigma$, $K2\sigma^2 8\sigma$ and $K2\sigma 1\pi^2$ configurations of the $X^2\Sigma^+$ state.

[‡] Contribution to $\langle x\rangle$ arising from terms between the above configurations.

TABLE III. MgH $(A^2\Pi - X^2\Sigma^+)$ Electronic dipole-momentum and dipole-length transition moments and transition energy[*]

R	ΔE	$-i\langle p_x \rangle$	[†]	$\langle x \rangle$	[‡]
1.75	0.0694	0.061	0.066	0.966	0.975
2.25	0.0813	0.077	0.082	1.019	1.033
2.75	0.0879	0.081	0.088	0.999	1.013
3.25	0.0923	0.080	0.086	0.946	0.974
3.75	0.0953	0.075	0.085	0.875	0.900
4.25	0.0971	0.067	0.078	0.782	0.816
4.75	0.0974	0.054	0.066	0.695	0.722
5.25	0.0983	0.040	0.045	0.515	0.482

[*]Entries are in a.u.

[†]Contribution to $-i\langle p_x \rangle$ arising from terms between the $KL4\sigma^2 2\pi$, $KL4\sigma^2 5\pi$, $KL4\sigma^2 6\pi$, $KL4\sigma 5\sigma 5\pi$ and $KL4\sigma 5\sigma 7\pi$ configurations of the $A^2\Pi$ state and the $KL4\sigma^2 5\sigma$ configuration of the $X^2\Sigma^+$ state.

[‡]Contribution to $\langle x \rangle$ arising from terms between the above configurations.

297

TABLE IV. BeH ($A^2\Pi - X^2\Sigma^+$) Relative Franck-Condon Factors and Band Oscillator Strengths

v' \ v"	0	1	2	3	4	5
0	1.000 *	0.807-3	0.346-5	0.158-7	0.115-8	0.168-8
	1.000 †	0.253-2	0.675-4	0.597-6	0.218-7	0.261-7
	1.000 ‡	0.441-2	0.128-4	0.262-6	0.515-8	0.810-10
	1.000 #	0.735-2	0.116-3	0.234-5	0.800-8	0.292-7
1	0.810-3	0.998	0.177-2	0.119-4	0.782-7	0.153-8
	0.257-2	0.996	0.404-2	0.199-3	0.303-5	0.462-7
	0.887-4	0.952	0.989-2	0.406-4	0.105-5	0.484-9
	0.193-3	0.954	0.136-1	0.313-3	0.103-4	0.318-7
2	0.439-6	0.178-2	0.996	0.294-2	0.302-4	0.253-
	0.248-4	0.419-2	0.993	0.461-2	0.389-3	0.925-5
	0.438-5	0.303-3	0.898	0.168-1	0.965-4	0.248-5
	0.518-4	0.435-4	0.906	0.190-1	0.549-3	0.276-4
3	0.146-9	0.137-5	0.298-2	0.993	0.436-2	0.712-4
	0.945-7	0.947-4	0.488-2	0.993	0.435-2	0.625-3
	0.593-8	0.183-4	0.745-3	0.835	0.257-1	0.226-3
	0.591-7	0.182-3	0.883-5	0.852	0.238-1	0.779-3
4	0.235-8	0.139-8	0.357-5	0.445-2	0.990	0.603-2
	0.106-6	0.570-7	0.231-3	0.471-2	0.993	0.343-2
	0.534-8	0.317-7	0.505-4	0.161-2	0.760	0.371-1
	0.120-6	0.314-6	0.407-3	0.759-3	0.792	0.283-1
5	0.150-8	0.589-8	0.136-7	0.106-4	0.62?-2	0.986
	0.207-7	0.454-6	0.941-7	0.449-3	0.381-2	0.995
	0.111-8	0.253-7	0.139-6	0.112-3	0.332-2	0.668
	0.207-7	0.494-6	0.885-6	0.712-3	0.322-2	0.726

*Theoretical $q_{v'v''}/q_{00}$ ($q_{00} = 0.999$)

†RKR $q_{v'v''}/q_{00}$ ($q_{00} = 0.997$)

‡Theoretical $f_{v'v''}/f_{00}$ ($f_{00} = 0.112$)

#Semitheoretical $f_{v'v''}/f_{00}$ ($f_{00} = 0.114$)

TABLE V. MgH ($A^2\Pi - X^2\Sigma^+$) Relative Franck-Condon Factors and Band Oscillator Strengths

v' \ v''	0	1	2	3	4	5
0	1.000 *	0.376-1	0.207-2	0.145-3	0.132-4	0.153-5
	1.000 †	0.546-1	0.405-2	0.396-3	0.529-4	0.114-4
	1.000 ♦	0.456-1	0.248-2	0.170-3	0.143-4	0.139-5
	1.000 #	0.647-1	0.483-2	0.466-3	0.609-4	0.120-4
1	0.398-1	0.924	0.700-1	0.590-2	0.554-3	0.624-4
	0.589-1	0.888	0.984-1	0.115-1	0.169-2	0.337-3
	0.317-1	0.899	0.849-1	0.706-2	0.644-3	0.680-4
	0.482-1	0.860	0.116	0.137-1	0.197-2	0.387-3
2	0.667-4	0.785-1	0.853	0.959-1	0.110-1	0.131-2
	0.209-3	0.116	0.778	0.135	0.221-1	0.450-2
	0.939-6	0.598-1	0.804	0.117	0.132-1	0.151-3
	0.285-4	0.906-1	0.725	0.158	0.263-1	0.525-2
3	0.630-6	0.164-3	0.115	0.790	0.115	0.170-1
	0.608-6	0.562-3	0.177	0.662	0.164	0.357-1
	0.137-5	0.417-6	0.831-1	0.717	0.141	0.203-1
	0.219-5	0.369-4	0.132	0.587	0.190	0.425-1
4	0.866-8	0.390-5	0.238-3	0.148	0.734	0.129
	0.675-7	0.225-6	0.107-2	0.248	0.535	0.185
	0.124-7	0.699-5	0.259-4	0.101	0.639	0.158
	0.726-7	0.568-6	0.205-4	0.175	0.444	0.209
5	0.129-8	0.230-7	0.136-4	0.247-3	0.178	0.660
	0.523-6	0.249-5	0.157-4	0.187-2	0.331	0.400
	0.114-7	0.662-8	0.201-4	0.150-3	0.114	0.567
	0.649-6	0.260-5	0.171-5	0.171-5	0.221	0.303

*Theoretical $q_{v'v''}/q_{00}$ ($q_{00} = 0.962$)

†RKR $q_{v'v''}/q_{00}$ ($q_{00} = 0.944$)

♦Theoretical $f_{v'v''}/f_{00}$ ($f_{00} = 0.192$)

#Semitheoretical $f_{v'v''}/f_{00}$ ($f_{00} = 0.188$)

TABLE VI. BeH ($A^2\Pi - X^2\Sigma^+$) Band Transition Probabilities and Wavelengths

v' \ v"	0	1	2	3	4	5
0	0.153+8* 4990‡	0.914+5 5538	0.115+4 6193	0.183+2 6985	0.482-1 7958	0.132+0 9174
1	0.358+4 4536	0.146+8 4985	0.171+6 5509	0.318+4 6127	0.835+2 6863	0.202+0 7748
2	0.113+2 4172	0.801+2 4549	0.139+8 4982	0.242+6 5482	0.569+4 6063	0.231+3 6744
3	0.150+1 3876	0.394+2 4199	0.161+3 4565	0.131+8 4981	0.305+6 5457	0.825+4 6002
4	0.348+1 3630	0.782+0 3912	0.938+3 4228	0.138+5 4583	0.122+8 4982	0.365+6 5433
5	0.674+0 3425	0.139+2 3675	0.216+2 3952	0.150+5 4260	0.579+5 4603	0.111+8 4986

* $A_{v'v''}$ (sec^{-1})

‡ $\lambda_{v'v''}$ (Å)

300

TABLE VII. MgH $(A^2\Pi - X^2\Sigma^+)$ Band Transition Probabilities and Wavelengths

v' \ v"	0	1	2	3	4	5
0	0.233+8* 5187‡	0.129+7 5604	0.822+5 6071	0.671+4 6595	0.739+3 7186	0.127+2 7855
1	0.131+7 4805	0.202+8 5160	0.236+7 5553	0.239+6 5989	0.295+5 6473	0.493+4 7014
2	0.888+3 4488	0.247+7 4796	0.172+8 5134	0.327+7 5504	0.472+6 5910	0.815+5 6355
3	0.770+2 4221	0.115+4 4493	0.360+7 4788	0.141+8 5108	0.400+7 5456	0.783+6 5833
4	0.285+1 3994	0.198+2 4237	0.634+3 4499	0.479+7 4780	0.108+8 5083	0.446+7 5409
5	0.281+2 3800	0.101+3 4019	0.592+2 4254	0.528+2 4505	0.607+7 4773	0.740+7 5059

*$A_{v'v"}$ (sec^{-1})

‡$\lambda_{v'v"}$ (A)
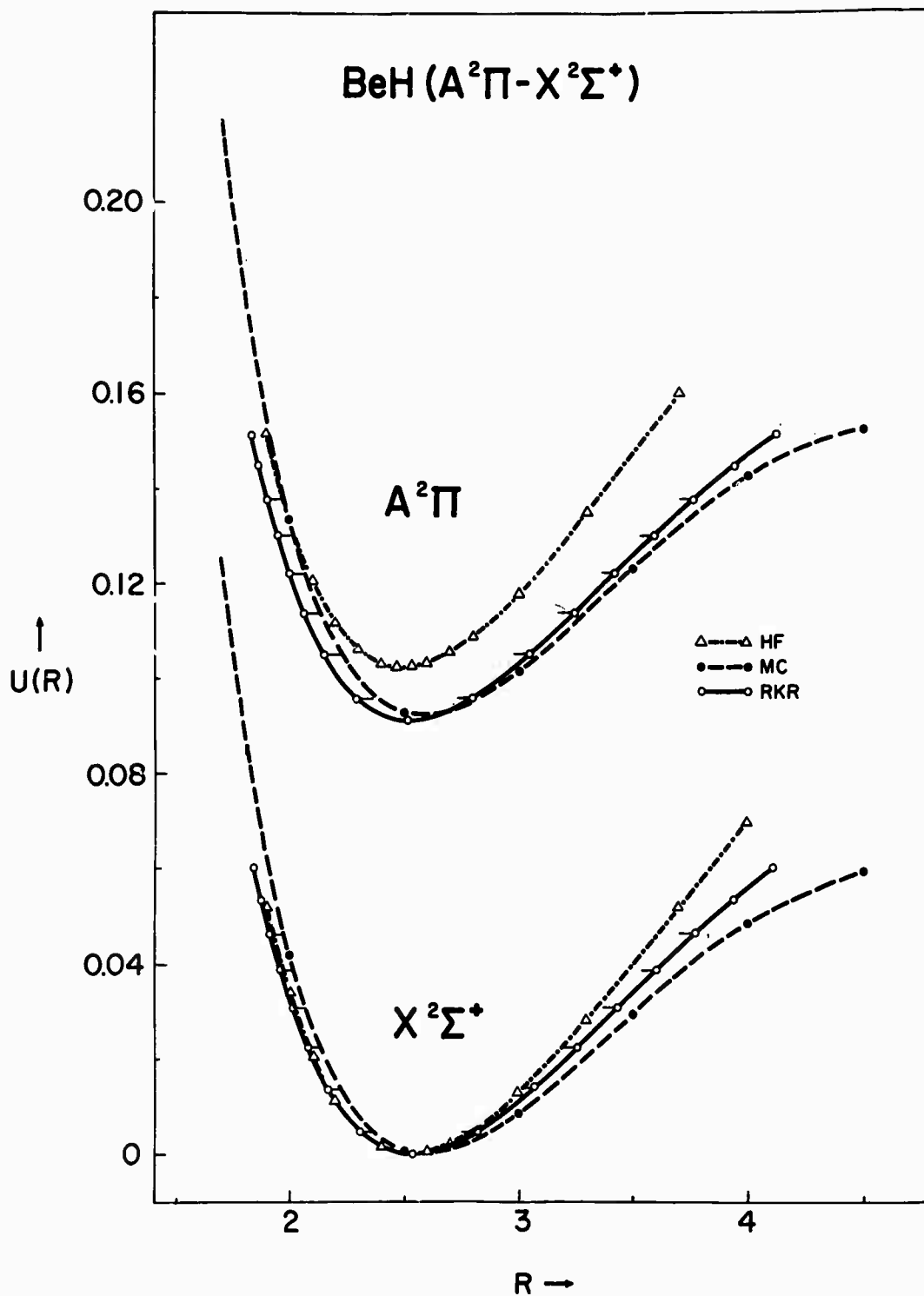
FIGURE 1. BeH ($A^2\Pi$—$X^2\Sigma^+$) potential energy curves. The excited state curves are measured relative to the minimum in the ground state curves. For the RKR curves the lower vibrational levels are indicated.

302
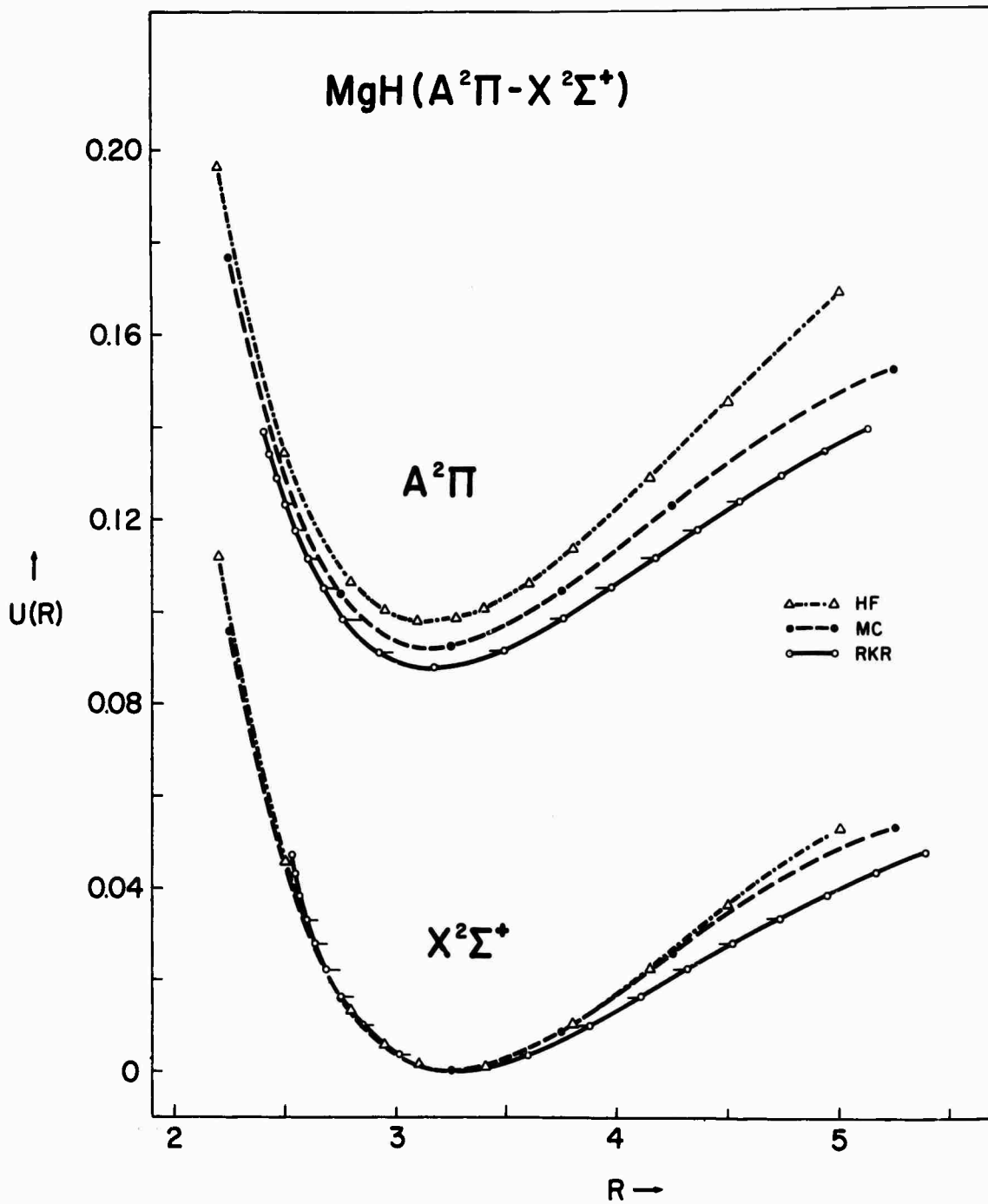
FIGURE 2. MgH ($A^2\Pi$—$X^2\Sigma^+$) potential energy curves. The excited
state curves are measured relative to the minimum in
the ground state curves. For the RKR curves the lower
vibrational levels are indicated.

303
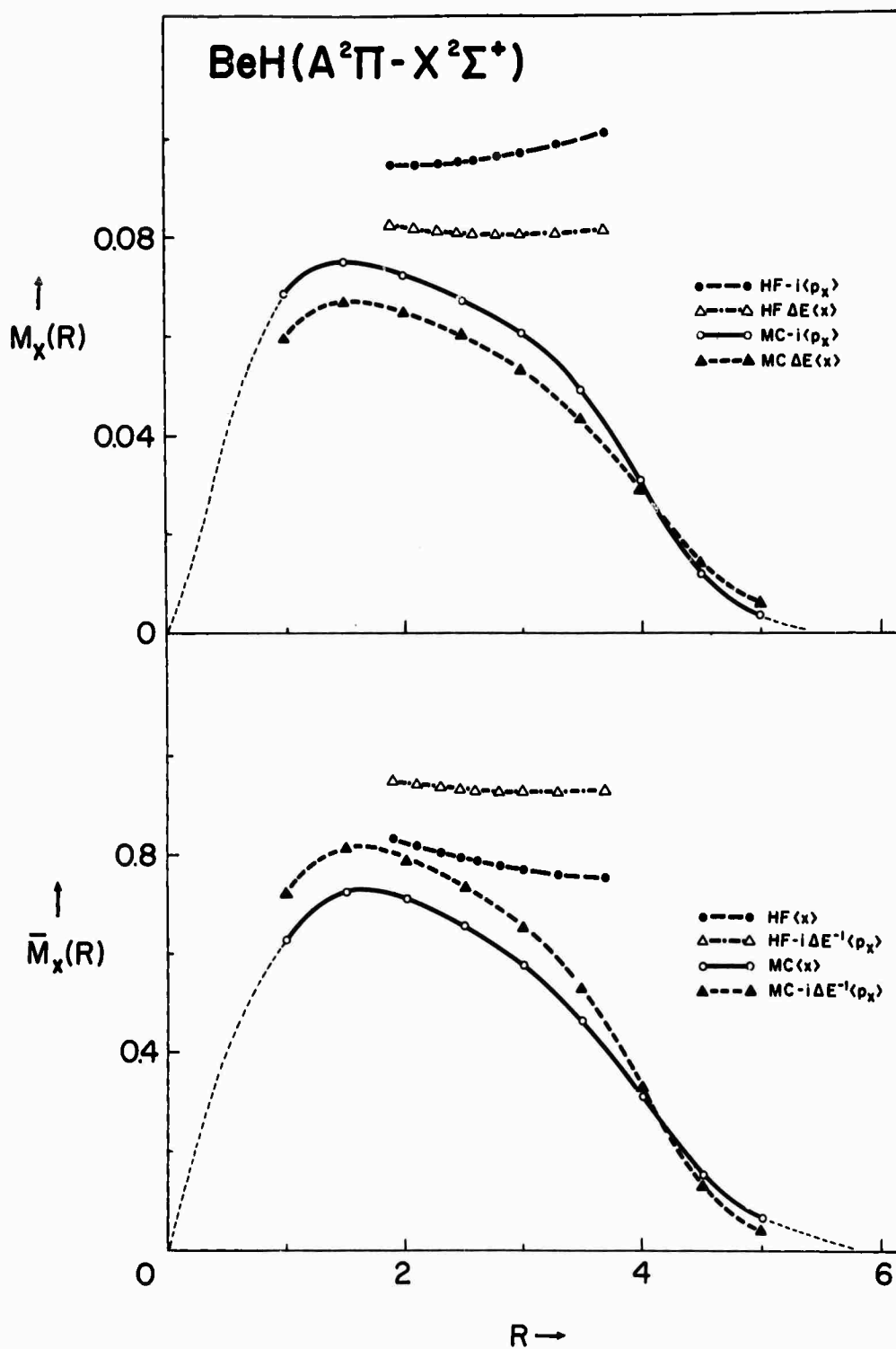
FIGURE 3. BeH ($A^2\Pi$—$X^2\Sigma^+$) dipole-momentum and dipole-length transition moment curves.
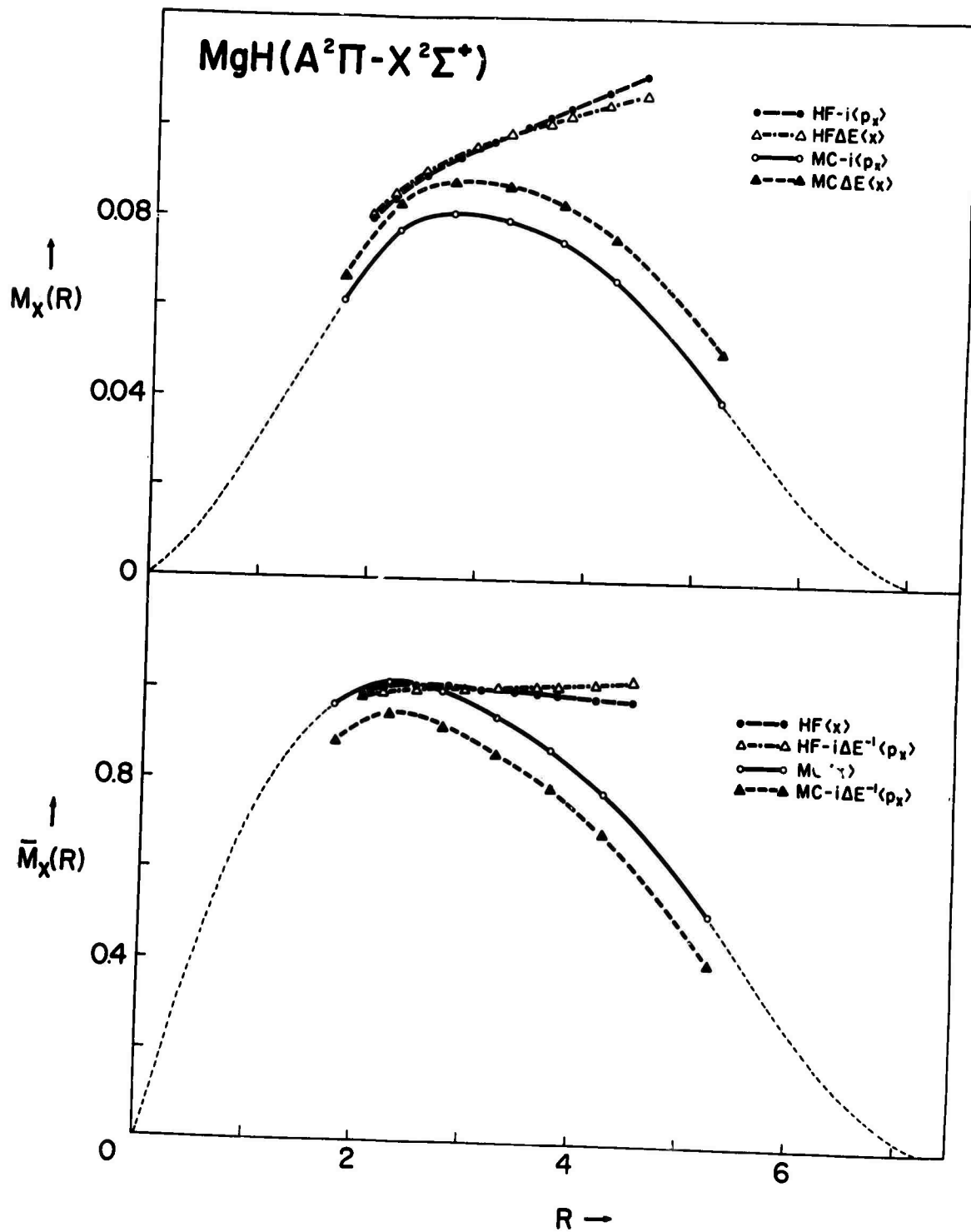
FIGURE 4. MgH $(A^2\Pi - X^2\Sigma^+)$ dipole-momentum and dipole-length transition moment curves.

305

THE ROLE OF KINETIC ENERGY IN THE FRANCK-CONDON PRINCIPLE; WITH APPLICATIONS TO THE IODINE MOLECULE EMISSION SPECTRUM

R. S. MULLIKEN

Laboratory of Molecular Structure and Spectra, Department of Physics,
University of Chicago, Chicago, Illinois 60637, USA

It is shown that for electronic states with high vibrational energy the Franck–Condon principle can predict high intensity for spectral emission to continuum states of high kinetic energy. A series of diffuse bands in the I_2 spectrum is explained.

According to the Franck principle, the nuclear positions and momenta (hence kinetic energies) tend to remain fixed during an electronic transition in a molecule [1]‡. According to the quantummechanical Franck-Condon principle [1] the *most probable* changes in vibrational quantum numbers or nuclear energy should conform to the Franck principle. Using the Born-Oppenheimer approximation, the probability per unit time dp/dt of a transition between an upper electronic-state nuclear wave function χ' and a lower state function χ'' is then given for a diatomic molecule by:

$$\frac{dp}{dt} = C\nu^n [\int Q_{,1}(R) \, \chi'(R) \, \chi''(R) dR]^2 , \quad (1)$$

where $n = 0$ or 3 according as the transition is in absorption or in emission. Although in general the variation of the electronic transition moment Q_{el} with R is important, for the moment let us assume it constant. Then dp/dt is proportional to the square of the FC overlap integral $\int \chi'(R)\chi''(R)dR$.

In the usual implementation of the FC principle, it is noted that $\chi'(R)$ and $\chi''(R)$ are especially large for R values near the classical turning point (for unbound states) or turning points (for bound states), so that the FC overlap integral is especially large if $\chi'(R)$ and $\chi''(R)$ overlap strongly near such R values. Also, in absorption, transition from the state with $v'' = 0$ (v = vibrational quantum number) are especially strong to

‡ For a review of the Franck-Condon principle, see ref. [2].

an upper state function having a classical turning point near the equilibrium R, R_e, of the lower electronic state.

Attention will be concentrated here on the emission spectrum of a diatomic molecule in a particular discrete vibrational state χ' of total energy E'. (Generalization to other cases can be made readily.) A particular initial rotational state may also be assumed, but this feature will not be further considered since the results are not seriously dependent on it. The energy levels of the final nuclear state χ'' may be discrete vibrational levels and/or continuum levels. The *total* transition probability per unit time summed over all the final nuclear levels is given by

$$dP/dt = CQ_{el}^2 \, \bar{\nu}^3 . \quad (2)$$

To apply the Franck principle, we first contemplate the classical vibrations of the molecule in its initial state on a potential curve $U'(x)$, where $x = R - R_e$. For the moment disregarding a factor ν^3 and assuming Q_{el}^2 independent of x, the Franck principle says (i) the probability that the electronic transition will take place has a constant value in time, proportional to Q_{el}^2, the same at all phases of the classical vibration; (ii) when the electron does jump, the positions and momenta (hence the kinetic energy) of the nuclei are momentarily unchanged. In quantum mechanics, of course, item (ii) becomes a statement of maximum probability and not of certainty.

If the electron jump occurs when the nuclei are at position x, their kinetic energy is

$K(x) = E' - U'(x)$. According to the Franck principle, K is the same after the electron jump, while the total energy becomes $E''(x) = U''(x) + K(x)$. Quantum-mechanically, $h\nu = E' - E''$, so that if the jump occurs at x, the semi-classical frequency is

$$\nu(x) = [E' - E''(x)]/h = [E' - U''(x) - K(x)]/h . \qquad (3)$$

What we are interested in is the spectral density $dP/d\nu$ - the probability per unit frequency interval. If we accept the Franck principle and its probabilistic carry-over to quantum mechanics,

$$\frac{dP}{d\nu} = \frac{dP}{dt}\frac{dt}{dx}\frac{dx}{d\nu} = \frac{CQ_{el}^2 \nu^3}{(dx/dt)(d\nu/dx)} , \qquad (4)$$

where dx/dt can be obtained from the classical equation for vibration on $U'(x)$, and $d\nu/dx$ can be obtained using eq. (3) with $K(x)$ obtained classically and $U''(x)$ specified or known experimentally.

Let us consider three model cases, all with $U'(x) = \frac{1}{2}kx^2$, and with $U''(x)$ respectively (a) zero, (b) repulsive, and (c), attractive. In case (a), shown in fig. 1 (where $W = h\nu$), ν varies between a maximum value $\nu_{max} = E'/h$ corresponding to the classical turning points $x = \pm A$, at which $K = 0$, and a minimum value $\nu_{min} = E' - \frac{1}{2}kA^2$ corresponding to $x = 0$. Here, with $x = A \sin 2\pi ft$, $f = (1/2\pi)(k/\mu)^{1/2}$, μ being the reduced mass of the molecule, dx/dt and $d\nu/dx$ are readily obtained. Eq. (4) then leads to $dP/d\nu = \infty$ at ν_{max} and at ν_{min}; integration over equal finite intervals of 0.1 $(\nu_{max} - \nu_{min})$ near these two points gives probabilities which are equal and maximal in these two regions, and smaller for intervals of equal size in intermediate regions (see fig. 2). Similar results are obtained
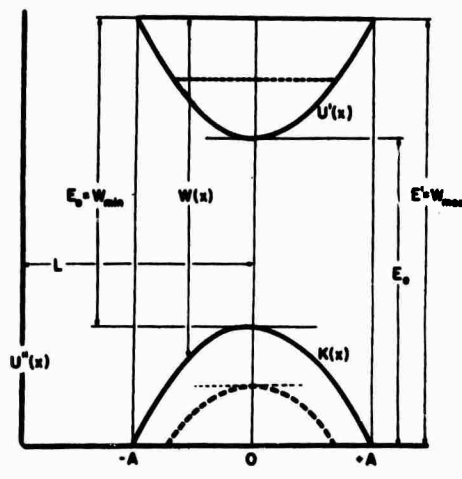
Fig. 1.
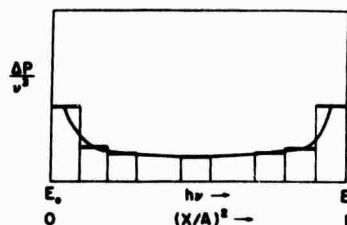
Fig. 2.

in cases (b) and (c), except that now there may be three regions of maximum intensity, one around ν_{min}, the other around two larger frequencies which correspond to $x = \pm A$ [‡]. If $U'(x)$ is replaced by a more realistic function than $\frac{1}{2}kx^2$, all the results are qualitatively similar, in particular the occurrence of a maximum of intensity around $\nu = \nu_{min}$.

A result which can be seen from fig. 1, and which often remains true in cases (b) and (c), and in realistic cases, is that ν_{min} is independent of E' [see the dashed line in fig. 1 for an alternative E', and the dashed curve for the corresponding $K(x)$]. In realistic cases, ν_{min} may correspond to a transition either to a discrete vibrational level or to a continuum energy, depending on the form of $U''(R)$. Further details will be given in another paper [3].

The present work grew out of an effort to explain the "diffuse bands" in the emission spectrum of the iodine molecule. These are structureless symmetrical regions mostly of about 100 cm^{-1} width. They can be excited either electrically or as part of a fluorescence spectrum resulting from absorption of an atomic line or lines [4]. Even when excited electrically, the spectrum is apparently due mainly to absorption of an iodine atomic line or lines [5]. There is evidence [6] that the fluorescence spectrum consists of a *primary spectrum* which results at low pressures from absorption to a highly excited vibrational level of the D state of I_2, plus a secondary spectrum of diffuse bands due to emission from other electronic states than the D state, reached by collisions. The primary fluorescence spectrum consists in a series of resonance doublets extending from the exciting

[‡] However, if $U''(R)$ is sufficiently steep at $x = -A$, $E''(R)$ ceases to have a maximum, and there are now only two ν regions of maximum intensity. The analogue of ν_{min} of fig. 1 now no longer exists.

line towards longer wavelengths, followed by a somewhat irregular series of diffuse bands which end in a relatively intense set of several regularly spaced diffuse bands near $\lambda 3250$. This spectrum can be explained by an application of the considerations given above, as follows.

The D state is one of ion-pair type with large R_e, perhaps 4.1 Å, while the ground state (X) has $R_e = 2.67$ Å. At R equal to R_e of state D, $U''(R)$ for state X is close to dissociation, and ν_{min} corresponds to an energy E'' in the continuum of state X some distance above dissociation, while ν_{max} corresponds to $v = 0$ of state X. The complete spectrum then consists in the observed resonance series (from ν_{max} to ν_{med}) and a continuum consisting of the observed diffuse bands (from ν_{med} to ν_{min}) culminating in the relatively intense group at $\lambda 3250$, which represents ν_{min}; ν_{med} corresponds to dissociation of state X. The banded structure of the continuum is a quantum-mechanical diffraction effect (see below). It can be show [6] that the position of ν_{min} is in good agreement with other evidence on the energy E_0 of the minimum of the $U(R)$ curve of state D, to which it is related.

The striated group near $\lambda 3250$ consists of some half dozen peaks and valleys with sinusoidal intensity variation and a peak spacing or "fluctuation interval" of about 224 cm^{-1} under conditions which are believed to correspond to excitation by the iodine atom line $\lambda 1830.4$ ($E' = 54\,600$ cm^{-1}). Excitation by longer wavelength atomic lines gives patterns of smaller spacing (165 cm^{-1} for Hg $\lambda 2537$ excitation) [7], but with only a very slight shift in average position. This invariance of ν_{min} is exactly what is predicted (see third preceding paragraph). Further, as will now be shown, the magnitude of the fluctuation interval and its variation with exciting wavelength are in excellent agreement with theoretical predictions.

To deal with the striated structure of the continuum we must go over to quantum mechanics. For simplicity, consider case (a). Quantum-mechanically, the intensity at any frequency is proportional to the square of $\int \chi'(x)\chi''(x)dx$. It is clear that major contributions to this integral occur in regions of x where the de Broglie wavelengths $\lambda = h/\mu\dot{x}$ of χ' and χ'' are, (i) equal or nearly so, (ii) in phase or nearly so (constructive overlap of χ' and χ''). Regions where these two conditions are not fulfilled make only minor or negligible contributions (destructive overlap). Condition (i) is fulfilled when the Franck principle of equal kinetic energy K for χ' and χ'' is satisfied, since $\lambda = h/(2\mu K)^{1/2}$. This matching of λ's between

χ' and χ'' can occur at any value of x between $+A$ and $-A$ in fig. 1, for frequencies corresponding to transitions from E' to points lying on the curve $E''(x) = K(x)$ in fig. 1, but it is especially good near $x = 0$.

Now consider condition (ii). The phase of the χ'' waves depends on the distance $L + x$ from x to the vertical part of $U''(x)$ shown at the left in fig. 1. Now the Franck principle is not exact; quantum-mechanically the energy E'' can deviate somewhat from the locus given by $K(x)$ in fig. 1; this locus corresponds only to maximum probability. Small variations of E'', hence of ν, permit shifting the phase of the χ'' waves. Starting from a ν value which gives best matching of phases of the χ' and χ'' waves, hence a maximum intensity, one can compute how much shift of ν is needed to produce a phase shift of $\pi/4$ (zero intensity) or of $\pi/2$ (a new peak). Let us call the latter shift $\delta\nu$. This $\delta\nu$ is the predicted fluctuation interval. It is easily shown that

$$\delta\nu = \frac{h}{2\mu\lambda(L+x)} = \frac{(2K/\mu)^{1/2}}{2(L+x)}. \qquad (5)$$

In general (case b or c), L is replaced by an effective length L^*. Note also that in general, $+|x|$ and $-|x|$ yield two different values of $\delta\nu$. However, we are especially interested in $\delta\nu$ at ν_{min}, which in case (a) occurs at $x = 0$. Given $K = E_0 + D$ approximately (D is the dissociation energy of state X), L^* can be calculated from eq. (5) with L^* instead of $L+x$. If R_e of state D is 4.1 Å, E_0 is 42 400 cm^{-1}, and K is $E' - E_0$ = 12 200 cm^{-1} assuming $E' = 54\,600$ cm^{-1}. Then $L^* = 1.79$ Å, which is very reasonable. [L^* should be somewhat less than the distance from the R value (about 2.2 Å) at the left hand limb of $U''(R)$ at an energy corresponding to $U'' + K$ to an R value slightly greater than R_e of state D.] Thus the major aspects of the primary fluorescence spectrum are in excellent agreement with the theoretical predictions. The diffuse bands of the secondary fluorescence spectrum can be attributed to transitions from various secondary excited states of ion-pair type to some of the very numerous predicted repulsion curves of iodine. Details will be given in another paper [6].

REFERENCES

[1] J. Franck, Trans. Faraday Soc. 21 (1925) 536.
[2] G. Herzberg, Spectra of diatomic molecules, 2nd Ed. (Van Nostrand, Princeton. 1950).
[3] R. S. Mulliken, to be published.
[4] O. Oldenberg. Z. Physik 18 (1923) 1.

[5] K. Asagoe. Sci. Repts. Tokyo Burnika Daigaku 2 (1935) 9;
M. Kimura and K. Tonomura, Pieter Zeeman volume (Nijhoff, The Hague, 1935) p. 241.

[6] R. S. Mulliken, Iodine revisited, to be published.
[7] F. Duschinsky and P. Pringsheim, Physica 2 (1935) 633.

Molecular Charge Distributions and Chemical Binding. IV.
The Second-Row Diatomic Hydrides AH

Paul E. Cade

Laboratory of Molecular Structure and Spectra, Department of Physics, University of Chicago, Chicago, Illinois 60637

AND

R. F. W. Bader, W. H. Henneker,* and I. Keaveny†

Department of Chemistry, McMaster University, Hamilton, Ontario, Canada

(Received 1 August 1968)

An interpretation of the binding in the second-row diatomic hydrides NaH, MgH, AlH, SiH, PH, SH, and HCl is presented based on the molecular charge distributions and the forces exerted on the nuclei. The total density distributions are discussed in relation to "molecular" size and the arbitrary partitioning of the total charge between different spatial regions. Density difference maps are employed to compare the Hartree–Fock *molecular* charge distribution with the appropriate Hartree–Fock *separated-atom* charge densities and also the corresponding Hartree–Fock united-atom charge density. In addition, for SiH, PH, SH, and HCl, *two-center* Hartree–Fock molecular charge distributions are compared with extensive *one-center* charge distributions. The molecular orbital charge densities are classified as binding, nonbinding, or antibinding on the basis of their partial contributions to the force acting on each nucleus. The orbital forces provide a quantitative assessment of the relative binding abilities of the orbital charge densities for a given molecule, through a complete series of molecules, or between homologous series of molecules. In terms of the total charge distributions, the various density difference maps, and the partial forces exerted on the nuclei, a qualitative and quantitative comparison is made between the bonding in the first- and second-row hydrides. The bonding in NaH is classified as ionic, that in SiH, PH, SH, and HCl as covalent, and for the second row both MgH and AlH appear transitional between the limiting classifications of ionic or covalent. Particular attention is paid to the role of the large and diffuse KL-shell core on A and the *increased* role of the proton in determining the details of the molecular charge distribution in the second-row hydrides. The latter two features account for the major differences in AH bonds between the first- and second-row hydride congeners.

I. INTRODUCTION

The previous members of this series have dealt with the first-row homonuclear diatomic molecules,[1] the first-row diatomic hydrides,[2] and several members of the 12- and 14-electron isoelectronic series.[3] These studies employed the detailed molecular charge distributions and forces acting on the nuclei to interpret and discuss chemical bonding. In the present investigation, this study is extended to include the hydrides, NaH, MgH, AlH, SiH, PH, SH, and HCl. This interpretive study is complimentary to the energetic considerations and the treatment of certain molecular properties presented elsewhere for the second-row hydrides.[4,5]

The *additional* perspectives the present paper attempts to explore are: (a) the relationship between two entire rows of homologous molecules, and (b) the role of an atomiclike "core" in chemical bonding. Thus, a critical study of the second-row hydrides in parallel with the preceding study of the first-row hydrides provides an excellent opportunity to examine in some detail the changes in the nature of the chemical bonding across the row between the two sequences LiH to HF versus NaH to HCl. Aspects of the relative internal trends between these two homologous series have already been discussed in relation to energy considerations and certain molecular properties, but the comparison can be more fully appreciated in terms of the relevant charge distributions themselves instead of a single sequence of relative numbers, e.g., the dipole moments, which are averages over the complete charge distributions. The second additional aspect involving the atomiclike "core" centered about the heavy nucleus in AH seems to offer an attractive and promising approach to relative bonding situations. The atomiclike (K- or KL-shell) "core" has until recently been relatively neglected as an *important* agent to probe or gauge the details of the electronic charge distribution and chemical bonding. But stimulating new experimental results of Siegbahn *et al.*[6] using the ESCA method (which essentially is an x-ray photoelectron technique) reveal an important new role for the atomiclike "core" as "our man in the molecule." The authors

* Present address: Laboratory of Molecular Structure and Spectra, Department of Physics, University of Chicago, Chicago, Ill. 60637.

† Present address: Department of Chemistry, University of California, San Diego Campus, La Jolla, Calif. 92037.

[1] R. F. W. Bader, W. H. Henneker, and P. E. Cade, J. Chem. Phys. 46, 3341 (1967).

[2] R. F. W. Bader, I. Keaveny, and P. E. Cade, J. Chem. Phys. 47, 3381 (1967).

[3] R. F. W. Bader and A. D. Bandrauk, J. Chem. Phys. 49, 1653 (1968), Paper III in this series.

[4] P. E. Cade and W. M. Huo, J. Chem. Phys. 47, 634 (1967).

[5] P. E. Cade and W. M. Huo, "Electronic Structure of Diatomic Molecules. VII.B. Certain Expectation Values and Molecular Properties for the Ground States of the Second-Row Hydrides AH" (unpublished).

[6] K. Siegbahn *et al.*, Nova Acta Regiae Soc. Sci. Upsaliensis 20, 275 (1967), (contains many related references).

believe the "core" will provide a relatively nonparticipating gauge of the details of the noncore or "valence-shell" electronic charge distribution as valuable as, and potentially more informative than, for example, the quadrupole coupling constants. Except for hydrogen, *all* atoms bring an atomiclike "core" into the molecule, but not all have nuclei with quadrupole moments which are either known or nonzero.

The difference between the total molecular density distribution and the total density distribution of the separated atoms at the same internuclear distance can play a central role in the comparative study of molecules. This difference density, which would in principle be observable if the atoms could be held at the correct internuclear· separation without mutual electrostatic disturbance, reflects the rearrangement of the electronic charge which accompanies molecular formation. Two extreme limiting topological forms can be recognized for such difference densities and the words "ionic" and "covalent" can be retained to identify these two taxonomic categories. The numerous results accumulating strongly indicate that many systems and/or states fall in between these two guide posts. Thus, while the explicit form of the difference density map is an interesting basic piece of information, alone it provides only *part* of a basic background which the authors feel must undergird the understanding of chemical bonding. The single most important concept about understanding the nature(s) of chemical bonds is that *relative* quantities or gauges, *relative* behavior, and *relative* changes are the fundamental data. In this regard we have tried to concentrate on approximation-independent, flexible, and versatile basic quantities to examine these comparative properties of molecules, i.e., charge densities and electrostatic forces.

In the first-row hydrides, LiH to HF, there is a steady change in the total density, the various orbital densities and in particular in the difference density maps. The latter change from LiH, which is a prototype of the "ionic" form, to BeH, which is a "covalent" or transitional type, and then to BH through HF where a form polarized in the direction opposite to LiH gradually intensifies. The characteristics of the 2σ, 3σ, and 1π molecular orbitals as "binding," "antibinding," and "nonbinding" have also been followed across the sequence revealing a progressive change of behavior or intensity of behavior. In the present paper the parallel internal changes in the sequence NaH, MgH, AlH, SiH, PH, SH, and HCl are followed and the binding characteristics of the 4σ, 5σ, and 2π molecular orbitals are compared to their first-row hydride congeners. There is no abundance of experimental data concerning the physical properties of the second-row hydrides, e.g., only the dipole moments of SH and HCl are known,[7] and no major interpretive effort addressed to this group of molecules is known to the authors.

The molecular charge distributions involved here are based on calculations which are alleged to be close approximations to the true Hartree–Fock wave-functions.[4] These results are for the NaH ($X\ ^1\Sigma^+$), MgH ($X\ ^2\Sigma^+$), AlH ($X\ ^1\Sigma^+$), SiH ($X\ ^2\Pi_r$), PH ($X\ ^3\Sigma^-$), SH ($X\ ^2\Pi_i$), and HCl ($X\ ^1\Sigma^+$) states at R_e(exptl). For this sequence, R_e(calc) is only slightly different from R_e(exptl), so that no significant misrepresentation is likely to result from using R_e(exptl) and vertical improvements can thus be compared more easily in future studies. The second-row hydride wavefunctions were obtained using expansion basis sets for the various molecular orbitals which, relatively speaking, were not quite as extensive as in the case of the first-row hydride results. Thus, Cade and Huo[4,6] have more carefully qualified the second row results; e.g., as shown below, the total force on each nucleus is somewhat larger than for the first row hydride results, although still small and the vector sum of forces departs more from zero. A subsequent more exhaustive calculation for HCl by McLean and Yoshimine[8] has shown that except for obtaining a smaller value for the forces and different results for certain higher polarizabilities, the representation of HCl by Cade and Huo is satisfactory (to Hartree–Fock approximation). The results presented below show no evidence of any deterioration of the quality of the wavefunctions for the second-row hydrides.

II. THE MOLECULAR CHARGE DENSITY: TOTAL, PARTIAL, AND CERTAIN DIFFERENCE DENSITIES

A. The Total and Orbital Molecular Charge Density

The total molecular charge density distributions for NaH→HCl are shown in Fig. 1 and they display the expected one-to-one close correspondence with the first-row hydrides. If the atomiclike "cores" are neglected, the second-row hydrides appear as straightforward enlargements of their first-row counterparts.[9] In Table I certain useful properties of the total density distribution are given and a comparison between first- and second-row quantities is pictured in Fig. 2.

The first member of the sequence (NaH) once again looks atypical compared to the rest of the sequence, but a glance at Fig. 3 where the atomiclike KL core and the 4σ and 5σ molecular orbitals appear, suggests the explanation. Thus the LK core in NaH can be superimposed on the *total* density distribution to show that the relatively steep rise of $\rho(x, y)$ is principally that of the core. The 4σ molecular orbital (which is occupied) has little probability density on the nonbonded side of

---

[7] A. Carrington, D. H. Levy, and T. A. Miller, J. Chem. Phys. 47, 3801 (1967).

[8] A. D. McLean and M. Yoshimine, J. Chem. Phys. 47, 3256 (1967).

[9] In comparing Fig. 1 above and Fig. 1 of Ref. 2, it should be recognized that while each figure has all *internal* density contours to the same scale of length, the two figures are *not* to the same scale as published.
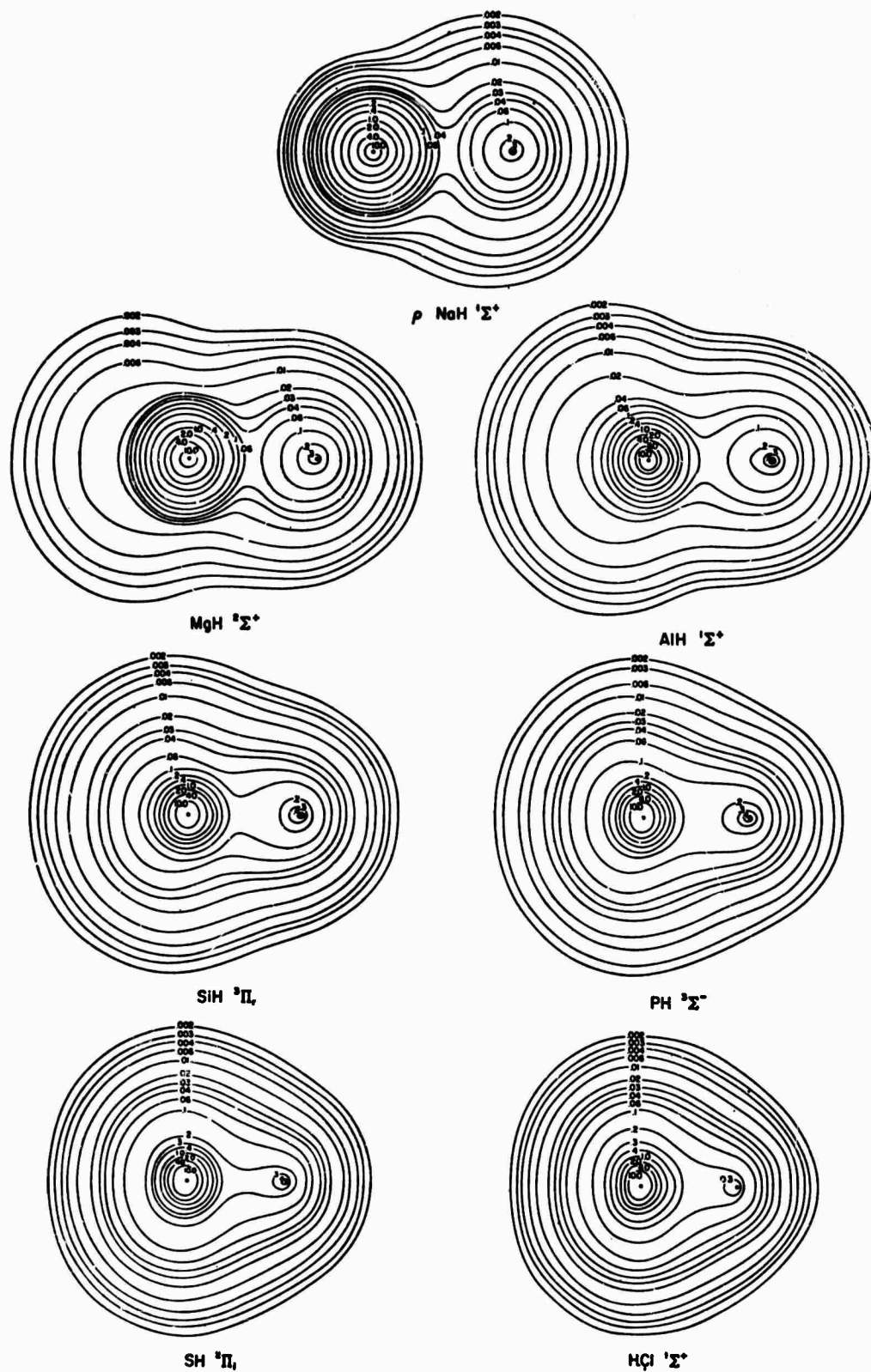
FIG. 1. Total molecular charge density contours for the second-row diatomic hydrides in atomic units (1 a.u. = 6.749 $e/Å^3$). All maps are drawn to the same scale of length (1 bohr = 0.529172 Å). The A nucleus is on the left in this and in all succeeding figures.
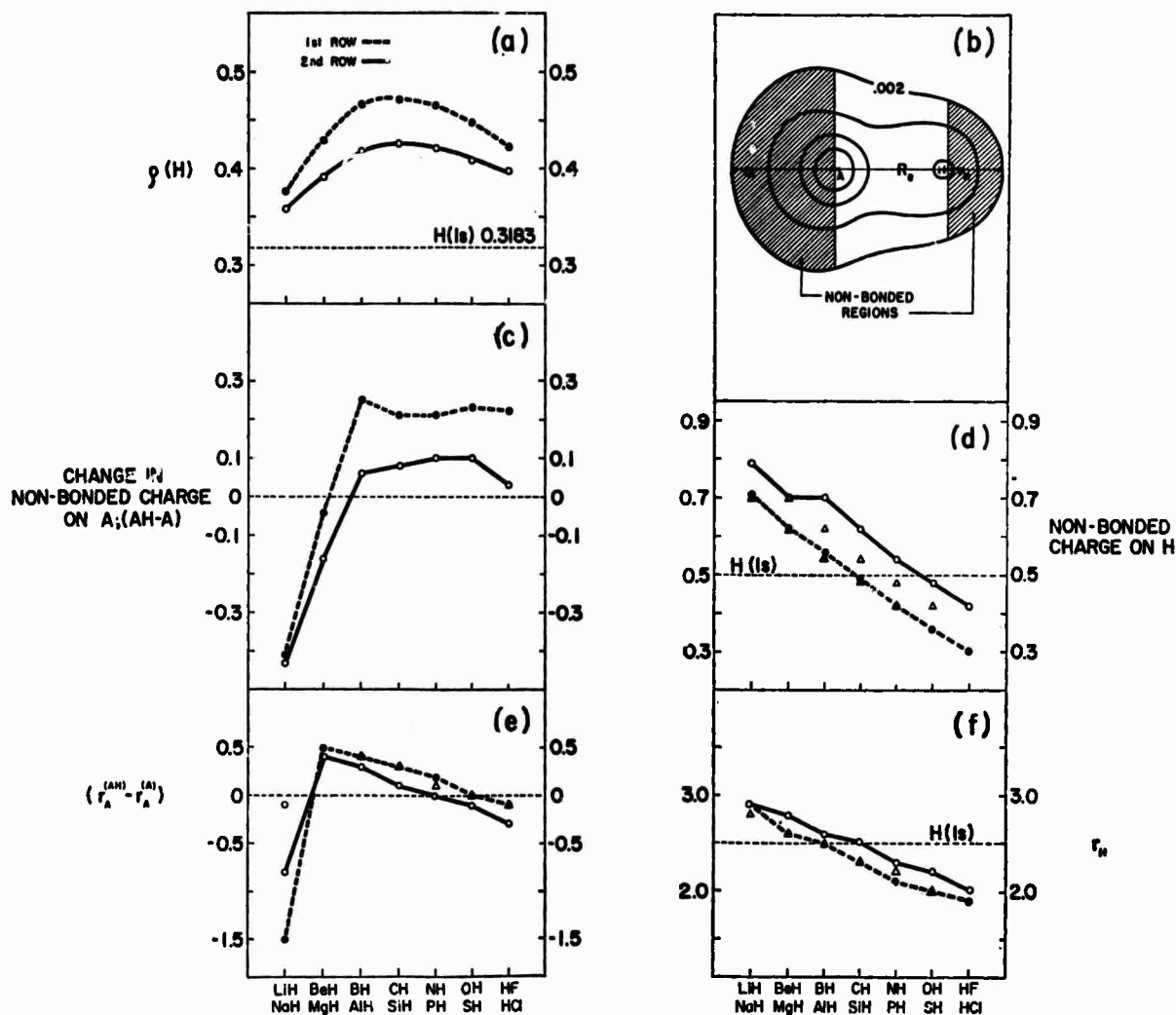
FIG. 2. Comparison of properties of the total charge densities of the second-row versus the first-row hydrides: (a) The total density at the proton; total density for H(1s) also shown. (b) Definition of the nonbonded regions around A and H; also r_A and r_H are here defined. (c) The total nonbonded charge around A in AH, minus the nonbonded charge around A for the free atom. (d) The total nonbonded charge around H; the corresponding quantity for H(1s) also shown. (e) The change in r_A in AH versus r_A for the atom (extraneous point o is using $Na^+ r_A$). (f) The nonbonded radius, r_H; the corresponding quantity for H(1s) also shown. In Figs. (d), (e), and (f) the triangles $\triangle$ or $\blacktriangle$ refer to shifting second-row quantity one or two places to the left.

Na and the 5σ molecular orbital which has a substantial, but diffuse probability density on the nonbonded side of Na is *unoccupied* in the ground state of NaH. Thus, NaH fits regularly into the sequence, as examination of $\rho(x, y)$ and the probability densities of the 4σ and 5σ molecular orbitals in MgH and AlH indicates.

The total electron density at the various nuclei, $\rho(H)$ and $\rho(A)$, is related to the hyperfine splitting structure in atoms and diatomic molecules. Thus, the absolute value and the trend *across* and *between* rows of $\rho(H)$ provide a relationship between hyperfine splitting (if relevant) and the chemical bonding, although the relationship is not straightforward. The *change* in $\rho(A)$ for the molecule compared to the free atom is very small (e.g., for SH about 1 part in 2500), and although $\rho_{AH}(A) < \rho_A(A)$ in almost all cases, the

actual numbers may have no significance. The density at the proton is much more sensitive to the bonding situation as Fig. 2(a) indicates. It is useful to note that $\rho(H)$ is always lower for the second-row hydride (the percent decrease ranges from $\sim 5\%$ for the LiH:NaH to about 10% for the BH:AlH, CH:SiH, and NH:PH pairs).

The nonbonded charge on A and H and the nonbonded radii, r_A and r_H, are defined in Fig. 2(b) and compared within the second-row sequence and between the two rows of hydrides in Figs. 2(c), 2(d), 2(e), and 2(f). The nonbonded charge is just the charge contained in the shaded regions near the A and H nuclei and the numerical integration over the pseudo-hemispheres is in practice carried out to the 0.002 or 0.001 contour, but no substantial fraction of an electron

313

TABLE I. Properties of the total density distribution.[a]

AH	μ (D)[b]	R_e (bohr)	L (bohr)[e]	Nonbonded radius[d]			Nonbonded charge[d]		Charge density at nucleus	
				r_A	r_A (atom)	r_H	On A	On H	$\rho(H)$	$\rho(A)$
NaH	−6.962	3.566	8.9	2.4	3.2	2.9	5.07	0.79	0.3579	833.399
MgH	−1.516	3.271	10.3	4.4	4.0	2.8	5.84	0.70	0.3905	1092.423
AlH	0.170	3.114	10.2	4.4	4.1	2.6	6.56	0.69	0.4183	1401.787
SiH	0.302	2.874	9.4	4.1	4.0	2.5	7.08	0.62	0.4259	1764.332
PH	0.538	2.708	8.8	3.8	3.8	2.3	7.60	0.54	0.4205	2184.889
SH	0.861	2.551	8.2	3.6	3.7	2.2	8.10	0.48	0.4077	2666.340
HCl	1.197	2.4087	7.7	3.3	3.6	2.0	8.53	0.42	0.3966	3214.481

[a] Atomic units are employed; 1 bohr $=0.52917$ Å $=a_0$, 1 unit of charge density $=e/a_0^3=6.749$ $e/$Å^3. Except for the dipole moment, μ, which is given in debyes.

[b] The sense of the sign of the dipole moment is $\mu<0\rightarrow$A$^+$H$^-$, $\mu>0\rightarrow$ A$^-$H$^+$, or the center of negative charge is right or left of the midpoint of R_e in A–H.

[e] The molecular lengths computed from Eq. (2.1), and R_e of the second-row hydrides are 10.6, 10.1, 9.6, 8.8, and 8.3 bohrs, for MgH, AlH, SiH, PH, and SH, respectively.

[d] The nonbonded regions on A and H are as defined on Fig. 2(b) (the shaded regions bounded partly by the 0.002 contour).

charge is neglected. (The explicit values are given in Table I.) In Fig. 2(c) the *change* in the amount of nonbonded charge in the molecule versus the atom A is given for internal comparison and the result is strikingly similar to the figure given by Cade and Huo[10] for the electric dipole moments. That is, for LiH and NaH almost 0.5e^- exactly (which would correspond to loss of one electron, e.g., convential ideal "ionic" case) has been removed from around A relative to the free atom. The BeH and MgH systems are also deficient in nonbonded charge on A compared to their separated atoms. The remainder of the two series both evidence a net *gain* which is $\sim$0.22e^- for the first row and $\sim$0.1e^- for the second row.

The absolute values of the nonbonded charge associated with the proton in Fig. 2(d) can be compared with the free-hydrogen-atom value of 0.5e^-. In both rows some hydrides show an increase of the nonbonded charge on H, and some show a decrease. Relatively large amounts of charge (0.41e^- for LiH, 0.43e^- for NaH, and 0.16e^- for MgH) have been removed from near A, and relatively large amounts of charge 0.21e^- for LiH, 0.29e^- for NaH, and 0.20e^- for MgH) have appeared as nonbonded charge on H. From Fig. 2(c) one sees a more or less constant *increase* in the non-bonded charge on A for BH→HF or AlH→HCl with about twice as much increase in the first-row hydrides as for second row hydrides. The nonbonded charge on H in AH does not keep pace, however, and for several systems (BH for the first row and AlH, SiH, and PH from the second row) nonbonded charge is increased on *both* A and H in the hydride as if the bond formation spills charge over to both ends of the molecule with an acutal decrease in the total *bonded* charge between the two nuclei. This paradox, contrary to canons of bonding theory, results from the oversimplified picture

[10] P. E. Cade and W. M. Huo, J. Chem. Phys. **45**, 1063 (1966).

and requires a more detailed assessment of the rearrangement of charge upon molecule formation.

The distance from the A or H nucleus, in a direction away from the other nucleus, to the 0.002 charge density contour is the definition of r_A and r_H, respectively. The total molecular length, $L=r_A+r_H+R_e$, also makes use of the arbitrary 0.002 contour in defining the molecular "size." While such a choice is completely arbitrary, such a contour contains $\sim$95% of the total molecular charge, and in several cases where van der Waals' radii can be compared, the results are quite reasonable.[1] This definition is less useful if the charge density falls off very slowly with distance or a smaller "size" is effective by virtue of violent collisions or strong interactions, but the r_H and r_A quantities are convenient numbers to compare various molecules or sequences of molecules. The pronounced contraction in r_A for LiH and NaH [Fig. 2(e)] results because the valence-shell electron is stripped away leaving an r_A more characteristic of the "core." Neglecting the LiH and NaH members, both sequences show a gradual decrease in Δr_A and Δr_H. If in Fig. 2(f) the *second*-row abscissa scale, designating the molecule, is shifted one place to the *left* (as the triangles show), the first- and second-row sequences of points are near coincidence. Therefore, to good approximation, Δr_H for the second-row hydride is equivalent to Δr_H for the regular first-row congener hydride, *minus* one. A similar striking association holds for Δr_A as the triangles of Fig. 2(e) illustrate. Thus, if the points for Δr_A for the second-row hydrides are shifted one place to the *right* (e.g. MgH→BH, AlH→CH, $\cdots$ SH→HF), the two sequences of points are again nearly coincident; thus Δr_A for the second-row hydride is approximately given by Δr_A for the regular first-row congener, *plus* one. These gross morphological features suggest that to gauge the changes in certain aspects of the total molecular charge distribution for a *second*-row hydride (e.g., SiH) the hydrogen end from
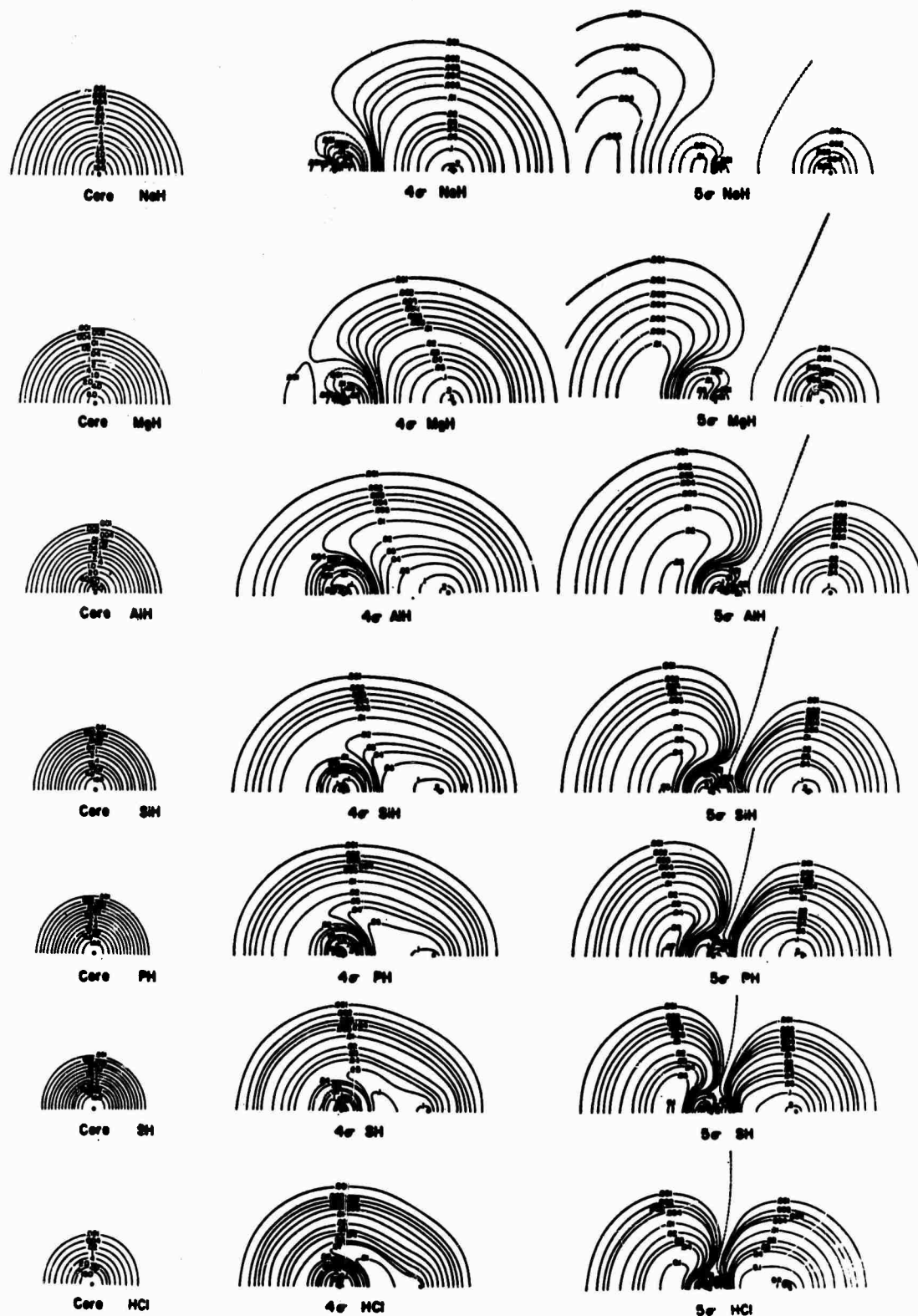
FIG. 3. Contour maps of the $(1\sigma^2 2\sigma^2 3\sigma^2 1\pi^4)$ "core" densities, the 4σ, and 5σ molecular orbital densities for the second-row hydrides. (N.B. The 5σ molecular orbital is unoccupied in NaH and is included for reference only.)
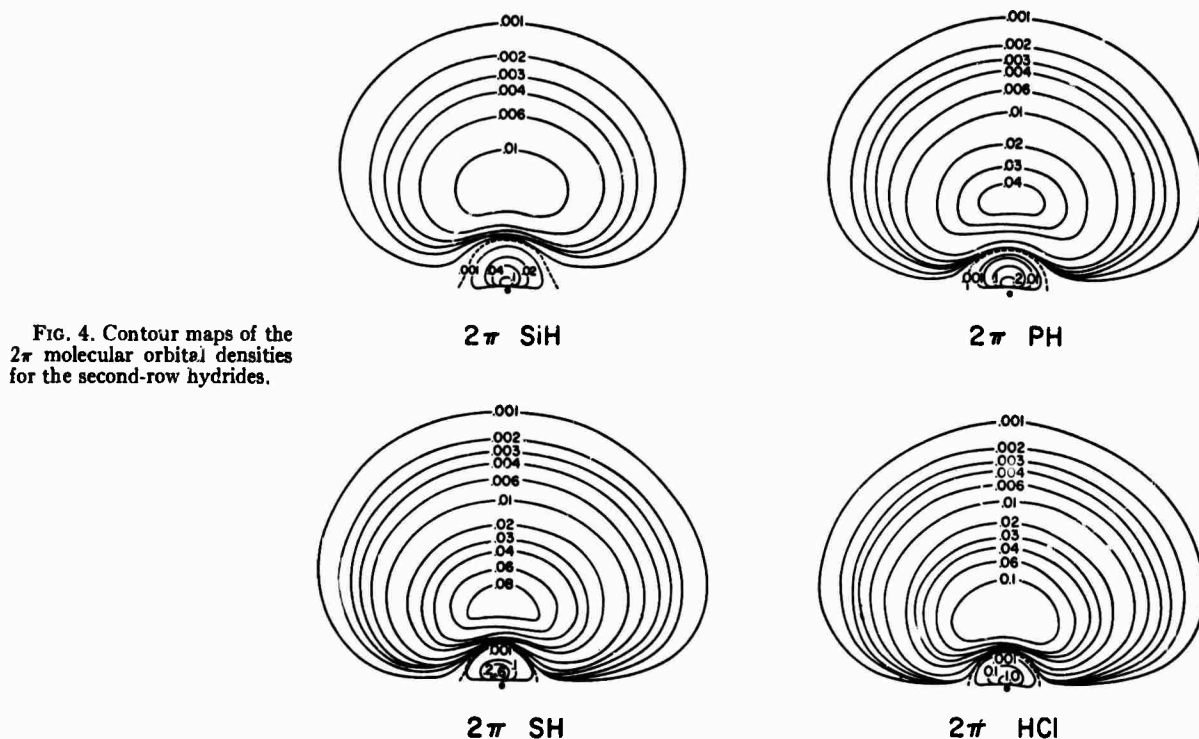
FIG. 4. Contour maps of the 2π molecular orbital densities for the second-row hydrides.

2π SiH

2π PH

2π SH

2π HCl
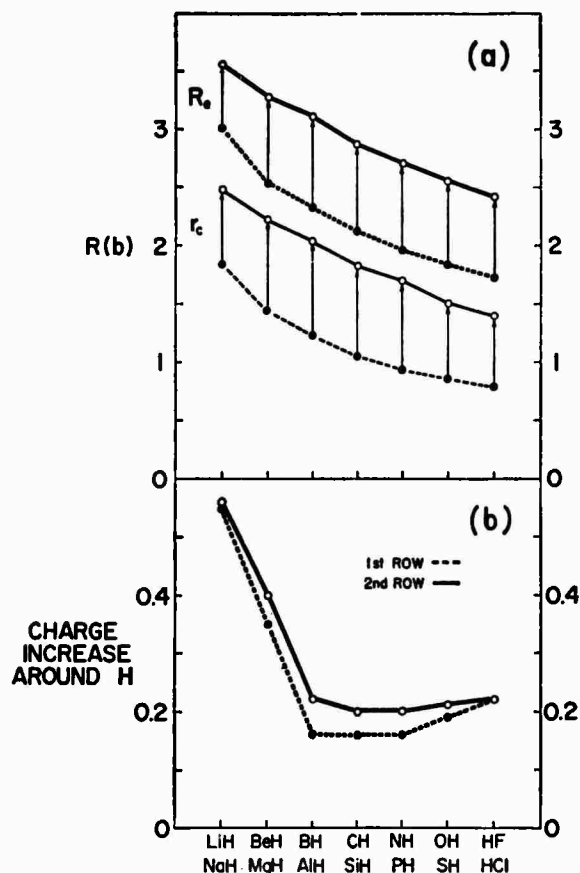
FIG. 5. (a) The change in R_e and the "core size" for the first-row versus the second-row hydrides. (b) The variation of the increase of charge around the proton (the ⑱ region of Fig. 6), and the intra- and interrow comparisons.

the first-row congener, *minus* one (e.g., BH) and the change in the heavy atom end from the first-row congener, *plus* one (e.g., NH) may be used. Similarly, the molecular "size" of a second-row hydride (e.g., SiH) can be estimated from

$$L(\text{SiH}) = R_e(\text{SiH}) + r_H(\text{BH}) + r_A(\text{Si}) + \Delta r_A(\text{NH}).$$

$$(2.1)$$

(In Footnote c of Table I, the second-row L values calculated in this way are given.)

We now consider the r_A or Δr_A values, the r_H or Δr_H values in concert with the nonbonded charge or change in nonbonded charge on A and H as A+H→AH, i.e., the changes in *size* versus the changes in amount of *electronic charge*. The LiH and NaH members are simple to characterize; nonbonded charge on A is depleted by almost the classical "ionic" limit of $0.5e^-$ and the value of r_A drops to near the Li^+ or Na^+ "core" values. This decrease in size, i.e., in r_A, and in the nonbonded charge on A is accompanied by an increase in size, r_H, and in nonbonded charge on H [i.e., in the shaded region of Fig. 2(b)].

The five pairs of hydrides [BH:AlH], [CH:SiH], [NH:PH], [OH:SH], and [HF:HCl], are not as simple to understand interrow or intrarow. For these subsequences the amount of increase of nonbonded charge on A is roughly constant, ~$0.2e$ for the first row and ~$0.1e$ for the second row, but the actual *size* as gauged by r_A or Δr_A increases, remains unchanged or decreases. Near the proton, the size and amount of nonbonded charge on H steadily decreases and relative

FIG. 6. Contour maps of the molecular bond density $\Delta\rho_{BA}(x, y)$ (molecule at R_e minus undistorted separated atoms also at R_e) in atomic units for the second-row diatomic hydrides. Dotted lines correspond to deficit regions and solid lines denote where charge density has increased.
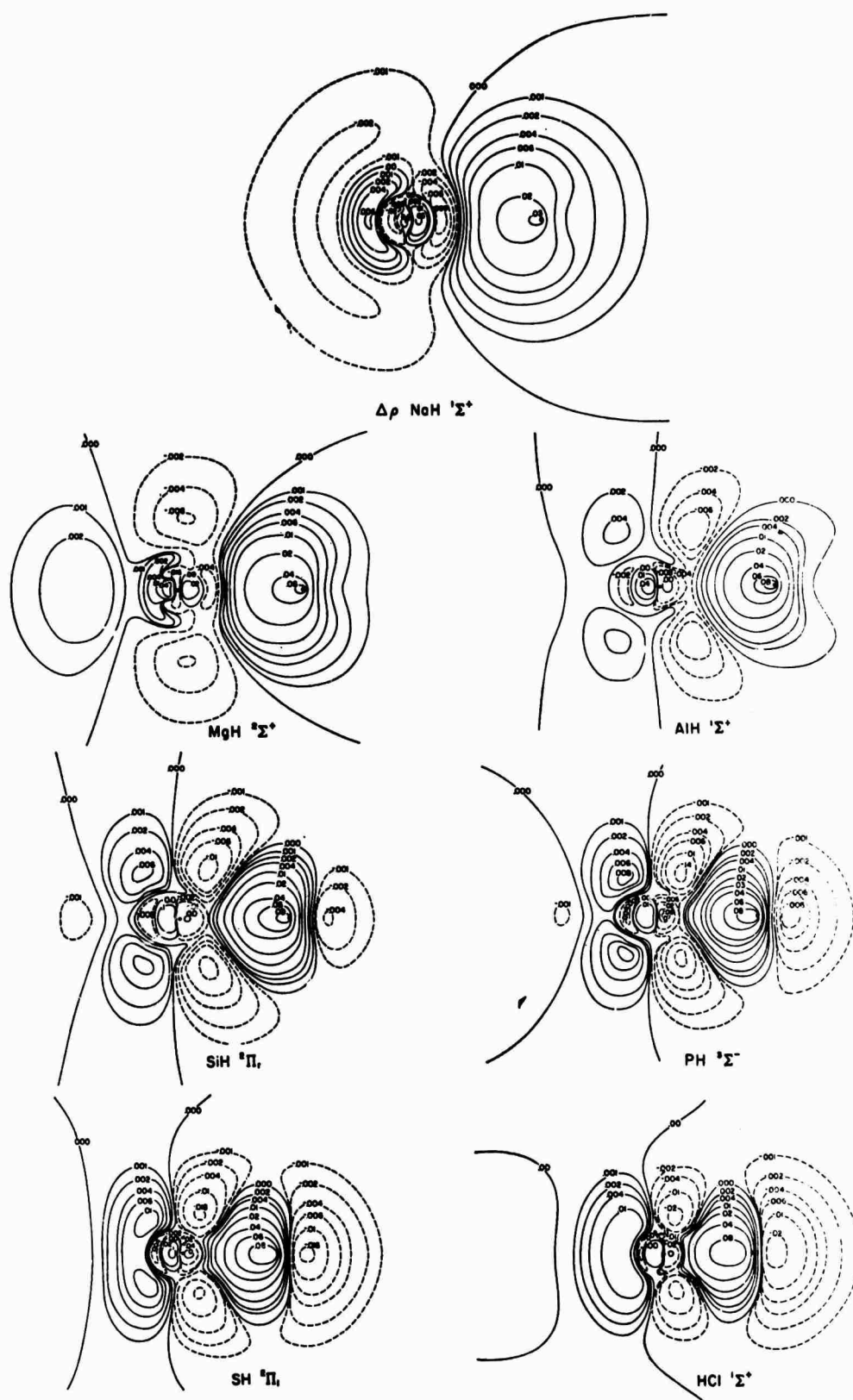
to the corresponding H(1s) values, a variable behavior obtains. These rough indices from the total charge distribution suggests that the proton is progressively less important in determining the details of the total charge distribution in the sequence BH→CH→NH→OH→HF as a *tendency* towards a polar (A⁻H⁺) model (opposite to that for LiH or NaH) is evident. It is clear from Fig. 2(d) that in the second row the proton is relatively more important in determining the details of the total charge distribution near the proton. Thus, a given second-row hydride A nucleus and KL "core" is about as effective in influencing the total charge distribution near the proton as is the nucleus and K "core" of the first-row congener one to the left. In terms of *size* this seems reasonable [see Fig. 2(f)], but in terms of the *amount* of charge in the shaded region near H in Fig. 2(b) this association seems inadequate. If the abscissa scale of the second-row hydrides is shifted one place to the left in Fig. 2(d) (open triangles, △), it is apparent that using the first-row congener *one* to the left would lead to an *underestimate* of the nonbonded charge on H for each second-row hydride. But if the abscissa scale goes *two* places to the left (solid triangles, ▲) in Fig. 2(d), the correspondence is again surprisingly good. Apparently, then, the influence of the A nucleus and the KL core in determining the details of the total molecular charge distribution near the proton for a given second-row hydride (e.g., PH), is similar in certain respects to the first-row congeners, one [CH] *and* two [BH] to the left. This relatively crude measure plainly indicates the generally weakened effect of the larger physical core in the second-row hydrides and suggests that in certain gross features the first-row congener is less important than first-row hydrides to the left of the regular congener.

For consideration of these second-row hydrides trapped as impurities in rare gas or other molecular crystals, the molecular sizes given in Table I may be instructive, especially when compared to the molecular sizes of Ne, Ar, Kr, or N_2 potential hosts. It is also noteworthy that like HF, the HCl molecule is not far different from being spherical so that rotation in a lattice site in Ar, for example, is possible. The crystal structure of HCl has recently been studied by Sándor and Farrow[11] and apparently hydrogen bonding plays a significant part in the crystal. The use of the molecular size for HCl is thus not particularly useful, except that any –Cl···Cl– distance should exceed $2r_{Cl}$ (6.6 bohr or 3.5 Å from Table I).

The charge distributions for the $(1\sigma^2 2\sigma^2 3\sigma^2 1\pi^4)$ core, the 4σ and 5σ molecular orbitals, and the 2π molecular orbital are given in Figs. 3 and 4. (The 4σ and 5σ molecular orbital densities do not show all of the nodal surfaces for practical reasons.) The 4σ and 5σ molecular orbitals progressively approach $3s\sigma$ and $3p\sigma$ atomic

[11] E. Sándor and R. F. C. Farrow, Nature 213, 171 (1967); 215, 1265 (1967).
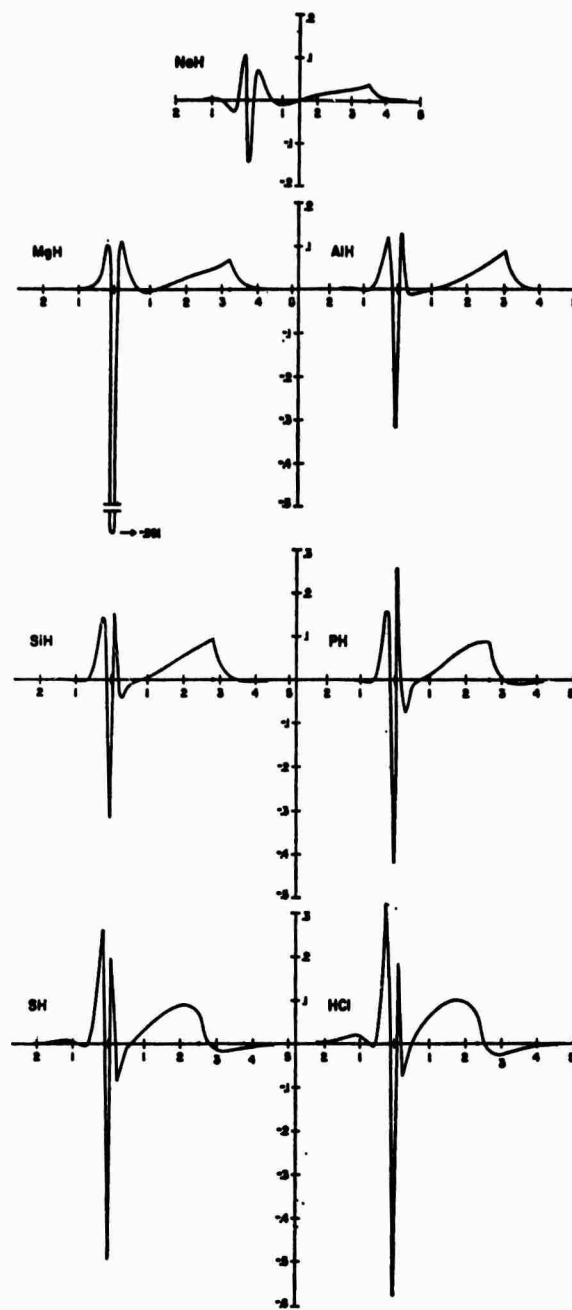
FIG. 7. Profiles of $\Delta\rho_{BA}(x, y)$ in atomic units along the internuclear axis. The abscissa (distance along internuclear axis) is in bohrs with the A nucleus at the origin.

orbitals on A, respectively. in the sequence MgH→HCl. Although not shown, the 2σ, 3σ, and 1π molecular orbitals are very little changed from the 2s, 2pσ, and 2pπ atomic orbitals on A except for small polarization effects. The 2π molecular orbital is essentially a perturbed $3p\pi$ atomic orbital on A.

The neonlike KL core decreases regularly in size with Z_A and from Fig. 3 one can discern no significant polarization of the core except very slightly for NaH. The latter will be discussed in Sec. III and only the

relative sizes are considered here in relation to bond distances in the second-row hydrides. Two questions considered are: "Does the bond distance across a row, e.g., LiH→HF or NaH→HCl, decrease for the most part simply because the "core" decreases?" and "Is the relative size of the two cores (KL versus K) the major reason for the increase in bond length for second-row hydrides relative to their first-row congeners?" In Fig. 5(a) the relevant quantities are plotted together for both the first- and second-row hydrides, namely, R_e and the "size" of the K and KL core. The "core" is a convenient artifice to consider charge localized very near the nuclei from all sources and this is dominated by either $1\sigma^2$ density in the first-row or the ($1\sigma^2 2\sigma^2 3\sigma^2 1\pi^4$) density in the second-row hydrides. To speak of the "size" of a "core" is to define an arbitrary criterion and a number which gauges the effective radius of the charge near the nucleus. A plot of the $1\sigma^2$ density of the first-row hydrides and that of the ten electrons of the neonlike core of the second-row hydrides is a very compact, sharply pointed quantity which falls to values of $\rho(x, y) \approx 0.002$ or 0.001 very rapidly with a more noticeable tail in the KL shell of NaH to HCl sequence. Therefore, a "size" for the core is a useful quantity and we shall employ the radius of the core r_e defined by the 0.001 contour as the "size." These are the "sizes" employed in Fig. 5(a).

It is strikingly seen in Fig. 5(a) that ΔR_e for HCl compared to HF, SH compared to OH, PH compared to NH, etc., is almost identical to the increase in the "size" of the core (so defined) for each pair of molecules. If another criterion is used to define a core "size," both curves for the core "sizes" will move up or down, but the correlation shown in Fig. 5(a) will not change significantly. It thus does appear that the greater bond length of the second-row hydrides relative to the bond length of the first-row hydrides can be ascribed in large part to the increased core "size" in the second-row hydrides. (A case could also be made on the same grounds that the gradual decrease in bond length across both rows is due to the gradual decrease in the core "sizes.")

B. The Molecular Bond Density Maps

The molecular bond density maps presented in Figs. 6 and 7 are defined by

$$\Delta\rho_{BA}(x, y) = \rho_{AB}(x, y; R_e)$$

$$-[\rho_A(x, y) + \rho_B(x, y)]_{R=R_e}, \quad (2.2)$$

and such difference densities are widely appreciated as a key characterization of a chemical bond if a stable state is involved. The quantity $\Delta\rho_{BA}(x, y)$ is a direct indication of how the charge density of the two atoms separated by R_e is rearranged either to obtain a state of electrostatic equilibrium and a chemical bond or to minimize *dominant* repulsive forces in a purely repulsive interaction.

It is necessary to consider carefully what is subtracted from $\rho_{AB}(x, y; R_e)$ to avoid introducing artifactual changes. It is desirable to use as good a wavefunction as possible for AB, A, and B and to have some idea of the errors in $\Delta\rho_{AB}(x, y)$ introduced as a result of using approximate wavefunctions. Bader and Chandra[12] have compared $\rho_{AB}(x, y)$ calculated from Hartree–Fock wavefunctions with $\rho_{AB}(x, y)$ calculated using the generalized Hartree–Fock wavefunctions of Das and Wahl and Das[13] for H_2 and Li_2. The result is that "no serious error is introduced when Hartree–Fock molecular charge densities are employed····." The point to be noted is that the slight change in $\rho_{AB}^{(GHF)}(x, y) - \rho_{AB}^{(HF)}(x, y)$ is much less than the changes involved in molecular formation from the atoms (e.g., 0.0001 versus 0.007 for Li_2). In the difference density maps given here, the unpublished wavefunctions of Bagus[14] for the second-row atoms were used, and as for the *first*-row hydrides the $M_L = 0$ component was employed for Na, Mg, Al, P, and Cl and an equal mixture of the $M_L = \pm 1$ components were employed for Si and S atoms.

Such "bond density" maps are also being considered experimentally mainly via x-ray crystallography. Although such efforts will doubtlessly improve in quality and a better understanding of the extent and nature of false detail or temperature effects will develop before quantitative "bond densities" are available, the present theoretical $\Delta\rho_{BA}$ maps nicely compliment these and other experimental efforts. Brill[15] has recently given a review of such efforts and a paper by O'Connell, Rae, and Maslen[16] also considers this general problem.

The bond density maps in Figs. 6 and 7 present a striking portrait of the rearrangement of electronic charge which accompanies formation of the second-row hydrides. There are two major regions where charge is accumulated in AH relative to A+H and as for the first-row hydrides, these are designated the α and $\mathcal{B}$ regions [these three-dimensional volumes are bonded by the surfaces with $\Delta\rho_{BA}(x, y) = 0$; see Fig. 2(b), Ref. 2]. The $\mathcal{B}$ region encloses the proton and for the various members NaH→HCl has the appearance of a doorknob of varying design, but always protracted towards the A nucleus. This $\mathcal{B}$ region is the most distinctive feature, in size and proximity, associated with formation of the A–H bonds.

The sequence, NaH→HCl, in Figs. 6 and 7 shows a

[12] R. F. W. Bader and A. K. Chandra, Can. J. Chem. **46**, 953 (1968).

[13] G. Das and A. C. Wahl, J. Chem. Phys. **44**, 87 (1966); G. Das, *ibid.* **46**, 1568 (1967).

[14] P. Bagus (private communication). These wavefunctions were the "skeleton" building blocks for obtaining the second-row hydride wavefunctions and have considerable merit of employing a smaller and very carefully optimized basis set (with no sacrifice in quality) compared to other wavefunctions that are available.

[15] R. Brill, in *Solid State Physics*, F. Seitz and D. Turnbull, Eds. (Academic Press Inc., New York, 1967), pp. 1–35.

[16] A. M. O'Connell, A. I. M. Rae, and E. N. Maslen, Acta Cryst. **21**, 208 (1966).

gradual transition, from NaH where charge has transferred from around the Na$^+$ core to around the proton, to HCl in which the region of charge accumulation is clearly peaked between the two nuclei and the proton is near the edge of this large accumulation. The proton is shifted from near the *center* of the $\mathcal{B}$ region for NaH to a region of a sharp gradient in $\Delta\rho_{BA}(x, y)$ for HCl. In HCl the charge has been primarily removed from the nonbonded side of the proton *and* the toruslike or doughnut region around the bond axis near A. The properties of the HCl bond density map represent one extreme in the series and the steady progression from NaH→HCl goes in unison with the change in sign and magnitude of the dipole moment and the electric field gradients at the hydrogen nucleus.

Comparison of Figs. 6 and 7 with the corresponding Figs. 3 and 4 for first-row hydrides[2] shows a very closely parallel behavior, but with some noticeable differences. Significant differences are associated with the K-shell versus KL-shell core *and* valence-shell 2σ and 3σ molecular orbitals versus the 4σ and 5σ molecular orbitals. The amount of charge contained in the $\mathcal{B}$ region [Fig. 5(b)] is greater for the second-row than for the first-row hydrides, except for NaH versus LiH and HCl versus HF. In the latter two cases the charge accumulated near the proton is almost the same for the two rows. Not only does the *amount* of charge contained in the $\mathcal{B}$ region around the proton differ, but the details of the topography of the $\mathcal{B}$ region are somewhat different (see especially Fig. 7) for the second-row hydrides. The profiles (Fig. 7 versus Fig. 4 of Ref. 2) of the second-row hydrides do not exhibit the sharp peak *in* $\mathcal{B}$ near the A nucleus so characteristic of the profiles of the first-row hydrides; this comparison is most pronounced for HCl versus HF. This latter, apparently sharp difference, can be attributed to the larger ratio of "core" size to molecule "size" in the second-row hydrides and especially to the accommodation of another shell in the second-row "core" on A. Thus the sharp peak just to the right of the A nucleus in Fig. 4 of Ref. 2 is *also* present in Fig. 7 (and due mostly to the K-shell and inner-lobe differences) but now a new feature has been interposed (and due to L-shell and further inner-lobe differences) in the second-row hydrides. Alternatively viewed, one might redefine the $\mathcal{B}$ region in the second-row hydrides to contain *two* lobes, although the small *inner* lobe would not be very important in characterizing the A–H bond. A further characteristic difference is that the $\mathcal{B}$ volume (as defined—not with a lobe structure) penetrates much nearer the heavy nucleus and accumulates charge more efficiently along the bond axis for the first-row hydrides than for the second-row hydrides. This again arises because of the larger core in the second-row hydrides compared to the first-row hydrides and is most evident from the profiles but is also striking in the projection (Fig. 6) for BH→OH in which the progressive penetrating extension of the $\mathcal{B}$ region towards A is evident.

The details of the $\mathcal{C}$ region show more relative differences between the first- and second-row hydrides. This region of charge accumulation as well as the toruslike (or doughnut) region of charge decrease about the molecular axis are both much less pronounced, and are less in absolute magnitude for the second-row hydrides. This is consistent with the decreased importance of removing charge centered on A from between the nuclei to reduce electrostatic repulsion and is the result of a sizeable buffering "core" localized around the A nucleus. Thus those features which characterized the $\mathcal{C}$ region for the first-row hydrides are present but subdued for the second-row hydrides, as less charge is accumulated in the $\mathcal{C}$ region for the MgH→HCl sequence. (Again, a two-lobe structure might be introduced to characterize the $\mathcal{C}$ region for the second-row hydrides as contrasted to the first-row hydrides.)

The preceding section suggested that the features on the nonbonded [shaded regions in Fig. 2(b)] region around A and H for a given second-row hydride (e.g., SiH) were more similar to the nonbonded region around A for the first-row congener *plus* one (e.g., NH) and to the nonbonded region around H for the first-row congeners *minus* one or two (e.g., BH and BeH), respectively. In considering Figs. 6 and 7 and Figs. 3 and 4 of the first-row hydrides paper,[2] this appears only roughly to hold. The four numbers, r_A and r_H, and the nonbonded charge on A and H, mask a considerable amount to detail and the usefulness of such a simple relationship is blunted.

The NaH molecule exhibits a rather large transfer of charge from around the Na nucleus to around the proton and also shows a very interesting polarization behavior about the Na nucleus. Neglecting certain details near the Na nucleus, NaH typifies the characteristic "ionic" type of molecular bond density and very closely parallels LiH[17] and LiF. The distinguishing features of the "ionic" bonding type are very obvious: (i) a clear-cut transfer of charge ($1.0e$) from the proximity of one nucleus to the other to simulate Na$^+$ and H$^-$ ions, and (ii) the accompanying mutual polarization of the approximate Na$^+$ and H$^-$ parts by one another. However, compared to LiH the polarization effects on the H$^-$-like part are more pronounced, and the Na$^+$-like part has a substructure of polarization effects.

The specific pattern of the density difference diagrams around the A nucleus, even in an orbital perspective, is a complicated mélange of competing effects. The presence of the 5σ molecular orbital plays a key role in parallel to the behavior of the 3σ orbital in the first-row hydrides [the latter shows a more dramatic appearance in the $\Delta\rho_{BA}(x, y)$ map for BeH], but obviously there are other important factors and all

[17] R. F. Bader and W. H. Henneker, J. Am. Chem. Soc. **88**, 280 (1966).
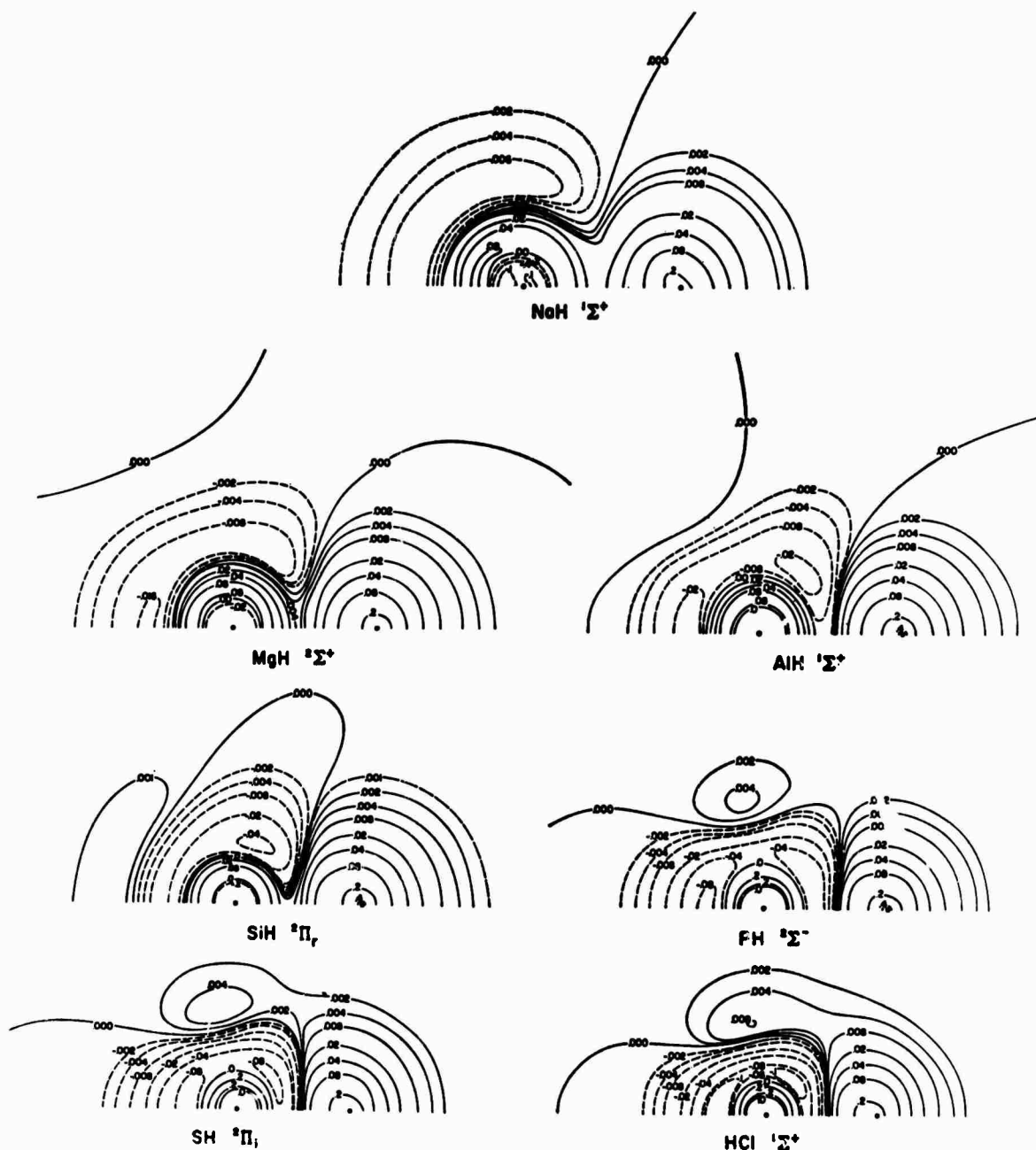
FIG. 8. Contour maps of the difference density $\Delta\rho_{UA}(x, y)$ (molecule–united atom) in atomic units for the second-row hydrides.

vary across the entire row. Whereas BeH seemed a clear-cut example of a transition between the case where charge is transferred from A to H and the cases where charge is transferred to between the nuclei and accumulates behind A, both MgH *and* AlH appear transitional in both the projection and profile maps. The distinctive appearance of the α region for MgH compared to NaH coincides with the first appearance of the 5σ orbital in the series and suggests that the α region accumulation occurs mainly from 5σ charge density. The deficit right at the A nucleus for MgH is out of sequence in *size*, and, the *position* of the A

nucleus is right in the center of the decrease, not left of center (as in NaH), or right of center (as in AlH→ HCl). Only for MgH (and BeH) does formation of the molecule involve such a pronounced *new* feature [e.g., corresponding to what might be called the promotion $\mathrm{Mg}(KL3s^23p^0)\rightarrow\mathrm{Mg}(KL3s3p)$]. Thus the charge transferred to around the proton now has strong and nearly even competition in polarizing the charge near the A nucleus due to the occupied 5σ molecular orbital. An oversimplified picture of the situation would be to imagine an electron in the $\mathrm{Mg}(KL3s^2)$ atom jumping to a $3p\sigma$ orbital as the hydrogen atom ap-

321
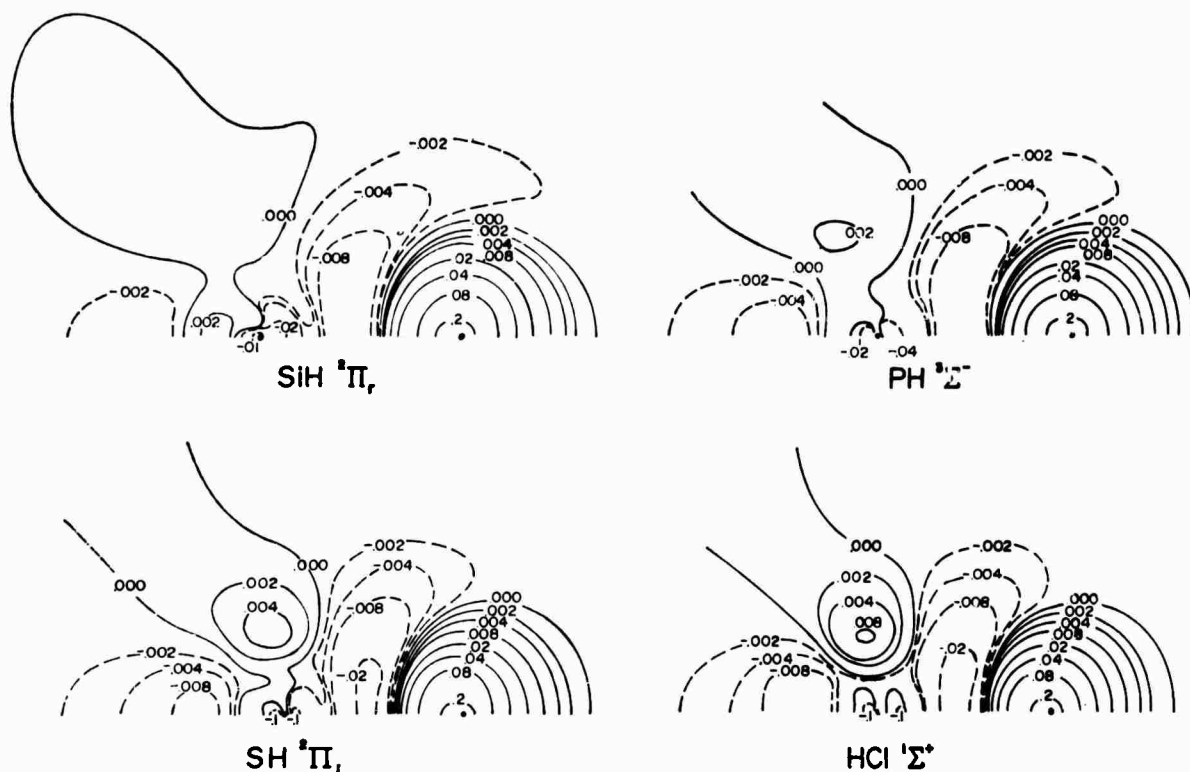
FIG. 9. Contour maps of the difference density of a two-center expansion charge density, minus a one-center expansion charge density for SiH, PH, SH, and HCl (see Ref. 18).

proaches and the $3p\sigma$ orbital is modified and transformed into a 5σ orbital.

In summary, the second-row hydride bond density maps suggest that the binding in NaH is ionic and the binding in SiH, PH, SH, and HCl are covalent. This latter characterization is based on the indication that the charge accumulation between the nuclei is shared, albeit undemocratically. A more accurate statement, particularly evident from these second-row results, is that the charge in the ⑬ region is shared between the proton and the neonlike "core" about the A nucleus. In this perspective, although the total electronic charge is rearranged so that the forces on the *nuclei* are zero (or parctically, very small), it should also mean that the force on the neon'ike KL-shell core is near zero. The MgH and AlH molecules appear less clearly defined in terms of ionic or covalent templates although neither seems as transitional as BeH. In comparison to the binding across the first-row hydrides, the second-row hydrides show a parallel behavior in the details of the $\Delta\rho_{SA}(x, y)$ maps and their trends.

C. Difference Density Maps: United Atom versus AH and One-Center versus Two-Center Expansion Densities

The difference density defined by the relation

$$\Delta\rho_{UA}(x, y) = \rho_{AH}(x, y; R_e) - \rho_{UA}(x, y; R=0), \quad (2.3)$$

is given in Fig. 8. The united atom nucleus is placed at the A nucleus in the subtraction [Eq. (2.3)] and for AlH and SiH the ^1D excited state UA of Si and ^2D excited state UA of P, respectively, are used. In detail then one can consider the change in the charge distribution as the hydride is formed from the united atom—an expecially important reference state for hydride molecules.

The most pronounced feature in $\Delta\rho_{UA}(x, y)$ of Fig. 8 is, of course, the accumulation of charge about the proton in AH. This parallels the first-row results and again the major features near the proton in $\Delta\rho_{UA}(x, y)$ do not change much from one hydride to another. The comparison of $\Delta\rho_{UA}(x, y)$ for the second-row hydrides with those for the first-row hydrides (Fig. 6, Ref. 2) reveals no substantial differences in the charge accumulated around the proton.

The features of $\Delta\rho_{UA}(x, y)$ very near the heavy nucleus are more complicated and have to do with the decrease in size of corresponding K- and L-shell orbitals in the UA and the polarizations of the $1\sigma^2$, $2\sigma^2$, $3\sigma^2$, and $1\pi^4$ orbitals in AH discussed above. The outer deficit region near A, which finally becomes enclosed at HCl, is clearly associated with the valence-shell atomic orbitals of the united atom not being suitably polarized as in bond formation (e.g., if the charge density of Ar in an axial electric field was used and compared with HCl, the polarization of this deficit region vould be reduced). It is interesting to note that right on the heavy nucleus there is a big deficit

region not easily visible in Fig. 8 surrounded by a low wall of accumulation in AH relative to UA. This behavior reflects the increase in nuclear charge $Z_A(AH) \rightarrow (Z_A+1)(UA)$ and particularly the shifting, polarization, and internal competitive rearrangement of nodal surfaces in AH versus the related nodal surfaces in UA.

The final set of difference density maps given in Fig. 9 is the result of subtracting for each molecule an extensive one-center expansion SCF density from the Hartree–Fock density of Cade and Huo.[4] The one-center results were obtained explicitly for this comparison to allow a better assessment of the one-center density than wavefunctions in the literature would have permitted.[18] The results in Fig. 9 are intended as a gauge of the ability of the one-center expansion to achieve the two-center expansion results—a much more limited question of mostly practical value. It is conceivable that a really Herculean one-center expansion calculation may remove many of the substantial differences in Fig. 9 and in principle in the limit it must remove all differences. Hake and Banyard[19] have discussed the merits and characteristics of one-center calculations and Bishop[20] has given a lengthy review of one-center wavefunctions, but the implications of Fig. 9 must also be weighted against any practical advantages or energy results obtained.

The most obvious defect of the one-center result is, as expected, the relative inability to place nearly enough charge near the proton. If the specific contours in Fig. 9 are compared to those in Fig. 1 of the *total* density, it is clear that this error is substantial. The accumulation region *off* the axis near A and the two deficit regions around the molecular axis reveal the relative incapacity of the one-center expansion to effectively place charge between the nuclei or, more accurately, to *preferentially* place charge along the bond axis between the nuclei. Thus, to accumulate any charge near the proton (via STF's with high quantum numbers, l, perhaps in diffuse orbitals), the one-center expansion has to also accumulate extraneous charge elsewhere.

[18] The calculations for $SiH(X\,^2\Pi_r)$, $PH(X\,^3\Sigma^-)$, $SH(X\,^2\Pi_i)$, and $HCl(X\,^1\Sigma^+)$ each involved 16 σ-type STF's and eight π-type STF's centered on the heavy nucleus. The two-center basis sets of Cade and Huo (Ref. 4) were used with the functions centered on the proton replaced by further nd and nf STF's in σ and π symmetry on A. No optimization of orbital exponents was carried out and it is apparent that these results are not to Hartree–Fock quality, but are substantially better than one-center expansions for these molecules available in the literature. Thus, it was felt desirable to obtain these wavefunctions to permit a better quality assessment of the one-center expansion. The energy results were −289.2999 (−289.4362), −341.1685 (−341.2932), −397.9889 (−398.1015), and −460.0077 (−460.1103) hartrees for SiH, PH, SH, and HCl, respectively, with the two-center expansion results of Cade and Huo (Ref. 2) given in parentheses. These one-center wavefunctions are available from P. E. Cade upon request.

[19] R. B. Hake and K. E. Banyard, J. Chem. Phys. **45**, 3199 (1966).

[20] D. M. Bishop, Advan. Quantum Chem. **3**, 25 (1967).

III. A COMPARISON OF THE BINDING IN THE FIRST- AND SECOND-ROW HYDRIDES

As explained previously,[1,2] a measure of the extent to which an orbital charge density, ϕ_i^2, binds nucleus A in a diatomic molecule AB is given by the partial force f_{iA} defined by

$$f_{iA}(R) = R^2 N_i \int \phi_i^*(\mathbf{r}_\mu) \frac{\cos\theta_{\mu A}}{r_{\mu A}^2} \phi_i(\mathbf{r}_\mu) d\mathbf{r}_\mu. \quad (3.1)$$

Each partial force *on* the A nucleus f_{iA} is numerically equal to a point charge q_B which, placed *at* the B nucleus, would exert the same electrostatic force on the A nucleus as does the density in the ith molecular orbital. (*Nota bene* the *actual* force exerted on A by all electrons in ϕ_i is $R^{-2} f_{iA}$ and *not* f_{iA}.) The terms *binding*, *nonbinding*, and *antibinding* are defined with reference to the *change* in the value of f_{iA} as R is changed from ∞ to R_e, i.e., with reference to the change in the equivalent point charge at the B nucleus effective in binding the A nucleus when the molecule is formed from the separated atoms. Of equal interest to the binding-antibinding character of the orbital densities within (intrarow) the second-row hydrides is the comparison of the binding in this series of molecules with that found for the first-row hydrides (interrow). Specifically, how is the binding of the nuclei affected by the increase in the number of core electrons from two to ten and by the more diffuse character of the valence density in the second-row hydrides?

A. Binding by the Core Density

In the Hartree–Fock approximation the electronic charge density near the A nuclei in the second-row hydrides is dominated by the $(1\sigma^2 2\sigma^2 3\sigma^2 1\pi^4)$ molecular orbital density. The fact that the core densities, as shown in Fig. 3, are nearly spherical and centered on the A nuclei with effective radii less than the bond length suggests that this group of orbitals be treated as a single entity in the discussion of the binding and its properties compared with those of the $1\sigma^2$ ($\sim 1s_A^2$) core of the first-row hydrides. A partial force for the core density, f_{core}, may be defined as the sum of the f_i values for the core orbitals. The charge equivalent of the total force exerted on the proton (column 7, Table II) by the core density, $f_{core,H}$, is in every case $\sim 10e^-$. Thus, $f_{core,H}(R)$ is unaltered by the formation of the molecules, i.e., $f_{core,H}(R_e) = f_{core,H}(\infty)$, and the core density simply screens an equivalent nuclear charge *on* A from the proton. This density is *nonbinding* for the proton in each case, consistent with its definition as a core density.

The nonzero values of $f_{core,A}$, however, show that the core density exerts a net repulsive or attractive force on the A nucleus as a result of the core polarization. The signs indicate that the *net* polarization of the core density is directed away from the proton in NaH

TABLE II. Analysis of the partial forces for the inner shell, 4σ, 5σ, and 2π molecular orbitals.

Molecular orbital(s)	AH	Forces on the A nucleus				Forces on the H nucleus			
		Total	Atomic	Overlap	Screening	Total	Atomic	Overlap	Screening
$(1\sigma^2 2\sigma^2 3\sigma^2 1\pi^4)$	NaH	−0.724	−0.963	0.238	0.001	9.982	0.002	0.030	9.950
Inner-shell	MgH	−0.217	−0.332	0.115	0.000	9.998	0.000	0.015	9.983
"core"	AlH	0.171	0.169	0.002	0.000	9.983	0.000	0.002	9.981
	SiH	0.172	0.175	−0.003	0.000	10.006	0.000	0.002	10.004
	PH	0.177	0.179	−0.002	0.000	10.009	0.000	0.001	10.008
	SH	0.181	0.184	−0.003	0.000	10.005	0.000	0.000	10.005
	HCl	0.185	0.191	−0.006	0.000	10.005	0.000	0.000	10.005
4σ	NaH	1.791	0.571	−0.133	1.353	1.015	0.526	0.381	0.108
	MgH	1.960	0.624	0.223	1.113	1.783	0.609	0.903	0.271
	AlH	1.831	0.629	0.565	0.637	2.370	0.447	1.202	0.721
	SiH	1.567	0.611	0.577	0.379	2.542	0.328	1.135	1.079
	PH	1.270	0.550	0.508	0.212	2.540	0.224	0.941	1.375
	SH	1.033	0.479	0.426	0.128	2.474	0.161	0.767	1.546
	HCl	0.868	0.429	0.357	0.082	2.411	0.119	0.630	1.662
5σ	MgH	−0.696	−0.699	−0.052	0.055	0.266	0.006	−0.060	0.320
	AlH	−1.084	−1.226	−0.311	0.453	0.668	0.170	−0.198	0.696
	SiH	−0.877	−1.234	−0.206	0.563	1.011	0.286	0.082	0.643
	PH	−0.627	−1.191	0.003	0.561	1.424	0.339	0.428	0.657
	SH	−0.435	−1.108	0.162	0.511	1.806	0.376	0.679	0.751
	HCl	−0.304	−1.022	0.270	0.448	2.100	0.378	0.841	0.881
2π	SiH	0.024	0.015	0.009	0.000	0.497	0.000	0.009	0.488
	PH	0.075	0.057	0.018	0.000	1.135	0.000	0.018	1.117
	SH	0.130	0.054	0.073	0.003	1.812	0.002	0.084	1.726
	HCl	0.191	0.065	0.120	0.006	2.549	0.005	0.143	2.401

and MgH

(A–H)

and directed towards the proton

(A–H)

in AlH, SiH, PH, SH, and HCl. The core density is, therefore, *antibinding* for the Na and Mg nuclei and slightly *binding* for the remaining A nuclei. The binding of the nuclei by the density in the core orbitals varies in an identical manner through the first- and second-row hydrides, the $1s_A$-like core of the first-row molecules being *nonbinding* for the proton, *antibinding* for the Li and Be nuclei, and slightly *binding* for the remaining A nuclei.

The $\Delta\rho_{8A}(x, y)$ maps, Fig. 6, and particularly the profiles of these maps, Fig. 7, illustrate that the detailed polarization of the cores is more complex than indicated simply by the $f_{core,A}$ values, which reflect only the net polarization effect. Inasmuch as the $(1\sigma^2 2\sigma^2 3\sigma^2 1\pi^4)$ density in AH is almost identical[21] with the $(1s^2 2s^2 2p^6)$ density in A, it is sensible to speak of the changes noted in $\Delta\rho_{8A}(x, y)$ near the A nucleus as arising largely from the very slight polarization of the neonlike KL shell relative to the free-atom situation. [However, it must be remembered that changes in the *inner* lobes of the $4\sigma^2$, $5\sigma^2$, and $2\pi^n$ MO densities versus the ancestral $3s^2$, $3p\sigma^2$, and $3p\pi^n$ AO densities also contribute to the $\Delta\rho_{8A}(x, y)$ map near the A nucleus.] As is seen below, a hierarchical structure of polarizations (each giving rise to a region of charge accumulation *and* deficit) usually obtains although not resolved.

The individual f_{iA} contributions to $f_{core,A}$ indicate the

[21] The close associations $1\sigma \sim 1s$, $2\sigma \sim 2s$, $3\sigma \sim 2p\sigma$, and $1\pi \sim 2p\pi$ between the inner-shell molecular orbitals in the second-row hydrides, AH, and the separated atom A, are clearly evident from a close comparison of the individual orbitals, either directly or in terms of the relative $C_{A\mu}$ coefficients in the wavefunctions.
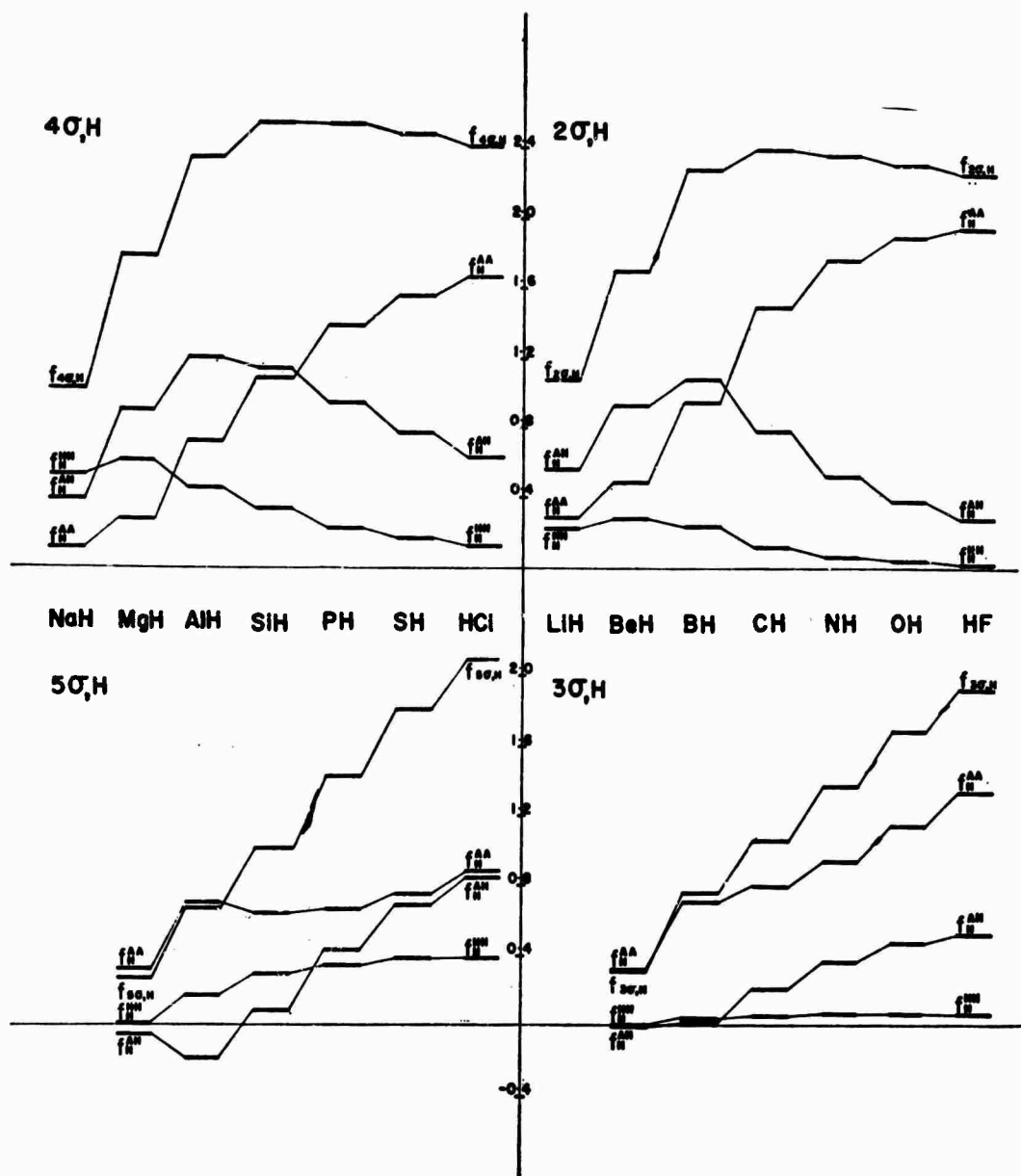
FIG. 10. Intrarow and interrow comparison of the partial forces on the H nucleus, $f_{n\sigma,H}$ and the atomic $f_{n\sigma,H}^{(HH)}$, overlap, $f_{n\sigma,H}^{(AH)}$, and screening, $f_{n\sigma,H}^{(AA)}$ contributions for the first-row hydrides ($n=2$ and 3) and the second-row hydrides ($n=4$ and 5).

presence of two opposing polarizations of the core.[22] Thus, for NaH and MgH the $1\sigma^2$, $2\sigma^2$, and $1\pi^4$ densities exert a repulsive effect on A tending to pull A and H apart, but the $3\sigma^2$ density exerts an attractive force. For the remainder of the series, AlH, SiH, PH, SH, and HCl, the roles are reversed with the $3\sigma^2$ density

now being repulsive and the $1\sigma^2$, $2\sigma^2$, and $1\pi^4$ densities attractive. The individual breakdown is associated entirely with the axial core ($3\sigma^2 \sim 2p\sigma^2$) versus spherical ($1\sigma^2$ and $2\sigma^2 \sim 1s^2$ and $2s^2$) and perpendicular ($1\pi^4 \sim 2p\pi^4$) core parts in response to accumulation of charge along the molecular axis; the spherical and perpendicular polarizations dominate the axial polarization in every case.

In summary, the transfer of valence density from around the Na⁺-like core to around the proton (as shown by the large, diffuse, and outermost charge decrease on the nonbonded side of Na and its associated

---

[22] A full table of the individual partial forces, $f_{i\lambda,A}$ and $f_{i\lambda,H}$, for the 1σ, 2σ, 3σ, and 1π MO's for each hydride is available from the authors upon request. Generally speaking, $f_{i\lambda,H} \approx f_{i\lambda,H}^{(AA)} \approx N_{i\lambda}$, i.e., all *screening* part, and $f_{i\lambda,A} \approx f_{i\lambda,A}^{(AA)}$, i.e., all atomic part, for the 1σ, 2σ, 3σ, and 1π core MO's, except for the $f_{i\sigma,A}$ values which have a dominant overlap part for NaH and MgH.

325
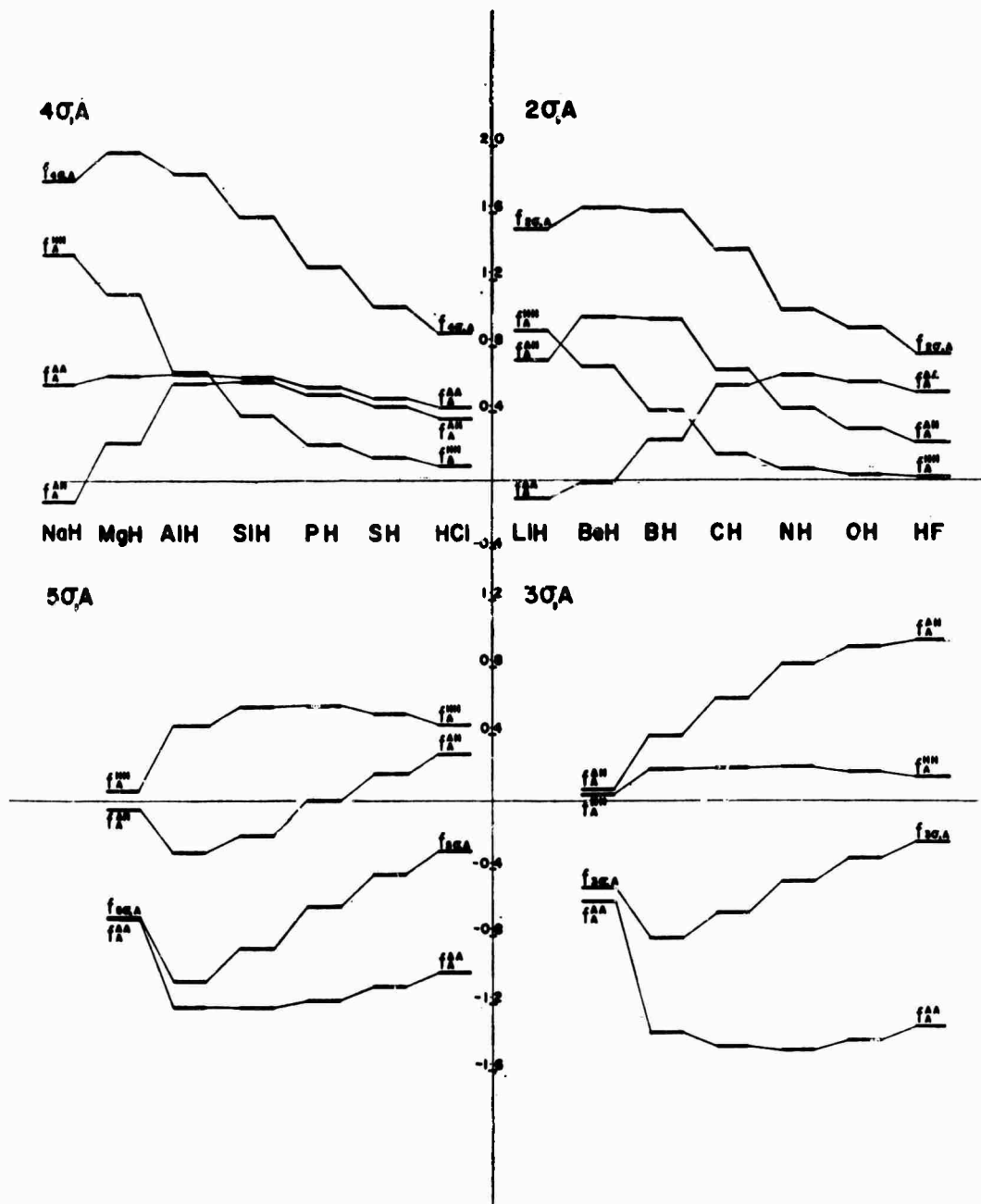
FIG. 11. Intrarow and interrow comparison of the partial forces on the A nucleus, $f_{ne,A}$ and the atomic, $f_{ne,A}^{(AA)}$, overlap, $f_{ne,A}^{(AH)}$, and screening, $f_{ne,A}^{(HH)}$, contributions for the first-row hydrides ($n=2$ and 3) and the second-row hydrides ($n=4$ and 5).

increase on H) induces an opposing polarization in the $2s^2$ and $2p\pi^4$ densities

$$(\overset{\leftharpoonup}{A}-H)$$

which in turn is countered by a deeper axial attractive polarization of the $2p\sigma^2$ density

$$(\overset{\rightharpoonup}{A}-H),$$

which is opposed by a smaller back-polarization of the $1s^2$ density

$$(\overset{\leftharpoonup}{A}-H)$$

in the immediate vicinity of the Na nucleus. As the direction, extent, and loci of the charge transfer comprising the Ⓑ region changes, the response of the core changes, as is shown by these three polarizations.

326

In MgH the polarizations are reduced in value from those in NaH and are more evenly balanced. Through the sequence AlH→HCl an increasing amount of charge is transferred from H→A with an increasing axial contribution and the *directions* of the polarizations are reversed. Thus at the other extreme, in HCl, the outermost core polarization, that attributed to the $2\sigma^2$ and $1\pi^4$ densities, is now directed *towards* the proton in response to the transfer of valence density from H to behind Cl, the axial polarization is directed away from H, and the inner $1\sigma^2$ polarization is directed towards H.

While the charge equivalent of the net field exerted by the "A nucleus+core" is equal to the number of valence electrons on A for both K-shell and KL-shell cores, the strength of the "A nucleus+core" electric field is reduced in the second-row hydrides because of the increased size of the KL-shell core relative to molecular size as compared to that of the K-shell core. As will become apparent in the following discussion of the binding, the reduction in the effective field which the A nuclei of the second row exert on the valence density is largely responsible for the differences between the binding of the *proton* in the first- and second-row hydride congeners.

B. Binding by the Valence Orbital Density

The comparison of the binding of the nuclei by the valence-shell molecular-orbital density between the two series of hydrides is facilitated by Figs. 10 and 11 which show the variation in the partial forces (and their population contributions) for corresponding valence orbitals in the two series. The binding by the valence-orbital density is considered below in three main parts: (i) the binding of the proton and A nucleus by the 2σ or 4σ density, (ii) the binding of the proton and A nucleus by the 3σ and 5σ density, and (iii) the rather dormant contribution of the 1π or 2π density. Throughout, a comparative perspective of the second-row versus the first-row hydrides is sought.

(i) The 4σ density (Fig. 3) is largely localized on the proton in NaH, MgH, and AlH, delocalized over both nuclei in SiH and PH, and, finally, localized in the region of the A nuclei in SH and HCl—a general trend similar to but less pronounced than that for the $2\sigma^2$ density in the first-row hydrides. Comparison of the partial force values at R_e with the limiting value $[f_{4\sigma,\text{H}}(\infty) = f_{2\sigma,\text{H}}(\infty) = 2.0]$ indicates that $4\sigma^2$ and $2\sigma^2$ densities are *antibinding* for the proton in MgH and BeH and *binding* for the proton in the remaining members of both series. A comparison of the atomic, overlap, and screening contributions (see Ref. 2 for definitions) to $f_{4\sigma,\text{H}}$ with those for $f_{2\sigma,\text{H}}$ indicates that the $4\sigma^2$ density distributions exhibit a greater reorganization relative to the limiting separated-atom spherical charge density centered on A than do the $2\sigma^2$ distributions of the first-row hydrides. (The limiting

forms are most closely approached by HCl and HF.) In HF the $2\sigma^2$ density screens 1.95 units of nuclear charge on F (i.e., $f_{\text{H}}^{\text{HAA}} = 1.95$ compared to the limiting value of 2.00) and the atomic (f_{H}^{HH}) and overlap (f_{H}^{AH}) contributions are both small in value. In HCl, on the other hand, the $4\sigma^2$ density screens only 1.66 of the Cl nuclear charges and the atomic and overlap contributions to the force binding the proton are more than double those for the $2\sigma^2$ density in HF. In fact, the binding of the proton by the $4\sigma^2$ density in HCl measured in terms of $f_{4\sigma,\text{H}}$ (and especially its components) resembles more nearly that of the $2\sigma^2$ density for CH or NH.

The forces exerted on the A nuclei by the $4\sigma^2$ and $2\sigma^2$ density distributions (Fig. 11) are *binding* in every case. (The *limiting* values of the 2σ and 4σ partial forces on A are unity for LiH and NaH, and zero for the remaining molecules in both series.) The greater binding by the $4\sigma^2$ density relative to the $2\sigma^2$ density for each congeneric pair results from an increased screening of the proton particularly in AlH→PH *and* an increase in the overlap contribution from PH→HCl. In the first-row series the $2\sigma^2$ overlap charge density contributes almost equally to the force on both the proton and the A nucleus (with the exception of the ionic case of LiH). In contrast to this, the 4σ overlap component to the force is substantially *larger* for the proton than for the A nucleus—a direct result of the large KL core. Its increased size and concomitant reduction in the effective field of the A nucleus results in the accumulation of the overlap charge density relatively nearer to the proton in the second-row than in the first-row hydrides.

(ii) The 5σ and 3σ orbital densities are strongly *antibinding* for the A nuclei (Fig. 11). (The limiting values, as $R\to\infty$, of the partial forces on A *and* H for the 5σ and 3σ orbitals are unity, i.e., $f_{3\sigma,\text{A}} = f_{3\sigma,\text{H}} = f_{5\sigma,\text{A}} = f_{5\sigma,\text{H}} = 1.0$.) Note that $f_{5\sigma,\text{A}}(R_e)$ and $f_{3\sigma,\text{A}}(R_e)$ are not only less than unity but also less than zero indicating that the 5σ and 3σ charge densities exert a *net*, as contrasted to only a relative, repulsive force on the A nuclei. This is a result of the large accumulation of charge density in the immediate vicinity behind the A nucleus so characteristic of the $5\sigma^2$ and $3\sigma^2$ density distributions. This is numerically evident from the negative values (Table II) for the *atomic* components $f_{5\sigma,\text{A}}^{\text{AA}}$ and $f_{5\sigma,\text{A}}^{\text{AA}}$. Large and negative atomic force contributions are characteristic of orbital densities which possess a dominant $2p\sigma$ or $3p\sigma$ component.[1,2] The screening of the nuclear field of the proton from the A nuclei (via $f_{5\sigma,\text{A}}^{\text{HH}}$) is uniformly low and considerably less than the limiting value of unity for the $3\sigma^2$ densities, indicating a substantial charge transfer from H→A in the formation of this orbital density for BeH→HF. In contrast, with the exception of MgH, the $5\sigma^2$ charge density screens approximately one-half of the proton charge, indicating a reduced transfer of

TABLE III. Total atomic, overlap, and screening contributions for AH.

AH	$\Sigma_i f_{i,H}^{(HH)}$	$\Sigma_i f_{i,H}^{(AH)}$	$\Sigma_i f_{i,H}^{(AA)}$	$Z_A - \Sigma_i f_{i,H}^{(AA)}$	$F_H{}^a$
		Forces on the proton			
NaH	0.528	0.410	10.059	0.941	+0.0002
MgH	0.615	0.858	10.574	1.426	−0.0043
AlH	0.617	1.006	11.426	1.574	−0.0050
SiH	0.614	1.227	12.214	1.786	−0.0067
PH	0.562	1.388	13.156	1.844	−0.0144
SH	0.540	1.529	14.029	1.971	−0.0151
HCl	0.502	1.613	14.949	2.051	−0.0108

AH	$\Sigma_i f_{i,A}^{(AA)}$	$\Sigma_i f_{i,A}^{(AH)}$	$\Sigma_i f_{i,A}^{(HH)}$	$Z_H - \Sigma_i f_{i,A}^{(HH)}$	$F_A{}^a$
		Forces on the A nuclei			
NaH	−0.392	0.105	1.354	−0.354	−0.0582
MgH	−0.407	0.286	1.168	−0.168	−0.0451
AlH	−0.430	0.257	1.090	−0.090	+0.1005
SiH	−0.433	0.378	0.942	0.058	+0.1903
PH	−0.406	0.528	0.773	0.227	+0.2204
SH	−0.390	0.659	0.642	0.358	+0.2090
HCl	−0.337	0.742	0.537	0.463	+0.1833

a Forces are expressed in atomic units. 1 a.u. $= e^2/a_0^2 = 8.2378 \times 10^{-3}$ dyn. A positive force is a force of repulsion.

charge from H→A in the formation of the second-row as compared to the first-row hydrides. The *overlap* contributions show this even more distinctly.

The $5\sigma^2$ density is *antibinding* for the proton in MgH and AlH, *nonbinding* in SiH, and increasing more *binding* as PH→SH→HCl (Fig. 10). This trend in the antibinding–binding character of the $5\sigma^2$ density parallels that for the $3\sigma^2$ density in the first-row hydrides. Characteristic differences in the component contributions should be noted from comparing Table II and Table IV of Ref. 2. For example, when compared in terms of the extent to which the screening of the nuclear charge is *changed* in molecule formation, i.e., via $f_{i,A}^{(BB)}$, HF tends more towards the "ionic" limit in which the screening of one nucleus increases by one and the other decreases by one, whereas HCl is more like the "covalent" model in which both nuclei are screened to comparable extents[1] and screened less in the molecule than in the separated atoms.

The atomic and overlap contributions to the force binding the proton are considerably larger for the $5\sigma^2$ density of the second-row hydrides than for the $3\sigma^2$ density of the first-row hydrides (Fig. 10)—again the increased "core" size in the second-row hydrides requires the valence density to accumulate further from the A nucleus. The force exerted on the A nuclei by the overlap component of the $3\sigma^2$ density in the

first row is approximately twice that exerted on the proton, but the overlap contribution to $5\sigma^2$ density is localized further from the A nuclei and exerts a considerably larger force on the proton than on the A nuclei.

(iii) The binding of the nuclei by the 2π orbital in the second-row hydrides is similar to that by the 1π orbital in the first-row series. In both series the valence-shell pi density is well described as atomiclike $2p\pi^n$ or $3p\pi^n$ ($n = 1, 2, 3, 4$) density centered on the A nuclei and slightly polarized towards the proton (Fig. 4). The small *binding* force exerted by the 2π orbitals on the A nuclei (because of the polarization of the density) is less than that for the 1π orbitals in the first row. The $w\pi$ orbitals are *antibinding* for the proton since at R_e the $w\pi^n$ density does not screen an equivalent number of nuclear charges on A from the proton (the $w\pi^n$ density being concentrated perpendicular to the bond axes). This antibinding effect is enhanced in the second row because of the more diffuse nature of the $2\pi^n$ compared to the $1\pi^n$ charge densities of the first-row hydrides.

In summary, the presence of a large and diffuse core in the second-row hydrides results in a weakened and slowly varying field exerted by the "A nucleus+KL-shell core." This is less effective in influencing the

details of the molecular charge distribution as compared to the "A nucleus+K-shell core" of the first-row congener. This is apparent in the differences in chemical binding between the two series as determined by the forces exerted on the proton and also in the enhanced role which the field of the proton plays in determining the distribution of charge in the $\otimes$ region of the bond density maps for the second-row hydrides. For example, a comparison of the total charge distributions or the bond density maps for HF and HCl shows that the F nucleus with a compact "K-shell core" exerts the dominant field on the charge distribution in HF, whereas the Cl nucleus with a "KL-shell core" is obviously in a more even competition with the field of the proton to determine the details of the molecular charge distribution in HCl.

C. Classification of the Binding: Summary

The manner in which electrostatic equilibrium is attained in the molecule may be classified as *ionic* or *covalent* by comparing the values of the total atomic, overlap, and screening forces exerted on the nuclei at R_e with their limiting values for the separated atoms ($R \to \infty$). This comparison isolates changes in the original atomic distributions responsible for the binding of the nuclei in the molecule. The forces exerted on the nuclei and the charge redistribution depicted in the $\Delta \rho_{BA}(x, y)$ maps are complementary characterizations of the binding. The three components to the *total* forces on the A and H nuclei at R_e are listed in Table III. For the reference state of the separated atoms the atomic and overlap contributions are equal to zero and the screening contributions are:

$$\sum_i f_{i,H}{}^{(AA)}(\infty) = Z_A$$

and

$$\sum_i f_{i,A}{}^{(HH)}(\infty) = Z_H = 1, \qquad (3.2)$$

i.e., the electric field of the electronic charge distribution of a neutral atom must exactly cancel the electric field of the nucleus as $R \to \infty$.

The more dominant role of the proton in determining the charge distribution in the second-row hydrides is evident in the values of $Z_A - \sum_i f_{i,H}{}^{(AA)}$ and $Z_H - \sum_i f_{i,A}{}^{(HH)}$ (Table III) which measure the extent to which the *total* screening of the nuclear charge in the molecule changes relative to the limiting separated-atoms values. The total screening in the *molecule* is often less than Z_A or Z_H, and so the screening is *reduced* or the nucleus is *descreened*. The descreening of the A nuclei is larger than that found for their first-row counterparts, e.g., the F nucleus in HF is descreened by only $0.88e^-$ compared to $2.05e^-$ for Cl in HCl. In parallel there is a reduced descreening of the proton in the second-row hydrides as compared to the first row. The screening contribution $\sum_i f_{i,A}{}^{(HH)}$ has the effect

of *increasing* the effective charge at the proton by $0.35e^-$, $0.17e^-$, and $0.1e^-$, and exerts a net *negative* field (attraction) at the A nuclei in NaH, MgH, and AlH, respectively.

Unlike the first-row hydrides, the overlap density exerts a *larger* force on the proton than on the A nuclei in the second row. Thus the binding of the nuclei in the second-row hydrides, as gauged by the sum of atomic, overlap, and screening forces exerted on the nuclei, differs considerably from that found in the first-row series. In the first row, the descreening of the A nuclei and the overlap forces on both A and H exhibit a plateau at BH and CH. These two molecules are representative of covalent binding; both nuclei are descreened and the resulting repulsive forces [which would prevail if only $\sum_i f_{i,H}{}^{(AA)}$ and Z_A or $\sum_i f_{i,A}{}^{(HH)}$ and Z_H were contributing] on the nuclei are balanced by large and approximately equal forces exerted by the density which is shared between the nuclei, the overlap density. In LiH, the binding is ionic and to the right, from NH $\to$ HF, the binding becomes more polar, with the A nucleus increasingly dominating the charge distribution. In the second-row the electrostatic field of the A nuclei is *not* dominant in determining the charge distribution and the more pronounced polar binding found in OH and HF does not appear. The HCl, SH, PH, and SiH molecules (SiH being borderline) fulfill the electrostatic requirements of covalent binding in the second-row hydrides. However, the binding in these molecules differs from that in CH and BH of the first row in that the distribution of the valence density is dominanted by the field of the proton.

The transitional character of BeH in the first row is extended to include *both* MgH and AlH in the second-row hydrides. The binding of the proton in both BeH and MgH by the $2\sigma^2$ and $4\sigma^2$ densities, respectively, is ionic in character as is the case for LiH and NaH, but this feature is masked in over-all characteristics. The *total* charge distributions do not exhibit this because of the presence of the *unshared electron* in the 3σ (BeH) or 5σ(MgH) orbitals, the charge densities of which are concentrated behind the Be and Mg nuclei. In view of the dominant role played by the field of the proton in determining the nature of the $2\sigma^2$ and $4\sigma^2$ densities in BeH and MgH and the unshared electron in the 3σ and 5σ orbital, the attachment of another hydrogen atom to form BeH$_2$ and MgH$_2$ is easily understood. Thus, the unshared electron in the 3σ and 5σ is dominated by the proton of the second hydrogen atom and each Be–H and Mg–H bond in BeH$_2$ and MgH$_2$ is very near the ionic limit (e.g., as LiH and NaH). The relationship between the binding in the second-row versus the first-row *diatomic* hydrides, AH, which centers around the large and diffuse KL-shell core and the increased role of the proton in determination of the valence density for the second-row

systems, suggests promising approaches to understanding the differences between AH_n or other polyatomic hydrides for the first-row versus the second-row central atoms (e.g., SiH_4 versus CH_4, PH_3 versus NH_3, etc.).

The contributions to the force on the proton in NaH are characteristic of ionic binding. The electric field exerted by the *atomic* charge density on Na effectively screens 10.06 of the 11 nuclear charges on Na from the proton, resulting in a field characteristic of the Na^+-like ion. The force of repulsion exerted on the proton by the descreened Na nucleus is balanced by an inwards polarization (Fig. 6) of the charge density localized on the proton. The descreened Na nucleus exerts a repulsive field of $0.94/R_e^2$ at the proton, a field which is balanced by a force of $-0.94/R_e^2$ originating in the polarization of the charge increase localized around the proton.[23] The electric fields exerted on the proton by the Na nucleus and the atomic density on Na in NaH *correspond* to the point-charge distribution $Na^{+0.9}H^{-0.9}$ close to the ionic limit of $Na^{+1}H^{-1}$ (compare with the results[2] for LiH, $Li^{+0.8}H^{-0.8}$ and LiF, $Li^{+1}F^{-1}$). Since the charge distribution on an anion is very diffuse while that on a cation is contracted (both relative to a neutral system), a molecular charge distribution appears to be *less* ionic when viewed in terms of the effective field exerted on the *cation* (A nucleus) than when viewed from the anion (as above). Thus the point-charge equivalents of the fields exerted on the Li and Na nuclei in LiF, LiH, and NaH are $Li^{+0.9}F^{-0.9}$,

$Li^{+0.6}H^{-0.6}$, and $Na^{+0.6}H^{-0.6}$ [but in this case the *overlap* contribution is included so that the effective charge seen by the A nucleus is $Z_A - \sum_i (f_{iA}^{(AH)} + f_{iA}^{(HH)})$]. NaH now appears to be *less* ionic than LiH, a result of the more diffuse nature of the charge increase on H in NaH compared to LiH. Table II indicates that the polarization of the Na core density alone exerts a field of $+0.96/R_e^2$ on the Na nucleus, close to the limiting ionic value of $+1/R_e^2$ necessary to balance the attractive force of $-1/R_e^2$ resulting from the transfer of unit charge to the proton. Further reference to Table II shows that the repulsive *atomic* force on Na (-0.96) is reduced by a large attractive atomic contribution (0.57) from the $4\sigma^2$ density. The contour diagram of the $4\sigma^2$ density of NaH (Fig. 3) indicates that this orbital density is localized on the proton, but the inner lobe of charge density remaining in the immediate vicinity of the Na nucleus is strongly polarized *towards* the proton. This distinctive inner lobe of the $4\sigma^2$ density in the immediate region of the Na nucleus (and of the Mg nucleus in MgH) is, of course, absent in the corresponding $2\sigma^2$ density of LiH. In the latter case the valence density remaining in the vicinity of Li is encompassed by a *single* node and the density is polarized *away* from rather than towards the proton. Thus the more diffuse character of the charge increase around the proton in NaH and its apparently reduced effective electric field compared to that found in LiH may be largely explained by the differences in the valence density which remains in the vicinity of the A nucleus.

ACKNOWLEDGMENTS

---

[23] The charge density which a population analysis describes as an *overlap* population is actually contained within the charge buildup localized on the proton by the zero contour encompassing the proton on the $\Delta\rho_{BA}(x, y)$ map for NaH and defined by the map as an *atomic* density on H. Thus, if the charge density and its forces are to be partitioned in a manner suggested by the $\Delta\rho_{BA}(x, y)$ maps in the ionic case (a partitioning which is independent of the orbital basis set), the *overlap* population should be added to the atomic population on H and the forces exerted by this combined density equated to that of the density localized on the proton in the bond density map.

Analytic Optimization in Atomic SCF Calculations[*][†]

Joseph P. Olive[‡]

Laboratory of Molecular Structure and Spectra, Department of Physics, University of Chicago, Chicago, Illinois 60637

(Received 21 May 1969)

For self-consistent field calculations by the expansion technique, equations were derived which incorporate the optimization of the exponents as well as the coefficients of the Slater-type basis functions. The equations were programed for a computer, and the program was tested for small atoms.

I. INTRODUCTION

In the classical Hartree–Fock procedure for calculating atomic wavefunctions, the orbitals are subjected to a full functional variation. Roothaan[1] has introduced an expansion technique for the orbitals in terms of basis functions; a recent formulation of this technique has been presented by Roothaan and Bagus.[2] In this formulation, the variation principle is applied to the expectation value of the total energy, and self-consistent field (SCF) equations are obtained for the expansion coefficients.

Ideally, it should be possible to obtain expanded orbitals which are indistinguishable from the numerical orbitals obtained from the solution of the classical Hartree–Fock equations, but the quality of the solution obtained will be highly dependent on the basis set chosen. It has been shown[3] that results of excellent quality can be obtained with a small set of Slater-type basis functions, as long as the basis function exponents are optimized carefully.

Numerous empirical–numerical methods exist for the

optimization of the exponents. One such method[2] consists of calculating the energy at different values of one or several exponents which are varied, and interpolating for the value of the exponent at the minimum. Since a complete SCF calculation has to be carried out at each point used in the interpolation, this method is inefficient; this is especially true when it is necessary to optimize two or more exponents simultaneously. Other empirical methods[4,5] also require numerous complete SCF calculations to determine the optimum value of the exponents.

This paper suggests a new method for optimizing the exponents which is more accurate and efficient than any method used before. The variation principle is applied to the total energy expression, and differentiation is performed with respect to both coefficients and exponents. The resulting equations enable us to obtain solutions for the coefficients and exponents simultaneously.

An added benefit of this process is that optimized exponents can be obtained with much greater accuracy than is otherwise possible. Although these more carefully optimized exponents do not contribute significantly to a lowering of the energy, they often do improve the orbitals and make comparison between related systems (isoelectronic series) more meaningful.

II. GENERAL THEORY

The total electron wavefunction of an atom is constructed from orthonormal shell functions[6] which are

[1] C. C. J. Roothaan, Rev. Mod. Phys. 23, 69 (1951).

[2] C. C. J. Roothaan and P. S. Bagus, *Methods in Computational Physics* (Academic Press Inc., New York, 1963), Vol. 2, p. 47.

[3] P. S. Bagus *et al.* (private communication).

[4] B. J. Ransil, Rev. Mod. Phys. 32, 239 (1960).

[5] U. Kaldor, J. Chem. Phys. 49, 6 (1968).

[6] J. Hinze and C. C. J. Roothaan, Progr. Theoret. Phys. (Kyoto) 40, 37 (1967).

expanded in terms of basis functions according to

$$P_{\lambda i}(r) = \sum^p R_{\lambda p}(r) c_{\lambda i p}. \quad (1)$$

The symmetry species is defined by λ; i labels the orbitals which cannot be distinguished by symmetry. The basis functions are Slater-type functions given by[7]

$$R_{\lambda p}(r) = [\zeta_{\lambda p}/(2n_{\lambda p})!]^{1/2}(\zeta_{\lambda p}r)^{n_{\lambda p}} \exp(-\zeta_{\lambda p}r), \quad (2)$$

where the exponent $\zeta_{\lambda p}$ is a continuous variable and $n_{\lambda p}$ is a fixed integer.

In order to obtain expanded wavefunctions which are indistinguishable from the numerical wavefunctions obtained from the solution of the classical Hartree–Fock equations, the basis set has to be chosen carefully. This can be achieved by optimization of the exponents $\zeta_{\lambda p}$, combined with some experimentation with the choice of $n_{\lambda p}$ and the expansion length in Eq. (1). In this paper, we shall present a new formalism where the exponent optimization is incorporated into the SCF process, and solutions are obtained simultaneously for both the expansion coefficients and the basis-function exponents.

The following integrals enter the calculations: the overlap, one-electron Hamiltonian, and the two-electron interaction integrals, defined by

$$S_{\lambda pq} = \int_0^\infty dr\, R_{\lambda p}(r) R_{\lambda q}(r), \quad (3a)$$

$$H_{\lambda pq} = \int_0^\infty dr\,\{\tfrac{1}{2}R'_{\lambda p}(r)R'_{\lambda q}(r) \\ + [\tfrac{1}{2}\lambda(\lambda+1)r^{-2} - Zr^{-1}]R_{\lambda p}(r)R_{\lambda q}(r)\}, \quad (3b)$$

$$J_{\lambda pq,\mu rs,\nu} = \int_0^\infty dr \int_0^\infty ds\, U_\nu(r,s) R_{\lambda p}(r) \\ \times R_{\lambda q}(r) R_{\mu r}(s) R_{\mu s}(s), \quad (3c)$$

$$K_{\lambda pq,\mu rs,\nu} = \frac{1}{2}\int_0^\infty dr \int_0^\infty ds\, U_\nu(r,s)[R_{\lambda p}(r)R_{\lambda q}(s) \\ \times R_{\mu r}(r)R_{\mu s}(s) + R_{\lambda p}(r)R_{\lambda q}(s)R_{\mu r}(s)R_{\mu s}(r)]. \quad (3d)$$

where $R'_{\lambda p}(r) = dR_{\lambda p}(r)/dr$, Z is the nuclear charge, and

$$U_\nu(r,s)\begin{cases} = r^{-\nu-1}s^\nu, & r \geq s \\ = r^\nu s^{-\nu-1}, & r \leq s. \end{cases} \quad (4)$$

Clearly, the integrals are functions of the exponents. Note that the index structure specifies the variables, for instance, $S_{\lambda pq}$ is a function of $\zeta_{\lambda p}$ and $\zeta_{\lambda q}$. In addition to the integrals (3), which suffice for the ordinary expansion technique, we shall need for the present analysis various differential quotients with respect to one or two exponents. For example

$$J_{\lambda p'q,\mu rs',\nu} = \int_0^\infty dr \int_0^\infty ds\, U_\nu(r,s)[\partial R_{\lambda p}(r)/\partial\zeta_{\lambda p}] \\ \times R_{\lambda q}(r)R_{\mu r}(s)[\partial R_{\mu s}(s)/\partial\zeta_{\mu s}]. \quad (5)$$

[7] This definition of the Slater function is different from the customary (Ref. 2) definition by a factor of r.

where the prime on the index indicates that a differentiation has been performed with respect to the exponent which is defined by that index (two primes imply a second derivative). Since the two-electron interaction integrals will always be used in a combination which is unique for the state of the atom which is being calculated, it is convenient to introduce the following integral

$$I_{\lambda i pq,\mu j rs} = \sum_{\nu=0}^{\min(\lambda,\mu)}(a_{\lambda i,\mu j,\nu} J_{\lambda pq,\mu rs,2\nu} \\ - x_{\lambda i,\mu j,\nu} K_{\lambda pq,\mu rs,|\lambda-\mu|+2\nu}), \quad (6)$$

where $a_{\lambda i,\mu j,\nu}$ and $x_{\lambda i,\mu j,\nu}$ are coupling coefficients which depend on the construction of the configuration state function from the Slater determinants.

The expectation value of the energy can be written in terms of the integrals,[3] namely

$$E = \sum_{\lambda i} N_{\lambda i}\sum_{pq} c_{\lambda i p}(H_{\lambda pq} + \tfrac{1}{2}\sum_{\mu j}N_{\mu j}\sum_{rs} c_{\mu j r} \\ \times I_{\lambda i pq,\mu j rs}c_{\mu j s})c_{\lambda i q}, \quad (7)$$

where $N_{\lambda i}$ is the occupation number of the shell λi. The orthonormality of the shell functions is expressed by

$$\sum_{pq} c_{\lambda i p}S_{\lambda pq}c_{\lambda j q} = \delta_{ij}. \quad (8)$$

The SCF equations for the coefficients and the exponents are obtained by applying the variation principle to Eq. (7). To honor the constraints, Eq. (8), Lagrange multipliers $e_{\lambda ij}$ are introduced, where $e_{\lambda ij}=e_{\lambda ji}$ (we assume them real as well). Because of the transformation properties of the total wavefunction(s), the solution of the SCF equations is not unique. In the case of closed shells for example, solutions can be obtained for different linear combinations of the shell functions; in this case we choose the canonical form for which the off-diagonal Lagrange multipliers vanish.

Since numerous summations over the basis function indices will be necessary, an appropriate matrix notation will facilitate the orderly and compact presentation of the formalism. Accordingly, we introduce, for each λi, the column vector

$$[c_{\lambda i}]_p = c_{\lambda i p} \quad (9)$$

Defining

$$[f_{\lambda i}]_p = N_{\lambda i}\sum_q (H_{\lambda pq} + \sum_{\mu j}N_{\mu j}\sum_{rs} c_{\mu j r} \\ \times I_{\lambda i pq,\mu j rs}c_{\mu j s})c_{\lambda i q}, \quad (10a)$$

$$[f'_\lambda]_p = \sum_i N_{\lambda i}c_{\lambda i p}\sum_q(H_{\lambda p'q} + \sum_{\mu j}N_{\mu j}\sum_{rs}c_{\mu j r} \\ \times I_{\lambda i p'q,\mu j rs}c_{\mu j s})c_{\lambda i q}, \quad (10b)$$

and

$$[s_{\lambda i}]_p = \sum_q S_{\lambda pq}c_{\lambda i q}, \quad (11a)$$

$$[s'_{\lambda i}]_p = \sum_q c_{\lambda i p}S_{\lambda p'q}c_{\lambda i q}, \quad (11b)$$

TABLE I. SCF results for small basis sets.

	He		Be		Ne	
	Present results[a]	Bagus et al.[b]	Present results	Bagus et al.	Present results	Bagus et al.
Energy	-2.861673	-2.861673	-14.57209	-14.57209	-128.5195	-128.5195
$\zeta_1(1S)$	2.90624	2.906	3.38572	3.386	9.35304	9.354
$\zeta_2(1S)$	1.45296	1.453	5.7796	5.781	$\cdots$	$\cdots$
$\zeta_3(2S)$			0.974829	0.975	12.2236	12.23
$\zeta_4(2S)$					2.95212	2.952
$\zeta_5(2P)$					4.68319	4.683
$\zeta_6(2P)$					2.05352	2.053
$C_{1,1S}$	0.18159	0.18159	0.87843	0.87859	1.06248	1.06232
$C_{2,1S}$	0.84291	0.84289	0.13339	0.13322	-0.06678	-0.06661
$C_{3,1S}$			-0.00052	-0.00051	0.00437	0.00439
$C_{1,2S}$			-0.21593	-0.21603	-0.24539	-0.24534
$C_{2,2S}$			0.00245	0.00249	-0.02403	-0.02408
$C_{3,2S}$			1.02624	1.02625	1.03690	1.03688
$C_{4,2P}$					0.36881	0.36896
$C_{5,2P}$					0.71703	0.71694

[a] The present results are given with all converged significant figures.   [b] See Ref. 3.

the SCF equations can be written as

$$f_{\lambda i} = \sum_j \epsilon_{\lambda ij} s_{\lambda j}, \qquad (12a)$$

$$f'_\lambda = \sum_{ij} \epsilon_{\lambda ij} s'_{\lambda ij}. \qquad (12b)$$

Equation (12a) is not written in the ordinary manner, namely as a pseudoeigenvalue equation, because the second (exponent) equation cannot be written in any way resembling that form. Hence, we chose to write the equations in a way which maintains a certain parallelism between them. From Eq. (8) and Eq. (12a), we can easily obtain an explicit expression for the Lagrange multipliers in terms of the SCF solution, namely

$$\epsilon_{\lambda ij} = \epsilon_{\lambda ji} = \tfrac{1}{2}(c_{\lambda i}{}^\dagger f_{\lambda j} + c_{\lambda j}{}^\dagger f_{\lambda i}). \qquad (13)$$

For solving the SCF equations, we formulate a method analogous to a multidimensional Newton–Raphson scheme. In this method, corrections are computed from and for approximate solutions. A similar scheme has been used to solve the pseudoeigenvalue equation for the coefficients, but since the dependence of the Fock matrix on the coefficients is implicit, it is customary[2] to make the approximation that the correction to the Fock matrix is small enough to be neglected. If this process converges, it is justified since a new Fock matrix is repeatedly computed in the iterative procedure, and when self consistency is achieved, the Fock matrix is constructed from coefficients which are the true solution. In order to obtain a better convergence, Hinze and Roothaan[6] included the correction to the Fock matrix in their formalism. It should be noted that since the exponents are implicit, nonlinear variables of the integrals, they can only be determined by a Newton–

Raphson-type scheme, whereas when solving for the coefficients only, other schemes could be employed.

Experience has shown that for the SCF solution, the vectors and exponents of a given symmetry are strongly dependent only on the coefficients and exponents of the same symmetry, and much less on those of another symmetry. This strong coupling within a symmetry is mainly due to the orthonormality constraints within that symmetry. For this reason we simplify the Newton–Raphson-type process by solving for the corrections approximately, for one symmetry at a time. For the ultimate convergence of the solution, we rely upon iterating the entire procedure.

Dropping for the time being the symmetry indices, let $c_i{}^0$, ζ^0 constitute an approximation to the desired solution, and let δc_i, $\delta\zeta$ be the correction, so that

$$c_i = c_i{}^0 + \delta c_i, \qquad (14a)$$

$$\zeta = \zeta^0 + \delta\zeta. \qquad (14b)$$

We define $s_i{}^0$, $f_i{}^0$, etc. in terms of $c_i{}^0$ and ζ^0 by the obvious analogues of Eqs. (10) and (11). For the approximate Lagrange multipliers we adopt

$$\epsilon_{ij}{}^0 = \epsilon_{ji}{}^0 = \tfrac{1}{2}\Delta_{ij}(c_i{}^{0\dagger}f_j{}^0 + c_j{}^{0\dagger}f_i{}^0), \qquad (15)$$

where

$$\Delta_{ij} \begin{cases} = 0, & \epsilon_{ij} = 0 \\ = 1, & \epsilon_{ij} \neq 0. \end{cases} \qquad (16)$$

The quantity Δ_{ij} is introduced to force $\epsilon_{ij}{}^0$ to vanish whenever ϵ_{ij} vanishes.

In order to obtain the final equations which will be used to solve for δc_i and $\delta\zeta$, we expand all the quantities in Eqs. (12) and (13) in terms of the approximations and their corrections. The expanded Eq. (13) is then

substituted into Eqs. (12) and all terms of second order and highers are neglected. The equation

$$\sum_{ij}(\mathbf{s}_i{}^\dagger\delta c_j+\mathbf{s}'_{ij}{}^\dagger\delta\zeta)=0, \qquad (17)$$

which is obtained from Eq. (8), is used to symmetrize the results. The final equations can be written in the form

$$\sum_j \mathbf{M}_{ij}\delta c_j+\mathbf{M}'_i\delta\zeta=\mathbf{m}_i, \qquad (18a)$$

$$\sum_j \mathbf{M}'_j{}^\dagger\delta c_j+\mathbf{M}''\delta\zeta=\mathbf{m}'. \qquad (18b)$$

The square matrices $\mathbf{M}_{ij}$, $\mathbf{M}'_i$, and $\mathbf{M}''$, and the vectors $\mathbf{m}_i$, and $\mathbf{m}'$ are defined by

$$\mathbf{M}_{ij}=-\mathbf{G}_{ij}+\tfrac{1}{2}\Delta_{ij}(\mathbf{s}_j\mathbf{m}_i{}^\dagger+\mathbf{m}_j\mathbf{s}_i{}^\dagger)$$
$$+\tfrac{1}{2}\sum_k[\Delta_{ik}\mathbf{s}_k(\mathbf{g}_{ikj}{}^\dagger+\mathbf{g}_{kij}{}^\dagger+\delta_{ij}\mathbf{m}_k{}^\dagger)$$
$$+\Delta_{jk}(\mathbf{g}_{ijk}+\mathbf{g}_{ikj}+\delta_{ij}\mathbf{m}_k)\mathbf{s}_k{}^\dagger], \quad (19a)$$

$$\mathbf{M}'_i=-\mathbf{G}'_i+\tfrac{1}{2}\sum_{kl}\Delta_{kl}(\mathbf{g}_{ikl}+\mathbf{g}_{ikl})\mathbf{s}'_{kl}{}^\dagger$$
$$+\tfrac{1}{2}\sum_k\Delta_{ik}[\mathbf{s}_k(\mathbf{g}'_{ik}{}^\dagger+\mathbf{g}'_{ki}{}^\dagger)+\mathbf{m}_k(\mathbf{s}'_{ik}{}^\dagger+\mathbf{s}'_{ki}{}^\dagger)], \quad (19b)$$

$$\mathbf{M}''=-\mathbf{G}''+\tfrac{1}{2}\sum_{kl}\Delta_{kl}[\mathbf{s}'_{kl}(\mathbf{g}'_{lk}{}^\dagger+\mathbf{g}'_{kl}{}^\dagger)$$
$$+(\mathbf{g}'_{kl}+\mathbf{g}'_{lk})\mathbf{s}'_{kl}{}^\dagger], \quad (19c)$$

$$\mathbf{m}_i=\mathbf{f}_i-\Sigma_j\epsilon_{ij}\mathbf{s}_j, \qquad (20a)$$

$$\mathbf{m}'=\mathbf{f}'-\Sigma_{ij}\epsilon_{ij}\mathbf{s}'_{ij}, \qquad (20b)$$

where

$$[\mathbf{G}_{\lambda ij}]_{pq}=\delta_{ij}N_{\lambda i}(H_{\lambda pq}+\sum_{\mu j}N_{\mu j}\sum_{rs}c_{\mu jr}I_{\lambda ipq,\mu jrs}c_{\mu js})$$
$$+2N_{\lambda i}N_{\lambda j}\sum_{rs}c_{\lambda jr}I_{\lambda ips,\lambda jrq}c_{\lambda is}-\epsilon_{\lambda ij}S_{\lambda pq}, \quad (21a)$$

$$[\mathbf{G}'_{\lambda i}]_{pq}=N_{\lambda i}\Sigma_l[\delta_{pq}H_{\lambda p'l}+\delta_{q'}H_{\lambda pl'}+\sum_{uj}N_{\mu j}\sum_{rs}$$
$$\times c_{\mu jr}(\delta_{pq}I_{\lambda ip'l,\mu jri}+\delta_{ql}I_{\lambda ipl',\mu jrs})c_{\mu js}]c_{\lambda il}$$
$$+2N_{\lambda i}\sum_j N_{\lambda j}\sum_{rs}c_{\lambda jr}I_{\lambda ips,\lambda jrq'}c_{\lambda is}c_{\lambda jq}$$
$$-\sum_j\epsilon_{\lambda ij}\sum_l(\delta_{pq}S_{\lambda p'l}+\delta_{ql}S_{\lambda pl'})c_{\lambda jl}, \quad (21b)$$

$$[\mathbf{G}''_{\lambda}]_{pq}=\sum_i N_{\lambda i}c_{\lambda ip}\sum_l[\delta_{pq}H_{\lambda p''l}+\delta_{ql}H_{\lambda p'l'}+\sum_{\mu j}N_{\mu j}$$
$$\times\sum_{rs}c_{\mu jr}(\delta_{pq}I_{\lambda ip''l,\mu jrs}+\delta_{ql}I_{\lambda ip'l',\mu jrs})c_{\mu js}]c_{\lambda il}$$
$$+2\sum_{ij}N_{\lambda i}N_{\lambda j}c_{\lambda ip}\sum_{rs}c_{\lambda jr}I_{\lambda ip's,\lambda jrq'}c_{\lambda is}c_{\lambda jq}$$
$$-\sum_{ij}\epsilon_{\lambda ij}c_{\lambda ip}\sum_l(\delta_{pq}S_{\lambda p''l}+\delta_{ql}S_{\lambda p'l'})c_{\lambda jl}, \quad (21c)$$

and

$$\mathbf{g}_{ijk}=\mathbf{G}_{ij}c_k, \qquad \mathbf{g}_{ijk}{}^\dagger=c_i{}^\dagger\mathbf{G}_{jk},$$
$$\mathbf{g}'_{ij}=\mathbf{G}'_ic_j, \qquad \mathbf{g}'_{ij}{}^\dagger=c_i{}^\dagger\mathbf{G}'_j{}^\dagger. \qquad (22)$$

III. RESULTS AND DISCUSSION

The equations given in the preceding section were programmed for the IBM 7094 computer. The program was then tested for small atoms.

TABLE II. Three calculations of helium with saturated basis sets.

Iteration No.	$\zeta_1(1S)$	$\zeta_2(2S)$	$\zeta_3(2S)$	Energy
Case a (divergence)				
1	1.6	2.8	1.88	−2.8126
2	1.53	2.39	1.86	−2.86165
3	1.35	3.53	1.88	−2.68009
4	1.38	2.11	1.82	−2.85986
5	4.80	18.14	8.84	+56.91233
Case b (convergence to a minimum different from Bagus et al.[a])				
1	1.9	2.8	1.5	−2.8616753
2	2.042	2.948	1.595	−2.8615236
3	2.054	2.974	1.584	−2.8616774
4	2.116	3.021	1.619	−2.8616728
5	2.114	3.032	1.615	−2.8616772
6	1.999	2.760	1.575	−2.8616564
7	2.001	2.798	1.576	−2.8616789
8	1.960	2.756	1.557	−2.8616786
9	1.957	2.756	1.555	−2.8616794
10	1.886	2.665	1.522	−2.8616727
11	1.886	2.665	1.522	−2.8616797
Case c (convergence to minimum near to the one given by Bagus et al.[a])				
1	1.45	2.64	1.72	−2.8616793
2	1.4500	2.6411	1.7233	−2.8616796
3	1.4520	2.6455	1.7288	−2.8616795
4	1.4514	2.6437	1.7271	−2.8616796
5	1.4511	2.6428	1.7261	−2.8616796
6	1.4516	2.6445	1.7277	−2.8616797
7	1.4511	2.6431	1.7262	−2.8616795
8	1.4513	2.6437	1.7269	−2.8616796
9	1.4517	2.6446	1.7279	−2.8616798
10	1.4505	2.6412	1.7243	−2.8616795
11	1.4520	2.6454	1.7289	−2.8616795
12	1.4521	2.6459	1.7292	−2.8616793
13	1.4521	2.6456	1.7291	−2.8616795
14	1.4519	2.6452	1.7285	−2.8616796

[a] See Ref. 3.

For helium, beryllium, and neon, approximated by two, three, and five basis functions, respectively, rapid convergence was obtained. Table I shows the results of these computations and compares them with results given by Bagus et al.[3]

In these calculations, the energy converged well before the exponents did. In the case of He, for example, the energy converged to eight significant figures in three iterations, while the exponents required 11 iterations to converge to six significant figures. This phenomenon implies that a determination of the exponents by a numerical interpolation cannot produce wavefunctions which are as good as those produced by this method since the energy is not sensitive enough. Furthermore, a similar phenomenon is known to occur in the calculation of the expansion coefficients, since in this case the quality of the coefficients is better than the energy can reflect.

When the basis set was enlarged, the calculations were not as well behaved as for the smaller sets. Table II demonstrates the behavior of three different calculations with three different sets of exponents. This table

TABLE III. SCF results for large basis sets.

	He		Be		Ne	
	Present results[a]	Bagus et al.[b]	Present results	Bagus et al.	Present results	Bagus et al.
Energy	−2.861680	−2.861680	−14.57299	−14.57299	−128.5470	−128.5471
$\zeta_1(1S)$	1.886	1.450	6.238	6.225	13.68	15.439
$\zeta_2(1S)$	...	...	3.4388	3.437	9.152	8.806
$\zeta_3(3S)$	...	...	1.77512	1.776	5.658	10.995
$\zeta_4(2S)$	2.665	2.641	0.86707	0.869	2.76	3.764
$\zeta_5(2S)$	1.522	1.732			1.91	2.301
$\zeta_6(2P)$					8.96	10.542
$\zeta_7(2P)$					4.365	4.956
$\zeta_8(2P)$					2.25	2.793
$\zeta_9(2P)$					1.35	1.623
$C_{1,1s}$	0.91821	1.36211	0.09711	0.09806	0.11195	0.09218
$C_{2,1s}$	−0.09564	−0.10724	0.91345	0.91256	0.89234	0.94891
$C_{3,1s}$	0.22297	−0.28189	0.00168	0.00150	0.00484	−0.04499
$C_{4,1s}$			−0.00064	−0.00055	−0.00030	0.00308
$C_{5,1s}$			...	...	0.00037	−0.00003
$C_{1,2s}$			−0.00860	−0.00855	−0.00078	0.00645
$C_{2,2s}$			−0.18780	−0.18811	−0.25577	−0.28821
$C_{3,2s}$			0.26687	0.26309	0.23875	−0.02632
$C_{4,2s}$			0.77394	0.77745	0.69244	0.56972
$C_{5,2s}$			...	...	0.13723	0.53066
$C_{6,2P}$					0.02130	0.00930
$C_{7,2P}$					0.35791	0.24154
$C_{8,2P}$					0.56588	0.48233
$C_{9,2P}$					0.15468	0.36532

[a] The present results are given with all converged significant figures.　　[b] See Ref. 3.

indicates that the course of the calculations, and their results, depend highly on the initial guesses. We can infer from this table that the exponents, in the case of He approximated by three basis functions, are ill-determined, and simultaneous solutions cannot always be obtained for them.

With the use of certain input parameters for the computer program, some exponents can be held fixed while others are being varied. With some experimentation, we learned that solutions can be obtained rapidly if the exponents of the more important basis functions, i.e., those with large expansion coefficients for at least some orbitals, are varied first. Table III shows a sample of such calculations.

The dependence of the accuracy of the exponents on the size of the basis set can be seen in the calculations of Be for example, where for a set of two, three, four, and five basis functions, the exponents converged to eight, six, five, and three significant figures, respectively. It should be noted that even though the accuracy

of the exponents decreases as the basis set is enlarged, the quality of the orbitals improves until the basis set is saturated.

When the basis set is saturated, as in the case of Ne approximated by nine basis functions, the calculations have to be performed with great care. In this case, the ill-determinacy of the exponents may cause the calculation to diverge if too many exponents are varied simultaneously; furthermore, the exponents which are obtained from these calculations converge with few significant figures. As can be seen in Table III, in the case of saturation, there is more than one set of exponents for the desired solution.

ACKNOWLEDGMENTS

Ab initio Calculations on Small Hydrides Including Electron Correlation.

IV. A Study of the Molecules BeH$_2$, Be$_2$H$_4$ and Be$_3$H$_6$

Reinhart Ahlrichs*

Lehrstuhl für Theoretische Chemie der Universität Göttingen, Germany

* Present address: Laboratory of Molecular Structure and Spectra, University of Chicago, Chicago, Illinois.

336

The molecules BeH_2, Be_2H_4 and Be_3H_6 are investigated by means of *ab initio* calculations including the electron correlation of the valence shell electrons. It is found that BeH_2 shows a strong tendency to polymerize in linear chains. The polymerization energy is estimated to be 40 Kcal/Mol.

Die Moleküle BeH_2, Be_2H_4 und Be_3H_6 werden mit Hilfe von *ab initio* Rechnungen unter Einschluß der Elektronenkorrelation der Valenzelektronen untersucht. Es zeigt sich, daß BeH_2 eine starke Tendenz hat, in linearen Ketten zu polymerisieren. Die Polymerisationsenergie wird zu 40 Kcal/Mol abgeschätzt.

Les molécules BeH_2, Be_2H_4 et Be_3H_6 sont étudiées au moyen de calculs *ab-initio* avec corrélation électronique des électrons de la couche de valence. On trouve que BeH_2 présente une forte tendance à polymériser en chaînes linéaires. L'énergie de polymérisation est estimée à 40 Kcal/mole.

1. Introduction

In some recent publications [1, 7–10, 18] rather detailed studies of the ground state of BeH_2 have been reported. Though all the investigations show that the BeH_2 molecule is very stable with respect to dissociation into $BeH + H$ or $Be(gas) + H_2$, it has not been observed experimentally so far. The difficulty to detect BeH_2 is mainly due to the low BeH_2 partial vapor pressure under normal experimental conditions [1].

Solid BeH_2 can be synthesized [4, 17]. Unfortunately almost nothing is known about its physical properties because one has not yet obtained sufficient pure samples. From the investigation of a product containing about 76% BeH_2 it has been suggested [14], that this sample contained $(BeH_2)_x$ chains with $x \approx 70$, but no X-ray diffraction pattern has been obtained. The IR-spectrum showed a broad absorption at $1758\ cm^{-1}$ which can possibly be interpreted as a BeH_2Be vibration [3, 14].

The aim of the investigations reported in the present paper was to study whether BeH_2 has a tendency to polymerize via H bonds, as has been supposed [17]. We further wanted to get a better understanding of the high cohesion energy of solid BeH_2 which has been estimated at 48 Kcal/Mol [1].

The computations have been performed with a method that starts from an SCF calculation and then includes the correlation energy within the independent

337

electron pair approach (IEPA) [15, 16]. A short description of the present computer program is given in [12], a detailed treatment of the theoretical background will be published elsewhere [13]. Our computer program differs mainly in three aspects from the conventional IEPA computation schemes.

1. As starting point for the treatment of pair correlation energies ε_{ij} we always use localized SCF orbitals rather than the canonical SCF orbitals. The localization procedure follows the method proposed by Foster and Boys [6].

2. The computation of pair correlation functions and energies is based on a direct calculation of approximate natural orbitals of the corresponding two electron functions, which have been denoted as quasi-NO's [2, 12].

3. The pair functions under consideration are always chosen to have a definite spin (singlet or triplet), which is different from Nesbets approach [15] who uses simple product-type pair substitutions.

The present method is an extension of the one described previously [2] which accounted for the intrapair correlation only.

As the K shell intrapair and the K shell-valence shell interpair correlation is not expected to have a considerable effect on binding energies and equilibrium geometries for the molecules considered in this paper we have decided to treat the valence shell correlation only. This makes the computations considerably shorter.

2. Basis Functions

As basis functions $\varphi_i(r)$ we used linear combinations of gaussian functions $f_\nu(r)$:

$$\varphi_i(r) = \sum_\nu C_{i\nu} f_\nu(r), \quad f_\nu(r) = N e^{-\eta_\nu (r - r_\nu)^2}$$

as indicated in Table 1. The s-type gaussians centered at Be and H are taken from Huzinaga's optimized atomic s-basis [11]. The contraction coefficients $C_{i\nu}$ for the functions $1s(\text{Be})$, $4s(\text{Be})$ and $1s(\text{H})$ were obtained from pilot calculations with uncontracted basis sets. The parameters which specify the groups $1p\sigma(\text{Be})$, $2p\sigma(\text{Be})$ and b (see Table 1) were determined by optimizing the SCF energy of BeH_2 for basis set A and B respectively (see Table 2). During this procedure the ratio of η values for the $p\sigma(\text{Be})$ functions was kept fixed. The basis sets A' and B' (see Table 2) differ from A and B by the further contraction of $1s(\text{H})$ and $2s(\text{H})$ to $1s'(\text{H})$. For the computation of correlation energies the functions $p\pi(\text{Be})$ and $p\sigma(\text{H})$ and $p\pi(\text{H})$ were added to the SCF basis. The parameters specifying these additional basis functions were varied to optimize the valence shell intrapair correlation energy of BeH_2.

3. Results

A. BeH$_2$

Although we have already reported a detailed study of the ground state of BeH_2 [1] it seems worthwhile to discuss briefly the new results summarized in Table 3. As a consequence of the careful basis optimization the SCF and correlation energies obtained with basis set B or B' are slightly better than in our best

Table 1. *Basis functions*

η	d^a	c^a	Label
1741.4	—	0.00261	1s(Be)
262.14	—	0.01988	
60.3255	—	0.9594	
17.6240	—	0.31652	
5.9326	—	0.70247	
2.1847	—	1.0	2s(Be)
0.8590	—	1.0	3s(Be)
0.20		0.45520	4s(Be)
0.06		0.76145	
0.28	0.5	1.6244	1pσ(Be)
1.4	0.2	0.5000	
0.9	0.5	1.1870	2pσ(Be)
4.5	0.2	0.2425	2pσ(Be)
0.233	0.5	1.0	1pπ(Be)
30.2	—	0.0579	1s(H)
4.76	—	0.3830	
1.24	—	1.3092	
0.377	—	1.0	2s(H)
0.118	—	1.0	3s(H)
30.2	—	0.0145	1s'(H)
4.76	—	0.0960	
1.24	—	0.3273	
0.377	—	0.6300	
0.4	0.4	1.0	pσ(H), pπ(H)
0.27	middle of BeH-bond		b

^{a} c are the coefficients with which the lobes are contracted to groups. $2d$ is the distance between two lobes forming a p-orbital.

Table 2. *Specification of the different basis sets*

Basis	HF-part		Correlation-part
A	Be: 1s, 2s, 3s, 4s, 1pσ	H: 1s, 2s, 3s	
A'		H: 1s', 3s	Be: pπ H: pσ, pπ
B	Be: 1s, 2s, 3s, 4s, 2pσ	H: 1s, 2s, 3s; b	
B'		H: 1s', 3s; b	

For the notation of basis functions see Table 1.

339

Table 3. HF *and correlation energies for* BeH$_2$, Be-H-*distance* 2.5 a.u.

Basis	$-E_{HF}$	$-\varepsilon_{vv}$	$-{}^1\varepsilon_{vv'}$	$-{}^3\varepsilon_{vv'}$	$-\varepsilon_{vv'}$	$-\varepsilon$	NHF, NT, NG		
A	15.7617	0.0308	0.0022	0.0026	0.0048	0.0664	11	19	39
A'	15.7570	0.0305	0.0021	0.0025	0.0046	0.0656	9	17	39
B	15.7698	0.0312	0.0024	0.0030	0.0054	0.0678	13	21	41
B'	15.7691	0.0309	0.0024	0.0029	0.0053	0.0671	11	19	41

ε_{vv}: Intrapair correlation per valence pair.

${}^1\varepsilon_{vv'}$, ${}^3\varepsilon_{vv'}$, $\varepsilon_{vv'}$: Singulett-, triplett and total interpair correlation energies for valence electrons. $\varepsilon_{vv'} = {}^1\varepsilon_{vv'} + {}^3\varepsilon_{vv'}$.

ε: Total valence shell correlation energy.

NHF: Number of basis functions (groups) for HF-calculation.

NT: Total number of basis functions.

NG: Total number of gaussian lobes.

previous calculation, though the latter was performed with a larger number of basis functions, namely 53 gaussians contracted to 29 groups.

In our previous paper on BeH$_2$ [1] we have in a crude way guessed the inter-pair correlation energy between the valence electrons to be $\varepsilon_{vv'} = -0.013 \pm 0.005$ a.u. The actual calculation performed now leads to $\varepsilon_{vv'} = -0.0068 \pm 0.0008$ a.u. The unexpected smallness of $\varepsilon_{vv'}$ is a consequence of the good localizability of the SCF-MO's of the valence electrons (see Fig. 1) (This result does not affect the estimate for the total energy of BeH$_2$ given in [1]). For a comparison of the different basis sets let us recall that the SCF-limit for BeH$_2$ is approximately 15.7730 a.u. [8], whereas the valence shell correlation energy ε can be estimated from the present calculations to be $\varepsilon = 0.080 \pm 0.004$ a.u.[1].

The SCF-energies given in Table 3 differ from the SCF-limit by 0.016 a.u. (basis A') to 0.003 a.u. (basis B), whereas the error of the correlation energy ε varies from 0.014 a.u. (basis A') to 0.012 a.u. (basis B). The basis set A' is hence rather poor with respect to the calculation of the SCF energy but it accounts for almost the same amount of correlation energy as the more refined basis sets B and B'. This discussion indicates that it is sufficient to use the basis set A' for the calculation of correlation energies whereas one should use the basis set B' or B (without the correlation part of course, see Table 2) to obtain reliable SCF energies.

The plots of contour lines of the quasi NO's given in Fig. 1 show very clearly that the NO's describing the intrapair correlation are concentrated in the same region of space as the localized SCF-MO's are. The NO's of the interpair correlation functions are of course extended over the region where the two localized SCF-MO's are essentially different from zero, which is the whole molecule in this case.

B. Be$_2$H$_4$

Our first task was to determine the ground state equilibrium geometry for this unknown molecule. Previous experience has suggested that for a molecule of this kind certain simplifications can be made which do not significantly change the results but lead to a considerable reduction of computation time.

---

[1] The error bounds given in this paper have been estimated from the experience of calculations on systems like H$_2$ and LiH where rather exact data are available [2].
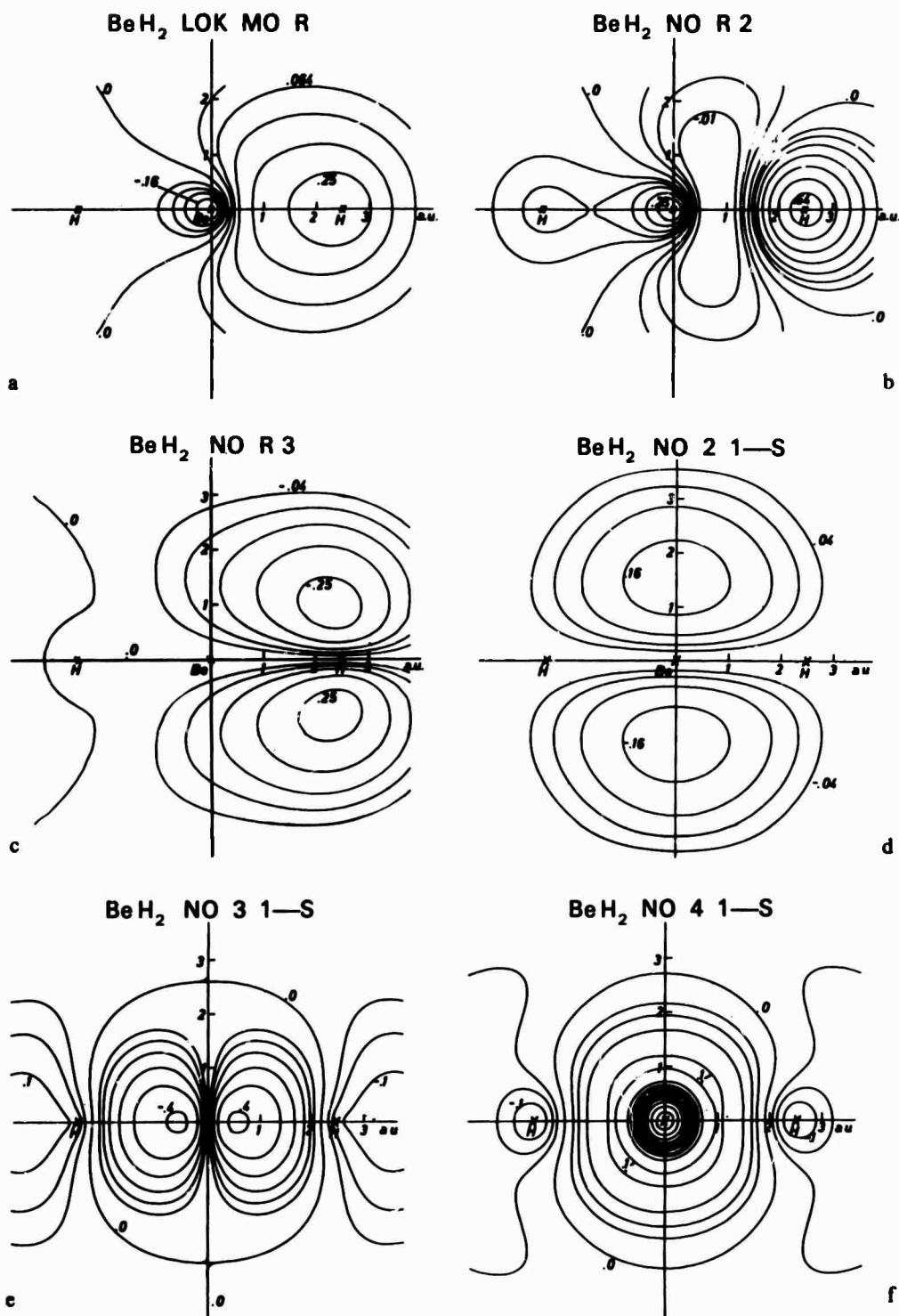
Fig. 1 a–h. Contour lines of localized SCF-MO's and some important NO's of pair functions for BeH₂.
a) Localized valence shell SCF-MO, b–c) NO's of the corresponding intrapair correlation function,
d–f) NO's of the singlett interpair correlation-function, g–h) NO's of the triplett interpair correlation
function. – The corresponding numerical values of the contour lines are: 0.0, ±0.04, ±0.064, ±0.1,
±0.16, ±0.25, ±0.4, ±0.64

BeH$_2$ NO 2 1—T   BeH$_2$ NO 2 1—T

g   h
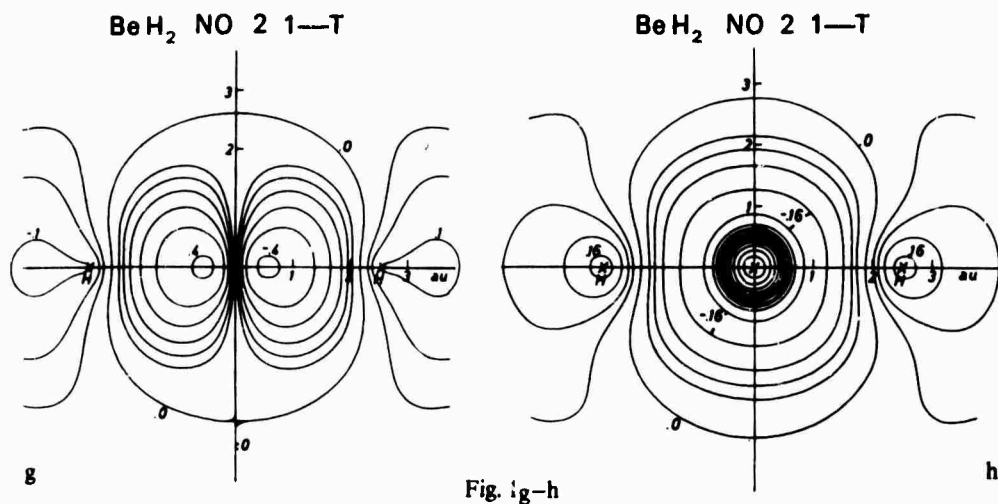
Fig. g–h
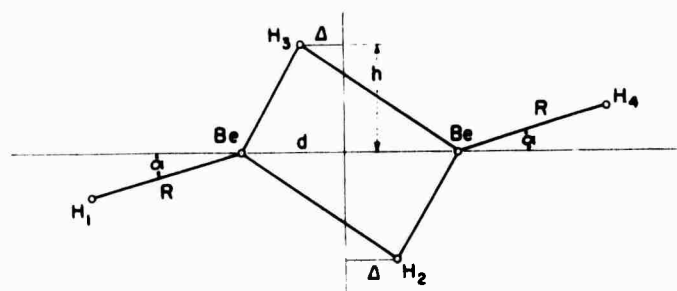
Fig. 2. Nuclear Coordinates of Be$_2$H$_4$
Equilibrium geometry: $R = 2.5$, $d_0 = 3.9$, $h_0 = 2.0$, $\Delta_0 = \alpha_0 = 0$ (in a. u.)

Table 4. HF-*energies for* Be$_2$H$_4$, *basis A*. $R = 2.5$, $\Delta = 0$, $\alpha = 0$

h \ d	2.5	3.2	3.9	4.6
1.5	− 31.3154	− 31.4409	− 31.5060	− 31.5012
2.0	−- 31.3494	− 31.5111	− 31.5448	− 31.5262
2.5	− 31.3462	− 31.4923	− 31.5200	− 31.5021

For the meaning of R, h, d, Δ, α see Fig. 2.

Only the planar configuration of Be$_2$H$_4$ was considered. The bond distance
for the terminal BeH bond was kept fixed at $R = 2.5$ a.u. as in BeH or BeH$_2$ [1].
Only SCF-energies were calculated. The basis set A was used (see Table 2) which
should contain enough flexibility to give reliable results at least for the bond
distances.

As the lowest electronic energy was expected for D_{2h} symmetry a series of
calculations for several values of d and h (see Fig. 2) was performed first. From
the results, which are given in Table 4, the following equilibirium distances have

342

Table 5. HF-*energies for* Be_2H_4, *basis A*. $R = 2.5, d = 3.9, h = 2.0$

$R \cdot \alpha$ ╲ Δ	0.0	0.2
0.0	-31.5448	-31.5418
0.1	-31.5446	-31.5410

For the meaning of R, d, h, Δ, α see Fig. 2.

been obtained:

$$d_0 = 3.9 \pm 0.2 \text{ a.u.}, \quad h_0 = 2.0 \pm 0.1 \text{ a.u.} .$$

Some results for the subsequent calculations for the lower symmetry $C_{2h}(\Delta \neq 0,$ $\alpha \neq 0$, see Fig. 2) are collected in Table 5. These did not lead to a lowering of the energy and suggest that the molecule has in fact D_{2h} symmetry.

From the values for d_0 and h_0 the H_2BeH_3 equilibrium bond angle (see Fig. 2) is calculated to be 89°. The BeH bond distance in a BeH_2Be bridge is 2.8 a.u., which is about 10% larger than the corresponding value for a terminal bond. For the B_2H_6 molecule, which should be comparable to Be_2H_4 in this context, the corresponding experimental [5] data are 97° and 12%. The slight increase of this bridge bond angle (in going from Be_2H_4 to B_2H_6) can be explained easily: with increasing nuclear charge of the first row atom the p-character of the hydrogene bond increases (in LiH a rather pure s-bond is formed whereas FH is mainly $p\sigma$ bonded) and the bond becomes more directed. Consequently the bond angles in B_2H_6 are closer to the tetrahedral angle than in Be_2H_4. For the latter molecule even a 120° bond angle could have been expected in the case of a strongly directed bond as only sp^2 hybridization is necessary.

After having determined the equilibrium geometry of Be_2H_4 further calculations were performed to obtain correlation energies and more reliable results for the SCF energy. From the experience with the BeH_2 calculations it seemed to be sufficient to use the basis A' for the treatment of correlation energies, whereas the basis set B' was taken for a more precise SCF calculation (see Table 6). The most striking fact is the relatively large deviation of SCF energies obtained with different basis sets. This effect becomes still more apparent from Table 7, where the contributions to the energy difference ΔE of the reaction $2 BeH_2 \rightarrow Be_2H_4 + \Delta E$ obtained with different basis sets are listed. The large variation of ΔE_{HF} (see Table 7) was not expected to that extent before the computations were done. This demonstrates drastically the disadvantage of small basis sets with respect to the calculation of binding energies. Nevertheless one would assume ΔE_{HF} obtained with basis set B' to be in error by not more than 0.005 a.u.

The slight decrease of the intrapair correlation energy (in going from $2 BeH_2$ to Be_2H_4) has been expected of course, since in Be_2H_4 only one $2p$-AO at each Be atom is completely available for substitutions describing electron correlation, whereas in BeH_2 there are two.

The rather large contribution of the interpair correlation to the dimerisation energy (see Table 7) is mainly due to the fact that the number of interpair con-

343

Table 6. *HF- and valence shell correlation energies of* Be_2H_4 *for the equilibrium configuration* $d = 3.9, h = 2.0$

Basis	$-E_{HF}$	$-\varepsilon_{11}$	$-\varepsilon_{22}$	$-{}^1\varepsilon_{12}$	$-{}^3\varepsilon_{12}$	$-\varepsilon_{12}$	$-{}^1\varepsilon_{23}$	$-{}^3\varepsilon_{23}$	$-\varepsilon_{23}$	$-\sum_i \varepsilon_{ii}$	$-\sum_{i<j} \varepsilon_{ij}$	$-\sum_{i\leq j} \varepsilon_{ij}$
A	31.5448	—	—	—	—	—	—	—	—	—	—	—
A'	31.5296	0.0303	0.0300	0.0011	0.0022	0.0033	0.0026	0.0048	0.0075	0.1206	0.0207	0.1413
B'	31.5726	—	—	—	—	—	—	—	—	—	—	—

ε_{ii} = intrapair correlation energy of localized pair i.

${}^1\varepsilon_{ij}$, ${}^3\varepsilon_{ij}$: singulett and triplett interpair correlation energy.

$\varepsilon_{ij} = {}^1\varepsilon_{ij} + {}^3\varepsilon_{ij}$.

(Labeling of the localized MO's corresponds to that of H-atoms in Fig. 2).

Table 7. *Contributions to the dimerisation energy of* BeH_2

Basis	ΔE_{HF}	$\Delta \sum_i \varepsilon_{ii}$	$\Delta \sum_{i\leq j} \varepsilon_{ij}$
A	-0.0214	—	—
A'	-0.0156	0.0014	-0.0101
B'	-0.0344	—	—

$\Delta E_{HF} = E_{HF}(Be_2H_4) - 2 E_{HF}(BeH_2)$

$\Delta \sum_i \varepsilon_{ii} = \sum_i \varepsilon_{ii}(Be_2H_4) - 2\sum_i \varepsilon_{ii}(BeH_2)$

$\Delta \sum_{i\leq j} \varepsilon_{ij} = \sum_{i\leq j} \varepsilon_{ij}(Be_2H_4) - 2 \sum_{i\leq j} \varepsilon_{ij}(BeH_2)$

tributions is 5 for Be_2H_4 but only one for each BeH_2. (We have not considered $\varepsilon_{14}{}^2$, because the corresponding localized MO's are not next neighbours and are separated by a distance of about 4.0 a.u. which causes ε_{14} to be very small.) The different contributions to the dimerisation energy listed in Table 7 should rather be considered as upper bounds to the exact numbers, since the basis sets were all optimized for BeH_2 and are hence more appropriate for this molecule than for Be_2H_4. Having this in mind one can estimate the dimerisation energy (see Table 8):

$$2\,BeH_2 \rightarrow Be_2H_4 + 0.05 \text{ a.u.} \pm 0.01 \text{ a.u.} (31 \pm 6 \text{ Kcal/Mol}).$$
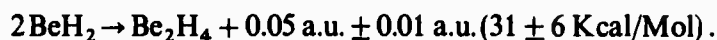
The contour lines of the localized MO's and some NO's describing the intrapair correlation of the BeHBe bridge electron pair are given in Fig. 3. The dominant feature of these plots is the good localizability of the SCF-MO's for Be_2H_4 which expains the smallness of the interpair correlation energies. Obviously only the MO's describing the bridge bonds have a considerable differential overlap which makes it understandable that ε_{23} is twice as large as ε_{12} (see Table 6). We further note, that the localized SCF-MO's describing a terminal BeH bond are almost the same in BeH_2 and Be_2H_4 (see Fig. 1, Fig. 3).

C. Be_3H_6

SCF calculations on Be_3H_6 were performed for two different molecular geometries: a linear chain (Fig. 4) and a cyclic structure (Fig. 5). No attempt was made to find out exactly the equilibrium geometry because of the relatively large amount of computer time necessary for these calculations. For the chain structure the bond distances were simply taken to be the same as found for Be_2H_4 ($d = 3.9$ a.u., $h = 2.0$ a.u., see Fig. 2 and Fig. 4). The result of the SCF calculation using basis set B' was

$$E_{SCF} = -47.3847 \text{ a.u. (chain structure)}.$$

For the cyclic structure all angles and the bond distances of the terminal BeH bonds were kept fixed but the BeHBe bridge bond distance $S = 2.74$ a.u. was obtained from a series of SCF calculations with basis set A'. The final SCF calculation with basis set B' yielded the energy

$$E_{SCF} = -47.3494 \text{ a.u. (cyclic structure)}.$$

The large difference of SCF energies in the two geometries (0.0353 a.u.) shows that the chain structure is more stable. Even by inclusion of correlation energies it is hardly conceivable the SCF energy difference is overcompensated. Consequently no further calculations on the cyclic structure were performed.

Concerning the pair correlation energies ε_{ij} of Be_3H_6 in its linear conformation it was first of all realized that the localized SCF-MO's describing a terminal BeH or a BeHBe bridge bond hardly change in going from Be_2H_4 to Be_3H_6. One would thus expect the corresponding pair correlation energies in Be_2H_4

---

[2] ε_{ij} denotes the interpaircorrelation energy between the electron pairs occupying the localized SCF-MO's i and j. The localized SCF-MO's are labeled in the same way as the H atoms (see Fig. 2) at which they are centered.
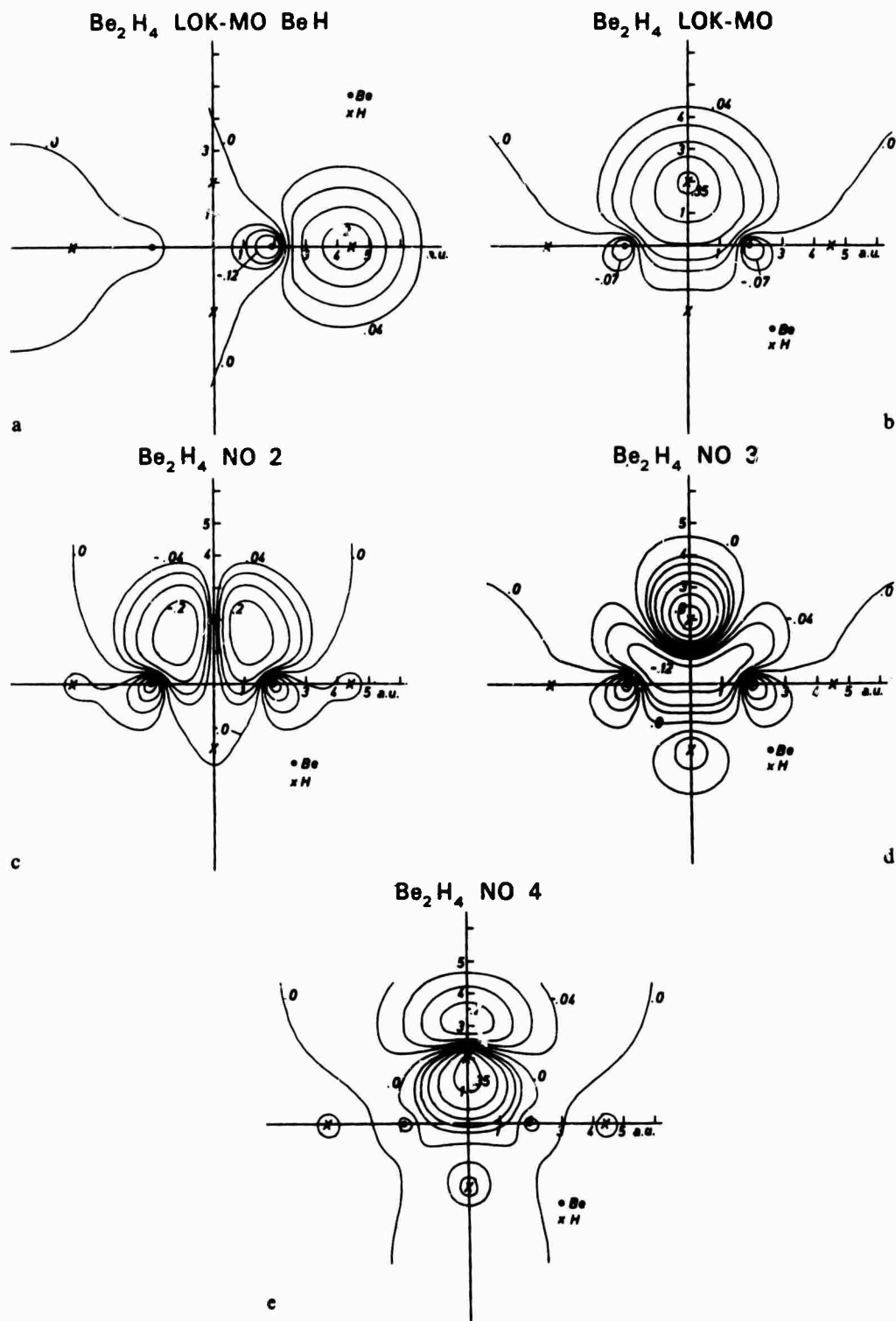
Fig. 3a–e. Contour lines of localized SCF-MO's and NO's of pair functions for Be_2H_4. a) localized SCF-MO of terminal Be-H bond. b) localized SCF-MO of Be-H-Be bridge bond. c–e) NO's of the intrapair correlation function of the Be-H-Be bridge bond pair. – The corresponding numerical values of the contour lines are: 0.0, ±0.04, ±0.07, ±0.12, ±0.2, ±0.35

25*
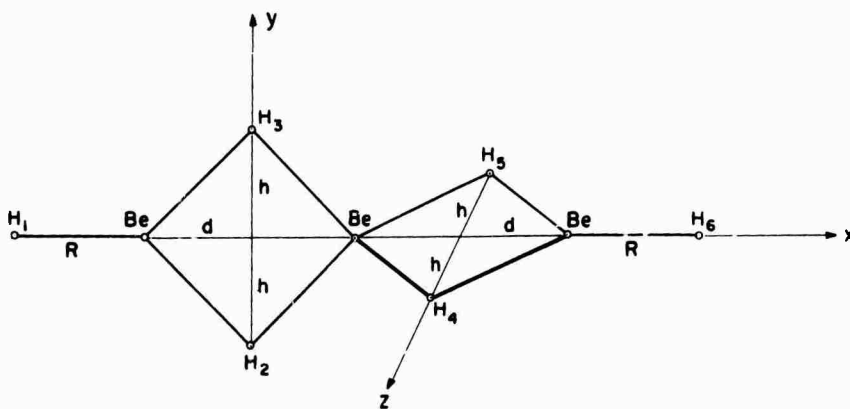
Fig. 4. Chain structure geometry of Be_3H_6
$R = 2.5$, $d = 3.9$, $h = 2.0$ (in a. u.)
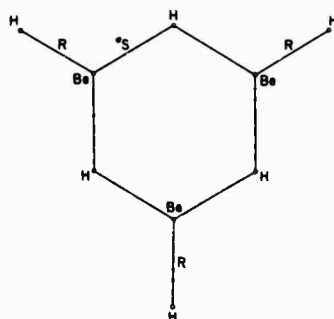
Fig. 5. Cyclic structure geometry of Be_3H_6
$S_0 = 2.74$, $R = 2.5$ (in a. u.)

and Be_3H_6 to be quite the same. This assumption was indeed confirmed by the computation of ε_{22} and ε_{23} for Be_3H_6 (using basis set A') which differ by less than 0.3% (maximal 0.0001 a.u.) from the corresponding values for Be_2H_4 listed in Table 6. Deviations of this order of magnitude are of course negligible for the purpose of the present investigation. The surprisingly good transferability of ε_{ij}'s from Be_2H_4 to Be_3H_6 furthermore is a confirmation of the original ideas of Foster and Boys [6] that properties of corresponding localized electron pairs should not change significantly in going from one molecule to another. Consequently it is not necessary to compute all ε_{ij}'s for Be_3H_6, it is sufficient to treat ε_{24} only which has no counterpart in Be_2H_4. A calculation using basis set A' gave the following results:

$$^1\varepsilon_{24} = -0.0008 \text{ a.u.}, \quad ^3\varepsilon_{24} = -0.0018 \text{ a.u.}, \quad ^1\varepsilon_{24} + {}^3\varepsilon_{24} = -0.0026 \text{ a.u.}.$$

Taking for the other pair correlation energies the corresponding ε_{ij} values from the Be_2H_4 calculation (Table 6) one obtains the following valence shell correlation energies for Be_3H_6 (in the chain structure, see Fig. 4).

$$\sum_i \varepsilon_{ii} = -0.1806 \text{ a.u.}, \quad \sum_{i<j} \varepsilon_{ij} = -0.0386 \text{ a.u.}, \quad \sum_{i \leq j} \varepsilon_{ij} = -0.2192 \text{ a.u.}$$

347

Table 8. ΔEn values (in atomic units) of the reactions $2\,BeH_2 \to Be_2H_4 + \Delta E_1$ and $Be_2H_4 + BeH_2 \to Be_3H_6 + \Delta E_2$ obtained in different approximations

	SCF[a]	% error[b]	SCF + intrapair[c]	% error[b]	total[d]	estimated
ΔE_1	0.0344	23	0.0330	26	0.0445	0.050 ± 0.010 $(31 \pm 6\,\text{Kcal/Mol})$
ΔE_2	0.0430	22	0.0420	24	0.0553	0.063 ± 0.015 $(40 \pm 10\,\text{Kcal/Mol})$

[a] From the SCF energies calculated with basis set B'.

[b] Percentage errors with respect to the total ΔE values given in Column 5.

[c] Including the valence shell intrapair correlation energies ε_{ii}.

[d] Including the total valence shell correlation energies calculated with basis A'.

(Here we have again neglected the interpair correlation energies between non-neighbouring localized SCF-MO's which are expected to be very small, see discussion above.)

In Table 8 we finally summarize the energy differences for the reactions $2\,BeH_2 \to Be_2H_4$ and $Be_2H_4 + BeH_2 \to Be_3H_6$ obtained within different approximations. The most striking effect is that inclusion of intrapair correlation gives even slightly poorer results than the SCF approximation and that about 25 % of the dimerisation and trimerisation energies are due to interpair correlation effects. The importance of the interpair correlation for the reactions considered in Table 8 is easily explained, if we observe that the number of pairs of neighbouring localized SCF-MO's which give rise to non-negligible interpair correlation energy contributions increases from 1 in BeH_2 to 5 in Be_2H_4 and to 10 in Be_3H_6. Though each individual $\varepsilon_{ij}(i \neq j)$ is rather small (compared to the ε_{ii}) the increasing number of such terms makes the interpair correlation rather important for Be_2H_4 and Be_3H_6.

4. The Polymerization Energy of the Hypothetical $(BeH_2)_\infty$ Chain

From the results reported above one can give at least a rough estimate for the energy difference ΔE_n of the reaction

$$(BeH_2)_n + BeH_2 \to (BeH_2)_{n+1} + \Delta E_n.$$
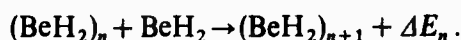
The geometry of $(BeH_2)_n$ is assumed to be that of a linear chain as in indicated for Be_3H_6 in Fig. 4. For the case $n \geq 2$ we rewrite the above reaction in the form

$$R_n BeH_2 BeH + BeH_2 \to R_n BeH_2 BeH_2 BeH + \Delta E_n$$
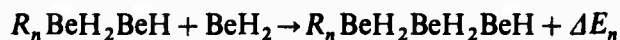
where R_n stands for $H(BeH_2)_{n-1}$. The investigations reported in the present paper have shown the shape of the localized SCF-MO's describing the BeH_2Be bridge bonds is quite the same for Be_2H_4 and Be_3H_6 and will probably not change if we go over to $(BeH_2)_n$ for general n. Consequently one would expect ΔE_n to be almost independent of n if $n \geq 2$, as the different R_n should have a rather small influence only. We arrive hence at the conclusion that the polymeriza-

tion energy of the hypothetical $(BeH_2)_\infty$ chain is approximately

$$\Delta E_n \approx -0.063 \text{ a.u. } (40 \text{ Kcal/Mol}) \ n \geqq 2,$$

which is the estimated value for E_2 given in Table 8.

The case $n=1$ is different from $n \geqq 2$ for two reasons. In the reaction $2 BeH_2 \rightarrow Be_2H_4 (n=1)$ the sp hybrid valence orbitals on each Be atom have to be promoted to sp^2 hybrids. In the case $n \geqq 2$ however one promotion from sp to sp^2 and one from sp^2 to sp^3 is involved. As the promotion from sp^2 to sp^3 requires less promotion energy than the one from sp to sp^2, it is evident that in the SCF approximation ΔE_1 is smaller than ΔE_n for $n \geqq 2$ (see Table 8).

Concerning the correlation energy contributions to ΔE_n we have already seen that the intrapair correlation has only a rather small effect on ΔE_n. The interpair correlation however is by no means negligible, which is due to the growing number of pairs of neighbouring localized SCF-MO's with increasing n. It is easily verified that for the reaction under consideration the number of pairs of neighbouring SCF-MO's increases by 3 if $n=1$ and by 4 for the case $n \geqq 2$.

5. Conclusions

The present investigations show that BeH_2 has a strong tendency to oligomerize via H bonds. The calculations performed for Be_3H_6 in a cyclic and a linear chain structure furthermore indicate that $(BeH_2)_n$ has probably a chain structure, at least if n is not too large.

From these results one can of course draw no conclusions concerning the possible crystal structures of solid BeH_2. The present results however do not contradict the assumption [17] that solid BeH_2 consists of $(BeH_2)_n$ chains (with large n) and has hence a SiS_2 like crystal structure. The estimated polymerization energy for the linear BeH_2 chain of 40 Kcal/Mol is in sufficient agreement with the cohesion energy of solid BeH_2 which has been estimated at 48 Kcal/Mol [1].

References

1. Ahlrichs, R., Kutzelnigg, W.: Theoret. chim. Acta (Berl.) **10**, 377 (1968), [Part I of this series].
2. — J. chem. Physics **48**, 1819 (1968).
3. Banford, L., Coates, G. E.: J. chem. Soc. (London) **1964**, 5591.
4. Barbaras, G. D., Dillard, C., Finholt, A., Wartik, T., Wilzbach, K. E., Schlesinger, H. I.: J. Amer. chem. Soc. **73**, 4585 (1951).
5. Bartell, L. S., Corroll, B. L.: J. chem. Physics **42**, 1135 (1965).
6. Foster, J. M., Boys, S. F.: Rev. mod. Physics **32**, 303 (1960).
7. Frost, A. A.: J. physic. Chem. **72**, 1289 (1968).
8. Goldberg, M. C., Ritter, J. R.: J. physic. Chem. **71**, 3111 (1967).
9. Harris, F. E., Michels, H. H.: Int. J. quant. Chemistry **1**, 329 (1967).

10. Hayes, E. F., Pfeiffer, G. V.: J. chem. Physics **47**, 5168 (1967).
11. Huzinaga, S.: J. chem. Physics **42**, 1293 (1965).
12. Jungen, M., Ahlrichs, R.: Theoret. chim. Acta (Berl.) **17**, 339 (1970) [Part III of this series].
13. Kutzelnigg, W., Jungen, M., Ahlrichs, R.: To be published.
14. Mounier, J.: C. R. Acad. Sc. Paris Ser. C **265**, 1261 (1967).
15. Nesbet, R. K.: Physic. Rev. **155**, 51 (1967).
16. Sinanoglu, O.: J. chem. Physics **36**, 706 (1962); **36**, 3198 (1962); Advances chem. Physics **6**, 315 (1964).
17. Wiberg, E., Bauer, R.: Z. Naturforsch. **6b**, 171 (1951).
18. Wu, A. A., Ellison, F. O.: J. chem. Physics **48**, 727 (1968).

Dr. R. Ahlrichs
Laboratory of Molecular Structure and Spectra
University of Chicago
Chicago, Illinois, USA

350

Rotational Analysis of the $C^2\Pi \to A'^2\Delta_r$ Electronic Transition
in LaO[1]

David W. Green

Laboratory of Molecular Structure and Spectra, Department of Physics

University of Chicago, Chicago, Illinois 60637

ABSTRACT

Rotational analysis of the (0,0) and (1,1) bands of two violet-degraded band systems between 6500 and 6825 Å has shown they are subbands of a $^2\Pi_r \to {}^2\Delta_r$ electronic transition. The upper state is in common with the upper state of the previously known $C^2\Pi \to X^2\Sigma^+$ transition. The transition is called $C^2\Pi_r \to A'^2\Delta_r$. The $A'^2\Delta_r$ state is probably the expected low-lying state deprived primarily from a (La dδ) molecular orbital configuration. The absolute electronic term values, T_e, of the $C^2\Pi_r$ and $A'^2\Delta_r$ state were not determined.

---

1. Presented, in part, at the Twenty-Fifth Symposium on Molecular Structure and Spectroscopy, Columbus, Ohio, 1970.

INTRODUCTION

The observed optical spectrum of LaO has bands extending from 3400 Å in the ultraviolet to 8800 Å in the near infrared[1]. Rotational analyses have been published on bands of the $A^2\Pi_r \rightarrow X^2\Sigma^+$ and $B^2\Sigma^+ \rightarrow X^2\Sigma^+$ by Åkerlind[2] and the $C^2\Pi_r \rightarrow X^2\Sigma^+$ by Carette and Blondeau[3]. Vibrational analyses of these systems and the systems designated[4] $D \rightarrow X$, $E \rightarrow$?, $F \rightarrow X$ and $G \rightarrow$? have been proposed[1, 4-7].

The ground state identification of ScO and LaO has been the subject of much discussion. The designations from rotational analyses for ScO[8], YO[9], and LaO[2] were originally $X^4\Sigma^+$, $X^2\Sigma^+$, and $X^4\Sigma^+$ respectively. The $A^2\Pi_r$ and $B^2\Sigma^+$ states of these three molecules are at similar energies relative to the X states as shown in Fig. 1. The rotational analyses show a correspondence of the other characteristics (spin-orbit splitting, spin-spin splitting, internuclear distance and Λ-doubling) of the A and B states among these three molecules. The expected similarity of electronic structure, the experimental similarity of the corresponding excited states and the difficulty of assigning a reasonable molecular orbital configuration to a low-lying $^4\Sigma^+$ state make the different X state assignments questionable.

The X state assignment of LaO has been criticized[10, 11] and a revision[12, 13] to $^2\Sigma^+$ with hyperfine splitting has been proposed. This reassignment is consistent with the reassignment[14] of the ScO X state as $^2\Sigma^+$.

It is expected that a $^2\Delta_r$ electronic state, primarily from the metal dδ molecular orbital, should be low-lying in these three molecules. This $^2\Delta$ state was proposed as the expected ScO ground state[15] although

more recent calculations[16] show it to be about 0.9 eV below the $A^2\Pi$ state. The correspondence of analysed LaO and ScO electronic states would suggest a low-lying $^2\Delta$ state in LaO.

Knowledge of the characteristics of this $^2\Delta$ is important to an understanding of the molecular electronic structure, yet no information is available about the energies of states from $d\delta$, $d\pi$ and $d\sigma$ orbitals for LaO[17]. A transition between the $^2\Delta$ and the $X^2\Sigma^+$ state is forbidden, but emission from excited $^2\Pi$ states should be allowed[18]. It was with this possibility in mind that a high resolution investigation of the "E" and "G" systems of LaO was undertaken.

EXPERIMENTAL

The LaO source was a reduced pressure arc between a lanthanum anode and copper cathode. Both electrodes were attached to brass water-colled holders tapered to fit ground glass joints. The distance between electrodes could be adjusted during operation. The arc was found to operate best in an atmosphere of about one Torr air and ten Torr oxygen. The use of this source decreased the observed line widths considerably from those obtained using an atmospheric pressure arc source.

The arc was in series with ballast resistors and a 220 volt dc power supply. Currents of about 1.5 Å were used.

Light from the arc was focused onto the slit of a predisperser which utilized a fused-silica Pellin-Broca prism. Dispersed light from the predisperser was focused onto the slit of a 3.4 m Ebert spectrograph. Both the "E" and "G" systems of LaO were photographed in the ninth-order on Kodak 103 a-F spectroscopic plates. Overlapping orders were entirely eliminated by the predisperser. Exposure times of about one hour were required for both systems. The reciprocal linear dispersion in ninth-order was 0.4-0.5 Å/min.

An electrodeless discharge in a fused-silica tube containing ThI_4 produced the thorium atomic spectrum which was used as the standard line source. The ninth-order Th spectrum was overlapped with the "E" system and the eleventh-order with the "G" system. Only interferometrically measured Th line wavelengths proposed as secondary standards were used to reduce the data[19].

Line positions were measured from the plates with a photoelectric

354

comparator. The Th line positions and known wavelengths were least-squares fitted by a computer program using a cubic polynomial. The standard air wavelength and vacuum wavenumbers of the LaO features were determined from the polynomial coefficients. The refractive index parameters of air were measured during the course of an exposure and were taken into account by the computer program using the formulas of Edlen[20].

RMS errors of fitting of the Th line wavelengths, errors due to comparator measurements, errors due to refractive index parameter variations and the RMS error among different measurements were all less than 0.01 cm^{-1} in ninth-order. The primary uncertainty in the reported frequencies of the LaO rotational lines is due to blending and the line widths.

ELECTRONIC ASSIGNMENT

Between the red-degraded bands of the $A^2\Pi_r \to X^2\Sigma^+$ and the $B^2\Sigma^+ \to X^2\Sigma^+$ transitions, weaker violet-degraded bands are evident. These bands have been classified into two systems[1, 4] designated "G $\to$?" and "E $\to$?". The proposed (0,0) heads of the "G" system are at 6825.5 and 6814.0 Å and those of the "E" system at 6607.73 and 6605.12 Å. The hypothesis[1] that the $X^2\Sigma^+$ state is the lower state of these systems is incorrect as shown immediately in high resolution by the absence of the characteristic hyperfine doubling of the $X^2\Sigma^+$ state.

A closer examination of the bands shows that the "E" system has two P heads per vibrational band and that both the "E" and "G" sytems have strong Q branches. The analysis reported here demonstrates that the two P branches of the "E" system arise from a large Λ-doubling. This doubling indicates a $^2\Pi$ state is involved in the transition. The strong Q branches observed eliminate a second $^2\Pi$ as the other state of the transition. The two P heads per band of the "E" system eliminate a $^2\Sigma$ as the second state of the transition because symmetry selection rules prevent both Λ-doublet components of the $^2\Pi$ from combining with a $^2\Sigma$ at the same rotational level[18].

So the "E" transition is either $^2\Pi \to {}^2\Delta$ or vice versa. Analysis of the "G" system gives lower state first difference values, $\Delta_1 F_v''(J)$, which are similar to those of the "E" system and which show no Λ-doubling. This would not be possible if the $^2\Pi$ state were the lower state with the observed large Λ-doubling. The "E" system is assigned as a $^2\Pi_{1/2} \to {}^2\Delta_{3/2}$ subband and the "G" system as $^2\Pi_{3/2} \to {}^2\Delta_{5/2}$ subband since

the Λ-doubling of a $^2\Pi_{1/2}$ should be very much larger than that of a $^2\Pi_{5/2}$. Both states are in Hund's coupling case a. Figure 2 shows schematically the first lines of the expected branches of this electronic transition with Λ-doubling resolved in the $^2\Pi$ state but not in the $^2\Delta$. Henceforth the $^2\Pi$ and $^2\Delta$ electronic states of this transition will be referred to as the $C^2\Pi$ and $A'^2\Delta$ (see Addendum). A portion of the $C^2\Pi_{1/2} \rightarrow A'^2\Delta_{3/2}$ transition is shown in Figure 3.

ANALYSIS METHODS

The term-energy exclusive of electronic and vibrational energies for a $^2\Pi_r$ state may be written as

$$F'_{1c}(J) = B'_1 J(J + 1) - D'_1 J^2(J + 1)^2 + \epsilon'_1(J)/2, \qquad (1a)$$

$$F'_{1d}(J) = B'_1 J(J + 1) - D'_1 J^2(J + 1)^2 - \epsilon'_1(J)/2, \qquad (1b)$$

$$F'_{2c}(J) = B'_2 J(J + 1) - D'_2 J^2(J + 1)^2 + \epsilon'_2(J)/2, \qquad (1c)$$

$$F'_{2d}(J) = B'_2 J(J + 1) - D'_2 J^2(J + 1)^2 - \epsilon'_2(J)/2, \qquad (1d)$$

where (1a) and (1b) refer to the $^2\Pi_{1/2}$ sublevel and (1c) and (1d) to the $^2\Pi_{3/2}$ sublevel; $\epsilon(J)$ represents the Λ-doubling and the primes indicate that the $^2\Pi$ is the upper state. An accurate evaluation of the Λ-doubling of a $^2\Pi$ state requires a knowledge of its interaction with all $^2\Sigma$ states of the molecule[21, 22]. This information is not available for LaO and it is assumed for the purpose of analysis that the Λ-components are equally and oppositely affected.

The Λ-doubling should be small in a $^2\Delta$ state[18, 21] especially one derived from a dδ orbital. If we assume that it is negligibly small, the term energy may be written as

$$F''_1(J) = B''_1 J(J + 1) - D''_1 J^2(J + 1)^2, \qquad (2a)$$

$$F''_2(J) = B''_2 J(J + 1) - D''_1 J^2(J + 1)^2. \qquad (2b)$$

where (2a) and (2b) refer to the $^2\Delta_{3/2}$ and $^2\Delta_{5/2}$ sublevels, respectively, and the double primes indicate that the $^2\Delta$ is the lower state.

All term energies depend on the vibration quantum number but this dependence will not be explicitly included in the nomenclature used here. The frequencies of rotational lines shown in Figure 2 are

358

appropriate differences of rotational, vibrational and electronic term energies.

The rovational constants, B, of the sublevels are related.

$$B_1' = B'(1 - B'/A'), \qquad (3a)$$

$$B_2' = B'(1 + B'/A'), \qquad (3b)$$

$$B_1'' = B''(1 - B''/2A''), \qquad (3c)$$

$$B_2'' = B''(1 + B''/2A''). \qquad (3d)$$

In this work the rotational analysis of the two subbands was done independently and Eq. (3) was used to determine whether the states are regular or inverted.

The theoretical expressions for $\epsilon(J)$ reduce to the following forms for the $^2\Pi_{1/2}$ and $^2\Pi_{3/2}$[21, 22] in Hund's coupling case a.

$$\epsilon_1'(J) = a_0(J + 1/2) + a_1(J + 1/2)(J + 3/2)(J - 1/2), \qquad (4a)$$

$$\epsilon_2'(J) = a_2(J + 1/2)(J + 3/2)(J - 1/2). \qquad (4b)$$

It is expected that a_1 and a_2 will be very much smaller than a_0[22]. The sign of the Λ-doubling coefficients cannot be obtained solely from the analysis of a $^2\Pi \rightarrow {}^2\Delta$ transition. The coefficients a_0 and a_2 are arbitrarily assumed positive and the sign of a_1 follows from that of a_0. Experimental values of $\epsilon(J)$ are obtained as follows:

$$\epsilon_1'(J) = Q_{1c}(J) - Q_{1d}(J), \qquad (5a)$$

$$= R_{1c}(J - 1) - R_{1d}(J - 1), \qquad (5b)$$

$$= P_{1c}(J + 1) - P_{1d}(J + 1). \qquad (5c)$$

359

A similar set of expressions holds for $\epsilon_2'(J)$.

Rotational constants, B and D, were obtained by least-squares fitting an equation of the following form for both electronic states.

$$y_1 = c_o + c_1 x_1, \tag{6}$$

where

$$y_1 = \frac{\Delta_1 F(J)}{2(J + 1)} \qquad x_1 = -2(J + 1)^2.$$

The values of c_o and c_1 obtained from the least-squares fit analysis are then equal to the rotational spectroscopic constants B and D.

For the $A'^2\Delta$ state with no Λ-doubling the experimental values of $\Delta_1 F''(J)$ were obtained from the observed frequencies as follows:

$$\Delta_1 F_1''(J) = R_{1c}(J) - Q_{1c}(J + 1), \tag{7a}$$

$$= R_{1d}(J) - Q_{1d}(J + 1), \tag{7b}$$

$$= Q_{1c}(J) - P_{1c}(J + 1), \tag{7c}$$

$$= Q_{1d}(J) - P_{1d}(J + 1). \tag{7d}$$

A similar set of equations holds for $\Delta_1 F_2''$.

For the $C^2\Pi$ upper state where Λ-doubling is observed, a modified procedure must be used. In this work the Λ-doubling $\epsilon'(J)$, was evaluated first from Eq. (5) by least-squares fitting the observed data to the appropriate form expected for $\epsilon'(J)$ [see Eq. (4)]. The values of $\Delta_1 F_1'(J)$ and $\Delta_1 F_2'(J)$ were then obtained by adjusting the observed branch differences using the computed $\epsilon'(J)$ value. This procedure avoids the additive uncertainties of obtaining first difference values directly using four observed frequencies.

$$\Delta_1 F_1'(J) = R_{1c}(J) - Q_{1c}(J) - \Delta\epsilon_1'(J)/2, \tag{8a}$$

$$= Q_{1c}(J + 1) - P_{1c}(J + 1) - \Delta\epsilon_1'(J)/2, \tag{8b}$$

$$= R_{1d}(J) - Q_{1d}(J) + \Delta\epsilon_1'(J)/2, \tag{8c}$$

$$= Q_{1d}(J + 1) - P_{1d}(J + 1) + \Delta\epsilon_1'(J)/2, \tag{8d}$$

where $\Delta\epsilon_1'(J) = [\epsilon_1'(J + 1) - \epsilon_1'(J)]$. A similar set of equations apply for $\Delta_1 F_2'(J)$. The rotational spectroscopic constants, B and D, were obtained for the $C^2\Pi$ state using Eq. (6).

The band origins $\nu^{(1)}$ and $\nu^{(2)}$ of the $^2\Pi_{1/2} \rightarrow {}^2\Delta_{3/2}$ and $^2\Pi_{3/2} \rightarrow {}^2\Delta_{5/2}$ subbands, respectively, are most accurately obtained by a least-squares quadratic fit of the lines of the P and R branches. The P_c and R_d lines fit a single equation in m (m = -J for the P branch; = J + 1 for the R branch) as do the P_d and R_c lines. The origin is the calculated position of the hypothetical line, m = 0, with a small correction applied for Λ-doubling.

For each vibrational band of each subband the value of the rotational constants B and D may be obtained from the experimental data. The values of $B(v)$ and $D(v)$ of each electronic state are derived from Eq. (3) for each vibrational level.

The dependence of $B(v)$ and $D(v)$ on the vibrational quantum number may be accurately approximated as follows for small quantum numbers.

$$B(v) = B_e - \alpha_e(v + 1/2) \tag{9}$$

$$D(v) = D_e + \beta_e(v + 1/2). \tag{10}$$

The (0,0) and (1,1) bands analysed in this work are sufficient to determine the spectroscopic constants α_e, β_e, B_e, D_e and the value of the equilibrium internuclear distances, r_e.

361

RESULTS

About five lines were measured for each 1.0 cm^{-1} over the range of the bands studied. This high density of lines combined with the observed line width makes assignment of some high and low J lines difficult. In many cases a line was observed near the expected frequency but was too strong or asymmetric. Assignment of lines was based on (1) comparison of the observed frequency of a line with that calculated from a fit of other lines in the same branch; (2) the qualitative intensity; (3) comparison of the observed Λ-doubling to that calculated from a fit of all observed lines; (4) most importantly, comparison of the first difference value, $\Delta_1 F(J)$, with that calculated from all the observed lines.

Table I contains those frequencies (in cm^{-1}) of lines of branches of the (0,0) band of the $C^2\Pi_{1/2} \to A'^2\Delta_{3/2}$ subband that are consistent with the requirements used above. Table II contains the frequencies of lines of branches of the (0,0) band of the $C^2\Pi_{3/2} \to A'^2\Delta_{5/2}$ subband. Further lines, especially of the Q type branches, were observed but are not reported because no check for consistency with other branches was available (i.e. no $\Delta_1 F(J)$ value could be obtained). The reported frequencies are the results of three independent measurements.

Table III and IV report the observed frequencies of the (1,1) bands of each subband. A large number of these lines are either totally obscured or blended, however there are enough lines to complete an analysis. No analysis of the (2,2) bands was attempted.

362

The strong La atomic spectrum overlaps the calculated frequency of some lines and those lines are indicated by "a" in Tables I-IV. Lines whose measured frequency is used for more than one assignment are indicated by "b" after the reported frequency. Lines overlapped by an apparent band head are indicated by "h". Lines whose calculated frequency is obscured by other LaO features and could not be accurately measured are omitted from the tables.

Special attention should be called to some systematic blends. The unresolved Λ-doublets at low J of the $C^2\Pi_{3/2} \rightarrow A'^2\Delta_{5/2}$ subband are not indicated as blends in Tables II and III. Lines of some P branches at low J going to the band head are systematically blended with those at higher J coming away from the head. The Q_{1c} and Q_{1d} branches are blended at low J where the Λ-doubling is nearly equal to the branch spacing.

Qualitative reasons for all the unreported (obscured) lines of the (0,0) bands (Tables I and II) were evident from an examination of a microdensitometer tracing with the exception of $R_{1d}(56.5)$. No confirmation of a perturbation was possible from the Q and P branches. No other evidence of perturbation was observed in the (0,0) band although the large number of blends prohibits a thorough evaluation. No information about possible perturbation in the (1,1) band could be obtained.

The rotational spectroscopic constants derived from the analysis of lines are reported in Table V, the Λ-doubling coefficients of the $C^2\Pi$ state (see Eq. 4) in Table VI and the (0,0) and (1,1) subband

origins in Table VII.

The relationship of the B values of the subbands [see Eq. (3)] indicates both the $C^2\Pi$ and $A'^2\Delta$ are regular states.

DISCUSSION

The vibrational quantum number assignments for the $C^2\Pi \rightarrow A'^2\Delta$ bands analysed in this work are unlikely to be incorrect for the following reason. The bands of the (0,0) sequence of the $B^2\Sigma^+ \rightarrow X^2\Sigma^+$ transition are much stronger[1, 7] than those of the (0,1) or (1,0) for small v. The equilibrium internuclear distances of 1.855 and 1.825 Å for the B and X states are not as close as the r_e values of the C and A' states (see Table V). The Franck-Condon factors for small v depend on the difference in r_e between states of the transition so it would be expected that the (0,0) sequence should be stronger than other sequences of the $C^2\Pi \rightarrow A'^2\Delta$ transition. Other bands of this transition should also be violet-degraded. The bands analysed in this work are the strongest violet-degraded bands of this spectral region[1]. So, in agreement with previous assignments[1, 4, 7] the bands are assigned to the (0,0) sequence.

The hypothesis that the unanalysed ultraviolet bands of LaO (called[1] D → X? and F → X?) may be the subbands of the $C^2\Pi_r \rightarrow X^2\Sigma^+$ transition is seen to be incorrect from a calculation of rotational lines using the spectroscopic constants of the $X^2\Sigma^+$ state[2] and the

$C^2\Pi$ state (Table V). Both ultraviolet transitions have the $X^2\Sigma^+$ as the lower state as is evident from the characteristic hyperfine splitting (0.48 cm^{-1}) of the band heads[23]. However, the calculated (0,0) and (0,1) band heads of the $C^2\Pi \rightarrow X^2\Sigma^+$ are degraded to longer wavelengths contrary to what is observed for the "D $\rightarrow$ X" and "F $\rightarrow$ X".

The analysis of the $A'^2\Delta_r$ state gives the first experimental information on a $^2\Delta$ in ScO, YO, or LaO. It is expected that this state is derived primarily from a La dδ molecular orbital although no final correlation can be made until the electronic energy, T_e, is known. It is the dδ $^2\Delta$ state of ScO which is calculated[16] to be below the $A^2\Pi$ with $^2\Delta$ states from other configurations at much higher energy.

The spectroscopic states[24] from the atomic d^{2}s and ds^2 configurations for Sc, Y, and La are shown in Figure 4. It is expected that this near degeneracy of atomic s and d orbitals will lead to low-lying $^2\Sigma^+$ and $^2\Delta_r$ electronic states in the diatomic oxides. The ScO calculations[16] and experimental analysis[14] show that the lowest $^2\Sigma^+$, $^2\Pi_r$ and $^2\Delta_r$ states may be approximated as being derived from a core of closed shells with a single unpaired electron (sδ, pπ or dδ orbital) centered on the metal atom (see Figure 1). The calculated electronic distribution of ScO at the equilibrium internuclear distance shows a considerable ionic character. Figure 5 shows that the d-orbital is lowered in energy relative to the s orbital as charge is removed from the metal atom. Data for Figure 5 were obtained from the atomic energy levels[25] using the "center of gravity" for the

configurations which yield more than one spectroscopic state. From these considerations it seems likely that both the $X^2\Sigma^+$ and $A'^2\Delta_r$ should be very low-lying states of ScO, YO and LaO.

Matrix isolation of ScO, YO, and LaO[25] and molecular beam work on LaO[26] give strong evidence that the $X^2\Sigma^+$ state is the molecular ground state. Therefore, on the basis of (1) the nature of the molecular orbitals of ScO, YO, and LaO, (2) the near degeneracy of the s and d metal orbitals, and (3) the experimental evidence that the $X^2\Sigma^+$ is the lowest energy electronic state, it is concluded that the $^2\Delta_r$ must be higher in energy but near the $X^2\Sigma^+$ state.

CONCLUSIONS

Nearly all observed LaO bands[1], with the exception of the ultraviolet bands "D → X" and "F → X", can now be assigned to transitions between rotationally analysed electronic states. The lower state of the $C^2\Pi_r \rightarrow A'^2\Delta_r$ transition probably corresponds to the $^2\Delta_r$ expected from the low-lying dδ orbital located primarily on the metal atom. Although the electronic energy of the $A'^2\Delta_r$ state could not be determined in this work, there is evidence that it should be near to the $X^2\Sigma^+$ state.

ADDENDUM

In work done subsequent to the submission of this paper for publication, it has been determined that the reported[3] $C^2\Pi \rightarrow X^2\Sigma^+$ analysis of LaO needs modification. The $C^2\Pi$ state is the upper state of the transition reported in this paper as well as of the $C \rightarrow X$ transition.

In light of this information, portions of the DISCUSSION Section of this paper are no longer applicable. The nomenclature of the upper state in this paper has been made consistent with this information. Justification of the $C^2\Pi$ revision and a complete reanalysis of the $C^2\Pi \rightarrow X^2\Sigma^+$ transition will be presented in detail later.

ACKNOWLEDGMENT

368

REFERENCES

1. A. Gatterer, J. Junkes, E. W. Salpeter, and B. Rosen, "Molecular Spectra of Metallic Oxides," Specola Vaticana, Vatican City, 1957.

2. L. Åkerlind, Ark. Fys. 22, 65 (1962).

3. P. Carette and J. Blondeau, C. R. Acad. Sci. Ser. B. 268, 1743 (1969); P. Carette, These, Univ. de Lille, 1969.

4. S. Hautecler and B. Rosen, Bull. Cl. Sci. Acad. Roy. Belg. 45, 790 (1959).

5. W. Jevons, Proc. Phys. Soc. London 41, 520 (1929).

6. L. W. Johnson and R. C. Johnson, Proc. Roy. Soc. London, Ser. A. 133, 207 (1931).

7. W. F. Meggers and J. A. Wheeler, Bur. Stand. U.S.J. of Res. 6, 239 (1931).

8. L. Åkerlind, Ark. Fys. 22, 41 (1962).

9. U. Uhler and L. Åkerlind, Ark. Fys. 19, 1 (1961).

10. R. A. Berg, L. Wharton, W. Klemperer, A. Buchler, and J. L. Stauffer, J. Chem. Phys. 43, 2416 (1965).

11. C. K. Jørgensen, Mol. Phys. 7, 417 (1963).

12. R. Bacis, C. R. Acad. Sci. Ser. B. 266, 1071 (1968).

13. P. H. Kasai and W. Weltner, J. Chem. Phys. 46, 3172 (1967).

14. A. Adams, W. Klemperer, and T. M. Dunn, Can. J. Phys. 46, 2213 (1968).

15. R. A. Berg and O. Sinanoglu, J. Chem. Phys. 32, 1082 (1960).

16. K. D. Carlson, E. Ludena, and C. Moser, J. Chem. Phys. 43, 2408 (1965).

17. C. J. Cheetham and R. F. Barrow, "Advances in High Temperature Chemistry," (L. Eyring, Ed.), p. 30, Academic Press, New York, 1967.

18. G. Herzberg, "Molecular Spectra and Molecular Structure of Diatomic Molecules," 2nd Ed., D. Van Nostrand, Princeton, New Jersey, 1950.

19. A. Giacchetti, R. W. Stanley, and R. Zalubas, J. Opt. Soc. Amer. 60, 474 (1970).

20. B. Edlen, Metrologia $\underline{2}$, 71 (1966).

21. L. Kovacs, "Rotational Structure in the Spectra of Diatomic Molecules," American Elsevier, New York, 1969.

22. R. S. Mulliken and A. Christy, Phys. Rev. $\underline{38}$, 87 (1931).

23. D. W. Green, unpublished results.

24. C. E. Moore, "Atomic Energy Levels," in Vol. I, II, and III, Nat. Bur. Stand. U. S. Circ. 467, 1949, 1952, and 1958.

25. P. H. Kasai and W. Weltner, J. Chem. Phys. $\underline{43}$, 2553 (1965); $\underline{46}$, 3172 (1967).

26. L. Brewer and R. M. Walsh, J. Chem. Phys. $\underline{42}$, 4055 (1965).

Table I. Rotational lines of $C^2\Pi_{1/2} \to A'^2\Delta_{3/2}$ (0,0) sub-band

J	$P_{1c}(J)$	$P_{1d}(J)$	$Q_{1c}(J)$	$Q_{1d}(J)$	$R_{1c}(J)$	$R_{1d}(J)$
9.5			15151.32b	15150.25b		
10.5			51.55b	50.38b		
11.5			51.96b	50.51b		
12.5			52.21b	50.62b		
13.5			52.49b	50.76b		
14.5	15141.85b		52.74b	50.94b		
15.5	41.43b	15139.49b	53.02b	51.14b		
16.5	41.04b	38.92b	53.30b	51.32b	15166.26	15164.88
17.5	40.61b	38.43b	53.64b	51.74b		65.80b
18.5	40.26b	37.95b	54.09b	51.96b	68.32	66.67b
19.5	39.91b	37.49b	54.67b	52.21b		67.61
20.5	39.54b	37.04b	54.97	52.49b	71.48t	68.54b
21.5	39.21b	36.49b	55.77	52.74b	72.53b	69.50b
22.5	38.92b	36.03b	56.17	53.02b	73.60	
23.5	38.59b	35.65b	56.60	53.30b		71.48b
24.5	38.30b	35.25b	57.01	53.64b		
25.5	38.01b	34.89	57.47	54.09b	75.82b	73.52
26.5	37.76b	34.51	58.42	54.67b	76.97	74.53
27.5	37.49b	34.14	58.91	55.07		75.52b
28.5	37.27b	33.78	59.40	55.45		
29.5	37.04b	33.45	59.94	55.84		77.63
30.5	36.84b	33.12	60.46	56.23	80.43	78.72
31.5	36.64b	32.81	60.95	56.66	81.66b	79.81b
32.5	36.49b	32.51	61.50	57.09	82.35	80.98
33.5	36.30b	32.22	62.12	57.54	84.00b	82.07
34.5	36.13b	31.95	62.69	58.02	85.29	83.19
35.5	36.03b	31.69	63.28	58.52	86.47b	
36.5	35.88b	31.46	63.89	58.98	87.75	85.49b
37.5	35.75b	31.23	64.51	59.49	89.04b	86.64
38.5	35.65b	31.00	65.14	60.03	90.27b	87.83
39.5		30.82	65.80b	60.56	91.53b	89.04b
40.5		30.64	66.47	61.10	92.91	90.27b
41.5		30.43b	67.14	61.68	94.19	91.53b
42.5		30.28b	67.83	a	95.51b	92.74b
43.5		30.13b	68.54b	62.85	a	93.97
44.5		30.01b	69.27	63.42		95.27
45.5		29.88b	69.99	64.05	99.57	a
46.5			70.71	64.68	201.01	97.83b
47.5			71.48b	65.33	02.33	99.13
48.5			72.26	66.00	03.76b	200.50
49.5			73.04	66.67b	05.22	01.80b
50.5			73.85	67.37	06.65b	03.17
51.5			74.67	68.05	08.07	04.50
52.5	35.65		75.52b	68.77	09.54	05.85
53.5	35.75		76.33	69.50	11.02	07.26
54.5	35.88		77.19	70.24	12.50	
55.5	36.03		78.06	70.99	14.00b	
56.5	36.13				15.53	
57.5	36.30				17.04b	
58.5	36.49				18.58	
59.5	36.64				20.18	

a-overlapped by atomic line; b-blended with LaO line; h-overlapped by band head.

Table I. (cont.)

J	$P_{1c}(J)$	$P_{1d}(J)$	$Q_{1c}(J)$	$Q_{1d}(J)$	$R_{1c}(J)$	$R_{1d}(J)$
60.5	15136.84b	15129.88b	15178.94	15171.77	15221.75	15214.38b
61.5	37.04b	30.01b	79.81b	72.53b	23.29	15.91
62.5	37.27b	30.13b	80.73	73.34	24.87	17.34
63.5	37.49b	30.28b	81.56b	74.16	26.49	18.87
64.5	37.76b	30.43b	82.61	74.98	28.10	20.37
65.5	38.01b	30.60	83.55	75.82b	29.75b	21.93
66.5	38.30b	30.77	84.49	76.68		23.43
67.5	38.59b	30.98	85.49b	77.57		25.02
68.5	38.92b	31.19	86.47b	78.42	34.74	26.60
69.5	39.21b	31.42	87.48	79.31	36.42	
70.5	39.54b	31.65	a	80.19	38.13	29.75b
71.5	39.91b	31.89	89.52	81.15	39.82	31.35
72.5	40.26b	32.16	90.58	82.07	41.54	32.97
73.5	40.61b	32.45	91.62	83.02	43.29	34.59
74.5	41.04b	32.75	92.74b	84.00b	45.07	36.22
75.5	41.43b	33.05	93.78	84.96	46.84	37.91
76.5	41.85b	33.39	94.90	85.97	48.57	39.58
77.5	42.31	33.72	96.01	86.99	50.39	41.28
78.5	42.74	34.09	97.12	88.00	52.20	42.93
79.5	43.20	34.45	98.28	89.04b		44.68
80.5	43.68	34.85	99.46	90.08		46.39
81.5	44.20	35.25b	200.59	91.11	55.88	48.13
82.5	44.68	35.65b	01.80b	92.22	57.70	49.89
83.5	45.29	36.03b	02.97	93.30	59.57	51.69
84.5	45.73	36.49b	04.18	94.41	61.42	53.41
85.5	46.28	37.04b	05.39	95.51b	63.30	55.24
86.5	a	37.49b	06.65b	a	65.21	57.05
87.5	47.43	37.95b	07.90	97.83b	67.14	58.85
88.5	48.01	38.43b	09.15	98.96	69.07	60.71
89.5	48.62	38.92b	10.45	200.14	70.99	62.52
90.5	49.23	39.49b	11.74	01.33	72.96	
91.5		40.01	13.04	02.53	74.90	
92.5	50.51	40.61	14.48b	03.76b	76.87	66.27
93.5		41.13	15.72	04.97		68.15
94.5		41.75	17.04b	06.23		70.06
95.5		42.31	18.41	07.48		71.93
96.5		42.95	19.80	08.77		73.91
97.5		43.61	21.15	10.05		75.84
98.5			22.54	11.38		77.80
99.5		44.91	24.02	12.64	80.89	79.76
100.5		45.60	25.43	14.00b	82.87	81.73
101.5		46.28	26.88	15.34	84.93	83.75
102.5			28.34	16.68	86.97	
103.5		a		18.07	89.01	85.78
104.5		47.71	32.79	19.50		89.79
105.5		48.45	34.30	20.85		91.86
106.5		49.23	35.83	22.30		93.93
107.5				23.68		96.02

a-overlapped by atomic line; b-blended with LaO line; h-overlapped by band head.

Table II. Rotational lines of $C\,^2\Pi_{3/2} \rightarrow A'\,^2\Delta_{5/2}$ (0,0) sub-band.

J	P₂c(J)	P₂d(J)	Q₂c(J)	Q₂d(J)	R₂c(J)	R₂d(J)
4.5	14668.20b	14668.20b				
5.5	67.59b	67.59b				
6.5	67.00b	67.00b				
7.5	66.36b	66.36b				
8.5	65.81b	65.81b				
9.5	65.25b	65.25b				
10.5	64.71b	64.71b				
11.5	64.19b	64.19b				
12.5	63.67b	63.67b				
13.5	63.17b	63.17b	14672.65	14672.65		
14.5	62.69b	62.69b	72.89	72.89		
15.5	62.24b	62.24b	73.11	73.11		
16.5	61.78b	61.78b	73.37	73.37		
17.5	61.35b	61.35b	73.64	73.64		
18.5	60.93b	60.93b	73.92	73.92		
19.5	a	a	74.21	74.21	14687.56	14687.56
20.5	60.14	60.14	74.53	74.53	88.63b	88.63b
21.5	59.77	59.77	74.86	74.86	89.64	89.64
22.5	59.41	59.41	75.19	75.19	90.65	90.65
23.5	59.07	59.07	75.55	75.55	91.68b	91.68b
24.5	58.74	58.74	75.92	75.92	92.74	92.74
25.5	58.43	58.43	76.30	76.30	93.83	93.83
26.5	58.13	58.13	76.71	76.71	94.91b	94.91b
27.5	57.84	57.84	77.12	77.12	96.02	96.02
28.5	57.57	57.57	77.57	77.57	97.11	97.11
29.5	57.32	57.32	78.03	78.03	98.26	98.26
30.5	57.09	57.09	78.48	78.48	99.36b	99.36b
31.5	56.87	56.87	78.95	78.95	700.55	700.55
32.5	56.66	56.66	79.45	79.45	01.77	01.77
33.5	56.47	56.47	79.96	79.96	02.90	02.90
34.5	56.30	56.30	80.49	80.49	04.13b	04.13b
35.5	56.13	56.13	81.03	81.03	05.40b	05.40b
36.5	55.98	55.98	81.58	81.58	06.59	06.59
37.5	55.86	55.86	82.15	82.15	07.86	07.86
38.5	55.73	55.73	h	h	09.14	09.14
39.5			83.36	83.36	10.38b	10.38b
40.5			83.94	83.94	11.73	11.73
41.5			84.60	84.60	13.00	13.00
42.5			85.20	85.20	14.30	14.30
43.5			85.87	85.87	15.69	15.69
44.5			86.55	86.55	17.01	17.01
45.5			87.24	87.24	18.37b	18.37b
46.5			88.03	87.94	19.80	19.80
47.5			88.73	88.63b	21.21b	21.21b
48.5			89.43	89.38	24.08	22.55
49.5			90.21	90.15	25.57	23.97
50.5			90.97	90.88		25.43
51.5			91.77	91.68b	28.41	26.87
52.5			92.57	92.45	29.95	29.88
53.5			93.37	93.27		31.35

a-overlapped by atomic line; b-blended with LaO line; h-overlapped by band head.

Table II. (cont.)

J	P'₂c	P₂d(J)	Q₂c'(J)	Q₂d(J)	R₂c(J)	R₂d(J)
54.5			14694.21	14694.08	14732.00	14732.86
55.5			95.06	94.91b	34.33	34.36b
56.5			95.94	95.77	36.06	
57.5			95.79	96.65	37.66	37.47
58.5			97.69	97.53		39.08
59.5			98.61	98.42	40.79b	40.68
60.5			99.54	99.36b		
61.5			700.47	700.28	44.10	43.90
62.5			01.43	01.19	45.73	45.52
63.5			02.40	02.15	47.37	47.16
64.5			03.36	03.15	49.03	48.83
65.5			04.37	04.13b	50.73	50.53
66.5			05.40b	05.12	52.43	52.19
67.5			06.42	06.16	54.15	53.91
68.5			07.47	07.20	55.86	55.62
69.5			08.55	08.24	a	57.36
70.5			09.60	09.30	59.37	59.09
71.5	14660.93b	14661.00	10.70	10.38b	61.12	60.89
72.5	61.35b	61.42	11.77	11.50	62.97	62.67
73.5	61.78b	61.84	12.93	12.57	64.77	64.45
74.5	62.24b	62.31	14.05	13.69	66.57	66.24
75.5	62.69b	62.79	15.21	14.85	68.43	68.07
76.5	63.17b	63.28	16.39	16.01		69.90
77.5	63.67b	63.77	17.55	17.19	72.11	71.75
78.5	64.19b	64.29	18.76	18.37b	74.04	73.58
79.5	64.71b	64.82	19.95	19.57	75.92	75.51
80.5	65.25b	65.39	21.21b	20.75		
81.5	65.81b		22.45	22.02	79.78	79.29
82.5	66.36b	66.49	23.70	23.23	81.69	81.19
83.5	67.00b	67.12	24.99	24.51	83.65	83.16
84.5	67.59b	67.71	26.27	25.76	85.68	85.13
85.5	68.20b	68.35	27.58	27.05	87.61	87.11
86.5	68.85	68.98	28.88		89.62	89.09
87.5	69.51	69.65	30.27		91.65	
88.5	70.20	69.65	31.57	29.70		
89.5	a	70.32	32.98	31.04		
90.5	71.59	71.02	34.36b	32.38		
91.5		71.75	35.74	33.72		
92.5			37.14	35.09		93.09
93.5			38.58	37.94		
94.5			39.99	39.35		
95.5			41.46	40.79b		
96.5			42.92	42.21		
97.5			44.43	43.69		
98.5			45.93	45.22		

a-overlapped by atomic line; b-blended with LaO line; h-overlapped by band head.

Table III. Rotational lines of $c\,^2\Pi_{1/2} \rightarrow X\,^2\Delta_{3/2}$ (1,1) sub-band.

J	$P_{1c}(J)$	$P_{1d}(J)$	$Q_{1c}(J)$	$Q_{1d}(J)$	$R_{1c}(J)$	$R_{1d}(J)$
20.5				15176.00		
21.5				76.25		
22.5				76.50		
23.5			15179.64	76.73		
24.5			80.02	77.02		15194.71b
25.5	a	h	80.43b	77.31		95.71
26.5	a	15159.68	80.89	77.63b		a
27.5		59.31	81.34	77.94		97.72
28.5	15161.93b	58.91b	81.73	78.30	15201.19b	
29.5	61.68b	58.52b	82.24	h	02.33b	
30.5	61.45b	58.18	82.68		03.47	99.77
31.5	61.29b	57.88	83.19b		04.66	200.80b
32.5	61.10b	57.54b	83.73		05.85b	01.87
33.5		57.23	84.22		07.08b	02.97b
34.5	60.75b	56.95	84.75	80.59	08.25	
35.5		56.66b	85.29b	80.98b	09.54b	
36.5	60.46b	56.38	85.88	81.42	10.78	
37.5	60.35b	56.17	86.47b	81.92	13.26	08.58b
38.5	60.26b		86.99b	82.37	14.52	09.69
39.5			87.63	82.85b		
40.5		55.31	88.25	83.35		
41.5			88.88	83.85	18.41b	12.08
42.5		54.97	88.52b	h	19.80b	13.26b
43.5			90.17	84.96	21.15b	14.52b
44.5		54.67b	90.86	85.49b	22.53b	15.74b
45.5		54.56	91.53b	86.04	23.84	18.24
46.5			92.22b	86.64b	25.26b	19.50b
47.5			92.91b	87.22	26.60b	
48.5			93.67	87.83b		22.10
49.5			94.41b	a	29.46	23.43b
50.5			95.15	89.75	30.93	24.74
51.5			95.92	90.42	32.36	26.07b
52.5	60.26b		a	91.11b		27.48
53.5	60.35b		97.48	91.79	35.28	28.85b
54.5	60.46b		98.28b	92.49	36.76	30.23
55.5			99.13b	93.23	38.38	31.62
56.5	60.75b		99.94	93.97b	39.82b	32.97b
57.5			200.80	94.71	41.36	
58.5	61.10b		01.65		44.44	35.88b
59.5	61.29b		02.53b	96.24	46.01b	37.35b
60.5	61.45b		03.39	a	47.61	38.79b
61.5	61.68b		04.32	97.83b	49.22	
62.5	61.93b		05.22b	97.83b		
63.5	a		06.17	98.66		41.74
64.5	a		07.08b	99.46b		43.22b
65.5	62.69b		08.07b	200.32		
66.5	62.99		09.03	01.19		

a-overlapped by atomic line; b-blended with LaO line; h-overlapped by band head.

Table III. (cont.)

J	$P_{1c}(J)$	$P_{1d}(J)$	$Q_{1c}(J)$	$Q_{1d}(J)$	$R_{1c}(J)$	$R_{1d}(J)$
67.5	15163.28b		15210.05b	15202.06		
68.5	63.62		11.02b	02.97b		
69.5			12.05	03.85		
70.5	64.30		13.04b	04.78		
71.5	64.68b		14.14	05.68		
72.5	65.05		15.17	06.65b		
73.5	65.41		16.24	07.59		
74.5	65.80b		17.34b	08.58		
75.5	66.26b		18.41b	09.54b		
76.5	66.67b		19.51	10.55		
77.5	67.14b		20.64	11.57		
78.5	67.61b		21.75b			
79.5	68.05b		22.93	13.66		
80.5	68.54b		24.06	14.72		
81.5	69.05		25.26	15.77		
82.5			26.49b	16.87		
83.5	70.11		27.69b	17.97		
84.5			28.85	19.07		
85.5	71.32		30.15	20.18b		
86.5	71.77b		31.35b	21.34		
87.5			32.60b	22.53b		
88.5	73.60b		33.89	23.68b		
89.5	74.22		35.18	24.87b		
90.5	74.91		36.46	26.07		
91.5			37.81	27.26		
92.5			39.13	28.47		
93.5			40.48b			
94.5			41.86			
95.5			43.22	32.24		
96.5			44.61	33.55		
97.5			46.01	34.84		
98.5			47.41	36.16b		
99.5			48.84	37.48		
100.5				38.79b		
101.5				40.19		
102.5				41.54b		
103.5				42.93b		
104.5				44.32		
105.5				45.72		

a-overlapped by atomic line; b-blended with LaO line; h-overlapped by band head.

Table IV. Rotational lines of the $C^2\Pi_{3/2} \rightarrow A'^2\Delta_{5/2}$ (1,1) sub-band.

J	$P_{2c}(J)$	$P_{2d}(J)$	$Q_{2c}(J)$	$Q_{2d}(J)$	$R_{2c}(J)$	$R_{2c}(J)$	$R_{2d}(J)$
10.5	14691.68b	14691.68b	14699.18	14699.18			
11.5	91.17b	91.17b	99.36b	99.36b			
12.5	90.65b	90.65b	99.54b	99.54b			
13.5	90.15b	90.15b	99.81	99.81			
14.5			99.81	99.81			
15.5	89.22b	89.22b	700.05	700.05			
16.5			00.28b	00.28b			
17.5	88.34b	88.34b	00.55b	00.55b			
18.5	87.94b	87.94b	00.84	00.84			
19.5			01.43b	01.43b	14715.46	14715.46	14715.46
20.5	87.14b	87.14b	01.77b	01.77b	16.50b	16.50b	16.50b
21.5	86.76b	86.76b	02.15b	02.15b	17.55b	17.55b	17.55b
22.5	86.42b	86.42b	02.48	02.48	18.54	18.54	18.54
23.5	86.06b	86.06b	02.90b	02.90b	20.72b	20.72b	20.72b
24.5	85.75b	85.75b	03.25	03.25	21.78	21.78	21.78
25.5	85.45b	85.45b	03.67	03.67	22.91b	22.91b	22.91b
26.5					23.97b		23.97b
27.5	84.89b	84.89b	04.52	04.52	25.10	25.10	25.10
28.5	84.60b	84.60b	04.99	04.99	26.27b	26.27b	26.27b
29.5	84.39b	84.39b			27.45b	27.45b	27.45b
30.5	84.15b	84.15b	05.93	05.93	28.62b	28.62b	28.62b
31.5	83.94b	83.94b	06.42b	06.42b			
32.5	83.76b	33.76b	06.94	06.94	31.04b	31.04b	31.04b
33.5	83.56b	83.56b	07.47b	07.47b	32.25	32.25	32.25
34.5			08.01	08.01	33.48	33.48	33.48
35.5	83.28b	83.28b	08.55	08.55	34.72b	34.72b	34.72b
36.5			09.14b	09.14b	36.02b	36.02b	36.02b
37.5			h	h			
38.5					38.58b	38.58b	38.58b
39.5			10.95	10.95	39.91b	39.91b	39.91b
40.5			11.62		41.21	41.21	41.21
41.5			12.26	12.26			
42.5			12.93b	12.93b			
43.5				13.55			
44.5			14.30b	14.30b	46.72	46.72b	
45.5			15.01				
46.5			15.78	15.69b	49.46b		
47.5			16.50b		51.00		
48.5			17.28	17.19b			
49.5			18.07	17.98	53.91b	53.91b	
50.5			18.86	18.76b			
51.5				19.57b	56.89b	56.89b	
52.5			20.50	20.36	55.30 / 56.79 / 58.29		
53.5	83.28b						

a-overlapped by atomic line; b-blended with LaO line; h-overlapped by band head.

Table IV. (cont.)

J	$P_{2c}(J)$	$P_{2d}(J)$	$Q_{2c}(J)$	$Q_{2d}(J)$	$R_{2c}(J)$	$R_{2d}(J)$
54.5	14683.56b		14721.33	14721.21b	14761.51	
55.5	83.76b		22.19	22.02b	63.06	14769.27b
56.5	83.94b		23.06	22.91		70.88
57.5	84.15b		23.97b	23.78		72.50
58.5	84.39b		24.85	24.68	66.24b	74.19
59.5	84.60b		25.76b	25.57b	67.84	
60.5	84.89b		26.69	26.54	69.46	
61.5			27.63	27.45b	71.09	
62.5			28.62b	26.41b	72.75b	
63.5	65.45b		29.54	29.39	74.40	80.06
64.5	85.75b		30.57	30.33	76.04	82.68
65.5	86.06b		31.57b	31.35b		84.41
66.5	86.42b		32.61	32.38b	79.45	86.17
67.5	86.76b		34.72b		81.19b	87.98
68.5	87.14b		35.74b	35.51	82.94b	
69.5			36.84	36.57		
70.5	87.94b		37.94b	37.66b	86.50	91.55
71.5	88.34b		39.08b	38.76	88.27	
72.5			40.22	39.91		
73.5	89.22b		42.51	41.01		95.19
74.5			43.69b	42.21b		
75.5	90.15b		44.90	43.37		
76.5	90.65b		46.09	45.73b		
77.5	91.17b		47.37b	46.93		
78.5	91.68b		48.56	48.18b		
79.5	92.26b		49.82	49.45		802.66
80.5			51.12			
81.5			52.43b	51.96		06.51
82.5			53.71b	53.21		
83.5			55.02	54.54		
84.5			56.35	55.86b		
85.5			a			
86.5			59.09b	58.53		
87.5			60.45	59.89		
88.5			61.81b	61.27		
89.5				62.67		
90.5			64.68			
91.5			66.12	65.53		
92.5			67.58b			
93.5			69.06	68.41b		
94.5			70.54	69.90b		
95.5						
96.5						
97.5						
98.5			73.58b			
99.5			75.12			
100.5			76.64			
101.5			78.20			
102.5			79.78b			
103.5			81.39			

a-overlapped by atomic line; b-blended with LaO line; h-overlapped by band head.

374

TABLE V
Summary of Rotational Constants of $C^2\Pi \rightarrow A'^2\Delta$ Transition

	$C^2\Pi_{1/2}$	$C^2\Pi_{3/2}$	$A'^2\Delta_{3/2}$	$A'^2\Delta_{5/2}$	Error
$B(v=0)$	0.3495_6	0.3511_4	0.3427_1	0.3435_2	±0.0001
		0.3503_2		0.3431_2	
$B(v=1)$	0.3479_2	0.3494_4	0.3410_0	0.3418_6	±0.0002
		0.3486_6		0.3414_2	
$D(0) \times 10^6$	0.27_6	0.28_2	0.28_1	0.28_0	±0.005
$D(1) \times 10^6$	0.24_9	0.24_2	0.25_2	0.25_4	±0.01
B_e		0.3511		0.3439	
α_e		0.0016		0.0016	
$D_e \times 10^6$		0.29_7		0.29_4	
$\beta_e \times 10^6$		-0.03_5		-0.02_7	
r_e (Å)		1.829		1.848	

TABLE VI
Λ-Doubling Coefficients in $C^2\Pi$ State

	$v=0$	$v=1$	$=0$	$v=1$	Error
a_0	0.120_6	0.120_7			±0.0002
$a_1 \times 10^6$	-0.78	-0.75			±0.02
$a_2 \times 10^6$			0.80	0.76	±0.02

TABLE VII
Band Origins of $C^2\Pi \rightarrow A'^2\Delta$ (0,0) and (1,1) Subbands

	$C^2\Pi_{1/2} \rightarrow A'^2\Delta_{3/2}$	$C^2\Pi_{3/2} \rightarrow A'^2\Delta_{5/2}$	Error
$v'' = v' = 0$	15 150.00	14 671.19	±0.01
$v'' = v' = 1$	15 174.26	14 698.10	±0.02
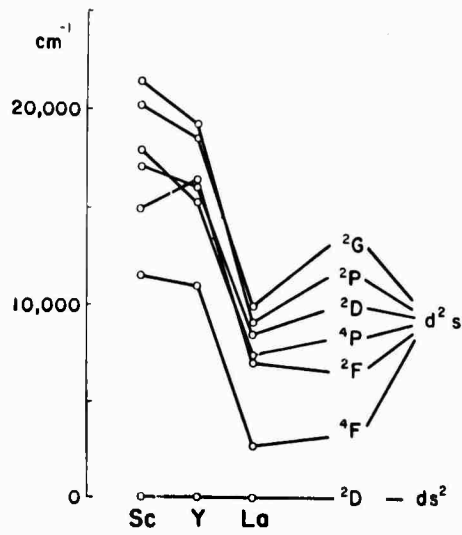
Fig. 4. Atomic energy levels of Sc, Y, and
La from the ds^2 and d^2s configurations.
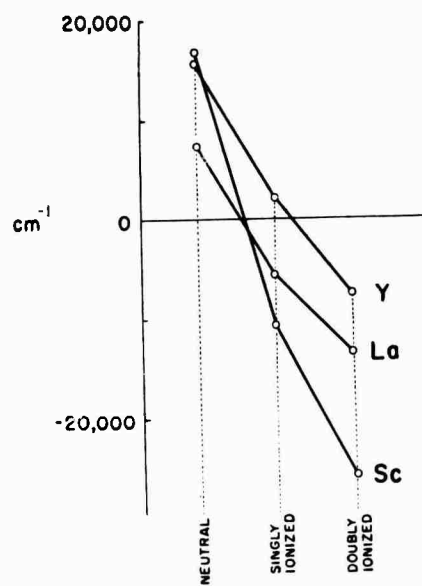
Fig. 5. Energy of a d orbital relative to an
s orbital for Sc, Y, and La atoms and
ions.

376
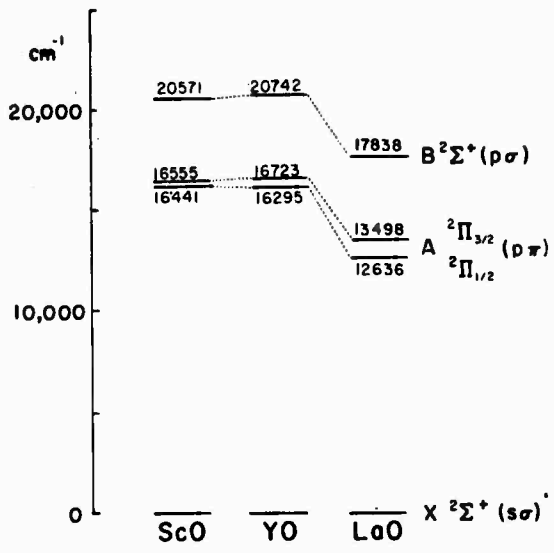
Fig. 1. Electronic energies and approximate
molecular orbital configurations
for three electronic states of
ScO, YO, and LaO.
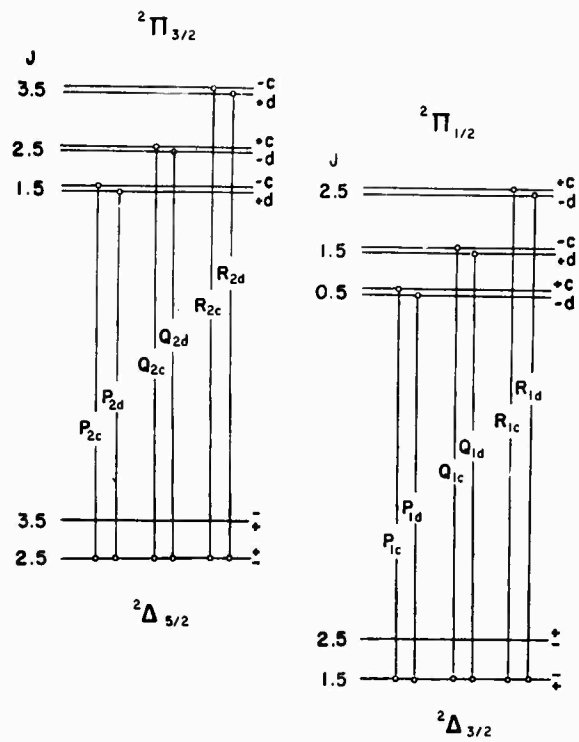
Fig. 2. Schematic representation of the
lines of the branches of a
$^2\Pi \rightarrow {}^2\Delta$ electronic transition for
both states in case a coupling.
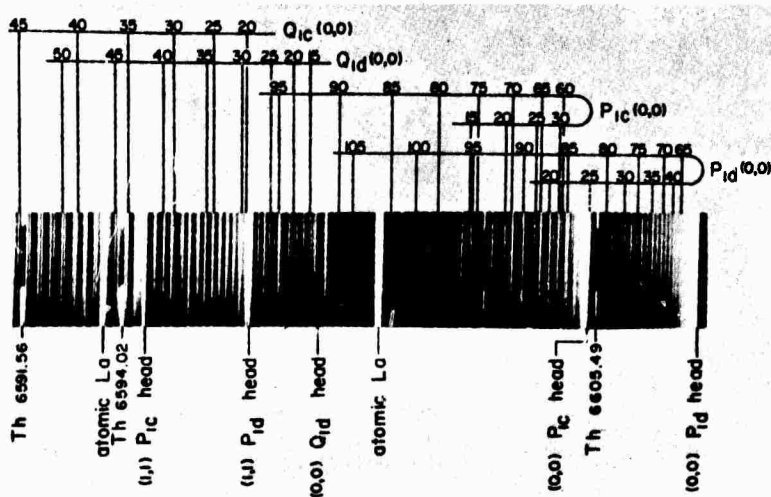
Fig. 3. A portion of the LaO $C^2\Pi_{1/2} \rightarrow A'^2\Delta_{3/2}$ (0,0) subband spectrum.

377